Novel Substituted Hydroxyapatites

A thesis

submitted in partial fulfilment

of the requirements for the degree

of

Doctor of Philosophy in Chemistry

at

The University of Waikato

by

Moh'd Yousef Beqain

THE UNIVERSITY OF
WAIKATO
Te Whare Wānanga o Waikato

2023

This thesis is dedicated to

My beloved wife Maysam Bqa'een and my children Lujain, Butros and Yousef Beqain. Without your love and support, I would not have reached this far

&

To the memories of my father Yousef Beqain and dear mother Khadra Madanat

Abstract

Hydroxyapatite (HAp) has been widely used as a bone replacement material for biomedical applications, in particular as a bone graft and coating for implants, because of its similarity in composition and crystal structure to natural bone.

The present study aims to develop of a novel method to prepare (unsubstituted and substituted) HAp by hydrolysis of monocalcium phosphate (MCP) using calcium hydroxide ($Ca(OH)_2$). Different techniques were used to characterize the prepared samples such as SEM, FTIR, XRD and ICP-MS. The presence of an apatitic phase in the sintered unsubstituted powders prepared by the hydrolysis of MCP/$Ca(OH)_2$ was confirmed by FTIR spectra, through detecting the fundamental vibrational modes of PO_4^{3-} group as well as by observation of the typical HAp lattice OH vibrations at 3572 and 631 cm^{-1}, so indicating formation of crystalline material. The XRD diffraction patterns of the sintered unsubstituted HAp powders were in a good agreement with the HAp patterns reported in the current literature, the standard HAp (reference card number 01-074-9780) as well as commercial HAp (Fluka) and showed the characteristic peaks of the HAp phase with a slight presence of the β-TCP phase that would have formed from the sintering process used to crystallise the HAp powders at 900 ˚C. The ICP-MS analyses of unsubstituted HAp powders showed that the Ca/P mole ratios of the unsubstituted HAp materials produced was 1.40, which is lower than the theoretical value of stochiometric HAp (1.67). This result can be ascribed to the substitution process of calcium ions by sodium ions in the HAp crystal lattice as a result of using sodium hydroxide to adjust pH in the reactions leading to the formation of HAp. The value of the (Ca+Na)/P when computed using elemental data obtained from the ICP-MS analyses was found to be 1.65 which is very close in value to of the value expected for stoichiometric HAp (1.67). SEM images showed that the sintered samples of unsubstituted HAp powders consist of particles with fine grains, spheroidal in shape associated with an irregular distribution of particle sizes. The degree of crystallinity and the numerical value of the crystallite size of the sintered unsubstituted HAp materials were 82.6% and 549.8 Å, respectively. The Rietveld refined values of lattice constants of the sintered unsubstituted HAp materials were a= 9.421±0.003 and c= 6.882±0.005 **Å**.

By means of the novel hydrolysis route (hydrolysis of MCP and $Ca(OH)_2$), three substituted "MHAp" materials were prepared with the following chemical formula: $Ca_{10-x}M_x(PO_4)_6(OH)_2$ (M=Zn, Sr and Cu, x=0.5, 1.0 and 1.5). FTIR spectra showed that there was:

- a presence of apatite phase in the prepared powders.
- a clear relation between the amount of M ions, and the intensities of OH^- vibration modes at 3572 cm^{-1} (stretching) and 630 cm^{-1}.
- A clear shift of phosphate bands in the unsubstituted HAp at 572 and 604 cm^{-1} to a lower wave number due to substitution of Sr^{2+} ions. This shift increases as the amount of Sr ions increases. Another shift of the OH librational band from 630 to 612 cm^{-1} was also observed with an increase in the percentage of Sr^{2+} ions in the substituted HAp.

The phase purity, crystallinity, crystallite size and lattice parameters of the prepared MHAp materials varied with increasing substitution levels. SEM images showed that ZnHAp and CuHAp materials consisted of agglomerated crystals which are spheroidal in shape. Spheroidal particles were seen in 0.5 SrHAp and 1.0 SrHAp samples, but a combination of spheroidal and rod like particles was recorded in the case of the 1.5 SrHAp materials. The results of ICP-MS measurements displayed clearly the presence of these ions (Zn^{2+}, Sr^{2+} and Cu^{2+} ions) in the HAp samples but did not offer explicit proof of substitution. The measured (actual) wt.% of Zn^{2+}, Sr^{2+} and Cu^{2+} ions that that were detected by ICP-MS analysis was lower than the theoretical value indicating how difficult it is for the small ions such as Zn^{2+} and Cu^{2+}as well as the large ions such as $Sr^{2+}$to be introduced and hosted by the HAp sample.

Also, in the present study different systems of cationic substituted HAp, namely 1% RbHAp (1 wt.% Rb^+), 1%EuHAp (1 wt.% Eu^{3+}) and 1,3 and 5% ScHAp (1, 3 and 5 wt.% Sc^{3+}), were prepared by using two different methods (precipitation and hydrolysis of MCP/$Ca(OH)_2$). The results of ICP-MS analysis showed that the presence of Rb^+, Eu^{3+} and Sc^{3+} ions in the HAp crystal was very low. In the case of the Sc-substituted HAp, the level of substitution was negligible.

Various systems of anionic and co substituted HAp, namely 1, 3 and 5% NbHAp, 1% B_4O_7HAp, bromapatite, sulfoapatite and NaClHAp were also prepared by using different preparation methods (precipitation, hydrolysis of MCP/$Ca(OH)_2$ and ion exchange routes). There was found to be a reduction of the intensity of the stretching mode of the OH^- group at 3572 cm^-

[1] due to the replacement process of phosphate and/or hydroxyl groups by monovalent and bivalent ions(Br^-, S^{2-} and $B_4O_7^{2-}$).

The mechanical strength and the particle size of specific systems of unsubstituted HAp, substituted and co substituted HAp powders prepared by the hydrolysis process of MCP and $Ca(OH)_2$ were also studied**.** The results of the mechanical properties in the present investigation showed clearly that particle size plays a fundamental rule in the value of mechanical strength, since an enhancement in the mechanical strength was recorded because of the reduction in particle size that occurred in some preparations.

Acknowledgements

First of all, I would like to express my most respectful gratitude to my chief supervisor, Associate Professor Michael Mucalo, Associate Dean Postgraduate (Division of Health, Engineering, Computing, & Science), for guidance, constant encouragement, feedback and patience throughout this project.

I am also equally thankful to my co-supervisor, Professor Kim Pickering and Dr. Amanda French, for their valuable feedback. I am also thankful to all the laboratory staff and technical persons (Helen Turner, Kirsty Vincent and Annette Rodgers) for providing technical assistance in characterising materials (SEM, XRD and Malvern Mastersizer instrument) whenever required.

Also, I would like to thank Dr. Chelsea Blickem and Andrea Haines for their assistance.

I want to offer my sincere special thanks to Cheryl Ward, for her assistance and support throughout my PhD journey.

Isaiah 41:13- "*For I am the LORD your God who takes hold of your right hand and says to you, Do not fear; I will help you*"

Table of Contents

Abstract i

Acknowledgements iv

Table of Contents v

List of Figures xviii

List of Tables xxvi

List of Abbreviations xxxiv

Chapter One Introduction to Hydroxyapatite and Substituted Hydroxyapatites. 35

1.1 Background: 35

1.2 Substituted HAp materials: 36

1.3 The Scope of the Present Investigation: 37

1.4 Broad objectives of this work: 40

Chapter Two Literature review. 42

2.1 Hydroxyapatite: 42

2.2 Structures of Hydroxyapatite: 45

2.3 Sources of HAp: 47

2.4 Some methods used for the preparation of Hydroxyapatite : 47

2.4.1 Precipitation method: 48

2.4.2 Solid state route : 48

2.4.3 Mechanochemical method: 48

2.4.4 Sol-gel synthesis: 49

2.4.5 Hydrothermal processes: 49

2.4.6 Hydrolysis: 50

2.5 Substituted Hydroxyapatites: 50

2.6 Summary of Synthetic Approaches to forming Substituted Hydroxyapatites: 52

2.7 Specific Systems of Substituted HAps 54

2.7.1 Some examples of XO_4 (anionic) substitutions in $M_{10}(XO_4)_6(Y)_2$: 54

2.7.1.1 Carbonate*:* 54

2.7.1.2 Si (as silicate) substituted HAp: 57

2.7.2 Examples for M substitution in $M_{10}(XO_4)_6(Y)_2$: 58

2.7.2.1 Ag: 58

2.7.2.2 Zn: 60

2.7.2.3 Fe: 61

2.7.2.4 Co and Cu: 62

2.7.2.5 Na substituted HAps:.....65
2.7.2.6 Sr.....65
2.7.2.7 Mg:.....67
2.7.2.8 Mn: 69
2.7.2.9 Lanthanide ion substituted HAps (La, Eu, Gd, and Tb): 69
2.7.2.10 Ti Substituted HAps:.....70
2.7.2.11 Bi HAps: 71
2.7.2.12 Ba substituted HAps:.....71
2.7.2.13 Nb: 72
2.7.3 Some Examples of Y Substitution in $M_{10}(XO_4)_6(Y)_2$:.....72
2.7.3.1 Fluoride (F^-): 73
2.7.3.2 Cl^-:.....75
2.7.4 Co-substitutions of hydroxyapatite (substitutions with two different or more several ions):.....76
2.7.4.1 Cationic co-substitutions (substitutions with two or more different cations):76
2.7.4.2 Anionic co-substitution (substitutions with two anions in the HAp lattice):...78
2.8 Research gaps in the current field of substituted HAps: 80
Chapter Three Materials and Methods 82
3.1 Research methodology 84
3.2 The common reagents and solvents that were used in this project to prepare the cationic, anionic and co-substituted HAp powders:.....95
3.2.1 Reagents used to prepare cationic substituted HAp with the following specific formulae: $Ca_{10-x}M_x(PO_4)_6(OH)_2$), where (M= Zn, Sr and Cu)and (X=0.5, 1.0 and 1.5)by the hydrolysis method: 99
3.2.2 Reagents that were used to prepare cationic substituted HAp (specifically 1% RbHAp (1 wt.% Rb^+), 1% EuHAp (1 wt.% Eu^{3+}) and 1, 3 and 5% ScHAp (1, 3 and 5 wt.% scandium ions) by the precipitation and hydrolysis methods:.....99
3.2.3 Reagents that were used to prepare anionic substituted HAp materials, namely (NbHAp, BHAp, Br_2Ap, and SAp powders) by the precipitation, hydrolysis and ion exchange methods:.....100
3.2.4 Reagents that were used to prepare co substituted HAp materials (NaClHAp) by the precipitation and hydrolysis methods:.....101
3.3 Characterization of the substituted HAps 101
3.3.1 Microstructural Characterization: 101
3.3.1.1 Microscopy: Scanning Electron Microscopy (SEM):.....101
3.3.1.2 Energy dispersive X-ray Analysis (EDX): 102
3.3.2 FTIR Spectroscopy:.....104
3.3.3 Inductively coupled plasma mass spectrometry (ICP-MS) analysis:.....105

3.3.4 Powder X-ray Diffraction 106
3.3.4.1 Sampling for XRD.....107
3.3.4.2 Phase Identification:.....108
3.3.4.3 Crystallinity and Crystallite size (D_{002} reflection plane):.....109
3.3.4.4 Lattice Parameter Determination and the volume of the hexagonal unit cell : 109
3.3.5 Mechanical tests: 111
3.3.5.1 Compression tests: 112
3.3.5.2 Laser Light Scattering Particle Size Analyzer: 114
Chapter Four The development of a novel method to prepare (unsubstituted) HAp by hydrolysis of monocalcium phosphate (MCP) using calcium hydroxide. 117
4.1 Introduction: 117
4.2 The Preparation and Characterization of the unsubstituted HAp material prepared via the novel hydrolysis method using MCP and $Ca(OH)_2$: 119
4.2.1 ICP-MS analysis of unsubstituted HAp materials prepared by hydrolysis of MCP/$Ca(OH)_2$ 121
4.2.2 FTIR studies of the unsubstituted HAp prepared by hydrolysis of MCP and $Ca(OH)_2$.....123
4.2.3 XRD diffraction analysis of the prepared unsubstituted hydroxyapatite materials (HAp) by the hydrolysis method (of MCP/$CaOH)_2$): 129
4.2.3.1 Phase identification of unsubstituted HAp materials prepared by hydrolysis of MCP with calcium hydroxide: 129
4.2.3.2 Crystallinity and Crystallite size of unsubstituted HAp materials prepared by the hydrolysis method. 134
4.2.3.3 Lattice parameter and volume of unit cell measurements of commercial HAp (Fluka) compared to sintered unsubstituted HAp materials prepared by the novel hydrolysis and conventional precipitation methods: 136
4.2.4 SEM of unsubstituted HAp materials prepared by hydrolysis method: 139
4.2.5 Previous results from other studies in the literature where the hydrolysis method has been used to prepare HAp: 144
4.3 Summary: 147
Chapter Five Preparation of (cationic) metal ion substituted HAp powders with the following chemical formula: $Ca_{10-x}M_xHAp$ (where M=Zn, Sr and Cu, X=0.5, 1.0 and 1.5) by a novel hydrolysis method using MCP/$Ca(OH)_2$. 149
5.1 Introduction: 149
5.2 The preparation of Zinc ion substituted hydroxyapatite (ZnHAp) materials by the novel MCP/$Ca(OH)_2$ hydrolysis method:.....151
5.3 Characterization of ZnHAp powders prepared with different Zn^{2+} content by the novel MCP/$Ca(OH)_2$ hydrolysis method.....151

5.3.1 ICP-MS studies of sintered ZnHAp materials prepared by hydrolysis of MCP/$Ca(OH)_2$ at 900 ˚C with different levels of Zn^{2+} substitution. 151
5.3.2 FTIR studies of ZnHAp prepared with different levels of Zn^{2+} substitution. 153
5.3.2.1 FTIR of non-sintered (as received) ZnHAp (prepared by hydrolysis of MCP/$Ca(OH)_2$) 153
5.3.2.2 FTIR spectra of ZnHAp after sintering at 900 ˚C: 155
5.3.3 XRD diffraction analysis of sintered ZnHAp (prepared by hydrolysis of MCP/$Ca(OH)_2$). 158
5.3.3.1 Phase Identification of the ZnHAp powders. 158
5.3.3.2 The degree of crystallinity and crystallite size of ZnHAp powders: 161
5.3.3.3 Lattice parameters and calculated volume of unit cell of the ZnHAp powders: 162
5.3.4 SEM of sintered ZnHAp materials with different levels of Zn^{2+} substitution as prepared by the novel hydrolysis method of MCP/$Ca(OH)_2$ 164
5.4 SrHAp materials generated by hydrolysis of MCP/$Ca(OH)_2$ 168
5.5 Characterization of SrHAp powders prepared with different levels of Sr^{2+} substitution by hydrolysis of MCP/$Ca(OH)_2$:.....168
5.5.1 ICP-MS analysis of sintered SrHAp materials after sintering at 900 ˚C: 168
5.5.2 FTIR Spectroscopy of SrHAp materials.....169
5.5.2.1 FTIR of non-sintered SrHAp materials.....169
5.5.2.2 FTIR of the SrHAp materials after sintering at 900 ˚C:.....171
5.5.3 -XRD diffraction analysis of the SrHAp materials after sintering at 900 ˚C. 174
5.5.3.1 Phase Identification of SrHAp powders. 174
5.5.3.2 Crystallinity and crystallite size of SrHAp powders:.....176
5.5.3.3 Lattice parameters and volume of unit cell of SrHAp powders:.....181
5.5.4 SEM investigation of SrHAp powders prepared by the novel hydrolysis method after sintering at 900 ˚C.....182
5.6 CuHAp materials by hydrolysis method:.....186
5.7 Characterization of CuHAp materials 187
5.7.1 5.6.1 ICP-MS of CuHAp materials after sintering at 900 ˚C 187
5.7.2 FTIR of CuHAp materials with different Cu^{2+} contents prepared by hydrolysis method.....189
5.7.2.1 FTIR of non-sintered CuHAp materials.....189
5.7.2.2 FTIR of CuHAp materials after sintering at 900 ˚C: 190
5.7.3 XRD diffraction analysis of CuHAp materials after sintering at 900 ˚C.....192
5.7.3.1 Phase Identification of CuHAp powders. 192
5.7.3.2 Crystallinity and crystallite size of CuHAp powders:.....194

5.7.3.3 Lattice parameters and volume of unit cell of CuHAp powders: 195
5.7.4 SEM of CuHAp materials after sintering at 900 ˚C 198
5.8 Summary: 200
Chapter Six Studies on cationic substitutions into HAp of little studied ions 203
6.1 Introduction: 203
6.2 1% RbHAp (1 wt.% Rb^{+}) powders prepared by hydrolysis and precipitation methods: 205
6.2.1 Characterization techniques of prepared 1%RbHAp (1 wt.% Rb^{+}) materials by hydrolysis and precipitation methods. 207
6.2.1.1 ICP-MS of 1% RbHAp (1 wt.% Rb^{+}) materials prepared by hydrolysis and precipitation methods after sintering at 900 ˚C. 207
6.2.1.2 FTIR of prepared 1%RbHAp (1 wt.% Rb^{+}) by hydrolysis method and precipitation method: 208
FTIR of the non- sintered 1% RbHAp (1 wt.% Rb+) materials prepared by hydrolysis and precipitation methods: 208
FTIR of 1% RbHAp (1 wt.% Rb^{+}) materials prepared by the novel hydrolysis and conventional precipitation methods after sintering at 900 ˚C: 210
6.2.1.3 XRD diffraction analysis of sintered and non-sintered 1%RbHAp (1 wt.% Rb^{+}) prepared by hydrolysis and precipitation method: 213
Phase Identification of 1% RbHAp (1 wt.% Rb^{+}) materials: 213
Crystallinity and crystallite size of sintered 1% RbHAp (1 wt.% Rb^{+}) materials: ... 217
Lattice parameters and volume of unit cell of sintered 1% RbHAp (1 wt.% Rb^{+}): 218
6.2.1.4 SEM of 1% RbHAp (1 wt.% Rb^{+}) materials prepared by hydrolysis and precipitation methods: 220
SEM of non-sintered 1% RbHAp (1 wt.% Rb^{+}) prepared by hydrolysis and precipitation methods. 220
SEM of 1%RbHAp (1wt.% Rb^{+}) materials prepared by hydrolysis and precipitation methods after sintering at 900 ˚C: 222
6.3 1%EuHAp (1 wt.% Eu^{3+}) powders prepared by hydrolysis and precipitation methods: 225
6.3.1 Characterization techniques of 1%EuHAp (1 wt.% Eu^{3+}) materials prepared by the conventional precipitation and novel hydrolysis methods: 227
6.3.1.1 ICP-MS of 1% EuHAp (1 wt.% Eu^{3+}) materials prepared by hydrolysis and precipitation method after sintering at 900 ˚C 227
6.3.1.2 FTIR of 1% EuHAp (1 wt.% Eu^{3+}) materials prepared by hydrolysis and precipitation methods: 229
FTIR of non-sintered 1% EuHAp (1 wt.% Eu^{3+}) materials prepared by hydrolysis and precipitation methods. 229
FTIR of 1%EuHAp (1 wt.% Eu^{3+}) materials prepared by hydrolysis and precipitation methods after sintering at 900 ˚C. 230

6.3.1.3 XRD diffraction patterns of non-sintered and sintered 1% EuHAp (1 wt.% Eu^{3+}) materials prepared by hydrolysis and precipitation methods: 232

Phase Identification of Sintered 1%EuHAp materials: 232

Crystallinity and crystallite size of sintered 1%EuHAp materials: 235

Lattice Parameters and volume of unit cell of 1%EuHAp materials: 237

6.3.1.4 SEM of 1%EuHAp (1 wt.% Eu^{3+}) materials prepared by hydrolysis and precipitation methods: 238

SEM of non-sintered 1%EuHAp (1 wt.% $Eu3^{+}$) materials prepared by hydrolysis and precipitation methods. 238

SEM of 1% EuHAp (1 wt.% Eu^{3+}) materials prepared by the novel hydrolysis and conventional precipitation methods after sintering at 900 ˚C: 240

6.4 1, 3 and 5% ScHAp (1, 3 and 5 wt.%Sc^{3+}) powders prepared by hydrolysis and precipitation methods: 244

6.4.1 1%ScHAp (1 wt.% Sc^{3+}) powders prepared by the novel hydrolysis and conventional precipitation methods: 247

6.4.1.1 Characterization techniques of 1% ScHAp (1 wt.% Sc^{3+}) materials prepared by the novel hydrolysis and conventional precipitation methods: 247

6.4.1.2 ICP-MS of 1%ScHAp (1 wt.% Sc^{3+}) materials prepared by hydrolysis and precipitation methods after sintering at 900 ˚C: 247

6.4.1.3 FTIR of 1% ScHAp (1 wt.% Sc^{3+}) materials prepared by the novel hydrolysis and conventional precipitation methods. 248

FTIR of non-sintered 1%ScHAp (1 wt.% Sc^{3+}) materials prepared by hydrolysis and precipitation methods. 248

FTIR of 1%ScHAp (1 wt.% Sc^{3+}) materials prepared by hydrolysis and precipitation methods after sintering at 900 ˚C: 250

6.4.1.4 XRD diffraction patterns of non-sintered and sintered 1%ScHAp (1 wt.% Sc^{3+}) materials prepared by hydrolysis and precipitation methods: 252

Phase Identification of 1%ScHAp (1 wt.% Sc^{3+}) materials: 252

Lattice parameters and volume of unit cell of sintered 1%ScHAp (1% wt. Sc^{3+}) materials: 256

6.4.1.5 SEM of 1%ScHAp (1 wt.% Sc^{3+}) materials prepared by hydrolysis and precipitation methods: 257

SEM of non-sintered 1%ScHAp (1 wt.% Sc^{3+}) materials prepared by hydrolysis and precipitation methods: 257

SEM of 1%ScHAp (1 wt.% Sc^{3+}) materials prepared by hydrolysis and precipitation methods after sintering at 900 ˚C: 260

6.4.2 3% ScHAp (3 wt.% Sc^{3+}) powders prepared by hydrolysis and precipitation methods: 264

6.4.2.1 Characterization techniques of 3% ScHAp (3 wt.% Sc^{3+}) materials prepared by hydrolysis and precipitation methods: 264

6.4.2.2 ICP-MS of prepared 3% ScHAp (3 wt.% Sc^{3+}) materials prepared by hydrolysis and precipitation methods after sintering at 900 ˚C: 264

6.4.2.3 …FTIR of 3% ScHAp (3 wt.% Sc^{3+}) materials prepared by the novel hydrolysis and conventional precipitation methods. 265

FTIR of non-sintered 3% ScHAp (3 wt.% Sc^{3+}) materials prepared by the novel hydrolysis and conventional precipitation methods. 265

FTIR of ScHAp (3 wt.% Sc^{3+}) materials prepared by the hydrolysis and precipitation methods after sintering at 900 ˚C: 267

6.4.2.4 XRD diffraction patterns of non-sintered and sintered 3% ScHAp (3 wt.% Sc^{3+}) materials prepared by hydrolysis and precipitation methods: 269

Phase identification of 3% ScHAp (3 wt.% Sc^{3+}) materials: 269

Crystallinity and crystallite size of sintered 3% ScHAp (3 wt.% Sc^{3+}) materials:.... 272

Lattice parameter and volume of unit cell of sintered 3% ScHAp (3 wt.% Sc^{3+}) materials: 273

6.4.2.5 SEM of 3% ScHAp (3 wt.% Sc^{3+}) materials prepared by hydrolysis and precipitation methods: 274

SEM of non-sintered 3% ScHAp (3 wt.% Sc^{3+}) materials prepared by hydrolysis and precipitation methods: 274

SEM of 3% ScHAp (3 wt.% Sc^{3+}) materials prepared by hydrolysis and precipitation methods and sintered after sintering at 900 ˚C: 276

6.4.3 5% ScHAp powders prepared by hydrolysis and precipitation methods: 280

6.4.3.1 Characterization techniques of prepared 5% ScHAp (5 wt.% Sc^{3+}) materials by hydrolysis and precipitation methods. 280

6.4.3.2 ICP-MS of prepared 5% ScHAp (5 wt.% Sc^{3+}) materials prepared by hydrolysis and precipitation methods after sintering at 900 ˚C. 280

6.4.3.3 FTIR of 5% ScHAp (5 wt.% Sc^{3+}) materials prepared by precipitation and hydrolysis methods. 281

FTIR of non-sintered of 5% ScHAp (5 wt.% Sc^{3+}) materials prepared by hydrolysis and precipitation methods. 281

FTIR of 5% ScHAp (5 wt.% Sc^{3+}) materials prepared by hydrolysis and precipitation methods after sintering at 900 ˚C: 283

6.4.3.4 XRD diffraction patterns of 5% ScHAp (5 wt.% Sc^{3+}) materials prepared by hydrolysis and precipitation methods: 285

Phase Identification of 5% ScHAp (5% wt. $Sc3^{+}$) materials: 285

Crystallinity and crystallite size of sintered 5% ScHAp (5 wt.% Sc^{3+}) materials:.... 287

Lattice parameter and volume of unit cell of sintered 5% ScHAp (5 wt.% Sc^{3+}) materials: 287

6.4.3.5 SEM of 5% ScHAp (5 wt.% Sc^{3+}) materials prepared by hydrolysis and precipitation methods..... 288

SEM of non-sintered 5% ScHAp (5 wt.% $Sc3^{+}$) materials prepared by hydrolysis and precipitation methods. 288

SEM of 5% ScHAp (5 wt.% Sc^{3+}) materials prepared by hydrolysis and precipitation methods after sintering at 900 ˚C:....291

6.5 Summary:....294

Chapter Seven Specific systems of anionic substituted HAp powders....297

7.1 Introduction:....297

7.2 1%, 3% and 5% NbHAp (1%, 3% and 5 wt.% niobate ions) powders prepared by precipitation and hydrolysis methods. 299

7.2.1 1% NbHAp (1 wt.% niobate ions) powders prepared by precipitation and hydrolysis methods:....302

7.2.1.1 Characterization techniques of prepared 1% NbHAp (1 wt.% niobate ions) materials by the precipitation and hydrolysis methods:....302

ICP-MS of 1%NbHAp (1 wt.% niobate ions) materials prepared by precipitation and hydrolysis methods after sintering at 900 ˚C:....302

FTIR of 1%NbHAp (1 wt.% niobate ions) materials prepared by precipitation and hydrolysis methods:....304

FTIR of non-sintered 1% NbHAp (1 wt.% niobate ions) materials prepared by precipitation and hydrolysis methods: 304

FTIR spectra of 1%NbHAp(1 wt.% niobate ions) materials prepared by precipitation and hydrolysis methods after sintering at 900 ˚C: 305

XRD diffraction analysis of 1%NbHAp (1 wt.% niobate ions) materials prepared by precipitation and hydrolysis methods: 306

Phase Identification of 1% NbHAp materials: 306

Crystallinity and crystallite size of sintered 1% NbHAp materials: 309

Lattice parameters and volume of unit cell of 1%NbHAp materials:....310

SEM of prepared 1%NbHAp(1 wt.% niobate ions) materials prepared by precipitation and hydrolysis methods: 310

SEM of non-sintered 1% NbHAp (1 wt.% niobate ions) materials prepared by precipitation and hydrolysis methods: 310

SEM of 1% NbHAp (1 wt.% niobate ions) materials prepared by precipitation and hydrolysis methods after sintering at 900 ˚C:....313

7.2.2 3% NbHAp (3 wt.% niobate ions) powders prepared by the precipitation and hydrolysis methods:....315

7.2.2.1 Characterization techniques of 3% NbHAp (3 wt.% niobate ions) materials prepared by precipitation and hydrolysis methods....316

ICP-MS of 3% NbHAp (3 wt.% niobate ions) materials prepared by precipitation and hydrolysis methods after sintering at 900 ˚C....316

FTIR of prepared 3% NbHAp (3 wt.% niobate ions) materials prepared by precipitation and hydrolysis methods: 317

FTIR of non-sintered 3%NbHAp (3 wt.% niobate ions) materials prepared by precipitation and hydrolysis methods: 317

FTIR of 3% NbHAp (3%wt. Nb^{5+}) materials prepared by precipitation and hydrolysis methods after sintering at 900 ˚C:.....319

XRD diffraction patterns of 3%NbHAp (3 wt.% niobate ions) materials prepared by precipitation and hydrolysis methods: 320

Phase Identification of 3% NbHAp materials: 320

Crystallinity and crystallite size of 3% materials: 323

Lattice parameters and volume of unit cell of prepared 3% NbHAp materials: .324

SEM of 3% NbHAp (3 wt.% niobate ions) materials prepared by precipitation and hydrolysis methods:.....324

SEM of non-sintered 3% NbHAp (3 wt.% niobate ions) materials prepared by precipitation and hydrolysis methods: 324

SEM of 3% NbHAp (1 wt.% niobate ions) materials prepared by precipitation and hydrolysis methods after sintering at 900 ˚C:.....327

7.2.3 5% NbHAp (**5** wt.% niobate ions) powders prepared by precipitation and hydrolysis methods:.....329

7.2.3.1 Characterization techniques of 5% NbHAp (**5** wt.% niobate ions) materials prepared by precipitation and hydrolysis methods.....330

ICP-MS of 5% NbHAp (5 wt.% niobate ions) materials prepared by precipitation and hydrolysis methods, after sintering 900 ˚C.....330

FTIR of 5% NbHAp (**5** wt.% niobate ions) materials prepared by precipitation and hydrolysis methods:.....331

FTIR of non-sintered 5%NbHAp (**5** wt.% niobate ions) materials prepared by precipitation and hydrolysis:.....331

FTIR of 5% NbHAp (**5** wt.% niobate ions) materials prepared by precipitation and hydrolysis methods after sintering at 900 ˚C:.....333

XRD diffraction patterns of 5% NbHAp (5 wt.% niobate ions) materials prepared by precipitation and hydrolysis methods: 334

Phase Identification of 5% NbHAp materials: 334

Crystallinity and crystallite size of prepared 5%NbHAp materials:.....337

Lattice parameters and volume of unit cell of prepared 5%NbHAp materials: ..338

SEM of 5%NbHAp (5 wt.% niobate ions) materials prepared by precipitation and hydrolysis methods:.....338

SEM of the non-sintered 5% NbHAp (5 wt.% niobate ions) materials prepared by precipitation and hydrolysis methods powders: 338

SEM of 5%NbHAp (5 wt.% niobate ions) materials prepared by precipitation and hydrolysis methods after sintering at 900 ˚C:.....341

7.3 1% B_4O_7HAp (1 wt.% $B_4O_7^{2-}$) powders prepared by precipitation and hydrolysis methods: 343

7.3.1 Characterization techniques of prepared 1% B_4O_7HAp (1 wt.% B_4O_7) materials prepared by precipitation and hydrolysis methods: 345

7.3.1.1 ICP-MS of 1% B_4O_7HAp (1 wt.% $B_4O_7^{2-}$) materials prepared by precipitation and hydrolysis methods, after sintering at 900 ˚C:.....345

7.3.1.2 FTIR of 1% B_4O_7HAp (1 wt.% B_4O_7) materials prepared by precipitation and hydrolysis methods. 346

FTIR of the non-sintered 1% B_4O_7HAp (1 wt.% B_4O_7) materials prepared by precipitation and hydrolysis methods at room temperature.....346

FTIR of 1% B_4O_7HAp (1 wt.% $B_4O_7^{2-}$) materials prepared by precipitation and hydrolysis methods after sintering at 900 ˚C.....348

7.3.1.3 XRD diffraction patterns of 1% B_4O_7HAp (1 wt.% $B_4O_7^{2-}$) materials prepared by precipitation and hydrolysis methods: 350

Phase Identification of 1% B_4O_7HAp materials:.....350

Crystallinity and crystallite size of 1% B_4O_7HAp materials: 352

Lattice Parameters and volume of unit cell of 1% B_4O_7HAp materials: 352

7.3.1.4 SEM of 1% B_40_7HAp (1 wt.% B_4O_7) materials prepared by precipitation and hydrolysis methods. 353

SEM of the non-sintered 1% B4O7HAp (1 wt.% B_4O_7) materials prepared by precipitation and hydrolysis methods. 353

SEM of sintered 1% B_4O_7HAp (1 wt.% B_4O_7) materials prepared by precipitation and hydrolysis methods at 900 ˚C.....356

7.4 Br_2Ap powders prepared by precipitation and hydrolysis: 358

7.4.1 Characterization methods of prepared Br_2Ap materials prepared by precipitation, hydrolysis and ion exchange methods.....361

7.4.1.1 ICP/MS of Br_2Ap materials prepared by precipitation, hydrolysis and ion exchange methods:.....361

7.4.1.2 FTIR of Br_2Ap materials prepared by precipitation, hydrolysis, and ion exchange methods:.....363

FTIR of the non-sintered Br_2Ap and BrHAp materials prepared by precipitation, hydrolysis, and ion exchange methods.....363

FTIR of Br_2Ap and BrHAp materials prepared by hydrolysis, precipitation, and ion exchange methods after sintering at 900 ˚C: 365

7.4.1.3 XRD diffraction analysis of Br_2Ap and BrHAp materials prepared by precipitation, hydrolysis and ion exchange methods. 367

Phase Identification of BrHAp and Br_2Ap materials prepared by precipitation, hydrolysis as well as ion exchange methods. 367

Crystallinity and crystallite size of prepared Br_2Ap and BrHAp materials:.....371

Lattice parameters and volume of unit cell of prepared Br_2Ap and BrHAp materials: 371

7.4.1.4 SEM of Br_2Ap and BrHAp materials prepared by precipitation, hydrolysis and ion exchange methods. 372

SEM of the non- sintered Br_2Ap and BrHAp materials prepared by precipitation, hydrolysis and ion exchange methods. 372

SEM of Br_2Ap and BrHAp materials prepared by precipitation, hydrolysis and ion exchange methods after sintering at 900 ˚C: 376

7.5 SHAp powders prepared by precipitation, hydrolysis and ion exchange methods: 380

7.5.1 Characterization techniques of prepared SAp materials by precipitation, hydrolysis and ion exchange methods. 382

7.5.1.1 ICP/MS of SAp materials prepared by precipitation, hydrolysis and ion exchange methods after sintering at 900 ˚C. 382

7.5.1.2 FTIR of SAp materials prepared by precipitation, hydrolysis and ion exchange methods. 383

FTIR of the non-sintered SAp materials prepared by precipitation, hydrolysis and ion exchange methods. 383

FTIR of SHAp materials prepared by precipitation, hydrolysis and ion exchange, after sintering at 900 ˚C: 385

7.5.1.3 XRD diffraction patterns of SAp materials prepared by precipitation, hydrolysis and ion exchange methods. 387

Phase Identification of the non-sintered and sintered SAp materials prepared by precipitation, hydrolysis and ion exchange methods. 387

Crystallinity and crystallite size of prepared SAp materials by precipitation, hydrolysis and ion exchange methods: 390

Lattice parameters and volume of unit cell of the sintered SAp materials prepared by precipitation, hydrolysis and ion exchange methods: 391

7.5.1.4 SEM of SAp materials prepared by precipitation, hydrolysis and ion exchange methods. 392

SEM of the non-sintered SAp materials prepared by precipitation, hydrolysis and ion exchange methods. 392

SEM of SAp materials prepared by precipitation, hydrolysis and ion exchange methods after sintering at 900 ˚C: 395

7.6 Co-substitution of NaClHAp ($Ca_9Na(PO_4)_6(OH)Cl$) powders prepared by precipitation and hydrolysis methods: 399

7.6.1 Characterization techniques of prepared NaClHAp ($Ca9Na(PO_4)_6(OH)Cl$) materials prepared by precipitation and hydrolysis methods. 401

7.6.1.1 ICP/MS of NaClHAp materials prepared by precipitation and hydrolysis methods after sintering at 900 ˚C: 401

7.6.1.2 FTIR of NaClHAp ($Ca_9Na(PO_4)_6(OH)Cl$) materials prepared by precipitation and hydrolysis methods. 403

FTIR of the non-sintered NaClHAp ($Ca_9Na(PO_4)_6(OH)Cl$) materials prepared by precipitation and hydrolysis methods. 403

FTIR spectra of NaClHAp materials prepared by precipitation and hydrolysis methods after sintering at 900 ˚C. 404

7.6.1.3 XRD diffraction analysis of sodium chloride co- substituted hydroxyapatite (NaClHAp) prepared by precipitation and hydrolysis methods: 405

Phase Identification of sintered NaClHAp materials prepared by precipitation and hydrolysis methods. 405

Crystallinity and crystallite size of NaClHAp materials prepared by precipitation and hydrolysis methods: 408

Lattice parameters and volume of unit cell of NaClHAp materials prepared by precipitation and hydrolysis methods: 408

7.6.1.4 SEM of NaClHAp materials prepared by precipitation and hydrolysis methods. 409

SEM of the non-sintered NaClHAp materials prepared by precipitation and hydrolysis methods. 409

SEM of NaClHAp materials prepared by precipitation and hydrolysis methods after sintering at 900 ˚C. 412

7.7 Summary: 416

Chapter Eight Mechanical properties of unsubstituted, substituted and co substituted HAp powders prepared by the Hydrolysis of monocalcium phosphate (MCP)/$Ca(OH)_2$. .418

8.1 Mechanical Properties: 418

8.1.1 Mechanical properties of sintered unsubstituted HAp powders at 900 ˚C prepared by the novel hydrolysis method using MCP and $Ca(OH)_2$ as starting materials: 419

8.1.2 Mechanical properties of ZnHAp powders at 900 ˚C ($Ca_{10-x}Zn_x(PO_4)_6(OH)_2$, where x= 0.5, 1.0 and 1.5) prepared by the novel hydrolysis of MCP/Ca(OH)2.: 421

8.1.3 Mechanical properties of sintered SrHAp powders ($Ca_{10-x}Sr_x(PO_4)_6(OH)_2$ at 900 ˚C, where x= 0.5, 1.0 and 1.5) prepared by the novel hydrolysis of MCP/$Ca(OH)_2$: 422

8.1.4 Mechanical properties of sintered CuHAp powders at 900 ˚C ($Ca_{10-x}Cu_x(PO_4)_6(OH)_2$, where x= 0.5, 1.0 and 1.5) prepared by the novel hydrolysis of MCP/$Ca(OH)_2$: 424

8.1.5 Mechanical properties of sintered 1%EuHAp (1 wt.% Eu^{3+}) and 1% ScHAp(1 wt.% Sc^{3+}) powders at 900 ˚C prepared by the novel hydrolysis of MCP/$Ca(OH)_2$: 426

8.1.6 Mechanical properties of sintered 1% B_4O_7HAp (1 wt.% $B_4O_7^{2-}$) and NaClHAp ($Ca_9Na(PO_4)_6ClOH$)powders at 900 ˚C prepared by the novel hydrolysis of MCP/$Ca(OH)_2$: 427

8.1.7 Mechanical properties of sintered SAp powders at 900 ˚C prepared by the novel hydrolysis of MCP/$Ca(OH)_2$: 429

8.2 Summary: 431
Chapter Nine Conclusions and Future work 432
9.1 Conclusion of this work: 432
9.1.1 The development of a novel method to prepare (unsubstituted) HAp by hydrolysis of monocalcium phosphate (MCP) using calcium hydroxide (Chapter 4): 432
9.1.2 Preparation of MHAp powders with the following chemical formula: $Ca_{10-x}M_xHAp$ (where M=Zn, Sr and Cu, X=0.5, 1.0 and 1.5) by the hydrolysis method(Chapter 5): 432
9.1.3 Cationic substituted HAp powders: 433
9.1.4 Anionic substituted HAp and co-substituted HAp powders: 434
9.1.5 Mechanical properties: 434
9.2 Further work: 434
References 436
Appendix A 452

List of Figures

Figure 2.1: Definition of the lattice parameters and their use in hexagonal crystal system [50]. 46

Figure 2.2: The atomic arrangement of calcium ions in $Ca_{10}(PO_4)_6(OH)_2$ [35] 47

Figure 2.3 : Schematic representation of substitution elements in apatites. The inner layer shows anionic substitutions, while outer layer – monovalent, divalent and trivalent cationic substitutions [64]. 51

Figure 2.4: The relative positions of F, OH and Cl atoms at the centre of the Ca_{II}triangles in F-apatite, OH-apatite and Cl-apatite [35] 52

Figure 2.5: The effects of the two types of carbonate substitution on the a-axis dimensions of synthetic apatites [35] 56

Figure 3-1 flowchart for the synthesis process of substituted and co substituted hydroxyapatite materials by using the precipitation method. 90

Figure 3-2 The synthesis process of substituted and co substituted hydroxyapatite materials by using an ion exchange method. 91

Figure 3-3 flowchart for the synthesis process of substituted and co substituted hydroxyapatite materials by using hydrolysis methods. 95

Figure 3-4 : The diffraction of X-rays by the planes in a crystal [141] 107

Figure 3-5 Sample holder as used in powder X-ray diffraction and the way powdered samples were packed into the holder with an even surface. 108

Figure 3-6: The cylindrical specimens of (10 mm) height and (11.2 mm) in diameter fabricated from prepared HAp material produced by the hydrolysis method. ... 114

Figure 4-1: The general appearance of the powders of non-sintered unsubstituted HAp materials synthesized by hydrolysis of MCP (monocalcium phosphate) and calcium hydroxide. 120

Figure 4-2: FTIR spectra of non-sintered unsubstituted HAp materials from (a) commercial HAp (Fluka) (b) prepared via the hydrolysis method (of $MCP/CaOH)_2$) and (c) prepared via the precipitation method. 124

Figure 4-3: FTIR spectra of sintered unsubstituted HAp materials prepared from (a) sintered commercial HAp (Fluka) at 900 ˚C(b) HAP prepared by the novel hydrolysis method (of $MCP/CaOH)_2$), (c) precipitation method, and (d) The non-sintered commercial (β-TCP). 126

Figure 4-4: The XRD diffraction patterns of as-prepared non-sintered and sintered (at 900 ˚C) unsubstituted HAp materials obtained from hydrolysis of MCP with calcium hydroxide compared to the pattern for standard HAp (reference card number 01-074-9780). 130

Figure 4-5: The XRD diffraction patterns of the both sintered unsubstituted HAp materials prepared by hydrolysis and precipitation methods at 900 °C, compared to commercial $Ca(OH)_2$, Na_2CO_3 and $CaCO_3$ compounds.....131

Figure 4-6: The XRD diffraction patterns of commercial β- TCP compared to the sintered commercial HAp (Fluka, at 900 ˚C) and both the sintered unsubstituted HAp materials prepared by the novel hydrolysis and conventional precipitation routes at 900 ˚C.....132

Figure 4-7: The XRD diffraction patterns of commercial Na_2HPO_4 and CO_3HAp compounds compared to the sintered commercial HAp (Fluka, at 900 ˚C) and both the sintered unsubstituted HAp materials prepared by the novel hydrolysis and conventional precipitation routes at 900 ˚C.....133

Figure 4-8: SEM images of (a) Unsubstituted HAp prepared from hydrolysis of MCP/$Ca(OH)_2$ sintered at 900 ˚C (b) Non-sintered unsubstituted HAp prepared by hydrolysis of MCP/$Ca(OH)_2$. 141

Figure 4-9: SEM images of sintered (a) Unsubstituted HAp prepared by a conventional precipitation route (b) Unsubstituted HAp prepared by hydrolysis of MCP/$Ca(OH)_2$ (c) commercial HAp (Fluka). 143

Figure 5-1: FTIR spectra of non-sintered zinc substituted hydroxyapatite with different Zn^{2+} content prepared by the MCP/$Ca(OH)_2$ hydrolysis method. 154

Figure 5-2: FTIR spectra of Zinc substituted Hydroxyapatite materials with different Zn^{2+} contents as prepared by the novel MCP/$Ca(OH)_2$ hydrolysis method after sintering at 900 ˚C.....156

Figure 5-3: The XRD diffraction patterns of ZnHAp materials with different Zn contents prepared by hydrolysis of MCP/$Ca(OH)_2$ after sintering at 900 ˚C. 159

Figure 5-4: SEM images from the present study of (a) unsubstituted HAp (b) 0.5 ZnHAp (c) 1.0 ZnHAp (d) I.5 ZnHAp, prepared by hydrolysis of MCP/$Ca(OH)_2$ after sintering at 900 ˚C. 167

Figure 5-5: FTIR spectra of the SrHAp powders (before sintering) with different levels of Sr^{2+} substitution as prepared by hydrolysis of MCP/$Ca(OH)_2$.....170

Figure 5-6: FTIR spectra of sintered SrHAp materials with different levels of strontium ion substitution as prepared by hydrolysis of MCP/$Ca(OH)_2$.....172

Figure 5-7: The XRD diffraction patterns of SrHAp powders prepared in this study by the novel hydrolysis method after sintering at 900 ˚C. 175

Figure 5-8: SEM images of (a) unsubstituted HAp (b) 0.5 SrHAp (c) 1.0 SrHAp (d) 1.5 SrHAp, prepared by hydrolysis of MCP/$Ca(OH)_2$ after sintering at 900 ˚C. 185

Figure 5-9: Colours of the non-sintered CuHAp materials containing different levels of Cu^{2+} ion substitution as prepared by the hydrolysis of MCP/$Ca(OH)_2$ 187

Figure 5-10: FTIR spectra of non-sintered copper substituted hydroxyapatite materials with different levels of Cu^{2+} substitution as prepared by the novel hydrolysis method of MCP/$Ca(OH)_2$ 189

Figure 5-11: FTIR spectra of CuHAp hydroxyapatite materials with different levels of Cu^{2+} substitution after sintering at 900 ˚C. 191

Figure 5-12: The XRD diffraction patterns of CuHAp materials after sintering at 900 ˚C. 193

Figure 5-13: SEM images of (a) unsubstituted HAp (b) 0.5 CuHAp (c) 1.0 CuHAp (d) 1.5 CuHAp, prepared by hydrolysis of MCP/$Ca(OH)_2$ after sintering at 900 ˚C. 200

Figure 6-1: FTIR spectra of non-sintered 1% RbHAp (1 wt.% Rb^{+}) materials prepared by the conventional precipitation and novel hydrolysis methods. 209

Figure 6-2: FTIR spectra of 1% RbHAp (1 wt.% Rb^{+}) materials prepared by precipitation and hydrolysis methods after sintering at 900 ˚C. 211

Figure 6-3: The XRD diffraction patterns of non- sintered 1% RbHAp (1 wt.% Rb^{+}) materials prepared by precipitation and hydrolysis methods. 214

Figure 6-4: The XRD diffraction patterns of 1% RbHAp (1 wt.% Rb^{+}) materials prepared by precipitation and hydrolysis methods after sintering at 900 °C. 215

Figure 6-5: SEM images of non-sintered (a) unsubstituted HAp by hydrolysis (b) unsubstituted HAp by precipitation (c) 1% RbHAp (1 wt. % Rb^{+}) by hydrolysis (d) 1% RbAHp (1 wt.% Rb^{+}) by precipitation. 222

Figure 6-6: SEM images of (a) unsubstituted HAp by precipitation (b) unsubstituted HAp by hydrolysis (c and d)1%RbHAp (1% wt. Rb^{+}) by precipitation (e) 1%RbHAp (1% wt. Rb^{+}) by hydrolysis, after sintering at 900 ˚C. 225

Figure 6-7: FTIR spectra of non-sintered 1%EuHAp (1 wt.% Eu^{3+}) materials prepared by precipitation and hydrolysis methods. 229

Figure 6-8: FTIR spectra of 1% EuHAp (1 wt.% Eu^{3+}) materials prepared by the conventional precipitation and novel hydrolysis methods after sintering at 900 ˚C. 231

Figure 6-9: The XRD diffraction patterns of non-sintered 1% EuHAp (1 wt.% Eu^{3+}) materials prepared by precipitation and hydrolysis methods. 233

Figure 6-10: The XRD diffraction patterns of 1% EuHAp (1 wt.% Eu^{3+}) materials prepared by the conventional precipitation and novel hydrolysis methods after sintering at 900 ˚C. 234

Figure 6-11: SEM images of non-sintered (a) unsubstitutedHAp by precipitation (b) unsubstituted HAp by hydrolysis (c) 1% EuHAp(1 wt.% Eu^{3+}) by precipitation (d) 1% EuHAp(1 wt.% Eu^{3+}) by hydrolysis. 240

Figure 6-12: SEM images of (a) unsubstituted HAp by precipitation (b) unsubstituted HAp by hydrolysis (c and d) 1 % EuHAp (1 wt.% Eu^{3+}) by precipitation (e) 1 % EuHAp (1 wt.% Eu^{3+}) by hydrolysis, after sintering at 900 ˚C. 243

Figure 6-13: FTIR spectra of non-sintered 1%ScHAp (1 wt.% Sc^{3+}) materials prepared by precipitation and hydrolysis methods. 249

Figure 6-14: FTIR spectra of 1%ScHAp (1 wt.% Sc^{3+}) materials prepared by precipitation and hydrolysis methods after sintering at 900 ˚C. 251

Figure 6-15. The XRD diffraction patterns of non-sintered 1% ScHAp (1 wt.% Sc^{3+}) materials prepared by conventional precipitation and novel hydrolysis methods. 253

Figure 6-16: The XRD diffraction patterns of 1%ScHAp (1 wt.% Sc^{3+}) materials prepared by precipitation and hydrolysis methods after sintering at 900 ˚C. 254

Figure 6-17: SEM images of non -sintered (a) unsubstituted HAp by precipitation (b) unsubstituted HAp by hydrolysis (c) 1 % ScHAp (1 wt.% Sc^{3+}) by precipitation (d) 1 % ScHAp (1 wt.% Sc^{3+}) by hydrolysis. 259

Figure 6-18: SEM images of (a) unsubstituted HAp by precipitation (b) unsubstituted HAp by hydrolysis (c+d+e) 1 % ScHAp (1 wt.% Sc^{3+}) by precipitation (f) 1 % ScHAp (1 wt.% Sc^{3+}) by hydrolysis, after sintering at 900 ˚C. 263

Figure 6-19: FTIR spectra of non-sintered 3% ScHAp (3 wt.% Sc^{3+}) materials prepared by precipitation and hydrolysis methods. 266

Figure 6-20: FTIR of 3% ScHAp (3 wt.% Sc^{3+}) materials prepared by precipitation and hydrolysis methods after sintering at 900 ˚C. 268

Figure 6-21: The XRD diffraction patterns of non-sintered 3% ScHAp (3 wt.% Sc^{3+}) materials prepared by the conventional precipitation and novel hydrolysis methods. 270

Figure 6-22: The XRD diffraction patterns of 3% ScHAp (3 wt.% Sc^{3+}) materials prepared by precipitation and hydrolysis methods after sintering at 900 ˚C. 271

Figure 6-23: SEM of images (a) unsubstituted HAp by precipitation (b) unsubstituted HAp by hydrolysis (c) 3 % ScHAp by precipitation (d) 3% ScHAp by hydrolysis. 276

Figure 6-24: SEM images of (a) unsubstituted HAp by precipitation (b) unsubstituted HAp by hydrolysis (c+d) 3 % ScHAp by precepitation (e) 3% ScHAp by hydrolysis, after sintering at 900 ˚C. 279

Figure 6-25: FTIR spectra of sintered 5% ScHAp (5 wt.% Sc^{3+}) materials prepared by precipitation and hydrolysis methods. 282

Figure 6-26: FTIR of 5% ScHAp (5 wt.% Sc^{3+}) materials prepared by precipitation and hydrolysis methods after sintering at 900 ˚C. 283

Figure 6-27: The XRD diffraction patterns of non-sintered 5% ScHAp (5 wt.5 Sc^{3+}) materials as prepared by the conventional precipitation and novel hydrolysis methods. 285

Figure 6-28: The XRD diffraction patterns of 5% ScHAp (5 wt.% Sc^{3+}) materials prepared by precipitation and hydrolysis methods after sintering at 900 ˚C. 286

Figure 6-29: SEM images of non-sintered (a) unsubstituted HAp by precipitation (b) unsubstituted HAp by hydrolysis (c) 5% ScHAp by precipitation (d) 5% ScHAp by hydrolysis. 290

Figure 6-30: SEM of (a) unsubstituted HAp by precipitation (b) unsubstituted HAp by hydrolysis (c+d) 5 % ScHAp by precipitation (e) 5% ScHAp by hydrolysis, after sintering at 900 ˚C. 293

Figure 7-1: $NbCl_5$ solution that resulted from dissolving Nb_2O_5 in 12 M HCl and heated at 200 ˚C with reflux for 10 hours. 300

Figure 7-2: FTIR spectra of non-sintered 1% NbHAp (1 wt.% niobate ions) materials prepared by precipitation and hydrolysis methods. 304

Figure 7-3: FTIR spectra of 1%NbHAp (1 wt.% niobate ions) materials prepared by precipitation hydrolysis methods after sintering at 900 ˚C. 305

Figure 7-4: The XRD diffraction patterns of non-sintered 1% NbHAp (1 wt.% niobate ions) materials prepared by precipitation and hydrolysis methods. 307

Figure 7-5: The XRD diffraction patterns of 1%NbHAp (1 wt.% niobate ions) materials prepared by precipitation and hydrolysis methods after sintering at 900 ˚C. 308

Figure 7-6: SEM images of non-sintered (a)unsubstituted HAp by precipitation (b) unsubstituted HAp by hydrolysis (c) 1%NbHAp by precipitation (d) 1%NbHAp by hydrolysis. 312

Figure 7-7: SEM images of (a) unsubstituted HAp by precipitation (b)unsubstituted HAp by hydrolysis (c) 1% NbHAp by precipitation (d) 1% NbHAp by hydrolysis after sintering at 900 ˚C. 315

Figure 7-8: FTIR of non-sintered 3%NbHAp (3 wt.% niobate ions) materials prepared by precipitation and hydrolysis methods. 318

Figure 7-9: FTIR spectra of 3%NbHAp (3 wt.% niobate ions) materials prepared by precipitation and hydrolysis methods after sintering at 900 ˚C. 319

Figure 7-10: The XRD diffraction patterns of the non-sintered 3%NbHAp (3 wt.% niobate ions) materials prepared by precipitation and hydrolysis methods. 321

Figure 7-11: The XRD diffraction patterns of 3%NbHAp (3 wt.% niobate ions) materials prepared by precipitation and hydrolysis methods after sintering at 900˚C. 322

Figure 7-12: SEM images of non-sintered (a) Unsubstituted HAp by precipitation (b)Unsubstituted HAp by hydrolysis (c) 3%NbHAp by precipitation (d)3%NbHAp by hydrolysis. 326

Figure 7-13: SEM of (a) Unsubstituted HAp by precipitation (b)Unsubstituted HAp by hydrolysis (c) 3%NbHAp by precipitation (d) 3%NbHAp by hydrolysis, after sintering at 900 ˚C. 329

Figure 7-14: FTIR of non-sintered 5% NbHAp (**5** wt.% niobate ions) materials prepared by precipitation and hydrolysis methods. 332

Figure 7-15: FTIR of 5% NbHAp (**5** wt.% niobate ions) materials prepared by precipitation and hydrolysis methods after sintering at 900 ˚C. 333

Figure 7-16: The XRD diffraction patterns of the non-sintered 5%NbHAp (5 wt.% niobate ions) materials prepared by precipitation and hydrolysis methods. 335

Figure 7-17: The XRD diffraction patterns of 5% NbHAp (5 wt.% niobate ions) materials prepared by precipitation and hydrolysis methods after sintering at 900 ˚C. 336

Figure 7-18: SEM images of (a)Unsubstituted HAp by precipitation (b)Unsubstituted HAp by hydrolysis (c) 5%NbHAp by precipitation (d)5%NbHAp by hydrolysis. 340

Figure 7-19: SEM images of (a) Unsubstituted HAp by precipitation (b) Unsubstituted HAp by hydrolysis (c) 5%NbHAp by precipitation (d) 5%NbHAp by hydrolysis, after sintering at 900 ˚C. 343

Figure 7-20: FTIR spectra of the non-sintered 1%B_4O_7HAp (1 wt.% B_4O_7) materials prepared by precipitation and hydrolysis methods. 347

Figure 7-21: FTIR spectra of 1% B_4O_7HAp (1 wt.% B_4O_7) materials prepared by precipitation and hydrolysis methods after sintering at 900 ˚C. 348

Figure 7-22: XRD diffraction patterns of the non-sintered of 1% B_4O_7HAp (1 wt.% $B_4O_7^{2-}$) materials prepared by precipitation and hydrolysis methods. 350

Figure 7-23: XRD diffraction patterns of 1% B_4O_7HAp (1 wt.% $B_4O_7^{2-}$) materials prepared by precipitation and hydrolysis methods after sintering at 900 ˚C. 351

Figure 7-24: SEM images of non-sintered (a) Unsubstituted HAp by precipitation (b) Unsubstituted HAp by hydrolysis (c) 1%B_4O_7HAp by precipitation (e) 1%B_4O_7HAp by hydrolysis. 355

Figure 7-25: SEM imaged of (a) Unsubstituted HAp by precipitation (b) Unsubstituted HAp by hydrolysis (c) 1% B_4O_7HAp by precipitation (d) 1%B_4O_7HAp by hydrolysis, after sintering at 900 ˚C. 358

Figure 7-26: FTIR spectra of the non-sintered Br_2Ap and BrHAp materials prepared by precipitation, hydrolysis and ion exchange methods. 364

Figure 7-27: FTIR spectra of Br_2Ap and BrHAp materials prepared by precipitation, hydrolysis and ion exchange methods after sintering at 900 ˚C. 366

Figure 7-28: The XRD diffraction patterns of the non-sintered Br_2Ap and BrHAp materials prepared by precipitation and hydrolysis methods. 368

Figure 7-29: The XRD diffraction patterns Br_2Ap and BrHAp materials prepared by precipitation and hydrolysis methods after sintering at 900 ˚C. 369

Figure 7-30: The XRD diffraction patterns of commercial HAp (fluka) and Br_2Ap materials prepared by ion exchange method. 370

Figure 7-31: SEM images of the non-sintered (a) Unsubstituted HAp by hydrolysis (b) Unsubstituted HAp by precipitation (c) BrHAp by precipitation (d) Br_2Ap by precipitation (e,f) Br_2Ap by hydrolysis (g) Br_2Ap by ion exchange. 376

Figure 7-32: SEM images of (a) Unsubstituted HAp by hydrolysis (b) Unsubstituted HAp by precipitation (c) Br_2Ap by precipitation (d) Br_2Ap by hydrolysis (e) Commercial HAp (Fluka) (f) Br_2Ap by ion exchange, after sintering at 900 ˚C. 379

Figure 7-33: FTIR spectra of the non-sintered SAp materials prepared by precipitation, hydrolysis and ion exchange methods. 384

Figure 7-34: *FTIR spectra SAp materials prepared by precipitation, hydrolysis and ion exchange methods after sintering at 900 ˚C.* 386

Figure 7-35: The XRD diffraction patterns of non-sintered SAp materials by precipitation and hydrolysis methods. 388

Figure 7-36: The XRD diffraction patterns of SAp materials prepared by precipitation, hydrolysis and ion exchange methods after sintering at 900 ˚C. 389

Figure 7-37: SEM mages of the non-sintered (a) Unsubstituted HAp by hydrolysis (b) Unsubstituted HAp by precipitation (c)SAp by hydrolysis (d) SAp by precipitation (e) SAp by ion exchange. 394

Figure 7-38: SEM images of: (a) Unsubstituted HAp by precipitation (b) Unsubstituted HAp by hydrolysis (c and d) SAp by precipitation (e) SAp by hydrolysis (f) SAp by ion exchange, after sintering at 900 ˚C. 398

Figure 7-39: FTIR spectra of non-sintered NaClHAp materials prepared by precipitation and hydrolysis methods. 403

Figure 7-40: FTIR of NaClHAp materials prepared by precipitation and hydrolysis methods after sintering at 900 ˚C. 404

Figure 7-41: XRD diffraction patterns of the sintered NaClHAp materials prepared by precipitation and hydrolysis methods. 406

Figure 7-42: XRD diffraction patterns of NaClHAp materials prepared by precipitation and hydrolysis methods after sintering at 900 ˚C. 407

Figure 7-43: SEM images of the non-sintered (a) Unsubstituted HAp by precipitation (b) Unsubstituted HAp by hydrolysis (c)NaClHAp by precipitation (d and e) NaClHAp by hydrolysis. 412

Figure 7-44: SEM images of (a) Unsubstituted HAp by precipitation (b) Unsubstituted HAp by hydrolysis (c + d) NaClHAp by precipitation (f) NaClHAp by hydrolysis, after sintering at 900 ˚C. 415

Figure 8-1: Compression strength against particle size of ZnHAp powders prepared by hydrolysis method with different substitution levels. 421

Figure 8-2: Compression strength against particle size for SrHAp powders prepared by the hydrolysis method at different substitution levels. 423

Figure 8-3: Compression strength against particle size of CuHAp powders prepared by hydrolysis method with different substitution levels. 425

Figure 8-4: Compression strength against particle size of of 1%EuHAp (1% wt. Eu^{3+}) and 1% ScHAp(1% wt. Sc^{3+}) powders prepared by hydrolysis method. 426

Figure 8-5: Compression strength against particle size of 1% B_4O_7HAp (1 wt.% $B_4O_7^{2-}$) and NaClHAp ($Ca_9Na(PO_4)_6ClOH$) powders prepared by hydrolysis method.. 428

Figure 8-6: Compression strength against particle size of SAp powders prepared by hydrolysis methods 430

List of Tables

Table 1-1: The cations and the anions that were substituted into HAps synthesized via the novel and conventional synthetic routes considered in this work. Synthetic routes will be described more in detail later on.....38

Table 2-1 Physico-chemical parameters of synthesized hydroxyapatite [34,46,47].....45

Table 3-1: Reagents that were used to prepare the cationic, anionic and co substituted HAp materials in this study by the different synthesis routes, namely precipitation, hydrolysis and ion exchange methods.....97

Table 3-2 Specific reagents that were used to substitute Zn^{2+}, Sr^{2+} and Cu^{2+} ions into HAp structure by the hydrolysis method with the following formula: $Ca_{10-x}M_x(PO_4)_6(OH)_2$), where (M= Zn, Sr and Cu)and (x=0.5, 1.0 and 1.5).....99

Table 3-3 Reagents that were used to substitute Rb^{+}, Eu^{3+} and Sc^{3+} ions into HAp crystal by the precipitation and hydrolysis methods:.....100

Table 3-4 Reagents that were used to substitute niobate, borate, bromo and sulfide ions into HAp structure by the precipitation, hydrolysis and ion exchange methods:100

Table 3-5 Reagents that were used to co-substitute sodium and chloride ions into the HAp structure by the precipitation and hydrolysis route:.....101

Table 4-1: Synthesis details of unsubstituted HAp materials by the MCP/$Ca(OH)_2$ hydrolysis method. 119

Table 4-2: Synthesis details of unsubstituted HAp materials by precipitation method.....120

Table 4-3: ICP-MS results of commercial HAp (Fluka) and unsubstituted HAp materials prepared by precipitation and hydrolysis (of MCP/$Ca(OH)_2$) methods after sintering at 900 ˚C. The concentration is reported in ppb (ug/L):.....121

Table 4-4: Assignments of main bands observed generally in the Infrared absorption spectra of unsubstituted HAp.....127

Table 4-5: The degree of crystallinity (%) and the crystallite size (in Angstroms) of sintered commercial HAp (Fluka, at 900 ˚C) compared to sintered unsubstituted HAp materials prepared by hydrolysis and precipitation methods at 900 ˚C.....135

Table 4-6: the value of crystallite size of HAp powders obtained from different synthesis routes.....136

Table 4-7: The lattice parameters and the volume of hexagonal unit cell of sintered commercial HAp (Fluka HAp sintered at 900 ˚C) compared to the sintered unsubstituted HAp materials prepared by MCP/$Ca(OH)_2$ hydrolysis and precipitation methods at 900 ˚C.....137

Table 4-8: The value of lattice parameters of HAp materials obtained from different investigations.....138

Table 4-9: the reaction conditions, crystallite size and lattice constants of the prepared samples in this investigation. 139

Table 4-10: investigation of hydroxyapatite materials by using a hydrolysis method based on OCP (ocatacalcium phosphate) and DCPD (dicalcium phosphate dihydrate) as starting materials and with water as well as 1 M of sodium phosphate solution as the hydrolyzing agent. 145

Table 5-1: Synthesis details of ZnHAp powders prepared by the MCP/$Ca(OH)_2$ hydrolysis method. 151

Table 5-2: ICP-MS results of ZnHAp materials from the present study which were at 900 ˚C with different levels of Zn^{2+} substitution as prepared by the hydrolysis reaction. Concentrations are quoted is in ppb (ug/L): 152

Table 5-3: The chemical analysis data of prepared ZnHAp materials after sintering at 900 ˚C with different Zn^{2+} contents by ICP-MS measurements. 152

Table 5-4: Phase composition of ZnHAp by hydrolysis method. 160

Table 5-5: The degree of crystallinity and the crystallite size of sintered ZnHAp materials with different Zn contents prepared by hydrolysis of MCP/$Ca(OH)_2$ at 900 ˚C. ..161

Table 5-6: The lattice parameters and the volume of hexagonal unit cell of ZnHAp materials after sintering at 900 ˚C with different levels of Zn^{2+} substitution by hydrolysis of MCP/$Ca(OH)_2$ 162

Table 5-7: The value of lattice parameters of ZnHAp powders prepared by different synthesis routes. 164

Table 5-8: Synthesis details of prepared SrHAp materials by hydrolysis of MCP/$Ca(OH)_2$. ..168

Table 5-9: ICP-MS results of SrHAp materials after sintering at 900 ˚C. The concentrations quoted are in ppb units (ug/L): 168

Table 5-10: The ICP-MS analysis data of SrHAp powders after sintering at 900 ˚C with different Sr^{2+} contents by ICP-MS measurements. 169

Table 5-11: The degree of crystallinity and crystallite size data for SrHAp materials generated by the novel hydrolysis method after sintering at 900°C 177

Table 5-12: Illustrates the results on the degree of crystallinity measurements of SrHAp materials obtained by studies in the literature. 178

Table 5-13: Illustrates the results of the crystallite size of SrHAp materials obtained by various studies. 180

Table 5-14: The lattice parameters and the volume of hexagonal unit cell of the SrHAp powders after sintering at 900 ˚C. 181

Table 5-15: llustrates the relationship between substitution level of Sr^{2+} ions and lattice parameters (a and c) as shown in other workers' studies. 182

Table 5-16: Synthesis details of prepared CuHAp materials by the novel hydrolysis method of MCP/$Ca(OH)_2$. 186

Table 5-17: ICP-MS results of CuHAp materials prepared using the novel hydrolysis method of MCP/$Ca(OH)_2$. Concentrations are expressed in ppb (ug/L): 188

Table 5-18: The chemical analysis data of CuHAp materials after sintering at 900 ˚C with different Cu^{2+} contents by ICP-MS measurements. 188

Table 5-19: The degree of crystallinity and the crystallite size of CuHAp materials after sintering at 900 ˚C. 194

Table 5-20: Illustrated the relationship between crystallinity and substitution of copper ions into HAp crystal. 195

Table 5-21: The lattice parameters and the volume of hexagonal unit cell of the CuHAp after sintering at 900 ˚C. 196

Table 6-1: Synthesis details of 1% RbHAp (1% wt. Rb^+) powders prepared by precipitation and hydrolysis methods. 206

Table 6-2: ICP-MS results of 1% RbHAp (1% wt. Rb^+) materials prepared by precipitation and hydrolysis methods after sintering at 900 ˚C. The concentration is given in ppb (ug/L): 207

Table 6-3: The chemical analysis data of 1% RbHAp (1 wt.% Rb^+) materials by ICP-MS measurements after sintering at 900 ˚C. 208

Table 6-4: The degree of Crystallinity and crystallite size of 1% RbHAp (1 wt.% Rb^+) materials prepared by precipitation and hydrolysis methods after sintering at 900 ˚C. 217

Table 6-5: The lattice parameters and the volume of hexagonal unit cell of 1% RbHAp (1 wt.% Rb^+) materials prepared by precipitation and hydrolysis methods after sintering at 900 ˚C. 218

Table 6-6: The lattice constants and the volume of unit cell of 1,3,5,7 and 10% RbHAp materials. 219

Table 6-7: Synthesis details of 1% EuHAp (1 wt.% Eu^{3+} ions) powders 226

Table 6-8: ICP-MS results of 1% EuHAp (1 wt.%Eu^{3+}) materials prepared by precipitation and hydrolysis methods after sintering at 900 ˚C. The concentration values are given in ppb (ug/L): 227

Table 6-9: The chemical analysis data of 1% EuHAp (1 wt.% Eu^{3+}) materials by ICP-MS measurements after sintering at 900 ˚C. 228

Table 6-10: The degree of crystallinity and crystallite size of 1% EuHAp (1 wt.% Eu^{3+}) materials prepared by precipitation and hydrolysis methods after sintering at 900 ˚C. 236

Table 6-11: The XRD results of Ce-doped HAp with different level of substitution of Ce^{3+} ions as reported by , Kaygili et al. [147].....237

Table 6-12: The lattice parameters and the volume of hexagonal unit cell of 1% EuHAp (1 wt.% Eu^{3+}) materials prepared by precipitation and hydrolysis methods after sintering at 900 ˚C.....237

Table 6-13: Synthesis details of 1%ScHAp (1 wt.% Sc^{3+}) powders.....245

Table 6-14: Synthesis details of 3%ScHAp (3 wt.% Sc^{3+}) powders.....245

Table 6-15: Synthesis details of 5%ScHAp(5 wt.% sc^{3+}) powders.....246

Table 6-16: ICP-MS results of 1%ScHAp (1% wt. Sc^{3+}) materials prepared by precipitation and hydrolysis methods after sintering at 900 ˚C. The concentration was in ppb unit (ug/L): 247

Table 6-17: The chemical analysis data of 1%ScHAp (1 wt.% Sc^{3+}) materials by ICP-MS measurements after sintering at 900 ˚C.....247

Table 6-18: The degree of crystallinity and the crystallite size of 1%ScHAp (1 wt.% Sc^{3+}) materials prepared by the conventional precipitation and novel hydrolysis methods after sintering at 900 ˚C.....255

Table 6-19: The effect of the low substitution levels of Zn^{2+} ions on the lattice constants and the crystallite size of the prepared HAp. 256

Table 6-20: The lattice parameters and the volume of hexagonal unit cell of 1%ScHAp (1 wt.% Sc^{3+}) materials prepared by precipitation and hydrolysis methods after sintering at 900 ˚C.....257

Table 6-21: ICP-MS results of 3% ScHAp (3 wt.% Sc^{3+}) materials prepared by precipitation and hydrolysis methods after sintering at 900 ˚C. The concentration was in ppb unit(ug/L). 264

Table 6-22: The chemical analysis data of 3% ScHAp (3 wt.% Sc^{3+}) materials by ICP-MS measurements after sintering at 900 ˚C.....265

Table 6-23: The degree of crystallinity and the crystallite size of 3% ScHAp (3 wt.% Sc^{3+}) materials prepared by precipitation and hydrolysis methods after sintering at 900 ˚C.....272

Table 6-24: The lattice parameters and the volume of hexagonal unit cell of 3%ScHAp (3 wt. % Sc^{3+}) materials prepared by precipitation and hydrolysis methods after sintering at 900 ˚C.....273

Table 6-25: ICP-MS results of 5% ScHAp (5 wt.% Sc^{3+}) materials prepared by precipitation and hydrolysis methods after sintering at 900 ˚C. The concentration was in ppb unit (ug/L): 280

Table 6-26: The chemical analysis data of sintered 5% ScHAp (5 wt.% Sc^{3+}) materials by ICP-MS measurements after sintering at 900 ˚C. 281

Table 6-27: The degree of crystallinity and the crystallite size of 5% ScHAp (5 wt.% Sc^{3+}) materials prepared by precipitation and hydrolysis methods after sintering at 900 ˚C. 287

Table 6-28: The lattice parameters and the volume of hexagonal unit cell of 5% ScHAp (5 wt.% Sc^{3+}) materials prepared by precipitation and hydrolysis methods after sintering at 900 ˚C. 288

Table 6-29: The measured wt.% of doped ions (Rb^{+}, Eu^{3+}, Sc^{3+} and Na^{+}) into HAp structure as confirmed by ICP-MS analysis. 295

Table 7-1: Synthesis details of 1% NbHAp powders by precipitation and hydrolysis methods. 301

Table 7-2: Synthesis details of 3% NbHAp powders by precipitation and hydrolysis methods. 301

Table 7-3: Synthesis details of 5% NbHAp powders by precipitation and hydrolysis methods. 301

Table 7-4: ICP-MS results of 1% NbHAp samples prepared by the precipitation and hydrolysis methods after sintering at 900 ˚C. The concentration was in ppb (ug/L): 302

Table 7-5: The chemical analysis data of 1% NbHAp materials by ICP-MS measurements after sintering at 900 ˚C. 303

Table 7-6: The degree of crystallinity and the crystallite size of 1% NbHAp (1 wt.% niobate ions) materials by precipitation and hydrolysis methods after sintering at 900 ˚C. 309

Table 7-7: The lattice parameters and the volume of hexagonal unit cell of 1% NbHAp (1 wt.% niobate ions) prepared by precipitation and hydrolysis methods, after sintering at 900 ˚C. 310

Table 7-8: ICP-MS results of 3%NbHAp (3 wt.% niobate ions) materials prepared by precipitation and hydrolysis methods after sintering at 900 ˚C. The concentration was in ppb unit (ug/L): 316

Table 7-9: The chemical analysis data of 3%NbHAp (3 wt.% niobate ions) materials by ICP-MS measurements after sintering at 900 ˚C. 316

Table 7-10: The degree of crystallinity and the crystallite size of 3% NbHAp (3 wt.% niobate ions) materials prepared by precipitation and hydrolysis methods after sintering at 900 ˚C. 323

Table 7-11: The lattice parameters and the volume of hexagonal unit cell of 3% NbHAp (3 wt.% niobate ions) prepared by precipitation and hydrolysis methods after sintering at 900 ˚C. 324

Table 7-12: ICP-MS results of *5*% NbHAp (5 wt.% niobate ions) materials prepared by precipitation and hydrolysis methods after sintering at 900 C˚. The concentration was in ppb (ug/L):.....330

Table 7-13: The chemical analysis data of 5%NbHAp (5 wt.% niobate ions) materials by ICP-MS measurements after sintering at 900 ˚C. 331

Table 7-14: The degree of crystallinity and crystallite size of 5%NbHAp (5 wt.% niobate ions) materials prepared by precipitation and hydrolysis methods after sintering at 900 ˚C.....337

Table 7-15: The lattice parameters and the volume of hexagonal unit cell of 5% NbHAp (5 wt.% niobate ions) prepared by precipitation and hydrolysis methods after sintering at 900 ˚C.....338

Table 7-16: Synthesis details of 1% B_4O_7HAp (1 wt.% $B_4O_7^{2-}$) materials prepatred by precipitation and hydrolysis methods. 344

Table 7-17: ICP-MS results of 1%B_4O_7HAp (1 wt.% $B_4O_7^{2-}$) materials prepared by precipitation and hydrolysis methods after sintering at 900 ˚C. The concentration is reported in ppb (ug/L): 345

Table 7-18: The chemical analysis data of 1% B_4O_7HAp (1 wt.% $B_4O_7^{2-}$) materials by ICP-MS measurements after sintering at 900 ˚C.....346

Table 7-19: The degree of crystallinity and crystallite size of 1% B_4O_7HAp (1 wt.% $B_4O_7^{2-}$) materials prepared by precipitation and hydrolysis methods after sintering at 900 ˚C. 352

Table 7-20: The lattice parameters and the volume of hexagonal unit cell of 1% B_4O_7HAp (1 wt.% $B_4O_7^{2-}$) materials prepared by precipitation and hydrolysis methods after sintering at 900 ˚C. 353

Table 7-21: Synthesis details of BrHAp and Br_2Ap materials prepared by precipitation, hydrolysis and ion exchange methods.....360

Table 7-22: ICP-MS results of Br_2Ap and BrHAp materials prepared by precipitation, hydrolysis and ion exchange methods after sintering at 900 ˚C. The concentration is in ppb (ug/L):.....361

Table 7-23: The chemical analysis data of Br_2Ap materials by ICP-MS measurements after sintering at 900 ˚C.....362

Table 7-24: The degree of crystallinity and crystallite size of Br_2Ap and BrHAp materials prepared by precipitation, hydrolysis and ion exchange methods after sintering at 900 ˚C. 371

Table 7-25: The lattice parameters and the volume of hexagonal unit cell of Br_2Ap and BrHAp materials prepared by precipitation, hydrolysis and ion exchange methods after sintering at 900 ˚C. 372

Table 7-26: Synthesis details of SAp materials prepared by precipitation, hydrolysis and ion exchange methods. 381

Table 7-27: ICP-MS results of SAp materials prepared by precipitation, hydrolysis and ion exchange methods after sintering at 900 ˚C. The concentration was in ppb unit (ug/L): 382

Table 7-28: The chemical analysis data of SAp materials by ICP-MS measurements after sintering at 900 ˚C. 383

Table 7-29: The degree of crystallinity and crystallite size of SAp materials prepared by precipitation, hydrolysis and ion exchange methods, after sintering at 900 ˚C. .390

Table 7-30: The lattice parameters and the volume of hexagonal unit cell of SHAp materials prepared by precipitation, hydrolysis and ion exchange methods, after sintering at 900 ˚C. 391

Table 7-31: Synthesis details of prepared NaClHAp materials by precipitation and hyfdrolysis methods. 400

Table 7-32: ICP-MS results of NaCl co substituted HAp materials prepared by precipitation and hydrolysis methods after sintering at 900 ˚C. The concentration was in ppb unit(ug/l): 401

Table 7-33: The chemical analysis data of prepared NaClHAp materials by precipitation and hydrolysis methods by ICP-MS measurements 402

Table 7-34: The degree of crystallinity and crystallite size of NaClHAp materials prepared by precipitation and hydrolysis methods after sintering at 900 ˚C. 408

Table 7-35: The lattice parameters and the volume of hexagonal unit cell of NaClHAp materials prepared by precipitation and hydrolysis methods after sintering at 900 ˚C. 409

Table 8-1: Mechanical results of unsubstituted HAp powders prepared by the hydrolysis of MCP/$Ca(OH)_2$. 419

Table 8-2: Mechanical results of ZnHAp powders prepared by hydrolysis method with different substitution levels. 421

Table 8-3: Mechanical results of SrHAp powders prepared by hydrolysis method with different substitution levels. 422

Table 8-4: Mechanical results of CuHAp powders prepared by hydrolysis method with different substitution levels. 424

Table 8-5: Mechanical results of 1%EuHAp (1% wt. Eu^{3+}) and 1% ScHAp(1% wt. Sc^{3+}) powders prepared by hydrolysis method. 426

Table 8-6: Mechanical results of 1% B_4O_7HAp (1 wt.% $B_4O_7^{2-}$) and NaClHAp ($Ca_9Na(PO_4)_6ClOH$) powders prepared by hydrolysis method. 428

Table 8-7: Mechanical results of SAp powders prepared by the novel hydrolysis methods.429

List of Abbreviations

Å	Angstrom
BCP	Biphasic calcium phosphate compound
β-TCP	Beta- Tricalcium phosphate
°C	Degrees Celsius
CDHA	Calcium-deficient hydroxyapatite
CaP	Calcium phosphate
Ca/P	Calcium/Phosphate mole ratio
E. coli	*Escherichia coli*
EDX	Energy-dispersive X-ray spectroscopy
FTIR	Fourier Transform infrared spectroscopy
FWHM	Full width at half maximum
g	Gram
HAp	Hydroxyapatite
ICP-MS	Inductively coupled plasma-mass spectrometry
IR	Infrared
MCP	Monocalcium phosphate
MCMP	Monocalcium phosphate monohydrate
mg	Milligram
ml	Millilitre
μm	Micrometre
mol	Mole
MPa	Mega Pascal = $1N/mm^2$
N/D	Not detected
nm	Nanometre
ppb	Parts per billion
S.aureus	*Staphylococcus Aureus*
SEM	Scanning electron microscopy
SBF	Simulated body fluid
TEM	Transmission electron microscopy
Wt.	Weight
XRD	X-ray diffraction

Chapter One

Introduction to Hydroxyapatite and Substituted Hydroxyapatites.

1.1 Background:

Due to factors such as age, disease, congenital birth defects and a growing population, there is an increasing clinical demand for bone replacement and repair materials. Normally bone replacement materials use the "gold standard" which is bone harvested from the iliac crest of the patient concerned. These are known as autologous bone implants and being the patient's own tissue constitute the least problematic material in terms of rejection. In previous research, there have been various efforts made to develop materials for use in biomedical applications, but which sometimes compromised biocompatibility, porosity, and at the same time a certain or significant level of strength/bioactivity. The development of suitable biomedical materials to replace autologous tissue has hence presented many challenges [1]. In the 1970s, when biomaterials science started to develop, a biomaterial initially was intended to be chemically inert towards the rest of the organism in which it was implanted. But when the first large-scale known bioactive material, Bio glass 45S5®, was able to produce a positive interaction with the biological environment: the term of "bioactivity" came into being, and this development led researchers to conclude that a biomaterial should not be inert but also elicit a positive response from the host organism [2]. The Consensus Conference of the European Society of Biomaterials [3] define a biomaterial as : "a material intended to interface with biological systems to evaluate, treat, augment or replace any tissue, organ or function of the body". It is clear that the purpose and goals of biomaterials are to be implanted and/or to interact with living tissue in the recipient host.

From a chemical point of view, biomaterials could belong to one of the following categories: ceramics (glasses), metals, polymers and composites. Each category has its own application. Metals are commonly used to replace hard, load-bearing tissues, The most commonly used implant metals are the 316L stainless steels. due to their elasticity, Composites have been

extensively used in dentistry and prosthesis designs, while polymeric materials have been used as implants or part of implant systems such as polymethyl methacrylate (PMMA) which has been employed as acetabular cups for hip prosthesis. Ceramics have been more widely used for bone replacement in non-load-bearing applications, due mostly to their brittleness which hindered their use in high load bearing areas of the body such as in hip or knee implants. The main applications of these less strong bioceramics are seen in the reconstruction of smaller sized bones, as for example in maxillofacial surgery and in dental applications [2].

However, hydroxyapatite as will be discussed extensively later (see chapter two for details) can be considered as one of the most studied bioactive ceramics for dental and skeletal purposes due to its biocompatibility and bioactivity behaviors that mimic the biological apatite. On the other hand, the biological apatites in mammals are characterized by several properties that they are calcium-deficient, carbonated, substituted and nonstoichiometric powders, therefore the aim of mimicking biological apatites materials has resulted in different versions of calcium HAp materials, with chemical and microstructural characteristics resembling those of biological ones [4].

1.2 Substituted HAp materials:

Many studies have been carried out which have investigated the synthesis and characterization of various substituted HAps. In certain areas of application (e.g. as in the biomedical sciences) the utility of generating these substituted HAps has also been discussed. The bone mineral can be represented as hydroxyapatite ($Ca_{10}(PO_4)_6(OH)_2$), which is associated with secondary groups and elements (e.g. CO_3^{2-} , HPO_4^{2-} , Na^+, Mg^{2+}) and trace elements (e.g. Sr^{2+}, K^+, Cl^- and F^-), some of these elements may be found at ppm level [5], which play a an important role in the biochemical reactions. The bioactivity of HAp, biological performance, stability and other properties can be modified and improved through insertion, substitution and incorporation of other anions, cations, or even functional groups into the crystal structure without destroying the crystallographic characteristics of HAp. For example, silver can be considered as an antimicrobial agent [6] against a wide range of microorganisms, therefore, insertion of silver into the HAp structure enhanced the antimicrobial properties in an obvious manner[7]. Also incorporation of copper and zinc [8], can lead to reduction in infections after implantation and surgical operations.

Fe-doped HAp opened up new classes for biodevices to be used as anticancer therapies [9]. A/B carbonate hydroxyapatite (CHA) biomaterials preparation led to materials that aimed to balance implant resorption rate and nascent tissue formation for improving bone formation[10]. Improvement of biological efficiency in terms of enhanced bone apposition, bone in-growth and cell-mediated degradation had been confirmed by Bianco et al. [11]. Preparation of substituted HAp with 10 wt% of terbium (Tb) content had been proven to be suitable for biolabelling applications [12]. Also, Cl-HAp demonstrates encouraging potential as a bone grafting material due to its highly enhanced bioactivity and osteoconductivity compared with pure hydroxyapatite (HAp). This brief summary above serves to show that synthetic versions of **substituted** and **co-substituted HAP** are important biomaterials in dental and orthopedic procedures and have become an important biomaterial for tissue engineering and other biomedical applications. Also, substituted HAp materials have many other applications outside the field of biomedical materials. These have been described elsewhere (see Chapter two for details).

1.3 The Scope of the Present Investigation:

The scope for producing novel substituted HAps still exists with various anions and cations that are yet to be investigated. This project represents materials science/chemistry-based research which aimed to develop novel synthetic methods (i.e. “hydrolysis) of preparing substituted and co-substituted HAps from precursors (namely monocalcium phosphate or MCP) which have not been extensively considered before in this area of work and to compare these with products from other more well known methods of synthesis (e.g. precipitation). In addition to the usual cation (or anion) substituents employed for making substituted HAps, some novel substituents (e.g. from Nb-based, Sc-based, and others) were also considered and analysed to confirm if substitution had taken place. Comparisons were made also with unsubstituted HAps

The substituted (and unsubstituted) hydroxyapatite products synthesized in this study were subject to various spectroscopic, microscopic and mechanical testing characterization regimes in order to characterize the products (and furthermore to assess the efficacy of the synthesis method) and to confirm that substituted HAps had been formed. The following table (**Table 1-1**) illustrates the cations and anions that were investigated as part of this PhD project.

Table 1-1: The cations and the anions that were substituted into HAps synthesized via the novel and conventional synthetic routes considered in this work. Synthetic routes will be described more in detail later on.

Cations and anions amenable to this study for substitution work	Any previous work involving these cations or anions	Possible applications	Notes
Zn^{2+}	No previous works to the author's knowledge through using MCP (monocalcium phosphate) as a precursor and hydrolysis method as a synthesis route	Biomedical applications [13]	It was reported that the substitution process of Zn^{2+} into HAp crystal is of particular interest due to its diverse biological functions such as inhibiting osteoporosis [6]
Sr^{2+}	No previous works to the author's knowledge through using MCP (monocalcium phosphate) as a precursor and hydrolysis method as a synthesis route	Biomedical applications [13]	Strontium plays a fundamental role in bone mineralization processes [6]
Cu^{2+}	No previous work to the author's knowledge through using MCP (monocalcium phosphate) as a precursor and hydrolysis method as a synthesis route	Biomedical applications [13]	Characterized by its ability to act as an antimicrobial agent [6]
Sc^{3+} or Sc-based substituents	No previous works to the knowledge of the author by using hydrolysis method. but one work was mentioned in the literature using a precipitation method [14]	Optical application(luminescence application) [15] . Catalytic applications	Tite et al. [16] reported that rare – earth metals such as lanthanides and scandium are of great interest in biomedical applications especially in orthopedic areas because of their high biological activity as well as their ability to substitute for calcium ions in the HAp structure.

Rb^{+}	No previous works to the knowledge of the author were performed by using precipitation and hydrolysis methods. But, one work had been achieved by using a hydrothermal method [17]	Biomedical applications.	Liu et al. [17] reported that substitution of Rb^{+} ions into HAp may enhance cytocompatibility and antibacterial ability.
Eu^{3+}	Several previous works [18-22]	Biolabelling applications [12]	it is well known that doping of HAp compounds with rare earth elements enhances its photoluminescent response, therefore it would be suitable for biolabelling applications [12].
Br^{-}	No previous works involving synthesis of substituted HAps were performed by using hydrolysis, ion exchange or precipitation methods. But, one work had been performed through heating HAp powders at 900 ˚C in a flow of hydrogen bromide for 10 hours [23]	Flame Retardants [24]	
S^{2-}	No previous works were performed by using hydrolysis, ion exchange or precipitation methods. But, one work had been performed through a solid state reaction and also by flowing of H_2S over $Ca_3(PO_4)_2$ for 2 hours [25]	Possibly in biomedical applications [26]	Sulfur and sulfates have a great interest in the biomedical field that they can be considered as a biological cement, which is involved in building and rebuilding skin cells, hair, nails as well as cartilage [5,27].
Na^{+} and Cl^{-} co-substituted	No previous works to the author's knowledge by using hydrolysis	Biomedical applications [6]	While bone mineralization, bone resorption and cell

	method. but one work was performed by precipitation route [28]		adhesion are processes in which sodium ion can have important effects [29], the substitution process of chloride ion into HAp crystal has been reported by Ratnayake et al. [29] to enhance bioactivity due to its high solubility and greater osteoconductivity over stochiometric HAp
$B_4O_7^{2-}$	No previous works to the author's knowledge	Biomedical applications [30]	Boron has many biological effects such as modifications of calcium and bone metabolism[30]
Nb (substituted as niobate ion)	Two previous publications reporting synthesis by the precipitation method [31,32], but no work done using a hydrolysis approach.	Biomedical applications [33]	As reported by Tamai et al. [32], introduction of niobate ions into biphasic calcium phosphate (HAp and β-tricalcium phosphate) can enhance the calcification of normal human osteoblasts due to the enhancement process of ALP activity.

1.4 Broad objectives of this work:

In this project we aim to achieve the following broad objectives, while the specific objective of this study will be discussed extensively later (see chapter 2, for details):

1- To prepare new systems of both substituted and co-substituted HAp powders using different kinds of synthesis routes (precipitation, ion exchange and hydrolysis methods) . Comparison with "unsubstituted" HAps was also undertaken.

2- To develop a new approach (to an extent) to prepare HAp, substituted and co substituted HAp powders through using a single novel precursor, namely MCP (monocalcium phosphate) by a one-step synthesis.

3- To characterize the prepared systems of substituted and co-substituted HAp materials using different kinds of techniques such as Fourier transform infrared (FTIR), scanning

electron microscopy (SEM), X-ray powder diffraction (XRD) and inductively coupled plasma mass spectrometry (ICP-MS).

4- To investigate the effect of the substitution process and the substitution levels on the physiochemical properties of hydroxyapatite.

5- To study (in the case of some selected systems) the effect of the lattice substitutions on the mechanical properties of the generated HAps

Chapter Two

Literature review.

2.1 Hydroxyapatite:

Hydroxyapatite (HAp), a member of the family of apatites belongs to the family of calcium orthophosphates, which can exist in different forms with the difference being attributed to the Ca: P mole ratios, in addition to the presence of water in their structure (e.g. as in the non-apatitic compound, brushite $CaHPO_4.2H_2O$). The lower the Ca:P mole ratio in the calcium orthophosphate compound, the more acidic and more soluble is the calcium orthophosphate material [34].

Hydroxyapatite is the main component of teeth and bone minerals, it has the chemical formula $Ca_{10}(PO_4)_6(OH)_2$ with a Ca:P mole ratio of 1.67. It shows excellent biocompatibility with both hard and soft tissues such as skin and muscle. Moreover, bioactivity and osseointegration are prominent characteristics when directly implanted into bone [35]. Also it is used in musculoskeletal procedures because of its chemical composition and crystallographic structure that mimic biological apatites in human bone and teeth [36]. Pure HAp is a stoichiometric apatite phase and is regarded as the most thermodynamically stable calcium phosphate phase to exist at normal temperatures. It is stable in liquids from pH 4-12 [37]. Despite these preferred properties of bioactivity and biocompatibility, the classical issue has been that pure HAp has poor mechanical properties, especially when used in load bearing areas of the body. However, biologically, hydroxyapatite differs from synthetic hydroxyapatite in various properties such as its smaller grain size, exhibiting of carbonate substitution, available lattice vacancies and increased solubility that is required for bone remodelling [38]. It is also usually present (at least in bone tissue) interdigitated with collagen which gives the bone, as a living tissue, its flexibility and strength.

However, the synthetic versions of HAp are important biomaterials for use in dental and orthopedic procedures. In addition, HAp and apatites are employed as industrial catalysts,

adsorbents for removing toxic substances, fertilizers and other applications. Below some briefly described uses of HAp are given in various fields of application:

1- Chromatographic columns: Hydroxyapatite chromatography has been used extensively for the purification and fractionation of various biochemical substances such as protein and viruses, due to its high resolution based on the mixed modes of cation exchange and metal affinity. However, the spread of infectious diseases has become a global health concern [39] hence in order to diagnose infectious diseases quickly and with high accuracy , next-generation DNA techniques for genetic analysis of infectious viruses have been developed. Unfortunately, it takes a long time to prepare clinical samples for genetic analysis. On the other hand, clinical samples from patients contain many impurities which can inhibit the detection of viruses, so purification of viruses allows for sensitive detection. Additionally, in order to detect a virus infection at an early stage, it is very important to enrich the low-concentration virus suspension. Therefore, Niimi et al. [39] developed a method to purify and enrich viruses in samples by using hydroxyapatite particles packed in a micro-column. The results of their study revealed that the purification and enrichment of the viruses can be achieved by using hydroxyapatite chromatography at low cost.

2- Agricultural applications: Low phosphorus (P) availability is a major problem that reduces crop production in several agricultural areas in the world. It has been reported that approximately 67% of the arable soils in the world can be considered as P (phosphorus) deficient [40]. Nanotechnology has been proposed as a technology that has the ability to enhance fertilizer formulations. Due to the specific properties of nanoparticles, it is reasoned that nanofertilizers could be designed to prevent the immobilization of nutrients in the soil in addition to better release of nutrients with plant demand. However, Liu and Lal [41] reported that the use of hydroxyapatite nanoparticles, led to improvements in the growth of soybeans by 33% and in yield by 20%, compared with conventional phosphorus-based fertilizers.

3- Environmental application: Due to the extensive use of new technologies in several fields, such as in agricultural and industrial fields, soil and groundwater can become polluted with elements that cause serious problems to the environment. Therefore, Safatian et al. [42] prepared hydroxyapatite from egg shells by microwave irradiation technique to remove lead ions from water and wastewater samples. The effect of the experimental conditions such as pH, temperature, initial concentration of lead ions as well other variables were investigated. However, the results indicated that the prepared hydroxyapatite had high adsorption capacities for removal of lead ion from water samples.

4- Optical application (luminescence application): it has been reported that doping HAp and HAp-based, compounds with rare earth elements especially those of trivalent lanthanide ions (which have strong luminescence), such as (La^{3+}), (Eu^{3+}) , (Ce^{3+}), (Tb^{3+}) and erbium (Er^{3+})enhances its photo luminescent response. Therefore, these biomaterials could be used for biolabelling applications [43].

5- Catalytic applications: Many studies have revealed that the synthesis of gold supported hydroxyapatite catalysts and gold nanocrystals loaded on phosphate containing supports prevent the agglomeration of Au crystals and increase the activity for the oxidation of Domínguez et al. [44] fabricated gold/hydroxyapatite catalysts for CO oxidation, with the results revealing that the Au-supported catalyst shows an excellent activity for the oxidation of CO even at room temperature.

6- Fire retarding application: Polymer nanocomposites [45]have attracted much attention recently. Polycarbonate (PC) is an important thermoplastic and one with the most interest is bisphenol A PC which is widely used in many fields such as electrical and electronic devices, automobiles, and construction. For electronic and electric applications, higher flame retardancy is required. Dong et al. [45] studied the thermal properties, in addition to flame retardancy of both PC and

PC/HAp. The results revealed an improvement in thermal properties of PC/HAp composites due to the existence of HAp. They also suggested further study of this area to elaborate the flame retardancy mechanisms involved.

Table 2-1 Physico-chemical parameters of synthesized hydroxyapatite [34,46,47]

Parameters	Values	Notes
Chemical formula	$Ca_{10}(PO_4)_6(OH)_2$	Composition can be varied depending on substitution levels
Ca:P mole ratio	1.67	This value corresponds to that for stoichiometric HAp
Spatial groups	$P6_3/m$ (hexagonal) $P2_1/b$ (monoclinic)	The major differences between these structures (hexagonal and monoclinic)were discussed elsewhere [48,49].
Lattice parameters	a = b = 9.432, c = 6.881 Å α = β = 90˚, γ = 120˚	These are the typical values for the hexagonal structure.
Theoretical density	3.16 g/cm^3	Varies with HAp composition
Solubility at 25 ˚C, in g/L	~0.0003	

2.2 Structures of Hydroxyapatite:

The physico-chemical properties of HAp are summarized in Table 1 above. The crystal structure of HAp is hexagonal, having the $P6_3/m$ space group symmetry with lattice parameters of a = b=9.432, c= 6.881 Å, and γ =120˚ [37]. The other form of HAp is the monoclinic structure with space group $P2_1/b$ and unit cell parameters a = 9.4214(8), b= 2a, c = 6.8814(7) Å, and γ =120˚, where γ is the interaxial angle between length a and b as shown in **Fig 2.1** below [50]:

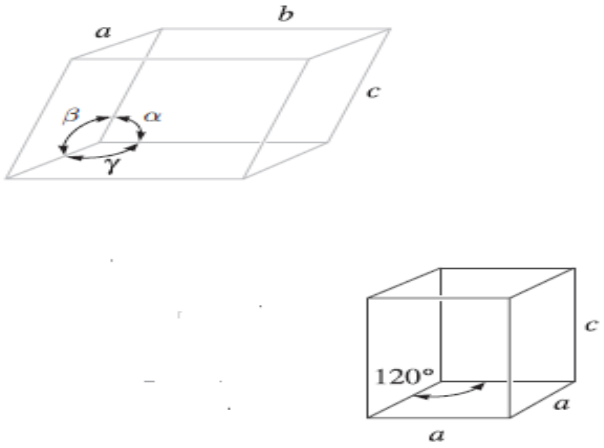

Figure 2.1: Definition of the lattice parameters and their use in hexagonal crystal system [50]**.**

The letters a, b and c represent the lattice parameters, which can be considered as the axial length of the unit cell, whereas the angles between these axial lengths are defined as the interaxial angles [50], and the Greek letters α, β and γ are used to describe these angles. As shown in **Figure 2.1,** α represents the angle between b and c lengths, whereas β is the angle between a and c, and γ is the angle between a and b.

The major difference between monoclinic and hexagonal HA is the orientation of the hydroxyl group, also the hexagonal HA is usually formed by precipitation from solutions of calcium ions and orthophosphate at 25-100°C, while the monoclinic form can be made by heating of the hexagonal form at 850°C in air and cooling to room temperature [37]. Although, the monoclinic phase of hydroxyapatite[49] is thermodynamically stable, the hexagonal form is the preferred phase, since the monoclinic form is destabilized by the presence of small amounts of foreign ions in the lattice [51] .

The hexagonal unit cell of HAp consists of Ca^{2+} and PO_4^{3-} groups distributed within the unit cell as shown in Fig**. 3.2** [35]. There are two types of Ca^{2+} cations residing within the unit cell, the first one is represented as a Ca(I) site which includes four calcium cations while the remaining six calcium cations are represented as Ca(II) sites, the Ca(I) can be substituted by smaller cations, whereas the other site of calcium, i.e. the Ca(II) ions, can be substituted by larger cations.

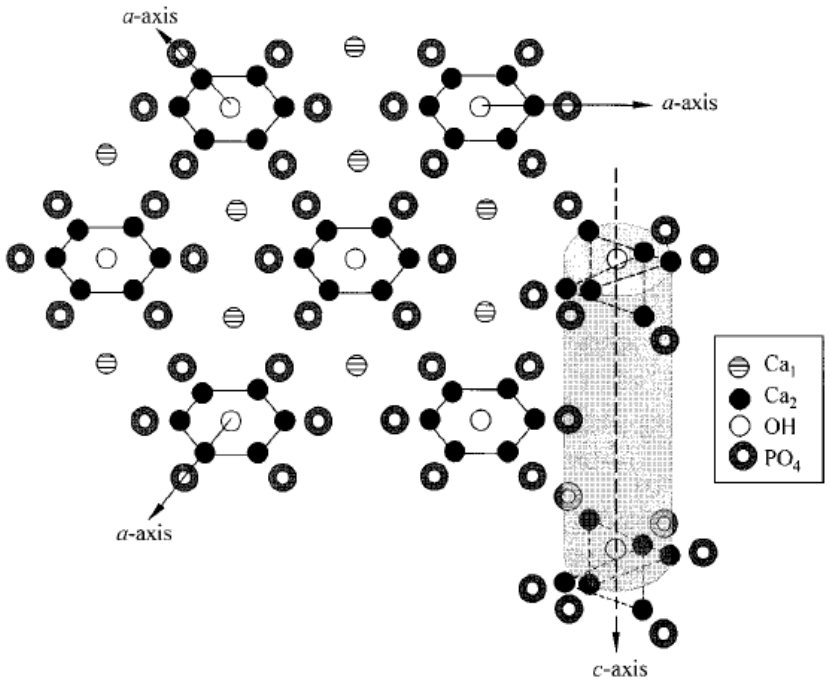

Figure 2.2: The atomic arrangement of calcium ions in $Ca_{10}(PO_4)_6(OH)_2$ [35]

2.3 Sources of HAp:

There are several sources for HAp materials, such as bio waste bovine bone which is considered as the most commonly available source, marine products such as shells and catfish, in addition to other types of calcium phosphates, that are easily transformed into HAp phases through various procedures [52]. The following HAp sources should also be added to this mix: oyster shell, and pig bone. Even extracted human teeth has been used for HAp fabrication into other forms [52].

2.4 Some methods used for the preparation of Hydroxyapatite :

As discussed in the current literature hydroxyapatite materials can be prepared through using different synthesis routes, various kinds of reactants as well as several processing conditions [35,53-59] . Below are described some of these methods: the final phase and composition of the hydroxyapatite product are highly dependent on the reaction conditions under which the

synthesis takes place [53]. Impurity elements or compounds present can become incorporated into the HAp lattice through substitution.

2.4.1 Precipitation method:

This is considered a simple and inexpensive method [53] to make HAp. It is usually performed in solutions at relatively high values of the pH (predominantly pH 8-11), with the temperature of reaction varying from room temperature to temperatures close to the boiling point of water (80-95 °C). It involves the reaction of calcium and orthophosphate ions which are produced from different sources of starting materials by dropwise addition of one reagent into another with stirring and controlling of the pH value. The final composition of the produced materials depend on many variables such as pH, the reactant addition rate, concentration, and temperature, therefore, all these parameters have to be controlled to form a homogeneous product of the correct phase.

2.4.2 Solid state route :

Solid-state reaction routes are simple and inexpensive methods of synthesis. They are based on solid diffusion of ions in powdered raw materials which require high temperatures (<1250°C) to initiate the diffusion reactions. The solid precursors can be various calcium- and phosphate-containing salts and oxides [54]. The main drawback of this method is the phase heterogeneity of the produced powder, due to low diffusion coefficients of ions within the solid phase [30]. Also, this method is characterized by low phase purity because of the high temperature that is required for the reaction to take place [54] . However, to prepare homogeneous powders, another step is required which can be achieved by the action of ball milling the starting materials for 16 hours although, some additives might also be used such as silicon dioxide, a binder (PVA) and an organic vehicle (acetone), to produce a slurry before milling. The slurry must then be dried and the resulting powder pressed into pellets at pressures of up to 135 MPa. Finally, sintering is performed up to 1250°C to crystallize the product [54].

2.4.3 Mechanochemical method:

While heterogeneous particles with irregular shape are usually obtained by the solid state method, a well-defined structure can be considered as a major characteristic of the

mechanochemical process [60]. The principle of the mechanochemical approach is attributed to the energy transfer by impaction that mill balls exert on powder particles toward the internal wall of the jar [61], whereas the temperature can vary from a few degrees Celsius to a hundred degrees Celsius in the collision region.

In other words, the mechanochemical route combines mechanical and chemical phenomena on a nano scale solid material, since chemical processing is obtained through the mechanical force. However, long processing times, contamination from the deformation instrument (e.g. the milling media), in addition to the lack of control of particle morphology generated are the major drawbacks of the ball milling process [59].

2.4.4 Sol-gel synthesis:

The first stage of the sol-gel synthesis method is to form a sol (colloids in a liquid). Metal alkoxides (such as tetraethoxysilane to produce silicon) and metal salts (calcium nitrate and ammonium phosphate) are used as the calcium and phosphorus precursors. Hydrolysis and polycondensation reactions occur to form the M-O-M bonds within the sol causing the viscosity to increase. The last step which is required to remove the liquid phase, can be executed by a drying process. This method has several advantages over the more conventional synthetic methods such as the ability to carry out homogeneous molecular mixing, the use of low processing temperatures (<400°C), and the ability to generate nano-sized particles [54]. However, the energy saving which is obtained from the low temperatures is offset by the high cost of the reactants involved in sol-gel processing. Major drawbacks of the sol-gel synthesis route are the existence of secondary phases, most often CaO, the high cost of starting materials (especially alkoxide based precursors) in addition to the long period of reaction required –this being 24 h or longer which has been reported as being needed to form the desired product [62]. The reasons for this long duration of reaction is due to the slow reaction between the calcium and phosphorus precursors in the sol-gel phase.

2.4.5 Hydrothermal processes:

Hydrothermal routes to synthesis of HAp use a solvent (water), which is heated in a sealed vessel capable of high pressures. The temperature of the solvent can be brought above its boiling point while the autogenous pressure within the vessel exceeds the ambient pressure [54]. These

methods have several advantages in that they can be performed at lower temperatures compared to solid-state reactions. Also, in comparison, other low temperature methods such as the precipitation route and sol-gel synthesis still require additional heat treatments to crystallize the HAp, but crystalline HAp can be produced in one step by a hydrothermal synthesis. Low cost reagents and short reaction times have also been reported for these hydrothermal processes, which is an advantage. The most notable drawbacks of the hydrothermal method is the poor capability to control the morphology and size distribution of any nanoparticles that may be produced [53].

2.4.6 Hydrolysis:

HAp may be prepared also by the hydrolysis of other (precursor) CaP solid phases, such as dicalcium phosphate dihydrate (DCPD, $CaHPO_4.2H_2O$) otherwise known as "brushite" and TCP (tricalcium phosphate, $Ca_3(PO_4)_2$ among other CaP phases. Historically, this type of conversion has not been considered to be of great interest as a method for the preparation of HAp particles, due to the slow rate of OCP [octacalcium phosphate] hydrolysis and the ability of OCP to incorporate impurity species, including additives and foreign ions used for its transformation to HAp. Hydrolysis of CaP phases into HAp can be realized via dissolution and reprecipitation processes [53].

2.5 Substituted Hydroxyapatites:

One of the most interesting properties of HAp is the flexibility/lability of its structure which gives it the ability to accept ionic substituents into the lattice and into vacancies [63]. The chemical formula of HAp is described as $M_{10}(XO_4)_6(Y)_2$, where M, XO_4, and Y are bivalent, trivalent, and monovalent ions respectively all of which can be substituted or co-substituted by using different techniques with different cations and anions. The present study delineated in this proposal will be focused on this lability of the HAp structure**. Fig. 2.3** shows [64] the various kinds of cations and anions that can substitute into the apatite structure.

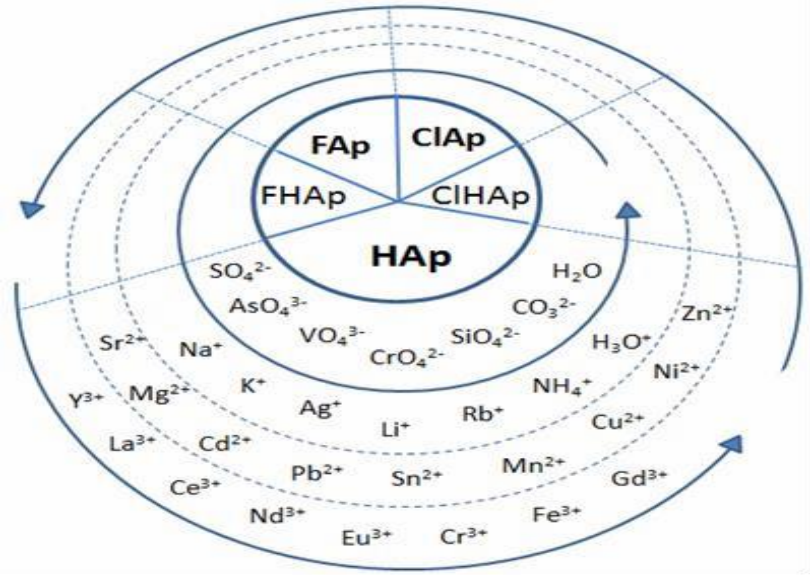

Figure 2.3 : Schematic representation of substitution elements in apatites. The inner layer shows anionic substitutions, while outer layer – monovalent, divalent and trivalent cationic substitutions [64].

Substitutions in the HAp lattice have significant effects on many properties such as physical properties due to noticeable changes in lattice parameters, crystal structure, morphology, solubility, and thermal stability relative to unsubstituted (stoichiometric) HAp [6]. Significant research has been performed on several cationic and anionic elements that have been substituted into the HAp lattice. Also biological HAp is calcium-deficient (Ca: P molar ratio is < 1.67) and is always carbonate substituted [35]. This may be attributed to the substitution of OH^- by CO_3^{2-} which leads to type A substitution or the charge balance due to the replacement of PO_4^{3-} with CO_3^{2-} which can be expressed as type B substitution [51]. Such substituted HAps occur in the body because these ions are inevitably made available in body fluids through various nutritional sources. Any substitution of any group in the hydroxyapatite will result, as highlighted earlier, in the changing of several properties, such as lattice parameters, crystallinity, morphology, solubility, in addition to physical, chemical and biological properties [65].

The changes in properties induced can be interesting and may offer improvements in properties exhibited by the stoichiometric HAp for example when fluoride or chloride ion substitute [2] for

the OH groups in the apatite structure, fluoro and chloro apatite would be produced. Therefore the positions of OH, Cl, or F in the crystal structure of each produced apatite , are completely different depending on the ionic radii of the substituted ions as shown below in Fig. 4 [2], which reveals that (F^-)is the smallest one to be located in the triangle plane (created by the Ca ions), that will affect the ionic interaction with the Ca(II),so that as a result, stronger interactions are produced, leading to the lower observed solubility of fluorapatite compared with the chloro substituted HAp and the stoichiometric HAp. The decrease in solubility provides the rationale for why fluoridated toothpaste is used to prevent dental caries in human teeth.

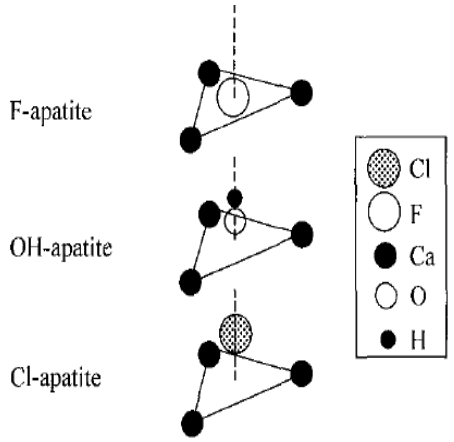

Figure 2.4: The relative positions of F, OH and Cl atoms at the centre of the Ca_{II}triangles in F-apatite, OH-apatite and Cl-apatite [35]

2.6 Summary of Synthetic Approaches to forming Substituted Hydroxyapatites:

During the past decade, several methods and routes have been investigated as being an effective way to prepare CaP powders. These methods can be divided into two groups: the first groups can be referred to as dry methods such as mechanochemical and solid-state routes. In these methods a solvent is not used and the properties of a powder are not strongly affected by the processing parameters such as pH [53]. The second group of methods is known as wet methods (such as precipitation, hydrolysis, sol gel, ion exchange and hydrothermal processing) in which the

crystallinity of the produced HAp particles can be varied and strongly depend on many parameters such as concentration of the initial reagent solutions, pH, temperature, etc.

Now in terms of the synthesis procedures for *substituted* and *co-substituted* HAp, the methodologies followed will be similar to the methods used to make unsubstituted HAp except that the substituent ions or functional groups of interest will be introduced at the time of the precipitation or synthesis etc for incorporation. Details of these main preparation routes have been covered above when discussing the general synthetic routes to HAp. For substituted HAp synthesis, the ions or functional groups can be introduced (as an "impurity") at point of preparation/precipitation with the intention of these entering the HAp lattice to prepare the substituted HAp compound. Hence a brief summary of the methodologies for achieving substituted HAps would be as follows:

Dry methods would be the label applied to "solid state" and "mechanochemical" routes which are characterized by the following features [35,53-59]:

1- All the starting materials or precursors are usually milled by using ceramic balls (e.g. zirconia) to produce homogeneous particles.
2- In mechanochemical preparations, several variables can affect the properties of produced HAp powders such as the type of reagents, the type of milling medium, and the rotational speed.

Wet methods, on the other hand would be the label applied to such synthesis processes for substituted HAps as "precipitation", "ion exchange" (via soaking), "hydrolysis", "sol gel" and "hydrothermal" approaches. These are characterized by the following features [35,53-59]:

1- The reactions can be performed at room temperature or elevated temperatures.
2- These reactions can be realized via various technical routes involving several kinds of chemicals and apparatus.
3- Stirring unsubstituted HAp solids with a solution of the desired substituent ion to achieve substitution can be achieved in the ion exchange method
4- Incorporating substituent ions in precursor phases to HAp during the synthesis route is used to prepare substituted HAp powders.

5- Hydrolysis methods tend to use a single precursor in the preparation.
6- A hydrothermal process, is characterized by the reaction of chemicals in an aqueous solution at high temperature and pressure.
7- The sol- gel method includes mixing alkoxides (or any other suitable precursors), followed by aging at room temperature, gelation, drying and finally removing of organic residues from the resulting dried gel using a heat treatment step (calcination).

Many studies exist where substituted HAps have been synthesized and studied. Many of these have found use in a variety of applications or have been found to have enhanced properties relative to unsubstituted HAp. The following is a review of reports where substituted HAps have been prepared and the properties that these systems have been found to have as a result of the substitutions.

2.7 Specific Systems of Substituted HAps

In this review, these have been classified by 1) anion, 2) cation and 3) multi ion substitutions

2.7.1 Some examples of XO_4 (anionic) substitutions in $M_{10}(XO_4)_6(Y)_2$:

Substitution within the HAp lattice can be obtained through the replacement of a calcium ion or any functional group such as hydroxyl or phosphate groups, which are considered to be the main constituent parts of the hydroxyapatite crystal lattice. Anionic substitutions involve the partial replacement of the XO_4 group, and as a result, new substituted hydroxyapatites with completely different chemical or physical properties can be obtained. These changes may also impact on hydroxyapatite's biological activity. Below are discussed some examples of these kind of substitutions:

2.7.1.1 Carbonate*:*

In nature, biological apatite can contain many other elements or functional groups in it with the most prevalent (functional group) being carbonate. The percentage of carbonate can be up to ~5.6 wt %, 3.5 wt % and 7.4 wt % in dentine, enamel and bone [66], respectively. It plays an important role in bone metabolism, hence the preparation of carbonate-substituted HAp (CO_3HAp) can be considered as a goal because it can be termed "bone-like apatite and considered for bone graft applications[6].

Carbonate can substitute in two ways in the hydroxyapatite lattice. The first is referred to as a type A substitution, due to the replacing of the smaller lattice hydroxyl ions by the larger carbonate ions. The second type is called a type B substitution and involves the replacement of the larger orthophosphate functional group ions by the smaller carbonate ion in the HAp lattice [6]. In general, type B substitutions are the most "preferred" carbonate substitution as it is commonly found in the bone of different kinds of living organisms [6], so biological apatite is generally regarded as consisting of type B-substituted carbonate. Type A substituted HAp can be produced most cleanly by heating HAp in a stream of dry CO_2 gas at ~900 ˚C for several days. The relevant reaction can be represented by the following equation [4]:

$$Ca_{10}(PO_4)_6(OH)_2 + xCO_2 \rightarrow Ca_{10}(PO_4)_6(OH)_{2-2x}(CO_3)_x + xH_2O \quad (1)$$

where B-type carbonate apatites, can be produced by precipitation from aqueous solutions, CO_3^{2-} replaces PO_4^{3-}, which leads to a reduction in the a- axis parameter, whereas the c-axis parameter is increased [67]. The neutrality in the lattice is achieved by incorporation of single valence cations such as (Na^+) or (K^+) into the Ca^{2+} positions [68], as described by the following formula:

$$(Ca_{10-x}Na_x)(PO_4)_{6\ x}(CO_3)_x\ (OH)_2 \quad (2)$$

The two types of carbonate substitution have opposite effects to each other on the HAp crystal lattice parameters. For example, as a Type A substitution involves the replacement of smaller hydroxide ions (OH^-)by larger carbonate ions (CO_3^{2-}), an expansion in the a-axis and contraction in the c-axis occur. Type B substitutions involve replacement of larger orthophosphate ions with smaller carbonate ions, and so will result in a contraction of the a-axis and expansion in the c-axis. This is shown in **Fig. 2-5** [35]. It is also possible to have mixed type A/ type B substituted carbonated apatites compounds [10]. As stated before, substitution of carbonate ion for lattice

OH group in hydroxyapatite will produce type A carbonate substituted HAp, whereas substitution of carbonate for phosphate will result in the forming of type B carbonate substituted HAp, but substitution of both groups, namely hydroxyl and phosphate by carbonate will lead to the formation of the so-called AB type carbonate substituted HAps. This kind of carbonated HAp has the following formula $Ca_{10-x}(PO_4)_{6-x}(CO_3)_x(OH)_{2-x-2y}(CO_3)_y$ and can be easily produced by using precipitation routes such as in the work reported by **Germaini et al. [10]**(see below for details).

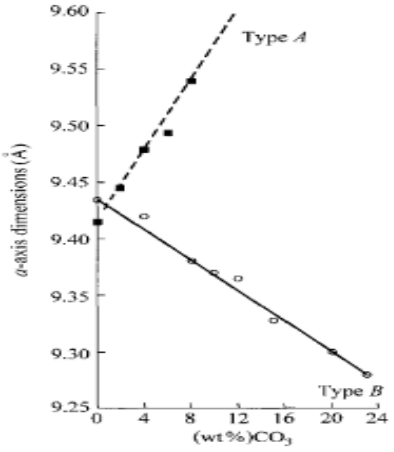

Figure 2.5: The effects of the two types of carbonate substitution on the a-axis dimensions of synthetic apatites [35]

Germaini et al. [10] studied the effect of the incorporation of 4.4 wt% of carbonate ions into the HAp lattice structure and produced mixed type A/type B carbonated apatites which had the chemical formula $(Ca_{9.5}(PO_4)_{5.5}(CO_3)_{0.5}(OH)(CO_3)_{0.25})$. By analyzing the response of pre-osteoblasts and osteoclast-like cells to these materials, they reported that these prepared materials were suitable for bone regeneration without any need for functionalization by proteins to stimulate the regeneration process, since the weight percentage of substitution is very close to that existing in typical biological apatites. They also reported that this type of carbonate substituted HAp (i.e. the type A/ type B substituted compounds) can be synthesized in a simple manner from HAp and β-TCP precursors. In addition, they found that carbonated hydroxyapatite materials, possessing 4.4 wt% substitution of carbonate showed an ideal balance between biodegradation/dissolution (that came about as a result of the action of osteoclasts) and

osteogenesis which was achieved by the action of osteoblasts so that bone remodelling could be induced.

2.7.1.2 Si (as silicate) substituted HAp:

In the $1970_{S,}$ electron microprobe studies revealed that 0.5 wt % (Si) is present in active growth areas (i.e. osteoid in new bone formation) of both mice and rats [6]. Also, it was shown that when there was a lack of or insufficient amounts of Si in the diet [69], abnormal skeletal growth was observed. In another study that had been applied in a rat model [70], a silicon deficiency was shown to cause skull deformations.

Many studies since then have shown that silicon plays a vital role in metabolic processes associated with growth and integrity of the extracellular matrix. In addition to this, several reports have revealed that Si is an influential factor in differentiation and proliferation of osteoblasts [5].

Nakata et al. [71] prepared silicon doped hydroxyapatite by a hydrothermal method using $Ca(OH)_2$, H_3PO_4 and $Si(OCH_2CH_3)_4$ (TEOS) as starting materials. The starting amounts of tetra-ethyl-orthosilicate (TEOS) were in the range of 0-15 weight%. In order to evaluate bioactivity of the prepared SiHAp, immersion in simulated body fluid (SBF) was carried out. SiHAp showed faster apatite forming ability than pure HAp, when the samples were immersed in SBF. Characterization of the samples was carried out by using several techniques such as transmission electron microscopy (TEM), X-ray powder diffraction (XRPD), Fourier transform infrared spectroscopy (FTIR) and X-ray absorption fine structure (XAFS). The authors reported that (i) the SiO_4^{4-} ion substituted for the PO_4^{3-} ion site in apatite structures, and (ii) the local structure of the nearby Ca, P, Si atoms were studied by XAFS, with the results showing that the energy position of the Si K edge XANES for 15% mass Si substituted hydroxyapatite had been shifted to that resembling amorphous SiO_2. The authors reported that the appropriate TEOS doping ratios were 5 and 10 mass% for superior biocompatibility. This was because in the case of 15 mass% TEOS doped samples, amorphous SiO_2 segregation was confirmed by XAFS analysis.

Bianco et al. [11] investigated the relationship between the synthesis process and composition and sinterability of pure (unsubstituted) and SiHAp samples (Si 1.4 wt%) when they were prepared by the following methods:

(i) Synthesis by a precipitation route: $Ca(NO_3)_2.4H_2O$ and $(NH_4)_2HPO_4$ were used as a starting material to prepare HAp, whereas $Si(CH_3CO_2)_4$ was used as a source of Si to fabricate the SiHAp samples. (ii) Synthesis by a titrimetric method: $Ca(OH)_2$, H_3PO_4 and $Si(OC_4H_9)_4$ were used as precursors.

The authors found that the chemical composition of HAp nanoparticles which have been produced by the first precipitation route (i) can be controlled. They reported that, a biphasic calcium phosphate material was formed due to the decomposition of both HAp and SiHAp around 1000 ˚C, since BCP (biphasic calcium phosphate) is produced when synthetic or biological calcium-deficient apatite is sintered at temperatures above 700˚C. In the synthesis method involving titration (ii), hydroxyapatites with higher Ca:P mole ratios and Ca/(P + Si) mole ratios were able to be produced in nanoparticulate dimensions. They reported that SiHAp produced by using $Ca(OH)_2$ as a starting material was thermally stable up to 1200 °C so showing that calcium hydroxide-derived nanoparticles had better thermal stability relative to calcium nitrate-derived nanoparticles. In other words, HAp and SiHAp which are prepared from $Ca(OH)_2$ revealed higher thermal stability, better sinterability, and more homogeneous microstructure compared to HAp and SiHAp which were prepared from calcium nitrate. Also, it was noted that a small increase in lattice parameters for both SiHAps (produced by the precipitation and the titrimetric method) was observed as a result of incorporation of the Si into the apatite lattice structure.

2.7.2 Examples for M substitution in $M_{10}(XO_4)_6(Y)_2$:

As mentioned previously HAp is the principal component of vertebrates' bones and teeth. The introduction of relevant ions into HAp crystal has been found to affect several properties such as the biological properties as well as many other characteristics [35]. The following are examples where cation substitution has been carried out in the HAp lattice structure, through replacing the calcium ions by other metal cations. These substitutions affected several properties of HAp, such as crystallinity, solubility, biological properties and so forth. Details about these kinds of substitutions have been discussed below:

2.7.2.1 Ag:

Since antiquity, silver has been used in many medical applications such as treatment for burns, and bacterial infections [6]. Also, it has been used for many years as a result of its ability and

efficacy as an antimicrobial agent to combat against bacteria, viruses, and fungi [72]. Despite these advantages, the concentration of silver ions must to be controlled when used in vivo to avoid cytotoxicity [37]. For example, in the literature a female [73] was reported as suffering from discoloured skin due to silver ingestion. At the age of 11, the patient was given nose drops of unknown composition for "allergies," which after three years of use caused her skin to become gray. The pigmentation extends to her waist and she was diagnosed as having Argyria, with a skin biopsy done at the age of 15 revealing the presence of Ag deposition [73]. This shows the importance of limiting Ag absorption in vivo as otherwise such conditions can arise.

Stanić et al. [7] synthesized and studied the antimicrobial efficacy of silver substituted hydroxyapatite samples $Ag_xCa_{10-x}(PO_4)_6(OH)_2$, $0.002 \leq x \leq 0.04$ for bone tissue engineering. Those studies revealed that all silver substituted hydroxyapatite samples showed excellent antimicrobial activity against several pathogens such as: *Staphylococcus aureus*, *E. coli*, and *Candida albicans*. The highest antimicrobial activity was recorded for the hydroxyapatite samples that contained the highest concentration of silver, to the extent that all cells of *E. coli* were killed on contact and with a more than 99% percent reduction in viable counts of *S. aureus* and *C. albicans* being observed. Atomic force microscope studies indicated that AgHAp samples cause obvious morphological changes to micro-organism cells which might be considered as the main reason for cell death. Also, hemolysis ratios (where hemolysis can be defined as a process occurring as a result of a specific group of proteins being produced by certain microorganisms, leading to the lysis or dissolution of the red blood cell membrane in the growth substrate) of the AgHAp-exposed samples were below 3%, indicating good blood compatibility.

As ionic silver along with copper and zinc ions exhibit excellent antimicrobial activities [74], in order to reduce the incidence of implant-associated infections, an antibacterial agent could be of great importance in managing infections associated with surgical implants [75].

Bir et al. [74] substituted the following ions (Zn^{2+} , Cu^{2+} , Ag^{+}) into fluoridated HAp (FHAp; $Ca_{10}(PO_4)_6(OH)_{2-x}F_x$, where $0 < x < 2$) and deposited it onto the surface of medical grade 316L stainless steel (18Cr– 8Ni– 2Mo with low carbon content) samples by using an electrochemical deposition method. The antimicrobial effects of FHA coatings against pathogen bacterial strains

S. aureus were tested in liquid media. The authors reported an enhancement of antimicrobial properties for all FHA samples tested.

2.7.2.2 Zn:

Zinc can be considered as the "second" trace element in the body; if one excludes or neglects the iron that is associated with hemoglobin, one will find that zinc becomes the most abundant trace element. The body contains approximately 1.4–2.3 g of zinc, with zinc having an obvious role in more than 300 enzyme reactions [37]. Zn in its divalent cationic form can also be substituted into CaHAp. The prominent use of ZnHAp is its potential to be used to treat people with osteoporosis to minimize reductions in bone mineral density or to improve the property of devices when coated with this material [4] as it can increase their longevity. ZnHAp is also used as a coating for implants; in particular, hip replacements [37], to prevent loosening of the hip implant device due to aseptic loosening [76].

Due to its efficacy also as an antimicrobial agent [77] Zn-HAp has been widely investigated due to the obvious effect of Zn^{2+} ions in metabolic processes. Zinc plays a vital role in growth before and after birth. Also, it has a clear effect in DNA and RNA, DNA polymerase, and RNA polymerase being responsible for DNA and RNA synthesis and cellular division [37]

Jallot et al.[78] doped HAp with Zn. In their study, four Zn concentrations (evaluated in terms of Zn/ (Zn+Ca) wt%) were prepared at 0.5, 1, 2, and 5 wt%. Then they immersed the Zn substituted hydroxyapatite into biological fluids for 1 - 20 days. After 20 days they noticed the formation of a calcium-phosphate (CaP) layer at the periphery of the HA doped with 5% of zinc. It was reported that (1) observation of the formation of the CaP–Mg layer indicates the specific bioactive properties of 5 % wt of Zn and (2) the biologically active layer formed led to the formation of a chemical bond between the ceramic and bone tissue.

Stanic´ et al. [8]synthesized CuHAp and ZnHAp by neutralization methods using $Ca(OH)_2$, H_3PO_4 and CuO or ZnO as starting materials. All samples were prepared with the amount [M + Ca] = 0.25 mol where M = Cu or Zn. Undoped and doped HAp with two different concentrations of M ions, namely ((MHAP1) and (MHAP2), were prepared, where M (Cu, Zn), and M/(Ca + M) = 0.0004 and 0.004 for MHAp1 and (MHAp2) respectively. The authors reported that all prepared samples were of nano sized dimensions and homogenous. They also found that copper and zinc

ions substituted into the hydroxyapatite lattice for calcium ions. In addition, the antimicrobial effects of Cu and Zn HAp against pathogen bacterial strains of *Escherichia coli*, *Staphylococcus aureus* and pathogen yeast *Candida albicans* were tested, with the result revealing that CuHAp and ZnHAp both had viable cell reduction ability for all tested strains in liquid media.

2.7.2.3 Fe:

In order to develop a new class of magnetic HAps, **Tampieri et al. [9]** prepared FeHAp nanoparticles (Fe = Fe^{2+} or Fe^{3+}) by a neutralization method to produce a material to assist bone and vascular remodelling during template or scaffold regeneration and to potentially apply it in anticancer therapies, to be used as an alternative source for the materials commonly used for this purpose. One conventionally used magnetic iron oxide was found to be very cytotoxic when it is used over the long term. Phosphoric acid, H_3PO_4, calcium hydroxide $Ca(OH)_2$, $FeCl_3$ $6H_2O$ and $FeCl_2.4H_2O$ were used as raw materials in the synthesis of FeHAps. In general, XRD, ICP and TEM analysis revealed that both Fe^2 and Fe^{3+} ions became incorporated into the HAp lattice and that the new FeHAp demonstrated very low crystallinity and thermal stability. Super paramagnetic effects were observed. Super paramagnetic or soft ferromagnetic nanoparticles, when placed under alternating current (AC) fields, (alternating current is an electric current which reverses the direction in periodic manner) can transform electromagnetic energy into heat. The generated heat can be used to destroy cancer cells or pathogenic microbes. In magnetic hyperthermia, the heating can occur due to several mechanisms such as frictional heating induced by the interaction between the magnetic nanoparticles (MNPs) and the surrounding medium. The authors reported that Fe-doped HA potentially opened new perspectives for biodevices aimed at bone regeneration and for anticancer therapies based on hyperthermia [9].

There is also a report from **Li et al. [79]** who synthesized manganese (II) and iron (III) substituted HAp nanoparticles using a wet chemical method. The results indicated that by increasing the initial metal ion concentration, the quantity of metal ion in the HAp lattice structure increased. In the same study, inductively coupled plasma (ICP) data revealed that Fe^{3+} ions were much more active than Mn^{2+} ions in replacing Ca^{2+} ions during the synthesis process. MnHAp and FeHAp did not, however demonstrate any toxic effects on osteoblast cells. An incorporation of Fe^{3+} ions into the HAp lattice increased the negative surface charge measured on pellets made from this

phase which led to an increase in osteoblast cell adhesion as compared to pure HAp and MnHAp phases.

Erica and Michael [80] studied and compared the sintering behaviour of FeHAp materials and pure HAp. In that study both pure HAp and FeHAp phases were fabricated by using a precipitation method and pressed into pellets after which they were sintered over two different temperature ranges (900-1300°C and 600-1100°C). It was reported that the FeHAp phase was less thermally stable than pure HAp, with decomposition beginning around 1200°C and 700°C, for pure HAp and FeHAp respectively. Also, it was indicated that the mechanical strength of FeHAp is much lower than that of pure HA. Upon immersion of FeHAp in cell culture media, it was observed that the FeHAp phases were still biocompatible materials. The authors reported that the biocompatibility of FeHAp combined with its magnetic characteristics could lead to a variety of biomedical applications such as uses in drug delivery and an agent for cancer hyperthermia.

Trinkunaite-Felsen et al. [81] synthesized FeHAp by using a sol–gel combustion technique. In that experiment *M. balthica* (L.) sea shells were used as a source of calcium. The authors found that the highest iron molar concentration that could be substituted without changing the apatite structure was 4 wt%. FTIR spectra revealed the formation of apatitic phases and SEM analysis indicated that the microstructure of the Fe/CHAp (Fe/carbonated hydroxyapatite) samples differs from that of stoichiometrically pure HAps. In addition, spherical particles < 500 nm in size were observed for Fe/CHAp samples which contained a low concentration of Fe (0.01–0.1%). Increasing Fe content in the CaHAp led to the formation of irregularly shaped particles with a lower particle size distribution (from ∼50 nm to ∼500 nm).

2.7.2.4 Co and Cu:

Cobalt is important in the human body as it constitutes one component of Vitamin B12, which is necessary for red blood cell production, DNA synthesis, and the protective covering of nerves, which is called myelin sheath generation [6]. Co ions have also been substituted into CaHAp.

Kramer et al. [82] synthesized cobalt doped hydroxyapatite by two methods: the first was a simple ion-exchange procedure while the second was achieved by a wet chemical method procedure. The results after substitution using the two various procedures showed, that the samples had an apatitic crystal structure. Cobalt substituted hydroxyapatite showed

paramagnetic properties, as opposed to the diamagnetism of pure HAp samples. Also, CoHAp did not exhibit any different mode of degradation behaviour from that of pure HAp. In addition, it was shown that the amount of cobalt released from the substituted hydroxyapatites over the period of a month was low (1024 µg/g CoHAp via wet chemical method and 1838 µg/g CoHAp via an ion exchange route), which allayed concerns about toxicity. The magnetic properties of cobalt substituted hydroxyapatite mean it can be used in several applications, such as magnetic imaging, drug delivery, and hyperthermia-based cancer treatments.

Ignjatovic et al. [83] analyzed the osteogenetic potential of synthesized HAp and CoHAp with different weight percents of Co^{2+} ions to produce HAp/Co5 and HAp/Co12 (i.e. containing 5 and 12 wt % Co^{2+}). They performed a quantitative study of the microscopic arrangement of newly formed tissue in a bone defect, after 12 and 24 weeks. A white female rat had been used during that investigation. A quantitative analysis of the Ca, Mg and P content in the defect was used as an evaluation of the mineral deposition after new bone reconstruction. They reported that after 24 weeks with using HAp/Co12, the defect was filled with new tissue matrix composed of dense collagen fibres containing centres of mineralization. It was also noted that the mineral deposition rate was higher when the defect was reconstructed from using CoHAp rather than pure HAp. In addition, it was noted that alveolar bone was recuperated and healed, this result had been revealed based on a histological analysis where the osteoporosis-induced defects were fixed and repaired using the CoHAp samples.

Copper is an essential micronutrient in living organisms since it is involved in metabolic processes. Hence copper substituted HAps could be of some use as an antibacterial against *E. coli* for CuHAp (3.3-wt % Cu) has been revealed from several studies. Although the results were considered promising, further studies were recommended to evaluate the toxicity of both Co^{2+} ions and Cu^{2+} ions before drawing conclusions on their suitability in therapeutic applications when incorporated into HAp [72] .

In other studies, **Saranya et al. [84]** prepared Cu-substituted hydroxyapatite by using the sol–gel route. XRD, FTIR and TEM analyses showed that the samples were of nano sized dimensions and homogenous. The XRD data showed that the crystallite size decreased with increasing content of Cu. Data also showed that the average crystallite size of Cu-doped samples was smaller than for

undoped HAp. It was also noted that the intensity of the XRD peaks decreased as the concentration of copper increased in the HAps. The formation of apatitic phases was confirmed by FTIR spectra. CuHAp demonstrated antimicrobial effects against the clinical pathogen *Shigella flexneri.* Thus, prepared metal-doped hydroxyapatite nano powders can be applied as antimicrobial materials for various applications such as in bone defects and implant coating in orthopedic surgery.

Li et al. [85] synthesized stoichiometric hydroxyapatite (HAp) and copper-substituted hydroxyapatite (CuHAp). The results of their XRD analyses indicated that Cu^{2+} ions had become incorporated into the lattice of HAp. The results of bacteriostatic annulus, bacteriostasis rate, minimum inhibitory concentration (MIC) and minimum bactericidal concentration (MBC) tests showed that Cu-HAp can be considered as an antibacterial agent against *E. coli and S. aureus*. In addition, the authors reported that there were two factors that can be considered as effective factors for playing a vital role in the antibacterial ability of these substituted apatites. The first is the electrostatic attraction which leads to bacteria adhering to the surface of Cu-HAp, while the other is attributed to copper ions that are slowly leached into the body medium which can inhibit and kill bacteria.

Li et al. [86] synthesized and studied the antimicrobial efficacy of CuHAp and TiHAp by wet chemical methods using various molar ratios (M_{added}/Ca_{added} = 0.01, 0.05, 0.10 and 0.15) . The following substances were used as starting materials $Ca(OH)_2$, H_3PO_4, $Cu(CH_3COO)_2{\cdot}H_2O$ and $TiBr_4$. In that study the authors indicated the following (i) the FTIR spectra showed the appearance of CO_3^{2-} ions (B-type carbonated HAp) which could be attributed to incorporation of dissolved CO_2 from the atmosphere, (ii) It was also noted that CuHAp is antibacterial but also cytotoxic even at low Cu ion concentrations. therefore, it is not suitable for using these nanoparticles as a coating for implants, (iii) TiHAp showed bactericidal properties at a molar ratio of M_{Ti}/M_{Ca} = 0.10, with only low toxicity being exhibited to osteoblasts.

2.7.2.5 Na substituted HAps:

The percentage of sodium ion substituted into HAp varies from 0.5-1 wt% in biological apatites [6]. Bone mineralization, bone resorption and cell adhesion are processes in which sodium ion can have important effects.

Sopyan et al. [87] synthesized and investigated the properties of Na-doped HAp by using a sol-gel method. They prepared different amounts of "Na" for substituting (i.e. 1, 5, 10 and 15 mol%) into HAp and reported that the addition of 5% Na led to a porous body of about 27% porosity and improved the compressive strength of HAp 17-fold compared with undoped HAp The synthesized scaffold had suitable pore interconnectivity associated with pore sizes ranging from 100 to 300 µm which can be considered as suitable for porous bone substitutes.

Cho et al. [88] investigated the effect of sodium substituted hydroxyapatite on osteoconductivity of HAp. NaHAp was prepared by using calcium hydroxide, phosphoric acid and sodium nitrate as starting materials followed by sintering. Based on ab initio computational chemistry methods the calculated total system energy of NaHAp phases was much higher than that of undoped hydroxyapatite, which indicated that the NaHAp was energetically less stable than pure HAp. NaHAp compared to pure hydroxyapatite, showed a higher solubility in simulated body fluid (SBF) and tris-buffered deionized water. NaHAp was also able to form hydroxy-carbonate apatite in SBF and showed higher osteoconductivity 4 weeks after implantation in the calvarial defects of New Zealand white rabbits compared to pure HAp. They reported that NaHAp can be considered as a non-cytotoxic material. These results showed that NaHAp can be considered as a bone grafting material because of its osteoconductivity.

2.7.2.6 Sr

Strontium has been referred to as a "bone seeking" element (can be introduced into HAp samples to replace the calcium in calcium sites). Also, Sr^{2+} ions play a fundamental role in bone mineralization processes, that has specific application as a treatment for osteoporosis, a disease characterized by a decrease in the density of bone. When strontium is used to prevent osteoporosis, it is supplied in the form of strontium ranelate because it can reduce bone resorption by controlling and increasing bone forming cells (osteblasts) whereas osteoclasts [13] are decreased. Strontium ranelate (SR) may play an important role by increasing bone mass for

patients who suffer from osteoporosis in order to reduce fracture risk [89]. The effect of remediation by SR (known commercially as Protelos) on human bone tissue and its quality of treatment were studied [90].

Landi et al. [91] prepared SrHAp by a neutralization method with the revelation that these materials have good mechanical properties to be considered for several applications such as a bone substitute and drug delivery agent. The authors reported that each substitution or co-substitution can cause specific changes, lattice effects and distortions in the HAp structure which are associated with the general properties of the material such as stoichiometry, crystallinity, etc. For example incorporation of Sr ion into the HAp lattice led to an increase in the c/a ratio (0.7317) compared to pure HAp (0.7309). In addition, the powders could be converted into resorbable materials. This observation had been revealed after performing solubility tests for SrHAp (400–600 nm in size) using a synthetic body fluid solution where Sr ions were released after 24 h, with a decrease in release rate followed by a plateauing of concentration. The higher solubility of the SrHAp reflects the higher release kinetics of the Ca ions that go into the solution together with Sr ions. It was also noted that the compressive strength of the prepared porous body was 4.52 ± 1.40 MPa with 45 vol.% of porosity.

Other work by **Xue et al. [92]** investigated the bioactivity of Sr-HAp ceramics and their effect on cellular attachment, proliferation, and differentiation of cells. Sr-HAp nanoparticles (containing 10 mol% Sr) were synthesized and the bioactivity evaluated by immersion in simulated body fluid (SBF). The results revealed that Sr-HAp has a greater ability than pure HAp to stimulate apatite precipitation on its surface. The effects on cell behaviour of SrHAp were also examined by culturing osteoprecursor cells (OPC1) on the material surfaces. Cell shape and cell-material interactions were analyzed by scanning electron microscopy (SEM) and an MTT assay was used to determine cell proliferation on samples. When compared with HAp, Sr-HAp promoted better OPC1cell attachment and proliferation, and showed no deleterious effects on extracellular matrix formation and mineralization. Confocal scanning microscopy was used to assess the expression of specific osteoblast proteins: alkaline phosphatase (ALP) and osteopontin (OPN). The results obtained indicate that the presence of Sr ion stimulates OPC1 cell differentiation and enhances ALP and OPN expression.

Cox et al. [93] synthesized pure and substituted hydroxyapatite nanoparticles with 2 mol% Sr, 10 mol% Mg, and 2 mol% Zn to make HAp, SrHAp, MgHAp and ZnHAp by using a precipitation method under the following conditions: pH 11 and 20°C. $(NH_4)_2HPO_4$ and $Ca(NO_3)_2$ were used as starting materials and suitable amounts of $Sr(NO_3)_2$, $Mg(NO_3)_2$, and $Zn(NO_3)_2 \cdot 6H_2O$ were adjusted to reflect the substitution levels (i.e. to make 2 mol% Sr, 10 mol% Mg and 2 mol% Zn). The results indicated that the ions were incorporated into the lattice structure of apatite. FTIR indicated that HAp and substituted HAp contained CO_3^{2-} ions due to the absorption of CO_2 during the synthesis process, whereas SEM studies indicated a bulk agglomeration of particles which led to particle sizes ranging from macro size (1.6-4.9 μm) to larger sizes (20-30 μm). The authors explained the observations in terms of the dominating surface properties associated with nanosized crystallites, which cause them to clump together. An indication of the bioactivity of samples was achieved by immersing samples in SBF for up to 28 days. Furthermore, a live/dead assay indicated the viability of seeded MC3T3 osteoblast precursor cells on HAp and substituted HAp substrates for up to 7 days of culture.

2.7.2.7 Mg:

Magnesium is considered a very important trace element to occur in biological apatite, where it exists in levels of up to 0.72% in bone, 0.44% in enamel, and 1.23% in dentin. Magnesium ion affects the process of bone metabolism by eliciting proliferation of osteoblasts in the first stages of osteogenesis [6].

Liangzhi et al. [94] used a hydrothermal method to synthesize Mg-HAp whiskers(0 – 6.14 mol% Mg), with lengths up to 50 μm through using acetamide as starting material. The Mg substitution level can be a achieved by changing the initial molar ratio of Mg/(Mg + Ca) in the raw materials. The results indicated that Mg^{2+} ions substituted for Ca^{2+} ions, with the lattice parameters in the unit cell decreasing through increases in the amount of the Mg-substitution. The cell culture results revealed that Mg-HAp whiskers adjusted the proliferation of MG-63 (human osteoblast cells) at certain concentrations of Mg^{2+} ions. This was noted especially for the Mg5-HAp (($Mg^{2+}/(Ca^{2+} + Mg^{2+})$) mole ratios of 0.05) component which can be considered as an ideal one for cell activity .

MgHAp samples were also synthesized by **Andres et al.** [95] in which the authors used a wet-chemical precipitation route, followed by a hydrothermal treatment to incorporate Mg^{2+} ions into the crystal lattice of HAp. They reported that Mg^{2+} ions occupied Ca(1) sites in limited amounts and stimulated the formation of calcium deficient HAp (cd-HAp). The amounts of Mg^{2+} incorporated into HAp affect several properties of MgHAp such as crystallinity degree, cell parameters, morphology, solubility, and degradation properties, depending on the degree of substitution. The results revealed that these prepared samples have a good biocomptability through displaying several properties which led to an optimal cellular viability, cell spreading, and proliferation. In addition, an enhancement of osteoblast adhesion was observed after incorporation of Mg^{2+} into the HAp lattice.

Ren et al. [96] substituted Mg in HAp using a wet-chemical precipitation method at 90°C. It was found that a limited amount of Mg (Mg/(Mg + Ca)) between 5 and 7 mol% could be successfully substituted for Ca in the HA lattice, and that as a result, HAp crystallites in the Mg-substituted solid became smaller, irregular, and formed greater agglomerates of material with Mg substitution. It was also noted that crystallinity and thermal stability decreased in HAp as a result of Mg substitution. As mentioned in other works, it was also noted that the Ca(1) sites in HAp were the preferred sites for Mg substitution.

In other work [97] **Mehrjoo et al.** synthesized magnesium substituted hydroxyapatite by using a wet chemical precipitation route, The authors investigated the effect of substituting different amounts of Mg^{2+} ions on biological properties of HAp samples by using various kinds of tests such as cellular proliferation, alkaline phosphatase (ALP) activity and gene expression . The cellular behaviour of MG-63 cells was improved by incorporation of Mg^{2+} into HA samples. The results revealed that the high amounts of Mg^{2+} in HAp cause improvements in cellular behaviour compared to that of pure HAp. It was reported that samples with high levels of Mg^{2+} ions in the HAp lattice showed the highest proliferation rate, ALP activity and gene expression. Biological tests revealed that 1.2% substituted (HAp-1.2Mg) and 1.6% substituted (HAp-1.6Mg) particles showed the best performance compared to pure HAp and 0.6% substituted (HAp-0.6Mg) particles. The result confirms the positive role of incorporation of Mg^{2+} ions into the HAp crystal lattice in terms of bone tissue engineering applications.

2.7.2.8 Mn:

It has been reported that addition of Mn^{2+} ion to hydroxyapatite improves the density of the produced ceramic body without any phase transformation being obtained even after sintering the HAp material or calcining it at 1300°C [79]. Further, Mn^{2+} ions are known to provide increased potential for ligand binding affinities to integrins, the receptor proteins that cells employ to bond to and respond to extracellular matrix. This can lead to improved cell adhesion and osteoblast bonding [98].

Zilm et al. [99] also investigated the thermal stability and mechanical properties of (MnHAp). Pure HAp and MnHAp pellets were sintered over two different temperature ranges, the first one being from 900 - 1300°C and the other from 700 to 1300 °C. The sintered pellets were characterized by various methods such as mechanical testing, X-ray diffraction, and field emission electron microscopy. The results revealed that MnHAp was less stable (i.e. it decomposes around 800 °C) than HAp which decomposed around 1200 °C. In addition, the flexural strength of MnHAp was weaker than stoichiometric HAp with this being attributable to the lower decomposition temperature of MnHAp compared to 1100 °C for HAp. The low thermal stability of MnHAp indicates that its expected dissolution rate will be higher compared to pure HAp.

2.7.2.9 Lanthanide ion substituted HAps (La, Eu, Gd, and Tb):

Jime´nez-Flores et al. [43]synthesized CDHA and Tb-doped CDHA (10 and 12 wt% Tb) by using a sol–gel procedure for luminescent purposes. The results confirmed the incorporation of terbium ions into HAp lattice, with good crystallinity, and clear effects on the cell parameters. The energy band gap was measured for all samples by using UV–Vis spectroscopy with the finding that the value of the band gap energy decreases as the amount of terbium ions substituted into HAp increases. They also reported that the maximum luminescent emission was obtained for the sample synthesized with 10 wt% of terbium. The samples that contain 10 wt% of terbium also have the best properties to be considered for biolabelling applications.

Chen et al. [100] prepared multifunctional Eu^{3+}/Gd^{3+} dual-doped HAp by using a microwave-assisted hydrothermal method. They reported (i) small levels of toxicity to cells, high drug adsorption capacity and sustained drug release by using ibuprofen as a model drug. (The acceptability of using Eu^{3+}/Gd^{3+}substituted HAp with photoluminescent properties

for in vivo imaging, was revealed by the noninvasive visualization using nude mice with a subcutaneous injection of the material. The Eu^{3+}/Gd^{3+} substituted HAp can be considered as a suitable material for biomedical applications such as multifunctional drug delivery systems with the benefit of imaging guidance.

Guo et al. [101] investigated the physicochemical properties and biocompatibilities of La-containing apatites (La-HAp). It was reported that the La^{3+} ion can be incorporated into the crystal lattice of HAp resulting in the formation of La-incorporated apatite by using a solid-phase synthesis procedure.

The La-incorporated apatites have a number of beneficial properties, such as higher thermal stability, higher flexural strength, lower dissolution rate, preferable osteoblast morphology and comparable cytotoxicity to La-free apatite. The sintered LaHAp was found to have a maximal flexural strength of 66.69 MPa at 5 wt% La content (95% confidence interval), which is equal to an increase of 320 percent over the undoped apatite. Based on these findings, the authors suggested that the La-incorporated apatite has potential application in developing a new type of bioactive coating material for metal implants. [101].

Li et al. [102] synthesized nanocrystalline hydroxyapatite (HAp), $Ca_{10}(PO_4)_6(OH)_2$, substituted with gadolinium (Gd^{3+}) and neodymium (Nd^{3+}) in different mole ratios (M = metal, $M_{added}/Ca_{added}=X_M$,0.01, 0.05, 0.1, and 0.2). These were synthesized via an anion-exchange method by using $Ca(OH)_2$, H_3PO_4, $GdCl_3.6H_2O$ and $NdCl_3.6H_2O$ as starting materials with all samples having the single phase of MHAp except for X_M= 0.2, which displayed a second phase of $M(OH)_3$. The GdHAp and NdHAp nanoparticles were elongated spheroids of approximately 70 nm, and it was noted also that the shape and size had not changed by increasing X_M. The M(III)-HAp had a higher electrical conductivity than of pure HAp. Also a cytotoxicity test indicated that all M(III)-HAp samples were non-cytotoxic except for the material made with X_{Gd} = 0.2.

2.7.2.10 Ti Substituted HAps:

Ergun Celaletdin [103] studied the interaction of titanium-containing (Ti) ions with HAp by performing two different kinds of experiments. In one, titanium substituted HAp was made using a precipitation method, where tetraethyl orthotitanate ($C_8H_2OO_4Ti$) was used as the source of titanium to prepare TiHAp. The precipitates were dried and sintered at different temperatures

(500 °C, 700 °C, 900 °C, 1100 °C, and 1300 °C) for 2 h. In the second experiment, powder mixtures of HA/$CaTiO_3$ and tri-calcium phosphate/$CaTiO_3$ were sintered in air at different temperatures (900 °C, 1100 °C, and 1300 °C) for 2 h. The authors found that XRD demonstrated that lattice parameters were contracted due to Ti incorporation into the apatite structure. The grain sizes of Ti substituted HAp particles were smaller than for pure HAp. Increasing the amount of the Ti- in Ti-substituted HAp led to the decomposition of HAp which converted to α-tricalcium phosphate and $CaTiO_3$. This process helped to improve the porosity of TiHAp compared to pure HAp.

2.7.2.11 Bi HAps:

In the past bismuth salts have been used to treat gastrointestinal disorders, syphilis and hypertension [104]. In the present day, bismuth is used as an antimicrobial agent and an anticancer agent. Due to its radio-opacity effect, bismuth compounds, are also added to bone and dental implants, catheters and surgical instruments to enhance and improve detection processes by X-rays and computed tomography [105].

Ciobanu et al. [106] synthesized new bismuth-substituted hydroxyapatite [$Ca_{10x}Bi_x(PO_4)_6(OH)_2$ where x = 0–2.5] nanoparticles by a co-precipitation method via the use of calcium hydroxide, orthophosphoric acid, and bismuth nitrate pentahydrate $Bi(NO_3)_3.5H_2O$ as starting materials. The results indicated that bismuth ions had been successfully incorporated into the HAp lattice. The prepared samples were a single phase with a hexagonal structure with crystal sizes being found to be smaller than 60 nm. In this compound the (Bi + Ca)/P atomic ratio equalled 1.67. The BiHAp samples were reported as being mesoporous in nature with a pore size of 2 nm and with a specific surface area in the range of 12–25 m^2 /g. The BiHAp samples were also found to be more effective against gram-negative *Escherichia coli* bacteria than gram-positive *Staphylococcus aureus* bacteria.

2.7.2.12 Ba substituted HAps:

Kikuchi et al. [107]synthesized Ba-HAp by a wet method with $Ba(OH)_2.8H_2O$ and $(NH_4)_2HPO_4$ as starting materials. The Ba-HAp was sintered at 800°C for 12h and was found to have a Young's modulus value of 27 GPa. Cytotoxicity tests using L-cells showed no cytotoxicity, with the cells reported to be in close contact with the surfaces of the sintered Ba-HAp suggesting that the Ba-

HAp exhibited non-cytotoxicity and could be applied as a potential, bioactive X-ray opaque material.

2.7.2.13 Nb:

Niobium is a rare, soft, malleable, ductile, gray-white metal. It has a body-centered cubic crystalline structure; Niobium alloys may be used in surgical implants because they do not react with human tissue. This metal has also been reportedly substituted into HAp.

Capanema et al. [31] synthesized niobium substituted hydroxyapatite by a precipitation method through using $Ca(OH)_2$, $Ca(H_2PO_4).2H_2O$ and $NbCl_5$ as starting materials, followed by thermal treatment. The results indicated that the precipitate dried at 110 °C contained a mixture of amorphous calcium phosphate and HA, with polydisperse particles that varied from micro to nano dimensions. After thermal treatment at 900°C, the solid phases converted into crystalline HA phases, with evidence shown of particle sintering and reduction of surface area. Addition of 10 mol% of a niobium salt precursor led to incorporation of the Nb (V) anions into the HAp crystal structure, in addition to clear changes in the original lattice parameters. In aqueous solutions Nb(V) ions are usually present as negatively charged niobates [32]. The increase in lattice parameters seen in NbHAp materials can be explained in terms of the substitution of PO_4^{3-} anions by niobate ions which have a higher ionic radii compared to PO_4^{3-}. As a result of the incorporation of niobate ions, a reduction in the average particle size of the HA was observed. Also, the cytocompatibility response of the Nb-HAp biomaterials was evaluated by using human osteoblast cell culture such as MTT and resazurin assays, which confirmed no cytotoxicity of the NbHAp was observed.

2.7.3 Some Examples of Y Substitution in $M_{10}(XO_4)_6(Y)_2$:

The bioactivity, osteoconductivity and therapeutic effects of HAp depend on the solubility in the biological environment. As indicated in the literature, the mineral phase in vertebrate calcified hard tissues is not pure stoichiometric hydroxyapatite but is partially substituted by some foreign ions. Among them, of great importance is fluorine substitution. Recent studies showed that the incorporation of fluorine into hydroxyapatite improved the mechanical properties of apatite ceramics and induced better biological response. On the other hand, and due to its highly

enhanced bioactivity and osteoconductivity compared with pure HAp ,Cl doped HAp has encouraging potential for use as a bone grafting material, which has been detailed below.

2.7.3.1 Fluoride (F^-):

Substitution within the HAp lattice can also occur via replacement of the OH^- group. Fluoride is an essential element in the diet and plays a vital role in bone and dental health [6]. Fluoride has been used in the remediation of osteoporosis though excessive fluoride intake can result in skeletal fluorosis (crippling bone disease) [108] [109] which is associated with osteosclerosis, calcification of tendons, ligaments and bone deformities.

Fluorapatite (FAp) and "fluoro hydroxyapatite" (half F substituted, half OH substituted hydroxyapatite) has been successfully synthesized in the past. Substitution of fluoride ions leads to an increase in the crystallinity and crystal size of HAp and a decrease in its solubility [6] as mentioned earlier in this literature review.

Karlis and Luis [110] found that incorporation of fluoride into biomaterials plays an important role in the physicochemical properties of implants. The most important aspects include solubility and mechanical properties. However, Gross studied the effect of fluoride substitution for hydroxyl groups on the mechanical properties and reported that the elastic modulus increases linearly with fluoride content. Improvement of fracture toughness was also observed due to fluoride incorporation.

Chander and Fuerstenau [111] have studied the mechanism of fluoride uptake from solution by HAp. It was reported that at low concentrations, fluoride ions were substituted by hydroxyl ions in the HAp lattice, while at higher concentrations, HAp dissolves and the solution becomes supersaturated with respect to FAp.

Tredwin et al. [112] prepared HAp, F-substituted HAp (F-HAp), and F-apatite by using the sol–gel technique. It was reported that an improvement in the coating properties [113] of the material was observed by increasing the amount of fluoride substitution in the apatite lattice with F-HAp and FAp potentially offering a superior alternative to coating titanium implants with HAp using plasma spraying. This is because the bond strength for $Ca_{10}(PO_4)_6F_2$ was 40 MPa, while the bond

strength for the HAp-plasma-sprayed coatings was (≈ 10–40 MPa). F-HAp, and F-apatite materials can also be considered as plausible bone-grafting materials [112].

Kim et al. [114] prepared Hydroxyapatite (HAp) and fluor-hydroxyapatite (FHAp) powders by using sol– gel route. calcium nitrate tetrahydrate ($Ca(NO_3)_2.4H_2O$) and triethyl phosphite (TEP,$(C_2H_5O)_3P$) were used to prepare HAp, while ammonium fluoride (NH_4F) was used as a precursor of F^- ions. However, two kinds of TEP solutions containing different amounts of fluorine ion were also obtained by dissolving the desired amount of ammonium fluoride (NH_4F), where P/F molar ratios were supposed to be 6 and 3 and labelled as FHA1 and FHA2, respectively. The aging process was performed at 40°C for 72 hours, after which the formed gel was dried at 80°C into the oven, followed by heat-treatment at 400°–1000°C for 1 hour. The following observations were recorded:

(i) As a result of heat treatment at 500°C, TEM analyses displayed that all HAp and FHAp powders (FHAp1 and FHAp 2) contained nanosized particles (30 –50 nm).

(ii) apatitic structure was confirmed in all heat treated samples through detecting the characteristic bands of the apatitic phases by FTIR spectra. While, the spectra showed a slight reduction in the intensity of the librational mode of OH^- at 640 cm^{-1} in the case of the FHAp1 compound, the stretching band of OH^- group at 640 cm^{-1} was not observed at all in the case of the FHAp2 compound, suggesting that the OH^- group had been fully replaced by F^-. Another observation seen from the FTIR analysis was that carbonated apatite had been produced for as-dried and heat treated powders subjected to temperatures of 400° and 500°C. Hence FTIR spectra showed the presence of the typical peaks of CO_3^{2-} (at 870 and 1460 cm^{-1}). The intensity of the observed carbonate bands in these compounds followed the order HAp > FHAp1 > FHAp2

(iii) XRD analysis revealed the tricalcium phosphate (TCP) phase that normally formed in the HAp samples above 800 ˚C was decreased in the case of FHAp powders, suggesting substitution of fluoride ion had made the apatite structure more stable to decomposition and hence more stoichiometric.

(IV) The XRD analysis also revealed that Increasing the concentration of F^- improved crystallinity and increased the crystallite size. Also, a detectable difference in the values of lattice parameters was observed due to substitution of F^- ions, that a gradual decrease in the lattice constant a was recorded, while a slight change in the value of c was observed with increasing fluoride addition.

2.7.3.2 Cl^-:

Pure chloroapatite cannot be a good biomaterial because total replacement of the hydroxyl groups by chloride ions will enhance the acidity of the local environment, leading to rapid solubilization of alkaline salts [5]. Chlorine is a vital trace element in the mineral phase of both bone and teeth and is present to a level of ~0.13 wt% in natural bone [6]. Partially substituted Cl-HAp, however, enhances bioactivity due to its high solubility and possesses greater osteoconductivity over stoichiometric HAp [115].

Cho et al. [116] studied the effect of chloride-substitution on bioactivity and osteoconductivity of hydroxyapatite. Chloride-substituted hydroxyapatites (ClAp) with different chloride concentrations, ranging from low to high were fabricated using $Ca(OH)_2$, H_3PO_4 and NH_4Cl as a source of chloride ion, with subsequent sintering of the materials produced. As the chloride substitution increased, an improvement in bioactivity was achieved, whereas, the OHAp had not showed any bioactivity at all during the testing period when immersed in SBF. The solubility tests in deionized water also showed that as the chloride substitution increases, the solid becomes more soluble, which influences bioactivity through increasing the degree of supersaturation of apatite in SBF. ClAp showed higher osteoconductivity within 4 weeks of implantation in calvarial defects created in New Zealand white rabbits than the equivalent stoichiometric HAp implants. Ab initio methods reveal that the calculated total energy of the chloride-substituting system has a higher value, which indicated that the ClAp was energetically less stable compared to stoichiometric HAp. This result indicated the higher solubility of ClAp compared to HAp in both SBF and in deionized water will improve bioactivity and osteoconductivity. Therefore, it can be concluded that ClAp has promising properties for use as a bone grafting material.

2.7.4 Co-substitutions of hydroxyapatite (substitutions with two different or more several ions):

Hydroxyapatite $Ca_{10}(PO_4)_6(OH)_2$ as mentioned previously, has been widely used in biomedical areas. Its brittleness and poor degradation rate in vivo, have encouraged researchers to perform a lot of studies in order to improve on its drawbacks. On the other hand, as is well known, biological apatite contains trace ions such as Na^+, Mg^{2+}, etc, which play an important role in biological process, therefore substitution of hydroxyapatite partially by these elements would be considered as a goal, to improve its characteristics through imitation of the chemical composition of bone mineral. However, the flexibility in the apatite structure leads to the possibility of developing a large number of hydroxyapatite materials with different chemical structures through substituting and co-substituting by several elements for specific applications [117] , below are listed some examples of co-substituted hydroxyapatite products.

2.7.4.1 Cationic co-substitutions (substitutions with two or more different cations):

Cationic co substitution represents an example of the previous work involving substituted HAps, that has been done to improve on the biological performance of HAp. Good results have been obtained with the substitution of calcium by different metallic ions, particularly those involved on biological processes and human health, such as Mg^{2+} and Zn^2. Some examples that illustrate these kinds of substitution are mentioned below.

Kulanthaivel et al.[[118] revealed an improvement in the osteogenic and angiogenic properties of synthetic hydroxyapatite by doping of magnesium (Mg^{2+}) and cobalt (Co^{2+}) ions using a precipitation technique. (i) ICP-OES analysis indicated that the extent of cobalt substitution was higher than for magnesium, (ii) slight distortions in the crystal lattice, increased the apatite–water interaction and decreased the thermal stability of the substituted hydroxyapatite materials, and (iii) a preliminary evaluation showed that the doped samples had higher protein adsorption capacity compared to pure HAp. The analysis that related to the bone cell (MG-63) compatibility and differentiation indicated that the doped hydroxyapatite enhanced both the cell proliferation and differentiation. Therefore, the improved osteogenic and angiogenic properties of the dual doping of magnesium and cobalt ions into HAp led to a better biomaterial for use in bone tissue engineering.

Geng et al. [117] synthesized a series of Sr/Mg-co-substituted HAps by a hydrothermal route. Four different samples were prepared (5Mg25Sr, 10Mg20Sr, 20Mg10Sr and 25Mg5Sr). Magnesium ion was considered to be a destabilizing ion during the co-substitution process, since a decrease in crystallinity, thermal stability and lattice parameters of HAp was observed by introduction of Mg ions into the lattice. A good and acceptable biocompatibility for the fabricated samples after 14 days of culture had been achieved through in vitro studies with MG63 cells cultured in CLL, which was derived from synthesized samples incubated in the culture medium, especially 10Mg20Sr, which displayed better cell attachment, proliferation, and differentiation than pure HAp.

Lowry et al. [119] prepared nanoparticles of HAp, i.e. Sr10% nHAp, Zn10% nHAp and Sr5%/Zn5% nHAp using a precipitation method. The results revealed (i) all prepared materials were nanosized, with ZnHAp being found to have the smallest crystals (27 nm long and 8 nm wide), (ii) Sr^{2+} and Zn^{2+} were incorporated into the lattice in both cases (substitution and co- substitution), and (iii) presence of carbonate within all prepared samples was confirmed by FTIR. They also suggested further research was needed to (i) determine optimal strontium and zinc concentrations, within the co-substituted HA and (ii)investigate osteoblast cytotoxicity and viability on each of the fabricated substituted and co-substituted HA.

Using a microwave irradiation techniques, **Gopi et al. [120]** successfully synthesized Ca/Sr/Ce–HAp as a bioactive and antibacterial material. $Ce(NO_3)_3.6H_2O$ and $Sr(NO_3)_2.6H_2O$ were used as a precursor for Ce and Sr. They reported that (i) the formation of HAp, Ca/Sr–HAp and Ca/Sr/Ce–HAp (where $[Ce^{3+}]$= 0.05, 0.075 and 0.1 M) was revealed by using several techniques such as (FTIR), (XRD) and (SEM), (ii) XRD and HRTEM results which indicated that the crystallinity and size of the HAp nanoparticles were decreased by incorporation of the Sr^{2+} and Ce^{3+} ions into the HA lattice, (iii) the incorporation of Ce^{3+} into Ca/Sr–HAp with various concentrations (0.05, 0.075 and 0.1 M) led to enhanced antibacterial activity of the co-substituted nanoparticles (Ca/Sr/Ce–HAp), and (iv) the strong antibacterial activity against *E. coli* and *S. aureus* was associated with Ca/Sr/Ce-HAp (0.1 M Ce^{3+}). Moreover, the presence of Sr^{2+} and Ce^{3+} ions in the Ca/Sr/Ce–HAp nanoparticles enhanced the thermal stability of the materials up to 1200 °C.

Huang et al. [121] developed SrCuHAp coatings on CP-Ti (commercially pure titanium). The results of the following techniques FTIR, XRD, SEM, EDX, and ICP confirmed the formation of SrCuHAp coatings on CP-Ti. The authors reported that (i) the synthesized coatings can be considered as totally crack-free and compact, which caused a decrease in the corrosion current densities of CP-Ti in physiological media, (ii) the antibacterial behaviour is not ideal because the antimicrobial ratio of the SrCuHAp coating was below 91%, (iii) the biological tests confirmed that the co-substitution of Sr in CuHAp not only efficiently offsets the potential cytotoxicity of Cu, but also improves the osteogenic differentiation, and (iv)adjusting the Sr and Cu content in SrCuHAp coatings produces an improvement in the antibacterial activity and osseointegration ability.

Tamm et al. [122] investigated several systems such as singly substituted hydroxy- and fluorapatites and doubly substituted hydroxyapatites by using density- functional theory (DFT). The substitutions were Cd^{2+} and Zn^{2+} ions replacing Ca^{2+} in either or both of the structurally inequivalent positions. The authors reported that (i) a preference to occupy the Ca(1) and Ca(2) sites in fluorapatites and hydroxyapatites, respectively was observed in singly substituted cases, whereas the doubly substituted hydroxyapatites indicated a preference to occupy the Ca(2) site for both substitutions, (ii) a displacement of the hydroxide ion chain from the hexagonal axis of the ion channel prefers some situations in which both substitutions are occupied in the same side of the channel, this observation allowed the authors to explain the orientation and location of the incorporated ions around the axis, (iii) the preference of single and double substitutions to take place around the ion channel in HAp led to the supposition that migration might occur via these channels, and (iv) the authors explained the reason for choosing the Ca(1) site as the preferred one in fluorapatites because of the poorer sorption characteristics of fluorapatites.

2.7.4.2 Anionic co-substitution (substitutions with two anions in the HAp lattice):

Co-substituted HAp has gained much attention during the recent years, since these forms of substitution have much more potential to combine several desirable properties than a single substituted HAp. Many ionic substitutions have been investigated, but selecting ions for co-substitution must be performed carefully, as many variables have to be taken into consideration such as substitution sites and the biological impacts. Below are some examples that illustrate these kinds of substitutions:

Kannan et al. [123] synthesized fluoride and chloride co-substituted hydroxyapatites by using a precipitation procedure. $Ca(NO_3)_2.4H_2O$, $(NH_4)_2HPO_4$, NH_4F, and NH_4Cl, were used as the starting materials. They reported that (i) the apatite structure was not destroyed as a result of the substitutions, this observation was confirmed by the calculated unit cell parameters for the F^- and Cl^- co-substituted apatites, whereas a steady increase in the c-axis parameter was observed due to increases in the doping concentration level of the anions. XRD, FTIR and elemental analysis confirmed (i) the formation of single apatitic phases; (ii) the successful incorporation of the substituted anions, and (iii) the calculated crystallite sizes for all the fabricated apatite samples are lower than 50 nm, in good agreement with the typical crystallite size of bone mineral phases.

Ibrahim et al. [124] prepared a synthetic multi-substituted hydroxyapatite (Si-HAp and Si-CHAp) by a wet chemical method using $Ca(NO_3)_2.4H_2O$, $(NH_4)_2HPO_4$, $Si(OCH_2CH_3)_4$ TEOS, and $NaHCO_3$ as a starting materials. The chemical analysis indicated that substituted atoms are incorporated into the HAp powders. As a result of the incorporated ions into crystal lattice of Hap, a change in the unit cell parameters were obtained. The results revealed that the HAp with the substituted silicon and carbonate ions, had the highest solubility with a greater rate of ion release, compared with carbonate-free powder,(the substituting amounts of silicon were 0.523 wt% and 4.0 wt% for Si-CHAp and Si-HAp respectively).

Zhu et al. [108] synthesized co-substituted hydroxyapatite, namely (CO_3FHAp) by a precipitation route, using $(NH_4)_2HPO_4$, NaF, $NaHCO_3$ and $Ca(NO_3)_2{\cdot}4H_2O$ as starting materials. The authors wished to evaluate the influence of incorporating CO_3^{2-} and F^- ions on the substitution type and the content. They concluded the following: (i) a non linear increase in the fluoride and carbonate contents of CFHAp with the dopant concentrations was observed, (ii) the carbonate substitution compared to fluoride has much more influence in terms of morphology, (iii) the ion radii of F^- and OH^- are so close to each other, therefore F^- will occupy the OH^- sites of HAp crystals which forces CO_3^{2-} to locate to type B substitution sites (replacing phosphate) instead of on the type A sites.

Landi et al. [125] investigated the effect of silicate/carbonate co-substitutions in the HAp lattice on the properties of the as-synthesized samples and when using with human osteoblasts. The authors reported that osteoblastic behaviour is associated with the ion release from the $SiCO_3$HA

apatite, which depends on the physico-chemical surface properties of the material, (ii) SiCHA-1 exhibited a toxic effect (0.88 wt % of Si), whereas CHA and SiCHA-2 (0.55 wt % Si) prevented osteoblast proliferation at worst with no toxicity being observed. The higher toxicity of SiCHA-1 could be explained in terms of a higher ion release due to the improved solubility of the Si-substituted powder. The best osteoblast behaviour was recorded for the sample $SiCO_3$HA-2 (0.55 wt % Si) and Si-free CHA.

2.8 Research gaps in the current field of substituted HAps:

It is well known that the chemical, the structural as well as the morphological properties of pure, substituted and co-substituted HAp depend on many variables such as chemical composition and processing temperature. Many studies have been carried out which have investigated the possible approaches to synthesis HAp, substituted and co-substituted HAp materials [53,54,58,126,127], as well as several sources for HAp materials, such as biowaste bovine bone and marine products, in addition to other types of calcium phosphates, that are easily transformed into HAp phases [89]have been used for that goal.

Therefore, many ions had been substituted into HAp structures as discussed in the current literature [16] to enhance several properties of HAp materials such as the biological, the mechanical and the thermal stability, but the ability for preparing novel substituted and co substituted HAps still exists with various anions and cations to be investigated. Also, further studies and investigations to develop an effective synthetic route should be taken place, because only a few of them are satisfactory in terms of economics or performance , due to several reasons such as the cost of the preparation method and the phase impurities which occur in the crystal structure [53]. The necessity to investigate the effect of substitution levels as well as the preparation method on the properties of substituted HAp materials are also required, since such these factors effect on the many characteristics of HAp powders such as the chemical composition, the morphology and the mechanical properties.

However, this study hence aims to achieve the following specific objectives:

1- Develop a new approach (to an extent) to prepare HAp, substituted and co substituted HAp powders by using the hydrolysis method. The novel hydrolysis route was used in a direct manner (just one step) to prepare HAp, substituted and co-substituted HAp samples through using monocalcium phosphate and calcium hydroxide as starting materials. However, the full description of that route will be discussed later (see Chapter 3 for details).

2- Preparation of (cationic) metal ion substituted HAp powders with the following chemical formula: $Ca_{10-x}M_xHAp$ (where M=Zn, Sr and Cu, X=0.5, 1.0 and 1.5) by the novel hydrolysis method using MCP/$Ca(OH)_2$ as starting materials.

3- Prepare specific systems of cationic substituted hydroxyapatite materials, namely 1% RbHAp (1 wt.% Rb^+), 1%EuHAp (1 wt.% Eu^{3+}) and 1,3 and 5% ScHAp (1, 3 and 5 wt.% Sc^{3+}), by using two different approaches (precipitation and hydrolysis methods) followed by sintering process in a 900°C muffle furnace.

4- Synthesis of specific systems of anionic and co substituted HAp samples, namely: 1, 3 and 5% NbHAp, 1% B_4O_7HAp and NaClHAp ($Ca_9Na(PO_4)_6(OH)Cl$) by using two different preparation methods (precipitation and hydrolysis routes) followed by sintering process in a 900°C muffle furnace.

5- Prepare Calcium-Bromapatite(Br_2HAp) and Calcium- Sulfoapatite (SAp) materials by using precipitation, hydrolysis and ion exchange methods, since such these materials had already been prepared, but by using completely different approaches [23,25].

6- Investigate the effect of the preparation method on several properties of the prepared substituted HAp powders such as the chemical composition, the morphology, the thermal stability, the mechanical strength and the crystallographic properties.

7- Study the mechanical properties of specific systems of substituted and co substituted materials, which were prepared by using the novel hydrolysis method through performing the compression test. The Laser Diffraction Particle Size Analyzer was also employed to measure the particle size of these systems in order to study the effect of particle size on the mechanical strength.

Chapter Three

Materials and Methods

This chapter outlines the detailed experimental procedures and protocols that were used in:

- The preparation process of unsubstituted HAp by two methods, namely precipitation and a novel hydrolysis route involving a calcium phosphate precursor which has not been used widely before.

  Two samples of unsubstituted hydroxyapatite (HAp) were prepared by two different synthesis approaches (precipitation and hydrolysis) and then characterized by using different kinds of analysis techniques such as: SEM, FTIR, XRD and ICP-MS analysis. The prepared unsubstituted HAp materials by precipitation and hydrolysis routes were used throughout this study as a means of comparison, in order to investigate the effect of ion substitution and co substitution on various characteristics of hydroxyapatite.
- The preparation process of cationic, anionic and co substituted hydroxyapatites by using different synthesis routes (precipitation, hydrolysis and ion exchange methods).
- The experimental techniques that were used to characterize the prepared substituted and co substituted hydroxyapatites.

The following techniques were used to characterize the prepared materials:

- Fourier transform infrared spectroscopy (FT-IR) was used to identify the functional groups present in the prepared unsubstituted, substituted and co-substituted HAp powders.
- Scanning Electron Microscopy (SEM) was used to analyze the surface morphology of any synthesized powders.
- Powder X-ray diffraction (XRD) was used to ascertain the phase purity, degree of crystallinity, crystallite size, the lattice parameters (which are important to measure when synthesizing these compounds) and the volume of the unit cell of all generated unsubstituted, substituted and co substituted hydroxyapatites made in this study.

- Inductively coupled plasma mass spectrometry (ICP-MS) analysis was used to calculate the concentrations of Ca, P and “M” content (The symbol “M” refers generally to the cations and anions that had already been substituted into the HAp crystal).
- Compression testing was used to evaluate specific systems of prepared samples mechanically, while the Laser Diffraction Particle Size Analyzer was also employed to measure the particle size of these systems in order to investigate the effect of particle size on the values obtained with compression testing. The compression test and particle size measurements were used to study the following systems:
    1. Unsubstituted HAp powders ($Ca_{10}(PO_4)_6(OH)_2$) prepared by the hydrolysis route (Chapter 4 6)
    2. Cationic substituted materials prepared by hydrolysis method: $Ca_{10-x}M_x(PO_4)_6(OH)_2$), where (M= Zn, Sr and Cu)and (X=0.5, 1.0 and 1.5), EuHAp (1 wt.% Eu^{3+}) and ScHAp (1 wt.% Sc^{3+}) powders (Chapters 5 and 6 6)
    3. Anionic and co substituted HAp materials prepared by the hydrolysis method: 1%NbHAp (1 wt.% niobate anions, which (as suggested by Tamai et al. [32]), could enter the phosphate-ion-occupied site replacing it with the $H_4NbO_6^{3-}$ ion , which is an anionic monomer. Hence, the expected chemical formula might be $Ca_{10}(PO_4)_{6-x}(H_4NbO_6^{3-})_x(OH)_2$, where x= 0.055), BHAp (1 wt.% borate anions with the following chemical formula: $Ca_{10}(PO_4)_{6-x}(B_4O_7)(OH)_2$, where x= 0.065) and NaCl co-substituted HAp powders ($Ca_{10-x}Na_x(PO_4)_6(OH)_{2-x}Cl_x$, where x=1.0) (Chapter 7).
    4. Bromide and sulfide anion-substituted HAp materials prepared by hydrolysis methods: Br_2Ap ($Ca_{10}(PO_4)_6Br_2$)and SAp ($Ca_{10}(PO_4)_6S$) (Chapter 7).

Please note that all of the above chemical formulas stated above are theoretical or putative formulae, and the details of these calculations, which show where the values of X have originated from, can be found in Appendix A (see appendix A) through two computed examples involving unsubstituted HAp ($Ca_{10}(PO_4)_6(OH)_2$) and 1% EuHAp ($Ca_{9.93}Eu_{0.07}(PO_4)_6(OH)_2$) .

3.1 Research methodology

Hydroxyapatite, as mentioned previously, can be prepared by several methods using a wide range of starting materials. In this study, cationic, anionic and co substituted hydroxyapatite were synthesized via different routes, namely precipitation, hydrolysis and ion exchange methods. The following provides the experimental details of these synthetic methods:

1- Unsubstituted HAp by two different methods (precipitation and hydrolysis, see Chapter 4)
2- Cationic substituted hydroxyapatite: Different systems of cationic substituted hydroxyapatite materials (MHAp, where M= Zn, Sr and Cu) with different substitution levels have been prepared by a hydrolysis method using MCP as a single novel precursor. The chemical formula of such MHAp powders were ($Ca_{10-x}M_x(PO_4)_6(OH)_2$), where x=0.5, 1.0 and 1.5, see Chapter 5).
3- Cationic substituted hydroxyapatite: Different systems of cationic substituted hydroxyapatites namely RbHAp (1 wt.% Rb^+ with the following chemical formula: $Ca_{10-x}Rb_x(PO_4)_6(OH)_2$, where x=0.13), EuHAp (1 wt.% Eu^{3+} with the following chemical formula: $Ca_{10-x}Eu_x(PO_4)_6(OH)_2$, where x=0.07) and ScHAp (1,3 and 5 wt.% Sc^{3+} with the following chemical formula: $Ca_{10-x}Sc_x(PO_4)_6(OH)_2$, where x=0.25, 0.69 and 1.13) were prepared by using two different synthesis routes (precipitation and hydrolysis, see Chapter 6).
4- Anionic substituted hydroxyapatite: Different systems of anionic substituted hydroxyapatites namely NbHAp (1, 3 and 5 wt.% niobate anions with the following chemical formula: $Ca_{10}(PO_4)_{6-x}(H_4NbO_6)_x(OH)_2$, where x=0.055, 0.160 and 0.270) and BHAp (1 wt.% borate anions with the following chemical formula: $Ca_{10}(PO_4)_{6-x}(B_4O_7)_x(OH)_2$, where x=0.065) were prepared by two methods namely (precipitation and hydrolysis, see Chapter 7).
5- Calcium bromoapatite ($Ca_{10}(PO_4)_6Br_2$ with 14.14 wt.% Br^- ions) were prepared by three different synthesis methods (precipitation, hydrolysis and ion exchange methods), bromo hydroxyapatite ($Ca_{10}(PO_4)_6BrOH$ with 7.48 wt.% Br^- ions) was also prepared by precipitation (see Chapter 7). Calcium sulfoapatite ($Ca_{10}(PO_4)_6S$ with 3.20 wt.% of S^{2-} ions) was prepared by three different synthesis methods (precipitation, hydrolysis and ion exchange routes).

6- Co-substituted hydroxyapatite: NaClHAp with the following chemical formula : ($Ca_{10-x}Na_x(PO_4)_6(OH)_{2-x}Cl_X$, where x=1) has been synthesized by two different preparation methods namely precipitation and hydrolysis methods (see Chapter 7).

5 g of each of unsubstituted HAp, substituted and co substituted HAp powders were prepared by using the following approaches (i.e. the precipitation, hydrolysis and ion exchange methods).

The following standard synthesis procedures for substituted HAps as mentioned above, which were adopted throughout the present study and reported in this thesis, are as follows:

Route (1): Substitution of HAp by the chemical precipitation method during HAp synthesis:

This approach can be considered conventionally as the most popular and widely used technique for the preparation process of unsubstituted HAp, substituted and co-substituted HAp materials [55] . The aqueous solutions of certain concentrations of calcium and phosphate ions as well as the desired ions for substitution were mixed together under magnetic stirring and with control of the pH, to form by the precipitation process substituted HAp and multi substituted HAp materials. After achieving this, filtration and oven drying of the precipitate were also required, but in the final step of the synthesis (if this be required), a calcination (high temperature heating) step was undertaken to produce highly crystalline material[128]. In specific conditions such as when using the hydrothermal route to prepare HAp or substituted HAp, this particular step (calcination) is not required because a high degree of crystallinity would be achieved anyway with this synthesis route.

Many suitable salts are available to be used as a source of precursor ions or doping agents in order to prepare substituted or co-substituted hydroxyapatite materials by the precipitation route. These precursors are dissolved in Ca^{2+} or PO_4^{3-} ion-containing solutions (obtained from either dissolving calcium or phosphate containing salts). Often calcium nitrate and ammonium dihydrogen phosphate are utilized as the calcium and phosphate ion sources in such substitution reactions. They have been used because of the following reasons: 1) they are highly soluble in water at ambient temperatures and 2) nitrate ion will not substitute into the HAp lattice as it is too large an anion to enter the lattice. The pH of the reaction environment in which the formation of HAp takes place, plays a very important role in the synthesis process of

substituted and co-substituted HAps, therefore sodium hydroxide was used to adjust the pH value. The description of and rationale of the typical synthesis procedure followed with the precipitation method of generating HAps are described below in steps (1) to (8) as reported by Riccardo Gallo [2]and discussed in the current literature [7-11,80,91,119,129-133]:

(1) A stoichiometric amount of Ca^{2+} precursor, (calcium nitrate ($Ca(NO_3)_2$) is added under magnetic stirring to a certain volume (100 mL) of deionized water to form a Ca^{2+} ion- containing solution.

(2) A phosphate ion-containing solution is also prepared by dissolving a stoichiometric amount of PO_4^{3-} precursor (sodium phosphate dibasic (Na_2HPO_4) with constant stirring in 100 mL of deionized water.

(3) To bring about precipitation in the solutions described in (1) and (2) above, the pH of each of the solutions, i.e. the [PO_4^{3-}]-containing solution, and the [Ca^{2+}]-containing solution were adjusted to and maintained within the range of pH = 10.00 – 11.00 using a sodium hydroxide, NaOH (1 M) solution. Sodium hydroxide was used to adjust pH value rather than ammonia because sodium hydroxide (NaOH) is a stronger base compared to ammonia.

(4) When the pH of both solutions had been adjusted to the required value as stated in (3), the [PO_4^{3-}] containing solution was added dropwise to the [Ca^{2+}]- containing solution by means of a burette, with stirring and attention paid to maintaining pH within the range 10 – 11 if the purpose of the synthesis procedure is to obtain *anionic substituted* HAp samples.

The reason for the need to maintain pH in this range during the precipitation was to avoid formation of other non apatitic phases such as brushite ($CaHPO_4.2H_2O$) which would otherwise co-deposit with the desired (substituted HAp) product.

(5) At the end of the addition process (as described in (4)), the precipitate solution was left to stir for 2-3 hours at room temperature to let the precipitate age, while ensuring the pH in the solution was kept above 10. This ageing process allows development of the apatitic phase by

phase-transformation of initially formed phases and avoids formation of any non-apatitic by-product phases like tricalcium phosphate which could form initially.

(6) After executing the steps above, the resultant precipitate was subsequently extracted from the solution by filter paper or, where possible, by decanting. The precipitate was generally washed with deionized water several times, followed by ethanol. The ethanol serves to remove residual water and evaporates more quickly than water so leaving a dry sample that will not phase-transform any further. Alternatively, suspending the precipitated mass of solid in water for washing followed by centrifugation and decanting was also done because separating the fine powders from water by filtration was a time-consuming procedure.

(7) The filtered precipitates formed of whichever substituted HAp targeted were then dried in an oven (~100 °C) overnight and then manually ground, if necessary, in an agate mortar and pestle to reduce the particle size followed by further drying in an oven to remove any moisture picked up during the grinding process.

(8) As a final step, the obtained poorly crystalline and substituted HAps were then calcined at 900 ˚C or higher for a certain length of time, in order to obtain a high crystallinity powder. This was then followed by the usual solid state structural characterization methods like X-ray powder diffraction for instance.

Synthesis procedure for preparation of substituted and co substituted HAp by precipitation method:

The more exact *experimental description* (for the current study) of the typical synthesis procedure (described generally above) followed with the precipitation method of generating substituted and co substituted HAps is hence given below in steps (p-1) to (p-9):

(p-1) A stoichiometric amount of Ca^{2+} precursor, (calcium nitrate ($Ca(NO_3)_2$) is added under magnetic stirring to a certain volume (100 mL) of deionized water to form a Ca^{2+} ion- containing solution.

(p-2) In the case of a cation substitution into hydroxyapatite, a stoichiometric amount of the desired metal salt (containing the metal cation M^{n+} to be substituted for Ca^{2+}) is added to the Ca^{2+} containing solution with constant stirring to produce a [Ca^{2+} + M^{n+}] containing solution. A

phosphate-containing solution is also prepared by dissolving a stoichiometric amount of PO_4^{3-} precursor (sodium phosphate dibasic (Na_2HPO_4) with constant stirring in (100 mL) of deionized water.

(p-3) In contrast, for effecting an anionic substitution into hydroxyapatite, a suitable amount of an anion salt [Z^{n-}] is added to a PO_4^{3-} containing solution (prepared as indicated in (p-2) above) with stirring to produce a [PO_4^{3-}+ Z^{n-}] containing solution.

(p-4) To bring about precipitation in the solutions described in (p-2) and (p-3) above, the pH of each of the solutions, i.e. the [PO_4^{3-} + Z^{n-}]-containing solution, and the [Ca^{2+} + M^{n+}]-containing solution was adjusted to and maintained within the range of pH = 10.00 – 11.00 using a sodium hydroxide, NaOH (1 M) solution.

(p-5) When the pH of both solutions had been adjusted to the required value as stated in (p-4), the [PO_4^{3-}+Z^{n-}] containing solution was added dropwise to the [Ca^{2+}]- containing solution by means of a burette, with stirring and attention paid to maintaining pH within the range 10 – 11 if the purpose of the synthesis procedure is to obtain *anionic substituted* HAp samples.

For preparing *cationic substituted* HAp, the procedure followed was to add [Ca^{2+} + M^{n+}]-containing solution drop by-drop to the [PO_4^{3-}]- containing solution with the same care paid to maintaining pH to within the range of 10-11.

The reason for the need to maintain pH in this range during the precipitation was to avoid formation of other non apatitic phases such as brushite ($CaHPO_4.2H_2O$) which would otherwise co-deposit with the desired (substituted HAp) product.

(p-6) At the end of the addition process for any of the anion or cation substituted HAp synthesis procedures mentioned above (as described in (p-5)), the precipitate solution was left to stir for 2-3 hours at room temperature to let the precipitate age, while ensuring the pH in the solution was kept above 10. This ageing process allows development of the apatitic phase by phase-transformation of initially formed phases and also avoids formation of any non-apatitic by-product phases like tricalcium phosphate which could form initially.

(p-7) After executing the steps above, the resultant precipitate was subsequently separated from the solution by filter paper or, where possible, by decanting. The precipitate was generally washed with deionized water several times, followed by ethanol. The ethanol serves to remove residual water and evaporates more quickly than water so leaving a dry sample that will not phase-transform any further. Alternatively, suspending the precipitated mass of solid in water for washing followed by centrifugation and decanting was also done because separating the fine powders from water by filtration was a time-consuming procedure.

(p-8) The filtered precipitates formed of whichever substituted HAp targeted were then dried in an oven (~100 °C) overnight and then manually ground if necessary, in an agate mortar and pestle to reduce the particle size followed by further drying in an oven to remove any moisture picked up during the grinding process.

(p-9) As a final step, the obtained poorly crystalline and substituted HAps were then calcined at 900 ˚C or higher for a certain length of time, in order to obtain a high crystallinity powder. This was then followed by the usual solid-state structural characterization methods like X-ray powder diffraction for instance.

The flowchart for the synthesis process of substituted and co substituted hydroxyapatite materials by using the precipitation method is shown in **Fig.3-1**.

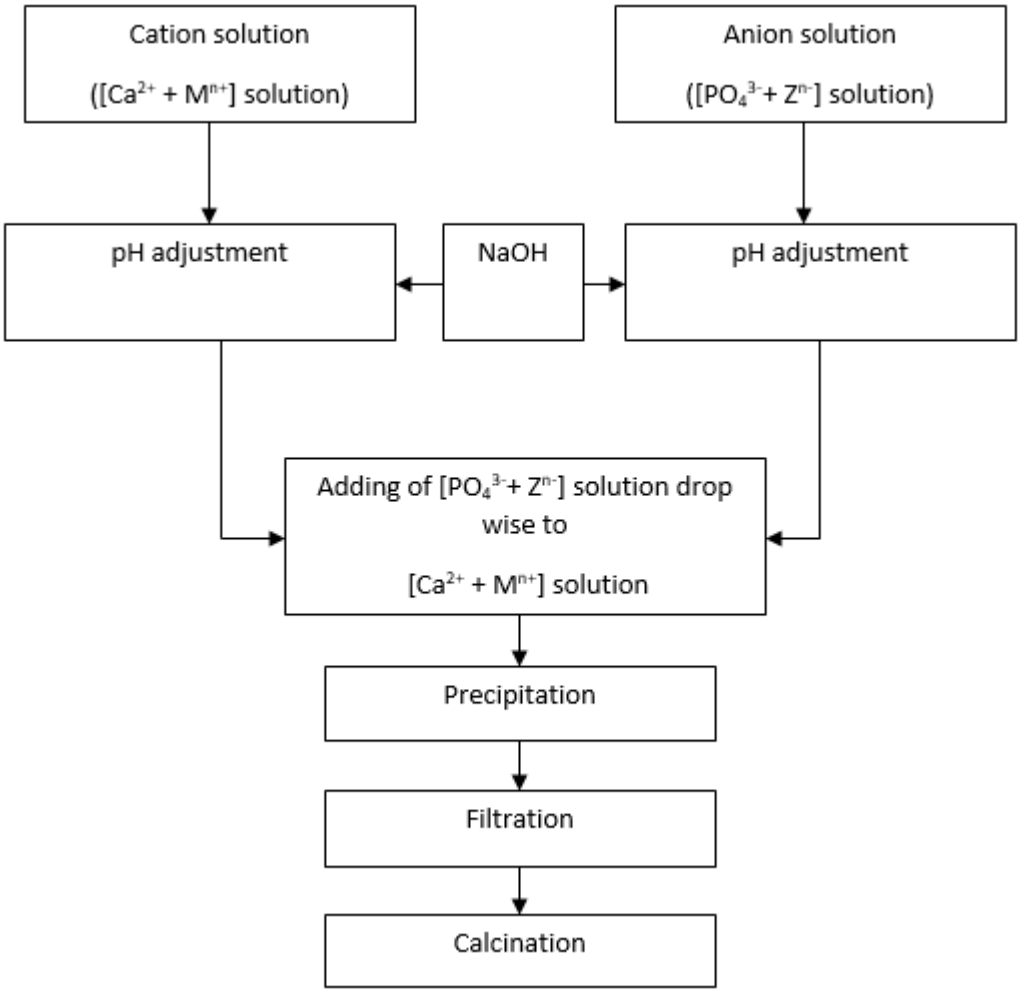

Figure 3-1 flowchart for the synthesis process of substituted and co substituted hydroxyapatite materials by using the precipitation method.

Route (2): Substitution of hydroxyapatite by an ion exchange procedure:

Substituted HAp powders can be easily achieved by using commercially sourced HAp powders, followed by immersion of the powders in solutions containing different dissolved metal ions. This then allows ion exchange of these ions to occur with ions from the HAp crystallites. The full description of the standard synthesis procedure to prepare substituted hydroxyapatite by ion exchange procedures is given in the following steps (i-1) to (i-3) which were adapted from synthesis routines as described in the current literature [82,134-136]:

(i-1)-Different solutions of metals salts (from which the substituting ions are taken) were prepared, by dissolving a stoichiometric amount of salts (1 M) in (1000 mL) of deionized water with stirring for 1 hour at room temperature.

(i-2)- Solid commercially sourced HAp was subsequently soaked in the prepared metal ion solutions (in the ratio of 200 mL solution per gram of HAp solid) with constant stirring for 3 hours to achieve the substituted MHAps.

(i-3)- The ion exchanged solid was then extracted from the solution by filter paper or by decanting. The ion-exchanged solid material is generally washed with deionized water several times, followed by ethanol. As described earlier, the ethanol removes residual water and evaporates quickly leaving a dry sample that will not transform any further. Alternatively, suspending the dried powder in water for washing followed by centrifugation and decanting was also done as washing and filtering the fine powders were found on occasion to be time consuming.

(i-4) After this, any ion exchanged solid formed of whichever substituted HAp targeted for was then dried in an oven (~100 °C) overnight then manually ground (where necessary) in an agate mortar and pestle to reduce the particle size and then redried again in an oven to remove any moisture absorbed during the grinding process.

Fig.3-2 is an illustration of the synthesis process of substituted and co substituted hydroxyapatite materials by using the ion exchange route.

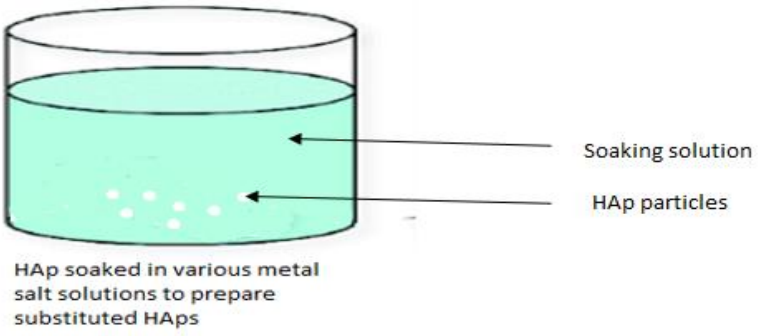

Figure 3-2 The synthesis process of substituted and co substituted hydroxyapatite materials by using an ion exchange method.

Route (3): Formation of substituted HAps via hydrolysis of precursor CaP phases:

As discussed in the literature [53], HAp powders can be prepared through a hydrolysis process of several types of calcium phosphate compounds. For example, dicalcium phosphate dihydrate (DCPD)as well as many other precursors can be hydrolyzed to obtain calcium-deficient HAp materials[53]. This approach has several advantages in that only a single precursor is required, and it can lead to calcium-deficient HAps as products which are more soluble compared to "stoichiometric" HAp.

The hydrolysis method is an effective route when the major goal of any researcher is to convert a commercially available CaP compounds such as tricalcium phosphate into HAp [53]. HAp material synthesized by hydrolysis methods is said to possess a good composition and morphology of crystals, because of the fact that there is only a limited number of variables that play an important role in the hydrolysis process such as temperature, ratio and composition of the starting reagents, as well as pH[137].

To the author's knowledge no previous work has been specifically performed to prepare substituted and co substituted HAp powders via the hydrolysis route of synthesis when using a specific reagent such as MCP (monocalcium phosphate) as a precursor. Like other CaP precursors such as brushite, octacalcium phosphate or tricalcium phosphate that have been subject to hydrolysis procedures in the past [35], MCP can be hydrolysed to produce HAp but previous reports do not exist for it, especially in regard to making substituted HAps. Therefore, it has been the aim in this study to explore the use of this precursor as a novel synthesis route for preparing substituted and co substituted hydroxyapatite at room temperature by using monocalcium phosphate (MCP, $Ca(H_2PO_4)_2$) together with calcium hydroxide ($Ca(OH)_2$).

The procedure used involved the use of equimolar amounts of monocalcium phosphate (MCP) and $Ca(OH)_2$ to prepare the substituted hydroxyapatite. As mentioned previously [35], calcium deficient HAp ($Ca_{10-x}(PO_4)_{6-x}(HPO_4)_x(OH)_{2-x}$, $0 \leq X \leq 1$) is generally expected from syntheses involving the hydrolysis approach[35] therefore, in the present study, calcium hydroxide ($Ca(OH)_2$) was used with monocalcium phosphate to supplement the calcium level in any resultant HAp products (and hence avoid the production of calcium deficient HAp).

This approach also leads to a mixture with a raised pH which is a stimulus for the hydrolysis reaction to take place. As shown below, steps (1) to (5) provide the full description of the synthesis procedure as developed in the present study for preparing unsubstituted HAps from MCP and $Ca(OH)_2$.

(1) A stoichiometric amount of $Ca(OH)_2$ powder was added to (100 mL) of doubly distilled hot water heated to 50-70 ˚C with stirring, after which a stoichiometric amount of MCP was also added. This step can be considered as a dissolution and "pre-doping" step.

(2) The reaction temperature of the solution was maintained within a certain range, i.e. 50-70 ˚C for two hours and at pH ˜ 11, during the hydrolysis process to encourage formation of the HAp phase through hydrolysis of the precursor compounds.

(3) After the two hours of reaction to allow hydrolysis as described in (2) had passed, the reaction mixture was magnetically stirred for a further 24 hours. After that, the precipitate was separated from the solution by filtering through Whatman filter paper or by decanting. The precipitate was then rinsed with deionized water several times, followed by ethanol rinsing which removes any residual water and evaporates quickly leaving a dry sample that does not phase transform any further. As done with the precipitation synthesis procedure described earlier, suspending the produced solid in water for washing followed by centrifugation and decanting was also used as an alternative for washing the product powder because any filtration procedures involving the finer powder products could be very time consuming.

(4) After this washing procedure, the precipitate was dried in an oven (~100 °C) overnight then manually ground (where necessary) in an agate mortar to reduce the particle size and then re-dried in an oven to remove any residual solvent traces picked up during grinding.

(5) The obtained HAp powders were then calcined at 900 ˚C or at other temperatures for 1 hour (as an example), in order to obtain high crystallinity HAp powders. This was also carried out with later analysis to determine their thermal stability at high temperature (i.e. the ability of metals to stabilize HAp with respect to other phases such as TCP (beta or alpha form) for instance.

Synthesis procedure for preparation of substituted and co substituted HAp by a novel hydrolysis method in detail:

The *experimental description* (for the current study) of the typical synthesis procedure (described generally above) followed with the hydrolysis method of generating substituted and co substituted HAps is hence given below in steps (h-1) to (h-5):

(h-1) A stoichiometric amount of $Ca(OH)_2$ powder was added to (100 mL) of doubly distilled hot water heated to 50-70 ˚C with stirring, after which a stoichiometric amount of MCP was also added, followed by the addition process of the required amount of metal salt precursor to prepare substituted HAp materials. This step can be considered as a dissolution and "pre-doping" step.

(h-2) The reaction temperature of the solution was maintained within a certain range, i.e. 50-70 ˚C for two hours and at pH ˜ 11, during the hydrolysis process to encourage formation of the HAp phase through hydrolysis of the precursor compounds.

(h-3) After the two hours of reaction to allow hydrolysis as described in (h-2) had passed, the reaction mixture was magnetically stirred for a further 24 hours. After that, the precipitate was separated from the solution by filtering through Whatman filter paper or by decanting. The precipitate was then rinsed with deionized water several times, followed by ethanol rinsing which removes any residual water and evaporates quickly leaving a dry sample that does not phase transform any further. As done with the precipitation synthesis procedure described earlier, suspending the produced solid in water for washing followed by centrifugation and decanting was also used as an alternative for washing the product powder because any filtration procedures involving the finer powder products could be very time consuming.

(h-4) After this washing procedure, the precipitate was dried in an oven (~100 °C) overnight then manually ground (where necessary) in an agate mortar to reduce the particle size and then re-dried in an oven to remove any residual solvent traces picked up during grinding.

(h-5) The obtained substituted HAp (M-HAp) powders were then calcined at 900 ˚C or at other temperatures for 1 hour (as an example), in order to obtain high crystallinity HAp powders. This was also carried out with later analysis to determine their thermal stability at high temperature

(i.e. the ability of metals to stabilize HAp with respect to other phases such as TCP (beta or alpha form) for instance.

The flowchart for the synthesis process of substituted and co substituted hydroxyapatite materials via the hydrolysis route is shown in **Fig.3-3**.

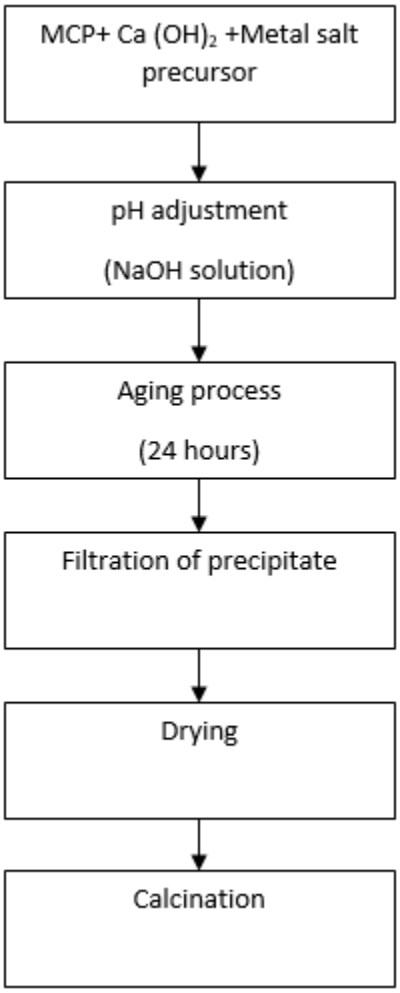

Figure 3-3 flowchart for the synthesis process of substituted and co substituted hydroxyapatite materials by using hydrolysis methods.

3.2 The common reagents and solvents that were used in this project to prepare the cationic, anionic and co-substituted HAp powders:

During this project various chemical reagents were used. The specific amounts of the reagents (i.e. weights) that were used in the various preparations have been indicated elsewhere (see Chapters 4, 5, 6 and 7) which represent the results and discussion chapters of the present study).

The following **Table 3-1** displays the common chemical reagents that were used to prepare and characterize all substituted and co substituted HAp materials during this project by the precipitation, hydrolysis and ion exchange methods discussed earlier:

Table 3-1: Reagents that were used to prepare the cationic, anionic and co substituted HAp materials in this study by the different synthesis routes, namely precipitation, hydrolysis and ion exchange methods.

Chemical name	Grade	Brand	Notes
Hydroxyapatite	>90% purity	Fluka	Used to prepare BrAp and Sap by the ion exchange method.
Tri-calcium phosphate	>99% purity	Fluka	Used to compare the XRD diffraction patterns with all substituted and co substituted materials.
Calcium nitrate anhydrous ($Ca(NO_3)_2$)	≥99.0 %	BDH	Used to prepare all substituted and co substituted materials by the precipitation method.
Disodium hydrogen phosphate (Na_2HPO_4)	≥99.0%	Sigma Aldrich	Used to prepare all substituted and co substituted materials by the precipitation method.
Calcium phosphate monobasic (MCP for monocalcium phosphate) ($Ca(H_2PO_4)_2$)	≥ 98.0%	Sigma Aldrich	Used to prepare the following systems by the hydrolysis method: • $Ca_{10-x}M_x(PO_4)_6(OH)_2$), where (M= Zn, Sr and Cu)and (X=0.5, 1.0 and 1.5). • RbHAp (1% wt. Rb^+). • BrAp ($Ca_{10}(PO_4)_6Br_2$)and Sap ($Ca_{10}(PO_4)_6S$)
Calcium phosphate monobasic monohydrate (MCPM) ($Ca(H_2PO_4)_2.H_2O$)	≥ 95.0%	Sigma Aldrich	Used to prepare the following systems by the hydrolysis method: • Used to prepare EuHAp (1% wt. Eu^{3+}) and ScHAp (1, 3 and 5% wt.Sc^{3+}). • Used to prepare NbHAp materials (1,3 and 5% wt. niobate ions) and BHAp (1% wt. borate ions). • NaClHAp ($Ca_{10-x}Na_x(PO_4)_6(OH)_{2-x}Cl_x$, where x=1.0).

Calcium hydroxide ($Ca(OH)_2$)	≥95.0%	Sigma Aldrich	Used in preparing all substituted and co substituted materials by the hydrolysis method
Sodium hydroxide (NaOH)	≥97.0%	Merck	Used to adjust the pH of reaction solutions of all substituted and co substituted HAPs prepared by the precipitation, hydrolysis and ion exchange methods
Potassium bromide (KBr)	IR spectroscopy grade	Sigma Aldrich	Used to make KBr disks in the IR characterization of all substituted and co substituted HAps
Nitric acid (HNO_3)	For analysis, 65%	EMSURE ™	Used to digest all substituted and co substituted HAps when analysed by ICP-MS methods

3.2.1 Reagents used to prepare cationic substituted HAp with the following specific formulae: $Ca_{10-x}M_x(PO_4)_6(OH)_2$), where (M= Zn, Sr and Cu)and (X=0.5, 1.0 and 1.5)by the hydrolysis method:

The following table (**Table 3-2**) shows the specific chemical reagents that were used to substitute Zn^{2+}, Sr^{2+} and Cu^{2+} ions into the HAp lattice by the hydrolysis method using different levels of substitution.

Table 3-2 Specific reagents that were used to substitute Zn^{2+}, Sr^{2+} and Cu^{2+} ions into HAp structure by the hydrolysis method with the following formula: $Ca_{10-x}M_x(PO_4)_6(OH)_2$), where (M= Zn, Sr and Cu)and (x=0.5, 1.0 and 1.5).

Chemical name	Grade	Brand
Zinc nitrate hexahydrate ($Zn(NO_3)_2.6H_2O$)	98.0%	Sigma Aldrich
Strontium chloride hexahydrate ($SrCl_2.6H_2O$)	99.0%	Sigma Aldrich
Copper (II) chloride ($CuCl_2$)	97.0%	Sigma Aldrich

3.2.2 Reagents that were used to prepare cationic substituted HAp (specifically 1% RbHAp (1 wt.% Rb^+), 1% EuHAp (1 wt.% Eu^{3+}) and 1, 3 and 5% ScHAp (1, 3 and 5 wt.% scandium ions) by the precipitation and hydrolysis methods:

The following Table (**Table 3-3**) displays the chemical reagents that were used to substitute Rb^+, Eu^{3+} and Sc^{3+} ions into HAp crystal by various preparation methods, namely by precipitation and hydrolysis methods:

Table 3-3 Reagents that were used to substitute Rb^+, Eu^{3+} and Sc^{3+} ions into HAp crystal by the precipitation and hydrolysis methods:

Chemical name	Grade	Brand	Notes
Rubidium chloride (RbCl)	≥99.0%	Sigma Aldrich	Used as a source of Rb^+ ions
Europium (III) nitrate pentahydrate ($Eu(NO_3)_3.5H_2O$)	99.9%	Sigma Aldrich	Used as a source of Eu^{3+} ions
Scandium (III) oxide (Sc_2O_3)	99.9%	Smart elements	Used as a source of Sc^{3+} ions
Hydrochloric acid (6 M HCl)	-	Merck	Used to convert Sc_2O_3 to $ScCl_3.(H_2O)_6$

3.2.3 Reagents that were used to prepare anionic substituted HAp materials, namely (NbHAp, BHAp, Br_2Ap, and SAp powders) by the precipitation, hydrolysis and ion exchange methods:

The following Table (**Table 3-4**) displays the chemical reagents that were used to substitute niobate, borate, bromide and sulfide ions into the HAp structure by various preparation methods, namely by the precipitation, hydrolysis and ion exchange methods:

Table 3-4 Reagents that were used to substitute niobate, borate, bromo and sulfide ions into HAp structure by the precipitation, hydrolysis and ion exchange methods:

Chemical name	Grade	Brand	Notes
Niobium (III) oxide (Nb_2O_5)	99.99%	BDH	Used as a source of niobate ions by using the precipitation and hydrolysis methods
Sodium tetraborate decahydrate ($Na_2B_4O_7.10H_2O$)	≥99.5%	Baker Analyzed reagents	Used as a source of borate ions by using the precipitation and hydrolysis methods
Sodium bromide (NaBr)	99.0%	Sigma Aldrich	Used as a source of Br^- ions by using the precipitation , hydrolysis and ion exchange methods
Sodium hydrosulfide hydrate (NaSH. $_xH_2O$)	99.0%	Sigma Aldrich	Used as a source of S^{2-} ions by using the precipitation ,

			hydrolysis and ion exchange methods
Hydrochloric acid (12 M HCl)	-	Merck	Used to convert Nb_2O_5 to $NbCl_5$

3.2.4 Reagents that were used to prepare co substituted HAp materials (NaClHAp) by the precipitation and hydrolysis methods:

The following Table (**Table 3-5**) shows the chemical reagents that were used to co substitute sodium and chloride ions into the HAp structure by the precipitation and hydrolysis methods:

Table 3-5 Reagents that were used to co-substitute sodium and chloride ions into the HAp structure by the precipitation and hydrolysis route:

Chemical name	Grade	Brand
Sodium chloride (NaCl)	99.0%	Sigma Aldrich

3.3 Characterization of the substituted HAps

During this project, an array of techniques has been used to characterize the substituted HAps to confirm 1) that HAp has actually formed, 2) that substitution of lattice ions or functional groups out of the HAp has actually taken place, and 3) to monitor the effect of the substituents on the HAp crystal lattice.

The following text details the techniques that were used in this study to characterize the prepared cationic, anionic and co substituted HAp powders. A brief introduction as to the utility of the technique is given first and then the equipment used in this study as well as sample preparation protocols.

3.3.1 Microstructural Characterization:

3.3.1.1 Microscopy: Scanning Electron Microscopy (SEM):

Microscopic analysis remains one of the most effective techniques for the characterization of biomaterials due to the information gained through visual analysis. Scanning electron microscopy (SEM) [138] is a widely used technique for imaging physical features of samples. It can be considered as a method for evaluating surface morphology and to determine the

microstructural and surface features of the materials. SEM imaging is based on scattered electrons, where these scattered electrons are classified as backscattered or secondary electrons. The principle of that technique depends on the information that is collected due to the scattering of electrons from the sample/test piece when the electron beam irradiates it. The emitted electrons from the electron shells from the materials under examination are considered a signal that contains all the required information about the sample's surface structure and composition. Generally, SEM is equipped with other instrumentation such as energy-dispersive X-ray spectroscopy (EDX) and/or wavelength-dispersive X-ray spectroscopy (WDS) detectors that are used for elemental analysis or chemical characterization.

The SEM was used to analyze the surface morphology of the substituted HAp compounds to check whether they were of porous or crystalline character. One way the observations from SEM could be used , for example, is that the detection of regular shape in the particles with clearer contours can give a good idea about crystallinity since it is related to increases in crystallinity, whereas irregular shapes with no obvious contours are related to a decrease in crystallinity [139]. Also, SEM can provide an idea about agglomeration that may occur as a result of substitution or whether the substituents are uniformly distributed throughout the HAp sample. Homogeneity of morphology and crystallite shape (e.g. whether spheres, needles or rods or other shapes are observed or not) can also be observed or confirmed using SEM.

In this project, samples for SEM analysis were prepared as follows: a thin layer of the sample powder was spread and adhered to double-sided conducting black carbon tape on the surface of 15 mm aluminium sample holder stubs. These were then sputter-coated with pure platinum and analysed using a Hitachi S-4700 Field Emission Scanning Electron Microscope [140], at 5 kV, but in the case of EDX analysis, 15 kV was used.

3.3.1.2 Energy dispersive X-ray Analysis (EDX):

Energy dispersive X-ray (EDX) spectroscopy [141] provides a semi-quantitative elemental analysis of the sample when it is examined by SEM. Combination of EDX with SEM provides elemental analysis combined with high resolution images of surface topography with spot analyses possible. EDX can be used to evaluate the elemental composition of a sample. Bombarding the sample's constitutional atoms with a high energy X-ray beam excites an electron in an inner shell and ejects

it from the shell leaving behind a hole or vacancy that a higher energy electron fills. The difference in energy between the higher and lower-energy shells may be released in the form of an X-ray, and by comparing the energy collected with a pattern related to atomic weight, a quantitative spectrum can be obtained. In other words, the EDX works by detecting x-rays characteristic of different elements and arranging them in an energy spectrum which EDX software then analyses to define and semi-quantify the elemental composition. The data that is generated by EDX analysis consist of spectra with peaks corresponding to all the different elements that are present in the sample. Hence, energy-dispersive X-ray analysis (EDX) was used for qualitative elemental analyses of any new substituted HAp materials prepared. Sometimes the sensitivity was not enough to detect low levels of substituted elements in the HAps in which case Inductively coupled plasma mass spectrometry (ICP-MS) (see later) was used to detect anything below the threshold sensitivity of the EDX technique.

In this project, the EDX technique was used to characterize specific systems of substituted and co substituted HAp powders, namely: 1% EuHAp (1 wt. % Eu^{3+}), 1% ScHAp (1 wt.% Sc^{3+}), SAp and NaClHAp powders that were prepared by the precipitation method.

EDX analysis was carried out and elemental mapping done to examine the distribution of sodium, carbon, calcium and phosphate ions in the microstructure of these systems and to obtain a clearer idea about their atomic percent in the prepared compounds. Although some elements of these systems could not be detected by EDX (such as scandium ions) due to the lower concentration of these ions, their presence in the prepared substituted HAp powders was confirmed by ICP-MS results.

3.3.2 FTIR Spectroscopy:

IR spectroscopy is a form of vibrational spectroscopy based on the interaction of IR radiation with the molecular vibrations of the chemical bonds in molecules that comprise the material [142]. This is a highly useful technique for probing the phases of calcium phosphate compounds. The substituted HAps prepared were investigated primarily via preparation of pressed KBr pellets and use of transmission IR spectroscopy on a Fourier transform infrared (FTIR) spectrometer.

FTIR analysis was performed to identify the functional groups present in the HAp particles. This provides information about the constitution and phase composition of the products. The FTIR spectra of the substituted and co substituted HAp contain in common several bands corresponding to hydroxyl (OH^-) and phosphate (PO_4^{3-}) groups of the HAp. In terms of certain substituents, CO_3^{2-} ion can easily replace OH^- (A sites) and PO_4^{3-} (B sites) to produce characteristic IR peaks at 1500–1545 cm^{-1} and 1420–1470 cm^{-1}, respectively which show the substituted carbonate moieties in so called carbonated HAp. In a number of preparations in this study this may be an unintended impurity because of the ease of formation of the carbonated HAp under the experimental conditions used to synthesize the substituted HAps [143] (i.e. with the reaction solution exposed to the ambient atmosphere). In this study, all samples were prepared for FTIR analysis via the following steps, 2 mg of each HAp sample was mixed with 300 mg of spectroscopic grade potassium bromide (KBr). These amounts were ground together to form a fine homogeneous powder using an agate mortar and pestle. They were then compressed (under a weight of 10 tons) using a KBr disk press to form semi-transparent pellets. The pellets were then placed in a disk holder and analyzed by FTIR in transmission mode using a Perkin Elmer 400 FT-IR/FT- FIR spectrometer which used Spectrum software for processing. The spectra were obtained between 400 and 4000 cm^{-1}, with a resolution of 4 cm^{-1}, with 3 scans. A background spectrum was recorded before each analysis by scanning an empty KBr disk sample holder in the pathlength of the beam and ratio-ing the sample spectrum by this spectrum.

Spectra were analysed to confirm the presence of the main chemical groups of HAp samples such as OH^- and PO_4^{3-} fundamentals as well (where detectable) as any peaks due to substituents (e.g carbonate) [140].

3.3.3 Inductively coupled plasma mass spectrometry (ICP-MS) analysis:

Confirmation of the incorporation of the substituent into the HAP lattice is only able to be possible in most cases by the use of elemental analysis techniques on digest solutions from the substituted HAp samples produced. They are required as the amount of substitution may be very small and not clearly detectable by other techniques such as EDX (see earlier comment on this).

Inductively coupled plasma mass spectrometry (ICP-MS) [144] is a widely used analytical technique and is commonly applied for trace elemental analysis where the Ca, P, and any elemental content from substituents can be determined. Acid digested samples are firstly converted to aerosols and then passed into a torch body and mixed with heated argon gas, producing an argon plasma flame. The atomized and ionized sample is then transferred into a pumped vacuum system through a quadruple mass filter and directed to a mass spectrometer.

ICP-MS provides a qualitative and quantitative analysis for a large part of the elements of the periodic table, with detection limits at or below the part per trillion (ppt) level. This technique is a very critically important one for the classical (destructive) chemical analysis of the substituted HAps. The results from analysis of substituted HAp digests need to be compared to that of unsubstituted HAp compounds to help confirm whether doping (substitution) of a certain element into the HAp lattice has actually occurred, because the substitution process of calcium ions (Ca^{2+}) or phosphate groups (PO_4^{3-}) by any other ions or functional groups causes a clear change in the value of Ca/P mole ratio of substituted HAp compared to that measured for stoichiometric or unsubstituted HAp.

The Ca, P and M contents (M represents the cations or anions that might be substituted into the HAp lattice) in the substituted HAps produced in the present study were analysed by using an Agilent 8900 Inductively Coupled Plasma - Mass Spectrometer (ICP-MS; Agilent Technologies, Santa Clara, California, USA) controlled by a MassHunter Workstation (version 4.5).

Typically, solid samples were weighed out (~0.1 g) into plastic tubes and completely digested in a mixture of concentrated nitric acid (2.0 mL, 68%) and distilled water (1.0 mL). These were then sealed and heated in a water bath (at 80 ˚C) to ensure complete digestion. The solutions in the tubes were then made up with distilled water to produce 50.0 mL of

prepared sample. A five-point calibration curve, consisting of concentrations of between 0.1 and 500 ppb was prepared for all trace elements using a stock standard IV71-A (standard multi-element solution from Inorganic Ventures). A separate calibration curve, consisting of concentrations between 100 and 10,000 ppb was prepared for the major elements (Ca, Si, P, S, K, Fe) using single-element standards (Inorganic Ventures). The ICP-MS standards were analysed every 20 samples and re-calibration was performed every 100 samples.

The analysis process of the prepared samples was performed under the following ICP-MS operating conditions:

Forward power (W) : 1570

Gas flows (Ar in L/min)

Plasma : 15

Auxiliary : 0.90

Nebuliser (carrier gas): 0.95

Makeup gas : 0.10

Sampling Depth (mm) : 8.0

The carrier, auxiliary and makeup gases were argon gas, but they were introduced at different points to ensure the plasma was hot enough, so that the ions generated are passed through in an accurate manner. On the other hand, the sample depth represents how far away the plasma is from the cones at the interface (It represents how far the torch is from the cones at the interface, to ensure optimum ion transmission from the torch through the cones at the interface).

3.3.4 Powder X-ray Diffraction

X-ray diffraction (XRD) is used to examine powdered inorganic crystals by measuring the degree of crystallinity, determining the size of crystallites and calculating the lattice parameters that are affected by the substitution process in the HAp lattice. Along with ICP-MS, it is thus a very

important technique for characterizing the substituted HAps and the impact the substituted atoms or functional groups have on the HAp crystal lattice.

In this technique, X-rays of a known wavelength are passed through a sample to examine its crystalline structure. The wave nature of the X-rays means that the lattice of the crystal gives a unique diffraction pattern, which results in a pattern of peaks of 'reflections' at different angles and with various intensities. The diffracted beams from atoms in successive planes cancel unless they are in phase, and the condition for this is given by Bragg's law [50].

$\lambda = 2.d.\sin\Theta$ …….. (1)

where λ is the wavelength of monochromatic radiation (λ = 1.54098Å), *d* is the distance between the different planes of atoms in the crystal lattice and *Θ* is the angle of diffraction (see **Fig. 3-4**)

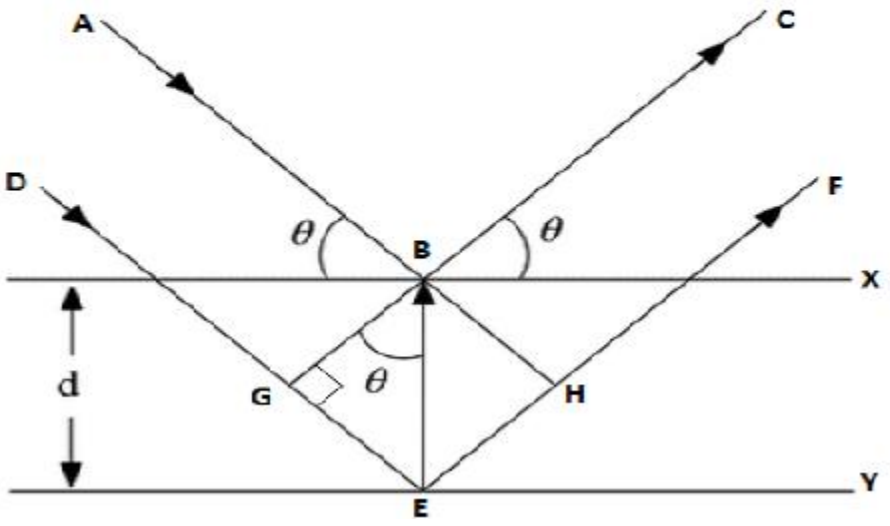

Figure 3-4 : The diffraction of X-rays by the planes in a crystal [140] .

3.3.4.1 Sampling for XRD

In this study, the prepared samples of substituted and co substituted HAp were ground into fine powders and packed into sample holders with even distributions of powder to obtain a flat surface in the sample holder (see below **Figure 3-5**). The diffractograms of these samples were

recorded using a Panalytical Empyrean Series 2 diffractometer, with the following instrument parameters:

Anode Material	:	Cu
Generator Settings	:	40 mA, 45 kV
Scan range	:	10-60 ˚
Scan step size	:	0.026 ˚
Time per step (ms):		236.64

Post diffractogram acquisition, calculations such as Rietveld refinement, phase identification, crystallite size (D_{002} reflection plane), the degree of crystallinity and determination of the lattice parameters (a, b and c) of the apatite hexagonal unit cell were carried out using the XPert High score Plus (Panalytical, the Netherlands) software.

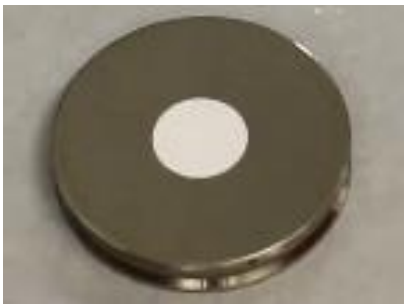

Figure 3-5 Sample holder as used in powder X-ray diffraction and the way powdered samples were packed into the holder with an even surface.

3.3.4.2 Phase Identification:

For the phase identification step, the X-ray diffraction patterns of the prepared cationic, anionic and co substituted HAp powders were directly compared to both XRD patterns of standard HAp (card no. 01-074-9780) and β-TCP (card no. 00-009-0169) through using XPert High score Plus software. Comparison was also made to any other phases that may have been present within the calcium phosphate compounds such as α-TCP (card no. 00-029-0359), mono calcium phosphate(MCP, card no. 00-009-0390), mono calcium phosphate monohydrate (MCPM, card

no. 00-003-0284), dicalcium phosphate anhydrous (DCPA, card no. 00-003-0428), octacalcium phosphate (OCP, card no. 04-013-3883), calcium oxide (CaO, card no. 04-017-9575), calcium hydroxide ($Ca(OH)_2$, card no. 04-014-7725) and calcium carbonate ($CaCO_3$, card no. 01-078-4615).

In addition, the X-ray diffraction patterns of the prepared cationic, anionic and co substituted HAp powders were compared directly with the experimentally acquired XRD patterns of various kinds of commercial compounds such as: β-TCP, CO_3HAp (carbonated hydroxyapatite), Na_2HPO_4, $Ca(NO_3)_2$, MCP, Na_2CO_3, $Ca(OH)_2$ and $CaCO_3$.

3.3.4.3 Crystallinity and Crystallite size (D_{002} reflection plane):

The degree of crystallinity is determined as a percentage from the XRD patterns obtained between 10° to 60° (2θ) and calculated using the following equation [145]:

$$X_c(\%) = \left(\frac{I_{300} - V_{112/300}}{I_{300}}\right) \times 100$$

……(2)

where: (I_{300}) is the intensity of (300) diffraction peak and ($V_{112/300}$) is the intensity of the hollow (valley) between the (112) and (300) diffraction peaks of HAp.

The crystallite size of each substituted and co substituted HAp materials were calculated using the Scherrer equation [146] which is given as:

$D = 0.9\lambda/\beta \cos \Theta$ ……..(3)

Where λ : is the wavelength of the incident X-ray (CuK_α radiation =0.154098 nm) , β : is the full width at half maximum (FWHM) in radians, and Θ : is the diffraction angle in degrees. The crystallite size (D_{002}) was calculated using the peak corresponding to the reflection plane of the (002) peak.

3.3.4.4 Lattice Parameter Determination and the volume of the hexagonal unit cell :

The spacing of the lattice points in a crystal is an important quantitative aspect of its structure and its investigation by X-ray diffraction. In the case of the hexagonal crystal structure of HAp, the lattice parameters are denoted by (*a=b*), and *c,* and are determined from the relationship between the distance (*d*) of two adjacent planes and the (*h k l*) Miller Indices by using equation

4 below [147]. The substitution process of any ions or functional groups into the HAp crystal lattice causes a clear change in the lattice parameters a and c.

$$\frac{1}{d^2} = \frac{4}{3}\left(\frac{h^2+hk+k^2}{a^2}\right) + \frac{l^2}{c^2} \quad \text{……(4)}$$

Where, (*d*) is the distance of two adjacent planes and (*h k l*) refer to the Miller Indices.

Hence calculations of lattice constants can be used as **obvious evidence of the ion replacement** process in the HAp crystal lattice.

In the present study the lattice parameters of the prepared HAp, "unsubstituted", substituted and co substituted HAps materials were calculated by using Highscore plus software that matches the Le Bail mode. The Le Bail whole powder profile fit can be performed to extract the unit cell parameters [148] through performing a Rietveld refinement process. The Rietveld refinement method considers the positions, the intensities and the shape of the powder diffraction peaks. The lattice parameters and the space group of the unit cell define the peak positions while the atom types, positions and vibrations define the peak intensities [148]. In the refinement process, an x-ray diffraction pattern is simulated based on the expected space group and lattice parameters of the sample. This simulated pattern is then compared to experimental data, and the differences between the simulated and experimental pattern are minimized in a least-squares fitting procedure [149]. In other words, for the application of the Le Bail method, pre-determined approximate lattice parameters, either from a structural model provided in the literature or deduced from indexing of the powder data, must be available. Ideally the space group of the crystal is also known. Therefore, the XRD patterns of the prepared HAp, substituted and co substituted HAp powders were refined as discussed in the literature [8] as a hexagonal structure (space group p63/m) with lattice parameters a=b= 9.4261 Å and c= 6.8971 Å and α = β= 90˚, whereas γ = 120 ˚through using the Highscore plus program. The results of the refined crystal constants (a and c) were identified and reported in result sections.

The volume (V) of the hexagonal unit cell of each substituted and co substituted HAp materials was then calculated using the following formula:

$V = 2.589a^2c$ [147] ……(5)

where a and c are the refined lattice parameters of the apatite structure. Changes in the overall volume of substituted and co substituted HAp materials display whether the dopant substituted into HAp crystal is smaller than the major lattice components of HAp (i.e. Ca^{2+}, PO_4^{3-} and OH^-) which can cause a contraction and shrinkage in the unit cell, or whether it is bigger which results in an expansion of the unit cell dimensions.

3.3.5 Mechanical tests:

Rationale for mechanical testing of substituted hydroxyapatites

Mechanical behaviour is an important factor when studying the performance of biomaterials that are used in biomedical fields such as in implant materials. As an example, the replacement process of the femoral stem of a total hip must bear static and cyclic loads imposed by body weight and muscle forces without failure for the lifetime of the implant [150]. Therefore, bone graft material with good mechanical properties and appropriate biological characteristics should also be developed to successfully perform bone replacement surgery [151]. HAp materials as mentioned previously, provide for a very desirable material for biomedical applications because of several properties such as bioactivity and biocompatibility, but some of its mechanical characteristics when in its pure state greatly limit its application, so it was of interest to study the effect of the substitution process on the value of mechanical strength [151] to see if any improvement (or worsening) of mechanical properties occurs as a result of substitution.

Mechanical properties of materials are characterized by the response of a material to applied loads commonly relating to stress and strain. While the stress is defined as the force acting per unit area over which the force is applied, the strain is considered as the change in dimension per unit length.

Even though the compressive strength of some HAp ceramics, which are widely used in medical applications, exceed those of natural bone [152], they are rarely used as implants in loaded parts of the skeleton because they are very brittle, liable to rapid crack growth, and not durable under load. For example, most of the loaded dental HAp implants when implanted in a past study, were observed to fail within one year [35]. The mechanical properties of HAp materials as reported in the literature [153]depend on many factors such as crystallinity, agglomeration, stoichiometry, impurities, substitution levels and particle size. The effect of impurities and substitution levels

on the mechanical properties of HAp powders has not been fully investigated yet. Therefore, in this project it was the aim to investigate the effect of such factors on the mechanical characteristics of HAp powders to see if significant changes occurred.

Experimental details of mechanical testing

In this project mechanical testing was performed for specific systems that were prepared by the hydrolysis method namely:

1- unsubstituted HAp powders prepared by the hydrolysis method.
2- Cationic substituted HAp materials prepared by the hydrolysis method: MHAp with the following chemical formula : $Ca_{10-x}M_x(PO_4)_6(OH)_2$ (where M=Zn, Sr and Cu, x= 0.5, 1.0 and 1.5), 1%EuHAp (1 wt.% Eu^{3+}) and 1% ScHAp (1 wt.% Sc^{3+}) powders.
3- Anionic substituted HAp materials prepared by the hydrolysis method: 1% B_4O_7HAp (1 wt.% $B_4O_7^{2-}$ ions, Br_2Ap ($Ca_{10}(PO_4)_6Br_2$) and SAp powders ($Ca_{10}(PO_4)_6S$).
4- Co-substituted HAp materials prepared by the hydrolysis method: NaClHAp ($Ca_9Na(PO_4)_6ClOH$) powders.

Only those systems that were prepared by the hydrolysis method could be studied due primarily to the limited amount of prepared substituted materials made available by the precipitation method which were not enough to perform such tests.

The following tests were used to evaluate samples for their mechanical properties. The required amount of substituted HAp materials to perform these tests (with allowance for replicates) was approximately 5 g per sample.

3.3.5.1 Compression tests:

Compression testing is applicable and suitable for biomaterials that are prone to or subjected to compressive forces and loads in vivo such as orthopaedic implants [154]. In compressive loading, the force is applied perpendicularly to the surface of the body or object. In vivo, it creates a shortening and widening of the bone as is commonly seen in human vertebra.

The purpose and goal of compression tests are to determine the behaviour or response of a material while it experiences a compressive load by measuring the fundamental variables: strain, stress, and deformation.

The compressive strength can be calculated using the following equation:

Compressive strength = F/A……..(6)

where F is a failure load (in Newtons, N), and A is the sample cross-sectional area (mm^2).
Although, the load applied in human bones is a complex combination of several forces such as bending, torsion, tension as well as compression load [155], the compressive strength can be considered as a major factor that is used to describe the mechanical behaviour of bone substitutes [5], especially when being used in load-bearing areas [6]**.**

Sample Preparation

Because of the limited amount of substituted and co substituted HAp powders that had been prepared during this project, the cylindrical specimens (of the HAp –based materials) of (10 mm) height and (11.2 mm) in diameter were compacted from the substituted and co substituted HAp powders in a hydraulic press through the use of standard dies customarily used in FTIR pellet preparation. Several researchers had also, used the standard die for pellets preparation in IR-spectroscopy to prepare their samples for mechanical investigation such as Dorozhkin et al. [156].

In the present study, 1.5 g of each material prepared by the hydrolysis method was compressed under a pressure of 3.4473 kN to generate the required dimension of the tested cylinders (10 mm × 11.2 mm).

Afterward, the produced cylinders were dried in an oven for 24 hours at 100 ˚C, followed by sintering of the specimens in an electrical furnace at 1000 ˚C. The temperature of the furnace was set to increase at a rate of 5°C/min up to the set plateau temperature (1000 °C) and it was held at this temperature for 2 hours. The sintered cylinders were cooled down to room temperature (at a cooling rate 5°C/min) and the compression tests were carried out using an Instron 5982 mechanical testing where a 5 kN load cell was secured in the Instron crosshead and the crosshead speed set to 1 mm / min (0.017 mm / s) in the downward direction for compression of the samples. A high load limit of 4.5 kN was set in the method software to protect the load

cell from damage. Three replicate samples of each material were prepared according to the previous procedure and the maximum load was measured. The average of the maximum loads was used to calculate the value of compressive strength.

Figure 3-6: The cylindrical specimens of (10 mm) height and (11.2 mm) in diameter fabricated from prepared HAp material produced by the hydrolysis method.

3.3.5.2 Laser Light Scattering Particle Size Analyzer:

Particle sizes of powders were measured using a Malvern Mastersizer instrument which is based on laser light scattering. The technique of Laser light scattering size analysis is based on the following principle that particles of a given size scatter light through a given angle where the angle increases with decreasing particle size. A narrow beam of monochromatic light (the laser) is passed through a suspension, and the scattered light is focused onto a detector that senses the angular distribution of scattered light intensity. The observed scattering intensity is dependent on particle sizes and diminishes in relation to the particle's cross-sectional area. Large particles therefore scatter light at narrow angles with high intensity, whereas small particles scatter at wider angles but with low intensity [157].

The particle sizes of prepared cationic, anionic and co substituted HAp particles were determined by means of a laser light scattering particle size analyzer (the Mastersizer 3000). The Mastersizer system consists of four basic components:

1- Optical measurement unit.
2- Computer system.
3- Malvern operating software.
4- Sample presentation unit.

The optical measurement unit is the main measurement facility for the system, which provides a collimated laser that passes through the sample to be measured. The scattered laser light from the sample is detected by the receiver of the optical measurement unit. The data from the receiver is transmitted to the computer system where the Malvern operating software calculates the size distribution.

The sample presentation unit disperses samples in approximately 500 mL of water, with ultrasonic action available to disperse aggregated samples. In a typical measurement using this method, less than 0.5 g of prepared HAp, substituted and co-substituted HAp powders were dispersed in water and ultrasonic bath in a Malvern Mastersizer 3000 instrument with the following parameters set: set refractive index: 1.629, particle absorption index: 0.010 and stirring speed :3000 RPM.

However, in order to understand the meaning of the results reported by the Malvern Mastersizer instrument, the following should be taken in the consideration:

The sample to analyze consists of a statistical distribution of particles of different sizes that is usually represented in the form of a frequency distribution curve or a cumulative distribution curve [158]. While the cumulative distribution curve shows the relative quantity (%) of particles smaller than or equal to size x, the frequency distribution curve provides information on how frequently each particle size is observed based on the number of particles, surface area or volume of the particles [158]. However, some statistical parameters are also reported. Such parameters are as follows:

• Mean - ‘Average’ size of population

• Median - Particle size where half of the population is below/above this point

• Percentile - Maximum particle size for a given percentage of sample volume, used particularly in volume-weighed distributions

The most common percentiles reported are Dv (10), Dv (50) and Dv (90), where D stands for diameter and v stands for volume-weighted distribution. Dv (50), the median, is the particle diameter where 50% of the population lies below/above this value. Similarly, Dv (90) indicates that 90% of the distribution is below this size and Dv (10) indicates the size where 10% of the population lies below this value. There can be several ways to define means which are based on the method of the collection of distribution data and the analysis. According to the results obtained from the Malvern Mastersizer 3000 laser light scattering method, they can be reported as shown below;

D [3,2] the surface weighted mean diameter

D [4,3] the volume weighted mean diameter.

When the result is displayed as a volume distribution, D [4,3] is appropriate for monitoring the coarse particulates in the size distribution, whilst D [3,2] is the most sensitive to the presence of fine particulates [158].

Chapter Four

The development of a novel method to prepare (unsubstituted) HAp by hydrolysis of monocalcium phosphate (MCP) using calcium hydroxide.

4.1 Introduction:

As discussed in the literature, hydroxyapatite materials can be prepared through using different synthesis routes, various kinds of reactants as well as several different processing conditions [35,53-58,127] (see Chapter 2 for details). The final phase and composition of the hydroxyapatite product are highly dependent on the reaction conditions under which the synthesis takes place [53].

The hydrolysis approach is one method that has been used to prepare HAp materials through the reaction of other calcium phosphate compounds such as dicalcium phosphate dihydrate (DCPD) and TCP [53]. This route is characterized by several features such as the forming of non-stoichiometric HAp powders and the generation of HAp with needle or plate like morphology in the micron size range (see Chapter 2 for details). In this project, monocalcium phosphate (MCP) was selected as a new precursor to prepare unsubstituted and substituted HAp materials because of the following reasons:

1- The cost of the MCP (monocalcium phosphate) compound is low. For example, the price of 100 g of MCP (mono calcium phosphate) and MCPM (monocalcium phosphate monohydrate) is about (NZ$206.00 and NZ$82.80 respectively according to Sigma- Aldrich prices) [159,160], compared to 10 g of β-TCP and 10 g of α- TCP (185 and 199 NZ$ respectively, according to Sigma- Aldrich prices) [161,162]. On the other hand, the price of 1 ton of MCP ((mono calcium phosphate) as an industrial grade chemical is 300-500 US $ according to Made-in-China prices [163], compared to 770-950 US $ for 1 ton of tricalcium phosphate (according to Made-in-China prices) [164].

2- MCP as a material is abundantly available. This is because MCP and MCPM are widely used in such applications as superphosphate fertilizers [165] and also as popular leavening agents in industrial baking practice [166].
3- The compound of MCP is very soluble in water and does not by dint of its dissolution, introduce any additional cations or anions into the prepared HAp. This is in direct contrast to other starting materials such as anhydrous calcium nitrate ($Ca(NO_3)_2$) and disodium hydrogen phosphate (Na_2HPO_4) which would introduce sodium ions (which can potentially substitute into the lattice) into HAp materials as well as nitrate ions (which will be a contaminant even though they do not substitute into the HAp lattice).

Therefore, in this study, a new route was developed to prepare initially unsubstituted HAp and later substituted and co-substituted HAp materials by using hydrolysis of monocalcium phosphate and calcium hydroxide as starting materials as this reaction was regarded as providing more of a direct route to the HAp. To the author's knowledge no previous work has been specifically performed to prepare unsubstituted, substituted and co substituted HAp powders via this reaction involving the hydrolysis of MCP (monocalcium phosphate) as a precursor with $Ca(OH)_2$.

In relation to this new hydrolysis method, this chapter provides the following insights:

1- To investigate the ability of the new preparation method (hydrolysis) to be used as an effectively new method to synthesize unsubstituted HAp powders by using the combination of monocalcium phosphate and calcium hydroxide.
2- To evaluate the effect of this new synthesis route on the general properties of unsubstituted HAp materials such as morphology, chemical composition, substitution levels, crystallinity, crystallite size, lattice parameters and phase purity, because such properties depend clearly on the preparation method employed to HAp[167]. This evaluation process has been carried out through comparing the general characteristics of unsubstituted HAp powders prepared by the new hydrolysis method with those of commercial HAp (Fluka-brand) and unsubstituted HAp prepared by the more conventionally (and more popularly) used *precipitation* synthesis routes (wet chemical method).

In order to achieve the aims of this chapter, the following techniques were used to characterize the prepared unsubstituted HAp powders and the results of these experiments are discussed extensively in this chapter:

1- Scanning electron microscopy (SEM)
2- FTIR spectroscopy.
3- Powder X-ray Diffraction (XRD).
4- Inductively coupled plasma mass spectrometry (ICP-MS) analysis

4.2 The Preparation and Characterization of the unsubstituted HAp material prepared via the novel hydrolysis method using MCP and $Ca(OH)_2$:

As discussed in the literature [25,53], HAp powders can be prepared through using different kinds of synthesis routes such as the hydrolysis route. A specific reagent such as MCP (monocalcium phosphate) as a precursor was used in the present study. The procedure involved the use of equimolar amounts of monocalcium phosphate (MCP) and $Ca(OH)_2$ to prepare the unsubstituted, substituted and co substituted hydroxyapatite powders (see Chapter 3 for experimental details on the reagents and general approaches taken to synthesis).

The details relating to the actual amounts of the reagents used to prepare the unsubstituted HAp by the new hydrolysis method are listed in **Table 4-1.**

Table 4-1: Synthesis details of unsubstituted HAp materials by the MCP/$Ca(OH)_2$ hydrolysis method.

Sample	MCP ($Ca(H_2PO_4)_2$) (g)	$Ca(OH)_2$ (g)	MCP($Ca(H_2PO_4)_2$) (mol)	$Ca(OH)_2$ (mol)	Expected Ca/P mole ratio
Unsubstituted HAp by hydrolysis	11.6487	3.6891	0.0498	0.0498	1.67

The typical appearance of the powders comprising the non-sintered unsubstituted HAp materials synthesized through hydrolysis of MCP (monocalcium phosphate and calcium hydroxide) is shown in **Fig. 4-1.**

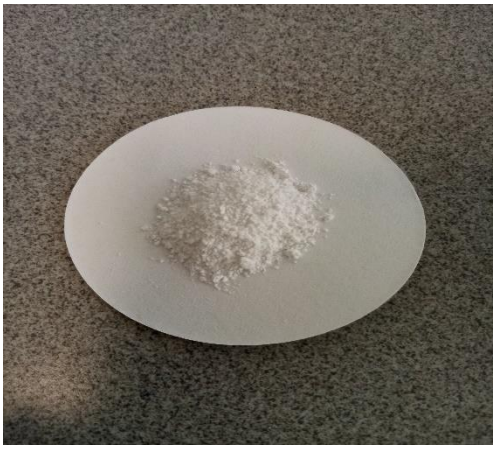

Figure 4-1: The general appearance of the powders of non-sintered unsubstituted HAp materials synthesized by hydrolysis of MCP (monocalcium phosphate) and calcium hydroxide.

In order to investigate the effect of the hydrolysis method on the general properties of prepared HAp such as crystallinity, crystallite size, the lattice constants, phase purity, morphology and the chemical composition, 5 g of unsubstituted HAp was also prepared by the precipitation method as mentioned previously in Chapter 3. The general characteristics of the unsubstituted HAp powders prepared by the novel hydrolysis method were compared directly also with both commercial HAp (Fluka) and unsubstituted HAp that was prepared by the more conventional precipitation route through using different kinds of analysis tests. The results of these tests are discussed later in this section.

The details relating to the actual amounts of the reagents used to prepare unsubstituted HAp by precipitation method are listed in **Table 4-2**

Table 4-2: Synthesis details of unsubstituted HAp materials by precipitation method.

Sample	$Ca(NO_3)_2$ (g)	Na_2HPO_4 (g)	$Ca(NO_3)_2$ (mol)	Na_2HPO_4 (mol)	Expected Ca/P mole ratio
Unsubstituted HAp by precipitation	8.1637	4.2335	0.0498	0.0298	1.67

The prepared materials were subjected to various kinds of analysis tests to confirm if hydroxyapatite had formed, to identify the phase purity, the crystallinity as well as the details of crystallographic properties such as the crystallite size and lattice parameters.

4.2.1 ICP-MS analysis of unsubstituted HAp materials prepared by hydrolysis of MCP/$Ca(OH)_2$

The results of the elemental analyses of a) sintered unsubstituted HAp samples prepared by the MCP/$Ca(OH)_2$ hydrolysis route, b) sintered commercial HAp (Fluka) and c) sintered unsubstituted HAp powders prepared by the conventional precipitation route are displayed in **Table 4-3**. Also, the starting (calculated) and actual (measured) chemical compositions of the prepared powders in terms of the calcium/phosphorus (Ca/P) molar ratios as well as the (Ca+Na)/P molar ratios as determined by ICP-MS are presented in **Table 4-3.**

Table 4-3: ICP-MS results of commercial HAp (Fluka) and unsubstituted HAp materials prepared by precipitation and hydrolysis (of MCP/$Ca(OH)_2$) methods after sintering at 900 ˚C. The concentration is reported in ppb (ug/L):

Sample	Ca44	P31	Na23	Ca/P ratio Theoretical	Ca/P ratio Measured	(Ca+Na)/ P ratio Measured
Unsubstituted HAp by precipitation	707795	401240	103797	1.67	1.36	1.71
Unsubstituted HAp by MCP hydrolysis	769928	423970	78396	1.67	1.40	1.65
Commercial HAp (Fluka)	557227	262446	298	1.67	1.64	1.64

Table 4-3 reveals that the unsubstituted HAp powders prepared by both routes (i.e. the hydrolysis and precipitation routes) contain more Na^+ ions. The measured Ca:P mole ratios of the samples generated by the precipitation and hydrolysis methods were (1.36 and 1.40), which are lower than the theoretical Ca:P molar ratios of the stoichiometric HAp powders $Ca_{10}(PO_4)_6(OH)_2$ (1.67). The lower Ca:P mole ratios are ascribable to the presence of Na^+ ions in the sample which might be substituting into the calcium ion sites in the HAp lattice as a result of using sodium hydroxide (NaOH) to adjust the pH value of the reaction during the synthesis process. Therefore, as a result, a reduction in the level of substituted Ca^{2+} ion in the HAp lattice has taken place which has led to a decrease in the experimental values of the Ca:P molar ratios and produced calcium deficient HAp. The details of these calculations can be found in Appendix A through the illustration of one computed example involving unsubstituted HAp that was prepared by hydrolysis of MCP/$Ca(OH)_2$. Also, it was found that the ICP-MS analysis data

displayed slightly higher values for the (Ca+Na)/P ratios for the unsubstituted HAp powders prepared by the conventional precipitation route, as the experimental values observed were found to be 1.71. In the case of the sintered samples prepared by the novel hydrolysis method involving MCP/$Ca(OH)_2$, the(Ca+Na)/P mole ratio was shown to be 1.65 which is very close to the standard value of hydroxyapatite (1.67). The Ca/P mole ratio of commercial HAp (Fluka) as measured by ICP-MS analysis was found to be 1.64.

Also, the results of the ICP-MS measurements in the present study, showed (**Table 4-3**) that the concentration of sodium ions in the case of unsubstituted HAp prepared by the conventional precipitation method was higher compared to that present in the HAp prepared by the hydrolysis of MCP/$Ca(OH)_2$ route. This result can be explained by the fact that **calcium hydroxide** was used with MCP as a starting material in the hydrolysis method to raise the pH value for the hydrolysis to take place . Therefore, a lesser amount of NaOH solution was used in the case of hydrolysis method, which resulted obviously in the detection of lower levels of sodium ions. In the case of unsubstituted HAp powders that were prepared by the conventional precipitation approach**,** a reduction in the phosphate ion concentrations was also observed in samples analysed by ICP-MS analysis (see **Table 4-3).** This result can be attributed to the substitution process of the phosphate ion by the carbonate ion that had taken place during the synthesis procedure. The replacement process of PO_4^{3-} by CO_3^{2-} was also confirmed by FTIR analysis of the unsintered powder. Therefore, as a result, a slightly higher value of (Ca+Na)/P mole ratio was observed because of that lower level of phosphate ions detected. The incorporation of carbonate during the preparation of HAp is the result of inevitable exposure of the alkaline solutions used for preparation of HAp materials to the atmosphere from where CO_2 can be taken up. The CO_3^{2-} ion as mentioned previously can replace OH^- (A-type substitution) and PO_4^{3-} (B-type substitution) at 1500–1545 cm^{-1} and 1410–1470 cm^{-1}, respectively to form the carbonated HAp. Formation of carbonated HAp powders were reported in the literature. As an example Stanic´ et al. [8] synthesized HAp by neutralization method (acid -base reaction) using $Ca(OH)_2$ and H_3PO_4 as a starting materials. The FTIR results showed in obvious manner the presence of carbonate group through detecting the typical peak of carbonate at 1430 cm^{-1}. Also, li et al. [86] prepared pure HAp using a wet chemical method (precipitation), in which their FTIR spectra showed in a

clear manner the presence of carbonate group through detecting two peaks between 1420 and 1451 cm^{-1} as an indication of the formation of B-type carbonated HAp.

4.2.2 FTIR studies of the unsubstituted HAp prepared by hydrolysis of MCP and $Ca(OH)_2$

As discussed previously, no earlier work has been specifically performed to prepare unsubstituted, substituted and co substituted HAp powders via the hydrolysis of MCP (monocalcium phosphate) and calcium hydroxide.

FTIR was used to characterize the HAp prepared by hydrolysis of MCP with calcium hydroxide and to compare it with the HAp prepared/supplied by other more conventionally used methods (e.g. by precipitation) or with HAp that had been procured from commercial sources.

Fig.4-2 shows the characteristic absorption bands of the non-sintered HAp materials in the prepared samples by using the novel hydrolysis and the precipitation methods compared to the non-sintered commercial HAp (Fluka).

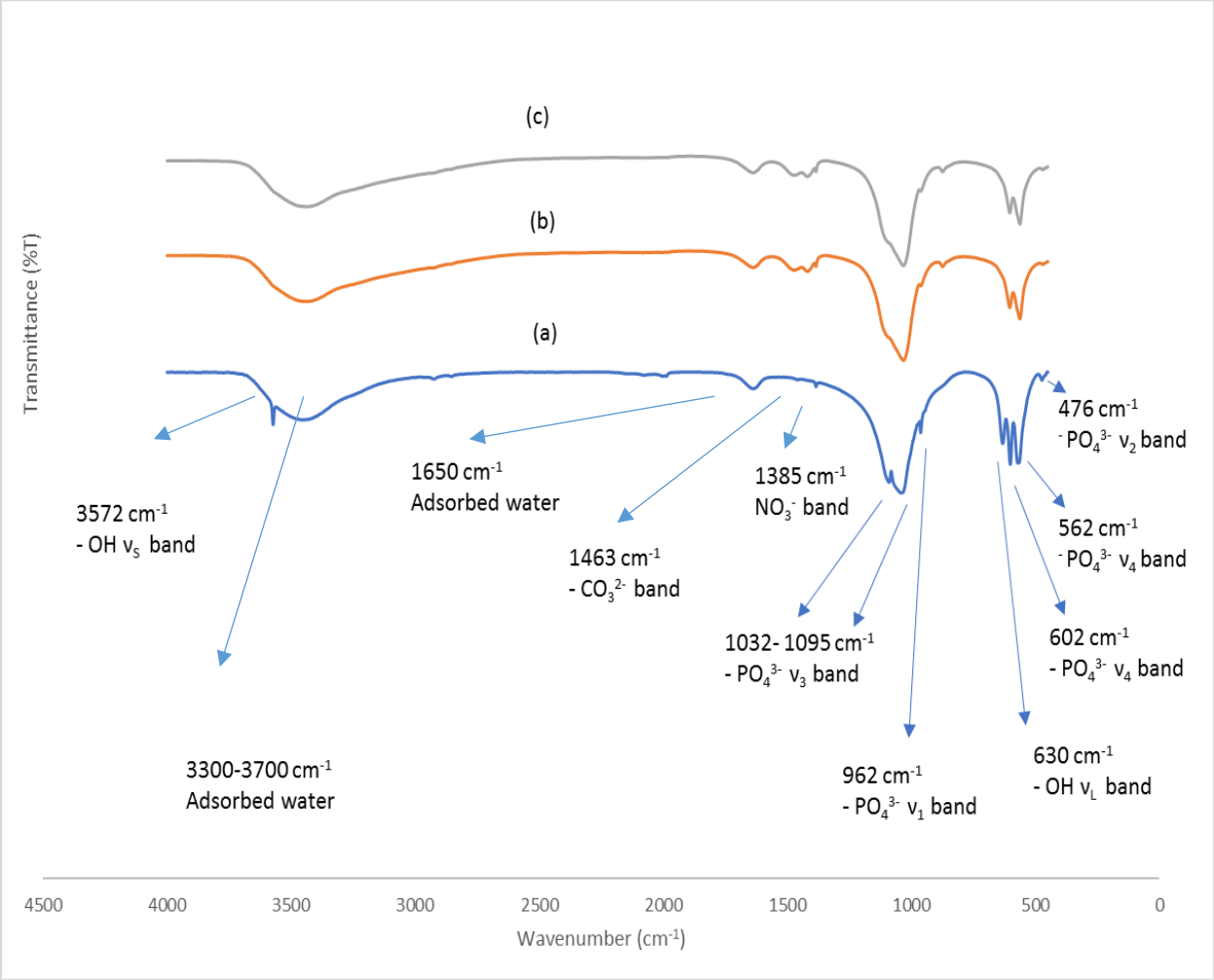

Figure 4-2: FTIR spectra of non-sintered unsubstituted HAp materials from (a) commercial HAp (Fluka) (b) prepared via the hydrolysis method (of MCP/CaOH)$_2$) and (c) prepared via the precipitation method.

As shown in **Fig. 4-2 (a)**, the characteristic bands of phosphate group were recorded at 1095, 1032, 962, 602, 562 and 476 cm^{-1}. The typical bands of hydroxyl group appeared at 3572 and 630 cm^{-1}, confirming the existence of the apatitic phase in the non-sintered commercial HAp (Fluka). Also, the bending vibration band of molecular H_2O at 1630 cm^{-1} and the broad band at 3300–3700 cm^{-1} were recorded as a result of adsorbed water. The carbonate peaks appeared at 1463, indicating substitution of phosphate sites in HAp by CO_3^{2-} (B-type). The typical peak of the nitrate group was also observed at 1385 cm^{-1}.

Also, **Fig. 4-2 (b and c)** shows that **t**he fundamental peaks at 562, 602, 962, 1026 and 1100 cm^{-1} were assigned to the/a phosphate group. The presence of the carbonate group was confirmed

by the appearance of typical bands of carbonate at 875, 1418 and 1470 cm^{-1}. The characteristic band of the nitrate group (NO_3^-) at 1385 cm^{-1}, was also detected by using the precipitation route. The recorded peak at 1385 cm^{-1} through using the hydrolysis method, is believed to be due to the N-O stretching vibration of nitrate ion which was a residual contaminant in the KBr powder used to make the pellets. The broad band at 3300–3600 cm^{-1} and a small band at about 1630 cm^{-1} are related to absorbed water.

Fig 4-3 illustrates the FTIR spectra of sintered unsubstituted HAp powders prepared by the (novel) hydrolysis and conventional precipitation methods compared to sintered commercial HAp (Fluka, at 900 ˚C).

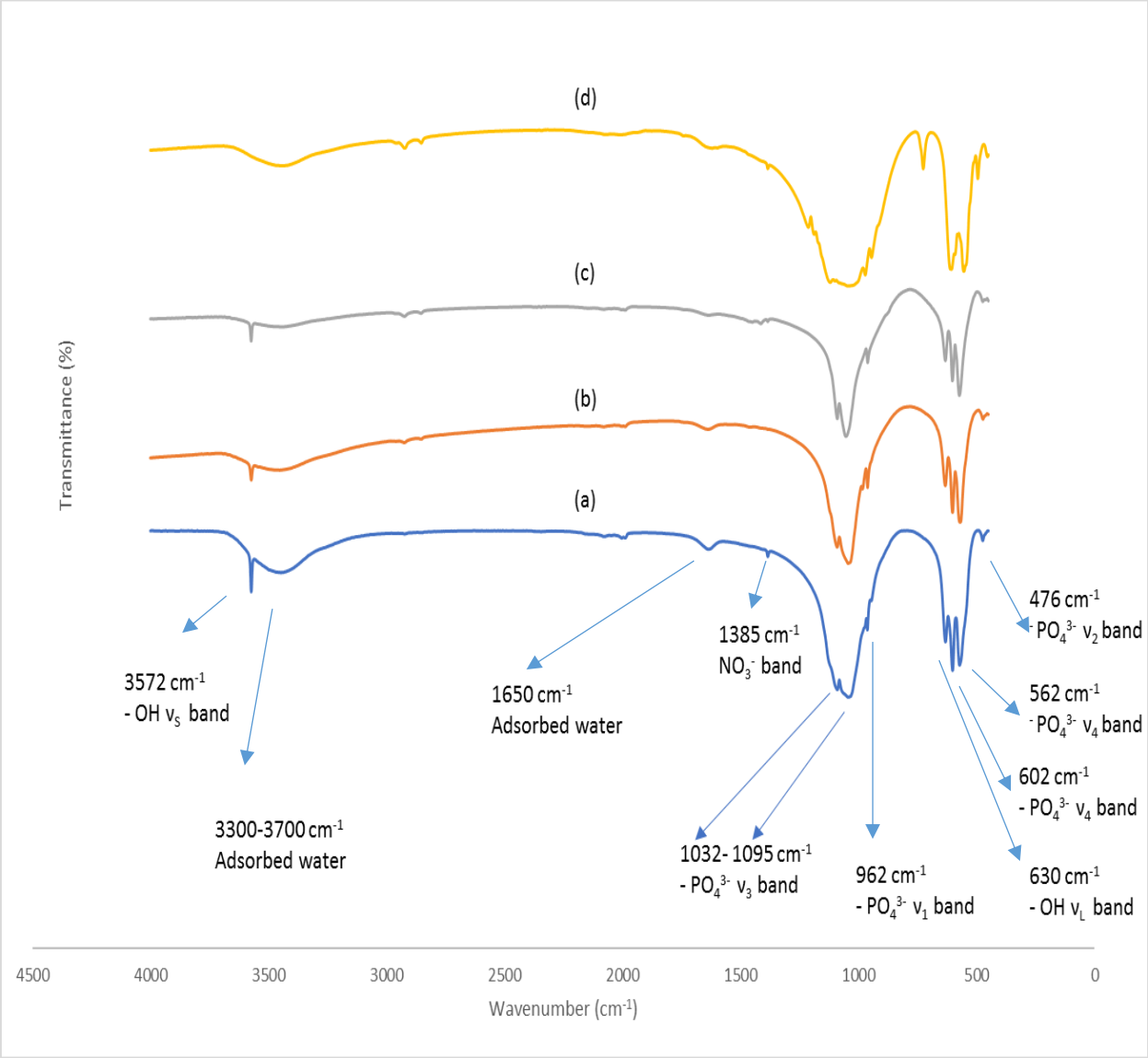

Figure 4-3: FTIR spectra of sintered unsubstituted HAp materials from (a) sintered commercial HAp (Fluka) at 900 ˚C (b) HAp prepared by the novel hydrolysis method (of MCP/$CaOH)_2$), (c) HAp prepared by the precipitation method, and (d) non-sintered commercial (β-TCP).

Fig.4-3 displays the characteristic absorption bands of HAp materials in the prepared samples by using the novel hydrolysis and the precipitation methods, in addition to the commercial HAp (Fluka). As shown in **Fig. 4-3 (a)**, the presence of apatitic phase in the commercial HAp powders (Fluka) can be a proven through detecting the fundamental vibrational modes of the PO_4^{3-} group at 476, 562, 602, 962 and 1032-1095 cm^{-1}, whereas the OH peaks in the commercial samples appeared were obvious at 630 and 3572 cm^{-1}. H_2O-associated vibrational bands due to adsorbed moisture on the powders were also detected at 1650 and 3300-3700 cm^{-1}, and the characteristic

band of nitrate ion (NO_3^-) was also, observed at 1385 cm^{-1}. On the other hand, the FTIR spectra of commercial HAp (Fluka) recorded one of the typical peaks of β-TCP at 944.8 cm^{-1} [168], this observation was associated with a clear change in the shape of P-O bands (v_4 and v_3 bands), indicating the presence of the β-TCP phase in commercial HAp (Fluka).

Fig. 4-3 (b) also, shows the presence of apatitic phase in the unsubstituted HAp powders, which were prepared by using the novel hydrolysis method. The typical bands of the phosphate group appear at 475, 572, 603, 962 and 1033-1090 cm^{-1} in the spectra, while the fundamental stretching and librational modes of the OH^- group at 630 and 3572 cm^{-1} are clearly visible in the prepared samples indicating the highly crystalline materials produced by the sintering process. In much of the research undertaken by others in this area the weak band at 1385 cm^{-1} is attributed to the nitrate ion, (NO_3^-) which comes from the starting calcium nitrate salt precursor [169], but in the case of the novel hydrolysis method described in this study, the small peak appearing at 1384 cm^{-1} can not have emanated from this source because no calcium nitrate source was used as a precursor. It is instead believed to be due to the N-O stretching vibration of nitrate ion which was a residual contaminant in the KBr powder used to make the pellets [169]. This follows given no nitrate group was detected in the MCP and $Ca(OH)_2$ compounds used in preparations by FTIR spectra. The bands that can be ascribed to the adsorbed water [169]were also detected by FTIR spectra at 3300-3700 and 1640 cm^{-1} as shown in **Fig. 4-3.**

The absorption band positions, and their assignments are summarized in **Table 4-4.**

Table 4-4: Assignments of main bands observed generally in the Infrared absorption spectra of unsubstituted HAp.

Peak (cm^{-1})	Assignment	References
3572	Stretching mode, v_s, of hydroxyl groups OH^-	**[170,171]**
1087	Triply degenerate asymmetric stretching mode, v_{3a}, of the P–O bond of phosphate groups PO_4^{3-}	**[171,172]**
1046	Triply degenerate asymmetric stretching mode, v_{3b}, of the P–O bond of phosphate groups PO_4^{3-}	**[171,173]**
1032 (shoulder)	Triply degenerate asymmetric stretching mode, v_{3c}, of the P–O bond of phosphate groups PO_4^3	**[171,173]**

962	v_1 (symmetric P-O stretch) of PO_4^{3-} in hydroxyapatite	**[171,173]**
632	Librational mode of the lattice – OH group within hydroxyapatite	**[171,174,175]**
602	v_4 P-O-P bending modes of PO_4^{3-} in hydroxyapatite	**[171,173,175]**
574 (shoulder)	Triply degenerate bending mode, v_{4b}, of the O–P–O bonds in phosphate groups PO_4^{3-}	**[171,173]**
561	Triply degenerate bending mode, v_{4c}, of the O–P–O bonds of the phosphate group	**[171,173]**
472	Doubly degenerate bending mode, v_{2a}, of the O–P–O bonds in phosphate groups PO_4^{3-}	**[171,173]**
462	Doubly degenerate bending mode, v_{2b}, of the O–P–O bonds in phosphate groups PO_4^{3-}	**[171,173]**

In the FTIR spectra of prepared unsubstituted HAp powders by the precipitation method, similar peaks were observed albeit with slightly different shape. It was hence possible to observe also the fundamental vibrational modes of the PO_4^{3-} group at 475 (v_2), 570 and 605 (v_4), 962 (v_1) and 1035- 1090 cm^{-1} (v_3). The presence of the OH group in the prepared samples was also detected through observation of the stretching vibrational and librational modes at around 3572 and 631 cm^{-1} respectively. The small band at 875 cm^{-1} and the doublet at 1416 as well as 1470 cm^{-1} displayed the presence of carbonate vibration modes and indicated the formation of CO_3HAp (B-type), which indicates a small amount of the PO_4^{3-} groups was replaced by CO_3^{2-}. The incorporation of carbonate during the preparation of HAp is the inevitable result of exposure of the solutions used for preparation of HAp materials to the atmosphere. The CO_3^{2-} ion as mentioned previously can replace OH^- (A-type substitution) and PO_4^{3-} (B-type substitution) at 1500–1545 cm^{-1} and 1410–1470 cm^{-1}, respectively to form the carbonated HAp. Hence, the so-named "**unsubstituted**" HAp produced does have this substituted carbonate in it as a contamination. This was evident in spectra of the powders prior to sintering. The observed band at 1385 cm^{-1} in the sintered unsubstituted powders prepared by precipitation method

can be attributed to the nitrate ion which is a residual from the starting precursor (calcium nitrate) [169].

The FTIR analysis showed clearly that the spectrum of HAp materials prepared by hydrolysis method using MCP and $Ca(OH)_2$ as starting materials were practically identical to that of the other spectra of HAp from other sources (HAp prepared by the precipitation route and the commercial HAp (Fluka)). The presence of the apatitic phase in the synthesized powders prepared by the novel hydrolysis method was evident through detecting the fundamental vibrational modes of PO_4^{3-} group at 562, 602, 962 and 1032-1095 cm^{-1} were detected by FTIR spectra, as well as the typical bands of HAp lattice OH^- group at 3572 and 631 cm^{-1} indicating the formation of crystalline HAp.

4.2.3 XRD diffraction analysis of the prepared unsubstituted hydroxyapatite materials (HAp) by the hydrolysis method (of MCP/$CaOH)_2$):

X-ray diffraction (XRD) as discussed previously (see Chapter 3) has been used to identify phase purity, measure the degree of crystallinity, determine the size of crystallites and to calculate the lattice parameters that are affected by the substitution processes in the HAp lattice. The discussion on this latter aspect is covered more extensively in later chapters. Work presented in this chapter establishes some baseline, "typical" values for "unsubstituted" HAp. (See below):

4.2.3.1 Phase identification of unsubstituted HAp materials prepared by hydrolysis of MCP with calcium hydroxide:

The XRD patterns of the non-sintered and sintered unsubstituted HAp powders that had been prepared by the novel hydrolysis method using MCP (monocalcium phosphate) as a precursor were compared to the XRDs of standard HAp (reference card number 01-074-9780) and commercially supplied MCP and are shown in **Fig. 4-4**. The overall diffraction patterns were in a good agreement with the current literature ([8], [80] as well as the standard HAp (reference card number 01-074-9780) and showed the characteristic peaks of HAp, but there was evidence of some β-TCP phase in the powders due to partial conversion of the pre sintered calcium phosphate phase to TCP during the sintering process at 900 ˚C (see later for evidence of this)**.**

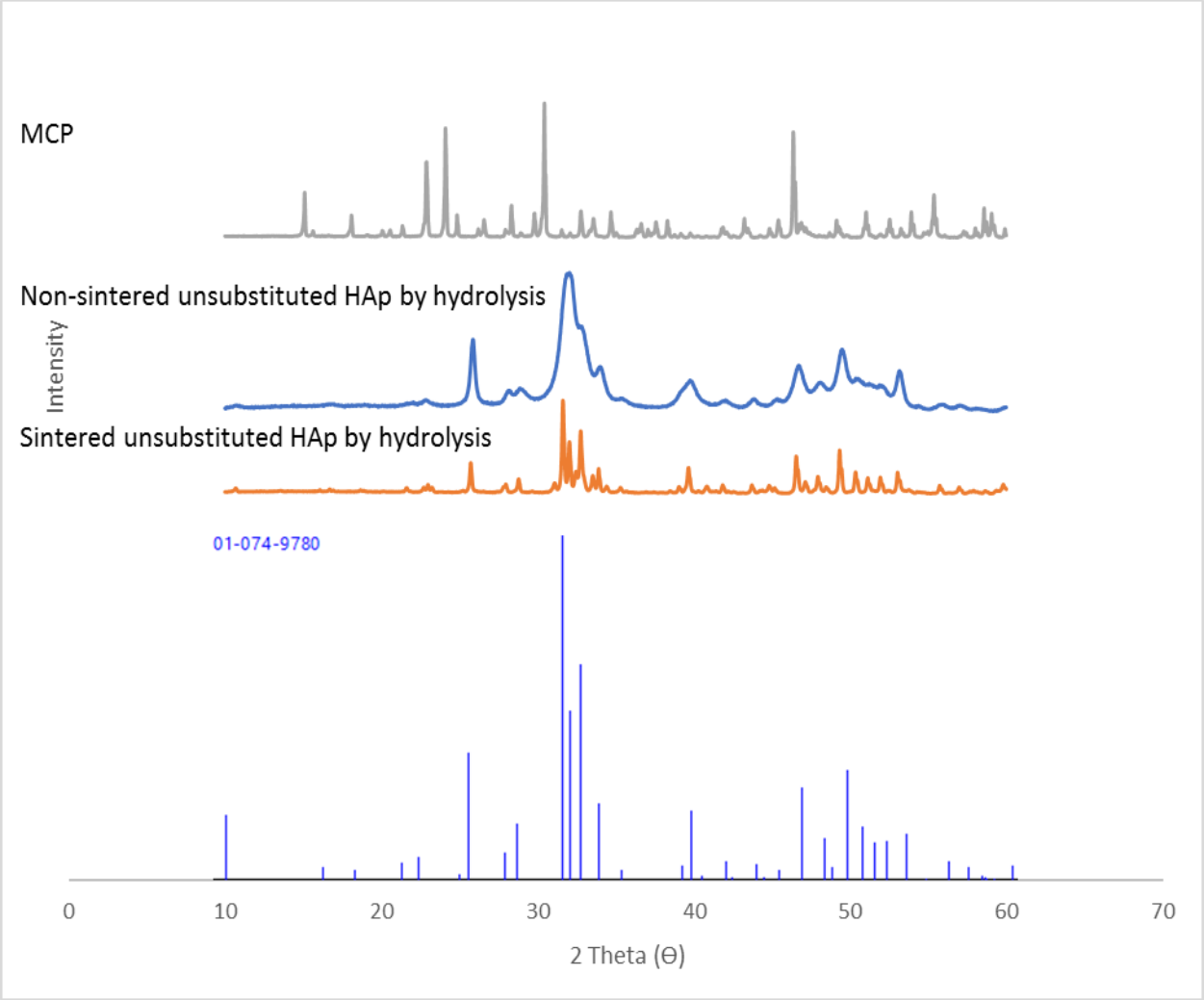

Figure 4-4: The XRD diffraction patterns of as-prepared non-sintered and sintered (at 900 ˚C) unsubstituted HAp materials obtained from hydrolysis of MCP with calcium hydroxide compared to the pattern for standard HAp (reference card number 01-074-9780).

The XRD diffraction patterns of sintered unsubstituted HAp materials prepared by hydrolysis of MCP/$Ca(OH)_2$ and the conventional precipitation methods at 900 °C compared to the patterns of commercial compounds namely, $CaCO_3$, $Ca(OH)_2$ and Na_2CO_3 are displayed in **Figure 4-5.** The diffraction patterns of unsubstituted HAp powders prepared by the novel hydrolysis method were also found to be in a good agreement with the patterns of unsubstituted HAp prepared by the precipitation route. The diffraction patterns of unsubstituted HAp powders prepared by the hydrolysis method did not contain any contributions from peaks that can be attributed to possible reaction by-product compounds such as $CaCO_3$, $Ca(OH)_2$ and Na_2CO_3 .

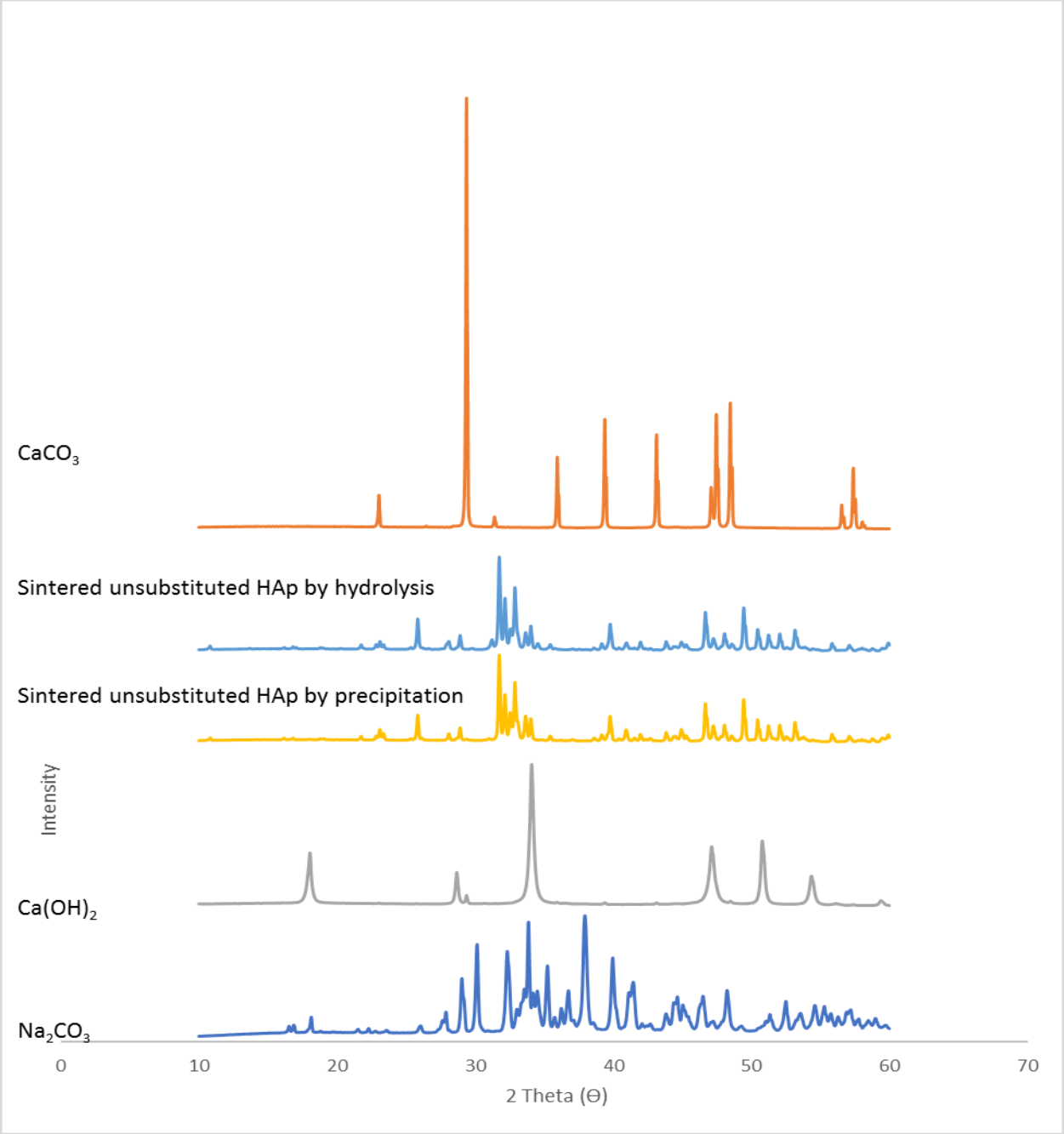

Figure 4-5: The XRD diffraction patterns of the both sintered unsubstituted HAp materials prepared by hydrolysis and precipitation methods at 900 °C, compared to commercial $Ca(OH)_2$, Na_2CO_3 and $CaCO_3$ compounds

The XRD diffraction patterns of commercial β- TCP compared to the sintered commercial HAp (Fluka, at 900 ˚C), non-sintered commercial HAp (Fluka) and both sintered unsubstituted HAp materials prepared by the novel hydrolysis and conventional precipitation routes at 900 ˚C are shown in **Fig.4-6**

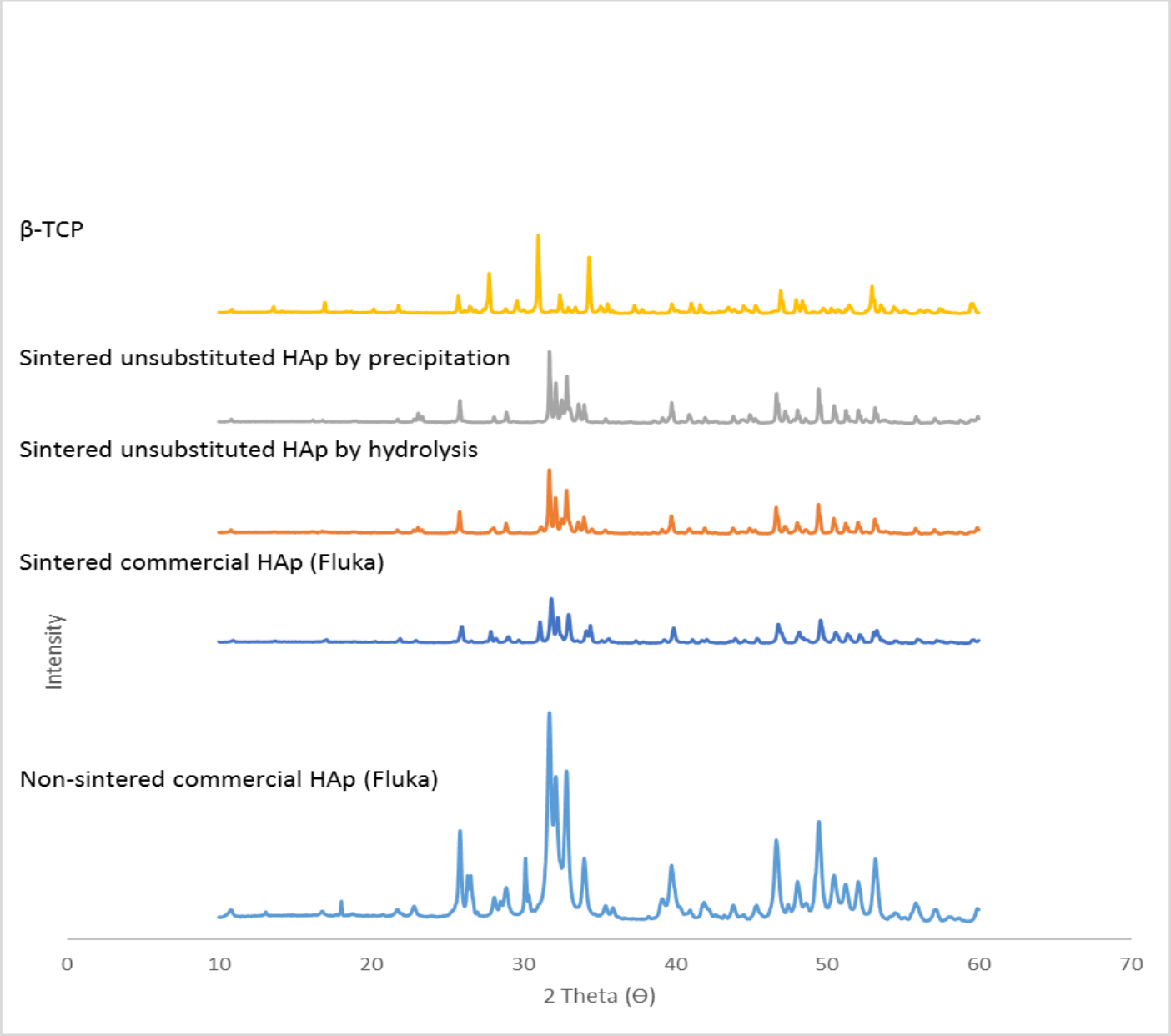

Figure 4-6: The XRD diffraction patterns of commercial β- TCP compared to the sintered commercial HAp (Fluka, at 900 ˚C) and both the sintered unsubstituted HAp materials prepared by the novel hydrolysis and conventional precipitation routes at 900 ˚C.

The XRD diffraction patterns of commercial Na_2HPO_4 and CO_3HAp compounds compared to the sintered commercial HAp (Fluka, at 900˚C) and both sintered unsubstituted HAp materials prepared by the novel hydrolysis and conventional precipitation routes at 900 ˚C are shown in **Fig.4-7.** The diffraction patterns of unsubstituted HAp powders prepared by the hydrolysis and the precipitation methods contained two peaks at 2 Theta = 23.1˚and 38.60˚. These peaks can be

attributed to the (Na_2HPO_4). In the case of the precipitation method, disodium hydrogen phosphate (Na_2HPO_4) was used as starting material. But, in the case of the novel hydrolysis route, these peaks are possibly produced as a by-product compound.

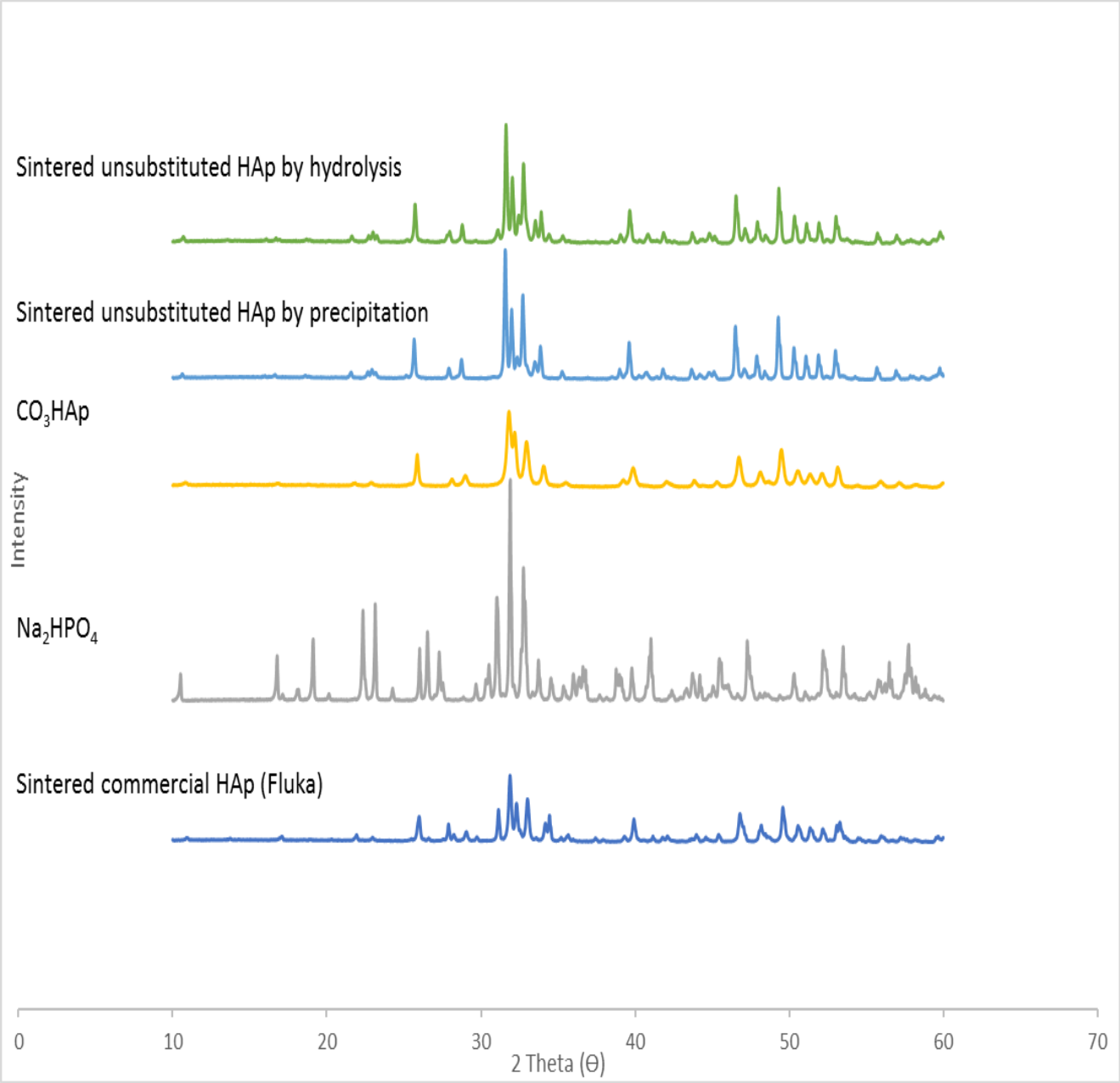

Figure 4-7: The XRD diffraction patterns of commercial Na_2HPO_4 and CO_3HAp compounds compared to the sintered commercial HAp (Fluka, at 900 ˚C) and both the sintered unsubstituted HAp materials prepared by the novel hydrolysis and conventional precipitation routes at 900 ˚C.

Fig. 4-6 revealed that the diffraction patterns of sintered unsubstituted HAp powders prepared by hydrolysis and precipitation methods were found to be in a good agreement with the patterns of sintered commercial HAp (Fluka), but it was evident that some β-TCP phase had formed in all powders due to the sintering process at 900 ˚C.

The presence of β-TCP was observed in the HAP made by both routes (i.e. the hydrolysis and precipitation routes) as indicated by the very weak observed intensities at 2 Theta = 17.19˚, 31.20˚, 32.80˚, 33.60˚, 41.14˚˚, 45.2˚ and 47.36˚. While an additional typical peak corresponding to β-TCP was detected by hydrolysis method at 2Theta= 34.57 ˚. It is well known that BCP (biphasic calcium phosphate compound that contains a mixture of HAp and β-TCP phase) is produced when a synthetic or biologic calcium-deficient apatite (Ca:P molar ratio ranging from 1.33 to 1.65 [176]) is sintered at temperatures ≥ 700 °C [177]. The ICP-MS analysis in the present investigation showed that the sintered unsubstituted HAp materials, which prepared by the hydrolysis and the precipitation methods can be considered as calcium deficient. Two additional peaks with very small intensity at 2 Theta = 23.1˚and 38.60˚ were also confirmed by XRD in both routes (hydrolysis and precipitation) as shown in **Fig. 4-7**. The detected peaks at 2 Theta = 23.1˚and 38.60˚ by using the precipitation routes can be ascribed to the commercial Na_2HPO_4, which was used as a starting material. In the case of hydrolysis route these peaks are possibly produced as by-product compound, due to the presence of these ions into the solution that was used to prepare unsubstituted HAp materials.

The XRD diffraction patterns of commercial HAp (Fluka) showed also, β-TCP in the powder and was an existing impurity phase in the powder despite the powder being labelled as "$Ca_5(PO_4)_5OH$" on the bottle which is the monomeric hydroxyapatite. It was also marketed as "hydroxyapatite" despite being misnamed "Tricalcium phosphate". The TCP phase was indicated by weak peaks at 2 Theta = 27. 90˚, 29.90˚, 31.15˚, 33.80˚, 34.70˚ and 37.6˚.

4.2.3.2 Crystallinity and Crystallite size of unsubstituted HAp materials prepared by the hydrolysis method.

The degree of crystallinity and the crystallite size of the sintered commercial HAp (Fluka, at 900 ˚C) materials compared to sintered unsubstituted HAp materials prepared by hydrolysis and precipitation methods at 900 ˚C are displayed in **Table. 4-5.**

Table 4-5: The degree of crystallinity (%) and the crystallite size (in Angstroms) of sintered commercial HAp (Fluka, at 900 ˚C) compared to sintered unsubstituted HAp materials prepared by hydrolysis and precipitation methods at 900 ˚C.

Sample	D_{002} (Å)	Crystallinity %
Unsubstituted HAp by precipitation	618.3±3.2	84.15±2.4
Unsubstituted HAp by MCP hydrolysis	549.8±3.6	82.57±2.1
Commercial HAp (Fluka)	395.0±2.8	77.31±4.2

The numerical value of crystallinity of the prepared unsubstituted HAp materials by the hydrolysis method as shown in **Table 4-5** indicated that the unsubstituted HAp samples was crystalline (≈82.6%), and that the value of the crystallite size (D_{002}) of the prepared powders as calculated by using the Debye Scherrer formula (see Chapter 3 for details) was ≈549. 8 Å. Both values of crystallinity and crystallite size of the unsubstituted HAp samples prepared by the MCP/$Ca(OH)_2$ hydrolysis route were found to be higher than the values for the sintered commercial HAp (Fluka, at 900 ˚C), but slightly lower than the value obtained by the precipitation method. The degree of crystallinity and the value of crystallite size of the sintered commercial HAp (Fluka) compared to sintered unsubstituted HAp samples prepared by hydrolysis and precipitation routes were as follows: Sintered unsubstituted HAp by precipitation > sintered unsubstituted HAp by hydrolysis > sintered commercial HAp (Fluka).

In the current literature, various values of crystallite size of HAp materials were reported by different studies that were performed through the use of different synthesis routes. In an effort to see any trends in preparation method on crystallite size of HAp produced, **Table 4-6** summarises some of the studies involving preparation and characterization of HAp powders, where the calculated values of crystallite size (D_{002}) for the unsubstituted HAp powders were also placed in that table. It can be seen clearly that different values of crystallite size were obtained even by using the same preparation method.

Table 4-6: the value of crystallite size of HAp powders obtained from different synthesis routes.

Authors	Preparation method	Year	Crystallite size(nm)
This study	Hydrolysis	2023	54.98
Kannan et al. [123]	Precipitation	2006	38.20
Othmani et al. [178]	Co-precipitation	2018	60.90
Capanema et al. [31]	Precipitation	2015	36.53
Maryam Louyeh [179]	Precipitation	2016	73.00
Kaygili et al. [146]	Sol gel	2014	27.46
Stojanović et al.[180]	Hydrothermal	2009	47.71
Nasser Y. Mostafa [181]	Two powders were prepared by chemical precipitation reactions (stoichiometric and calcium deficient HAp powders) and one powder was prepared by a mechanochemical method	2005	141.3 nm for stoichiometric HAp (precipitation). 211.9 nm for calcium deficient HAp (by precipitation). 57.4 for HAp (by a mechanochemical method)

4.2.3.3 Lattice parameter and volume of unit cell measurements of commercial HAp (Fluka) compared to sintered unsubstituted HAp materials prepared by the novel hydrolysis and conventional precipitation methods:

Table 4-7 displayed the lattice constants and volumes of the unit cell of sintered commercial HAp (Fluka, at 900 ˚C) compared to those from the sintered unsubstituted HAp materials prepared by the MCP/$Ca(OH)_2$ hydrolysis method developed in this study and the conventional precipitation methods. The Rietveld refined values of lattice constants for each sample (unsubstituted HAp samples prepared by the precipitation and hydrolysis methods as well as the commercial HAp (Fluka)) were calculated from three replicate samples in the present project and the mean values of the refined lattice constants with errors are summarised in **Table 4-7**.

Table 4-7: The lattice parameters and the volume of hexagonal unit cell of sintered commercial HAp (Fluka HAp sintered at 900 ˚C) compared to the sintered unsubstituted HAp materials prepared by MCP/$Ca(OH)_2$ hydrolysis and precipitation methods at 900 ˚C.

Sample	a [Å]	c [Å]	V[Å^3]
Unsubstituted HAp by precipitation	9.416±0.004	6.879±0.003	1579±0.004
Unsubstituted HAp by hydrolysis of MCP/$Ca(OH)_2$	9.421±0.003	6.882±0.005	1581±0.004
Commercial HAp (Fluka)	9.391±0.005	6.861±0.005	1566±0.005

Table 4-7 shows that the sintered commercial HAp (Fluka, at 900 ˚C) has a smaller volume in its lattice unit cell compared to both unsubstituted HAp powders prepared by the new hydrolysis and conventional precipitation approaches. The volume of the unit cell of the hexagonal structure of commercial HAp (Fluka) and both unsubstituted HAp powders prepared by hydrolysis and precipitation methods was as follows: **V (**unsubstituted HAp by hydrolysis) > **V** (unsubstituted HAp by precipitation) **> V (**commercial HAp (Fluka).

To compare the present results with those of other researchers who have prepared HAp powders via different synthesis methods, **Table 4-8** provides a summary of such investigations, with the refined values of the lattice parameters.

Table 4-8: The value of lattice parameters of HAp materials obtained from different investigations.

Authors	Preparation method	a [Å]	c [Å]	Notice
This study	Hydrolysis	9.4207	6.8823	-
Stojanović et al.[180]	Hydrothermal	9.4296	6.8837	-
Tang et al. [182]	Hydrothermal	9.4082	6.8755	Pure HAp phase.
Evis et al. [129]	Precipitation	9.4322	6.9050	-
Kannan et al. [123]	Precipitation	9.4197	6.8489	Pure HAp phase.
Stanić et al. [8]	Neutralization	9.4261	6.8971	Carbonated HAp as confirmed by FTIR.
Balamurugan et al. [183]	Sol gel	9.4182	6.8810	Pure HAp phase.
Kaygili et al. [146]	Sol gel	9.3950	6.8540	Carbonated HAp as confirmed by FTIR.
Adzila et al. [184]	Mechanochemical	9.4340	6.8860	Carbonated HAp as confirmed by FTIR.
Tian et al. [185]	Mechanochemical	9.4134	6.8818	-

As shown in **Table 4-6** and **Table 4-8,** the calculated values of crystallite size and the refined lattice constants of the prepared HAp samples varied, even though the same synthesis route was used across the different studies.

As an example, Kannan et al. [123] prepared HAp by using the conventional precipitation method. Their group used calcium nitrate tetrahydrate and diammonium hydrogen phosphate as starting materials. The results showed that the lattice parameters a and c were 9.4197 and 6.8489 Å respectively, and the volume V of the hexagonal unit cell was 1573.36 $Å^3$. Evis et al. [129] synthesized HAp samples by the precipitation method using calcium nitrate and ammonium phosphate as precursors. Their results revealed that the lattice constants of the resultant HAp powders were as follows: a = 9.4322 and c= 6.9050 Å, while the volume V of the hexagonal unit cell was 1590.5 $Å^3$. In another investigation Othmani et al. [178] prepared HAp by a co precipitation method using $Ca(NO_3)_2{\cdot}4H_2O$ and $(NH_4)_2HPO_4$ as starting materials. The crystallite size (D_{002}) of the HAp materials produced in that investigation was 60.9 nm. Also, Kannan et al. [123] prepared HAp by using a precipitation method, in which the crystallite size of HAp samples in that investigation was found to be 38.2 nm. The results of the mentioned examples showed

that although the researchers used the same preparation method, the refined values of the lattice constants and the numerical values of crystallite size were very varied. These results can be ascribed to the effect of reaction conditions such as the pH value and the temperature on the values of crystallite size and the lattice parameters (a and c). As an example, Martínez-Castañon et al. [186] prepared calcium deficient hydroxyapatite nanostructured powders with different crystallite sizes and lattice constants by using the precipitation method through varying the pH and temperature parameters. The researchers used $CaCl_2$ and $(NH_4)_2HPO_4$ as starting materials. The pH value as well as the temperature in this study were varied. The result of this investigation showed that the crystallite size and the lattice parameters varied depending on the pH and the temperature. **Table 4-9** shows the reaction conditions, crystallite size and lattice constants of the prepared samples in this investigation.

Table 4-9: the reaction conditions, crystallite size and lattice constants of the prepared samples in this investigation.

	Reaction conditions			Lattice parameters	
Sample label	**pH**	**Temperature (˚C)**	**Crystal size(nm)**	**a (Å)**	**c (Å)**
HA 1	7.00	25.0	19.15	9.47534	6.88520
HA 2	10.0	25.0	10.12	9.55656	6.81409
HA 3	11.0	25.0	16.68	9.58103	6.82260
HA 5	7.00	60.0	25.56	9.43544	6.88774
HA 6	7.00	80.0	26.40	9.48253	6.87898

Table 4-6 and Table 4-8 showed that the refined lattice parameters and the calculated values of crystallite size of the sintered unsubstituted HAp powders, which had been prepared by the novel hydrolysis method in this project were found to be consistent with the current literature and agreed with values obtained from other investigations performed by different researchers**.** This result showed that the novel; hydrolysis method using MCP and calcium hydroxide as precursors to be an effective method to prepare unsubstituted HAp.

4.2.4 SEM of unsubstituted HAp materials prepared by hydrolysis method:

Fig. 4-8 displayed the SEM images of the non-sintered and sintered unsubstituted HAp powders prepared by the novel hydrolysis method, using MCP/$Ca(OH)_2$ as a starting material**.** The SEM

analysis was used to study the surface morphology of the prepared samples at different magnifications (11.0 and 4.50 K) as seen below:

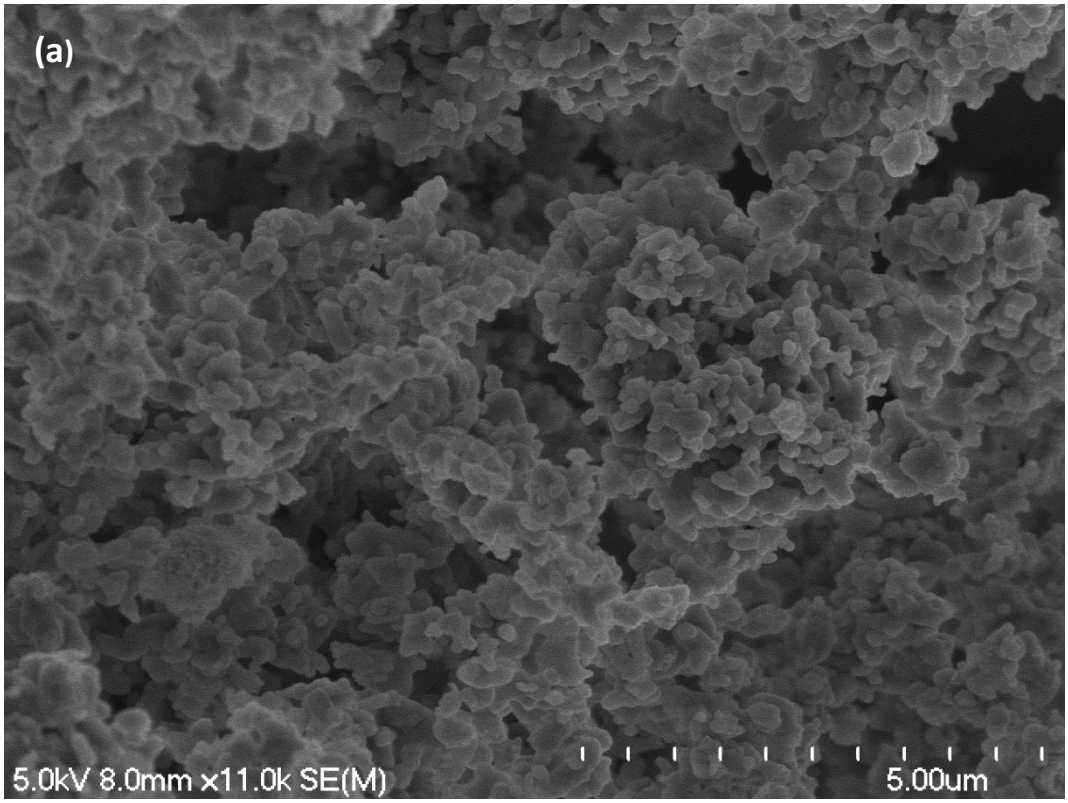

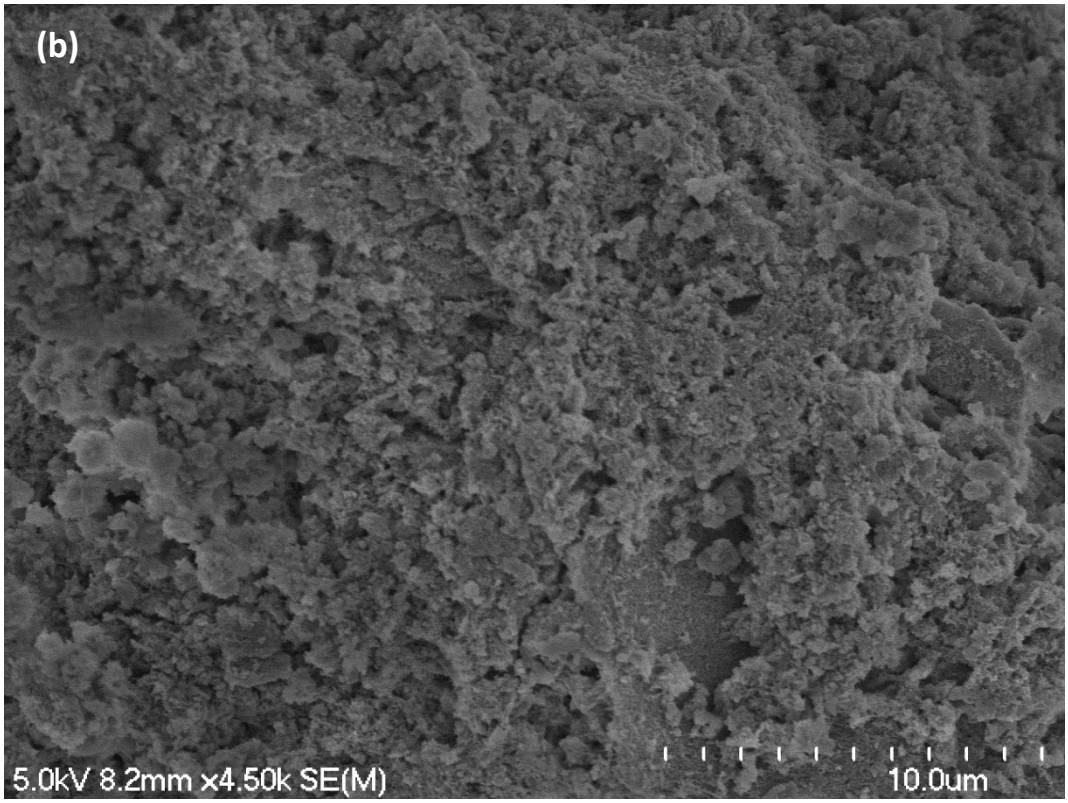

Figure 4-8: SEM images of (a) Unsubstituted HAp prepared from hydrolysis of MCP/$Ca(OH)_2$ sintered at 900 ˚C (b) Non-sintered unsubstituted HAp prepared by hydrolysis of MCP/$Ca(OH)_2$.

Figure 4-8 revealed that agglomeration and irregular distribution of particles were evident in the non-sintered unsubstituted HAp powders prepared by the MCP/$Ca(OH)_2$ hydrolysis route. An obvious enhancement in the crystallinity was confirmed by SEM images due to the heat treatment and calcination process (at 900 ˚C). The sintered samples of unsubstituted HAp samples prepared by hydrolysis of MCP/$Ca(OH)_2$ consist of particles with fine grains, which are spheroidal in shape and associated with an irregular distribution of particles.

The SEM images of sintered commercial HAp (Fluka, at 900 ˚C) compared to the sinteredunsubstituted HAp powders prepared by hydrolysis of MCP/$Ca(OH)_2$ and conventional precipitation routes at 900 ˚C are shown in **Fig. 4-9**.

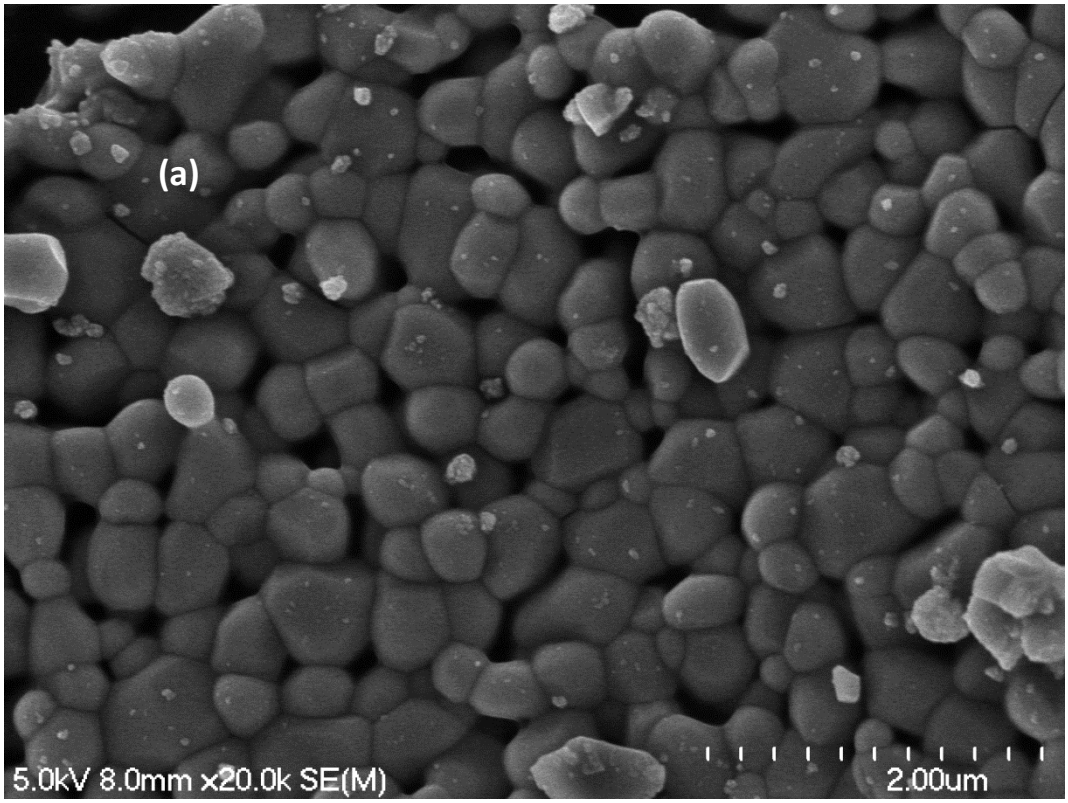
(a)
5.0kV 8.0mm x20.0k SE(M)
2.00um

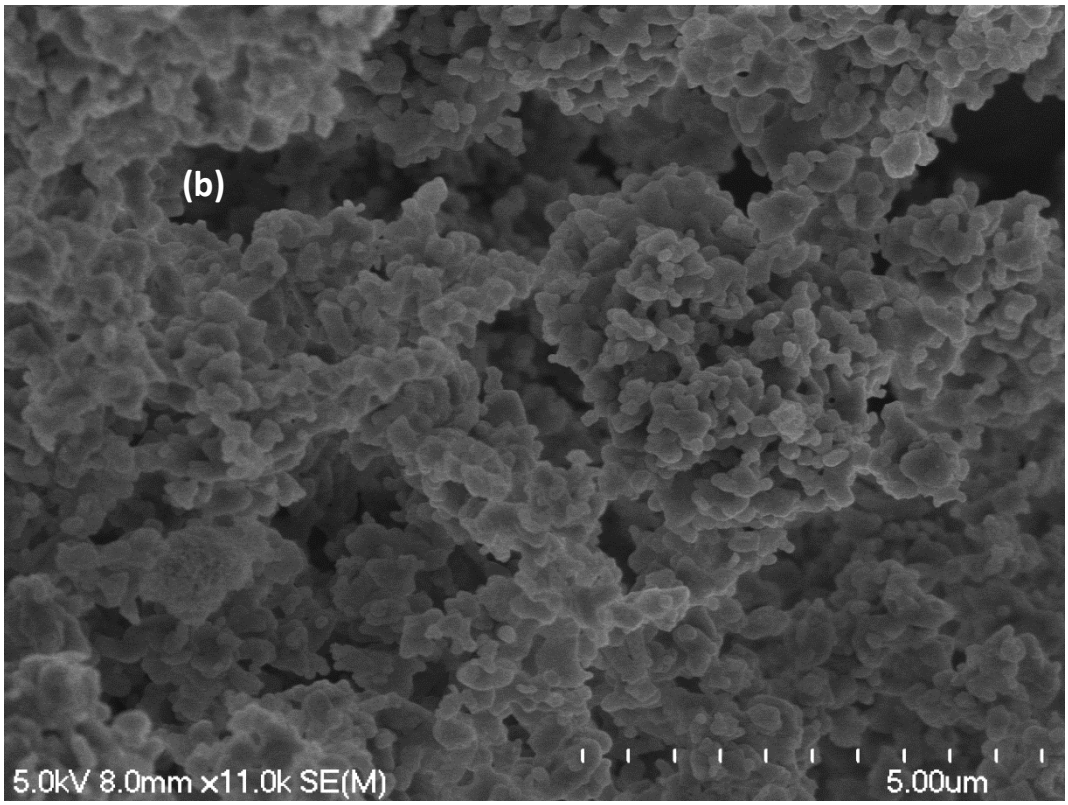
(b)
5.0kV 8.0mm x11.0k SE(M)
5.00um

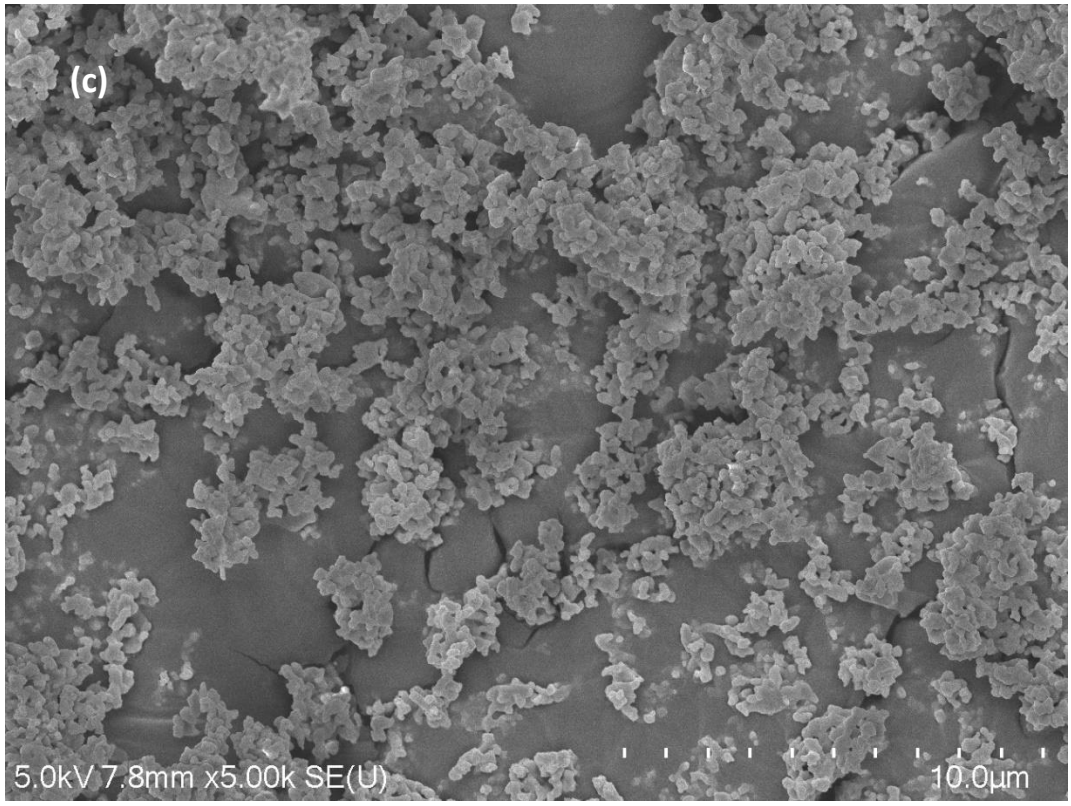

Figure 4-9: SEM images of sintered (a) Unsubstituted HAp prepared by a conventional precipitation route (b) Unsubstituted HAp prepared by hydrolysis of MCP/$Ca(OH)_2$ (c) commercial HAp (Fluka).

Fig.4-9 shows that the unsubstituted HAp materials prepared by the conventional precipitation method consist of a well-defined structure coupled with a homogeneous and regular distribution of particles. As a result, a well packed material was achieved by the precipitation synthesis approach compared to the more porous structure with a lower degree of packing obtained by the MCP/$Ca(OH)_2$ hydrolysis approach. On the other hand, the SEM image in **Fig. 4-9** showed that the sintered commercial HAp (Fluka) consists of fine particles associated with a porous structure and a clear trend to agglomerate. These observations may be attributed to the effect of the original synthesis route for the commercial HAp, starting materials and chemical composition, since the effect of the preparation method on the degree of crystallinity and the chemical composition was confirmed by XRD analysis and ICP-MS measurements. As shown in **Table 4-4,** the degree of crystallinity for both unsubstituted HAp powders prepared by hydrolysis of MCP/$Ca(OH)_2$ (≈82.6%) and the conventional precipitation (≈ 84.1%) methods was higher than for the commercial HAp (Fluka) (≈77.3%). This enhancement in the value of crystallinity

results in a well-defined structure with suitable arrangement of the atoms and also decreases the level of porosity.

4.2.5 Previous results from other studies in the literature where the hydrolysis method has been used to prepare HAp:

The use of hydrolysis as a method to prepare HAp is not new and previous reports do exist where different HAp precursors have been used. As reported by Shi Donglu [35], HAp powders can be obtained through the hydrolysis process of other calcium phosphate compounds such as dicalcium phosphate dihydrate (DCPD), octacalcium phosphate and tricalcium phosphate (TCP). Therefore, different researchers have prepared HAp materials through using the hydrolysis approach with these. Some examples of these investigation have been summarized in **Table 4-10** below:

Table 4-10: investigation of hydroxyapatite materials by using a hydrolysis method based on OCP (ocatacalcium phosphate) and DCPD (dicalcium phosphate dihydrate) as starting materials and with water as well as 1 M of sodium phosphate solution as the hydrolyzing agent.

Authors	Preparation method	The results
Stephan and Paul [187]	The authors studied the hydrolysis process of ocatacalcium phosphate (OCP) to HAp.	The result of their investigation showed conversion of OCP to HAp occurred by direct hydrolysis of OCP or by the hydrolysis process of OCP with other calcium phosphate compounds. The authors reported that i) the direct conversion of OCP to HAp phase occurred slowly. ii) The conversion process of OCP to HAp phase was more rapid when OCP was hydrolyzed with tetracalcium phosphate (TetCP), since the reaction of OCP with TetCP resulted in the formation of phase-pure HAp. iii) the rate of hydrolysis of OCP to an HAp phase was reduced when calcium hydroxide was present.
Fulmer and Brown [188]	The authors investigated the hydrolysis process of dicalcium phosphate dihydrate (DCPD) in water and in 1 M Na_2HPO_4 solution at temperatures from 25—60 °C.	The result of this investigation showed that the hydrolysis process of (DCPD) was incomplete in water i) at 25 °C, DCPD was partially hydrolyzed to hydroxyapatite (HAp), ii) at the higher temperatures, hydrolysis to HAp was more extensive and was accompanied by the formation of anhydrous dicalcium phosphate (DCP) iii) when hydrolysis was carried out in 1 M Na_2HPO_4 solution, the complete conversion to HAp phase had occurred in this solution. Also, the results of that investigation showed that the sodium phosphate solution caused a morphological change to the HAp. When the HAp, was formed by hydrolysis in water it had needle-like morphology when formed at 25 ˚C and a globular morphology when formed at 60 ˚C. In contrast, the HAp formed in the sodium phosphate solution exhibited a florette-like morphology.

H. Monma [189]	The researcher studied the conversion process of brushite (DCPD) into an HAp phase by a hydrolysis method. The preparation of HAp was studied through two stages as shown below: DCPD→ HAp (Ca/P < 1.67) … (I) DCPD→ HAp (Ca/P = 1.67) …(II)	In reaction (I), HAp formed rapidly at pH 7.5-8, with complete conversion observed at 40 ˚C within 2.5 hours of reaction, 1 hour of reaction at 60 ˚C and within 5 minutes of reaction at 80 ˚C. The composition of HAp was non-stoichiometric and had a Ca/P ratio below 1.60. In reaction (II), the reaction was carried out in alkaline solution with addition of $CaCl_2.2H_2O$ as a source of calcium ions to increase the Ca/P ratio. The result obtained showed that HAp with a stoichiometric Ca/P mole ratio was obtained at 40 ˚C after three hours of reaction at pH 9-10, and after 1 hour of reaction at pH =13. The SEM images displayed that the HAp powders prepared from DCPD were composed of dense aggregates consisting of irregular thin microcrystals.

4.3 Summary:

A summary of the findings for this chapter ca be outlined as the following:

1- A novel hydrolysis method to prepare HAp using monocalcium phosphate and calcium hydroxide as starting materials showed clearly that this route can be considered an effective approach for preparing unsubstituted HAp powders.

2- Different techniques were used to characterize the prepared samples such as SEM, FTIR, XRD and ICP-MS. This led to the following results:

- The presence of an apatitic phase in the sintered unsubstituted powders prepared by the MCP/$Ca(OH)_2$ hydrolysis method was confirmed by FTIR spectra, through detecting the fundamental vibrational modes of PO_4^{3-} group as well as by observation of the typical HAp lattice OH vibrations at 3572 and 631 cm^{-1}so indicating formation of crystalline material. This result was also confirmed through comparing the result of FTIR spectra of sintered unsubstituted HAp samples which was prepared by hydrolysis with those of sintered commercial HAp (Fluka) and unsubstituted HAp powders that were synthesized by a conventional precipitation route.
- The XRD diffraction patterns of sintered unsubstituted HAp powders that were prepared using the novel hydrolysis method were in a good agreement with the HAp patterns reported in the current literature ([8], [80], [190]), standard HAp (reference card number 01-074-9780) as well as commercial HAp (Fluka) and showed the characteristic peaks of the HAp phase, but also showed a slight presence of the β-TCP phase due to the sintering process at 900 ˚C. It is well known that BCP (biphasic calcium phosphate)which is a mixture of HAp and β-TCP phase, is produced when a synthetic or biogenically sourced calcium-deficient apatite is sintered at temperatures ≥ 700 °C [177].
- The ICP-MS analyses of HAp powders produced in the present study showed that the sintered unsubstituted HAp materials prepared by the novel hydrolysis method is calcium deficient because Ca/P mole ratios of 1.40 were measured which was ascribed to the substitution process of calcium ions by sodium ions in the HAp crystal lattice as a result of using sodium hydroxide to adjust pH in the reactions leading to the formation of HAp. Also, the value of (Ca+Na)/P when computed from the ICP-MS

analyses was found to be 1.65 which is very close in value to the value expected for stoichiometric HAp (1.67).

- SEM images revealed that agglomeration and irregular distributions of particles were evident in the non-sintered unsubstituted HAp powders prepared by the novel hydrolysis route, with an obvious enhancement in crystallinity being confirmed due to the sintering process (at 900 ˚C). The sintered unsubstituted HAp materials prepared by the hydrolysis of MCP/$Ca(OH)_2$ consist of particles with fine grains, which are spheroidal in shape and associated with an irregular distribution of particles.
- The degree of crystallinity and the value of the crystallite size of sintered unsubstituted HAp powders prepared by the novel hydrolysis method in the present study were found to be higher than that observed for the sintered commercial HAp (Fluka), since the measured values for the degree of crystallinity and the crystallite size of sintered unsubstituted HAp samples prepared by hydrolysis were found to be ≈ 82.6% and 549.8 respectively, compared to that of the sintered commercial HAp (Fluka) (77.3% and 395.0 um).

Chapter Five

Preparation of (cationic) metal ion substituted HAp powders with the following chemical formula: $Ca_{10-x}M_xHAp$ (where M=Zn, Sr and Cu, X=0.5, 1.0 and 1.5) by a novel hydrolysis method using $MCP/Ca(OH)_2$.

5.1 Introduction:

M doped hydroxyapatite powders (where M=Zn, Sr and Cu) with different level of substitutions were prepared by the novel hydrolysis method using $MCP/Ca(OH)_2$. No studies to the author's knowledge on the synthesis of Zn, Cu and Sr substituted HAp by the hydrolysis method using $MCP/Ca(OH)_2$ as a starting material have been published previously in the chemical literature. In previous scientific studies, ZnHAp, SrHAp and Cu-substituted HAps have been prepared using different synthesis methods [131,191-195] other than hydrolysis.

For the present study, strontium chloride hexahydrate ($SrCl_2.6H_2O$), zinc nitrate hexahydrate ($Zn(NO_3)_2.6H_2O$) and cupric chloride ($CuCl_2$) were used as source chemicals to substitute Zn^{2+}, Sr^{2+} and Cu^{2+} ions into the HAp lattice, due to their good solubility and availability. The stoichiometric amounts of the substituent metal ion precursors were added to monocalcium phosphate and calcium hydroxide-containing solutions to obtain substituted HAp powders, that were characterized by the following chemical formula $Ca_{10-x}M_x(PO_4)_6(OH)_2$, where (M = Zn, Sr or Cu) and ($0 \leq x \leq 1.5$). The unsubstituted hydroxyapatite was named unsubstituted HAp, whereas the samples where x= 0.5, 1.0 and 1.5 were named respectively 0.5 MHAp, 1.0 MHAP and 1.5 MHAp (where M= Zn, Sr or Cu). Gallo [2] also used this way to distinguish between his samples when he prepared FHAp materials with different levels of fluoride (F^-) ions.

This chapter aimed to:

1- Investigate the ability of the new MCP/$Ca(OH)_2$ hydrolysis preparation method to be used as an effective method to synthesize substituted HAp powders in a direct manner.

2- Prepare different systems of cationic substituted HAp materials (ZnHAp, SrHAp and CuHAp) with different substitution levels through using the new MCP/$Ca(OH)_2$ hydrolysis method with the following chemical formula ($Ca_{10-x}M_x(PO_4)_6(OH)_2$, where M= Zn^{2+}, Sr^{2+} and Cu^{2+}, whereas x=0.5, 1.0 and 1.5) at room temperature followed by calcination at 900 ˚C.

3- Investigate the effect of the new MCP/$Ca(OH)_2$ hydrolysis method on the chemical composition, morphology, crystallinity, crystallite size and phase purity of the prepared materials.
4- Study the effect of substitution levels on several characteristics of prepared substituted materials such as the chemical composition, the morphology, the crystallinity, crystallite size, lattice parameters and phase purity.
5- Investigate the relationship between the peak intensities of the lattice OH^- group in HAp (vibrational modes which appear at 3572 cm^{-1} and 630 cm^{-1}) and the level of substitutions, since an obvious decrease in the intensities of these peaks was observed as a result of the substitution process of Zn^{2+}, Sr^{2+} and Cu^{2+} ions into the HAp crystal. The details of this observation are discussed further in this chapter.
6- Study the relation between the substitution levels of some specific systems (SrHAp materials) and the clear shift of the phosphate bands at (572 and 604 cm^{-1}) to lower wavenumbers due to the substitution of Ca^{2+} ions with Sr^{2+} ions, where this shift increased as the level of substitution of Sr ions increased in the HAp lattice. The details of this observation are also discussed in this chapter.
7- Study the effect of the substitution of Ca^{2+} ions for Zn^{2+} ions into the HAp lattice on the phase purity, since results clearly showed that substitution of zinc ions can be used as a catalyst for the conversion process of HAp into a β-TCP phase.
8- Study the ability of Cu^{2+} ions to replace the proton on the OH lattice site as reported by Imrie et al. [196].

The following techniques were used to characterize the above substituted HAp powders and the results of these characterizations are discussed extensively in this chapter.

1- Scanning electron microscopy (SEM).

2- FTIR spectroscopy.

3- Powder X-ray Diffraction (XRD).

4- Inductively coupled plasma mass spectrometry (ICP-MS) analysis for probing elemental levels of powders. This provided an idea of what was "associated" with the powders element wise (aside from Ca and P) but was not actual proof of substitution.

5.2 The preparation of Zinc ion substituted hydroxyapatite (ZnHAp) materials by the novel MCP/$Ca(OH)_2$ hydrolysis method:

Three series of ZnHAp powders with different Zn^{2+} contents (0.5 ZnHAp, 1.0 ZnHAp and 1.5 ZnHAp powders) were prepared by the novel hydrolysis method. The exact amounts of reagents used to prepare these are listed T**able 5-1.**

Table 5-1: Synthesis details of ZnHAp powders prepared by the MCP/$Ca(OH)_2$ hydrolysis method.

Sample	MCP $Ca(H_2PO_4)_2$ (g)	$Ca(OH)_2$ (g)	$Zn(NO_3)_2.6H_2O$ (g)	$Ca(H_2PO_4)_2$ (mol)	$Ca(OH)_2$ (mol)	Zn (mol)	Expected Ca/P
Unsubstituted HAp	11.6487	3.6875	-	0.0498	0.0498	-	1.67
0.5 ZnHAp	10.9228	3.4603	0.7295	0.0467	0.0467	0.0025	1.58
1.0 ZnHAP	10.2268	3.2312	1.4434	0.0437	0.0436	0.0049	1.50
1.5 ZnHAp	9.5426	3.0307	2.1400	0.0408	0.0409	0.0072	1.42

5.3 Characterization of ZnHAp powders prepared with different Zn^{2+} content by the novel MCP/$Ca(OH)_2$ hydrolysis method.

5.3.1 ICP-MS studies of sintered ZnHAp materials prepared by hydrolysis of MCP/$Ca(OH)_2$ at 900 ˚C with different levels of Zn^{2+} substitution.

The results of the elemental analyses of the ZnHAp samples are displayed in **Table 5-2 .**

Table 5-2: ICP-MS results of ZnHAp materials from the present study which were at 900 ˚C with different levels of Zn^{2+} substitution as prepared by the hydrolysis reaction. Concentrations are quoted in ppb (ug/L):

Sample	Ca 44	P 31	Na 23	Zn 66
Unsubstituted HAp by hydrolysis	707795	401240	103797	-
0.5 ZnHAp by hydrolysis	697527	380678	112772	30472.3
1.0 ZnHAp by hydrolysis	649564	369636	106468	57649.5
1.5 ZnHAp by hydrolysis	647610	360929	88148	94942.8

The starting (calculated) and actual (measured) degree of chemical composition of the prepared powders in terms of wt.% of Zn^{2+} ions, the calcium/phosphorus (Ca/P) molar ratios as well as (Ca+Na+Zn)/P molar ratio were determined by ICP-MS and presented in **Tables 5-3.** The details of these calculations can be found in Appendix A (see appendix A) through one computed example involving 0.5 ZnHAp powders prepared by the novel hydrolysis method.

Table 5-3: The chemical analysis data of prepared ZnHAp materials after sintering at 900 ˚C with different Zn^{2+} contents by ICP-MS measurements.

Sample	Ca/P Theoretical	Ca/P Measured	(Ca+Na+Zn)/ P Measured	Wt.% of Zn^{2+} ions theoretical	Wt.% of Zn^{2+} ions measured
Unsubstituted HAp by hydrolysis	1.67	1.40	1.65	-	-
0.5 ZnHAp by hydrolysis	1.58	1.42	1.85	3.2%	1.5%
1.0 ZnHAp by hydrolysis	1.50	1.36	1.82	6.3%	2.9%
1.5 ZnHAp by hydrolysis	1.42	1.39	1.84	9.4%	4.7%

Tables 5-2 and **5-3** showed the detection of zinc and sodium ions in the HAp crystal samples, which indicated the replacement of calcium ions by sodium and zinc ions had taken place. Therefore, a clear reduction in the measured values of Ca:P mole ratios for the prepared ZnHAp powders was demonstrated by the ICP-MS measurements, but the measured values of (Ca+Na+Zn)/ P were found to be higher than the expected (stoichiometric) value (1.67) for hydroxyapatite. As this result could not be attributed to the formation of B-type-CO_3 substituted HAp powders, (FTIR spectra showed no evidence of the presence of carbonate ions in the sintered

ZnHAp powders), it is thus believed that this observation can be ascribed to the formation of biphasic compound mixtures as detected by XRD analysis which consequently affects the values of the (Ca+Na+Zn)/ P mole ratios.

On the other hand, **Table 5-3** displayed clearly that the measured (actual) wt.% of zinc ions that were presented into HAp samples is lower than the theoretical value indicating how difficult it is for the small ions such as Zn^{2+} to be introduced and hosted by the HAp. The details of these calculations can be found in Appendix A through the illustration of two computed examples involving unsubstituted HAp and 0.5 ZnHAp materials that were prepared by hydrolysis of MCP/$Ca(OH)_2$.

5.3.2 FTIR studies of ZnHAp prepared with different levels of Zn^{2+} substitution.

5.3.2.1 FTIR of non-sintered (as received) ZnHAp (prepared by hydrolysis of MCP/$Ca(OH)_2$)

The FTIR spectra of the Zn-substituted powders with different levels of substitution are shown in **Fig.5-1**.

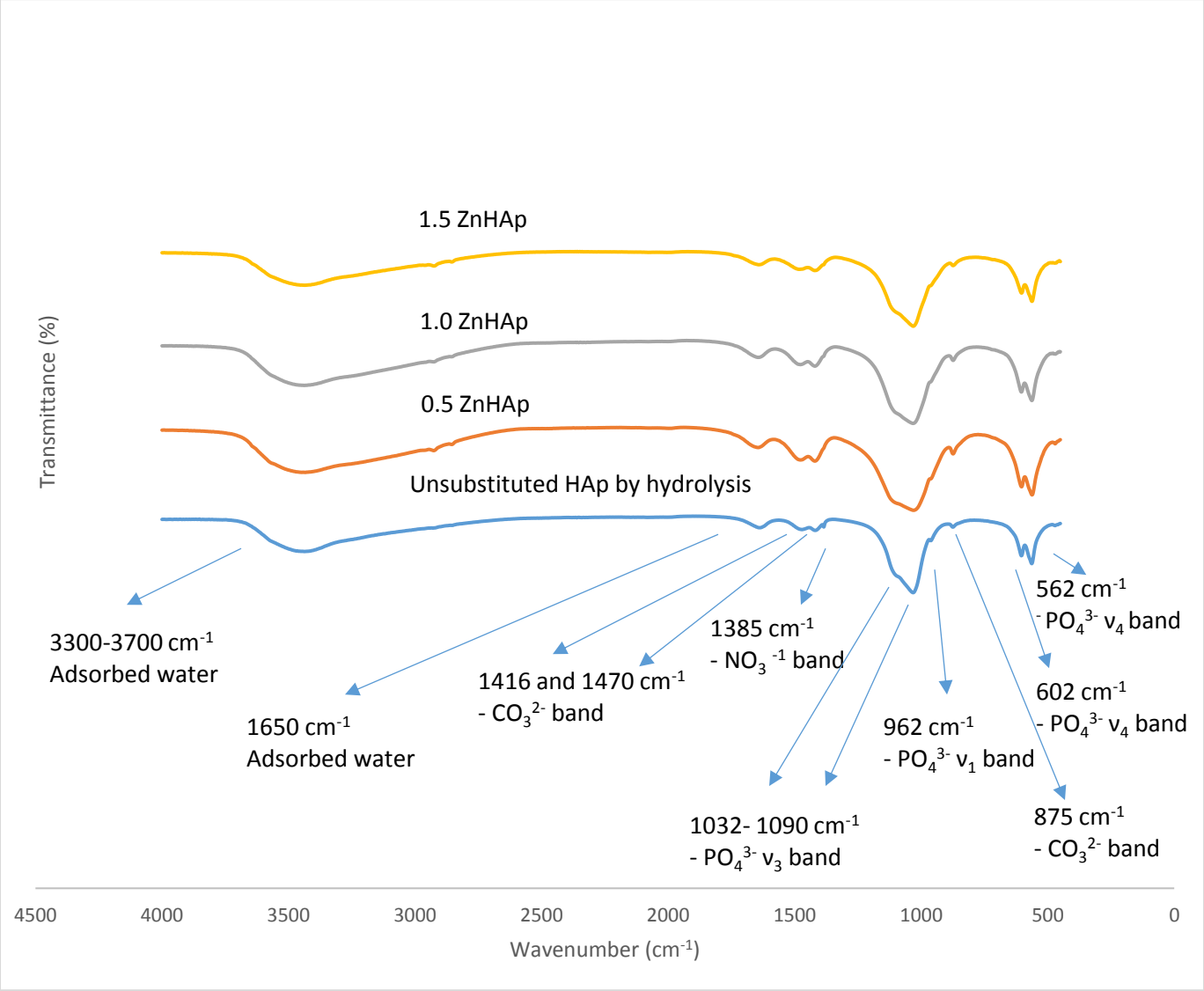

Figure 5-1: FTIR spectra of non-sintered zinc substituted hydroxyapatite with different Zn^{2+} content prepared by the MCP/$Ca(OH)_2$ hydrolysis method.

The FTIR is a common technique used to characterize and identify the covalent bonds, therefore any evidence or information related to the incorporation of metals cations into the crystal structure of HAp is not possible. As a result, the produced samples should have approximately the same FTIR spectral profiles with no obvious difference between samples in their spectra, since all powders have the same functional groups present (i.e. PO_4^{3-}, OH^- and CO_3^{2-}). The replacement process of the calcium site by metal ions could be confirmed by using other techniques such as XRD analysis, as the substitution of any ions or functional groups into the HAp crystal lattice should cause change in the lattice parameters a and c.

Fig.5-1 shows a broad band at 3000–3700 cm^{-1} as detected in all unsintered ZnHAp samples which was assigned to the O-H stretching band of adsorbed water with the peak at 1630 cm^{-1} attributed to the bending mode of H_2O. It was noted that sharp peaks expected to be at 3572 and 630 cm^{-1} due to lattice OH in HAp were not detected in the spectra of the non-sintered HAp materials which was taken as evidence of their amorphous/poorly crystalline state when initially prepared by the hydrolysis route. The presence of peaks at 562, 602, 962 and 1032-1090 cm^{-1} is due to the fundamental vibrational modes of phosphate group as discussed in Chapter 4. The carbonate-associated peaks appear in all samples at 875, 1416 and 1470 cm^{-1} and can be ascribed to the formation of carbonate-substituted hydroxyapatite where phosphate sites in HAp (B-type) are replaced by carbonate ions.

5.3.2.2 FTIR spectra of ZnHAp after sintering at 900 ˚C:

In contrast, The FTIR spectra of the sintered ZnHAp powders with different level of substitutions are shown in **Fig.5-2.** Spectra of other phases known to be present in the sintered HAp samples are also shown for comparison.

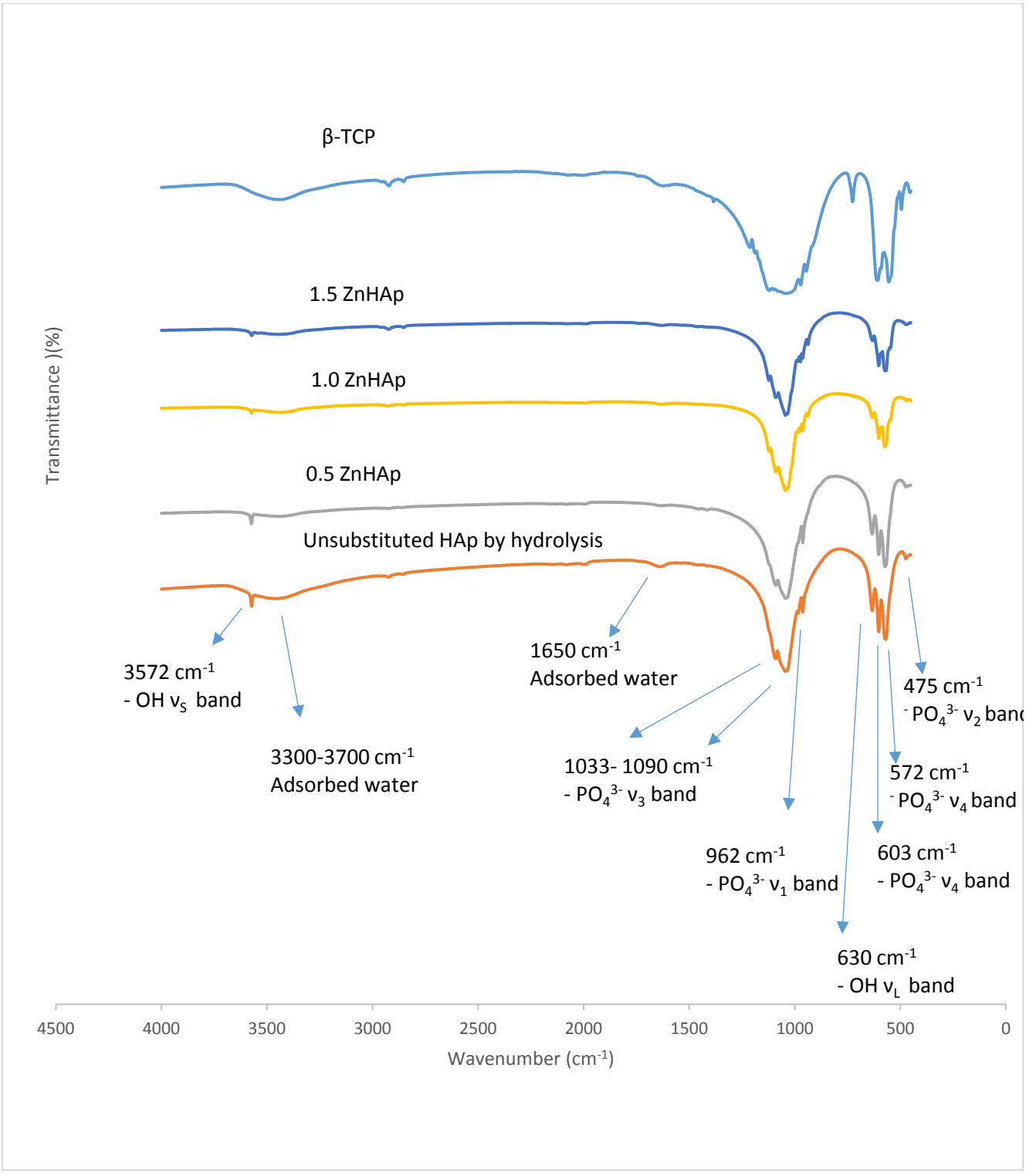

Figure 5-2: FTIR spectra of Zinc substituted hydroxyapatite materials with different Zn^{2+} contents as prepared by the novel MCP/$Ca(OH)_2$ hydrolysis method after sintering at 900 ˚C.

The relative intensities of both functional groups in the HAp samples, namely the hydroxyl and phosphate groups, decreased as the percentage of substitution of Zn^{2+} ions were increased in the hydroxyapatite lattice structure. The decrease of peak intensities at around 570, 603 and 1035 cm^{-1} in the FTIR spectra of the sintered ZnHAp materials occurred as the amount of substitution increased. Two additional peaks were observed in the case of the 1.0 ZnHAp and 1.5 ZnHAp powders at 946 and 1108 cm^{-1}; these peaks can be explained as being associated with the formation of β-TCP so forming a biphasic calcium phosphate (BCP) mix [168]. The broad band at 3000–3700 cm^{-1} and the small peak at about 1635 cm^{-1} that corresponds to adsorbed water were observed but in much lower intensity in all spectra of the sintered ZnHAp powders. The OH stretching and librational modes at 3572 and 631 cm^{-1} in the sintered ZnHAp samples were clearly detected in the FTIR spectra. The typical peaks of carbonate at (1454, and 1418 and 875 cm^{-1}) did not, however, appear in the sintered 1.0 ZnHAp and 1.5 ZnHAp samples due to the sintering process at 900°C. In other words, calcination leads to carbon dioxide release due to the decomposition of carbonate into CO_2[197]. On the other hand, the FTIR spectra also revealed that, as the amount of Zn substitution in the HAp increased, a decrease in the intensities of the HAp lattice OH^- stretching peak at 3572 cm^{-1} and the corresponding OH librational mode at 630 cm^{-1} was observed. This peak intensity decrease can be attributed to:

1- The change in the local environment of the OH groups, that occurs as a result of substitution of Ca^{2+} ions by Zn^{2+} ions. In other words, increasing the zinc ions concentration changes the local environment of the OH groups (Zn^{2+} ions substitute some of the calcium ions located on the CaII site). This indicates that not all of the calcium ions surrounding an OH group were replaced by Zn^{2+} ions. Therefore, Partial Zn^{2+} substitution for Ca^{2+} distorts the symmetric environment of the OH groups and, as a result, the intensity of stretching and librational modes of the OH^- group decreased.
2- As a result of increasing the zinc ions, less HAp phase was produced. Therefore, a reduction in the stretching and libration modes of OH^- group produced. Formation of BCP (biphasic calcium phosphate compound that contains a mixture of HAp and β-TCP phase) with increasing the substitution level of Zn^{2+} ions (see **Table 5-4**). As a result, less HAp phase was produced. Therefore, a reduction in the intensities of the HAp lattice OH^- stretching and libration modes at 3572 and 630 cm^{-1} were observed.

Bulina et al. [198] observed the same result when they prepared SrHAp by a mechanochemical method. They reported that as the strontium ion concentration in the HAp increased, the intensity of the OH librational bands (630 cm^{-1}) dropped sharply, while the intensity of the HAp lattice OH stretching vibration (3572 cm^{-1}) also decreased, albeit, slightly. They found that increasing the level of strontium ion substitution in the HAp lattice led to a change in the local environment of the OH groups, since Sr ion replaced some of the Ca^{2+} ions which are located at the Ca(II) site in the lattice. As a result, the partial Sr^{2+} substitution for Ca^{2+} distorts the symmetric environment of the OH groups. Therefore, the absorption band at 630 cm^{-1} (due to the OH librational mode), disappears.

Suchita et al. [199] made the same observation when they prepared ZnHAp by using a sol-gel method to study the effects of Zn ion on the physicochemical and in vitro behaviour of HAp.

Fig.5-2 also clearly displays that the amount of zinc ion substitution into the HAp structure can be used as a catalyst for the conversion process of HAp into another calcium phosphate phase of β-TCP. Paikaew et al. [200] prepared ZnHAp with different Zn levels (from 1 to 25 wt%) by a precipitation method. Their studies showed that increasing amounts of Zn substitution into the HAp crystal lattice accelerates the transformation of HAp to β-TCP when it is subjected to higher temperatures.

5.3.3 XRD diffraction analysis of sintered ZnHAp (prepared by hydrolysis of MCP/$Ca(OH)_2$).

5.3.3.1 Phase Identification of the ZnHAp powders.

The XRD diffraction patterns of sintered ZnHAp samples with different levels of zinc substitution are shown in **Figure 5-3.**

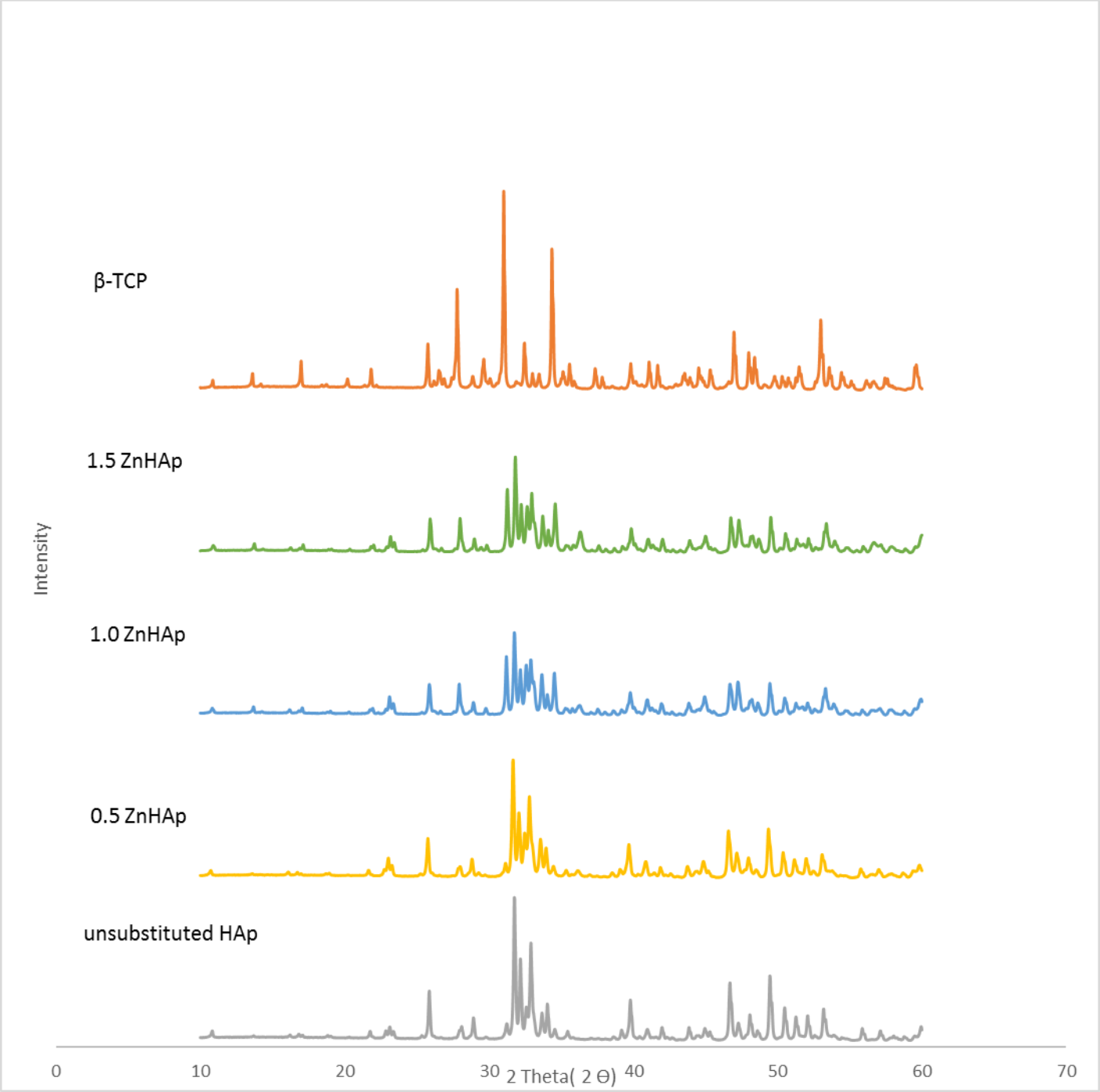

Figure 5-3: The XRD diffraction patterns of ZnHAp materials with different Zn contents prepared by hydrolysis of MCP/$Ca(OH)_2$ after sintering at 900 ˚C.

HAp's usual XRD pattern can be seen with the unsubstituted HAp, but it is apparent there is a small amount of β-TCP present when this is sintered as can be seen from peaks at 17.19˚, 31.20˚, 32.80˚, 33.60˚, 34.57 ˚, 41.14˚, 45.20˚ and 47.36˚. In the case of the 0.5 ZnHAp powders, an additional peak that corresponded to CaO phase detected at 2 Theta=

37.40˚ (reference card number 04-017-9575). But, in the case of 1.0 and 1.5 ZnHAp samples, new peaks that can be ascribed to β-TCP were confirmed by XRD at 2 Theta = 29.56˚, 30.08˚and 37.72˚, in addition to new peak that can be ascribed to CaO phase detected at 2 Theta= 37.40˚.

As the Zn content in the HAp lattice increases, it is evident that the level of beta TCP phase increases at the expense of the HAp phase. This can be seen by increases in the XRD peaks at 31.40˚, 32.66˚ and 34.57˚.

In summary we can note that:

1- Once the concentration of Zn^{2+} ions increased, both phases (HAp and β-TCP) have typical patterns were produced. It is evident from comparison with the Reference patterns for HAp and beta-TCP that the two phases present are HAp as a major phase and β-TCP as a minor phase. **Table 5-4** shows the phase composition of ZnHAp samples. It is obvious that the percent of HAp phase decreased with increasing the amount of substitution of Zn^{2+} ions.

Table 5-4: Phase composition of ZnHAp by hydrolysis method.

Sample	HAp %	β-TCP
HAp by hydrolysis	98.2	1.8
0.5ZnHAp by hydrolysis	98.0	2.0
1.0 ZnHAp by hydrolysis	57.8	42.2
1.5 ZnHAp by hydrolysis	58.7	41.3

2- At 900 ˚C, the outcome of sintering 1.0 ZnHAp and 1.5 ZnHAp solids is as a biphasic calcium phosphate (BCP) mixture consisting of the two phases HAp and β-TCP.

These observations were also noted by Nuamsrinuan et al. [201], who prepared ZnHAp samples by using a chemical precipitation method, where zinc nitrate ($Zn(NO_3)_2$ was used as the source of zinc ions. The different levels of zinc ions used in that experiment varied from 1 to 25 wt%. The results of that investigation showed that Zn can be used as a catalyst to transform HAp to β-TCP after heat treatment.

5.3.3.2 The degree of crystallinity and crystallite size of ZnHAp powders:

The degree of crystallinity and the crystallite size of the sintered ZnHAp containing different levels of Zn substitution are displayed in **Table 5-5**.

Table 5-5: The degree of crystallinity and the crystallite size of sintered ZnHAp materials with different Zn contents prepared by hydrolysis of MCP/$Ca(OH)_2$ at 900 ˚C.

Sample	D_{002} (Å)	Crystallinity %
Unsubstituted HAp by hydrolysis	549.8±3.6	82.57±2.1
0.5 ZnHAp by hydrolysis	474.0±5.3	75.29±4.2
1.0 ZnHAp by hydrolysis	461.1±3.8	70.72±2.8
1.5 ZnHAp by hydrolysis	470.4±4.1	74.52±5.2

The numerical values of % crystallinity were decreased due to the replacement process of zinc ions and slightly varied with increasing the level of substitution as shown in **Table 5-5**. Also, a clear reduction in the value of crystallite size was also due to the substitution of zinc ions into HAp lattice and slightly varied with increasing the level of substitutions. This result can be ascribed to the smaller ionic radius of Zn^{2+} (0.074nm) compared to Ca^{2+} ions (0.099 nm), which might have distorted the crystal structure of hydroxyapatite and inhibited the crystal growth of HAp [202] . Many previous studies ([191], [202], [199] and [203]), reported a decrease in both values of crystallite size and crystallinity with increasing Zn concentrations which aligns with our work. Guadalupe et al. [204] prepared ZnHAp powders by the precipitation method with different levels of substitutions [Zn/(Ca + Zn)= 0, 2.5, 5 and 10 mol%] and labelled them as 0-ZnHAp, 2.5-ZnHAp, 5.0- ZnHAp and 10-ZnHAp. The results showed the crystallite size decreased as a result of increasing the amount of Zn^{2+} ions in the HAp. The value of the crystallite size was calculated to be 40, 24, 14 and 13 nm for as 0-ZnHAp, 2.5-ZnHAp, 5.0- ZnHAp and 10-ZnHAp, respectively.

Miyaji et al. [191] prepared ZnHAp by precipitation with different Zn^{2+} concentrations (substitution in that study was done to a maximum of 15 mol%) The results showed that the crystallite size drastically decreased for samples containing 3 mol% Zn, and then were observed to gradually decrease in samples containing over 3 mol% Zn substitution .

Louyeh [179] prepared ZnHAp powders with different substitution levels (1, 5 and 10 wt%) by the precipitation method. The results showed that the measured crystallite size decreased with increasing of the level of Zn ion substitution in the HAp, and that the calculated values were 73, 72, 61.31 and 52.29 nm for unsubstituted HAp, ZnHAp 1%, ZnHAp 5% and ZnHAp 10% samples, respectively.

5.3.3.3 Lattice parameters and calculated volume of unit cell of the ZnHAp powders:

Table.5-6 displays the lattice parameters and the volume of the hexagonal unit cell of the sintered ZnHAp materials containing different substitution levels of Zn^{2+} in HAp prepared by hydrolysis of MCP/$Ca(OH)_2$

Table 5-6: The lattice parameters and the volume of hexagonal unit cell of ZnHAp materials after sintering at 900 ˚C with different levels of Zn^{2+} substitution by hydrolysis of MCP/$Ca(OH)_2$

Sample	a [Å]	c [Å]	V[Å^3]
Unsubstituted HAp by hydrolysis	9.421±0.003	6.882±0.005	1581±0.004
0.5 ZnHAp by hydrolysis	9.423±0.002	6.883±0.001	1582 ±0.002
1.0 ZnHAp by hydrolysis	9.417±0.005	6.879±0.006	1579±0.006
1.5 ZnHAp by hydrolysis	9.417±0.003	6.881±0.001	1580 ±0.002

A contraction was expected in both the value of lattice parameters (a and c), (as Zn^{2+} ions have a smaller ionic radius (0.074 nm) compared to Ca^{2+} ions (0.099 nm), but in **Table 5-6.** data have shown that there was a slight increase in the lattice constants (a and c) as observed in the case of the 0.5 ZnHAp solids. This observation can be explained as discussed previously through the following investigations:

1- Miyaji et al. [191] attributed such a result to the incorporation of H_2O into the apatite structure. They reported the H_2O that substitutes for OH sites in HAp has an effect on the value of the lattice parameters (a and c). However, the authors also prepared ZnHAp with different Zn levels in which the substituting limit of Zn was capped at 15 mol%. Their results revealed that the lattice parameter (a) measured for their solids decreased in value down to 5 mol% Zn, and then started to increase for solids that were substituted with > 5 mol% Zn. They explained this phenomenon as occurring as a result of water being incorporated into the HAp lattice when Zn ion substitution levels exceeded 5 mol%.

2- Other researchers such as LeGeros et al. [205] also observed the effect of the substitution of the OH site in the HAp lattice by H_2O on the value of the measured lattice parameters. Their studies [205] involved investigations of the types of "H_2O" existing in human enamel and in precipitated apatites through use of X-ray diffraction, infrared (IR) absorption spectroscopic and thermogravimetric analyses. They reported that the H_2O-for-OH substitution in the HAp lattice would be expected to cause an expansion in the unit-cell dimensions due to the following factors:

- The O-H bond length in the OH group of apatite crystal is smaller compared to its bond length in a H_2O molecule.
- The bent geometry of H-OH compared to O-H would occupy a larger volume (when substituted), causing lattice expansion. Therefore, the loss of "H_2O" upon pyrolysis (i.e. sintering) would cause a rearrangement of the apatite lattice to one with smaller unit cell dimensions, i.e. contraction in the a-axis dimension.

On the other hand, the result of this investigation showed due to as a result of increasing the level of substitution of Zn^{2+} ions (1.0 and 1.5 ZnHAp powders), the Rietveld refinement method displayed a reduction in the volume of cell unit of the ZnHAp powders. This result can be ascribed to the defect produced as a result of the replacement process involving zinc ions.

Several researchers prepared ZnHAp powders with different levels of substitution by using different preparation methods. The results of their studies revealed that the lattice constants (a and c) varied with the substitution levels. These results can be ascribed to several factors such as the preparation method, the level of substitutions and the phase purity. Below are summarised some of these investigations (see **Table 5-7**):

Table 5-7: The value of lattice parameters of ZnHAp powders prepared by different synthesis routes.

Authors	Preparation method	Results
Ren et al. [202]	prepared ZnHAp with the following chemical formula: $Ca_{10-x}Zn_x(PO_4)_6(OH)_2$ by a wet chemical method (precipitation) with different Zn contents (x=0.0, 0.5, 1.0, 1.5, 2.0, 4.0, 6, 8 and 10). The authors reported that the precipitates maintained the apatite phase up to a Zn:(Zn + Ca) ratio of 15–20 mol.%.	The results showed a decrease in both lattice parameters (a and c), with an increase being observed for both values (a and c) when the[Zn:(Ca + Zn)] ratio was higher than 10 mol.%.
Predoi et al. [206]	The researchers prepared Zn doped hydroxyapatite ZnHAp by using a co-precipitation method with the following chemical formula : $Ca_{10-x}Zn_x(PO_4)_6(OH)_2$, where $0.01 \leq xZn \leq 0.05$.	The XRD results revealed that the lattice parameter (a) increased as the percentage of zinc substitution increased, while the lattice parameter (c) decreased with increase of the Zn content.
Li et al. [207]	The authors prepared ZnHAp powders by a hydrothermal method with different levels of Zn substitution (3,5,10, 15 and 20 mol% Zn) inHAp.	The results revealed that the lattice parameter (a) decreased with increasing Zn substitution up to 10 mol%, but an increase over 10 mol % Zn had been observed. On the other hand, the lattice parameter (c) in this investigation was found to decrease with increasing Zn incorporation.

5.3.4 SEM of sintered ZnHAp materials with different levels of Zn^{2+} substitution as prepared by the novel hydrolysis method of MCP/$Ca(OH)_2$

The morphology of the 900 ˚C sintered ZnHAp samples with different Zn^{2+} content prepared by hydrolysis of MCP/$Ca(OH)_2$ was studied using scanning electron microscopy. The obtained images are displayed in **Fig.5-4**.

Based on these images, we can conclude that the produced materials consist of particles with fine grains, in which porous, irregular distribution, spheroidally shaped, and agglomerated

crystals were obtained in all samples. The morphology of the ZnHAp powders with different levels of Zn^{2+} ion was not dissimilar to each other with a porous structure being produced due to the replacement process of Zn^{2+} ions into the HAp lattice.

The shape of the particles remained unchanged as a result of the increase in concentration of Zn^{2+} ions in the HAp lattice. Several studies have been performed by different researchers in preparing ZnHAp powders with various levels of substitution. The results of these investigations showed clearly that the morphology remained unchanged due to the increasing Zn substitution level although the particles of the prepared powders in these studies demonstrated a trend to agglomerate. See below for details:

Predoi et al. [208] synthesized ZnHAp with the following chemical formula: $Ca_{10-x}Zn_x(PO_4)_6(OH)_2$ with $0.01 \leq X_{Zn} \leq 0.05$ using a co-precipitation method. SEM images of these particles revealed that there was no difference in the morphology for all ZnHAp samples studied. The morphology and the particles shape remained unchanged as a result of replacement process of zinc ions.

Fuzeng Ren et al. [202] prepared ZnHAp materials by the wet chemical method with the following formula : $Ca_{10-x}Zn_x(PO_4)_6(OH)_2$. Compounds with different values of x were prepared in the experiments (0, 0.5, 1, 1.5, 2, 4, 6, 8, 10). The precipitates maintained the apatite phase up to a Zn:(Zn + Ca) ratio of 15–20 mol.%. SEM images showed that pure HAp crystals had regular shapes, whereas the Zn-substituted apatite crystals had a clear tendency to agglomerate with increasing substitution of Zn^{2+} ions in the HAp lattice. This agrees with the observations made in the present study about agglomeration as a consequence of the substitution of zinc ions into the HAp lattice.

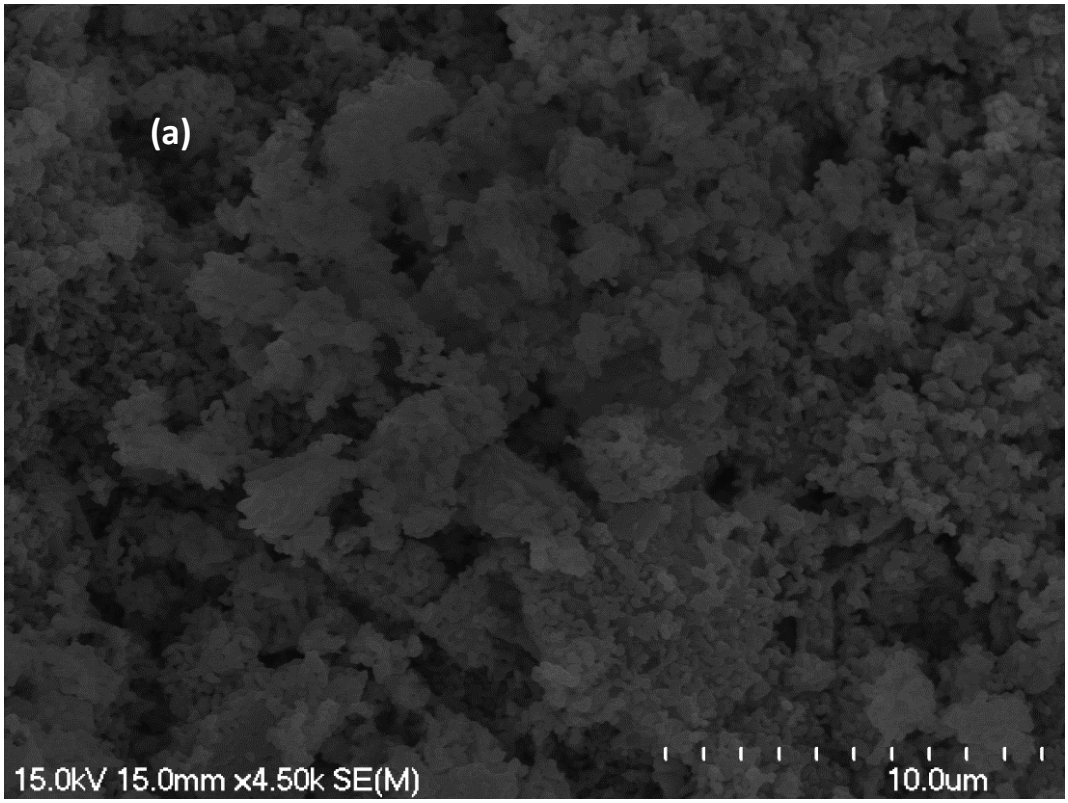
(a)
15.0kV 15.0mm x4.50k SE(M)
10.0um

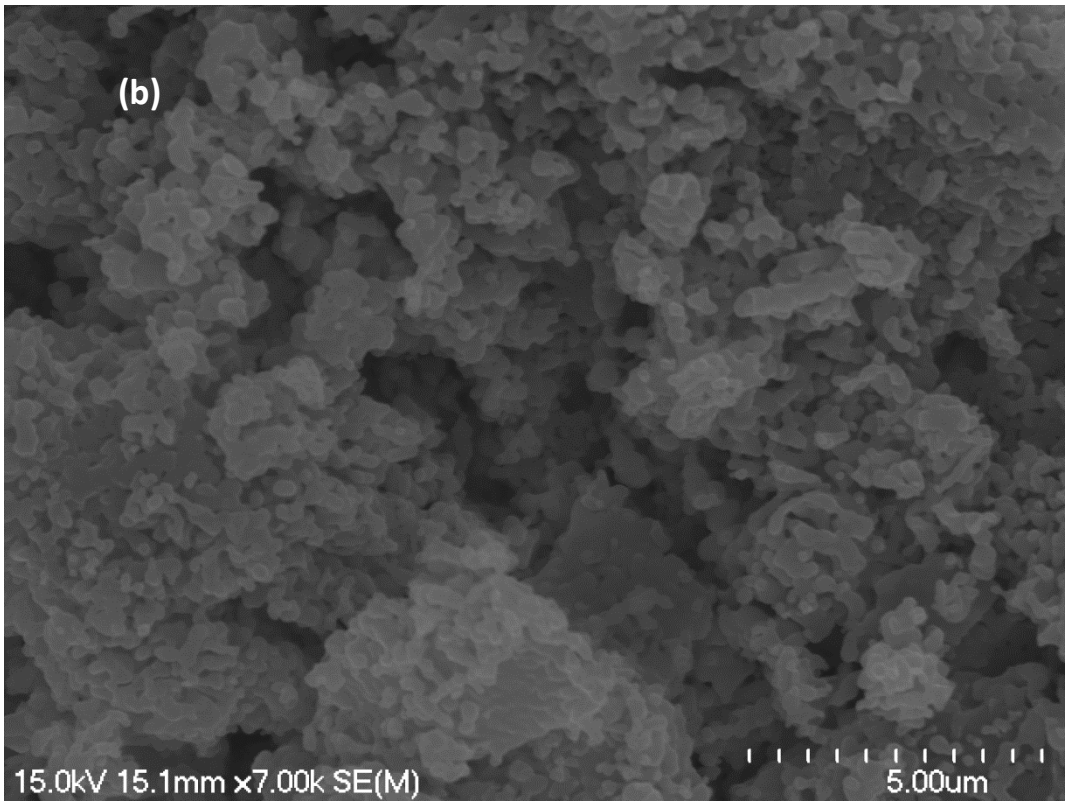
(b)
15.0kV 15.1mm x7.00k SE(M)
5.00um

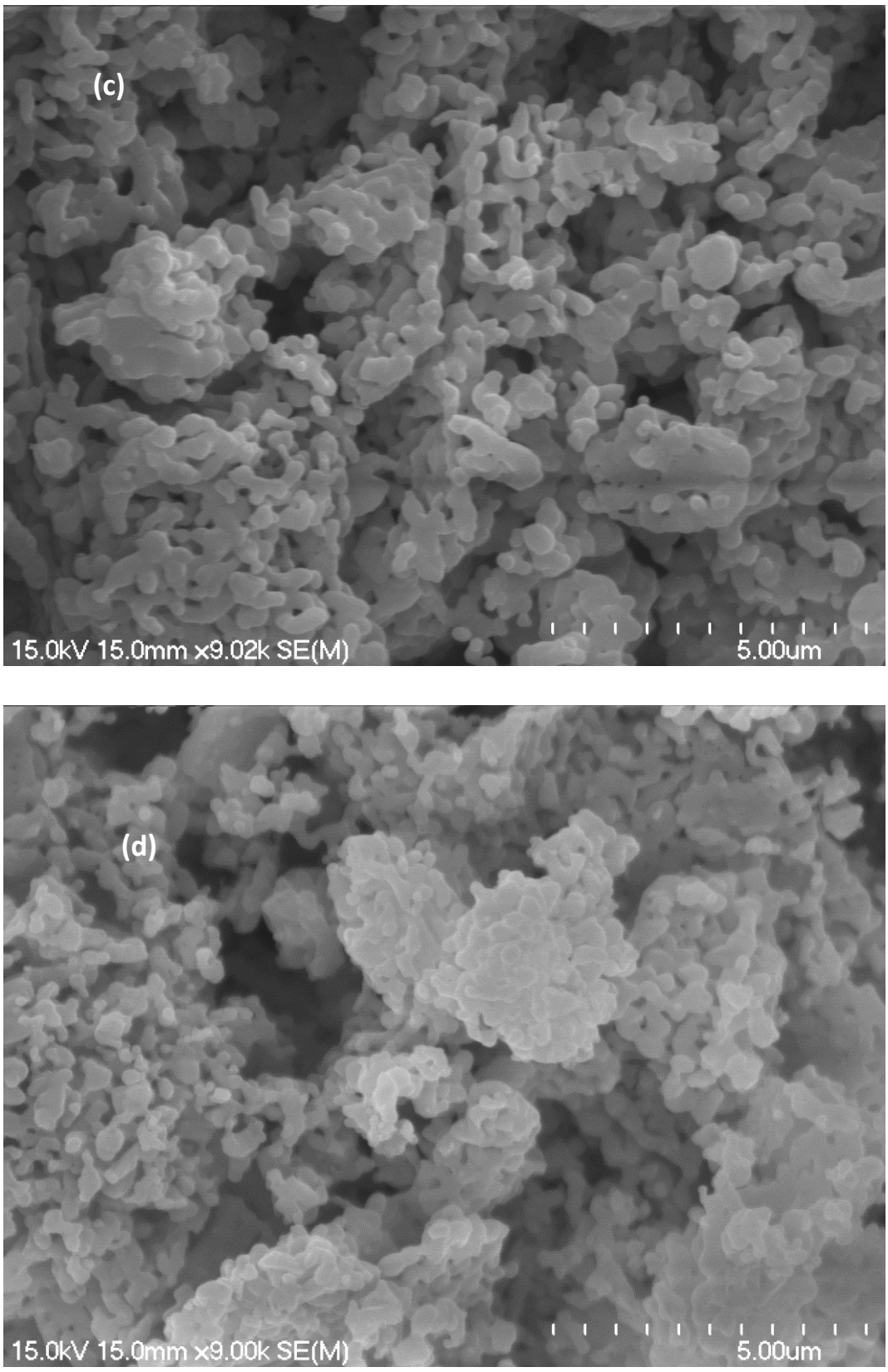

Figure 5-4: SEM images from the present study of (a) unsubstituted HAp (b) 0.5 ZnHAp (c) 1.0 ZnHAp (d) I.5 ZnHAp, prepared by hydrolysis of MCP/$Ca(OH)_2$ after sintering at 900 ˚C.

The images show the particles exhibiting increasing levels of agglomeration as the level of Zn ion substitution increases in the HAp lattice for samples.

5.4 SrHAp materials generated by hydrolysis of MCP/$Ca(OH)_2$

Three different series of SrHAp powders with differing levels of Sr^{2+} substitution (0.5 SrHAp, 1.0 SrHAp and 1.5 SrHAp) were prepared by hydrolysis of MCP/$CaOH)_2$, with the experimental details of the reagents used in their preparation being listed in the **Table 5-8.**

Table 5-8: Synthesis details of prepared SrHAp materials by hydrolysis of MCP/$Ca(OH)_2$.

Sample	MCP $Ca(H_2PO_4)_2$ (g)	$Ca(OH)_2$ (g)	$SrCl_2.6H_2O$ (g)	$Ca(H_2PO_4)_2$ (mol)	$Ca(OH)_2$ (mol)	Sr (mol)	Expected Ca/P
Unsubstituted HAp	11.6487	3.6522	-	0.0498	0.0493	-	1.67
0.5 SrHAp	10.8144	3.4227	0.6534	0.0462	0.0462	0.0025	1.58
1.0 SrHAP	10.064	3.1568	1.2748	0.0430	0.0426	0.0048	1.50
1.5 SrHAp	9.2413	2.9436	1.8682	0.0395	0.0397	0.0070	1.42

5.5 Characterization of SrHAp powders prepared with different levels of Sr^{2+} substitution by hydrolysis of MCP/$Ca(OH)_2$:

5.5.1 ICP-MS analysis of sintered SrHAp materials after sintering at 900 ˚C:

The elemental analyses of the SrHAp samples after sintering at 900°C are displayed in **Table 5-9.**

Table 5-9: ICP-MS results of SrHAp materials after sintering at 900 ˚C. The concentrations quoted are in ppb units (ug/L):

Sample	Ca 44	P 31	Na 23	Sr 88
Unsubstituted HAp by hydrolysis	707795	401240	103797	-
0.5 SrHAp by hydrolysis	711449	383124	93656.8	43563.3
1.0 SrHAp by hydrolysis	562155	361925	106468	88506.7
1.5 SrHAp by hydrolysis	647610	338452	88148	130086.1

The starting (calculated) and actual (measured) degree of chemical composition of the prepared powders in terms of wt.% of Sr^{2+} ions, the calcium/phosphorus (Ca/P) molar ratios as well as (Ca+Na+Sr)/P molar ratios were determined by ICP-MS and presented in **Table 5-10.**

Table 5-10: The ICP-MS analysis data of SrHAp powders after sintering at 900 ˚C with different Sr^{2+} contents by ICP-MS measurements.

Sample	Ca/P Theoretical	Ca/P Measured	(Ca+Na+Sr)/ P Measured	Wt.% of Sr^{2+} ions Theoretical	Wt.% of Sr^{2+} ions measured
Unsubstituted HAp by hydrolysis	1.67	1.40	1.65	-	-
0.5 SrHAp by hydrolysis	1.58	1.43	1.71	4.26%	2.18%
1.0 SrHAp by hydrolysis	1.50	1.20	1.71	8.34%	4.43%
1.5 SrHAp by hydrolysis	1.42	1.32	1.93	12.22%	6.50%

Table 5-10 shows the presence of Sr^{2+} and Na^{+} ions into HAp samples, as a result the measured value of Ca:P mole ratios for all prepared powders were lower than the theoretical value of the stochiometric Hap (1.67). The (Ca+Na+Sr)/ P mole ratios were found to be slightly higher than the expected value (1.67) for the 0.5 SrHAp and 1.0 SrHAp powders, but in the case of 1.5 SrHAp samples, the value of (Ca+Na+Sr)/ P mole ratios was significantly higher than the standard value of stochiometric HAp. The result was taken as evidence of the formation of carbonated HAp powders as confirmed by FTIR spectra. **Table 5-10** shows that the prepared unsubstituted HAp and SrHAp powders with different level of substitutions also contain Na^{+} ions. The presence of Na^{+} ions into the prepared powders can be ascribed to the substitution of sodium ions into calcium ion sites as a result of using sodium hydroxide (NaOH) to adjust the pH value of the reaction during the synthesis process.

5.5.2 FTIR Spectroscopy of SrHAp materials.

5.5.2.1 FTIR of non-sintered SrHAp materials.

The FTIR spectra of SrHAp powders before sintering with differing levels of Sr^{2+} substitution are illustrated in **Fig.5-5**.

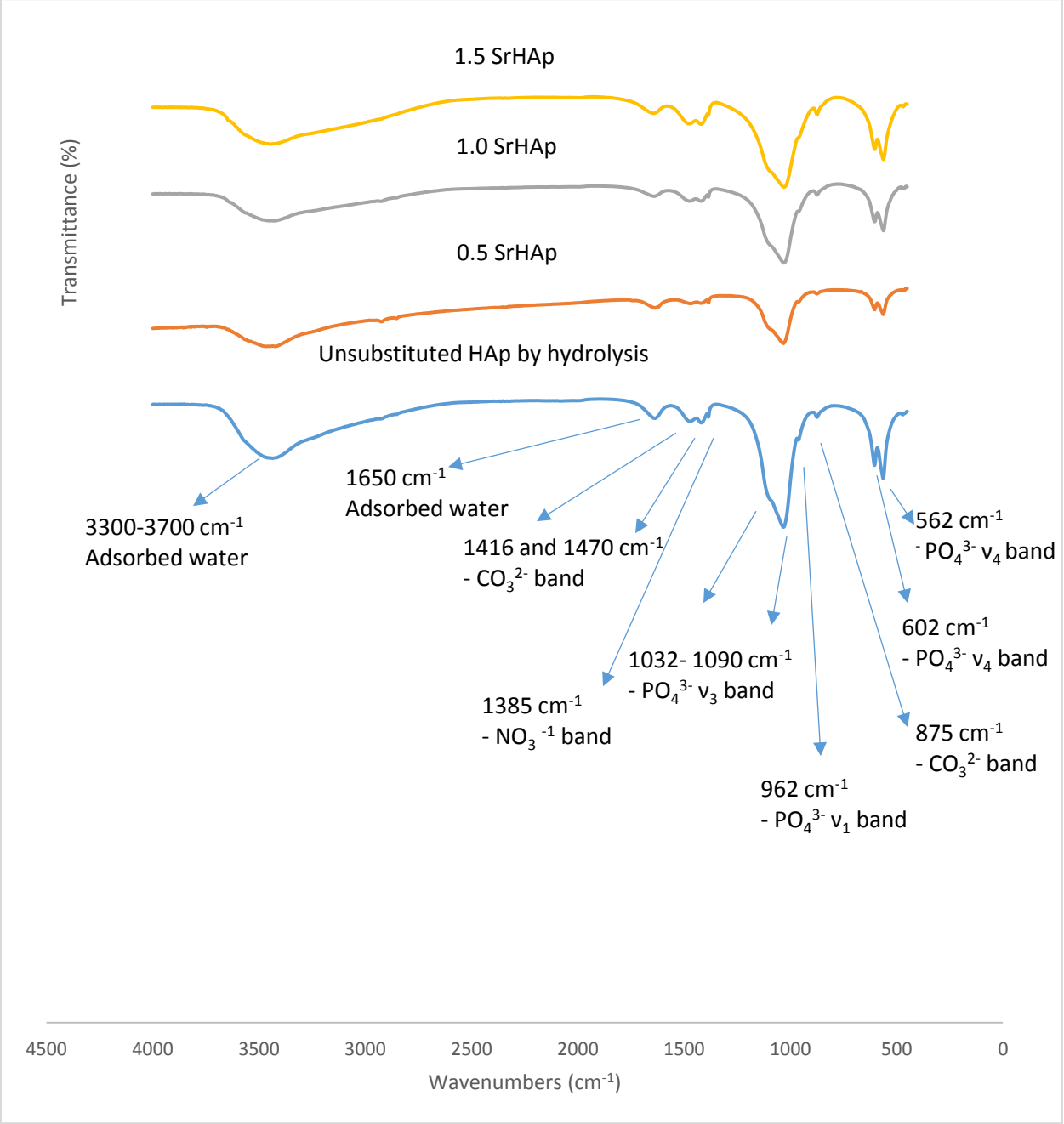

Figure 5-5: FTIR spectra of the SrHAp powders (before sintering) with different levels of Sr^{2+} substitution as prepared by hydrolysis of MCP/$Ca(OH)_2$.

In **Fig. 5-5**, the FTIR spectra of the prepared SrHAp powders before sintering have an approximately identical intensity scale, so can be compared in a direct manner. The spectra indicated the expected fundamental vibrational peaks of the phosphate group, i.e. v_3 and v_1 peaks at 1095/1032, and 962 cm^{-1}. The phosphate v_4 bands were also observed at 604 and 563

cm^{-1}. The carbonate v_3 band was also observed in spectra as two peaks at around 1416 and 1468 cm^{-1}, whereas the carbonate v_2 band featured as a single peak at 875 cm^{-1} in all samples. The characteristic sharp and low intensity band due to HAp lattice OH stretching at 3572 cm^{-1} did not appear (due to the samples being only poorly crystalline) or was obscured by the broad band between 3000–3700 cm^{-1} due to adsorbed moisture. The peak at 1640 cm^{-1} is the bending mode of water due to adsorbed moisture. The band that appeared at 1385 cm^{-1} in the unsintered powders is believed to be due to the N-O stretch of nitrate ion impurities [169].

5.5.2.2 FTIR of the SrHAp materials after sintering at 900 ˚C:

The FTIR spectra of the sintered SrHAp powders are shown in **Fig.5-6**.

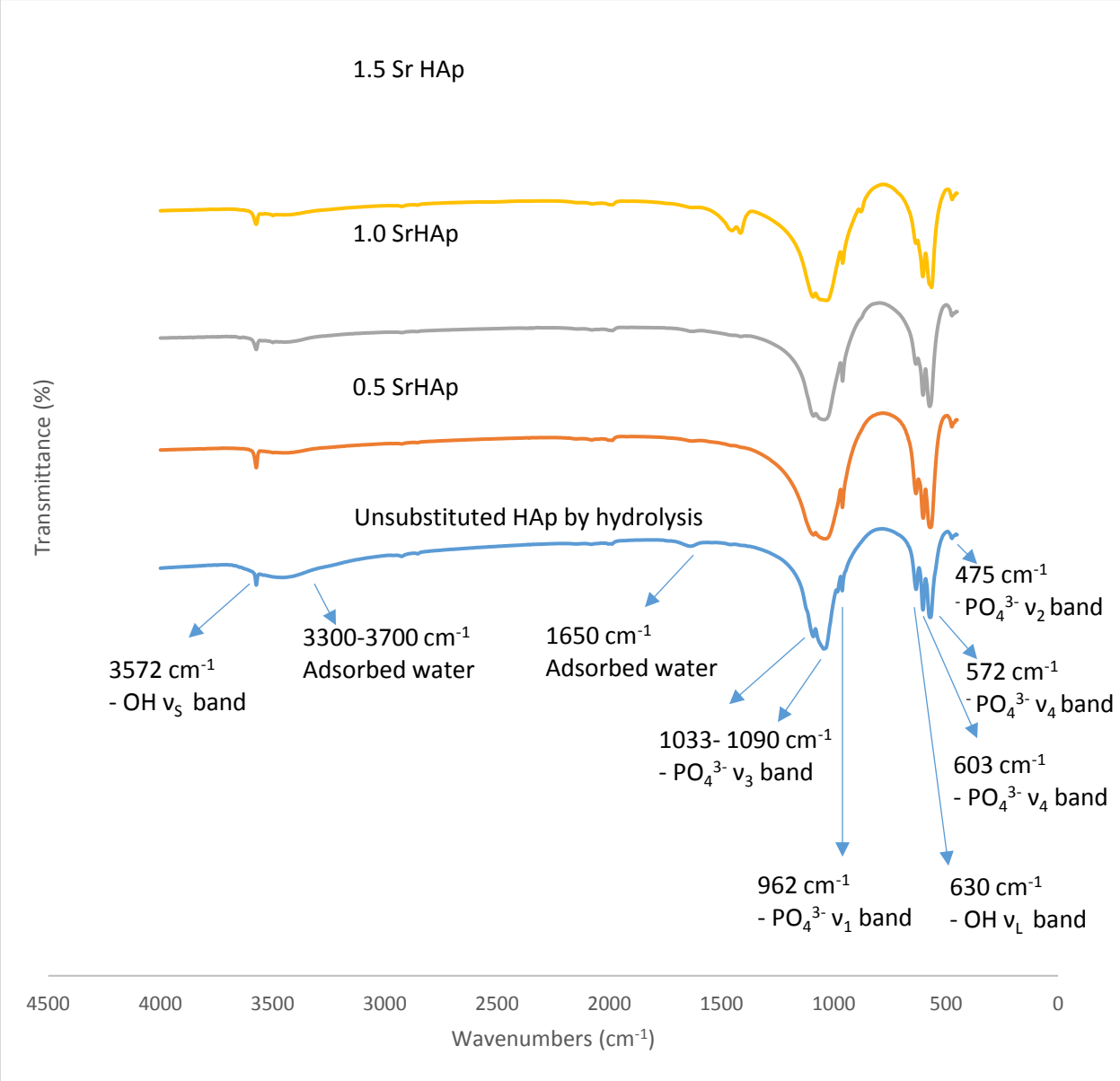

Figure 5-6: FTIR spectra of SrHAp materials with different levels of strontium ion substitution as prepared by hydrolysis of MCP/$Ca(OH)_2$ after sintering at 900 ˚C.

The FTIR spectra feature the expected characteristic molecular vibrations of the HAp phase, where the fundamental vibrational modes of the PO_4^{3-} group in HAp are detected at 562, 602, 962 and 1032-1095 cm^{-1}, as well the typical bands of the lattice OH^- group in HAp at 3572 and 631 cm^{-1} which appear in the sintered samples (as opposed to the unsintered samples). An important and unusual observation was the detection of peaks due to carbonate, at 875, 1412 and 1450 cm^{-1}, in the SrHAp powder containing the highest amount of strontium ions (1.5 SrHAp).

This phenomenon has been observed before by Zhang et al. [209] who prepared "Sr_xHAp" (where x = Sr/(Ca + Sr) = 0, 10, 40, 100 mol.%) by using a hydrothermal method. The presence of the CO_3^{2-} group in the non-sintered powders with increasing Sr content (Sr/(Ca+Sr)=40 and 100% mol) was confirmed by FTIR spectra. That result was explained in terms of the larger structural strain that is produced by partial substitution of Sr^{2+} for Ca^{2+} ions, as strontium has a larger ionic radius (113 pm) compared to calcium Ca (99 pm), therefore Sr–HAp (at higher substitution levels) can accommodate more carbonate to reduce this structural strain, resulting in the formation of a non-stoichiometric carbonated material.

Fig.5-6 showed that the intensity of the librational OH peak at 631 cm^{-1} in samples started to decrease with an increase in the substitution of Sr ions in the HAp structure. This IR spectral trend observed for Sr substituted HAps has been extensively discussed by Bulina et al. [198], who prepared Sr-Substituted Hydroxyapatite with the chemical formula : $Ca_{10-x}Sr_x(PO_4)_6(OH)_2$, where x = 0-2 and a mechanochemical method was used to synthesise it (see FTIR of ZnHAp powders).

Frasnelli et al. [192] prepared Sr-HAp nanopowders by a precipitation method with different Sr^{2+} content-(i.e. where the [Sr/(Sr + Ca) molar ratio = 0, 5, 10, 25, 50, 75 and 100%]. FTIR analysis showed:

1- The absence of carbonate bands in the prepared samples.
2- A change in the FTIR spectra where the peaks representing lattice OH groups at 3572 cm^{-1} (stretching) and 633 cm^{-1} (bending) started to gradually vanish at higher levels of Sr ion substitution.

Fig. 5-6 also, confirmed a clear shift of the phosphate bending modes at 572 and 604 cm^{-1} to lower wavenumber values upon Sr^{2+} ion substitution in the HAp lattice. It was found that this shift increased in extent as the substitution level of Sr ions increased in the HAp. In addition, the vibrational frequency of the OH librational mode at 632 cm^{-1} shifted to 612 cm^{-1} as the level of substitution of Sr^{2+} ions increased. This observation was in good agreement with another study performed by Bigi et al [131], who prepared SrHAp with Sr/(Ca + Sr) molar ratios ranging in value from 0 to 1 by using $Ca(NO_3)_2.4H_2O$, $Sr(NO_3)_2$ and $(NH_4)_2HPO_4$ as starting materials. The results of that investigation showed that the peak due to the OH librational mode shifted from 632 to

537 cm^{-1}, while the infrared absorption bands of the phosphate bending mode v_4 shifted from 603 (unsubstituted HAp) to 592 cm^{-1} as a result of increasing the levels of strontium ion in the lattice. The authors explained that the real factor causing shifts in the HAp-associated PO_4 vibrational frequencies to lower wavenumber values is the decreased anion–anion repulsion concomitant with an increase in the anion–anion separation in the HAp lattice because of the increasing cation radius. In other words, the shift of the infrared absorption bands of the phosphate groups with increasing concentration of Sr^{2+} ions can be directly attributed to the increasing mean dimensions of the Sr cation which is being incorporated into the HAp lattice.

5.5.3 -XRD diffraction analysis of the SrHAp materials after sintering at 900 ˚C.

5.5.3.1 Phase Identification of SrHAp powders.

Fig. 5-7. shows the XRD diffraction patterns of the sintered SrHAp materials prepared in this study.

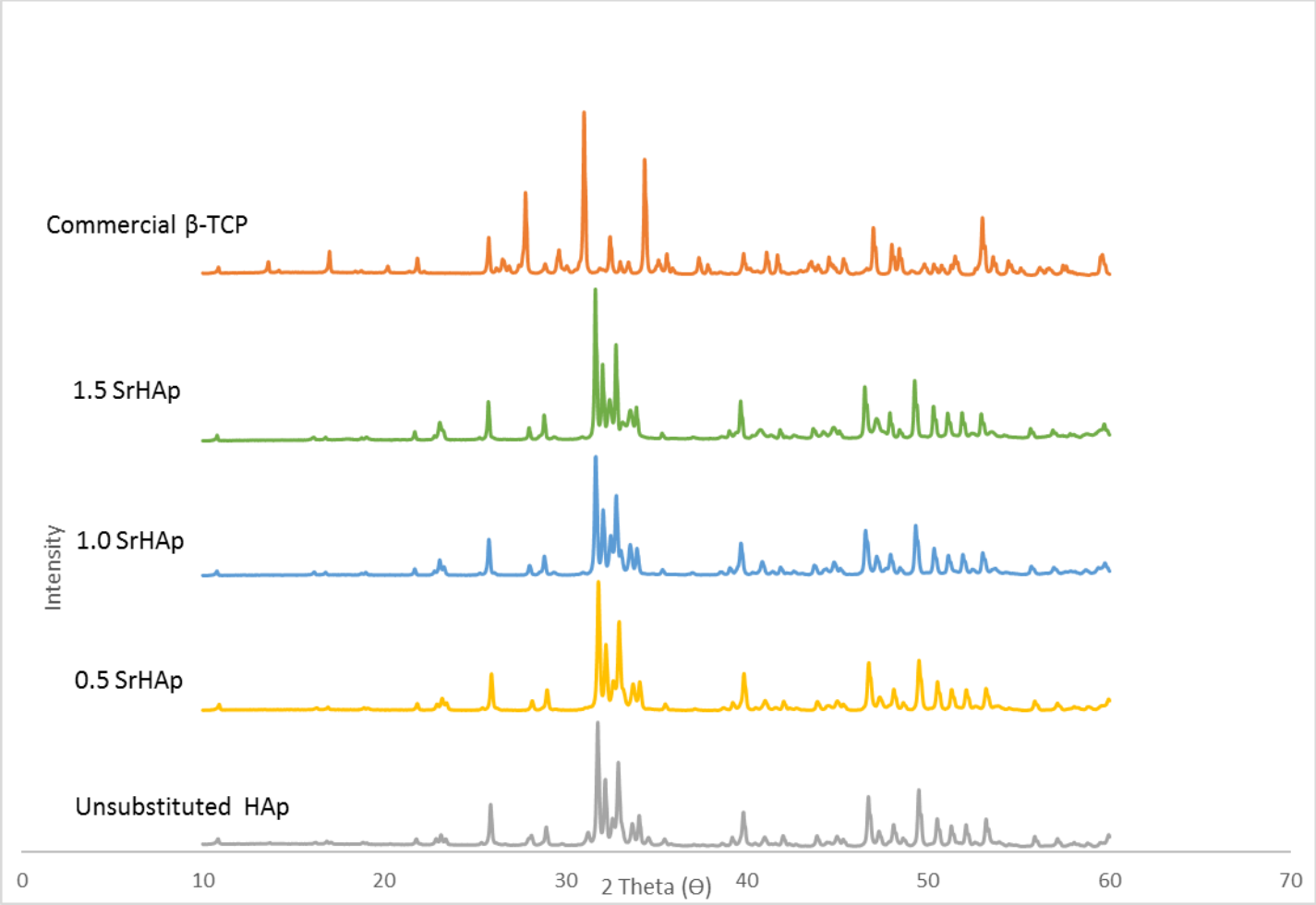

Figure 5-7: The XRD diffraction patterns of SrHAp powders prepared in this study by the novel hydrolysis method after sintering at 900 ˚C.

Fig.5-7 displays clearly that unsubstituted HAp powders contain more impurity phases (this being β-TCP) compared to SrHAp powders. The following observations were detected by XRD patterns:

1- In the case of 0.5 SrHAp we can see that some peaks that were ascribed to an impurity phase (β-TCP) at 2 Theta = 31.20˚ and 34.57˚ have vanished.

2- 2- At higher levels of substitution (1.0 SrHAp and 1.5 SrHAp), the disappearance of one typical peak of β-TCP at 2 Theta =34.57˚ as well as a clear reduction the intensity of another peak that is related β-TCP phase at 2 Theta = 31.20˚ were confirmed by XRD analysis. Also, weak peak beginning to emerge that can be attributed to the β-TCP phase at 2 Theta = 33.10˚ started to appear with small intensity.

In other words, substitution of Sr^{2+} ions into HAp structure into HAp structure led to produce an obvious enhancement in the thermal stability.

The literature studies described below refer to previous work by different researchers to prepare SrHAp samples with different substitution levels. It can be seen that these discussions supported what was observed in the present study regarding the stabilization of the HAp structure to sintering when Sr ion was incorporated into the HAp lattice.

Guo et al [210] prepared SrHAp with different Sr concentrations where the [Sr/(Sr+Ca) atom ratio = 0, 10, 20, 50 and 100%] by using a wet chemical method (i.e. precipitation). The result of that study revealed that none of the SrHAp materials with various Sr^{2+} contents were not decomposed below 900 ˚C. However, when the temperature of heat treatment was increased up to 1200˚C, the SrHAp (with Sr concentration [i.e. the Sr/(Ca+Sr) atom ratio] kept below 20%) showed good thermal stability to sintering to the extent that no other impurity phase (TCP) was detected in the sintered SrHAp materials containing Sr ion loadings below 20%. This investigation showed obviously that incorporation of Sr^{2+} ions into HAp enhances the thermal stability and hence the phase purity of the resultant sintered HAp, which agrees with the findings of the present study as discussed above.

Santos Tavares et al. [211] prepared SrHAp with different Sr fractions(0, 0.5, 1 and 5 mol %) by a wet chemical method (precipitation). The XRD patterns of the (0, 0.5, 1 Sr mol%) prepared samples showed the appearance of one typical peak of β-TCP at 2 Theta = 31.2, while in the case of 5 Sr mol%, that peak was not detected. This study also showed the replacement process of strontium ions into the HAp lattice enhances the thermal (and hence phase) stability of the HAp powders, which further agrees with the present study's results.

5.5.3.2 Crystallinity and crystallite size of SrHAp powders:

The degree of crystallinity and the crystallite size of the SrHAp materials after sintering at 900°C are summarised in **Table 5-11.**

Table 5-11: The degree of crystallinity and crystallite size data for SrHAp materials generated by the novel hydrolysis method after sintering at 900°C

Sample	D_{002} (Å)	Crystallinity %
Unsubstituted HAp by hydrolysis	549.8±3.6	82.57±2.1
0.5 SrHAp by hydrolysis	526.7±5.1	81.62±8.5
1.0 SrHAp by hydrolysis	569.4±1.5	79.45±2.5
1.5 SrHAp by hydrolysis	677.2±4.2	78.52±3.7

The crystallinity of the prepared SrHAp materials indicated a slight decrease in their values (from 82.6 to 78.5) with increases in the amount of strontium ion substituted into the HAp lattice. Other researchers using different preparation methods to make the substituted HAps have found the following in their reported studies. The results of their investigations are summarized in **Table 5-12** (see below).

Table 5-12: Illustrates the results on the degree of crystallinity measurements of SrHAp materials obtained by studies in the literature.

Authors	Preparation method	Results
Geng et al. [212]	The authors prepared Sr-substituted HAp with different levels of Sr ion substitution given by [Sr/(Ca + Sr)] = 10, 30 and 50 mol %) and used a hydrothermal method for the synthesis.	The result revealed that the crystallinity was slightly decreased with an increasing of the substitution levels of Sr^{2+} ions in the HAp. The calculated values of crystallinity were 54.5, 42.2 and 39.0% for 10, 30 and 50% Sr respectively. This result agrees with this investigation that a reduction in crystallinity was achieved due to substitution of strontium ions into the HAp lattice.
Bigi et al. [131]	The researchers prepared (SrHAp) by a precipitation method with [Sr/(Ca + Sr)] molar ratios varying from 0 to 1.	They reported a reduction in crystallinity, and stated how it can be considered as a measure to reflect how difficult it is for the larger ions such as Sr^{2+} to be introduced and hosted by the HAp lattice. In other words, substitution of strontium ions which have larger ionic radius (0.118 nm) values compared to calcium ions (0.100 nm) [192]into HAp lattice caused a decrease in crystallinity. Also, this result agrees with the present investigation

As shown in **Table 5-11**, the crystallite size of sintered SrHAp powders initially decreased with increasing substitution of strontium ions into the HAp lattice reaching a minimum value of (526.7 Å) for just the 0.5 SrHAp phase, and then started to increase as a result of increasing levels of strontium ion substitution in the HAp lattice to reach the maximum value of 677.19 Å for the 1.5 SrHAp phase. In the literature, various trends of crystallite size for SrHAp phases synthesized by other workers exist. The results of these investigations were summarized in **Table 5-13.**

Table 5-13: Illustrates the results of the crystallite size of SrHAp materials obtained by various studies.

Authors	Preparation method	The results
O'Donnell et al. [213]	The researchers prepared SrHAp materials with the following chemical formula $(Sr_xCa_{1-x})_5(PO_4)_3OH$, where x = 0.00, 0.25, 0.50, 0.75 and 1.00 by using a wet chemical route (precipitation).	The results showed the crystallite size decreased with addition of Sr^{2+} ions to the HAp lattice and reached a minimum value at around x = 0.5 then started to increase with Sr content. This result agrees with this investigation that substitution of Sr^{2+} ions into HAp structure caused a decrease in the numerical value of crystallite size and reached the minimum value at 0.5 SrHAp. Afterward, an increasing in the value of crystallite size was recorded with increasing the amount of strontium substitution and reached a maximum value at 1.5 SrHAp (677.186 Å) compared to unsubstituted HAp (549.770 Å)
Xu et a. [214]	The authors prepared undoped hydroxyapatite (HAp) as well as SrHAp materials with different levels of strontium ion substitution (from 1 to 20 mol.%) by using a hydrothermal method.	The results showed an increase in the numerical value of crystallite size due to substitution of Sr^{2+} ions in the HAp lattice where the crystallite size reached a maximum value of 755.1 Å with 20% mol of substitution process of Sr^{2+} ions compared to 401.9 Å for undoped/unsubstituted HAp. This agrees with the present investigation that substitution of strontium ions into the HAp lattice increases the crystallite size.

5.5.3.3 Lattice parameters and volume of unit cell of SrHAp powders:

The lattice parameters and the volume of hexagonal unit cell of the SrHAp materials by the novel hydrolysis method from the present study after sintering at 900 °C are shown in **Table 5-14.**

Table 5-14: The lattice parameters and the volume of hexagonal unit cell of the SrHAp powders after sintering at 900 ˚C.

Sample	a [Å]	c [Å]	V[Å³]
Unsubstituted HAp by hydrolysis	9.421±0.003	6.882±0.005	1581±0.004
0.5 SrHAp by hydrolysis	9.431±0.008	6.892±0.006	1586±0.007
1.0 SrHAp by hydrolysis	9.445±0.003	6.901±0.0002	1593±0.003
1.5 SrHAp by hydrolysis	9.453±0.005	6.909±0.003	1598±0.004

Table 5-14. displays that both lattice parameters (a and c) increased gradually with increasing of the level of substitution of Sr^{2+} ions in the HAp lattice. This is clearly related to the larger ionic radius of Sr^{2+} ions (0.118 nm) compared to that of the Ca^{2+} ions (0.100 nm) [192]. Several researchers reporting studies of SrHAp materials with different substitution levels showed in their lattice parameter data a clear expansion in both lattice constant values. The following table (**Table 5-15**) displays the results of some other workers' studies of strontium substituted HAp.

Table 5-15: llustrates the relationship between substitution level of Sr^{2+} ions and lattice parameters (a and c) as shown in other workers' studies.

Authors	Preparation method	Result
O'Donnell et al. [213]	These researchers prepared SrHAp materials with the following chemical formula $(Sr_xCa_{1-x})_5(PO_4)_3OH$, where x = 0.00, 0.25, 0.50, 0.75 and 1.00) by using a wet chemical route (precipitation).	The result of this investigation showed that both the lattice parameters (a and c) increased linearly with increasing Sr substitution in the HAp lattice, and this agrees with the result obtained in the present investigation.
Frasnelli et al. [192]	The researchers prepared SrHAp nanopowders by a precipitation approach with different fractions of Sr ions, to produce materials with a Sr/(Sr + Ca) molar ratio of 0, 5, 10, 25, 50, 75 and 100%.	The result of this investigation revealed that the lattice cell parameters (a and c) increased as the level of Sr ion substitution increased in the HAp lattice. Also, these results agree with the present study reported in this thesis.
Geng et al. [212]	The researchers prepared (using a hydrothermal method) Sr ion-substituted HAp with different levels of Sr ion substitution where [Sr/(Ca + Sr)] = 10, 30 and 50 mol %.	The results of their studies revealed that the lattice parameters (a and c) in the resultant substituted HAp increased with increasing addition of Sr^{2+}. This agrees also with the result obtained in the present study reported in this thesis.

5.5.4 SEM investigation of SrHAp powders prepared by the novel hydrolysis method after sintering at 900 ˚C.

Fig 5-8 displays SEM micrographs of the SrHAp powders after sintering at 900 ˚C.

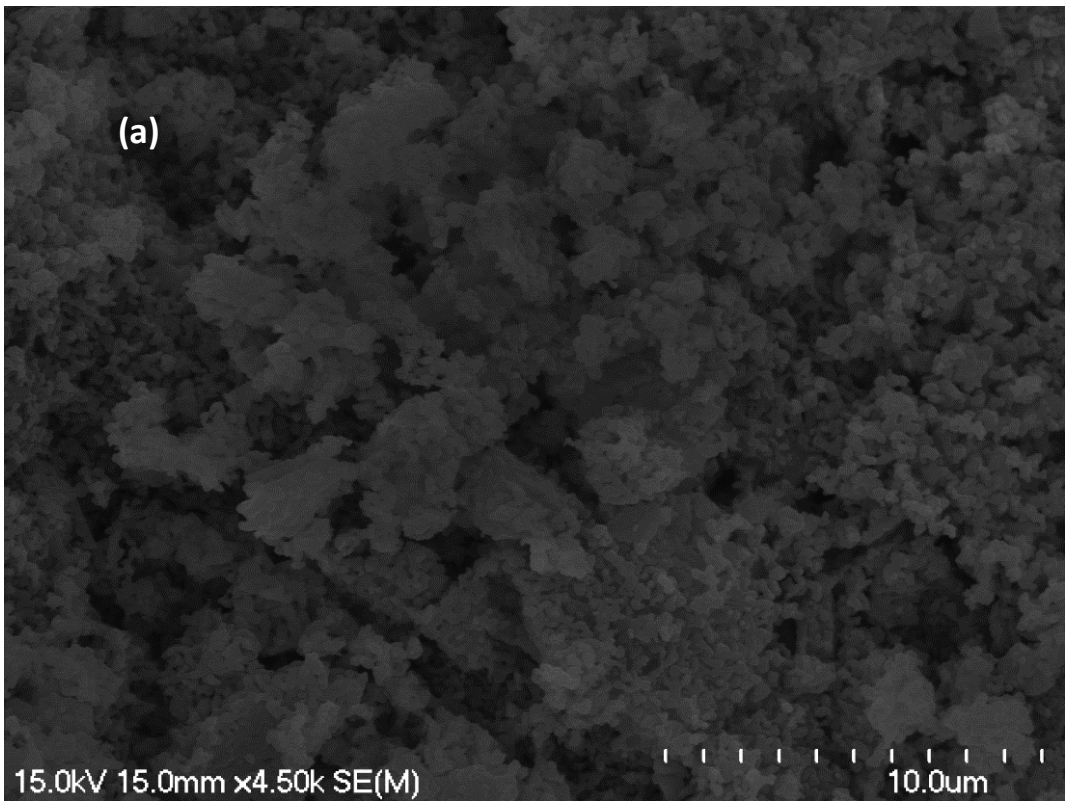
(a)
15.0kV 15.0mm x4.50k SE(M)
10.0um

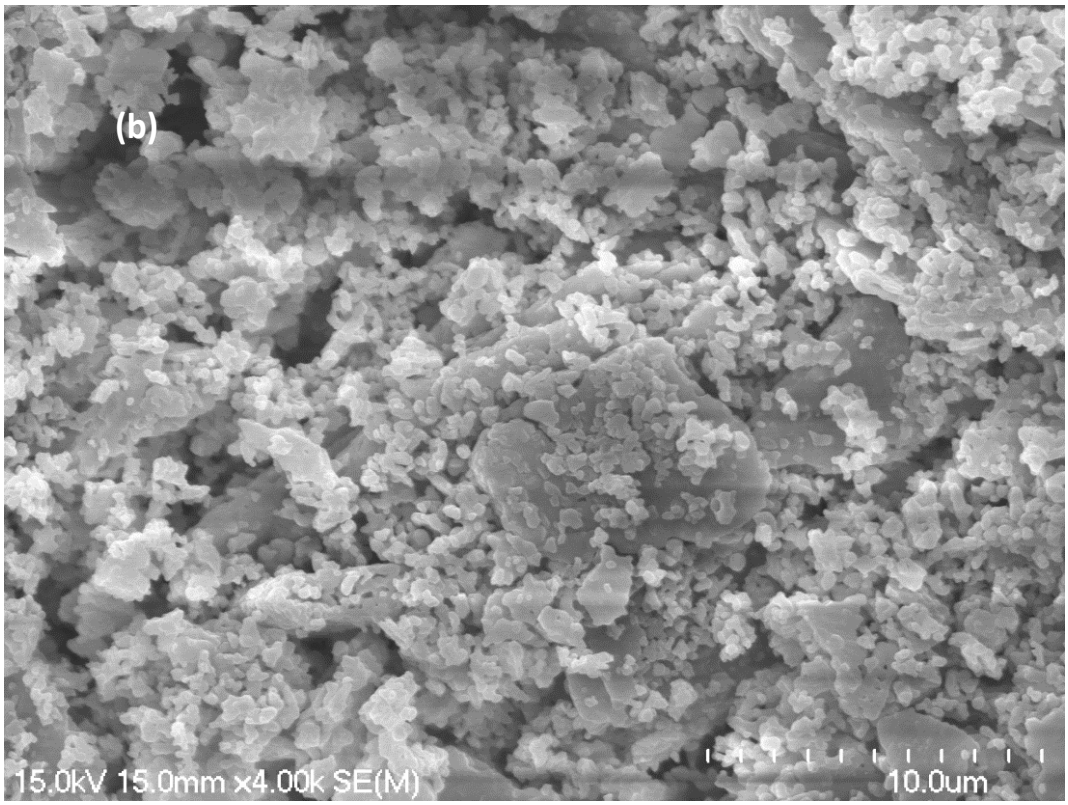
(b)
15.0kV 15.0mm x4.00k SE(M)
10.0um

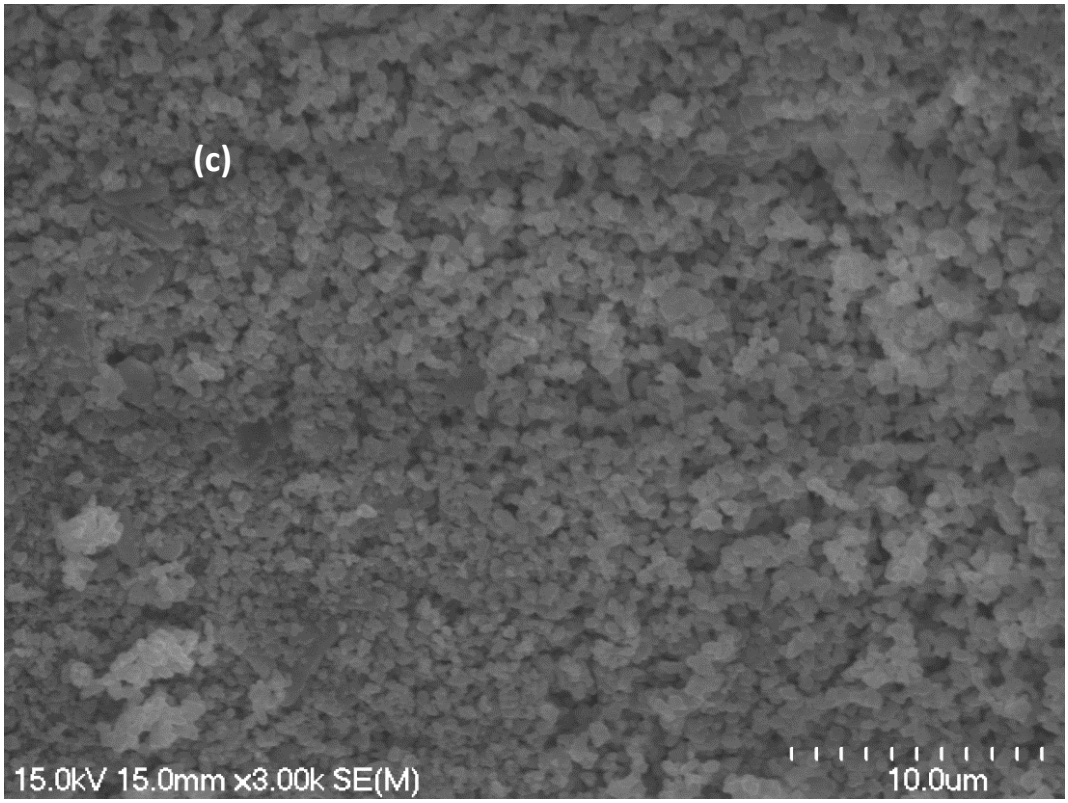
(c)
15.0kV 15.0mm x3.00k SE(M)
10.0um

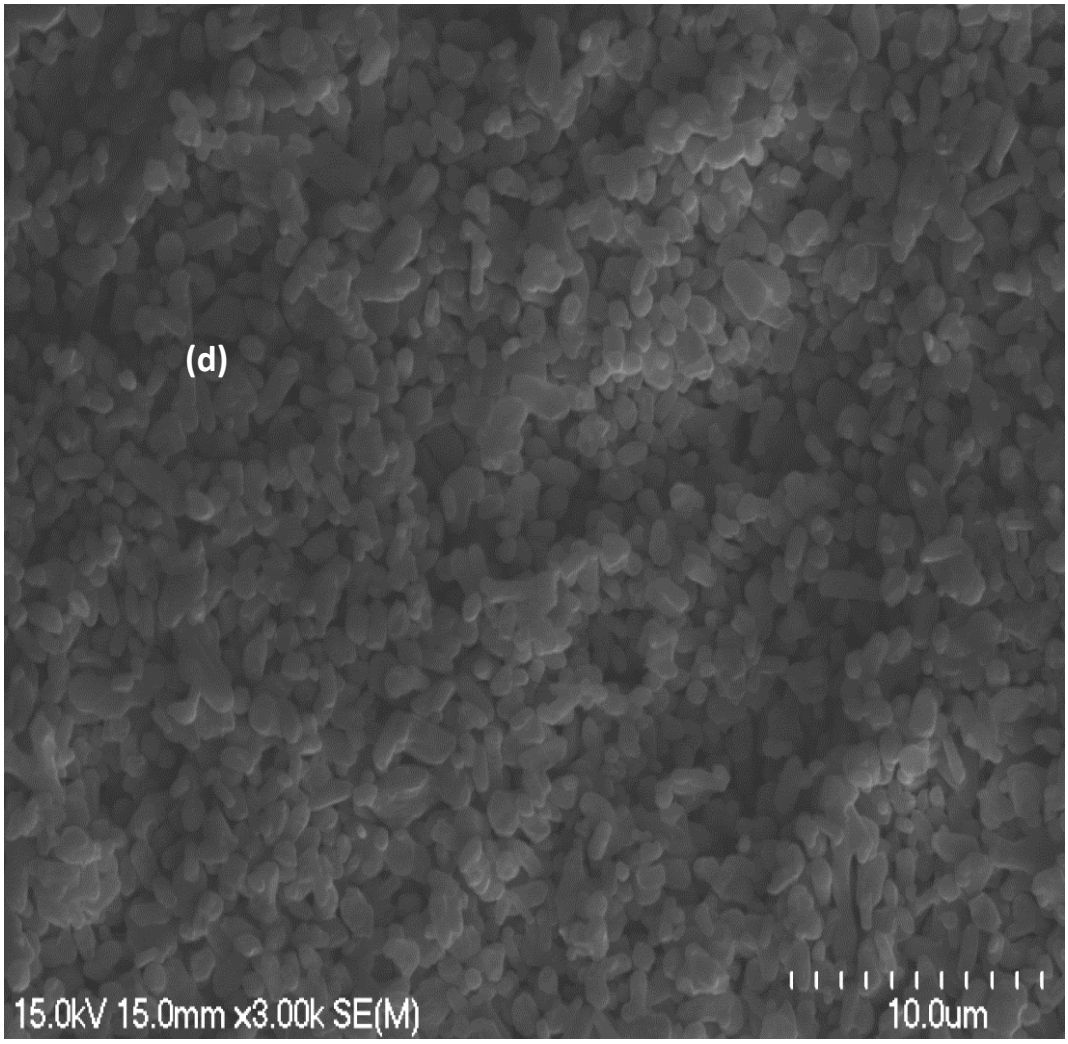

Figure 5-8: SEM images of (a) unsubstituted HAp (b) 0.5 SrHAp (c) 1.0 SrHAp (d) 1.5 SrHAp, prepared by hydrolysis of MCP/$Ca(OH)_2$ after sintering at 900 ˚C.

In general, the sintered HAp powders prepared with low levels of Sr ion substitution (e.g. 0.5SrHAp) were porous in nature and did not agglomerate readily. However, with increasing Sr^{2+} ion substitution, the SEM images of the HAp powders demonstrated that they became less porous in appearance and showed a uniform, regular distribution of particles with well packed materials being produced in the case of HAp powders produced with higher (i.e. 1.0 and 1.5 SrHAp) levels of Sr ion substitution. Spheroidal particles of HAp were seen in the cases of the 0.5SrHAp and 1.0 SrHAp powders while combinations of spheroidal and rod like particles were observed in the case of the 1.5 SrHAp powders.

Xu et al. [214], also noted that rod like particles were obtained when they prepared SrHAp samples with different levels of Sr ions (from 1 to 20 mol.%) by a hydrothermal route. However, their results revealed that all SrHAp samples prepared had a rod-like morphology which was different to the present study, since the present investigation displayed two kinds of morphology of SrHAp powders. Spheroidal particles of HAp were recorded in the cases of the 0.5SrHAp and 1.0 SrHAp powders, and combinations of spheroidal and rod like particles was observed in the case of the 1.5 SrHAp materials.

5.6 CuHAp materials by hydrolysis method:

Three different CuHAp powders with different levels of Cu^{2+} ion substitution (0.5 CuHAp, 1.0 CuHAp and 1.5 CuHAp powders) were prepared by hydrolysis of MCP/$Ca(OH)_2$, with the detailed amounts of the reagents listed in **Table 5-16.**

Table 5-16: Synthesis details of prepared CuHAp materials by the novel hydrolysis method of MCP/$Ca(OH)_2$.

Sample	MCP $Ca(H_2PO_4)_2$ (g)	$Ca(OH)_2$ (g)	$CuCl_2$ (g)	$Ca(H_2PO_4)_2$ (mol)	$Ca(OH)_2$ (mol)	Cu (mol)	Expected Ca/P
Unsubstituted HAp	11.5652	3.6522	-	0.0494	0.0493	-	1.67
0.5 CuHAp	10.9001	3.4532	0.3329	0.0466	0.0466	0.0025	1.58
1.0 CuHAp	10.2458	3.2364	0.6786	0.0438	0.0437	0.0050	1.50
1.5 CuHAp	9.5687	3.0412	0.9773	0.0409	0.0410	0.0073	1.42

An obvious difference between these powders and the other powders discussed thus far is the color of the CuHAp powders due to the replacement process of calcium ion by Cu^{2+} in the HAp crystals. While unsubstituted HAp (and the Sr and Zn substituted HAp powders) have a milky white color to them, the CuHAp powders have a distinct green color to them which varied in intensity from light green to dark green depending on the level of Cu ion substitution. This color can be considered as a telling sign that has proven that replacement of calcium ion by copper ions has actually taken place. **Fig 5-9** illustrates the powders obtained and their comparison with powders consisting of unsubstituted HAp**.**

Figure 5-9: Colours of the non-sintered CuHAp materials containing different levels of Cu^{2+} ion substitution as prepared by the hydrolysis of MCP/$Ca(OH)_2$

5.7 Characterization of CuHAp materials

5.7.1 5.6.1 ICP-MS of CuHAp materials after sintering at 900 ˚C

The results of the ICP-MS elemental analyses of the CuHAp samples are displayed in **Table 5-17.**

Table 5-17: ICP-MS results of CuHAp materials prepared using the novel hydrolysis method of MCP/$Ca(OH)_2$. Concentrations are expressed in ppb (ug/L):

Sample	Ca 44	P 31	Na 23	Cu 63
Unsubstituted HAp by hydrolysis	707795	401240	103797	-
0.5 CuHAp by hydrolysis	697314	381310	130778	26036.7
1.0 CuHAp by hydrolysis	662837	375921	131715	54955.6
1.5 CuHAp by hydrolysis	615229	361280	128236	81290.6

The starting (calculated) and actual (measured) degree of chemical composition of the prepared powders in terms of wt% of Cu^{2+} ions, the calcium/phosphorus (Ca/P) molar ratios as well as (Ca+Na+Cu)/P molar ratio were determined by ICP-MS and presented in **Table 5-18.**

Table 5-18: The chemical analysis data of CuHAp materials after sintering at 900 ˚C with different Cu^{2+} contents by ICP-MS measurements.

Sample	Ca/P Expected	Ca/P Measured	(Ca+Na+Cu)/ P	Wt.% of Cu^{2+} ions Theoretical	Wt.% of Cu^{2+} ions Measured
Unsubstituted HAp by hydrolysis	1.67	1.40	-	-	-
0.5 CuHAp by hydrolysis	1.58	1.41	1.91	3.1%	1.30%
1.0 CuHAp by hydrolysis	1.50	1.36	1.90	6.2%	2.74%
1.5 CuHAp by hydrolysis	1.42	1.32	1.90	9.2%	4.06%

The elemental composition of the prepared CuHAp materials as determined by ICP-MS are shown in **Table 5-18.** The Ca:P mole ratios were lower than the value expected from stoichiometric HAp (1.67) and this is due to the substitutions also involving Na^+ ions. However when calculating the (Ca+Na+Cu)/P ratio, this was found to be higher than the expected value of stochiometric HAp (1.67) and these higher values cannot be attributed to formation of carbonated HAp powders, because the prepared CuHAp samples, especially those labelled at 1.0 CuHAp and 1.5 CuHAp

were confirmed by FTIR spectra to be carbonate free materials. This result may be attributed to the phase purity, since another phase (CuO phase) was detected by XRD.

5.7.2 FTIR of CuHAp materials with different Cu^{2+} contents prepared by hydrolysis method.

5.7.2.1 FTIR of non-sintered CuHAp materials.

The FTIR spectra of the non -sintered CuHAp powders with different levels of Cu^{2+} substitution (as prepared by hydrolysis of MCP/$Ca(OH)_2$) are shown in **Fig.5-10**.

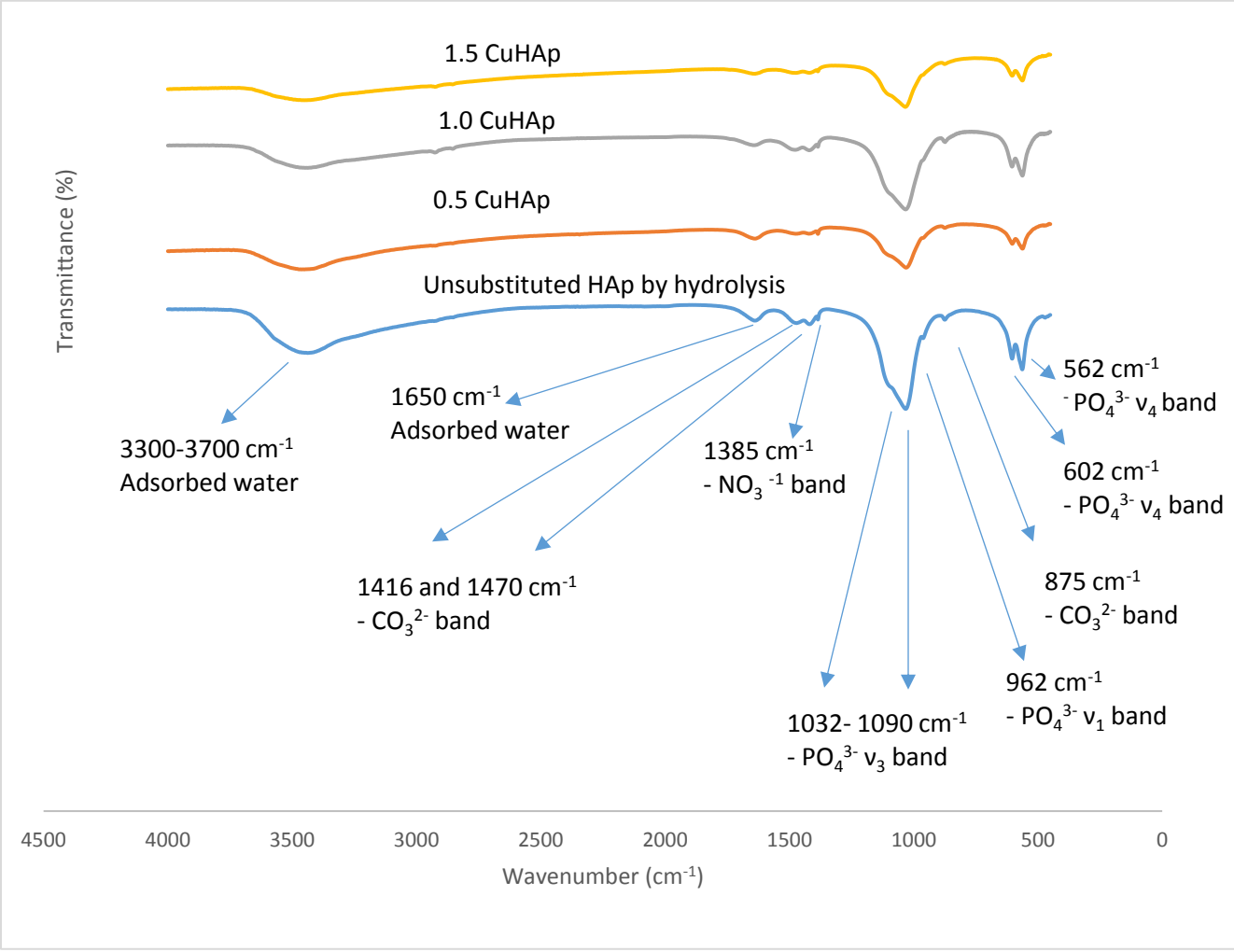

Figure 5-10: FTIR spectra of non-sintered copper substituted hydroxyapatite materials with different levels of Cu^{2+} substitution as prepared by the novel hydrolysis method of MCP/$Ca(OH)_2$

The broad band at 3000–3700 cm^{-1} and the small peak at about 1635 cm^{-1} are due to adsorbed water, while the bands with shoulder at 962– 1093 cm^{-1} were attributed to the P–O stretching vibration of phosphate (PO_4^{3-}). The band at 565–605 cm^{-1} that appears as a doublet was assigned to the PO_4^{3-} bending mode, and the carbonate modes detected at 875, 1416 and 1465 cm^{-1} served as an indication of the formation of CO_3HAp (B-type). The recorded band at 1385 cm^{-1} as discussed previously is believed to be due to the N-O stretching vibration of nitrate ion which could be a residual contaminant in the powders from starting materials or other sources.

5.7.2.2 FTIR of CuHAp materials after sintering at 900 ˚C:

The FTIR spectra of the sintered CuHAp powders with different levels of Cu^{2+} substitution are shown in **Fig.5-11**.

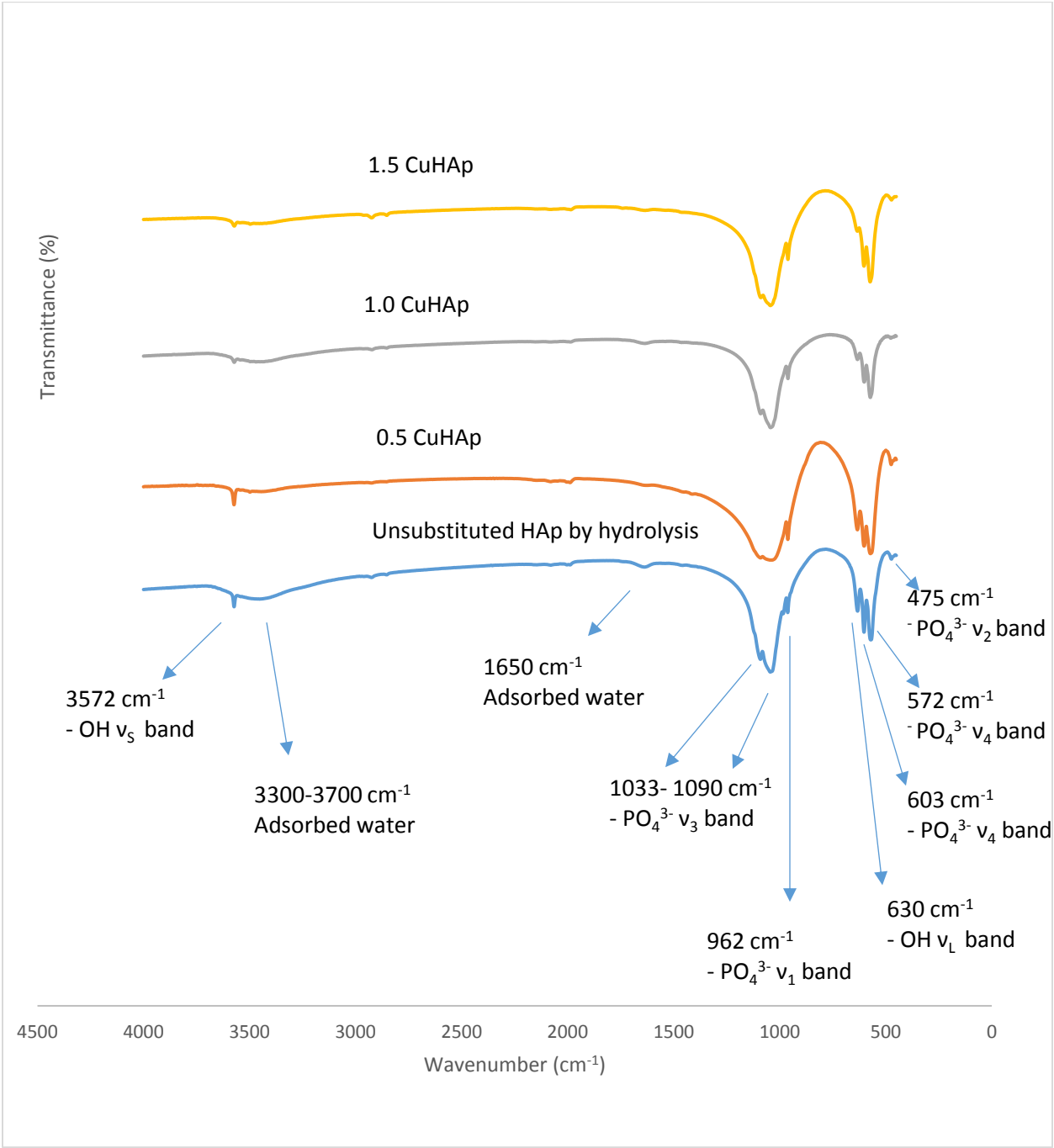

Figure 5-11: FTIR spectra of CuHAp hydroxyapatite materials with different levels of Cu^{2+} substitution after sintering at 900 ˚C.

Fig. 5-11. represents the FTIR spectra of sintered CuHAp powders. It is clear the characteristic peaks of adsorbed water (3000–3700cm^{-1}) and those due to the substituted carbonates (875, 1415 and 1470 cm^{-1}) disappear due to the sintering process. The fundamental vibrational modes of PO_4^{3-} group of all powders were all retained and are shown at 475 (v_2), 570, 605 (v_4), 962 (v_1)

and 1035- 1090 cm^{-1} (v_3). The presence of the lattice OH group in all CuHAp samples was detected by the observation of the OH stretching and librational modes at 3572 and 631 cm^{-1} respectively. Another observation from the FTIR spectra was that the intensity of both of the lattice OH-associated bands in the prepared CuHAp materials showed a decrease in intensity at 3572 cm^{-1} and 631 cm^{-1} as the substitution level of copper ion increased in the HAp lattice. This result has been observed in previous literature reports on CuHAp materials and can be attributed to the following possibilities:

1- Replacement process of hydroxyl group by chloride ions that were used as a source of copper ions ($CuCl_2$).
2- Replacement of the proton (H^+) in the compounds by copper ions. This will be discussed later in the section on XRD results.

Imrie et al. [196], reported the preparation of Copper-doped hydroxyapatite with the following nominal formula $Ca_{10}(PO_4)_6Cu_xO_yH_z$, where x = 0, 0.5, 0.75 and 1 which was prepared by using a solid state method. $CaHPO_4$, $CaCO_3$ and copper (II) oxide (CuO) were the starting materials. The FTIR investigations reported in that study displayed a clear reduction in intensity of the OH stretch (3572 cm^{-1}) and the OH librational peaks (631 cm^{-1}) as the level of copper ion substitution increased in the HAp compounds generated.

5.7.3 XRD diffraction analysis of CuHAp materials after sintering at 900 ˚C.

5.7.3.1 Phase Identification of CuHAp powders.

Fig. 5-12 illustrates the XRD diffraction patterns of the sintered CuHAp materials.

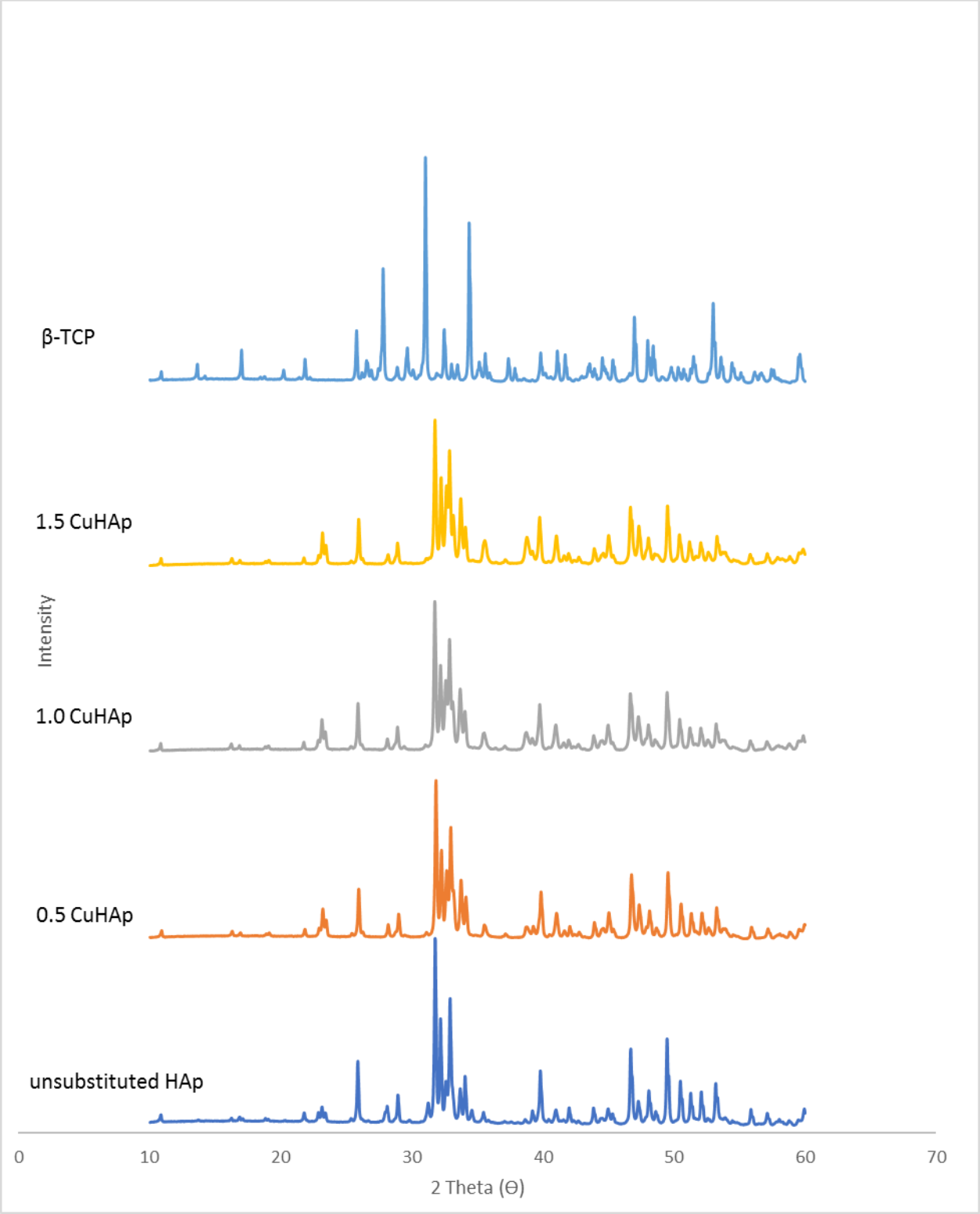

Figure 5-12: The XRD diffraction patterns of CuHAp materials after sintering at 900 ˚C.

The powder X-ray diffraction analysis (**Fig. 5-12**) showed the intensity of one peak at 2 Theta = 23.10˚ to start exhibiting a slight increase with an increase in the substitution levels of Cu^{2+} ions in the HAp lattice. In addition, the gradual decrease in intensity of one peak that corresponded

to the most intense peak in the β-TCP phase at 2Theta = 31.20˚ was also noted in the series of XRD patterns with increasing Cu^{2+} ion substitution. The following observations were also detected by XRD analysis:

1- An increase in the intensity of the peak at 2 Theta =33.60 corresponding to the impurity phase (β-TCP) was confirmed by XRD analysis in all prepared CuHAp powders with increasing the concentration of copper ions. This observation was associated with appearance of a new peak with very small intensity at 2 Theta = 38.80 ˚in all prepared CuHAp samples, this peak is related to an impurity phase (CuO) [215].

2- In the cases of 1.0 and 1.5 CuHAp samples, a new peak appeared at 2 Theta = 33.10 ˚, which can be attributed to the β-TCP phase. The intensity of this peak increased as the concentration of copper ions increased.

5.7.3.2 Crystallinity and crystallite size of CuHAp powders:

The degree of crystallinity and the crystallite size of the sintered CuHAp containing different levels of Cu^{2+} substitution are displayed in **Table 5-19.**

Table 5-19: The degree of crystallinity and the crystallite size of CuHAp materials after sintering at 900 ˚C.

Sample	D_{002} (Å)	Crystallinity %
Unsubstituted HAp by hydrolysis	549.8±3.6	82.57±2.1
0.5 CuHAp by hydrolysis	490.9±6.8	77.19±4.7
1.0 CuHAp by hydrolysis	474.0±1.5	73.40±4.6
1.5 CuHAp by hydrolysis	489.9±2.5	74.95±3.6

The XRD patterns in **Fig.5-12** also, show some broadening of peaks as the level of copper ion substitution in the HAp lattice increased. This was supported by the calculations of the degree of crystallinity which showed a clear reduction of the numerical value of crystallinity as the substitution level of Cu^{2+} ions increased in the HAp lattice (see **Table 5-19)**. This phenomenon was reported by several authors who also prepared CuHAp powders with different levels of

substitution via different synthetic methods. **Table 5-20** below illustrates some of these investigations.

Table 5-20: Illustrated the relationship between crystallinity and substitution of copper ions into HAp crystal.

Authors	Preparation method	Results
Othmani et al. [178]	The authors prepared CuHAp by a co-precipitation method with the following chemical formula: $Ca_{(10-x)}Cu_x(PO_4)_6(OH)_2$ ($0 \leq x \leq 4$).	They reported that substitution of copper ion into the HAp structure decreased the crystallinity.
Stanic´ et al. [8]	The authors reported the synthesis of CuHAp by neutralization methods (acid-base reaction, the authors used $Ca(OH)_2$ and H_3PO_4 to prepare the materials). HAp and doped HAp with two different concentrations of Cu ions, namely ((CuHAP1) and (CuHAP2) were prepared, and Cu/(Ca + Cu) = 0.0004 and 0.004 for CuHAp1 and (CuHAP2) respectively	The result of that investigation confirmed that incorporation of copper into HAp structure reduces the crystallinity. The numerical values of crystallinity were 86, 80 and 77% for HAp, CuHAp1 and CuHAp2, respectively.

In the present study, Table 5-19, also shows an obvious reduction in the value of crystallite size because of substitution of copper ions into HAp structure to reach the minimum value at 1.0 CuHAp (474.0 Å), a slight increase was obtained due to increasing the substitution level of copper in 1.5 CuHAp (489.9 Å).

5.7.3.3 Lattice parameters and volume of unit cell of CuHAp powders:

The lattice parameters and the volume of hexagonal unit cell of the sintered CuHAp materials are shown in **Table 5-21**.

Table 5-21: The lattice parameters and the volume of hexagonal unit cell of the CuHAp after sintering at 900 ˚C.

Sample	a [Å]	c [Å]	V[Å^3]
Unsubstituted HAp by hydrolysis	9.421±0.00	6.882±0.005	1581±0.004
0.5 CuHAp by hydrolysis	9.424±0.00	6.881±0.003	1582±0.003
1.0 CuHAp by hydrolysis	9.431±0.00	6.877±0.001	1583±0.002
1.5 CuHAp by hydrolysis	9.374±0.00	6.899±0.004	1569±0.004

In the cases of 0.5 and 1.0 CuHAp **Table 5-21** reveals that the lattice parameter (a) increased as the level of Cu ion substitution increased, while the lattice parameter (c) decreased. In the case of 1.5 CuHAp, the Rietveld refinement showed that the lattice parameter (a) decreased in a clear manner while lattice (c) increased.

Based on the ionic radius of Cu^{2+} (73 pm) which is smaller than that of Ca^{2+} (100 pm) [178], a reduction in both lattice parameters (a and c) of HAp materials should be expected, but Rietveld refinement, however, displayed an opposite result(an expansion in the volume of unit cell was recorded). This result can be attributed to the following:

1- The occurrence of the substitution process of hydroxyl group by chloride ions which have a larger ionic radius (0.168 nm) [216] compared to that of the OH^- ion (0.153 nm). The source of chloride ions was copper (II) chloride ($CuCl_2$), which was used as the Cu-containing starting material.

2- Well-known phosphates with apatite structure $\mathbf{A_5(PO_4)_3X}$ are widely investigated and show high potential for several applications such as biomedical ones [217]. While **A-**position, alkaline earth or other large cations are normally situated such as calcium and strontium, the channels are usually filled with the **X** units such as hydroxyl group (OH^-) and halogen anions. In the phosphate apatite structure, copper was known to substitute cations in **A-**position [218]. Even though there is no evidence up to now on a possibility to introduce copper or any other metal cations in the channels [217], the Rietveld analysis of our investigation showed an increase in the volume of unit cell with increasing Cu^{2+} concentrations which may indicate of substitution of copper ions by the

OH sites in the hexagonal channels of the apatite structure. In other words, this result provides an evidence of the possibility of copper ions ***to replace the smaller proton on the hydroxyl site which will cause an expansion in the volume of unit cell because of the larger ionic radius of Cu^{2+} (73 pm) compared to the smaller ionic radius of H^{+}.*** As a result, an expansion in the volume of unit cell of hexagonal structure of CuHAp powders was recorded. Similar results were obtained in the literature as detailed below:

Imrie et al. [196] prepared copper-doped hydroxyapatite with the following nominal formula $Ca_{10}(PO_4)_6Cu_xO_yH_z$, where x = 0, 0.5, 0.75 and 1 by using a solid state method. The authors used $CaHPO_4$, $CaCO_3$ and copper (II) oxide (CuO) as a starting material. They reported that as the level of Cu substitution increased in the HAp lattice, both lattice parameters (a and c) were observed to increase and stated that this observation confirmed the substitution of the Cu^{2+} ion for the smaller proton on the OH lattice site.

Bhattacharjee et al. [219] prepared copper-doped hydroxyapatite (CuHAp) with the following nominal composition $Ca_{10}(PO_4)_6[Cu_x(OH)_{2-2x}O_x]$ ($0.0 \leq x \leq 0.8$) by using two synthetic methods, namely solid-state and wet chemical methods (precipitation). The result of this investigation displayed that the volume of unit cell of the copper doped materials which were prepared by solid state reaction increased from 527.17 for HAp materials to 533.31 for CuHAp materials with the following composition ($Ca_{10}(PO_4)_6[Cu_{0.8}(OH)_{0.4}O_{0.8}$). On other hand, the wet chemical method displayed a slight expansion in the volume of unit cell compared to the solid-state route. The volume of unit cell was 528.30 for HAp materials to 529.3 of CuHAp materials with the following formula: $Ca_{10}(PO_4)_6[Cu_{0.8}(OH)_{0.4}O_{0.8}$. The authors reported that the unit cell expansion of CuHAp material, when prepared by a solid state route can be used as evidence that Cu enters the HAp channel X positions (OH- group), rather than the calcium sites (substitution of calcium site). Direct substitution of Cu^{2+} with smaller ionic radius (0.73 Å) for Ca^{2+} with larger ionic radius(0.99 Å) would lead to a contraction, but their investigation showed an increase in the volume of the unit cell of the hexagonal structure of copper doped HAp. The authors explained the slight increase in the volume of unit cell of CuHAp materials which were prepared by the wet chemical method in terms of the less complete Cu tunnel incorporation (this means Cu substitutes in the

channel (X) site) and partial of Cu in place of calcium (i.e. partial substitution of the calcium ion in its characteristic site by copper ions).

However, in the present study and in the case of 1.5 CuHAp, the Rietveld analysis showed a clear reduction in the volume of the unit cell of the 1.5 CuHAp powders. The lattice parameters (a and c) of the prepared 1.5 CuHAp samples were 9.374 and 6.899 Å, respectively compared to 9.421 and 6.882 Å for unsubstituted HAp materials. This reduction can be ascribed to defects and disorder achieved by substituting high levels of copper ions into the HAp structure.

5.7.4 SEM of CuHAp materials after sintering at 900 ˚C

Figure 5-13 displayed the SEM images of CuHAp powders after sintering at 900 ˚C.

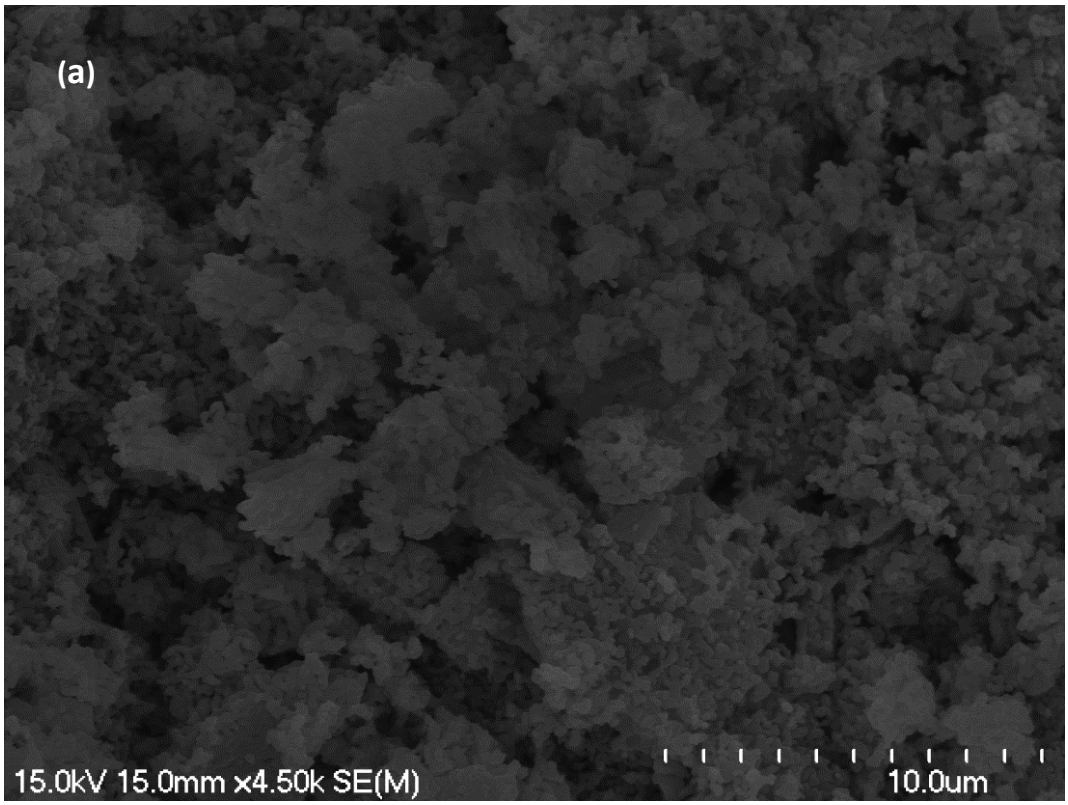

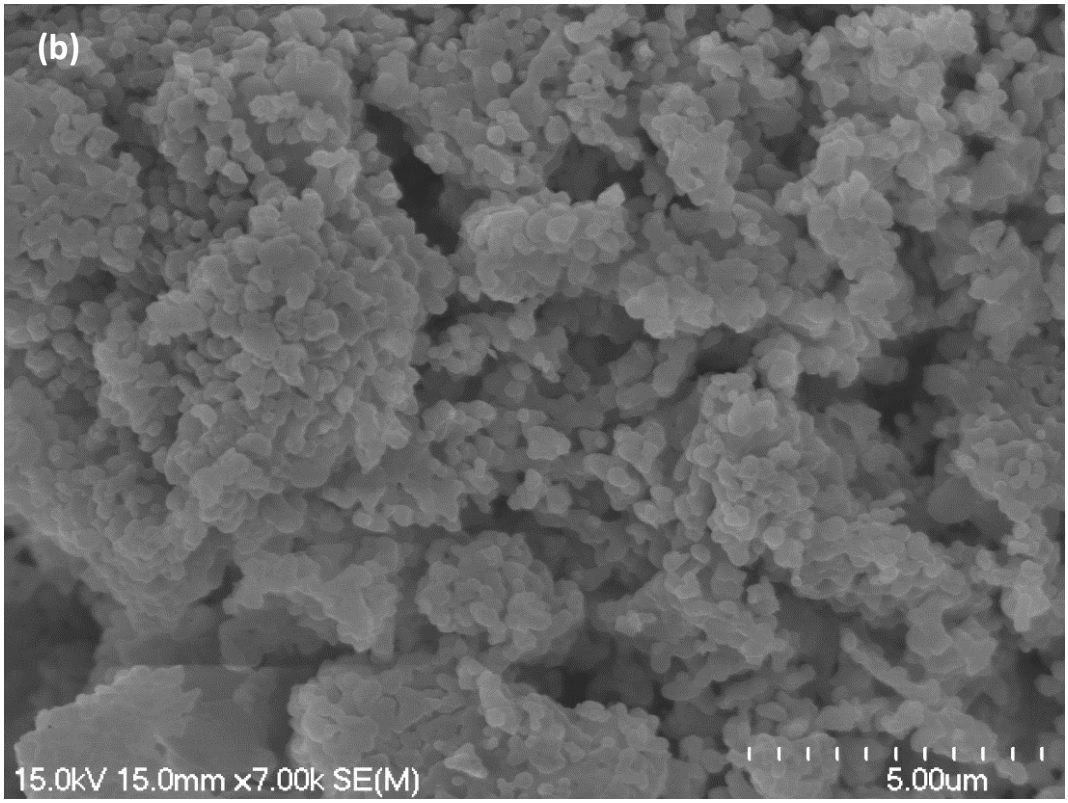
(b)
15.0kV 15.0mm x7.00k SE(M)
5.00um

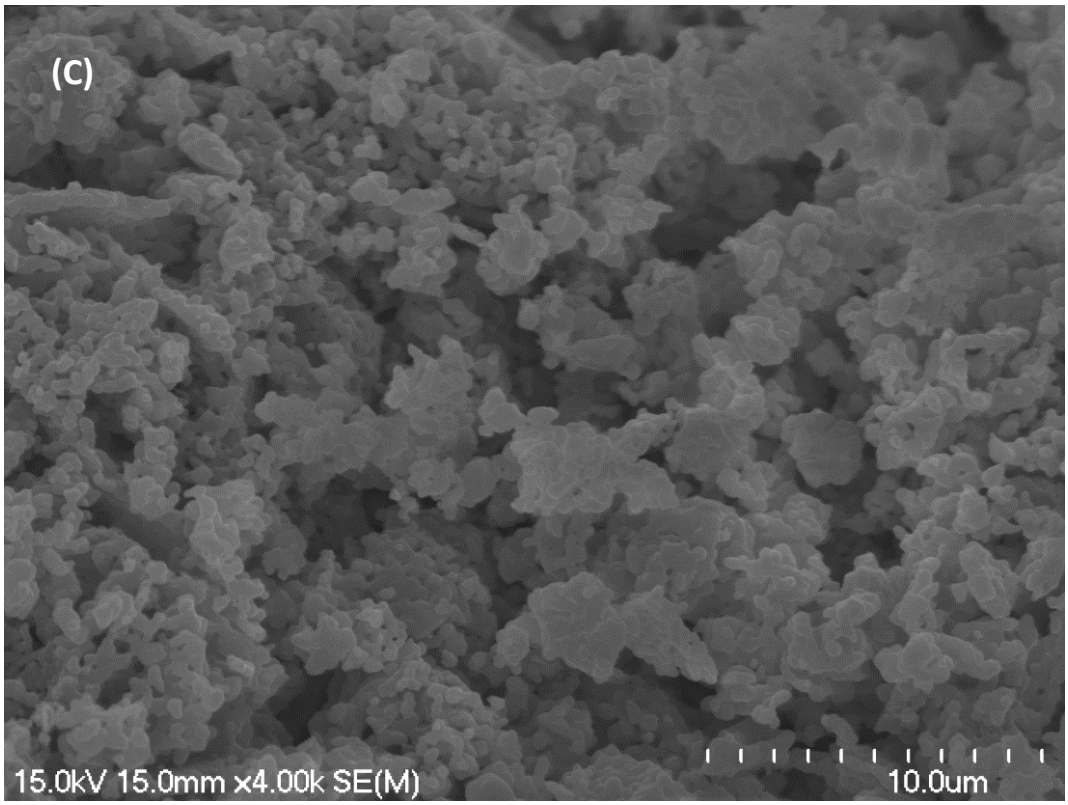
(C)
15.0kV 15.0mm x4.00k SE(M)
10.0um

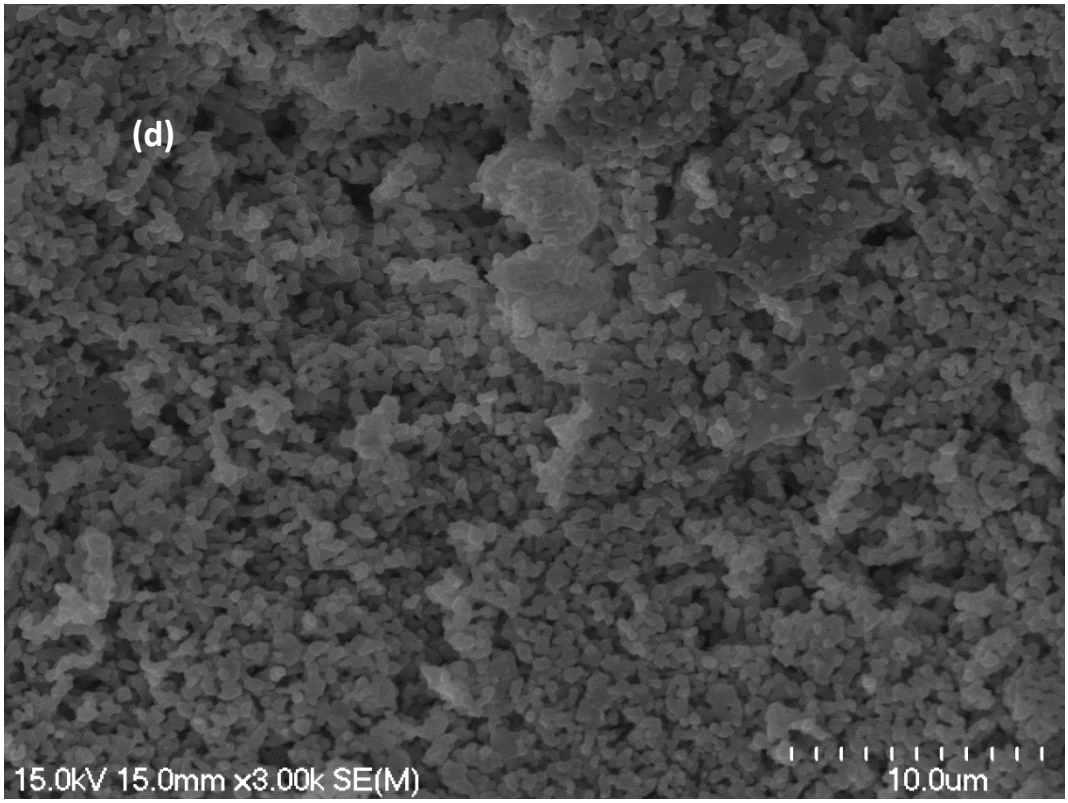

Figure 5-13: SEM images of (a) unsubstituted HAp (b) 0.5 CuHAp (c) 1.0 CuHAp (d) 1.5 CuHAp, prepared by hydrolysis of MCP/$Ca(OH)_2$ after sintering at 900 ˚C.

The SEM images revealed that porous, irregularly distributed, spheroidal shaped, and agglomerated structures were obtained for all samples. As a result of increasing the percent of cupper ions (Cu^{2+}), the morphology did not change; the particles remaining have elongated spheroids, whereas the level of porosity started to show a slight reduction.

5.8 Summary:

A summary of the findings for this chapter can be outlined as follows:

1- A new method to prepare HAps and substituted HAps by hydrolysis of MCP with $Ca(OH)_2$ is shown to be an effective new route to these powders. By means of this new synthetic route, three MHAp materials were prepared with the following chemical formula: $Ca_{10-x}M_x(PO_4)_6(OH)_2$ (M=Zn, Sr and Cu, x=0.5, 1.0 and 1.5), and were characterized by various methods to be HAp with one of them (ICP-MS) demonstrating the presence of the Zn, Sr and Cu ions in the associated with the HAp samples though not necessarily proving the different level of substitution.

2- As stated in 1, different techniques were used to characterize the prepared samples such as SEM, FTIR, XRD and ICP-MS.

The result of using these techniques showed:

- The formation of a hydroxyapatite phase was confirmed to result from the new hydrolysis method via detection of the fundamental vibrational modes of PO_4^{3-} group at 562, 602, 962 and 1032-1095 cm^{-1}, as well as by recording the typical HAp lattice-associated bands of the OH^- group at 3572 and 631 cm^{-1}. This result was confirmed by using FTIR analysis.
- The FTIR spectra of the prepared substituted MHAp materials (ZnHAp and SrHAp) also revealed a clear relationship between the concentration of M ions substituted, and the observed intensities of lattice OH^- vibrational modes at 3572 cm^{-1} (stretching) and 630 cm^{-1} (librational). This observation was attributed to the change in the local environment of the OH groups, that was obtained due to the substitution of Ca^{2+} ions by the Zn^{2+} and Sr^{2+} ions, which would also led to a change in the value of the frequency of librational mode.
- A clear shift of the phosphate bands at 572 and 604 cm^{-1} to lower wave numbers due to substitution of calcium ions by Sr^{2+} ions was detected by FTIR spectra. The magnitude of the shift increases as the concentration of Sr^{2+} ions substituted into the lattice increases. In addition, a shift of the OH librational mode band from 630 to 612 cm^{-1} was observed with increasing substitution of the Sr^{2+} ions into the HAp lattice. This result was in a good agreement with that obtained from another study performed by Bigi et al. [131].
- The phase purity, crystallinity, crystallite size and lattice parameters of the prepared MHAp materials with the following chemical formula: $Ca_{10-x}M_x(PO_4)_6(OH)_2$, (where M=Zn, Sr and Cu, X=0.5, 1.0 and 1.5) varied with increasing substitution levels and the details of these values were discussed in this Chapter.
- SEM images displayed that ZnHAp and CuHAp materials consist of agglomerated crystals which are spheroidal in shape. Also, spheroidal particles were seen in the cases of 0.5 SrHAp and 1.0 SrHAp samples, while a combination of spheroidal and rod like particles was observed in the case of 1.5 SrHAp materials.

- The varying presence of Zn^{2+}, Sr^{2+} and Cu^{2+} ions in the HAp samples was detected by ICP-MS analysis.
- ICP-MS analysis showed that Ca/P mole ratios of prepared MHAp powders with the following chemical formula: $Ca_{10-x}M_x(PO_4)_6(OH)_2$ (where M=Zn, Sr and Cu, x=0.5, 1.0 and 1.5), were found to be lower than expected from stoichiometry due to ion substitution processes occurring other than the ones of interest. These frequently involved Na^+ ions that would have come from the use of NaOH to adjust pH value. Also, Ca+Na+M/ P mole ratios (where M= Zn, Sr and Cu) were found to be higher than the value definitive of stoichiometric HAp. This result can be ascribed to the following:

  1- The additional formation of carbonated HAp as in the case of 1.5 SrHAp.

  2- The formation of biphasic compounds due to the replacement process of Zn^{2+} ions into HAp crystal as in the case of 0.5, 1.0 and 1.5 ZnHAp powders.

  3- The presence of another phase (CuO) as in the case of 0.5, 1.0 and 1.5 CuHAp materials.

  On the other hand, the results of ICP-MS measurements displayed clearly that the measured (actual) wt.% values of Zn^{2+}, Sr^{2+} and Cu^{2+} ions that had already been introduced into HAp samples were lower than the theoretical value introduced in terms of the synthesis parameters indicating how difficult it is for the small ions such as Zn^{2+} and Cu^{2+}as well as the large ions such as $Sr^{2+}$to be introduced and hosted by the HAp. It should also be mentioned that although ICP-MS may detect the presence of the introduced ions (for substitution) it does not prove they are actually substituted.

Chapter Six

Studies on cationic substitutions into HAp of little studied ions

6.1 Introduction:

As discussed previously calcium phosphate compounds have been used for many years in biomedical fields such as bone substitute materials for orthopaedic and dentistry [220]. The most used calcium phosphate compound is hydroxyapatite (HAp). Therefore, a novel method was developed to prepare (unsubstituted) HAp by hydrolysis of monocalcium phosphate (MCP) using calcium hydroxide as discussed in Chapter 4. Studies were described using this technique with ions which have been well studied for hydroxyapatite substitutions such as strontium, zinc and copper ions in Chapter 5

The stoichiometric HAp with $Ca_{10}(PO_4)_6(OH)_2$ formula is of great interest for researchers because of the flexibility/lability of its structure which gives it the ability to accept ionic substituents into the lattice and into vacancies [63]. Several attempts have been performed previously by other researchers and discussed extensively in the current literature [221], through substitution of other impurities into HAp crystal to enhance some properties of HAp such as the biological, the chemical and the mechanical characteristics. One of these methods is via cationic substitution. Cationic substitutions occur when the calcium site of HAp is partially replaced, or even occupied by another cation such as Zn^{2+}, Mg^{2+}, Na^{+},….etc [29]. As a result, different systems of MHAp powders with the following chemical formula: $Ca_{10-x}M_xHAp$ (where M=Zn, Sr and Cu, X=0.5, 1.0 and 1.5) were prepared by using the novel hydrolysis method. The details of analysis tests that were used to characterize these samples using the new hydrolysis method had been discussed in Chapter 5. Chapter six outlined the preparation method of new systems of cationic substituted hydroxyapatite materials. Specific systems of MHAp materials (where M= Rb, Eu and Sc) with different substitution levels were prepared using two different synthesis approaches, namely the novel hydrolysis and the conventional precipitation routes. The purpose of using these ions for the substitution process into HAp was mentioned in Chapter 1. No studies to the author's

knowledge on the synthesis of Rb, Eu and Sc substituted HAp by the hydrolysis method using MCP/$Ca(OH)_2$ as a starting material have been published in the chemical literature. Also, no studies to the author's knowledge on the preparation process of Rb and Sc substituted HAp by using the precipitation method have been reported. While, limited previous attempts were performed to prepare EuHAp powders as discussed in the literature [18,19,25,222,223], one paper was published describing the preparation of RbHAp by a hydrothermal method [224].

This chapter aimed to achieve the following:

1- To prepare specific systems of cationic substituted hydroxyapatite, namely 1% RbHAp (1 wt.% Rb^{+}), 1%EuHAp (1 wt.% Eu^{3+}) and 1,3 and 5% ScHAp (1, 3 and 5 wt.% Eu^{3+}), by using two different approaches (precipitation and hydrolysis methods).
2- To evaluate the effect of the synthesis route on some properties of HAp materials like the morphology, chemical composition, substitution levels, crystallinity, crystallite size, lattice parameters and phase purity, simply because the characteristics of HAp materials such as the physicochemical and morphological properties depend on the preparation method, as other research has established [167].
3- To provide an idea through using FTIR analysis about the relationship between the reduction of intensities of the stretching and librational modes of the OH^{-} group at (3572 and 630 cm^{-1}) and the requirement to keep the charge balance for the prepared substituted HAp powders due to the replacement process of the calcium ion in the HAP crystal lattice by the trivalent cation (Eu^{3+}) or the monovalent cation (Rb^{+}).

The following techniques were used to characterize the above substituted HAp powders and the results were discussed extensively:

1- Scanning electron microscope materials.

2- FTIR spectroscopy.

3- Powders X-ray Diffraction (XRD).

4- Inductively coupled plasma mass spectrometry (ICP-MS) analysis.

6.2 1% RbHAp (1 wt.% Rb^+) powders prepared by hydrolysis and precipitation methods:

Two series of RbHAp powders (1wt% RbHAp) were prepared by precipitation and hydrolysis methods, and the detailed amounts of the reagents are listed in T**able 6-1.**

Table 6-1: Synthesis details of 1% RbHAp (1% wt. Rb^+) powders prepared by precipitation and hydrolysis methods.

Sample	MCP (g)	$Ca(OH)_2$ (g)	$Ca(NO_3)_2$ (g)	Na_2HPO_4 (g)	RbCl (g)	MCP (mol)	$Ca(OH)_2$ (mol)	$Ca(NO_3)_2$ (mol)	Na_2HPO_4 (mol)	RbCl (mol)
1%RbHAp (1 wt.% Rb^+) by precipitation	-	-	8.0076	4.2145	0.0777	-	-	0.04880	0.0297	0.0006
1% RbHAp (1 wt.% Rb^+) by hydrolysis	11.4186	3.6087	-	-	0.0777	0.0488	0.0487	-	-	0.0006

6.2.1 Characterization techniques of prepared 1%RbHAp (1 wt.% Rb^+) materials by hydrolysis and precipitation methods.

6.2.1.1 ICP-MS of 1% RbHAp (1 wt.% Rb^+) materials prepared by hydrolysis and precipitation methods after sintering at 900 ˚C.

The results of the elemental analyses of 1% RbHAp (1 wt.% Rb^+) samples that were prepared by the conventional precipitation and the novel hydrolysis routes are displayed in **Table 6-2.**

Table 6-2: ICP-MS results of 1% RbHAp (1% wt. Rb^+) materials prepared by precipitation and hydrolysis methods after sintering at 900 ˚C. The concentration is given in ppb (ug/L):

Sample	Ca 44	P 31	Na 23	Rb 85
Unsubstituted HAp by precipitation	707795	401240	103797	-
1% RbHAp by precipitation	776621	378042	29600	1041.9
Unsubstituted HAp by hydrolysis	769928	423970	78396	-
1% RbHAp by hydrolysis	793212	392324	51192	141.4

The starting (calculated) and actual (measured) degree of chemical composition of the prepared powders in terms of wt% of Rb^+ ions, the calcium/phosphorus (Ca/P) molar ratios as well as (Ca+Na+Rb)/P molar ratio were determined by ICP-MS and presented in **Table 6-3.**

Table 6-3: The chemical analysis data of 1% RbHAp (1 wt.% Rb^+) materials by ICP-MS measurements after sintering at 900 ˚C.

Sample	Ca/P Theoretical	Ca/P Measured	(Ca+Na+Rb)/P Mole ratio	Wt.% Rb^+ ions theoretical	Wt.% Rb^+ ions Measured	Wt.% of Na^+ ions Measured
Unsubstituted HAp by precipitation	1.67	1.36	1.71	-	-	5.2%
1% RbHAp by precipitation	1.64	1.56	1.69	1%	0.05%	1.5%
Unsubstituted HAp by hydrolysis	1.67	1.40	1.65	-	-	3.9%
1%RbHAp by hydrolysis	1.64	1.48	1.74	1%	0.01%	2.6%

Table 6-3 displays that the Ca:P mole ratio for the prepared 1%RbHAp samples was lower than the expected value (1.64). This result can be attributed to the presence of Na^+ ions in the samples which are substituting into the calcium ion sites in the HAp lattice as discussed previously (see chapter four for details). Also, the ICP-MS analysis showed that the level of Rb^+ ions associated (though not necessarily substituted) with the HAp crystal was very low compared to the proposed percent of substitution (1%). This result was expected due to the larger ionic radius of Rb^+ (152 pm) compared to Ca^{2+} (100 pm) [225]. However, the **(**Ca+Na+Rb)/P mole ratios for the prepared RbHAp samples were slightly higher than the value of stochiometric HAp (1.67), due to formation of carbonated HAp in the prepared samples. Also, the ICP-MS analysis displayed that the measured wt.% of Rb^+ ions that was associated (though not necessarily substituted) with the HAp crystal by the precipitation method is higher compared to the hydrolysis method, indicating the effect of the preparation method on the incorporation of Rb as shown in **Table 6-3**.

6.2.1.2 FTIR of prepared 1%RbHAp (1 wt.% Rb^+) by hydrolysis method and precipitation method:

FTIR of the non- sintered 1% RbHAp (1 wt.% Rb+) materials prepared by hydrolysis and precipitation methods:

Fig.6-1 displays the FTIR spectra of the non-sintered 1% RbHAp (1 wt.% Rb^+) powders prepared by the conventional precipitation and novel hydrolysis methods.

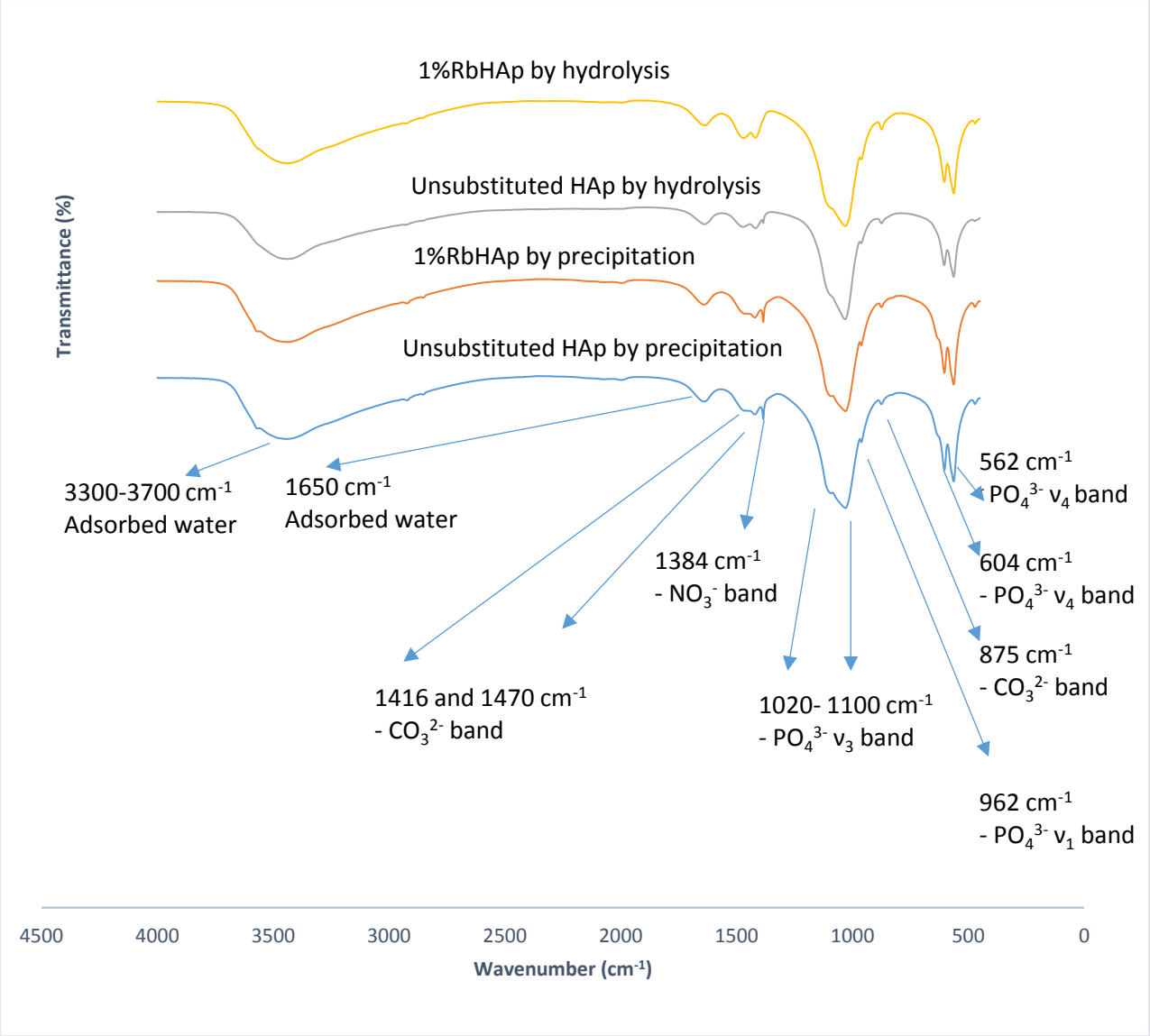

Figure 6-1: FTIR spectra of non-sintered 1% RbHAp (1 wt.% Rb^{+}) materials prepared by the conventional precipitation and novel hydrolysis methods.

The FTIR spectrum of the non-sintered 1%RbHAp materials which were prepared by the conventional precipitation method and the novel hydrolysis route was similar to the non-sintered unsubstituted HAp samples that were prepared by the precipitation and the novel hydrolysis methods as discussed in Chapter 4, as well as to the non-sintered MHAp materials with the following chemical formula: $Ca_{10-x}M_xHAp$ (where M=Zn, Sr and Cu, X=0.5, 1.0 and 1.5) that were synthesized by the novel hydrolysis method as shown in Chapter 5. The presence of the fundamental vibrational modes of PO_4^{3-} group at 562, 604, 962 and 1020-1100 cm^{-1}, were also

present in all samples, while the carbonate peaks appeared at 875, 1470 and 1416 $cm^{-1,}$ indicating substitution of phosphate sites in HAp by CO_3^{2-} (B-type). The typical peak of the nitrate group at 1384 cm^{-1} was also recorded in the HAP prepared by the precipitation method and emanate from the starting materials (nitrate salts). However, thobservation of this peak in HAp products resulting from the hydrolysis method (see Chapter four for details), is instead believed to be due to the N-O stretching vibration of nitrate ion which was a residual contaminant in the KBr powder used to make the pellets. In spectra the bending vibration band of molecular H_2O at 1630 cm^{-1} and the broad band at 3300–3700 cm^{-1} were also recorded and attributed to adsorbed moisture on the powders. The disappearance of the (lattice) hydroxyl stretching and bending peaks at 3572 and 630 cm^{-1} for all samples were confirmed by FTIR, as evidence of the amorphous/poorly crystalline materials that are initially produced by the hydrolysis and precipitation routes.

FTIR of 1% RbHAp (1 wt.% Rb^+) materials prepared by the novel hydrolysis and conventional precipitation methods after sintering at 900 ˚C:

The FTIR spectra of the sintered 1%RbHAp materials prepared by different synthesis routes (precipitation and hydrolysis) are displayed in **Fig.6-2**

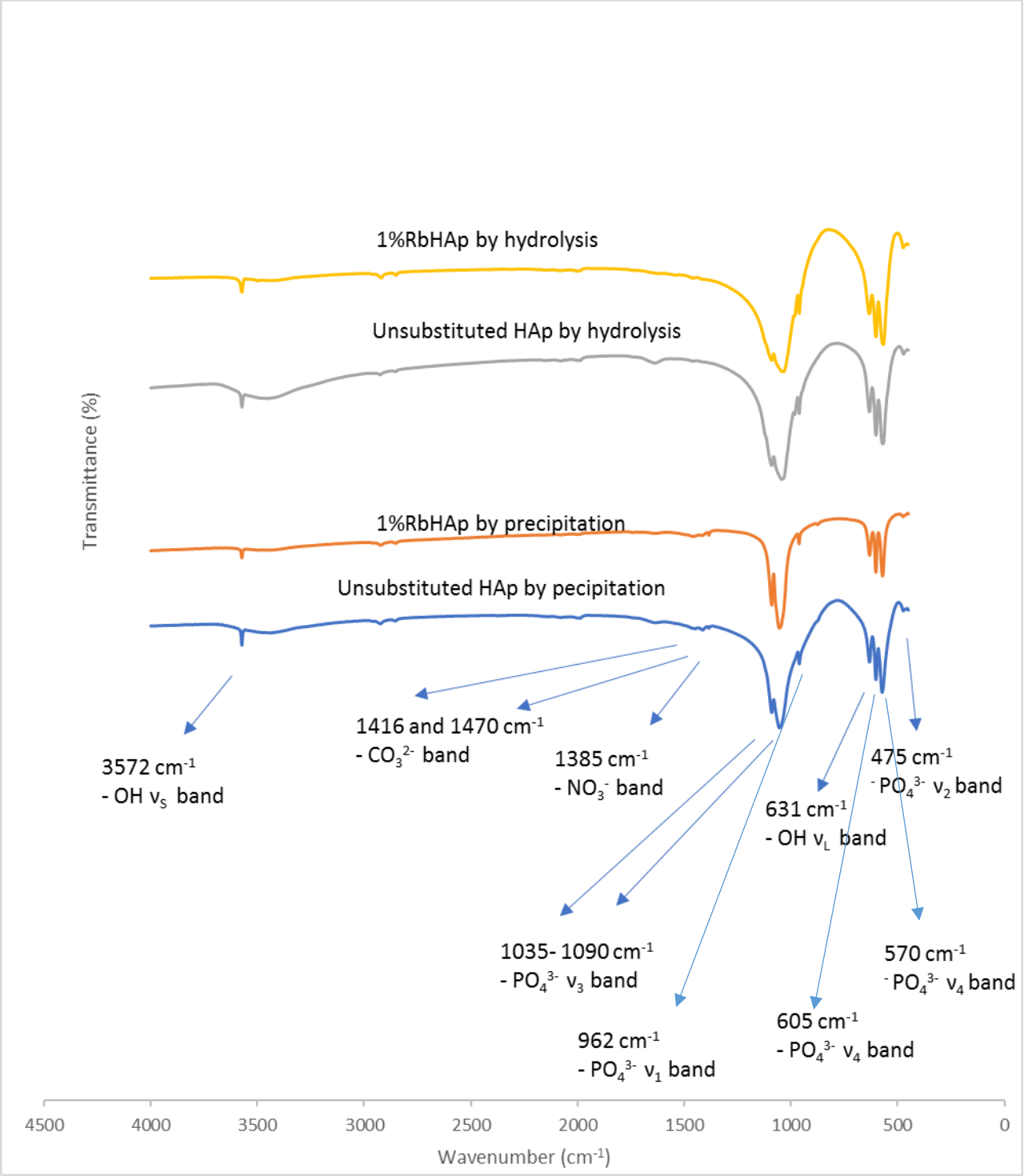

Figure 6-2: FTIR spectra of 1% RbHAp (1 wt.% Rb^{+}) materials prepared by precipitation and hydrolysis methods after sintering at 900 ˚C.

The FTIR spectra of sintered 1%RbHAp powders prepared by hydrolysis and precipitation methods displayed the presence of the apatitic phase. The bands at 570 and 603 cm^{-1} were

attributed to the bending mode (v_4) of the phosphate group. The (v_3) and (v_1) stretching modes of phosphate were observed at 1032-1090 and 962 cm^{-1}. The sharp peak at 3572 cm^{-1} related to the stretching vibration of lattice OH^-, as well as the peak at 630 cm^{-1} which corresponds to the OH^- librational mode. Well-defined peaks of carbonate at 875, 1412 and 1450 cm^{-1} were detected as a result of the substitution process of Rb^+ ions into the HAp structure by the precipitation method, but by using the hydrolysis method the carbonate bands disappeared. Other important observations confirmed by FTIR spectra were:

1- The intensity of the peak due to lattice OH (i.e. at 3572 cm^{-1}) stretching in the RbHAp materials prepared by the precipitation route at clearly decreased due to the substitution process of Rb^+ ions, while no any significant difference was obtained by hydrolysis method.
2- The increase of the peak intensities at 570, 603, 1032 and 1090 cm^{-1} of the prepared 1%RbHAp samples which were prepared by the precipitation route compared to the novel hydrolysis method can be considered as an enhancement of the crystallinity. This improvement in the crystallinity might be attributed to the higher wt.% of Rb^+ ions associated with the HAp crystals by using the precipitation route compared to the novel hydrolysis method as confirmed by ICP-MS analysis though ICP-MS cannot prove the Rb ions are substituted in the HAP lattice.

As discussed in the literature, the entry of other ions with different charges may be produced simply to restore the neutrality of HAp crystals that resulted from the substitution process of monovalent ions into the calcium sites [226]. The incorporation of Na^+ ions into HAp can be considered as an example of such a monovalent substitution process [226]. Several authors [226,227] described the proposed mechanism of replacement of sodium ions for calcium ions, suggesting Na^+ ions can promote the suitable conditions to accommodate the carbonate group (CO_3^{2-}) in phosphate sites. A reduction in the intensity of OH^- infrared absorption bands, as the levels of Na^+ ions increase in HAp structures, was reported in the literature [226]. However, the Na-containing B-type apatites ($NaCO_3$Aps) can be represented by the following formula : $Ca_{10-x}Na_{2x/3}(PO_4)_{6-x}(CO_3)_x(H_2O)_x(OH)_{2-x/3}$ [228], and the OH^- ion content was derived from the requirement to keep a charge balance. Therefore, the recorded reduction in the intensity of the stretching mode of the OH group that was associated with formation of carbonated HAp in the

present study's for prepared RbHAp materials by the precipitation route at (3572 cm^{-1}) can be attributed to :

1- the presence of sodium ions as confirmed by ICP-MS analysis associated with the formation of carbonated HAp in the prepared RbHAp materials as discussed above.
2- Also, the partial substitution of hydroxyl group by chloride ions as a result of using RbCl as a starting material to insert Rb^+ into the HAp crystal which can cause a reduction in the stretching mode of lattice OH at (3752cm^{-1}).

6.2.1.3 XRD diffraction analysis of sintered and non-sintered 1%RbHAp (1 wt.% Rb^+) prepared by hydrolysis and precipitation method:

Phase Identification of 1% RbHAp (1 wt.% Rb^+) materials:

Fig. 6-3 and 6-4 display the XRD diffraction patterns of non-sintered and sintered 1% RbHAp powders prepared by hydrolysis and precipitation methods.

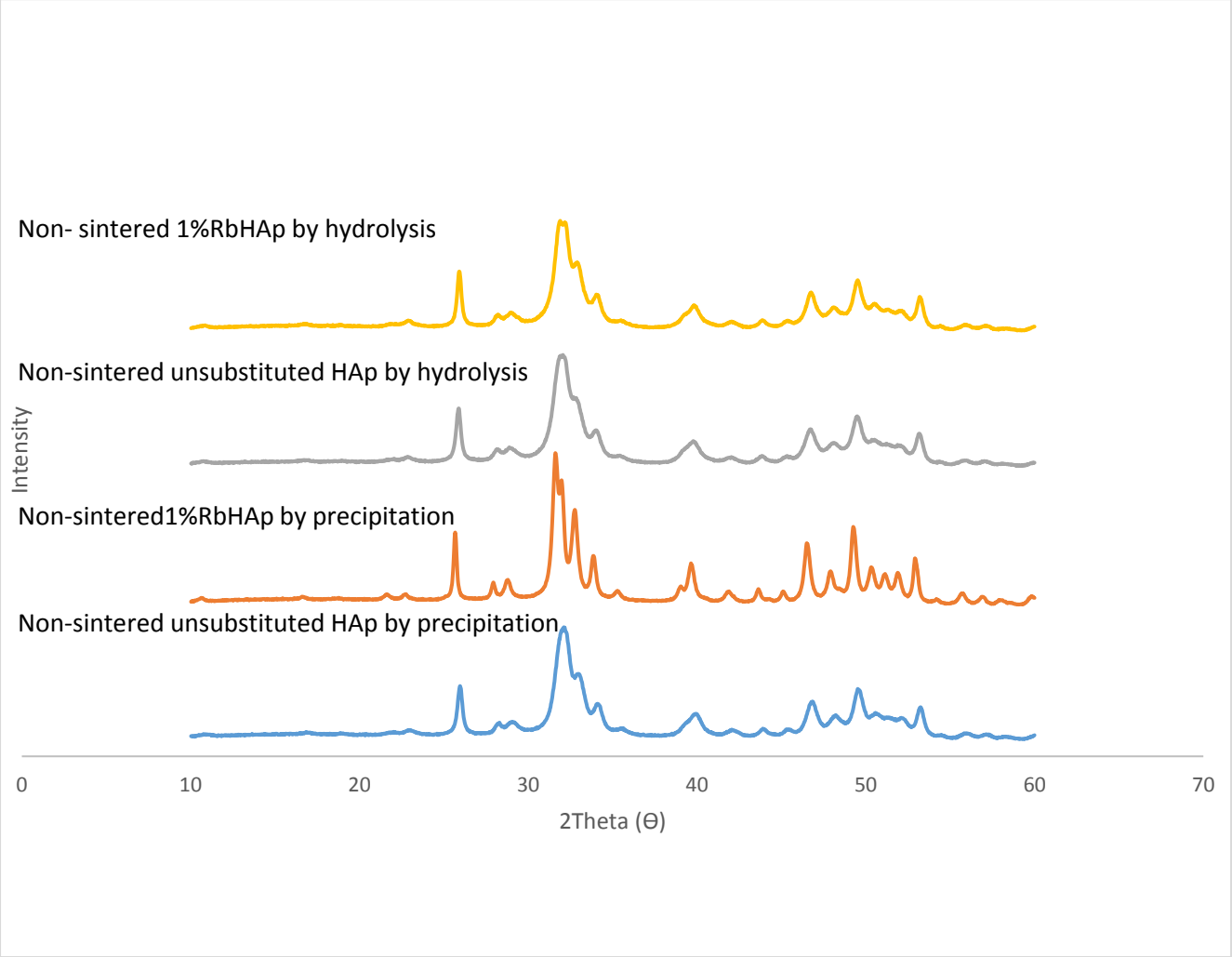

Figure 6-3: **The XRD diffraction patterns of non- sintered 1% RbHAp (1 wt.% Rb^{+}) materials prepared by precipitation and hydrolysis methods.**

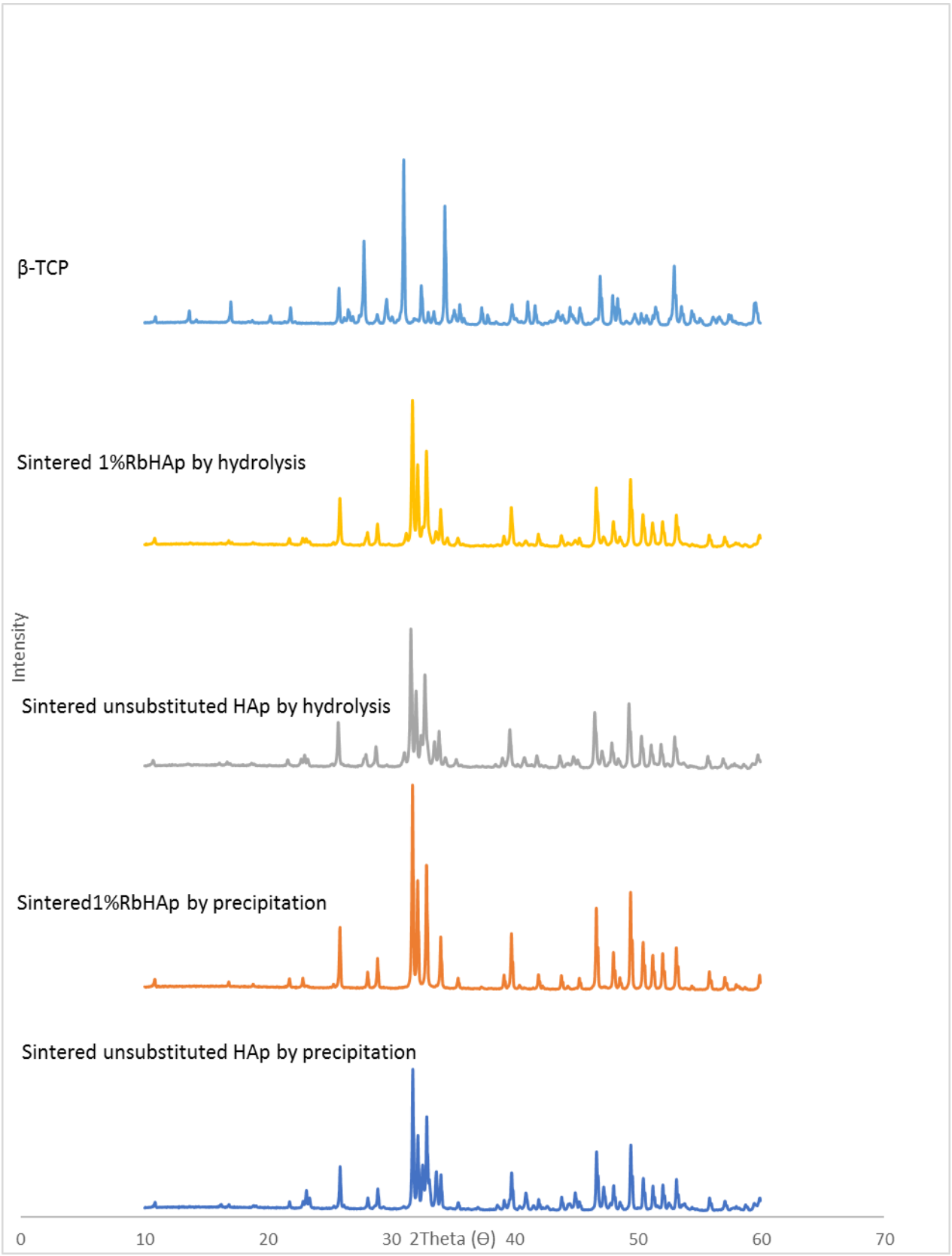

Figure 6-4: The XRD diffraction patterns of 1% RbHAp (1 wt.% Rb^{+}) materials prepared by precipitation and hydrolysis methods after sintering at 900 °C.

As a possible result of the substitution process of Rb^+ ions into HAp structure by the precipitation route (**Fig.6-4**) the absence of diffraction peaks that related to the impurity phase (β-TCP) at 2 Theta = 23.1˚ , 23.8˚, 31.2˚, 32.8˚, 33.6˚, 38.8˚, 41.14˚, 45.2˚ and 47.63˚ , is noticeable indicating the formation of a single phase with very high purity material achieved by preparing the Rb^+ substituted HAp crystal, in other words doping of Rb^+ ions into HAp structure appears to have produced a material of higher phase purity compared to unsubstituted HAp through using the precipitation method. Several studies reported an improvement in the thermal stability due to the substitution process of several cations into HAp crystal, for example Goldberg et al. [229] prepared AlHAp materials with various substitution levels of Al^{3+} (0, 0.5, 1.0, 5, 10 and 20 % mol) by using the precipitation method. They studied the influence of heat treatment in the range of 300–1400 ˚C on several properties of substituted Hap, such as the phase composition. The result of that study revealed that substitution of Al^{3+} ions into HAp lattice in the range (0.5–1.0 mol%) led to the production of an obvious enhancement in the thermal stability, that a 100 wt.% pure HAp phase was obtained as a result of heating AlHAp (0.5-1.0 Al mol%) at 1200 ˚C compared to 90 wt. % of HAp material and 10 wt.% of β-TCP that had already been achieved as a result of heating pure HAp powders (0.0 Al mol %) at the same temperature

Also, Bianco et al. [133] prepared pure HAp and ”half-F” substituted hydroxyapatite (with the following formula $Ca_{10}(PO_4)_6FOH$) by a precipitation route using $Ca(NO_3)_2.4H_2O$, $(NH_4)_2HPO_4$, and NH_4F as starting materials. The results revealed that pure HAp decomposed at around 1000 ˚C, while in the case of F-HAp, the introduction of F^- ions into the apatite lattice induced higher thermal stability, since the decomposition was observed to occur above 1300 ˚C. In the present study, the preparation of Rb^+ ion substituted HAp by the novel hydrolysis method also caused an enhancement in the thermal stability, since a visible reduction in the intensity of the XRD peaks that can be ascribed to an often observed impurity phase (i.e. TCP) were confirmed. This observation suggests that the substitution process of Rb^+, Na^+ and Cl^- ions into the HAp structure by hydrolysis method enhanced the thermal stability and hence the phase purity of the resultant HAp.

Crystallinity and crystallite size of sintered 1% RbHAp (1 wt.% Rb^+) materials:

Table 6-4 displays the degree of crystallinity and crystallite size of sintered 1% RbHAp (1 wt.% Rb^+) materials prepared by precipitation and hydrolysis methods at 900 ˚C.

Table 6-4: The degree of crystallinity and crystallite size of 1% RbHAp (1 wt.% Rb^+) materials prepared by precipitation and hydrolysis methods after sintering at 900 ˚C.

Sample	D_{002} (Å)	Crystallinity %
Unsubstituted HAp by precipitation	618.3±3.2	84.15±2.4
1% RbHAp by precipitation	711.9±1.1	91.10±1.5
Unsubstituted HAp by hydrolysis.	549.8±3.6	82.57±2.1
1% RbHAp by hydrolysis	571.9±3.1	83.62±1.8

The diffraction patterns of 1%RbHAp materials became sharper and narrower due to substitution of Rb^+ ions, suggesting a high degree of crystallinity was obtained by the precipitation method (**Fig. 6-4).** On the other hand, only a marginal improvement in crystallinity was recorded in the case of RbHAp prepared by the novel hydrolysis method. This observation was proven by the numerical value of crystallinity, that the calculated value of crystallinity of 1%RbHAp powders prepared by precipitation and hydrolysis was 91.1 and 83.6, compared to 84.1 and 82.5 for unsubstituted HAp materials prepared by precipitation and hydrolysis respectively.

As a general note, it has been found that the enhancement of crystallinity due to the substitution process of various ions into the HAp structure has been reported before in several studies. , For example, Kaygili et al.[146] compared unsubstituted HAp with Ce-substituted HAp samples that were prepared with different levels of Ce^{3+} ions (0.5, 1.0 and 2 at.%) by the sol–gel method. The XRD results of that study revealed that the degree of crystallinity of all prepared CeHAp samples were higher than that of HAp. Qiao et al. [230] substituted fluoride ions into porcine bone-derived hydroxyapatite (PHAp). which was prepared by using thermal treatment, followed by the incorporation of fluoride ions through soaking the prepared hydroxyapatite (PHAp) in different concentrations of sodium fluoride solutions (0.25, 0.50, and 0.75 mol l^{-1}) for 24 hours, and labelled as 0.25-FPHAp, 0.50-FPHAp, and 0.75-FPHAp. The XRD analysis showed an improvement

in crystallinity, and that result was also confirmed by the numerical value of crystallinity, since that value (Xc%) increased from 94.4 for PHAp to 98.7% for 0.75FPHAp.

In the present study**, Table 6-4**, also displays that a visible increase was recorded for the RbHAp samples in the value of crystallite size, when calculated by the Debye Scherrer equation, through using the conventional precipitation and novel hydrolysis routes. The effect of the synthesis route on such variables was also confirmed by **Table 6-4**, that the precipitation route produced materials with higher crystallinity and crystallite size, compared to those produced by the hydrolysis route. This can be ascribed to the higher wt.% of Rb^+ ions that associated with the HAp structure as prepared by the precipitation route compared to that prepared by the novel hydrolysis method as confirmed by ICP-MS results.

Lattice parameters and volume of unit cell of sintered 1% RbHAp (1 wt.% Rb^+):

The lattice parameters and the volume of hexagonal unit cell of the sintered 1% RbHAp (1 wt.% Rb^+) materials prepared by precipitation and hydrolysis methods at 900 ˚C are shown in **Table 6-5**.

Table 6-5: The lattice parameters and the volume of hexagonal unit cell of 1% RbHAp (1 wt.% Rb^+) materials prepared by precipitation and hydrolysis methods after sintering at 900 ˚C.

Sample	a [Å]	c [Å]	V[$Å^3$]
Unsubstituted HAp by precipitation	9.416±0.004	6.879±0.003	1579±0.004
1% RbHAp by precipitation	9.423+0.001	6.882 ±0.001	1581±0.001
Unsubstituted HAp by hydrolysis	9.421±0.003	6.882±0.005	1581±0.004
1% RbHAp by hydrolysis	9.424±0.001	6.882±0.002	1582±0.002

While an increase in both lattice constants (a and c) of 1%RbHAp (1 wt.%Rb^+) by the precipitation method was shown, the lattice parameter (a) in the case of hydrolysis method just showed a slight increase. However, an increase in the volume of unit cell of the whole prepared RbHAp powders by precipitation and hydrolysis methods was produced. This expansion in the unit cell can be ascribed to the following factors:

1- The substitution process of hydroxyl group by chloride ions because RbCl was used as a precursor of Rb^+ ions during the preparation method. This expansion can be attributed to the effect of chloride ions which have a larger ionic radius (1.81 Å) [123]compared to that of the hydroxyl group(1.68 Å).

2- Although the wt.% of Rb^+ ions associated with the HAp sample was very low as confirmed by ICP-MS analysis, the Rietveld analysis suggests that the expansion in the unit cell can possibly be attributed to the replacement process of Rb^+ ions which has a larger atomic radius (152 pm)[225] compared to Ca^{2+} (100 pm).

   Liu et al [224] prepared RbHAp materials by using the hydrothermal method. Different substitution levels of RbHAp materials were synthesized in this study: 1, 3, 5,7 and 10 % RbHAp samples through setting the atomic ratio of Rb/(Rb+Ca) at 1, 3, 5, 7 and 10%). The researchers used $Ca(NO_3)_2.4H_2O$, $RbNO_3$ and $(NH_4)_2HPO_4$ as starting materials. The Rietveld refinement showed an increase in the lattice parameters due to the substitution of Rb^+ ions into HAp as shown in **Table 6-6**. This result supports the present investigation that posits that substitution of Rb^+ ions caused an increase in the values of lattice parameters.

Table 6-6: The lattice constants and the volume of unit cell of 1,3,5,7 and 10% RbHAp materials.

Sample	a (nm)	c (nm)	V(nm^3)
HAp	0.9389	0.6865	0.5241
1%RbHAp	0.9401	0.6972	0.5261
3%RbHAp	0.9402	0.6974	0.5265
5%RbHAp	0.9405	0.6977	0.5268
7%RbHAp	0.9414	0.6977	0.5275
10%RbHAp	0.9425	0.6979	0.5290

6.2.1.4 SEM of 1% RbHAp (1 wt.% Rb^+) materials prepared by hydrolysis and precipitation methods:

SEM of non-sintered 1% RbHAp (1 wt.% Rb^+) prepared by hydrolysis and precipitation methods.

Fig.6-5. displays SEM images of non-sintered 1% RbHAp (1 wt.% Rb^+) powders prepared by hydrolysis and precipitation methods.

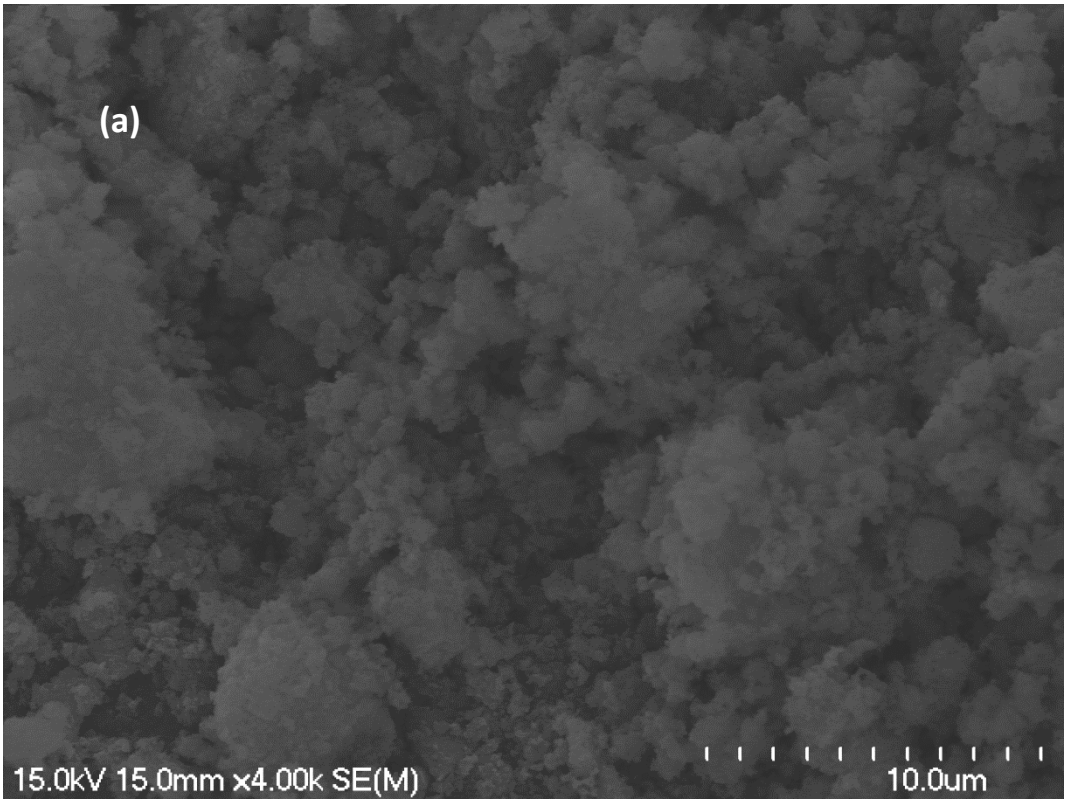

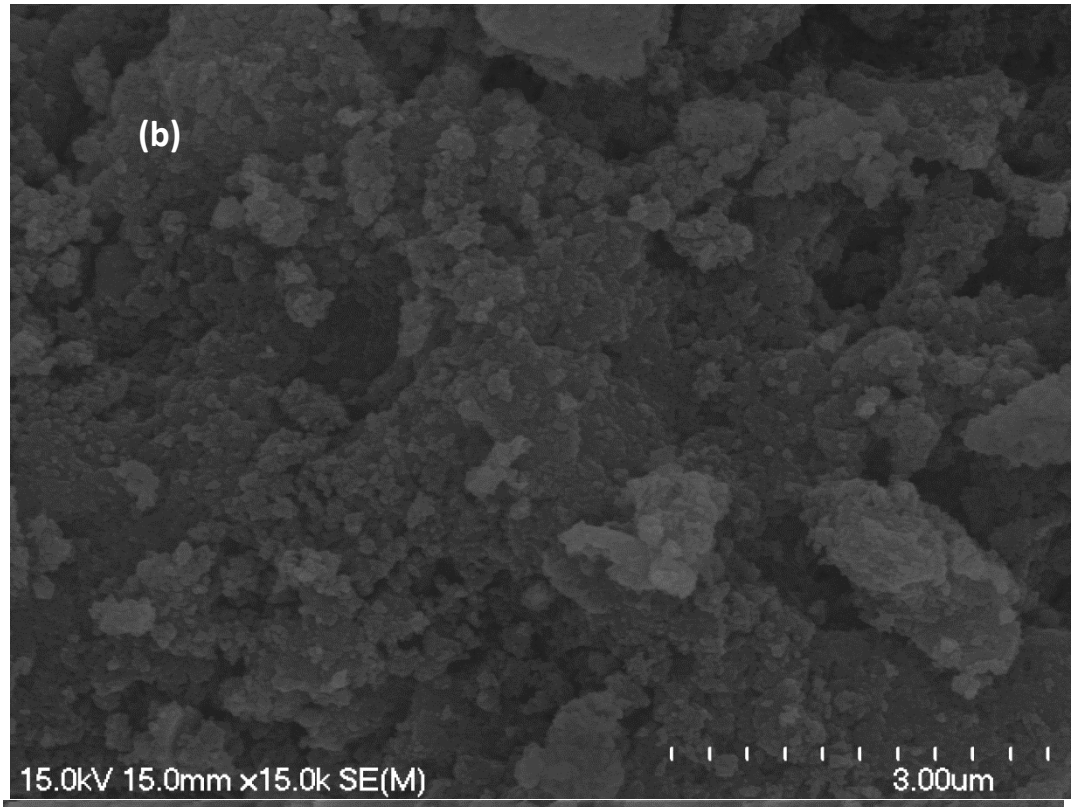
(b)
15.0kV 15.0mm x15.0k SE(M)
3.00um

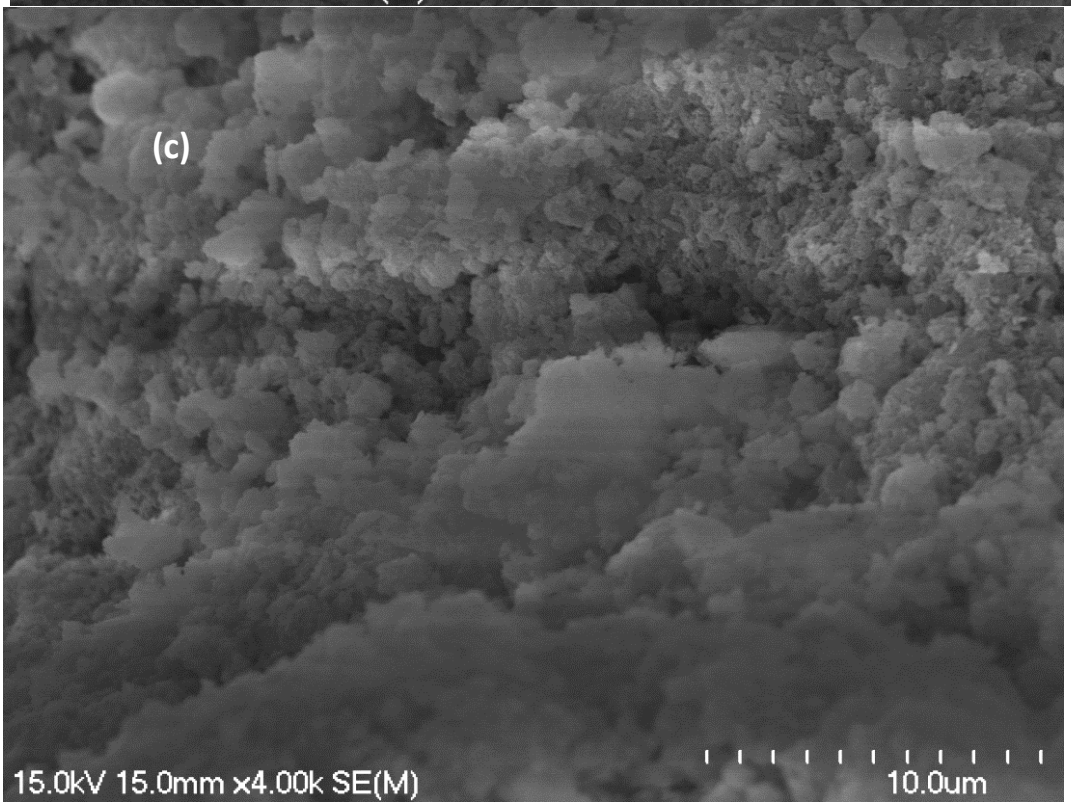
(c)
15.0kV 15.0mm x4.00k SE(M)
10.0um

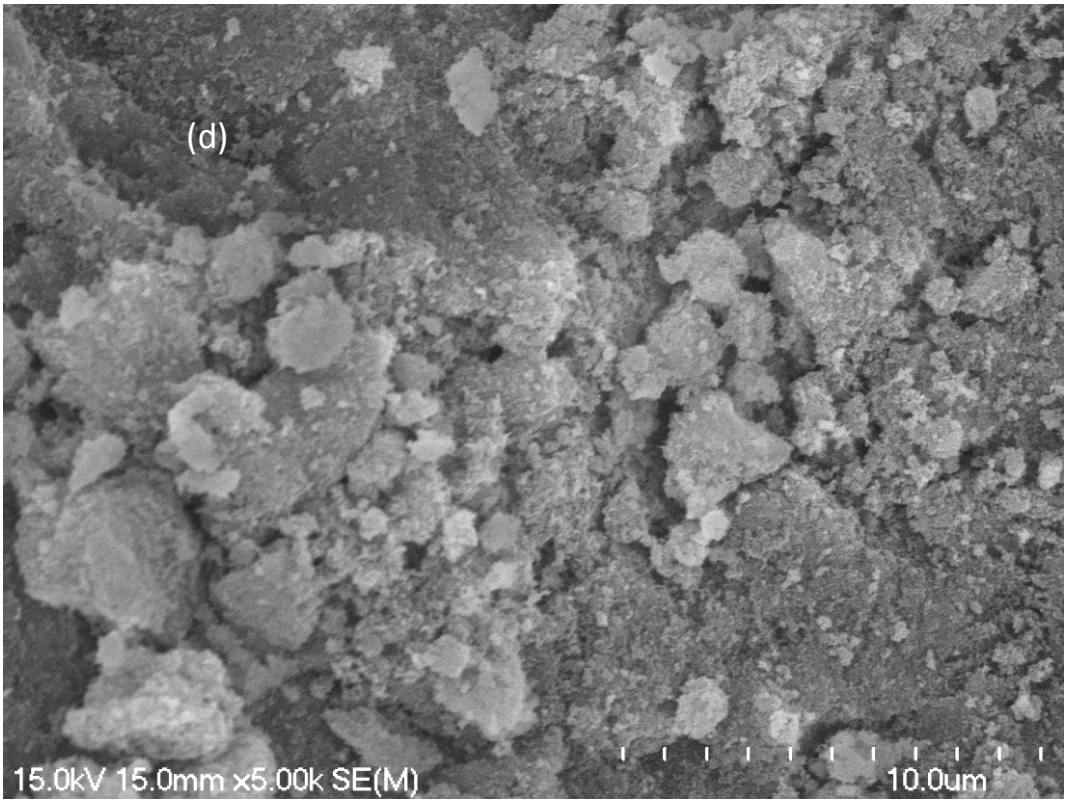

Figure 6-5: SEM images of non-sintered (a) unsubstituted HAp by hydrolysis (b) unsubstituted HAp by precipitation (c) 1% RbHAp (1 wt. % Rb^+) by hydrolysis (d) 1% RbAHp (1 wt.% Rb^+) by precipitation.

Irregular distribution and the ability to agglomerate were recorded for these samples by both methods as shown in **Fig 6-5**, whereas a reduction in the level of porosity was observed for 1% RbHAp powders by the hydrolysis method.

SEM of 1%RbHAp (1wt.% Rb^+) materials prepared by hydrolysis and precipitation methods after sintering at 900 ˚C:

The morphology of the sintered 1% RbHAp powders prepared by precipitation and hydrolysis methods at 900 ˚C are shown in **Fig. 6-6.**

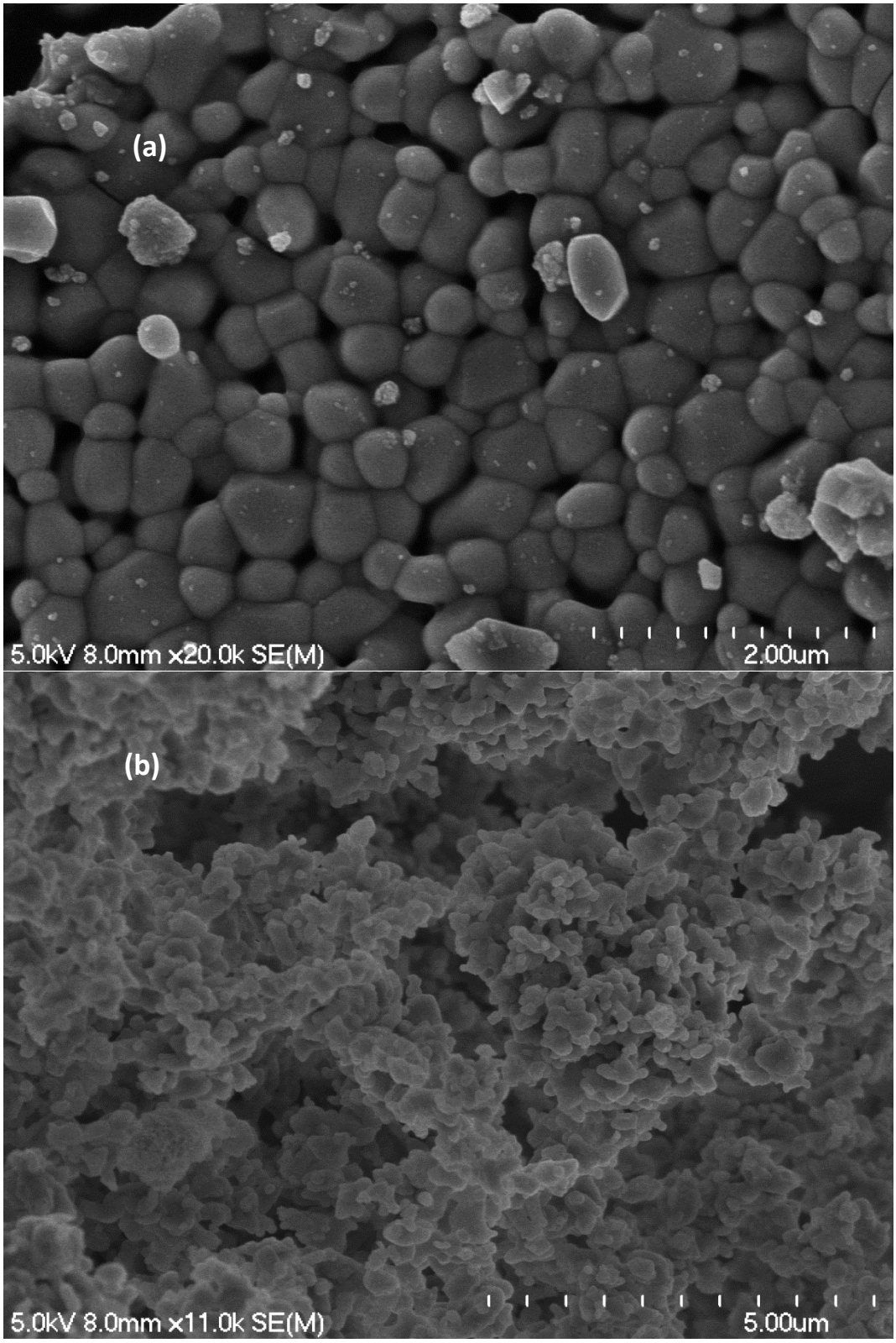
(a)
5.0kV 8.0mm x20.0k SE(M)
2.00um
(b)
5.0kV 8.0mm x11.0k SE(M)
5.00um

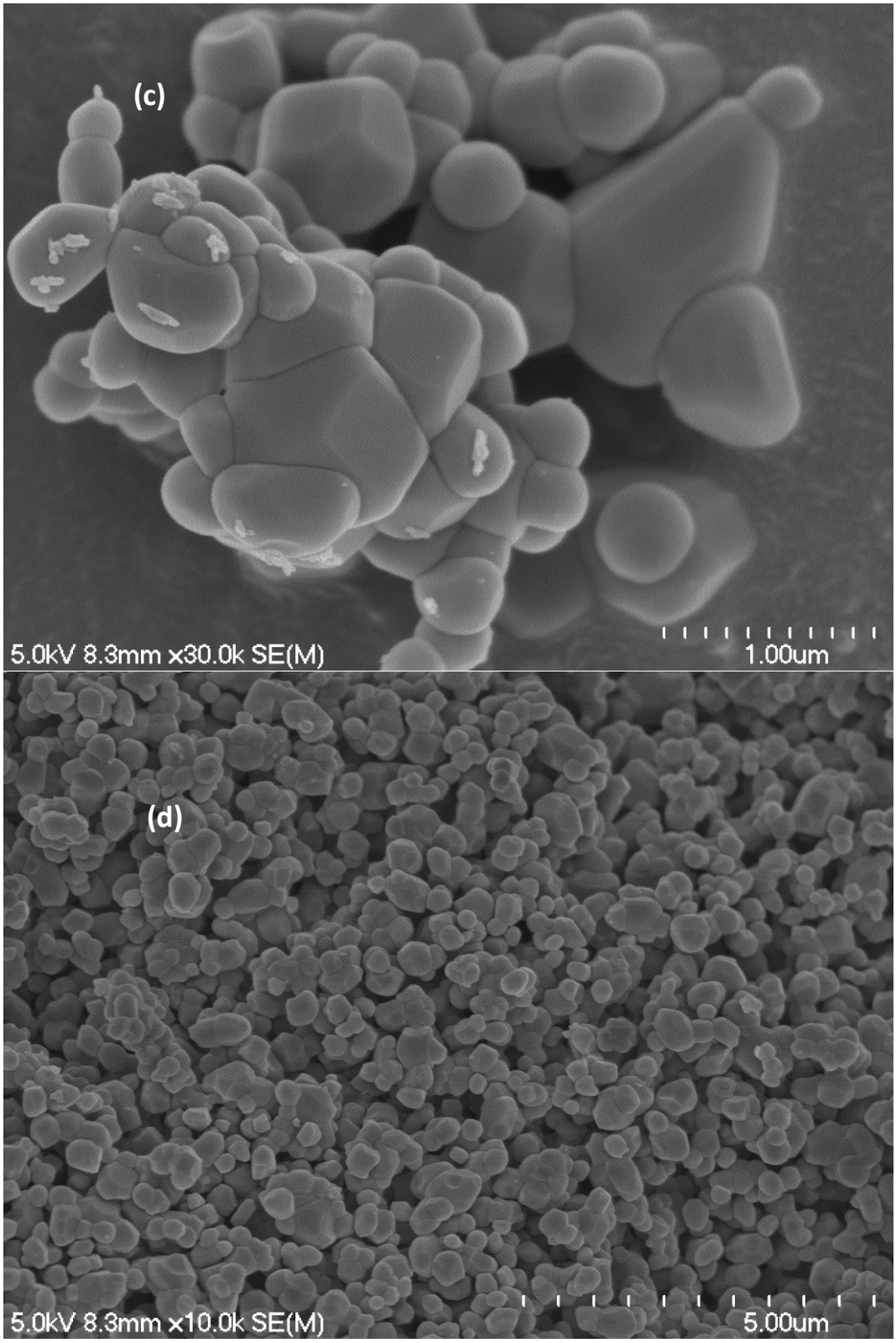
(c)
5.0kV 8.3mm x30.0k SE(M)
1.00um
(d)
5.0kV 8.3mm x10.0k SE(M)
5.00um

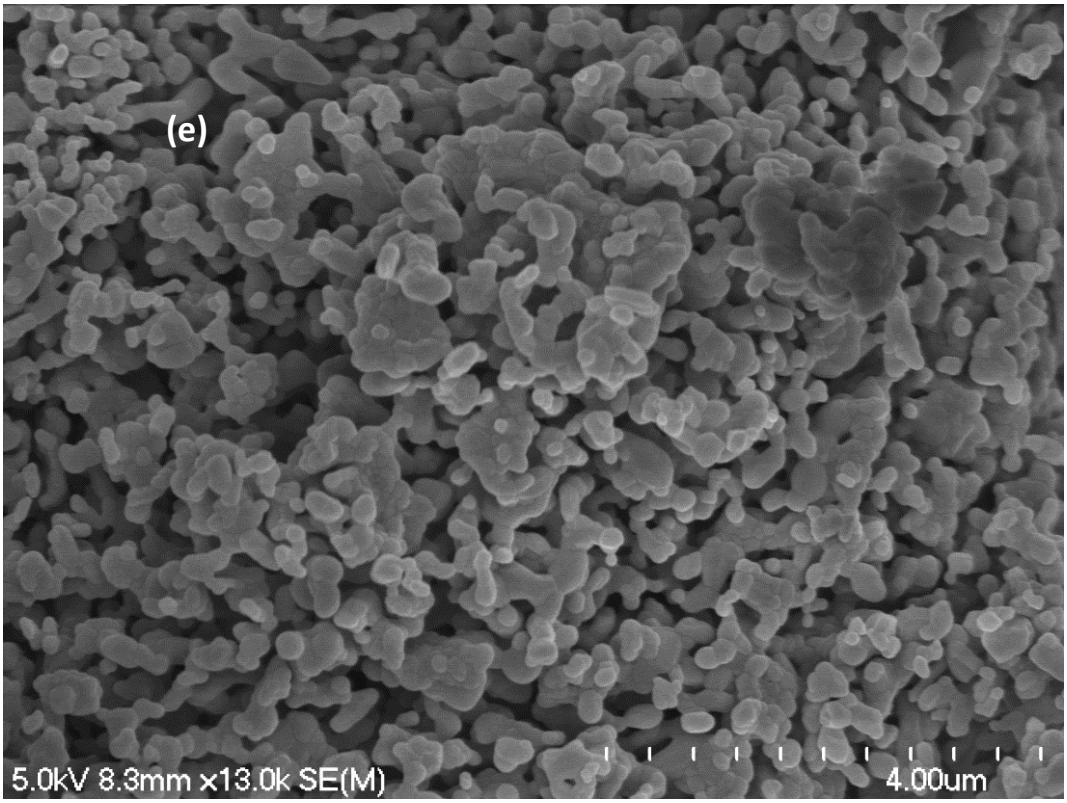

Figure 6-6: SEM images of (a) unsubstituted HAp by precipitation (b) unsubstituted HAp by hydrolysis (c and d)1%RbHAp (1% wt. Rb^{+}) by precipitation (e) 1%RbHAp (1% wt. Rb^{+}) by hydrolysis, after sintering at 900 ˚C.

It can be seen that the morphology of the prepared 1% RbHAp powders had not been affected by the preparation method and the supposed cationic substitution of Rb^{+} ions, since the level of Rb^{+} ions associated with the HAp was very low as confirmed by ICP-MS**.** The samples produced by the precipitation method consist of spherical particles with fine grains, while those prepared by the novel hydrolysis route led to the production of spherical particles which had a slight trend to agglomerate, which was associated with the enhancement in the level of porosity as confirmed by SEM images.

6.3 1%EuHAp (1 wt.% Eu^{3+}) powders prepared by hydrolysis and precipitation methods:

A series of 1%EuHAp powders (1 wt.% Eu^{3+} ions) was prepared by the precipitation and hydrolysis methods, and the detailed amounts of the reagents are listed in T**able 6-7.**

Table 6-7: Synthesis details of 1% EuHAp (1 wt.% Eu^{3+} ions) powders

Sample	$Ca(NO_3)_2$ (g)	$Ca(OH)_2$ (g)	MCPM (g)	Na_2HPO_4 (g)	$Eu(NO_3)_3.5H_2O$ (g)	$Ca(NO_3)_2$ (mol)	$Ca(OH)_2$ (mol)	MCPM (mol)	Na_2HPO_4 (mol)	$Eu(NO_3)_3.5H_2O$ (mol)
EuHAp (1 wt.% Eu) by precipitation	7.9921	-	-	4.1822	0.1452	0.0487	-	-	0.0295	0.0003
EuHAp (1 wt.% Eu) by hydrolysis	-	3.6244	12.328	-	0.1449	-	0.0489	0.0489	-	0.0003

6.3.1 Characterization techniques of 1%EuHAp (1 wt.% Eu^{3+}) materials prepared by the conventional precipitation and novel hydrolysis methods:

The prepared materials were subjected to various kinds of analysis tests to confirm the presence of hydroxyapatite and to calculate the crystallinity, crystallite size, lattice parameters, Ca:P mole ratio and the substitution level of the cation. See below for details:

6.3.1.1 ICP-MS of 1% EuHAp (1 wt.% Eu^{3+}) materials prepared by hydrolysis and precipitation method after sintering at 900 ˚C

The results of the elemental analyses of 1% EuHAp (1 wt.% Eu^{3+}) samples that prepared by precipitation and hydrolysis routes are displayed in **Table 6-8.**

Table 6-8: ICP-MS results of 1% EuHAp (1 wt.%Eu^{3+}) materials prepared by precipitation and hydrolysis methods after sintering at 900 ˚C. The concentration values are given in ppb (ug/L):

Sample	Ca 44	P 31	Na 23	Eu 153
Unsubstituted HAp by precipitation	707795	401240	103797	-
1% EuHAp by precipitation	750984	373050	65838	14904
Unsubstituted HAp by hydrolysis	769928	423970	78396	-
1% EuHAp by hydrolysis	710087	370113	72516	5103.4

The starting (calculated) and actual (measured) degree of chemical composition of the prepared powders in terms of wt.% of Eu^{3+}ions, the calcium/phosphorus (Ca/P) molar ratios as well as (Ca+Na)/P molar ratio were determined by ICP-MS and presented in **Table 6-9.**

Table 6-9: The chemical analysis data of 1% EuHAp (1 wt.% Eu^{3+}) materials by ICP-MS measurements after sintering at 900 ˚C.

Sample	Ca/P Theoretical	Ca/P Measured	(Ca+Na+Eu)/p	Wt.% Eu^{3+} ions theoretical	Wt.% Eu^{3+} ions measured	Wt.% Na^{+} ions measured
Unsubstituted HAp by precipitation	1.67	1.36	1.71	-	-	5.2%
1% EuHAp by precipitation	1.65	1.56	1.80	1%	0.74%	3.3%
Unsubstituted HAp by hydrolysis	1.67	1.40	1.65	-	-	3.9%
1%EuHAp by hydrolysis	1.65	1.48	1.75	1%	0.25%	3.6%

The ICP-MS results suggested (though did not prove conclusively) that Eu^{3+} as well as Na^{+} ions substituted for calcium ions. This was manifested by an observed reduction in the Ca:P mole ratios in HAp samples prepared using the precipitation and hydrolysis methods (1.56 and 1.48). The (Ca+ Eu+ Na) / P for the prepared powders (1.80 and 1,75) were higher than the proposed value of stochiometric HAp. However higher ratios of Ca:P were expected in CO_3HAp [185,231], due to the substitution of phosphate site by carbonate ions, and suggesting formation of B-type of carbonated HAp powders, which is in a good agreement with FTIR analysis that displayed the presence of CO_3^{2-} into HAp crystal.

On the other hand, **Table 6-9** displays that the doped concentrations of Eu^{3+} ions in the prepared samples were (0.74 and 0.25%) which were lower than the theoretical substituted value (1%), and the possible effect of the preparation method on the substitution levels was also demonstrated, because the levels of Europium ions associated with the HAp samples were found to be higher in HAps made by the precipitation method compared to those prepared by the novel hydrolysis route.

6.3.1.2 FTIR of 1% EuHAp (1 wt.% Eu^{3+}) materials prepared by hydrolysis and precipitation methods:

FTIR of non-sintered 1% EuHAp (1 wt.% Eu^{3+}) materials prepared by hydrolysis and precipitation methods.

The FTIR spectra of non-sintered 1%EuHAp powders prepared by hydrolysis and precipitation routes is displayed in **Fig.6-7.**

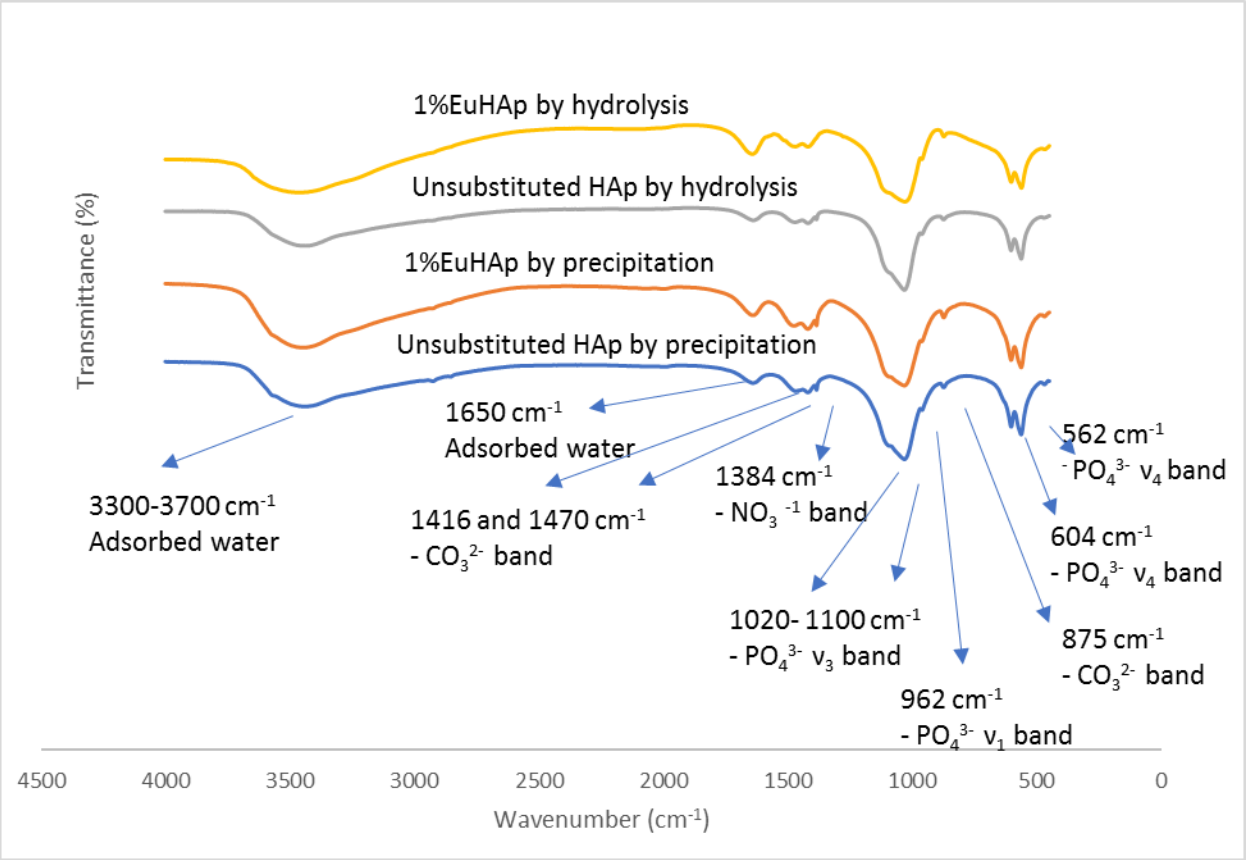

Figure 6-7: FTIR spectra of non-sintered 1%EuHAp (1 wt.% Eu^{3+}) materials prepared by precipitation and hydrolysis methods.

The FTIR spectra of all samples of the non-sintered 1%EuHAp materials that were prepared by the precipitation and the hydrolysis methods are similar to the other substituted HAp materials, which were prepared by the precipitation and the novel hydrolysis methods.

The FTIR spectra of the non-sintered 1%EuHAp samples prepared by different synthesis routes (precipitation and hydrolysis methods) displayed bands corresponding to the HAp structure as

confirmed in **Fig.6-7**. The broad band at 3300–3600 cm^{-1} and a small band at about 1630 cm^{-1} are related to absorbed water. The fundamental peaks at 562, 602, 962, 1026 and 1100 cm^{-1} were assigned to the phosphate group. The presence of the carbonate group was confirmed by the appearance of typical bands of carbonate at 875, 1418 and 1470 cm^{-1}, A typical band of the nitrate group (NO_3^-) at 1385 cm^{-1}, was also detected by using the precipitation route. The recorded peak at 1385 cm^{-1} through using the hydrolysis method, is instead believed to be due to the N-O stretching vibration of nitrate ion which was a residual contaminant in the KBr powder used to make the pellets.

FTIR of 1%EuHAp (1 wt.% Eu^{3+}) materials prepared by hydrolysis and precipitation methods after sintering at 900 ˚C.

Figure 6.8. shows the FTIR spectra of the sintered 1% EuHAp powders prepared by using different synthesis routes (the conventional precipitation and novel hydrolysis methods).

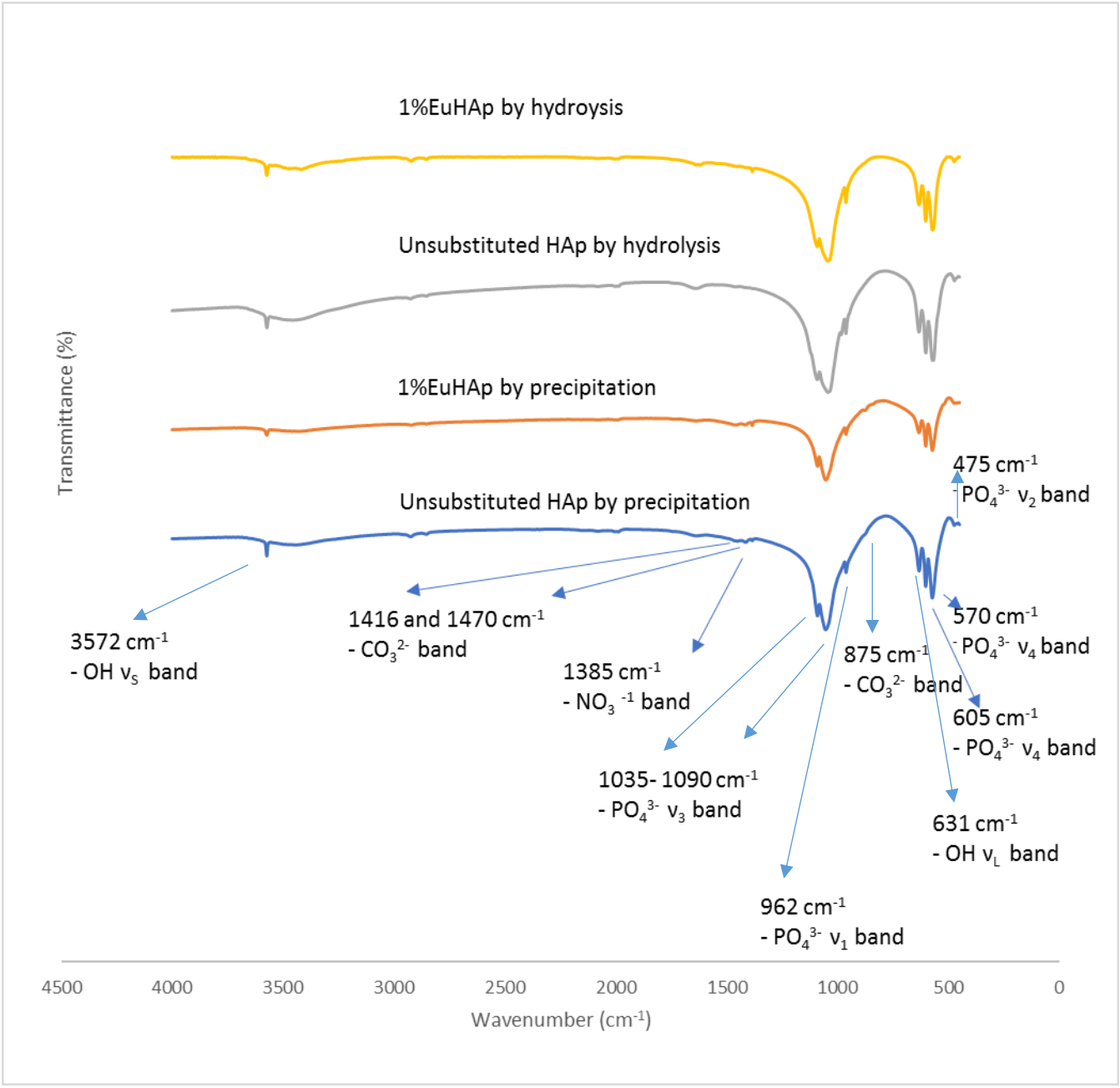

Figure 6-8: FTIR spectra of 1% EuHAp (1 wt.% Eu^{3+}) materials prepared by the conventional precipitation and novel hydrolysis methods after sintering at 900 ˚C.

Figure 6.8. shows the characteristic bands of phosphate group was recorded at 1091, 1035, 962, 602, 568 and 475cm^{-1}, whereas the typical bands of hydroxyl group appeared at 3571 and 634 cm^{-1}, confirming the existence of the apatitic phase by the hydrolysis and precipitation methods. Another important observation should be taken into account, was the reduction in the intensities of stretching and librational modes of the lattice OH^- group which may have occurred due to the substitution of calcium ions by the trivalent cation (Eu^{3+}) in the 1%EuHAp powders that were prepared by the precipitation method. Such an observation was also recorded by Serret et al.

[232], when they prepared LaHAp materials with chemical formula : $Ca_{10-x}La_x(PO_4)_6(OH)_y$ ($0 \leq x \leq 2$), by solid-state reaction. They used $CaCO_3$, $(NH_4)_2HPO_4$, and La_2O_3 for that purpose. The FTIR results revealed the absorption bands of hydroxyl ions at 3572 and 630 cm^{-1} were detected in a sample with x = 0. In the case of x = 0.5, just a weak band at 3572 cm^{-1} was observed, but at higher x values, absorption bands corresponding to hydroxyl ions were not observed. They reported that the substitution of Ca^{2+} by La^{3+} diminishes the number of OH^- ions, which they suggested was as a result of substitution of trivalent cation into HAp structure, and in order to keep the charge balance the transformation of the OH^- to O^{2-} ions can be considered as an acceptable possibility to increase the negative charge. Also, Han et al. [18] prepared EuHAp with different levels of Eu^{3+} ions(molar ratios of (Eu)/(Eu+Ca)=0.25–4%). They used $Ca(NO_3)_2$ $4H_2O$, $Eu(NO_3)_3$ $6H_2O$ and $Ca(H_2PO_4)_2$ $2H_2O$ as a precursors. The authors reported that the OH^- in the apatite structure can be replaced by O^{2-} ion to achieve charge compensation for the substitution, formulated as $Ca_{10-x}Eu_x(PO_4)_6(OH)_{2-x}O_x$.

6.3.1.3 XRD diffraction patterns of non-sintered and sintered 1% EuHAp (1 wt.% Eu^{3+}) materials prepared by hydrolysis and precipitation methods:

Phase Identification of Sintered 1%EuHAp materials:

The XRD patterns of the 1%EuHAp materials prepared by precipitation and hydrolysis methods are shown in **Fig.6-9** and **Fig.6.10.**

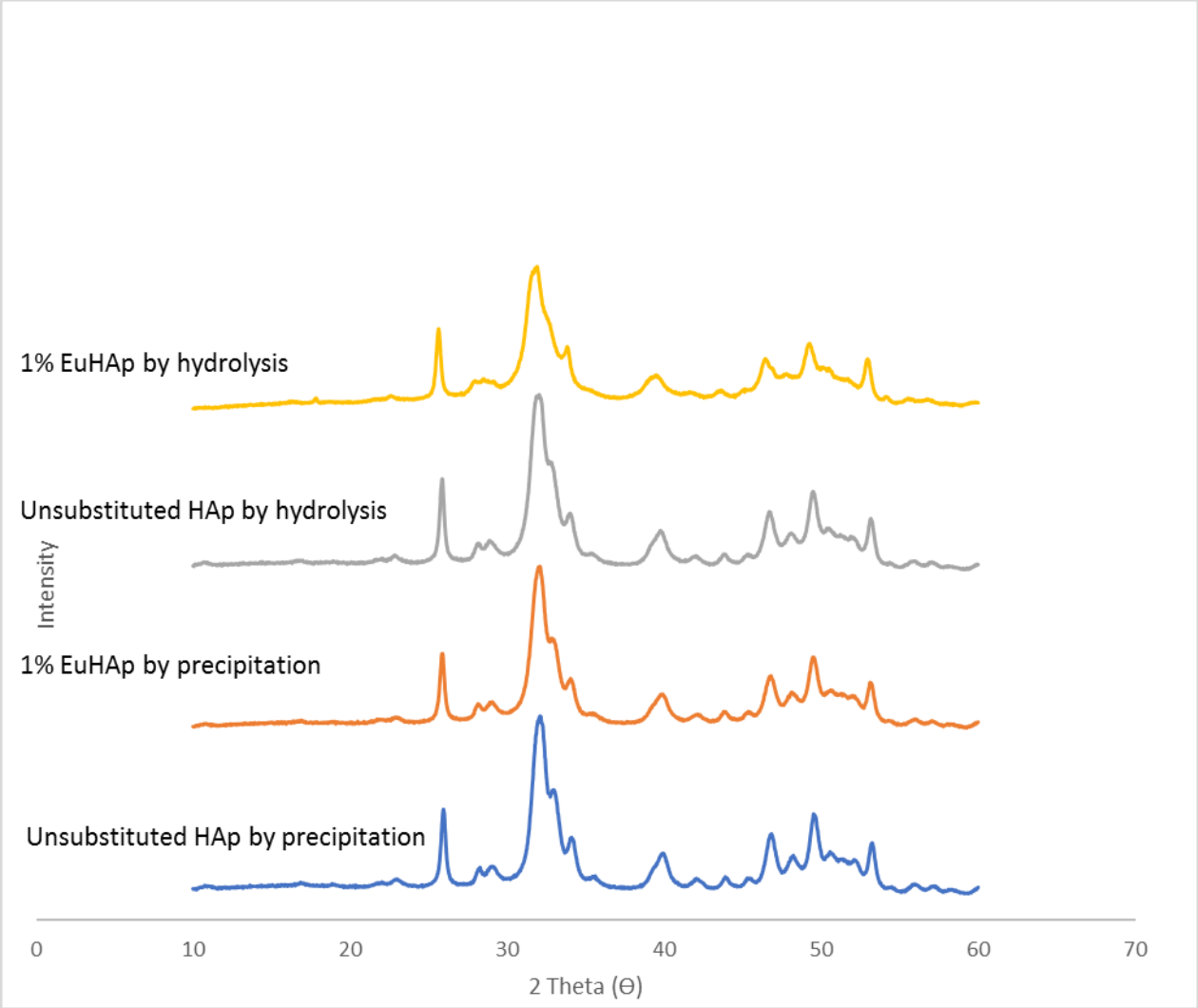

Figure 6-9: The XRD diffraction patterns of non-sintered 1% EuHAp (1 wt.% Eu^{3+}) materials prepared by precipitation and hydrolysis methods.

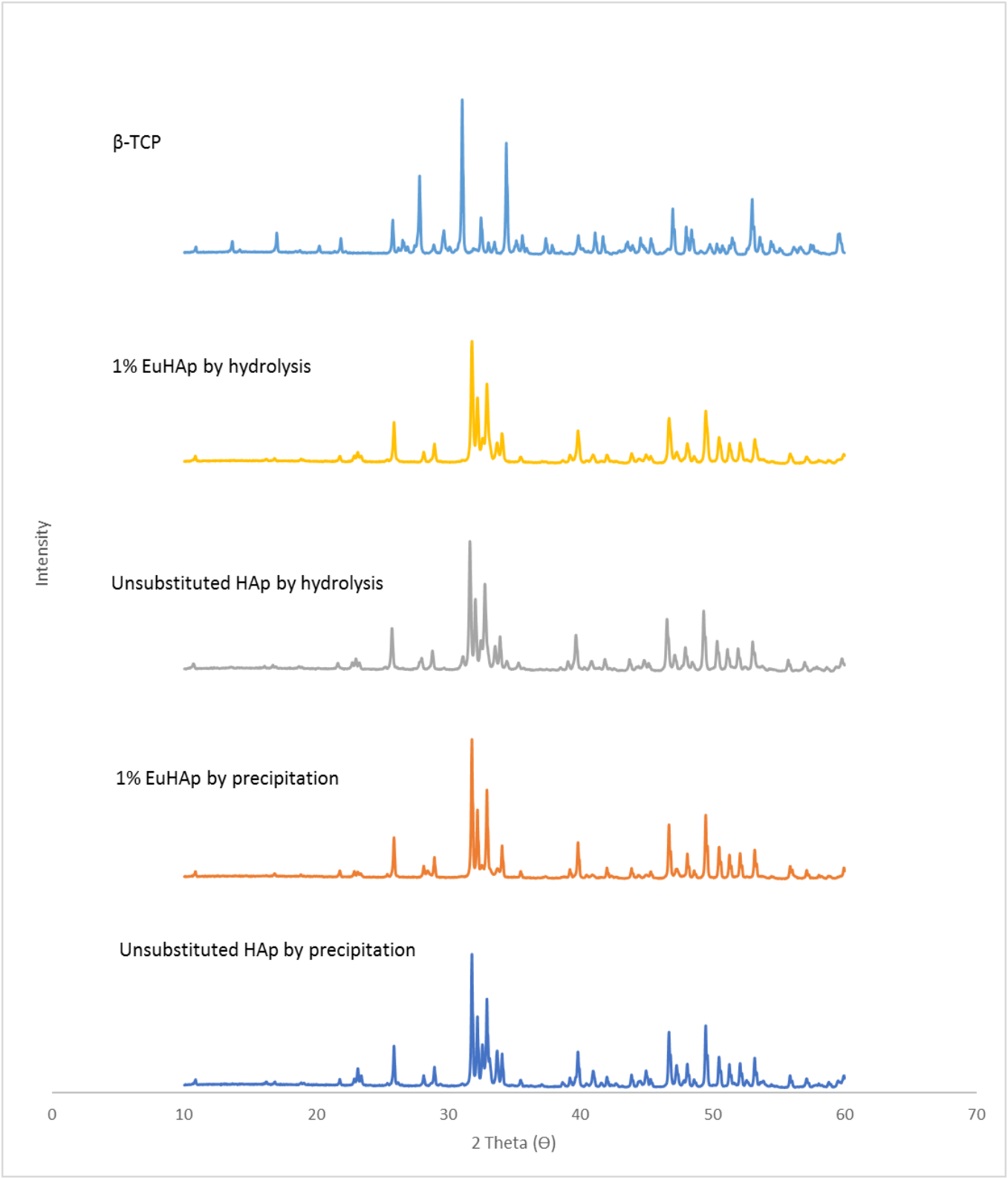

Figure 6-10: The XRD diffraction patterns of 1% EuHAp (1 wt.% Eu^{3+}) materials prepared by the conventional precipitation and novel hydrolysis methods after sintering at 900 ˚C.

In the case of the substituted samples of 1%EuHAp powders prepared by both routes, the characteristic diffraction peaks of unsubstituted HAp are still obvious, and the diffraction peaks can be well indexed and correspond to the hexagonal structure with p63/m space group as compared to standard patterns of HAp card no. 01-074-9780.

The effect of the introduction and possible substitution of Eu^{3+} ions into the HAp structure on the phase composition was confirmed by XRD patterns in both routes (precipitation and hydrolysis). The substitution process using the precipitation method reduced the intensities of most of the peaks related to β-TCP in a clear manner. This observation was also associated with disappearance of other characteristic peaks of impurity phase at 2 Theta = 38.8˚, 41.14˚ and 45.2˚. In the case of the hydrolysis method, **Fig. 6-10** displays that two peaks of an impurity phase (β-TCP) at 2 Theta = 31.20˚ and 34.57˚ completely vanished. These observations by both routes (precipitation and hydrolysis methods) suggest introducing of Eu^{3+} ions into HAp (and possibly in the HAp lattice) produced higher phase purity in the prepared 1% EuHAp materials compared to the unsubstituted HAp powders.

In other words, **Fig. 6-10** showed that the introduction of Eu^{3+} into the HAp crystal by the conventional precipitation and the novel hydrolysis methods produced more purer phase of HAp material and reduced β-TCP phase. The conventional precipitation route improved the phase purity of HAp and exhibited less β-TCP in the HApsamples relative to HAp prepared by the novel hydrolysis method. This observation can be attributed to the higher wt.% of Eu^{3+} ions associated with and possibly substituted into the HAp structure by using the precipitation route compared to the hydrolysis method as confirmed by ICP-MS results.

Crystallinity and crystallite size of sintered 1%EuHAp materials:

Table 6-10 displays the degree of crystallinity and crystallite size of sintered 1% EuHAp (1 wt.% Eu^{3+}) materials prepared by precipitation and hydrolysis methods at 900 ˚C.

Table 6-10: The degree of crystallinity and crystallite size of 1% EuHAp (1 wt.% Eu^{3+}) materials prepared by precipitation and hydrolysis methods after sintering at 900 ˚C.

Sample name	D_{002} (Å)	Crystallinity %
Unsubstituted HAp by precipitation	618.3±3.2	84.15±2.4
1%EuHAp by precipitation	677.2±5.2	83.32±4.7
Unsubstituted HAp by hydrolysis	549.8±3.6	82.57±2.1
%EuHAp by hydrolysis	476.0±3.5	77.04±3.1

In this project the calculated value of crystallinity was not strongly affected as a result of substitution of Eu^{3+} ions, especially in the case of precipitation route since it was 84.14 for unsubstituted HAp compared to 83.32 to 1%EuHAp. But, through using the hydrolysis process, the peaks became less intense and much broader confirming the relatively lower crystallinity.

However, **Table 6-10** shows that an increase in the value of crystallite size was produced by precipitation route due possibly to the substitution of Eu^{3+} ions into the HAp structure, but that the hydrolysis method caused a clear reduction in that value. This result can be ascribed to the effect of the preparation method on the value of crystallite size. As shown in **Table 6-9,** the conventional precipitation method produced higher wt.% of Eu^{3+} ions associated with theHAp sample (0.74 % of Eu^{3+}) compared to the novel hydrolysis method (0.25 % of Eu^{3+}). Therefore, there were different chemical compositions obtained through using the different synthesis routes. Also, **Table 6-10**, showed that the crystallite size and crystallinity are different to each other. While the crystallite size can be calculated through using the Debye Scherrer equation [146], the crystallinity refers to the degree of structural order in a solid. Several researchers obtained different values of crystallinity and crystallite size when studying substituted HAps. As an example, Kaygili et al. [146] prepared undoped HAp and Ce-doped HAp using by the sol–gel method. The amounts of Ce were 0 (undoped HAp), 0.5, 1.0 and 2.0 at.% and the samples were labelled as H1, H2, H3 and H4, respectively. The results of Kaygili's XRD analysis are shown in **Table 6-11**:

Table 6-11: The XRD results of Ce-doped HAp with different level of substitution of Ce^{3+} ions as reported by, Kaygili et al. [146].

Sample	D_{002} (Å)	Crystallinity %
H1	27.46	84.2
H2	29.76	89.2
H3	35.01	86.9
H4	28.42	85.4

Lattice Parameters and volume of unit cell of 1%EuHAp materials:

Table 6-12 displays the lattice parameters and the volume of the hexagonal unit cell of the sintered 1% EuHAp (1 wt.% Eu^{3+}) materials prepared by the precipitation and hydrolysis methods at 900 ˚C

Table 6-12: The lattice parameters and the volume of hexagonal unit cell of 1% EuHAp (1 wt.% Eu^{3+}) materials prepared by precipitation and hydrolysis methods after sintering at 900 ˚C.

Sample	a [Å]	c [Å]	V[$Å^3$]
Unsubstituted HAp by precipitation	9.416±0.004	6.879±0.003	1579±0.004
1%EuHAp by precipitation	9.419±0.001	6.881±0.002	1580±0.002
Unsubstituted HAp by hydrolysis	9.421±0.003	6.882±0.005	1581±0.004
1%EuHAp by hydrolysis	9.420±0.002	6.881±0.002	1580±0.002

Also, **Table 6-12.** shows a slight increase in both lattice parameters (a and c) due putatively to the replacement of Eu^{3+} ions into the HAp lattice structure by the precipitation method and this can be ascribed to the slightly bigger ionic radius of Eu^{3+} 1.087 Å [233] compared to (1.0 Å) of Ca^{2+}, A very slight decrease in both lattice parameters (a and c) resulted by using the hydrolysis process.

Carmen et al [234] prepared EuHAp materials by coprecipitation with the following chemical formula : $Ca_{10-x}Eu_x(PO_4)_6(OH)_2$, where X= 0, 0.01, 0.02, 0.1 and x = 0.2 (in terms of wt.% the substitution levels would be 0.15, 0.30, 1.50 and 3.00 wt.% of Eu^{3+} ions). However, the XRD analysis revealed that the lattice parameters did not modify significantly after substitution. The lattice parameters (a) and (c) for 1% EuHAp were found to be (0.9418 and 0.6884 nm), but in the

case of 2% EuHAp the calculated values were (0.9416 and 0.6881 nm) compared to standard data of JCPDS No. 09-0432 for pure HAp (0.9417 and 0.6883nm).

Sun et al. [222] prepared EuHAp powders, where (Eu^{3+}/(Eu^{3+}+ Ca^{2+}) = 1%). The results of the XRD analysis revealed that the calculated lattice constants of EuHAp were (a = b = 0.9416 nm and c = 0.6881 nm) compared to standard data of JCPDS No. 09-0432 for pure HAp (a = b = 0.9418 nm and c = 0.6884 nm).

6.3.1.4 SEM of 1%EuHAp (1 wt.% Eu^{3+}) materials prepared by hydrolysis and precipitation methods:

<u>SEM of non-sintered 1%EuHAp (1 wt.% $Eu3^{+}$) materials prepared by hydrolysis and precipitation methods.</u>

Fig.6-11. displays the morphology of 1%EuHAp materials prepared by precipitation and hydrolysis routes.

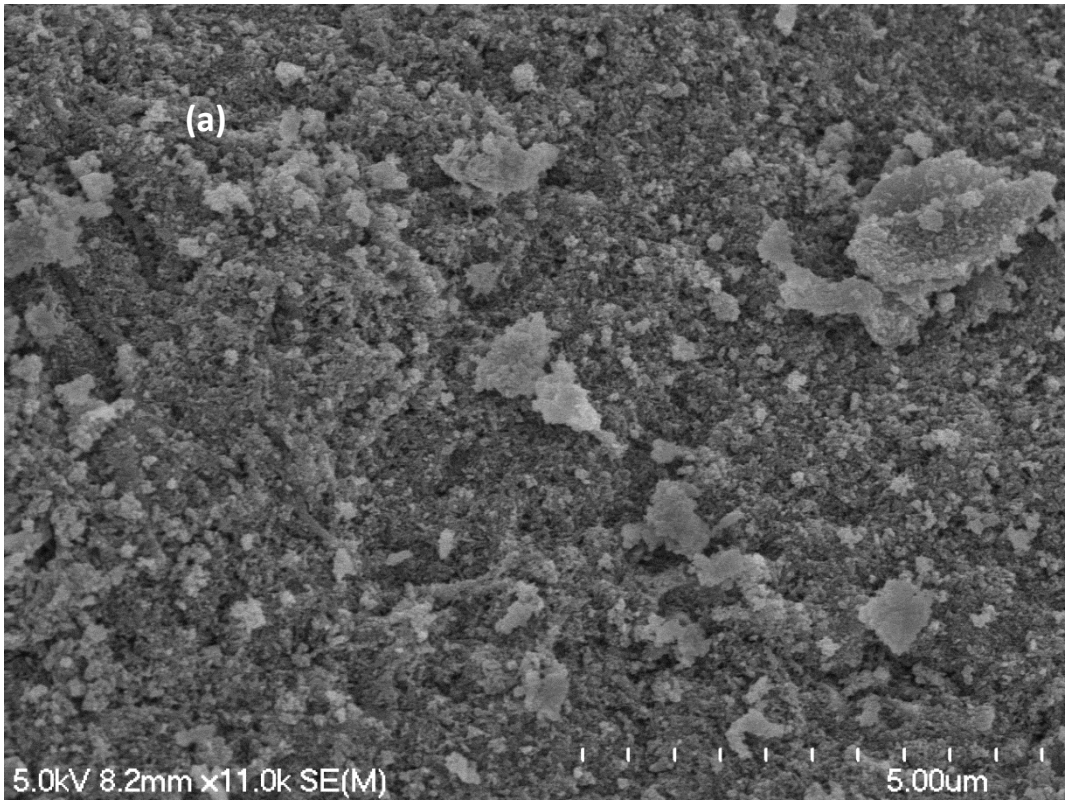

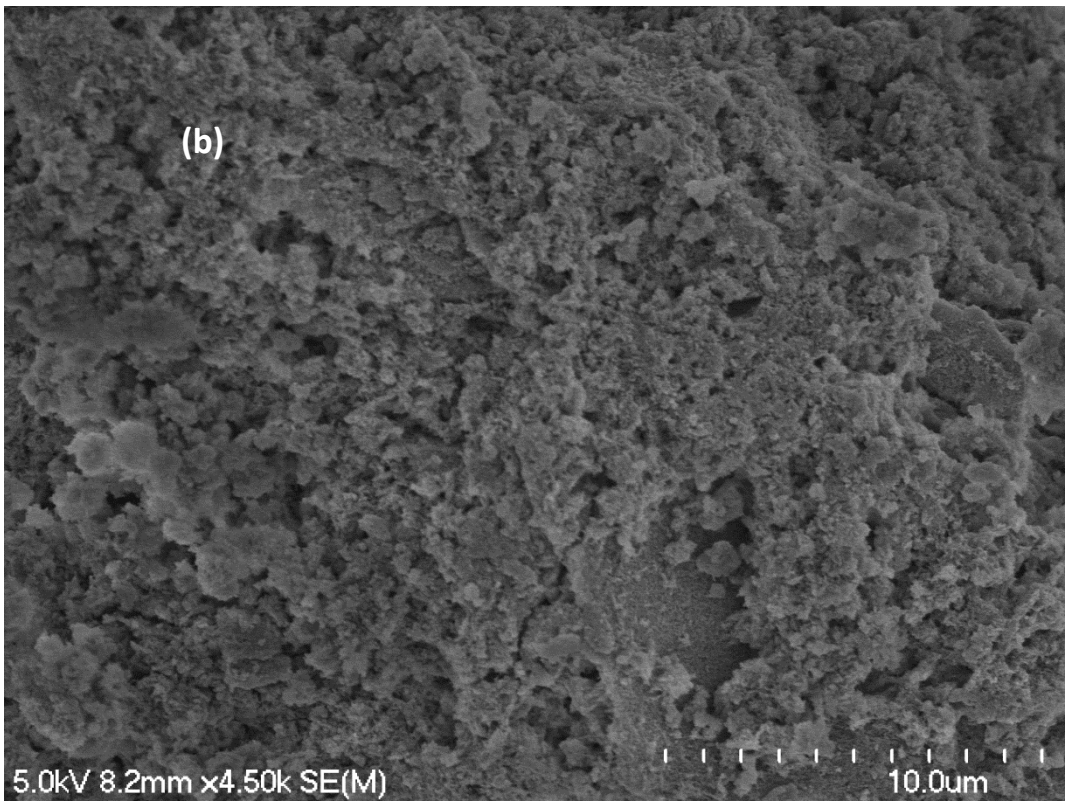
(b)
5.0kV 8.2mm x4.50k SE(M)
10.0um

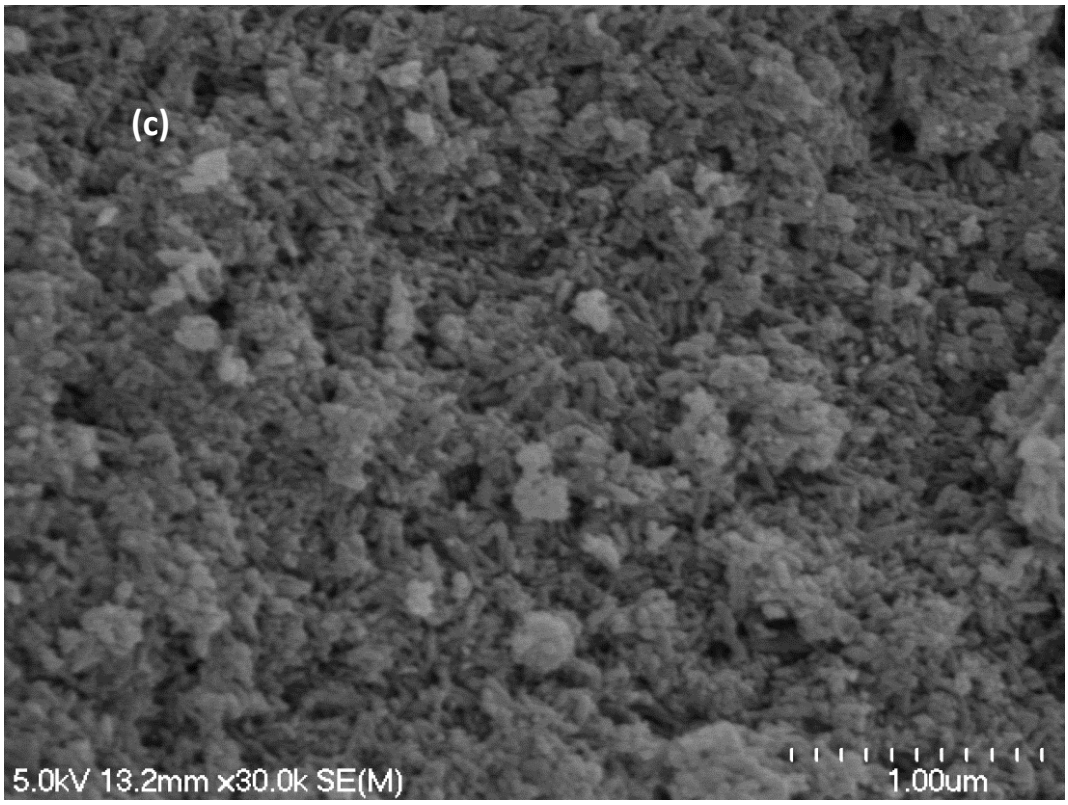
(c)
5.0kV 13.2mm x30.0k SE(M)
1.00um

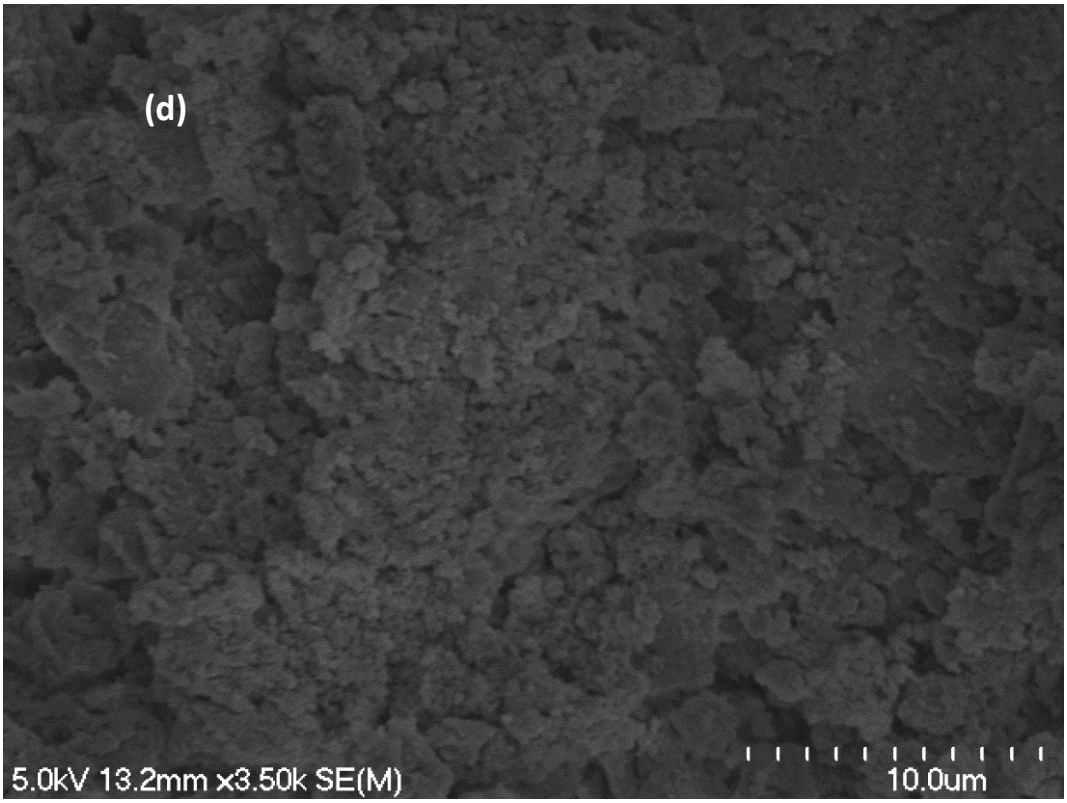

Figure 6-11: SEM images of non-sintered (a) unsubstitutedHAp by precipitation (b) unsubstituted HAp by hydrolysis (c) 1% EuHAp(1 wt.% Eu^{3+}) by precipitation (d) 1% EuHAp(1 wt.% Eu^{3+}) by hydrolysis.

As observed in **Fig.6-11,** the morphology of the prepared samples did not vary due to the substitution process of Eu^{3+} ions, since the EuHAp materials prepared by precipitation and hydrolysis routes appeared as porous materials with an irregular distribution coupled with a clear trend to agglomerate**.**

SEM of 1% EuHAp (1 wt.% Eu^{3+}) materials prepared by the novel hydrolysis and conventional precipitation methods after sintering at 900 ˚C:

Fig. 6-12 shows the morphology of 1%EuHAp samples prepared by the conventional precipitation and novel hydrolysis methods.

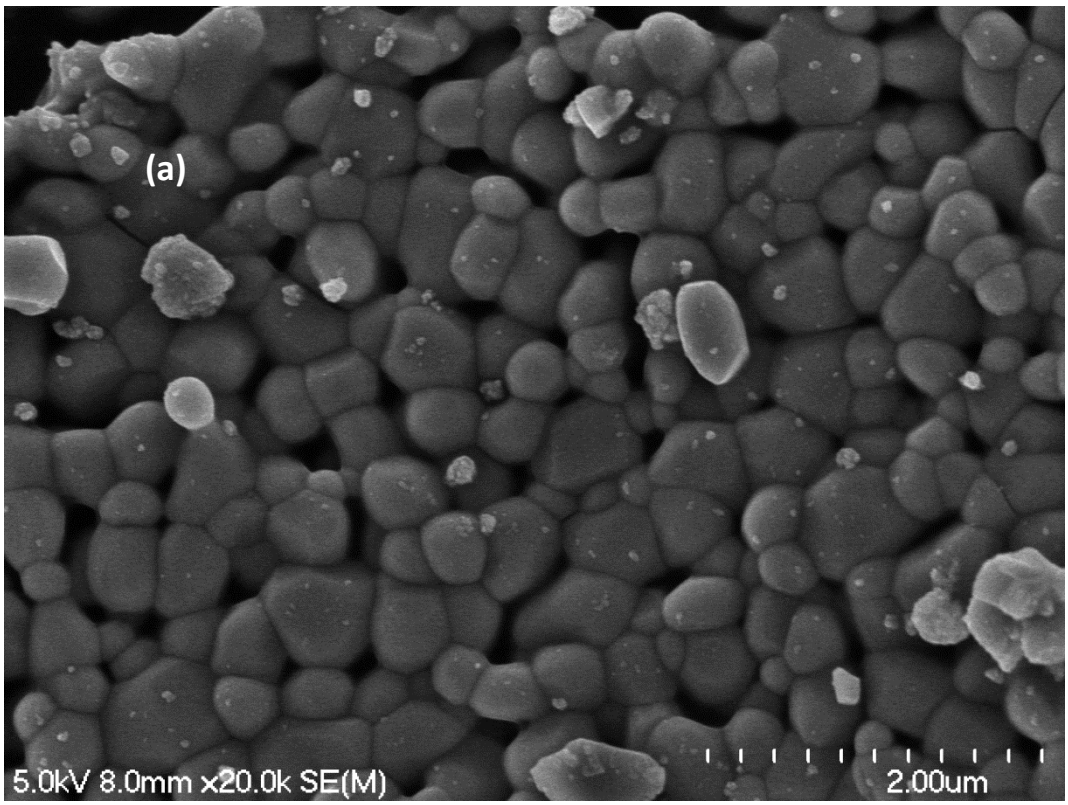
(a)
5.0kV 8.0mm x20.0k SE(M)
2.00um

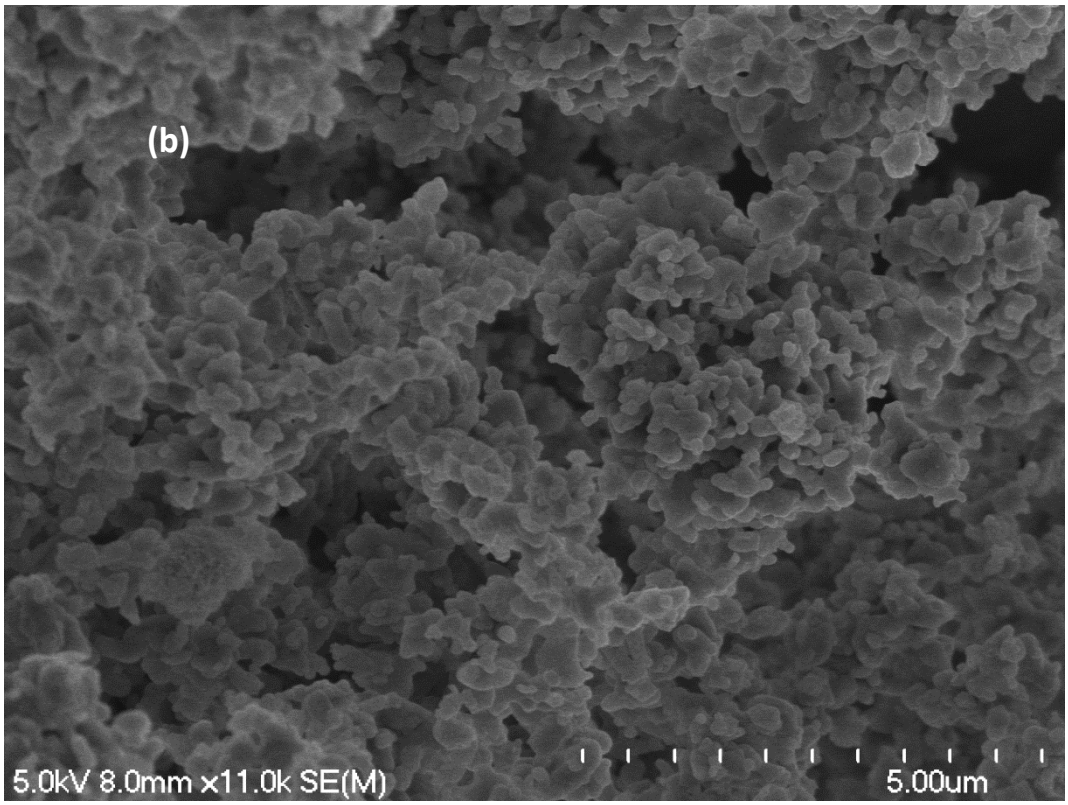
(b)
5.0kV 8.0mm x11.0k SE(M)
5.00um

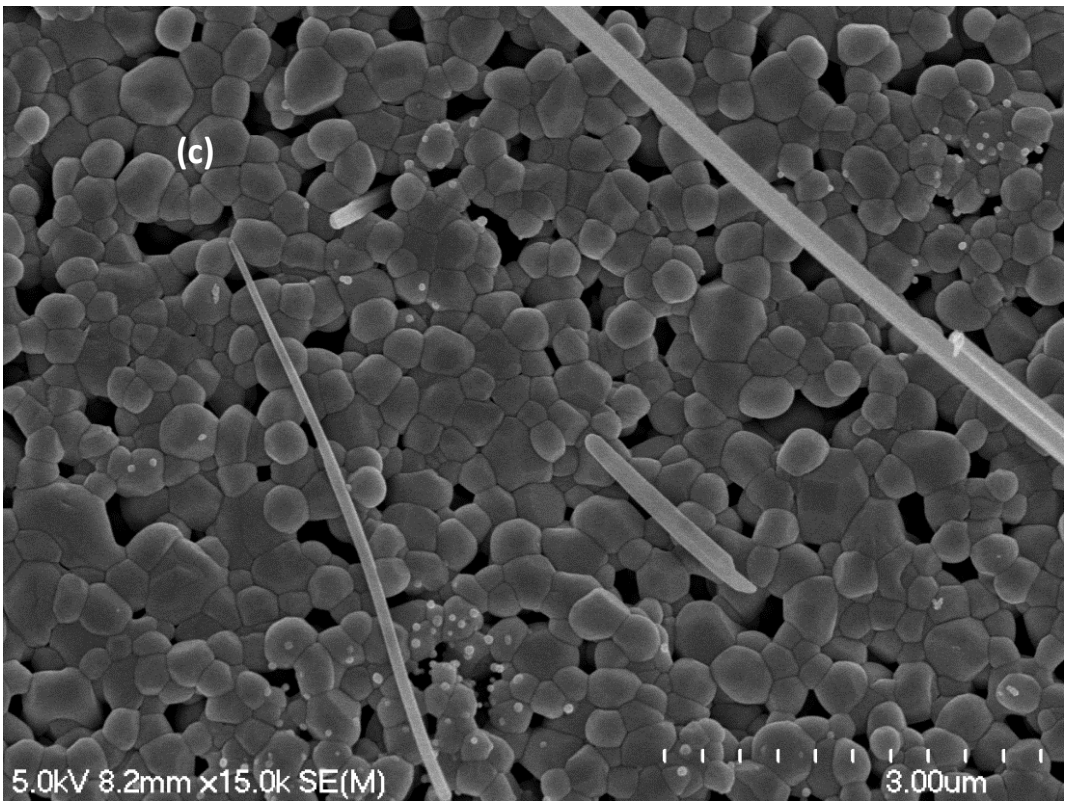
(c)
5.0kV 8.2mm x15.0k SE(M)
3.00um

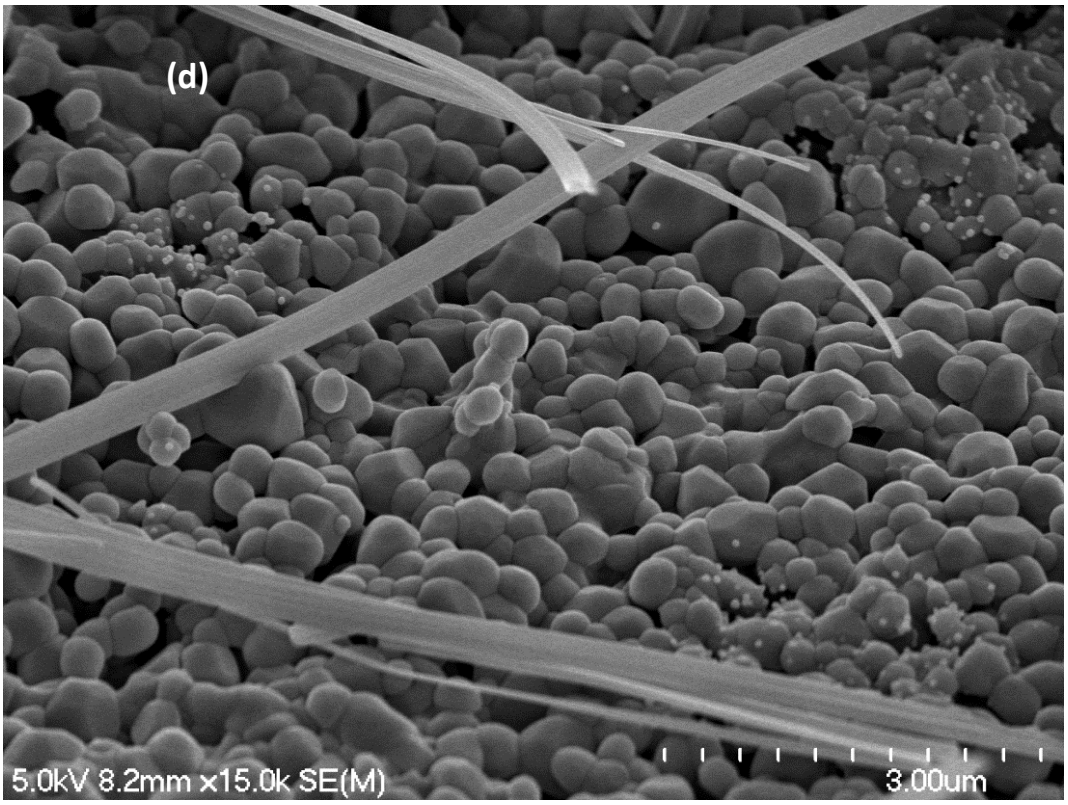
(d)
5.0kV 8.2mm x15.0k SE(M)
3.00um

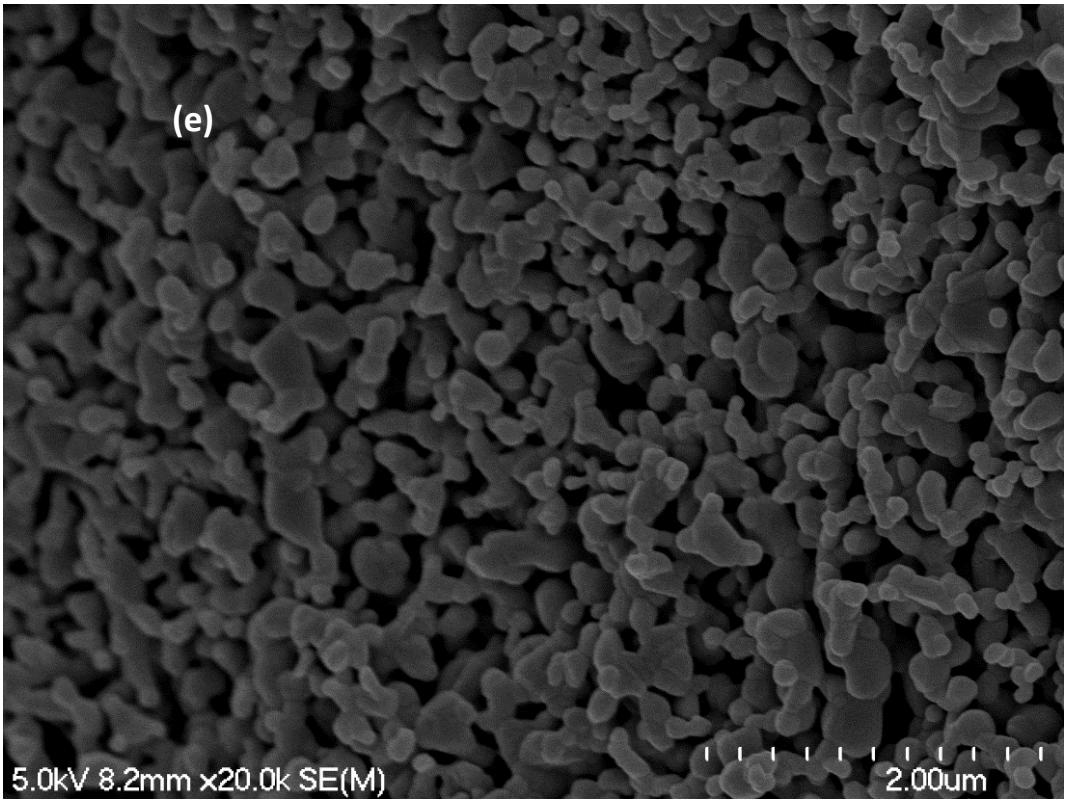

Figure 6-12: SEM images of (a) unsubstituted HAp by precipitation (b) unsubstituted HAp by hydrolysis (c and d) 1 % EuHAp (1 wt.% Eu^{3+}) by precipitation (e) 1 % EuHAp (1 wt.% Eu^{3+}) by hydrolysis, after sintering at 900 ˚C.

Fig.6-12. showed that the morphology of EuHAp powders is strongly influenced and affected by the synthesis route. A well-defined morphology had been obtained due to heat treatment of EuHAp materials at 900 ˚C by both methods (precipitation and hydrolysis). While, a spherical shape was obtained by the hydrolysis method, it can be seen that precipitation approach produced EuHAp materials that consist of particles with spherical shape and a small quantity of whiskers as observed by SEM images, but as a result of using hydrolysis method spheroidal like shapes with porous materials were recorded. It seems that replacement process of Eu^{3+} ions by precipitation method have a tendency to form whiskers. However, the SEM/EDX techniques was also used to get better idea about the elemental composition of the 1%EuHAp that was prepared by the conventional precipitation method. The results of SEM/EDX analysis for the above mentioned system can be found in Appendix (see appendix A). The SEM/EDX results showed that:

1- The whiskers consist of Ca^{2+}, PO_4^{3-}, OH^- and Na^+ ions.

2- Also, the weight percent of Na^+ ions (23.74%) in the whiskers were found to be higher than the spherical particles (2.22%).

3- The whiskers have lower Ca/P mole ratio (0.91) compared to spherical particles (1.40). The results of SEM/EDX analysis for the above-mentioned system can be found in Appendix A through the illustration of one computed example involving 1%EuHAp that was prepared by precipitation route.

6.4 1, 3 and 5% ScHAp (1, 3 and 5 wt.%Sc^{3+}) powders prepared by hydrolysis and precipitation methods:

Tite et al. [221] reported that rare – earth metals such as lanthanides and scandium are of great interest in biomedical applications especially in orthopedic areas because of their high biological activity as well as their ability to substitute for calcium ions in the HAp structure.

Three different series of ScHAp material (1, 3 and 5 wt.% Sc^{3+}) were prepared by using two different synthesis routes (precipitation and hydrolysis). Sc_2O_3 was used as the scandium precursor. 0.20 g of Sc_2O_3 was converted to $ScCl_3.(H_2O)_6$ by using (30 mL of 6M HCl) as described in [235], according to the proposed equation [235]:

$$Sc_2O_3 + 6\ HCl + 9\ H_2O \rightarrow 2\ ScCl_3.(H_2O)_6$$

The detailed amounts of the reagents are listed in the **Tables 6-13, 6-14 and 6-15.**

Table 6-13: Synthesis details of 1%ScHAp (1 wt.% Sc^{3+}) powders

Sample	$Ca(NO_3)_2$ (g)	$Ca(OH)_2$ (g)	MCPM (g)	Na_2HPO_4 (g)	$ScCl_3.6H_2O$ (g)	$Ca(NO_3)_2$ (mol)	$Ca(OH)_2$ (mol)	MCPM (mol)	Na_2HPO_4 (mol)	$ScCl_3.6H_2O$ (mol)
1% ScHAp (1 wt.% Sc^{3+}) by precipitation	7.9483	-	-	4.2304	0.3585	0.0484	-	-	0.0298	0.0014
1% ScHAp (1 wt.% Sc^{3+}) by hydrolysis	-	3.5819	12.1845	-	0.3585	-	0.0483	0.0483	-	0.0014

Table 6-14: Synthesis details of 3%ScHAp (3 wt.% Sc^{3+}) powders

Sample	$Ca(NO_3)_2$ (g)	$Ca(OH)_2$ (g)	MCPM (g)	Na_2HPO_4 (g)	$ScCl_3.6H_2O$ (g)	$Ca(NO_3)_2$ (mol)	$Ca(OH)_2$ (mol)	MCPM (mol)	Na_2HPO_4 (mol)	$ScCl_3.6H_2O$ (mol)
3% ScHAp (3 wt.% Sc^{3+}) by precipitation	7.5685	-	-	4.1976	0.9560	0.0461	-	-	0.0296	0.0037
3% ScHAp (3 wt.% Sc^{3+}) by hydrolysis	-	3.40562	11.5987	-	0.9560	-	0.0460	0.0460	-	0.0037

Table 6-15: Synthesis details of 5%ScHAp(5 wt.% sc^{3+}) powders

Sample	$Ca(NO_3)_2$ (g)	$Ca(OH)_2$ (g)	MCPM (g)	Na_2HPO_4 (g)	$ScCl_3.6H_2O$ (g)	$Ca(NO_3)_2$ (mol)	$Ca(OH)_2$ (mol)	MCPM (mol)	Na_2HPO_4 (mol)	$ScCl_3.6H_2O$ (mol)
5% ScHAp (5 wt.% Sc^{3+}) by precipitation	7.1998	-	-	4.2098	1.4340	0.0439	-	-	0.0297	0.0055
5% ScHAp (5 wt.% Sc^{3+}) by hydrolysis	-	3.2487	11.0598	-	1.4340	-	0.0438	0.0439	-	0.0055

6.4.1 1%ScHAp (1 wt.% Sc^{3+}) powders prepared by the novel hydrolysis and conventional precipitation methods:

One series of 1% ScHAp material (1 wt.% Sc^{3+}) was prepared by using two different synthesis routes (precipitation and hydrolysis), and the detailed amounts of the reagents are listed in **Table 6-13.**

6.4.1.1 Characterization techniques of 1% ScHAp (1 wt.% Sc^{3+}) materials prepared by the novel hydrolysis and conventional precipitation methods:

6.4.1.2 ICP-MS of 1%ScHAp (1 wt.% Sc^{3+}) materials prepared by hydrolysis and precipitation methods after sintering at 900 ˚C:

The results of the elemental analyses of 1%ScHAp (1 wt.% Sc^{3+}) samples prepared by precipitation and hydrolysis routes are displayed in **Table 6-16.**

Table 6-16: ICP-MS results of 1%ScHAp (1% wt. Sc^{3+}) materials prepared by precipitation and hydrolysis methods after sintering at 900 ˚C. The concentration was in ppb unit (ug/L):

Sample	Ca 44	P 31	Na 23	Sc 45
Unsubstituted HAp by precipitation	707795	401240	103797	-
1% ScHAp by precipitation	750385	375632	46230	226.4
Unsubstituted HAp by hydrolysis	769928	423970	78396	-
1% ScHAp by hydrolysis	796143	382950	59771	204.5

The starting (calculated) and actual (measured) degree of chemical composition of the prepared powders in terms of wt% of Sc^{3+}ions, the calcium/phosphorus (Ca/P) molar ratios as well as (Ca+Na+Sc)/P molar ratio were determined by ICP-MS and are presented in **Tables 6-17.**

Table 6-17: The chemical analysis data of 1%ScHAp (1 wt.% Sc^{3+}) materials by ICP-MS measurements after sintering at 900 ˚C.

Sample	Ca/P Theoretical	Ca/P Measured	(Ca+Na+Sc)/P Mole ratio	Wt.% Sc^{3+} ions theoretical	Wt.% Sc^{3+} ions measured	Wt.% Na^{+} ions measured

Unsubstituted HAp by precipitation	1.67	1.36	1.71	-	-	5.2%
1% ScHAp by precipitation	1.62	1.54	1.71	1%	0.01%	2.3%
Unsubstituted HAp by hydrolysis	1.67	1.40	1.65	-	-	3.9%
1%ScHAp by hydrolysis	1.62	1.61	1.81	1%	0.01%	3.0%

Table 6-17, displays that the Ca:P mole ratio of the prepared 1% ScHAp samples were lower than the expected value of stochiometric HAp (1.67). This result can be attributed to the presence of Na^+ ions in the samples which are substituting into the calcium ion sites in the HAp lattice as discussed previously (see chapter four for details). The **(**Ca+Na+Sc)/P mole ratios of the prepared 1%ScHAp samples were slightly higher than the stochiometric value of HAp (1.67). This observation can be ascribed to the presence of carbonate group as confirmed by FTIR spectra. Also, **Table 6-17**, showed that the substitution level of Sc^{3+} ions (if occurring) into HAp samples by both routes was expected to be very low compared to the proposed percent of substitution (1%). This result can be explained in terms of the lower concentration of Sc_2O_3 material that was used as a source of scandium ions (0.2 g of Sc_2O_3 were dissolved in 30 mL of 6M HCl to obtain the $ScCl_3.6H_2O$ solution).

6.4.1.3 FTIR of 1% ScHAp (1 wt.% Sc^{3+}) materials prepared by the novel hydrolysis and conventional precipitation methods.

FTIR of non-sintered 1%ScHAp (1 wt.% Sc^{3+}) materials prepared by hydrolysis and precipitation methods.

Figure 6-13 displays the FTIR spectra of the prepared non-sintered 1% ScHAp (1 wt.% Sc^{3+}) materials prepared by the precipitation and hydrolysis methods.

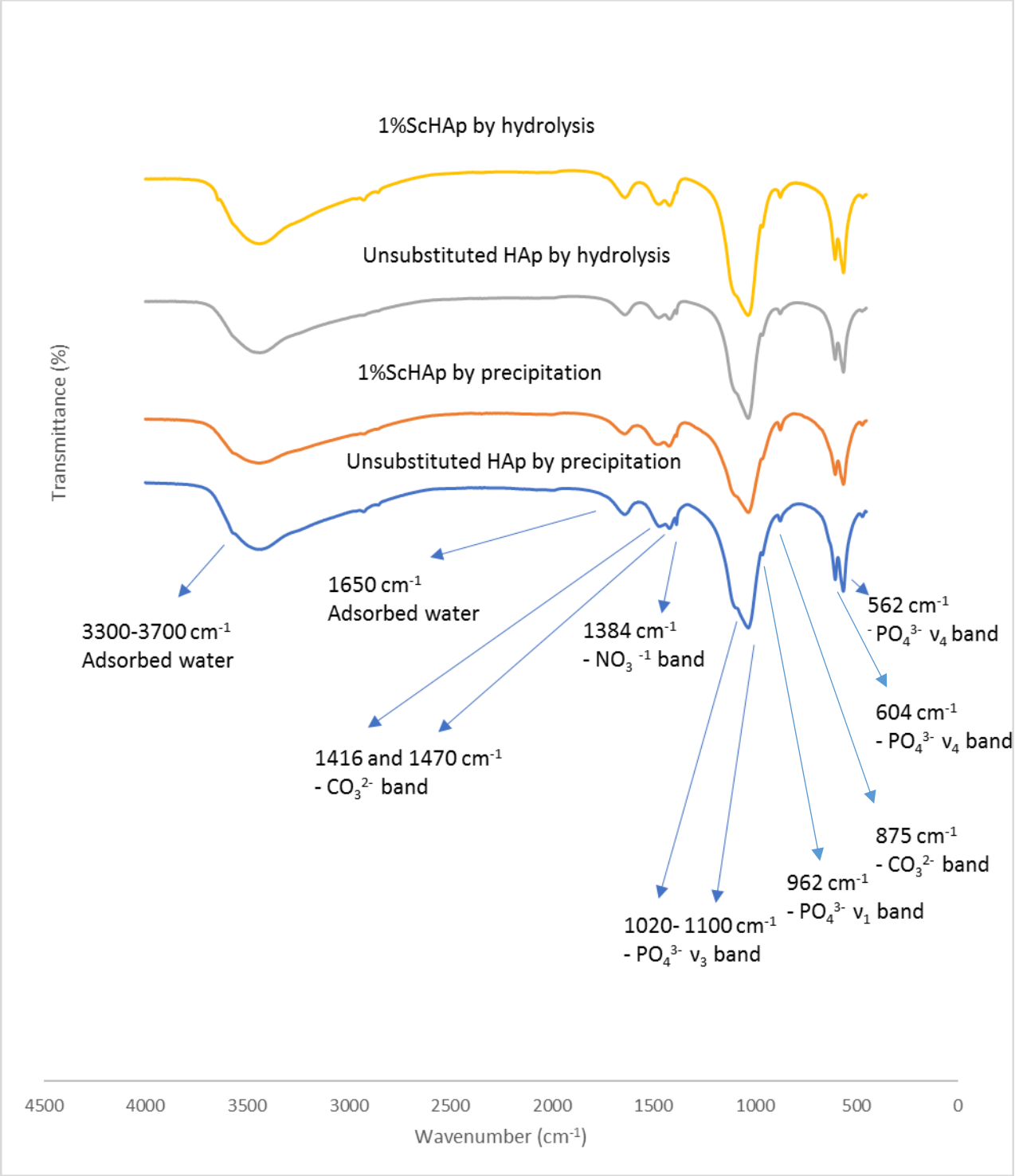

Figure 6-13: FTIR spectra of non-sintered 1%ScHAp (1 wt.% Sc^{3+}) materials prepared by precipitation and hydrolysis methods.

The FTIR analysis of all samples (**Fig. 6-13**) showed the characteristic bands of HAp. The broad band at 3300 - 3700 cm^{-1} and the peak at 1635 cm^{-1} were related to adsorbed water on the

powders. The band at 1028–1090 cm^{-1} was assigned to the P–O stretching vibration of the phosphate groups (PO_4^{3-}), while the band at 568–605 cm^{-1} which appears as a doublet was also attributed to the PO_4^{3-} bending mode. The small bands at about 1416 and 1465 cm^{-1} are related to the CO_3^{2-} group indicating the formation of CO_3HAp (B-type). In the case of the precipitation method, the band at 1385 cm^{-1} can be assigned to the nitrate group (NO_3^-) due to the starting materials using metal salts, but its observation in solids made by using the hydrolysis method, indicate it is likely due to the nitrate ion which was a contaminant in the KBr powder used to make the pellets.

FTIR of 1%ScHAp (1 wt.% Sc^{3+}) materials prepared by hydrolysis and precipitation methods after sintering at 900 ˚C:

Figure 6-14 displays the FTIR spectra of sintered 1%ScHAp (1 wt.% Sc^{3+}) materials prepared by the precipitation and hydrolysis methods.

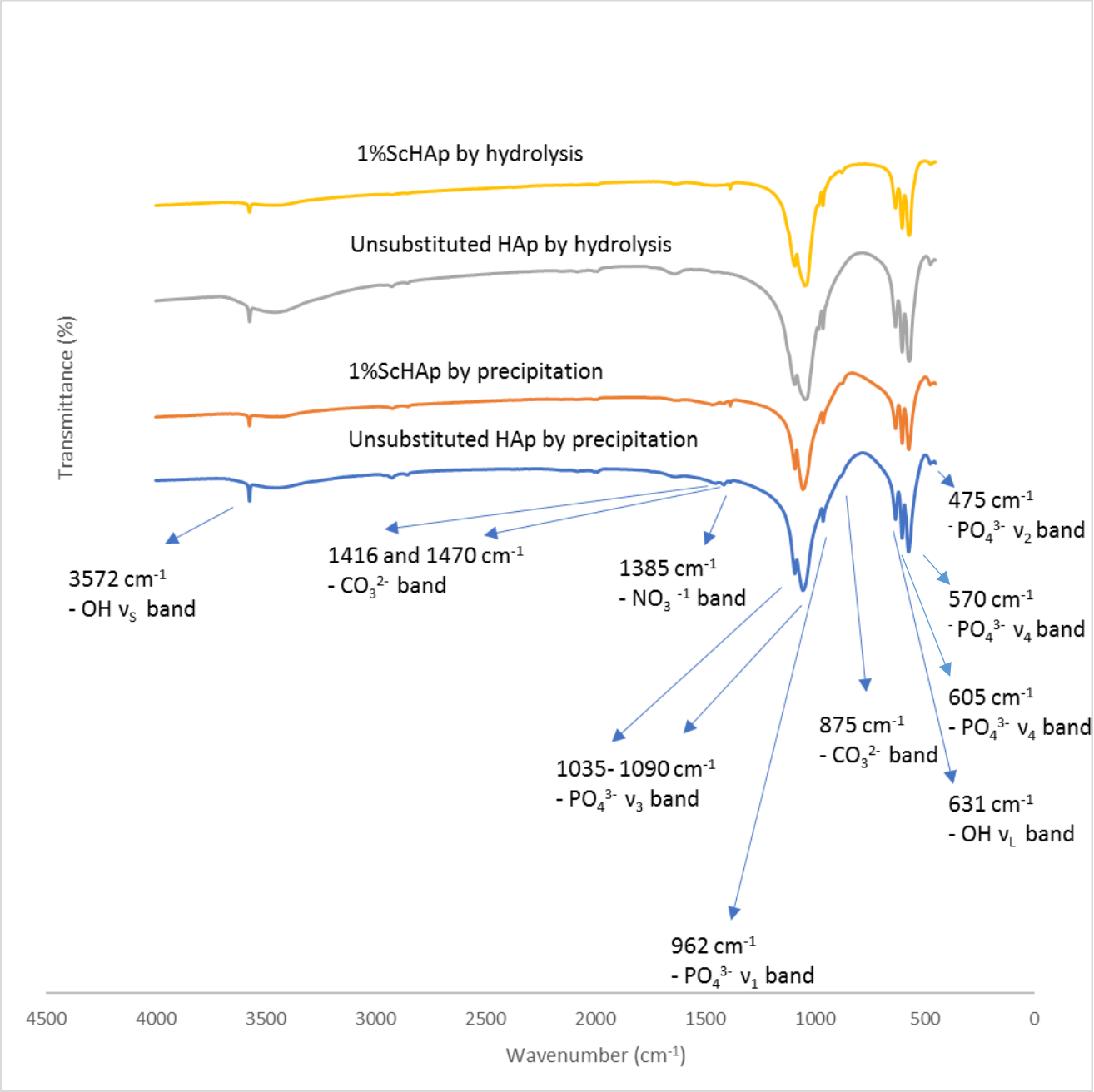

Figure 6-14: FTIR spectra of 1%ScHAp (1 wt.% Sc^{3+}) materials prepared by precipitation and hydrolysis methods after sintering at 900 ˚C.

The corresponding FTIR spectra (**Fig. 6-14**) of 1%ScHAp (1 wt.% Sc^{3+}) materials prepared by precipitation and hydrolysis methods displayed the characteristic vibrational modes of HAp materials. While the phosphate group appeared at (963, 472, 1104, 1035 cm^{-1}, 603 and 565 cm^{-1}), it can be seen the lattice OH stretching and librational bands appeared at (3572 and 631 cm^{-1}) indicating formation of high crystalline materials. Also, **Fig. 6-14** showed a clear reduction in the

intensity of the stretching mode of OH^- group at 3572 cm^{-1} due possibly to the substitution process by precipitation and hydrolysis methods at 3572 cm^{-1}. This observation can be discussed as follows:

1- The partial substitution of hydroxyl group by chloride ions as a result of using $ScCl_3$ as a precursor to substitute Sc^{3+} ions into HAp crystals.

2- The presence of sodium ions which comes from using sodium hydroxide to adjust pH value (confirmed by ICP-MS analysis) coupled with the formation CO_3HAp powders (as detected in FTIR spectra). These kinds of Na-containing B-type apatites ($NaCO_3$Aps) were discussed extensively (see FTIR of sintered 1%RbHAp), whereas the OH^- ion content was derived by the requirement to keep charge balance and to restore the neutrality of HAp crystals.

3- Although, the results of ICP-MS analysis showed that the measured wt.% of Sc^{3+} ions associated with the HAp was very low by both routes (the precipitation and the novel hydrolysis), the reduction in the intensity of the stretching mode of the OH^- group at 3572 cm^{-1} in HAP samples obtained by both preparation methods, might be attributed to the substitution process of a trivalent cation such as the trivalent scandium ion into the HAp structure as explained by Serret et al. [232] (see FTIR of sintered EuHAp materials).

6.4.1.4 XRD diffraction patterns of non-sintered and sintered 1%ScHAp (1 wt.% Sc^{3+}) materials prepared by hydrolysis and precipitation methods:

Phase Identification of 1%ScHAp (1 wt.% Sc^{3+}) materials:

The XRD diffraction patterns of non-sintered and sintered 1%ScHAp (1 wt.% Sc^{3+}) materials prepared by conventional precipitation and novel hydrolysis synthetic methods are shown in **Fig. 6-15 and 6-16**, respectively.

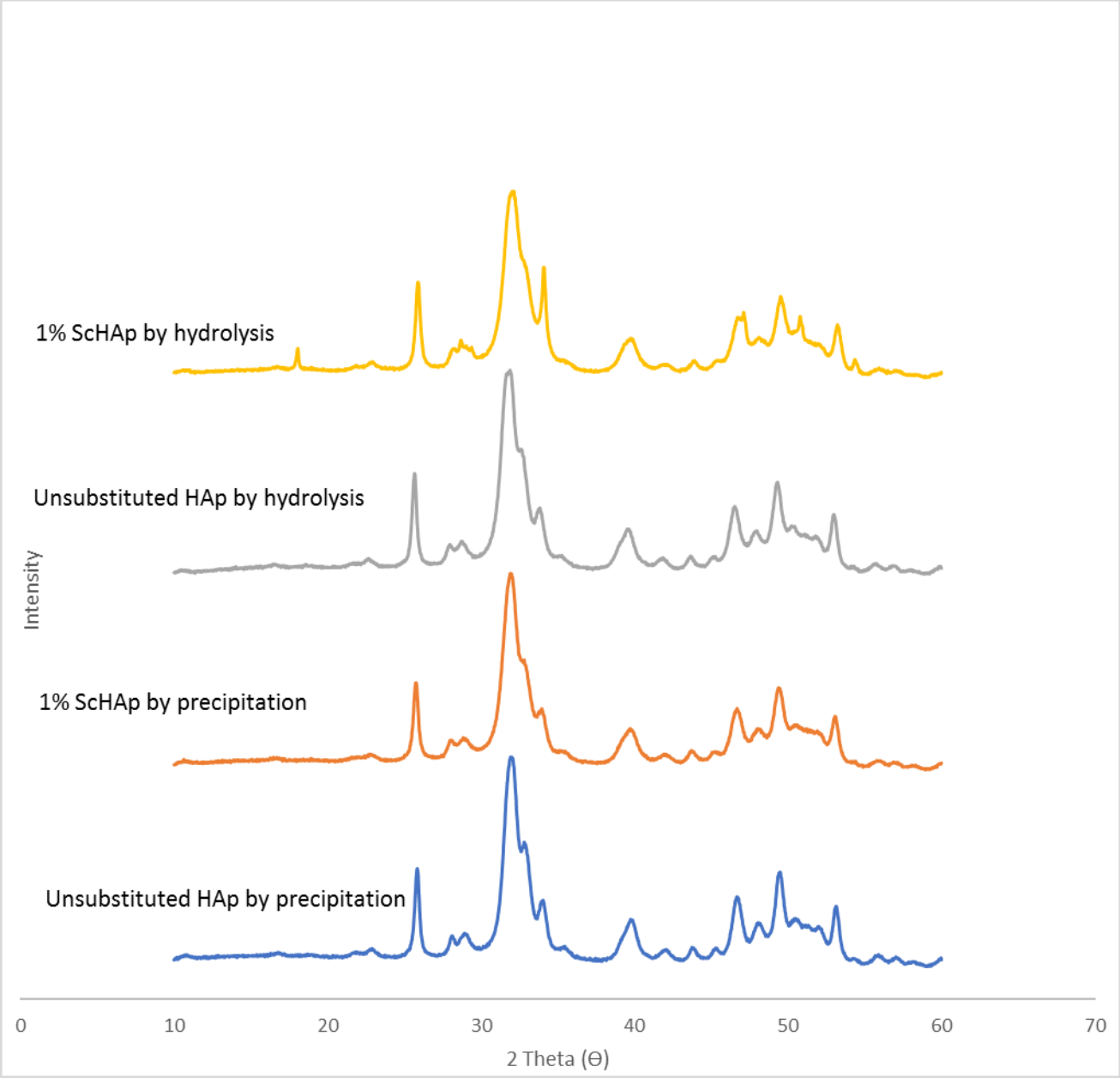

Figure 6-15. The XRD diffraction patterns of non-sintered 1% ScHAp (1 wt.% Sc^{3+}) materials prepared by conventional precipitation and novel hydrolysis methods.

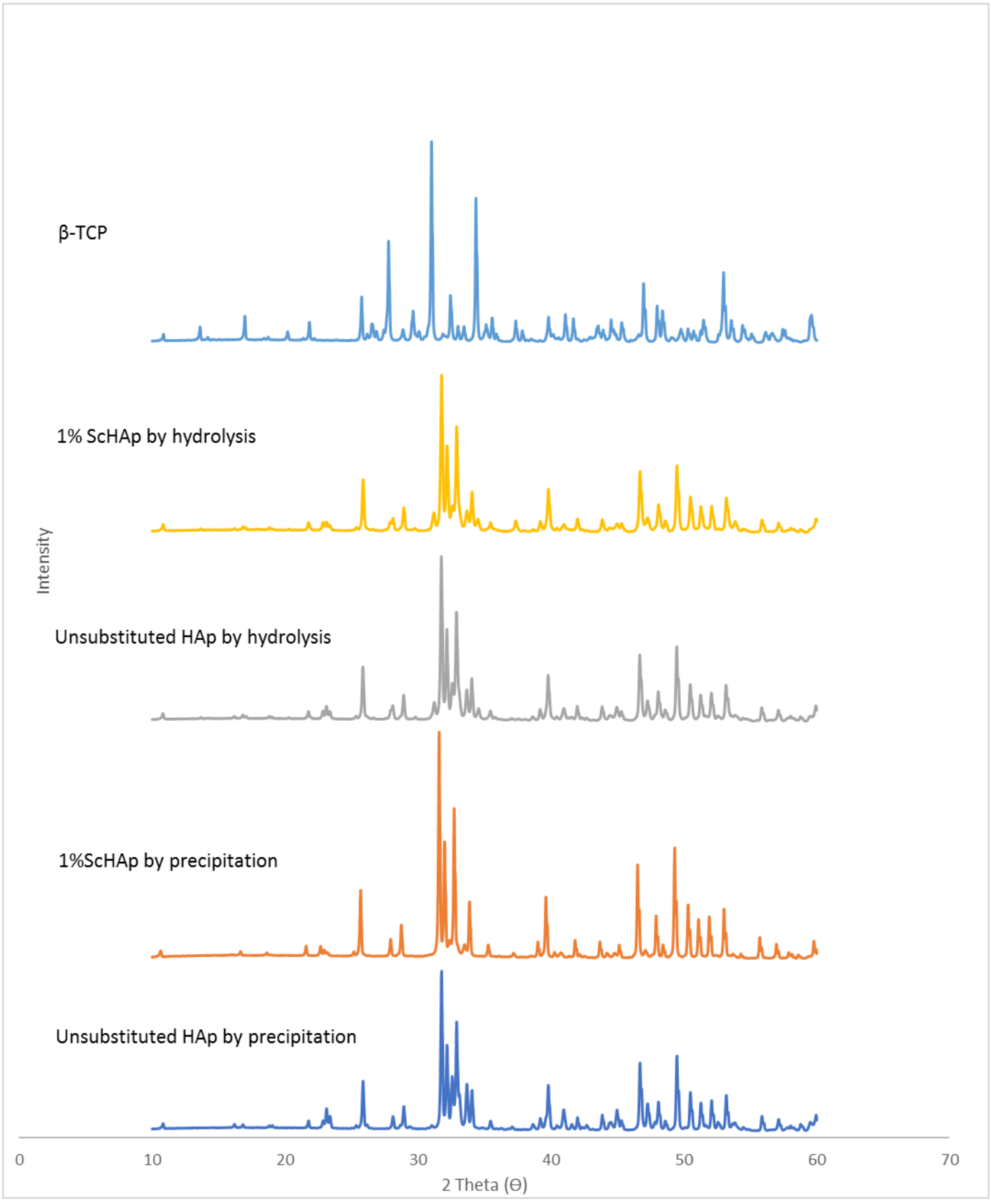

Figure 6-16: The XRD diffraction patterns of 1%ScHAp (1 wt.% Sc^{3+}) materials prepared by precipitation and hydrolysis methods after sintering at 900 ˚C.

Fig.6-16. shows a disappearance of some peaks of the impurity phase at 2 Theta = 31.24˚ and 38.8˚, and a reduction in the intensities of all other peaks that are related to impurity phase (β-TCP) due to substitution of Na^{+}, Cl^{-} and Sc^{3+} ions by precipitation route. In the case of the hydrolysis method, no clear difference was recorded in the phase purity due to the replacement process of Sc^{3+} ions into HAp crystal, except for an additional peak related to CaO at 2 Theta = 37.5 ˚ (reference card number 04-017-9575) that started to appear with small intensity in the ScHAp sample coupled with a reduction in the intensity of the other characteristic peaks of β-TCP at 2 Theta= 32.6˚ and 33.6˚.

Crystallinity and crystallite size of sintered 1% ScHAp (1 wt.% Sc^{3+}) materials:

Table 6-18 displays the degree of crystallinity and the crystallite size of sintered 1% ScHAp (1 wt.% Sc^{3+}) materials by the precipitation and hydrolysis methods.

Table 6-18: The degree of crystallinity and the crystallite size of 1%ScHAp (1 wt.% Sc^{3+}) materials prepared by the conventional precipitation and novel hydrolysis methods after sintering at 900 ˚C.

Sample	D_{002} (Å)	Crystallinity %
Unsubstituted HAp by precipitation	618.3±3.2	84.15±2.4
1% ScHAp by precipitation	711.9±5.5	88.30±5.3
Unsubstituted HAp by hydrolysis	549.8±3.6	82.57±2.1
1% ScHAp by hydrolysis	649.1±4.8	80.70±3.6

An increase in the numerical value of crystallinity was recorded, while a slight reduction of crystallinity produced by hydrolysis method as confirmed by **Table 6-18.** This might be due to the substitution of the trivalent scandium ion in the HAp samples at least via the precipitation method.

Also, **Table 6-18** suggests that the replacement process of Sc^{3+} ions into HAp crystals has possibly affected crystallite size, since an increase was achieved by both methods.

The effect of the low substitution levels on several properties of HAp materials such as the lattice constants and the crystallite size were reported in the literature. As an example: Daniela Predoi and others [206] prepared Zn doped hydroxyapatite ZnHAp by using co-precipitation method with the following chemical formula : $Ca_{10-x}Zn_x(PO_4)_6(OH)_2$, where $0.01 \leq x \leq 0.05$. The XRD results are shown in **Table 6-19.** The SEM images from Predoi et al.'s study indicated that the morphology of the non-sintered ZnHAp materials was similar for all zinc ion concentrations and the shape of particles remained unchanged.

Table 6-19: The effect of the low substitution levels of Zn^{2+} ions on the lattice constants and the crystallite size of the prepared HAp [206] .

Sample	a (Å)	b (Å)	Crystallite size (Å)
JCCD-PDF # 9-432	9.418	6.884	-
XZn = 0.00	9.4320	6.8838	231.879 ±1.000
XZn = 0.01	9.4325	6.8828	230.797±1.000
XZn = 0.03	9.4348	6.8818	224.182±1.000
XZn = 0.04	9.4365	6.8808	201.651±1.000

In the present study, the effect of substitution process on the numerical values of crystallinity and crystallite size can also be ascribed to:

1- the presence of Na^+, CO_3^{2-} in addition to the Sc^{3+} ions into HAp structure as confirmed by ICP-MS analysis and FTIR spectra.
2- Also, the existence of Cl^- ions in the HAp is expected because of the use of $ScCl_3.6H_2O$ as a precursor of Sc^{3+} ions.

Lattice parameters and volume of unit cell of sintered 1%ScHAp (1% wt. Sc^{3+}) materials:

Table 6-20 displays the lattice parameters and the volume of hexagonal unit cell of the sintered 1% ScHAp (1 wt.% Sc^{3+}) materials prepared by precipitation and hydrolysis methods.

Table 6-20: The lattice parameters and the volume of hexagonal unit cell of 1%ScHAp (1 wt.% Sc^{3+}) materials prepared by precipitation and hydrolysis methods after sintering at 900 ˚C.

Sample	a [Å]	c [Å]	V[$Å^3$]
Unsubstituted HAp by precipitation	9.416±0.004	6.879±0.003	1579±0.004
1%ScHAp by precipitation	9.417±0.002	6.879±0.002	1579 ±0.004
Unsubstituted HAp by hydrolysis	9.421±0.003	6.882±0.005	1581±0.004
1%ScHAp by hydrolysis	9.422±0.002	6.882±0.002	1581±0.002

Based on the given values of ionic radius of Sc^{3+} (87.1 pm) compared to Ca^{2+} ions (100 pm), we expected a contraction in both values, but the XRD analysis showed that no significant difference in the lattice parameters was recorded due to immersion of Sc^{3+} ions into HAp crystal by both routes**.** These results can be ascribed to lack of substitution of Sc^{3+} ions in the HAp lattice as suggested by the the ICP-MS analysis which shows a low level of Sc (about 0.01 wt.% Sc^{3+}) associated with the HAp sample, so increasing the level of substitution was performed to see whether a higher level of substitution could be achieved in the samples.

6.4.1.5 SEM of 1%ScHAp (1 wt.% Sc^{3+}) materials prepared by hydrolysis and precipitation methods:

SEM of non-sintered 1%ScHAp (1 wt.% Sc^{3+}) materials prepared by hydrolysis and precipitation methods:

The SEM technique was used to observe the surface morphology of the the non-sintered 1%ScHAp materials prepared by precipitation and hydrolysis methods and the resulting images are shown in **Fig.6-17.**

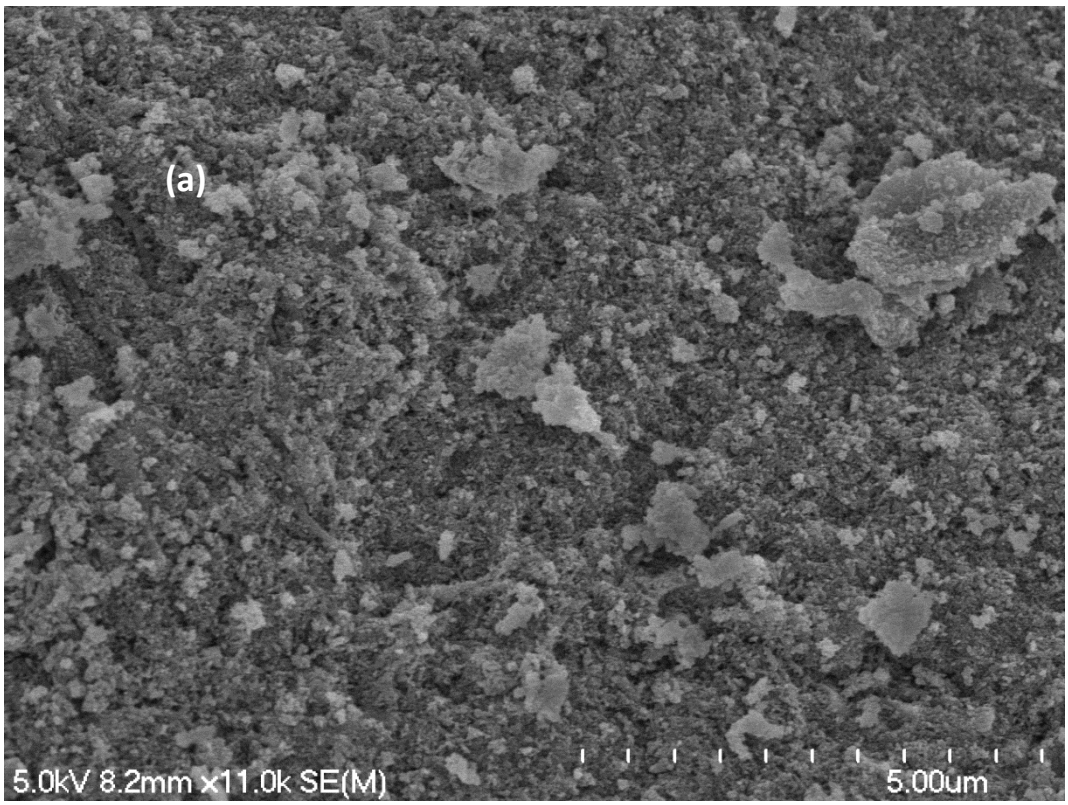
(a)
5.0kV 8.2mm x11.0k SE(M)
5.00um

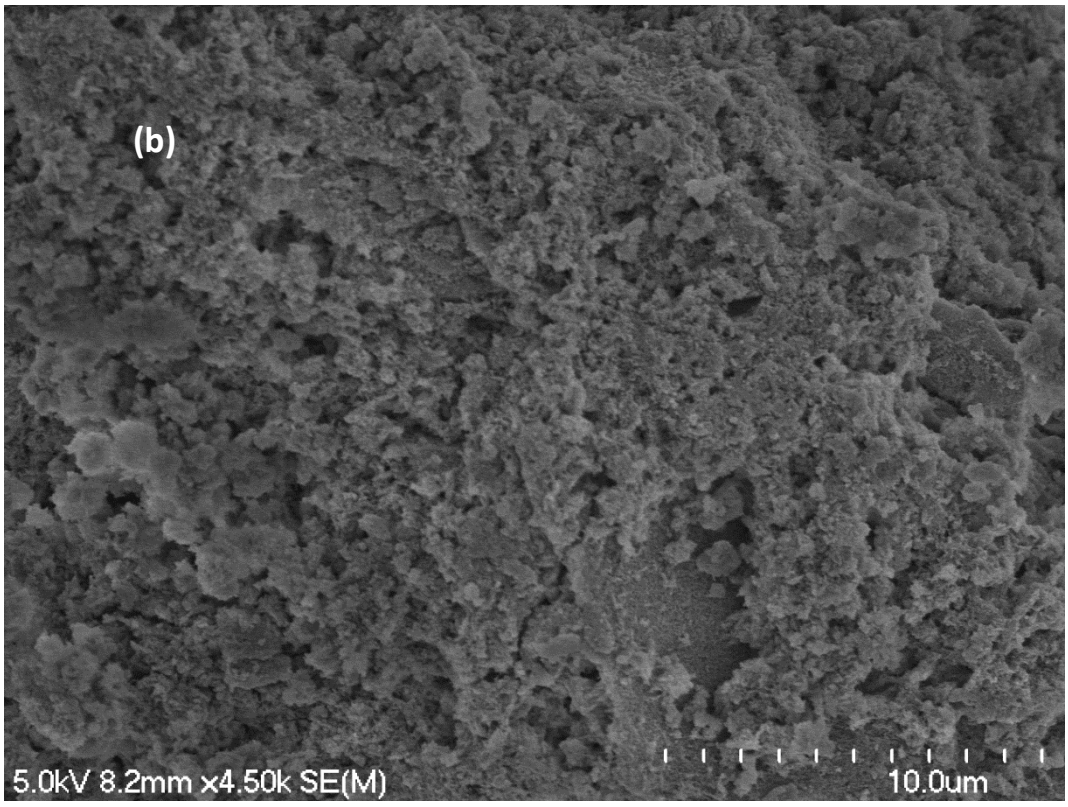
(b)
5.0kV 8.2mm x4.50k SE(M)
10.0um

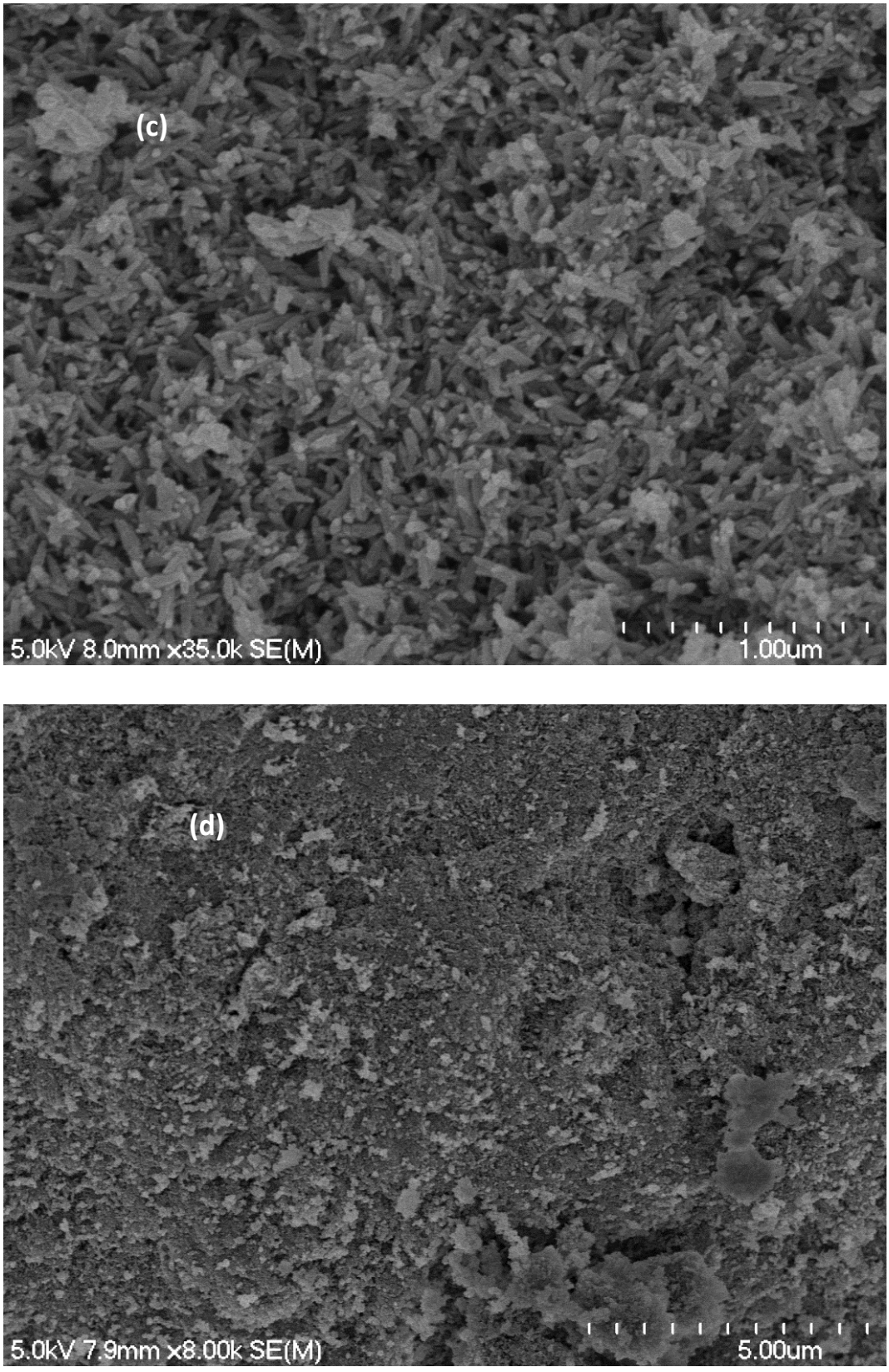

Figure 6-17: SEM images of non -sintered (a) unsubstituted HAp by precipitation (b) unsubstituted HAp by hydrolysis (c) 1 % ScHAp (1 wt.% Sc^{3+}) by precipitation (d) 1 % ScHAp (1 wt.% Sc^{3+}) by hydrolysis.

As shown in **Fig.6-17,** the morphology of the prepared samples did not appear to vary after substitution process of lattice ions by Sc^{3+} ions. The particles of ScHAp powders showed the ability to agglomerate in samples prepared by both routes (hydrolysis and precipitation methods).

SEM of 1%ScHAp (1 wt.% Sc^{3+}) materials prepared by hydrolysis and precipitation methods after sintering at 900 ˚C:

The following figure (Fig.6-18) shows the morphology of the sintered 1% ScHAp powders as prepared by the conventional precipitation and novel hydrolysis methods.

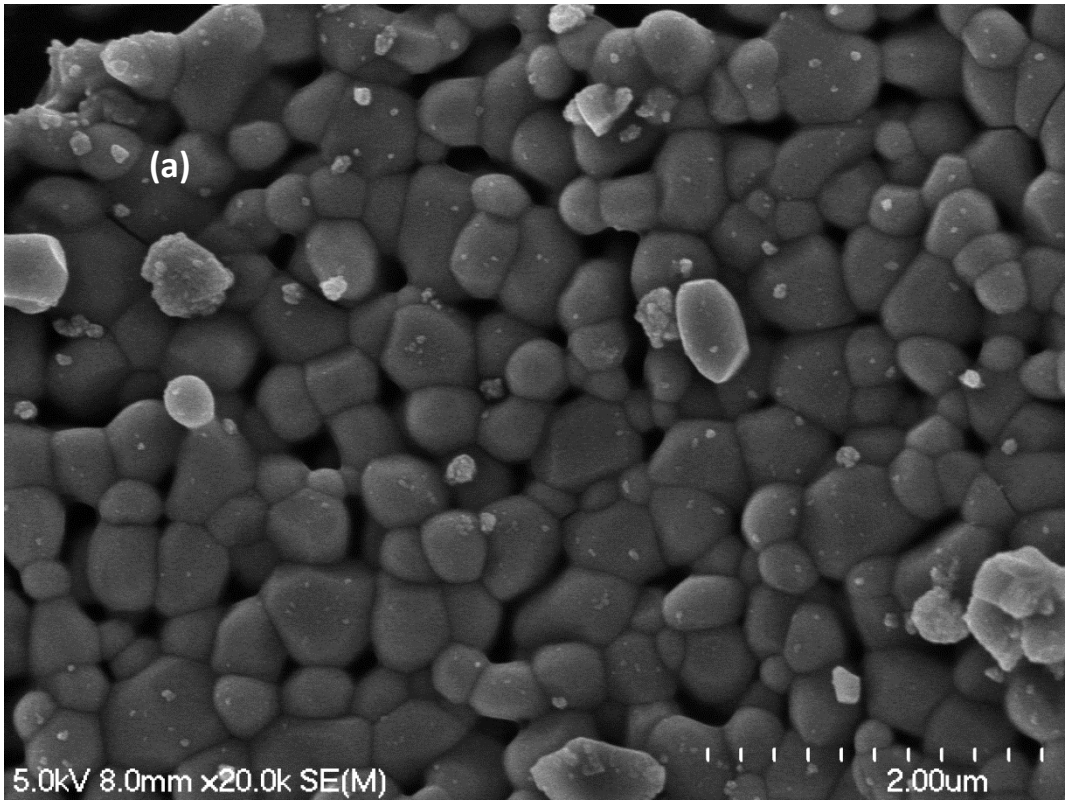

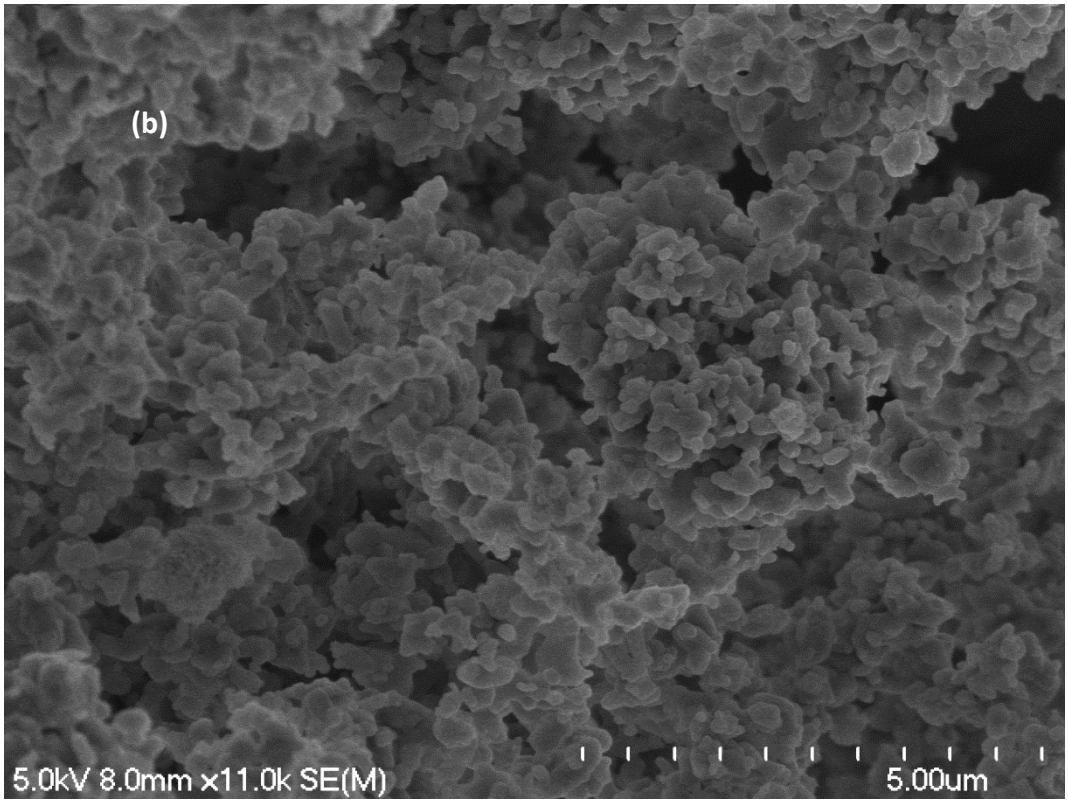
(b)
5.0kV 8.0mm x11.0k SE(M)
5.00um

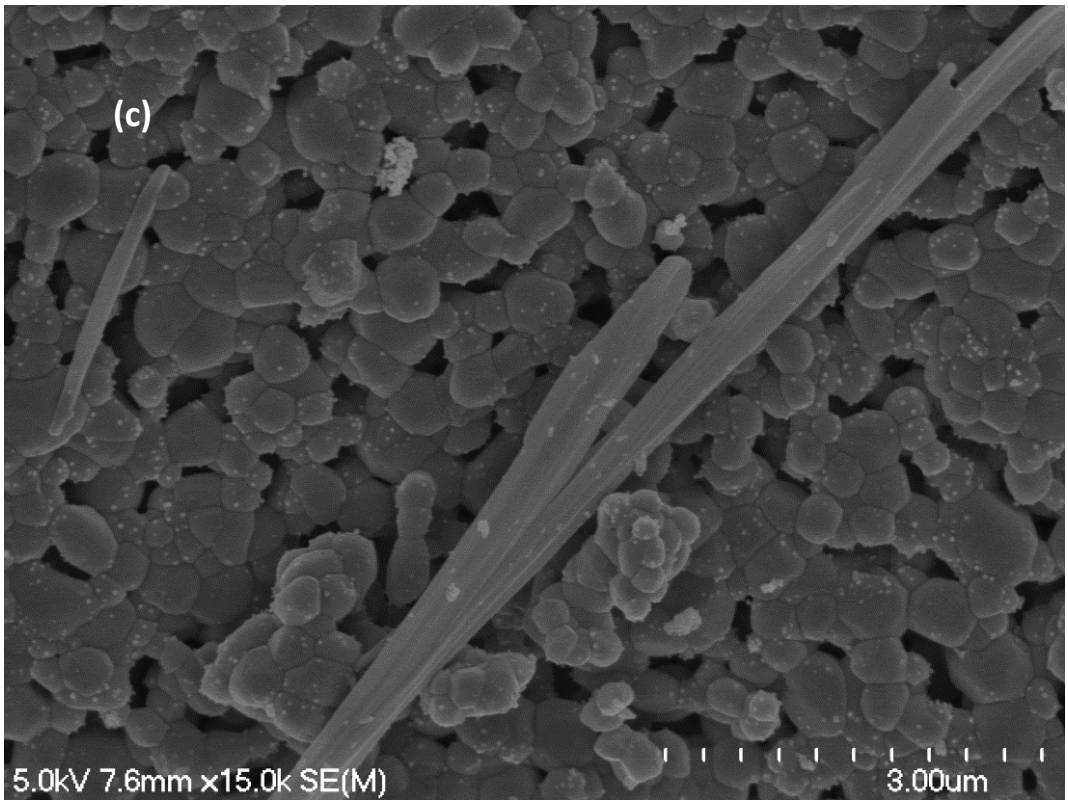
(c)
5.0kV 7.6mm x15.0k SE(M)
3.00um

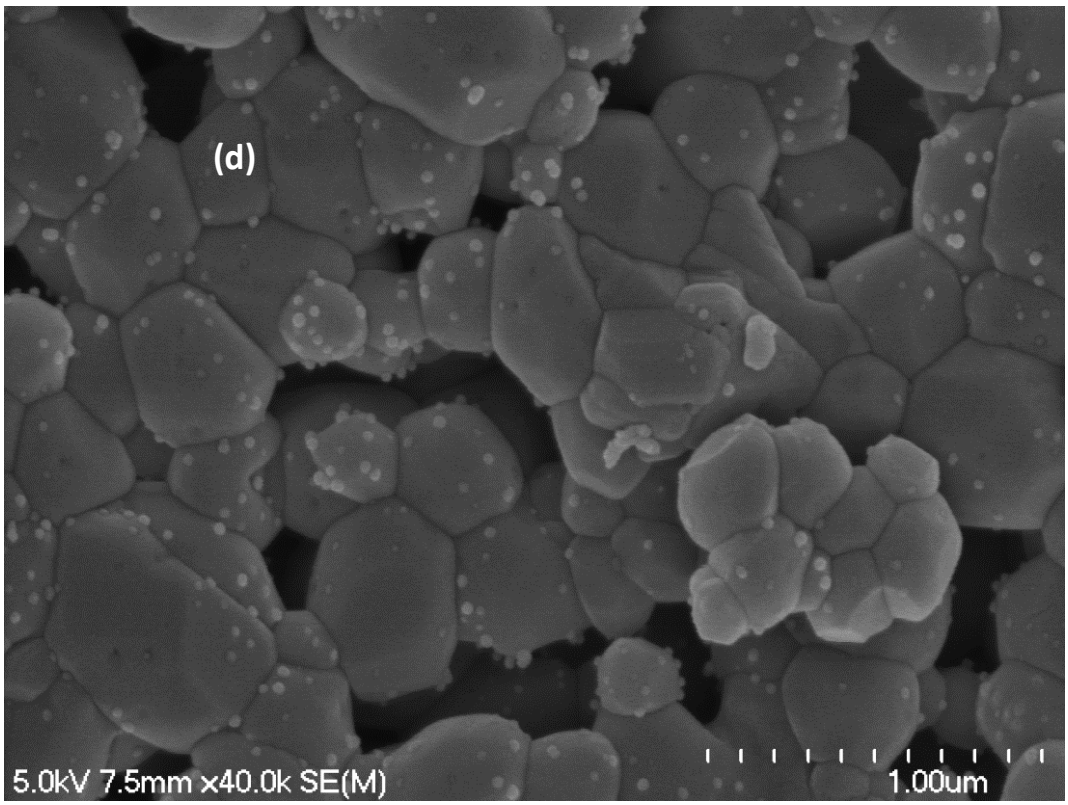
(d)
5.0kV 7.5mm x40.0k SE(M)
1.00um

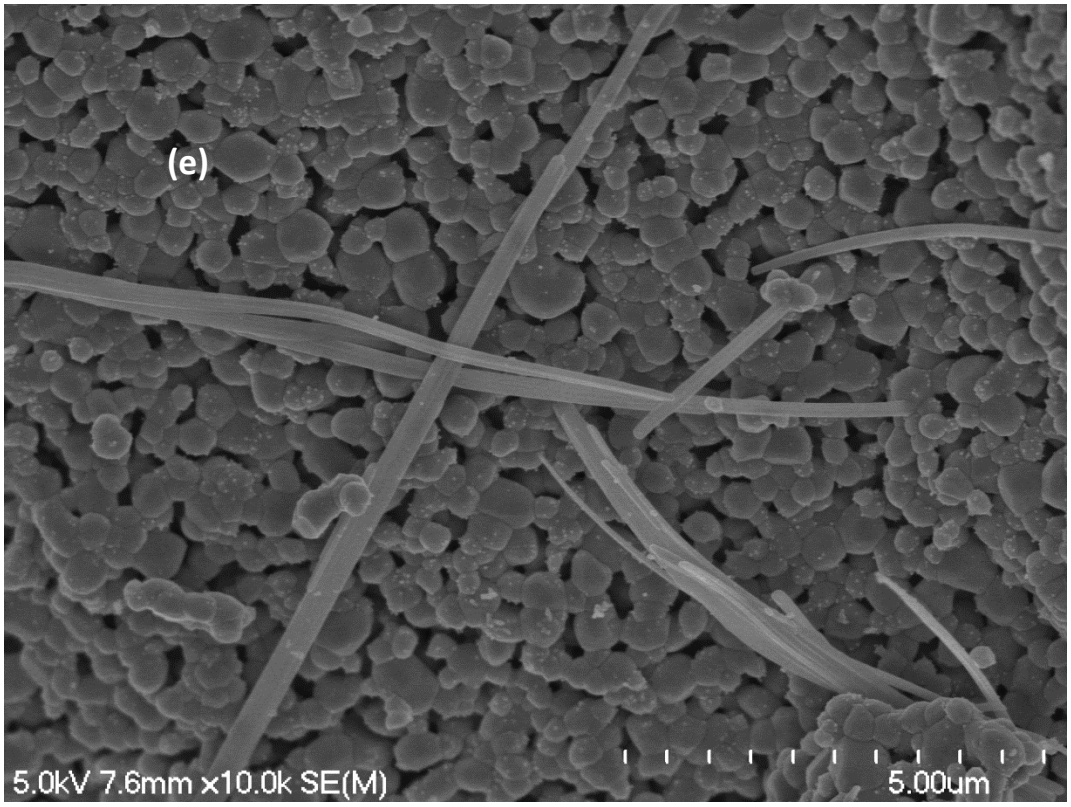
(e)
5.0kV 7.6mm x10.0k SE(M)
5.00um

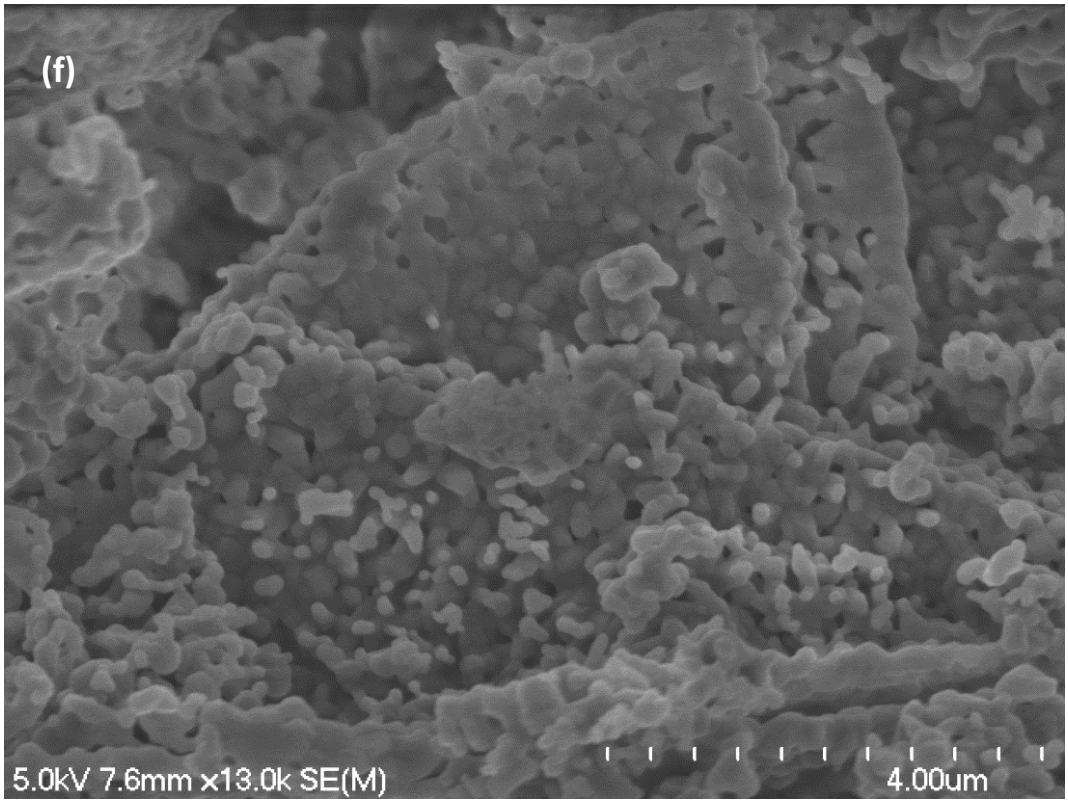

Figure 6-18: SEM images of (a) unsubstituted HAp by precipitation (b) unsubstituted HAp by hydrolysis (c+d+e) 1 % ScHAp (1 wt.% Sc^{3+}) by precipitation (f) 1 % ScHAp (1 wt.% Sc^{3+}) by hydrolysis, after sintering at 900 ˚C.

Fig.6-18. showed that the morphology of 1% ScHAp powders is highly dependent on the synthesis route. The prepared sample by precipitation method consists of particles with spherical shape and a small quantity of whiskers, indicating that the substitution of HAP lattice ions involving Sc^{3+} ions by precipitation tends to form solids which contain whiskers. On the other hand, **Fig.6-18(f)** shows that substitution processes of Sc-based species based on the novel hydrolysis method produced spherical shaped particles with an irregular distribution. The ability also to agglomerate and to form porous materials was also confirmed by SEM images. The SEM/EDX techniques was also used to get a better idea about the elemental composition of the 1%ScHAp that was prepared by the conventional precipitation method. The results of SEM/EDX analysis for the above-mentioned system can be found in the Appendix (see appendix A). The SEM/EDX results showed that:

1- The whiskers consist of Ca^{2+}, PO_4^{3-}, OH^- and Na^+ ions.

2- Also, the weight percent of Na^+ ions (2.17%) in the whiskers were found to be higher than the spherical particles (1.59%).

3- The Ca/P mole ratio of the whiskers is (1.47) compared to (1.50) of the spherical particles.

6.4.2 3% ScHAp (3 wt.% Sc^{3+}) powders prepared by hydrolysis and precipitation methods:

Two series of 3% ScHAp (3 wt.% Sc^{3+}) powders were prepared by precipitation and hydrolysis methods, and the detailed amounts of the reagents were listed in **table 6-14.**

6.4.2.1 Characterization techniques of 3% ScHAp (3 wt.% Sc^{3+}) materials prepared by hydrolysis and precipitation methods:

ICP-MS of prepared 3% ScHAp (3 wt.% Sc^{3+}) materials prepared by hydrolysis and precipitation methods after sintering at 900 ˚C:

The results of the elemental analyses of 3% ScHAp samples that were prepared by the precipitation and hydrolysis routes are displayed in **Table 6-21.**

Table 6-21: ICP-MS results of 3% ScHAp (3 wt.% Sc^{3+}) materials prepared by precipitation and hydrolysis methods after sintering at 900 ˚C. The concentration was in ppb unit(ug/L).

Sample	Ca 44	P 31	Na 23	Sc 45
Unsubstituted HAp by precipitation	707795	401240	103797	-
3% ScHAp by precipitation	660305	352548	129900	510.7
Unsubstituted HAp by hydrolysis	769928	423970	78396	-
3% ScHAp by hydrolysis	642181	367382	99800	215.9

The starting (calculated) and actual (measured) degree of chemical composition of the prepared powders in terms of wt.% of Sc^{3+}ions, the calcium/phosphorus (Ca/P) molar ratios as well as (Ca+Na+Sc)/P molar ratio were determined by ICP-MS and presented in **Table 6-22.**

Table 6-22: The chemical analysis data of 3% ScHAp (3 wt.% Sc^{3+}) materials by ICP-MS measurements after sintering at 900 ˚C.

Sample	Ca/P Theoretical	Ca/P Measured	(Ca+Na+Sc)/P	Wt.% Sc^{3+} ions theoretical	Wt.% Sc^{3+} ions Measured	Wt.% Na^{+} ions measured
Unsubstituted HAp by precipitation	1.67	1.36	1.71	-	-	5.2%
3% ScHAp by precipitation	1.55	1.45	1.94	3%	0.03%	6.5%
HAp by hydrolysis	1.67	1.40	1.65	-	-	3.9%
3%ScHAp by hydrolysis	1.55	1.35	1.72	3%	0.01%	5.0%

As shown in **Table 6-22**, the doped concentrations of Sc^{3+} ions (0.03 and 0.01% by precipitation and hydrolysis methods) in the prepared samples were very low and far away from the expected one (3%), whereas the Ca:P mole ratio of the prepared 3% ScHAp samples was lower than the expected value of stoichiometric HAp (1.67) due to the presence of sodium ions in the samples which are substituting into the calcium ion sites in the HAp lattice as discussed previously (see chapter four for details). The measured **(**Ca+Na+Sc)/P mole ratios of the prepared 3%ScHAp samples by the precipitation and the novel hydrolysis methods were found to be higher than the stoichiometric value of HAp (1.67) due to the formation of carbonated HAp as confirmed by FTIR spectra.

6.4.2.2 FTIR of 3% ScHAp (3 wt.% Sc^{3+}) materials prepared by the novel hydrolysis and conventional precipitation methods.

FTIR of non-sintered 3% ScHAp (3 wt.% Sc^{3+}) materials prepared by the novel hydrolysis and conventional precipitation methods.

FTIR spectra of the non-sintered 3%ScHAp powders prepared by the precipitation and hydrolysis methods are shown in **Fig.6-19**

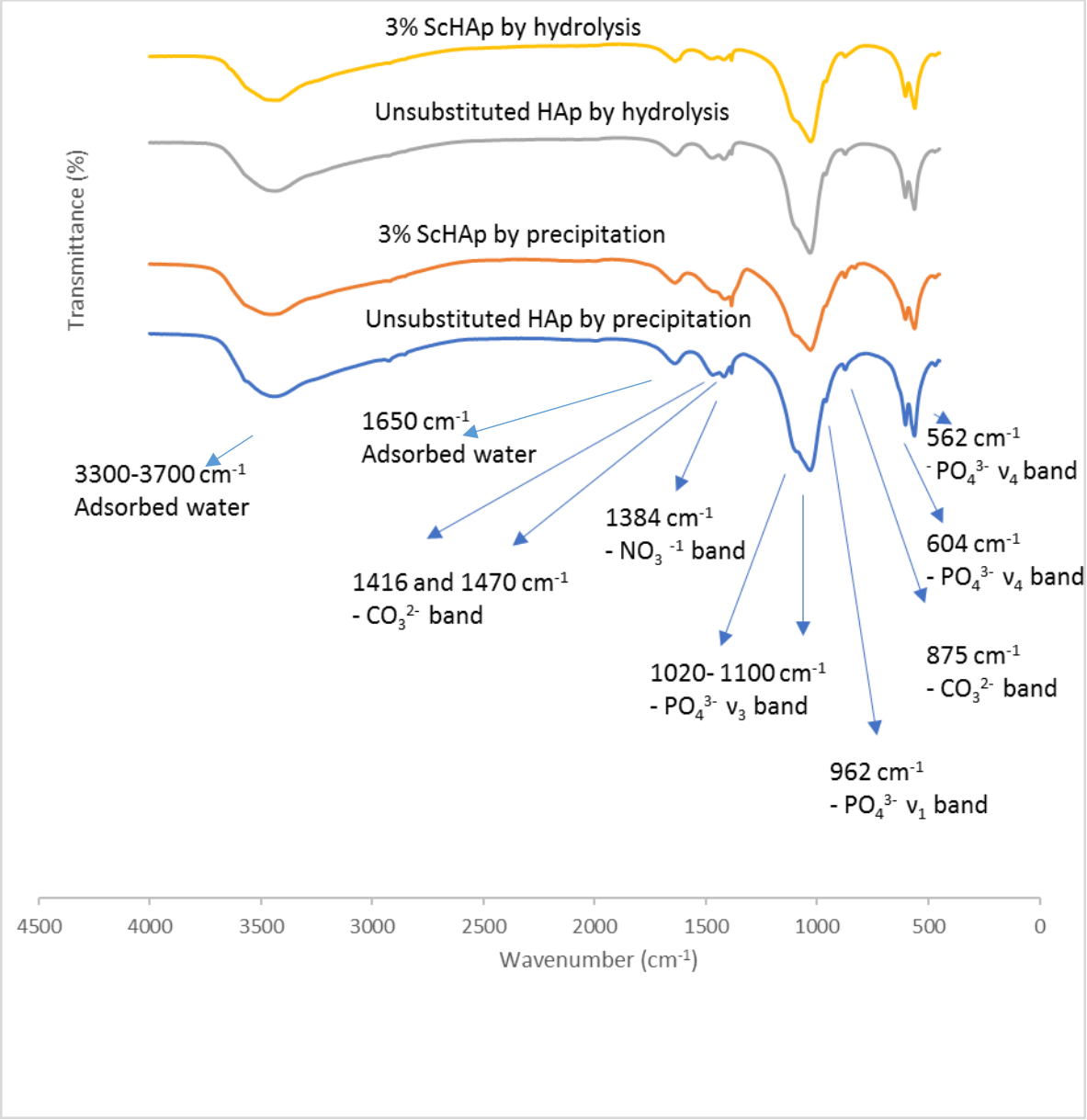

Figure 6-19: FTIR spectra of non-sintered 3% ScHAp (3 wt.% Sc^{3+}) materials prepared by precipitation and hydrolysis methods.

The spectra consist of the typical bands due to HAp. PO_4^{3-} bands were observed at 562, 603, 963, and 1032–1095 cm^{-1}. The FTIR spectra showed the presence of adsorbed water, through detecting the typical modes of water at 1640 and 3000–3700 cm^{-1}. The characteristic bands of carbonate were also detected at 875, 1415 and 1465 cm^{-1} as evidence of substitution of phosphate group by carbonate and also confirming the presence of B-type carbonated HAp. The typical band of the nitrate group at 1385 cm^{-1} was observed in the prepared samples from the precipitation route. This observation can be ascribed to the use of calcium nitrate as a precursor, but in the case of hydrolysis method that peak (at 1385 cm^{-1}), it is more possible that this impurity

may have existed in the KBr powder used to make the disks for IR analysis. However, a new, weak peak was observed to appear at 831 cm^{-1} in the Sc-substituted sample prepared by the precipitation method, while by hydrolysis route, the peak did not appear. In both spectra, the peak was interpreted to be due to the nitrate ion. In the solid phase prepared by precipitation, the co-appearance of the 831 cm^{-1} peak is merely because the level of nitrate contamination in this sample is higher than in the solid prepared by the hydrolysis method.

FTIR of ScHAp (3 wt.% Sc^{3+}) materials prepared by the hydrolysis and precipitation methods after sintering at 900 ˚C:

Figure 6-20 shows the FTIR spectra of the sintered 3% ScHAp (3 wt.% Sc^{3+}) materials prepared by the conventional precipitation and novel hydrolysis methods.

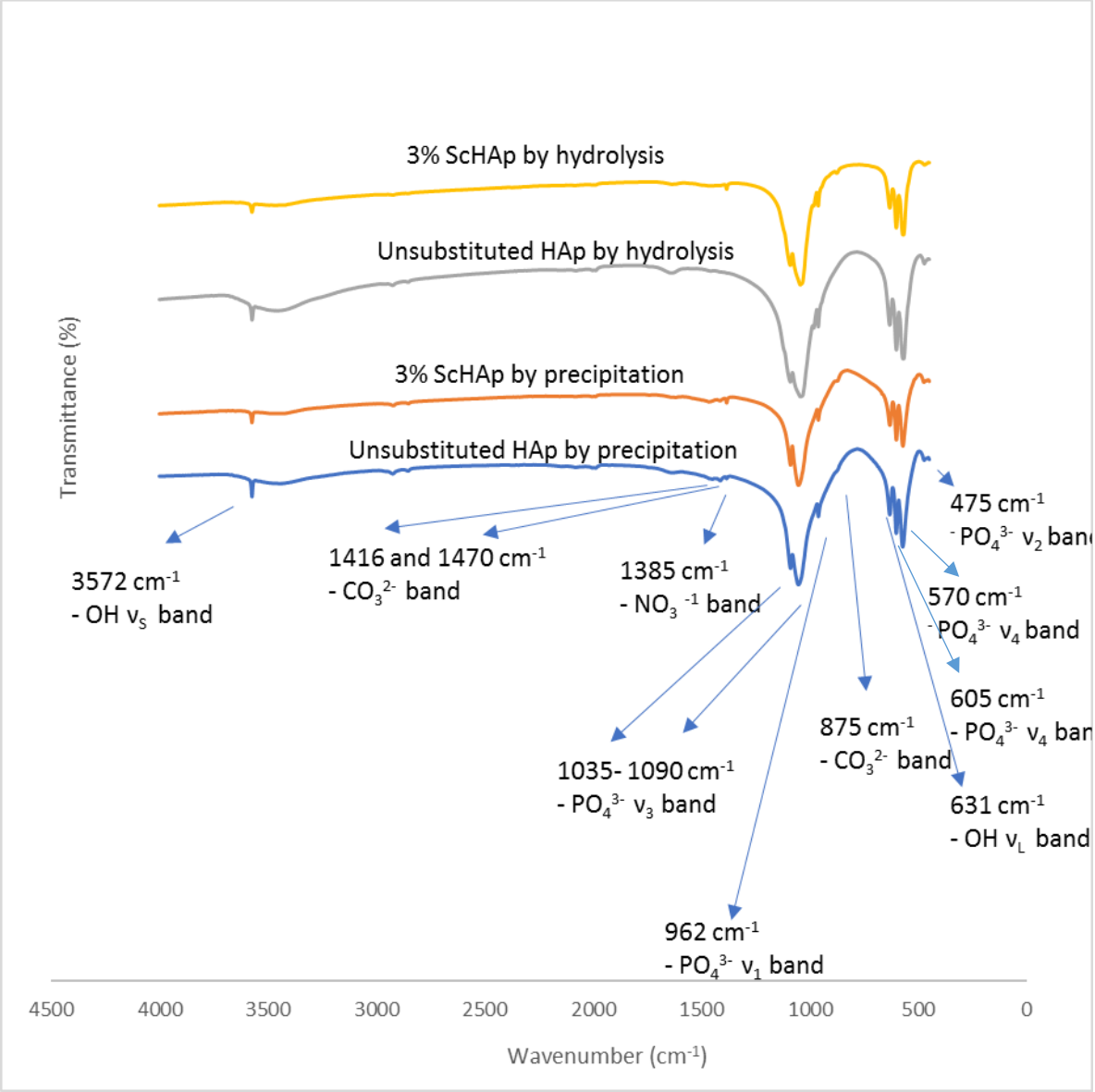

Figure 6-20: FTIR of 3% ScHAp (3 wt.% Sc^{3+}) materials prepared by precipitation and hydrolysis methods after sintering at 900 ˚C.

The corresponding FT-IR spectra **(Fig. 6-20)** of the prepared 3% ScHAp powders displayed the characteristic vibrational modes of the HAp phase. The typical peaks of phosphate group were observed at (472, 565, 603, 963, 1035 and 1092 cm^{-1}) by both routes, and weak peaks due to carbonate substitutions were detected at (875,1417 and 1456 cm^{-1}) in the case of the 3% ScHAp sample prepared by the precipitation method. Also, OH stretching and librational modes by both methods were observed at 3572 and 631 cm^{-1}.

Also, **Fig. 6-20** displayed in clearly a visible reduction in the intensity of the stretching mode of OH^- group at 3572 cm^{-1}.

This observation resulted from:

1- The partial substitution of hydroxyl group by chloride ions as a result of using $ScCl_3$ as a precursor to substitute Sc^{3+} ions into HAp crystals.
2- The presence of sodium ions as confirmed by ICP-MS analysis coupled with formation CO_3HAp powders as detected by FTIR spectra in the both ScHAp powders that were prepared by precipitation and hydrolysis methods. The OH^- ion content was derived by the requirement to keep charge balance and to restore the neutrality of HAp crystals (see the FTIR of sintered RbHAp materials for more details).
3- The ICP-MS results showed that the measured wt.% of Sc^{3+} ions that was associated with the HAp was very low by both routes (the precipitation and the novel hydrolysis routes). This could mean that scandium ion may not have substituted in the lattice given the amount of Sc associated with the HAp sample is low.

6.4.2.3 XRD diffraction patterns of non-sintered and sintered 3% ScHAp (3 wt.% Sc^{3+}) materials prepared by hydrolysis and precipitation methods:

Phase identification of 3% ScHAp (3 wt.% Sc^{3+}) materials:

The XRD patterns of non-sintered and sintered 3% ScHAp materials prepared by precipitation and hydrolysis methods are displayed in **Fig.6-21 and Fig.6-22**, respectively**.**

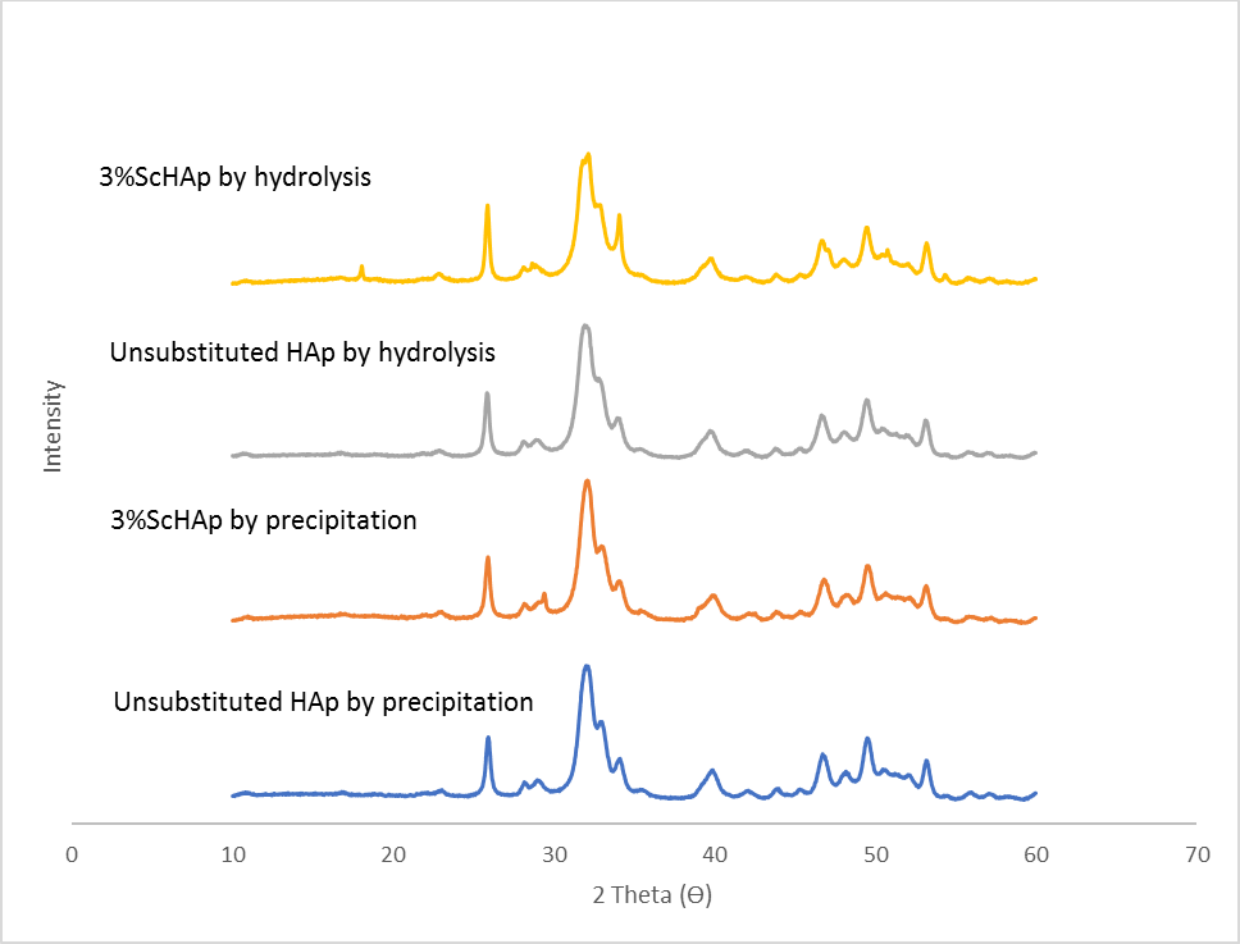

Figure 6-21: The XRD diffraction patterns of non-sintered 3% ScHAp (3 wt.% Sc^{3+}) materials prepared by the conventional precipitation and novel hydrolysis methods.

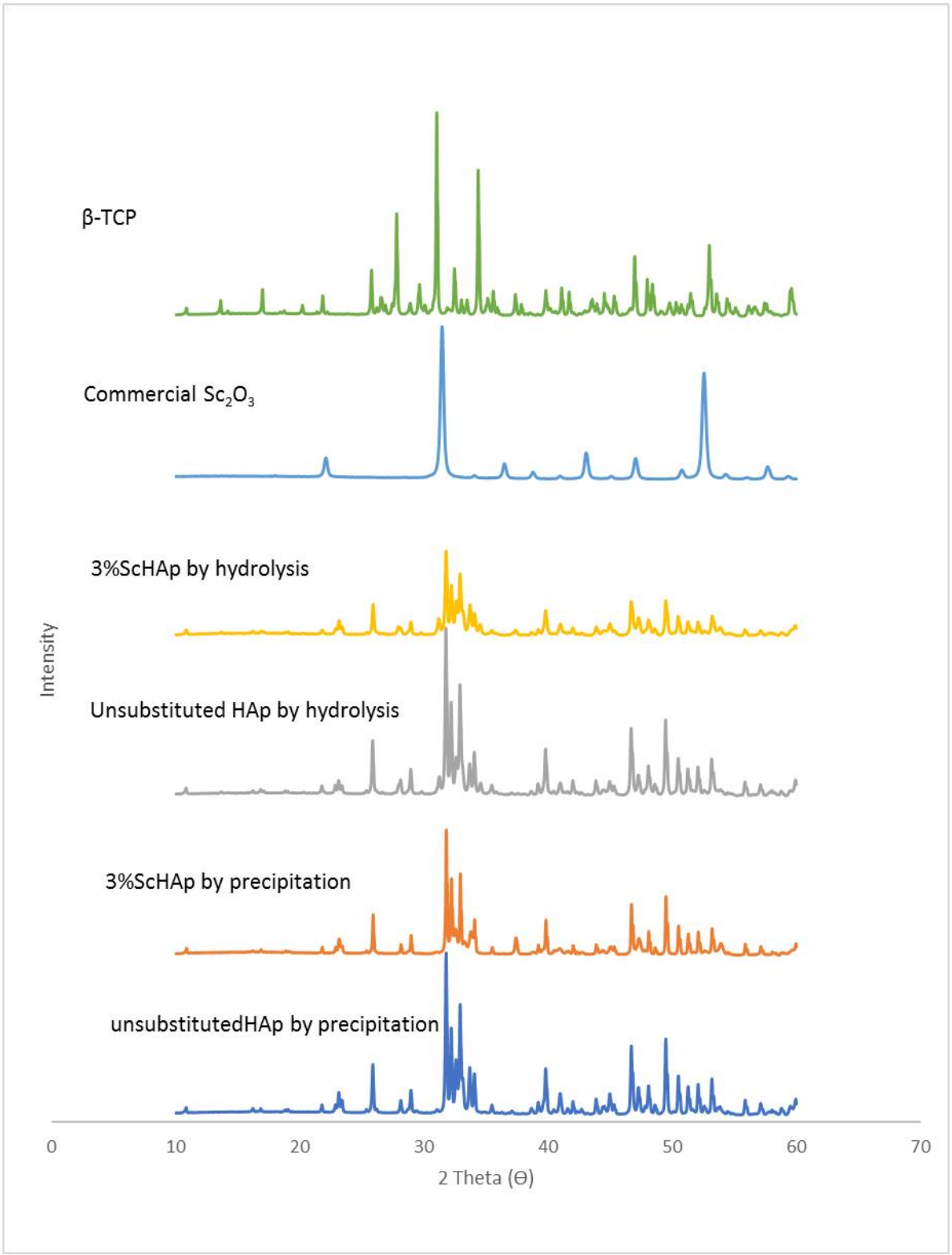

Figure 6-22: The XRD diffraction patterns of 3% ScHAp (3 wt.% Sc^{3+}) materials prepared by precipitation and hydrolysis methods after sintering at 900 ˚C.

Fig. 6-22, displays that the increasing levels of substitution process of Sc^{3+}ions caused a visible effect on the diffraction patterns of hydroxyapatite by both routes. A new peak appeared by precipitation method at 2Θ = 37.5˚ (This peak is related to CaO, reference card number 04-017-9575) associated with a decrease in the intensity of one typical peak that is related to impurity phase (β-TCP) at 2 Θ= 33.60˚. On the other hand, the diffraction patterns of impurity phase by hydrolysis method of 3%ScHAp powders had not shown any significant difference compared to HAp materials but an obvious reduction in the intensities of the whole peaks that were related to HAp structure were observed.

Crystallinity and crystallite size of sintered 3% ScHAp (3 wt.% Sc^{3+}) materials:

Table 6-23 displays the degree of crystallinity and the crystallite size of sintered 3% ScHAp (3 wt.% Sc^{3+}) materials prepared by precipitation and hydrolysis methods.

Table 6-23: The degree of crystallinity and the crystallite size of 3% ScHAp (3 wt.% Sc^{3+}) materials prepared by precipitation and hydrolysis methods after sintering at 900 ˚C.

Sample	D_{002} (Å)	Crystallinity %
Unsubstituted HAp by precipitation	618.3±3.2	84.15±2.4
3%ScHAp by precipitation	790.0±6.1	77.28±4.2
Unsubstituted HAp by hydrolysis	549.8±3.6	82.57±2.1
3%ScHAp by hydrolysis	444.4±4.5	70.32±3.8

Due to increasing the concentration of Sc^{3+} ions, a visible reduction in the intensities of the diffraction patterns were recorded by the hydrolysis route, associated with peaks broadening as an indication of decrease the degree of crystallinity. This observation was also confirmed by the numerical value of crystallinity as shown in (**Table 6-23**), that a clear reduction the value of crystallinity by both routes had been achieved due to increase in the amounts of Sc^{3+} ions. As confirmed by the ICP-MS analysis, the wt.% of Sc^{3+} ion that was associated with the HAp by both methods was very low, so the reduction in the crystallinity can be more likely be attributed to the presence of other ions such as Na^{+}, Cl^{-} and carbonate group (CO_3^{2-}). It was noted that an increase in the value of crystallite size of the prepared ScHAp samples by the precipitation route,

was observed but in the case of the hydrolysis method, a reduction in the value of crystallite size was shown.

As shown in **Table 6-23**, the numerical values of crystallinity and crystallite size were varied due to the substitution of Sc^{3+} ions into HAp samples. The effect of replacement process on the crystallinity and the crystallite size can be ascribed to the effect of the preparation method, the chemical composition and the phase purity as confirmed by ICP-MS, XRD and FTIR analysis.

Lattice parameter and volume of unit cell of sintered 3% ScHAp (3 wt.% Sc^{3+}) materials:

Table 6-24 shows the lattice parameters and the volume of hexagonal unit cell of 3%ScHAp (3 wt. % Sc^{3+}) materials prepared by precipitation and hydrolysis methods after sintering at 900 ˚C.

Table 6-24: The lattice parameters and the volume of hexagonal unit cell of 3%ScHAp (3 wt. % Sc^{3+}) materials prepared by precipitation and hydrolysis methods after sintering at 900 ˚C.

Sample name	a [Å]	c [Å]	V[Å^3]
Unsubstituted HAp by precipitation	9.416±0.004	6.879±0.003	1579±0.004
3% ScHAp by precipitation	9.424±0.003	6.884±0.003	1582±0.003
Unsubstituted HAp by hydrolysis	9.421±0.003	6.882±0.005	1581±0.004
3% ScHAp by hydrolysis	9.428±0.002	6.881±0.001	1583±0.002

An increase in both lattice parameters (a and c) were seen in samples prepared by the both routes (precipitation and hydrolysis). This result could not be ascribed to the substitution of Sc^{3+} ions into HAp materials with smaller ionic radius (87.1 pm) compared to Ca^{2+} ions (100 pm), because the ICP-MS results showed that the measured wt.% of Sc^{3+} ions that associated with the HAp was very low by the both preparation methods. The expansion that had taken place in the lattice constants as confirmed by the XRD analysis can be attributed to the effect of chloride ions (introduced into HAp crystal through using $ScCl_3$ as a starting material). These ions have a larger ionic radius (1.81 Å) [123] compared to the hydroxyl group(1.68 Å), since $ScCl_3$ was used as a precursor of Sc^{3+} ions during the preparation process

6.4.2.4 SEM of 3% ScHAp (3 wt.% Sc^{3+}) materials prepared by hydrolysis and precipitation methods:

SEM of non-sintered 3% ScHAp (3 wt.% Sc^{3+}) materials prepared by hydrolysis and precipitation methods:

Fig.6-23. displays SEM images of the non-sintered 3%ScHAp powders prepared by hydrolysis and precipitation methods.

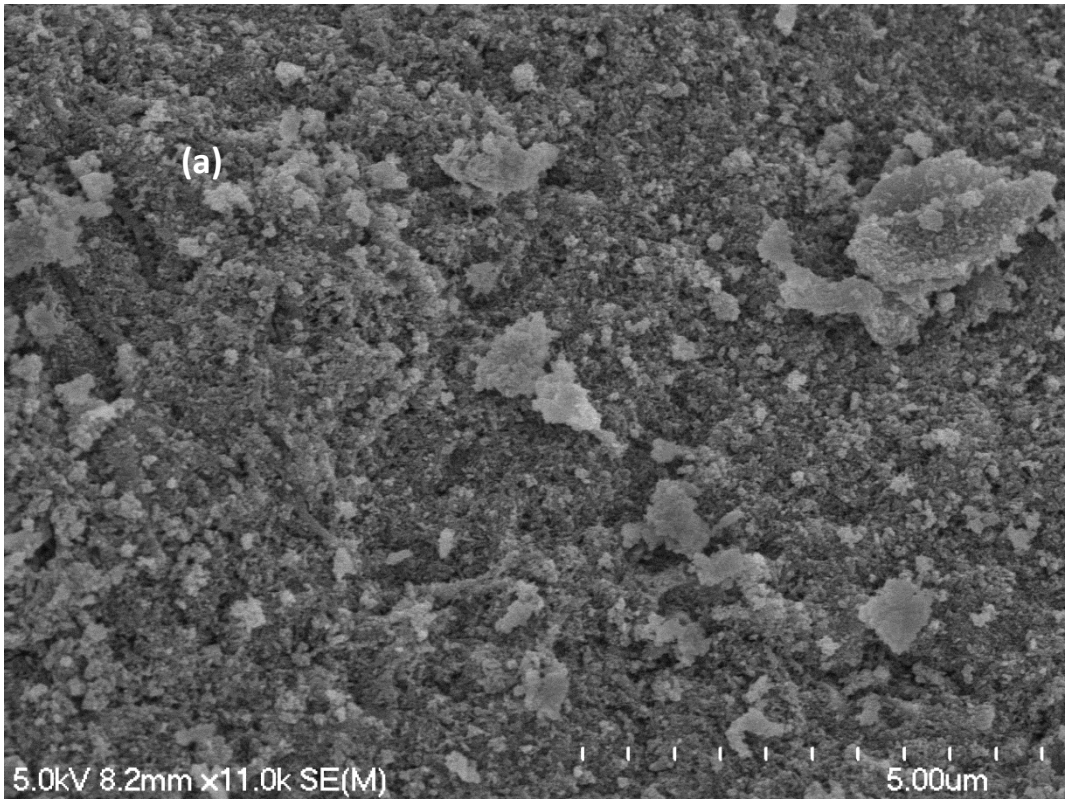

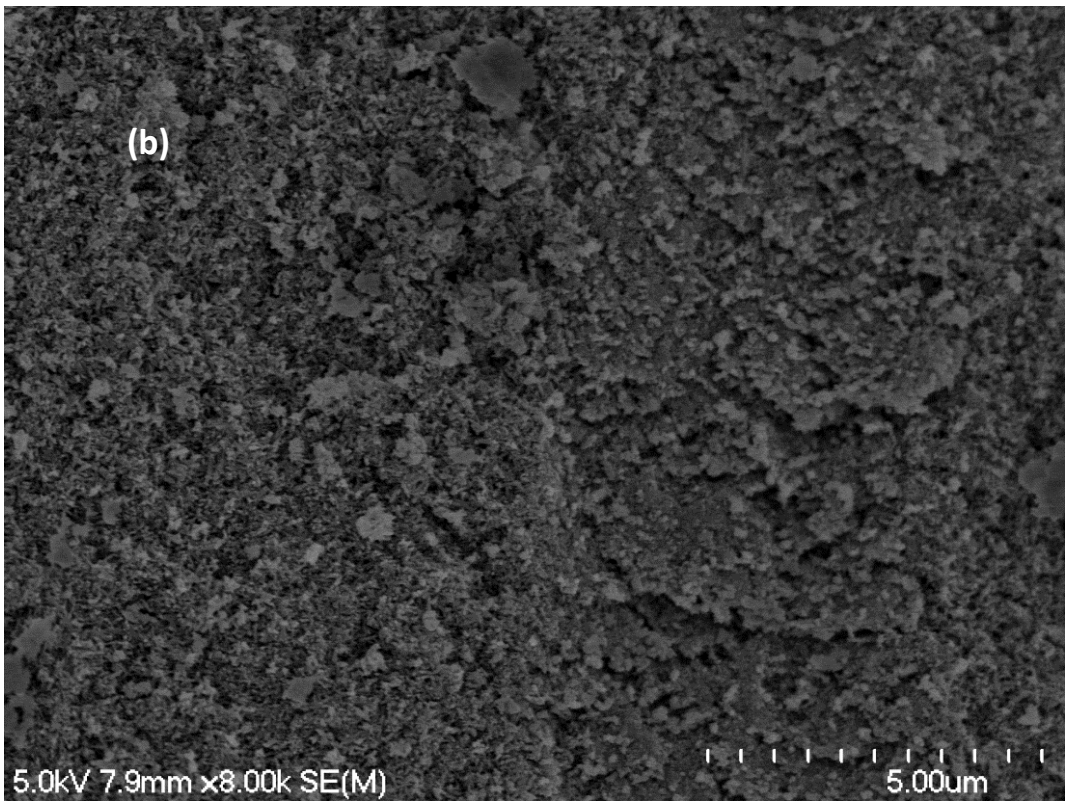
(b)
5.0kV 7.9mm x8.00k SE(M)
5.00um

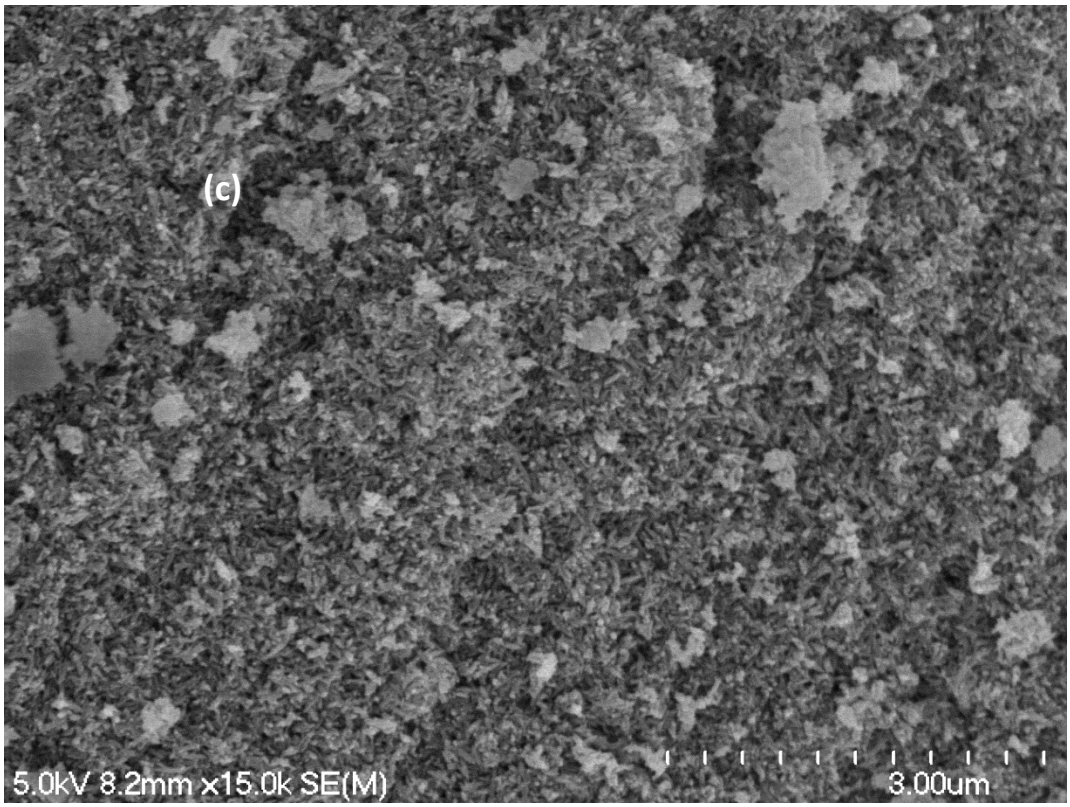
(c)
5.0kV 8.2mm x15.0k SE(M)
3.00um

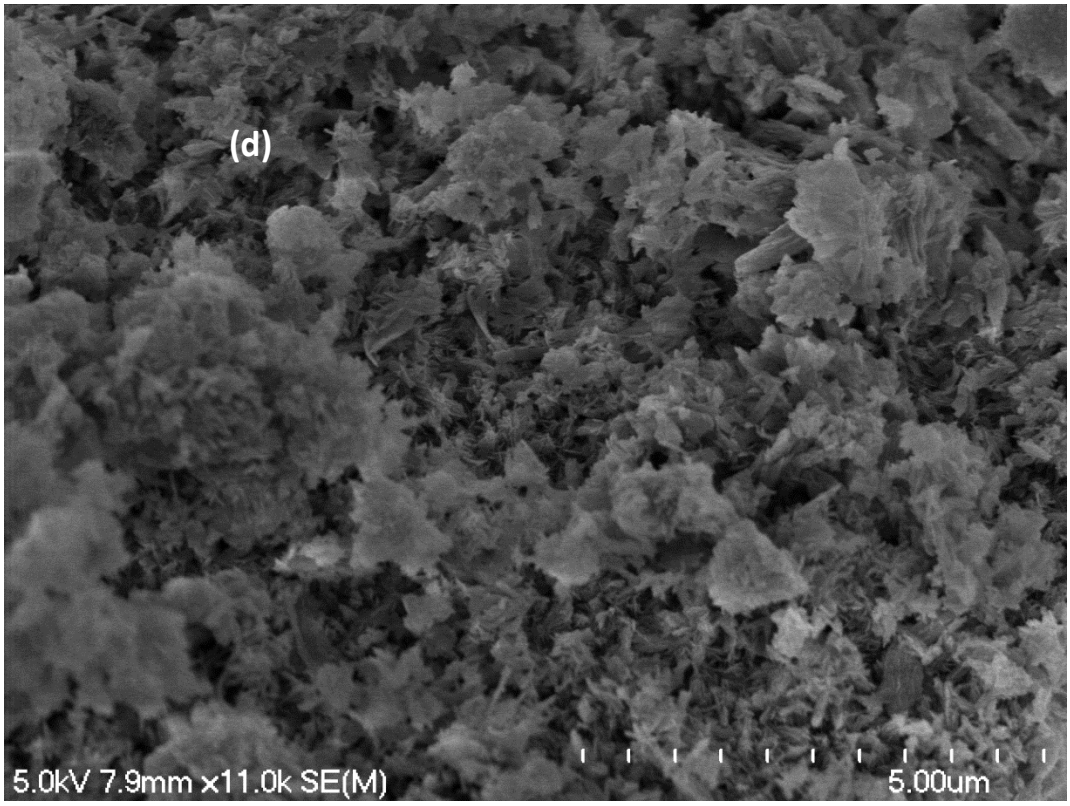

Figure 6-23: SEM of images (a) unsubstituted HAp by precipitation (b) unsubstituted HAp by hydrolysis (c) 3 % ScHAp by precipitation (d) 3% ScHAp by hydrolysis.

The morphology of the prepared samples by precipitation did not appear to vary due to the addition of Sc^{3+} ions into HAp samples and this was explained by the lower levels of Sc^{3+} detected as confirmed by ICP-MS results. Spheroidal like shapes associated with a trend to agglomerate were produced by the precipitation route. On the other hand, flake like shapes resulted in samples prepared by the hydrolysis method so confirming the effect of that synthesis route on the morphology.

SEM of 3% ScHAp (3 wt.% Sc^{3+}) materials prepared by hydrolysis and precipitation methods and sintered after sintering at 900 ˚C:

Fig.6-24. shows the morphology of sintered 3% ScHAp powders prepared by precipitation and hydrolysis methods.

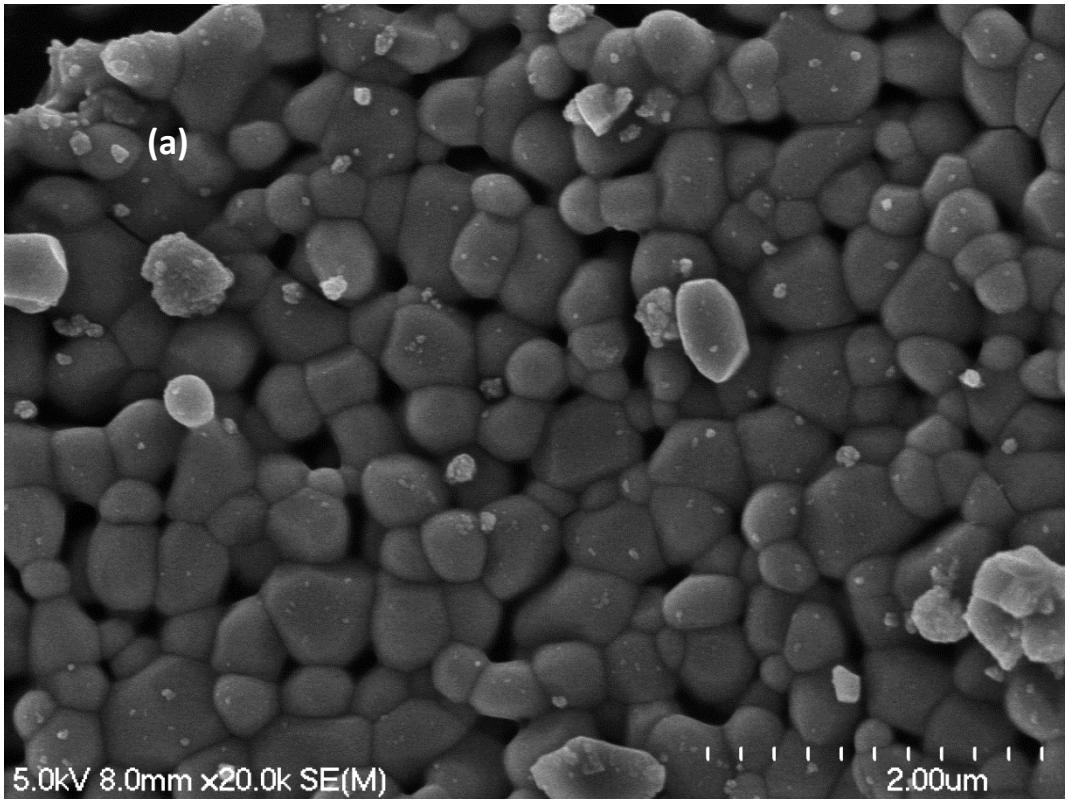
(a)
5.0kV 8.0mm x20.0k SE(M)
2.00um

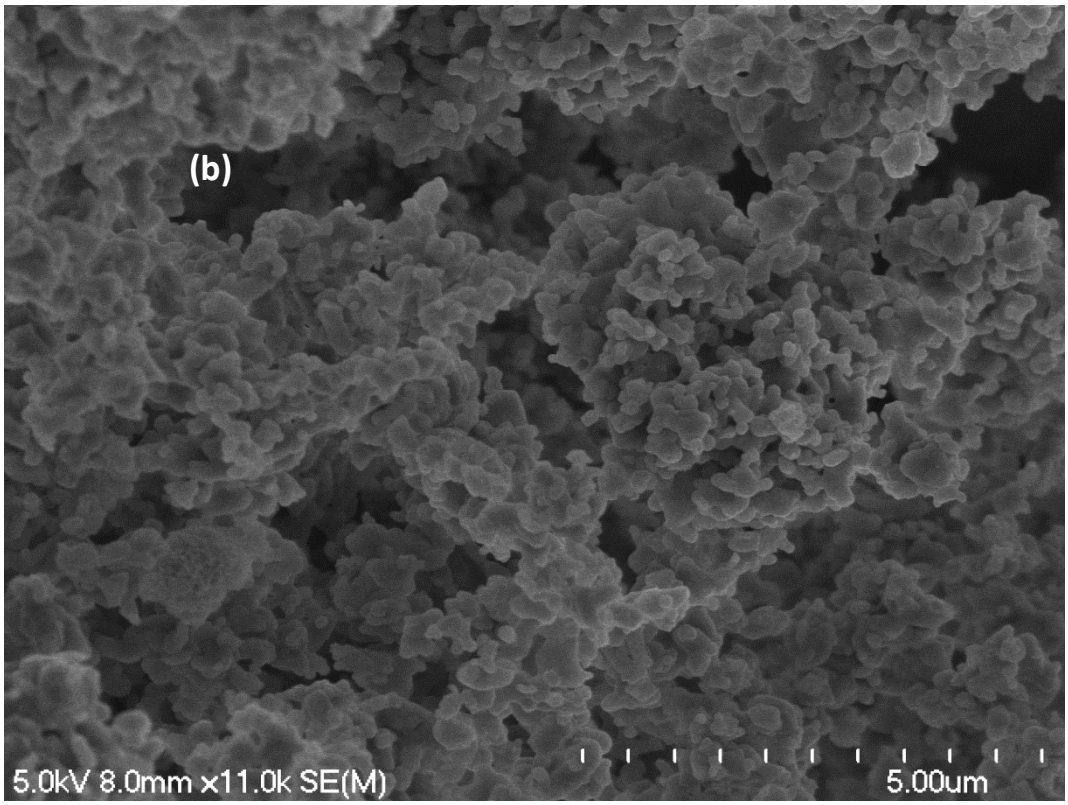
(b)
5.0kV 8.0mm x11.0k SE(M)
5.00um

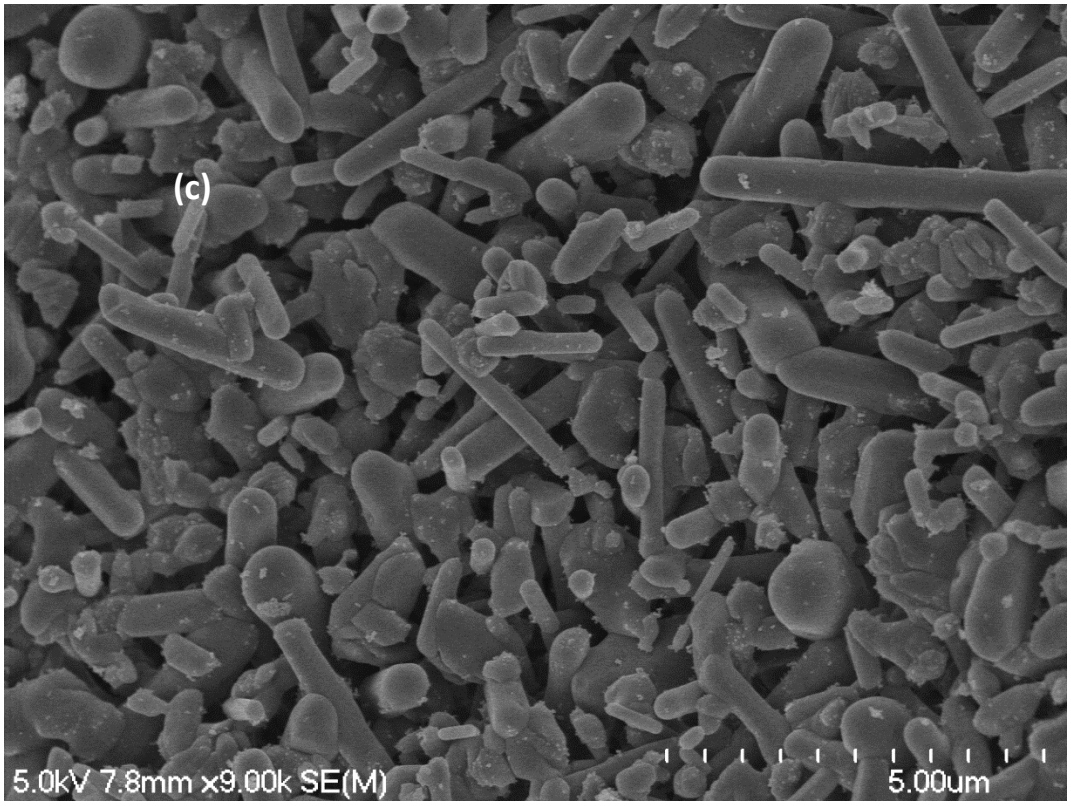
(c)
5.0kV 7.8mm x9.00k SE(M)
5.00um

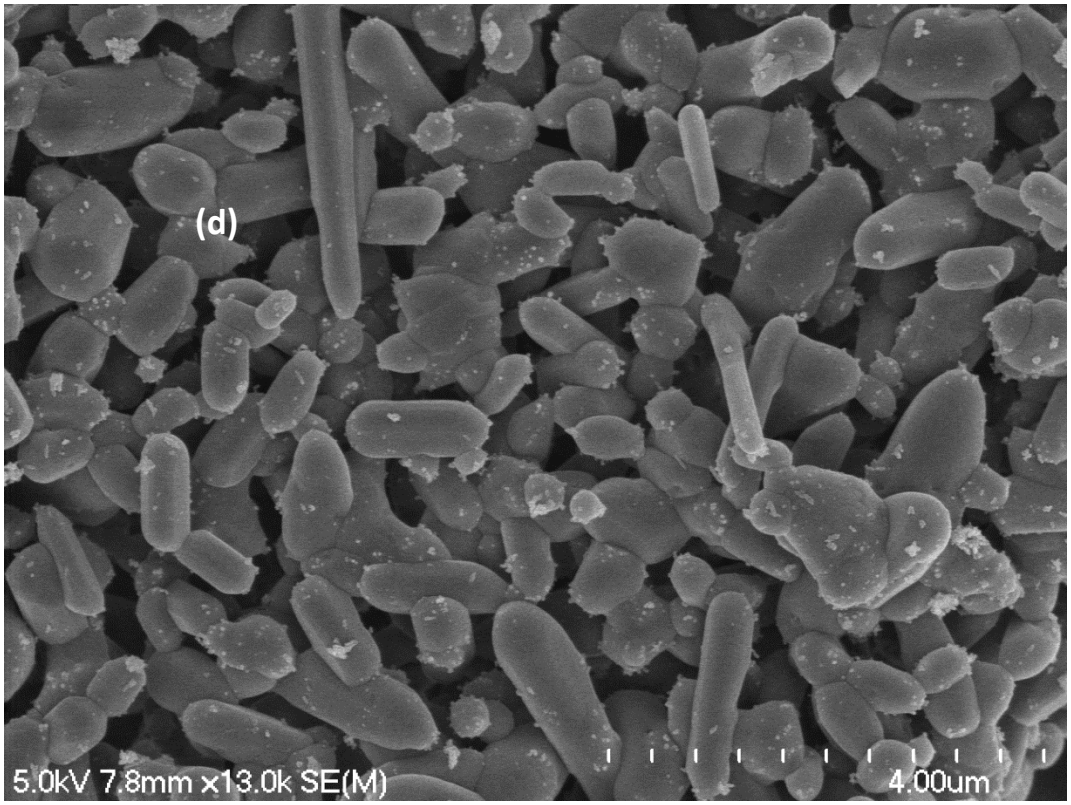
(d)
5.0kV 7.8mm x13.0k SE(M)
4.00um

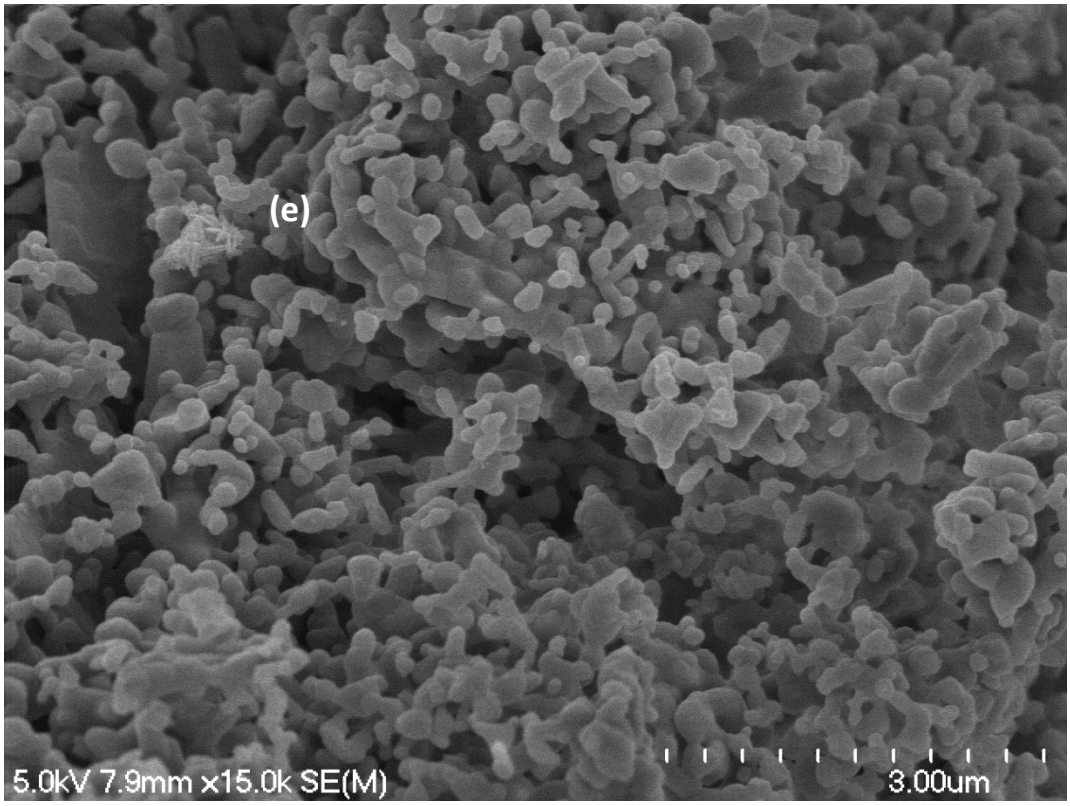

Figure 6-24: SEM images of (a) unsubstituted HAp by precipitation (b) unsubstituted HAp by hydrolysis (c+d) 3 % ScHAp by precipitation (e) 3% ScHAp by hydrolysis, after sintering at 900 ˚C.

Fig.6-24. showed that the morphology of 3% ScHAp powders depends on the synthesis route. While a well-defined morphology due to heat treatment of 3% ScHAp materials at 900 ˚C by precipitation had been produced, the SEM images showed that the prepared 3% ScHAp sample consists of particles with a rod like shape. On the other hand, the synthesis process of 3% ScHAp by the hydrolysis method produced particles with a spherical shape and with an irregular distribution. The high ability to agglomerate and to obtain porous material by the novel hydrolysis method was also confirmed by SEM images.

As discussed in the literature ([236] , [237], [238]), the morphology of the HAp depends on several variables used in the synthesis conditions such as temperature and the concentrations of calcium and phosphate ions. As an example Nathanael et al. [239] prepared hydroxyapatite (HAp) substituted with different levels of fluorine ions (P/F = 0, 6, 4 and 2) by the hydrothermal method, and labelled as FHAp1 (P/F ratio = 6), FHAp2 (P/F ratio = 4) and FHAp3 (P/F ratio = 2). FESEM displayed that some elongated crystals along with mostly spherical ones were visible for HAp,

but the effect of fluoride ions substitution was clearly visible in that the morphology of the rod-shaped crystals increased with increasing levels of fluoride ions.

6.4.3 5% ScHAp powders prepared by hydrolysis and precipitation methods:

One series of 5% ScHAp (5 wt.% Sc^{3+}) powders were prepared by two different synthesis methods (precipitation and hydrolysis), and the detailed amounts of the reagents are listed in Table **6-15**.

6.4.3.1 Characterization techniques of prepared 5% ScHAp (5 wt.% Sc^{3+}) materials by hydrolysis and precipitation methods.

6.4.3.2 ICP-MS of prepared 5% ScHAp (5 wt.% Sc^{3+}) materials prepared by hydrolysis and precipitation methods after sintering at 900 ˚C.

The results of the elemental analyses of sintered 5%ScHAp samples that were prepared by precipitation and hydrolysis routes are displayed in **Table 6-25.**

Table 6-25: ICP-MS results of 5% ScHAp (5 wt.% Sc^{3+}) materials prepared by precipitation and hydrolysis methods after sintering at 900 ˚C. The concentration was in ppb unit (ug/L):

Sample	Ca 44	P 31	Na 23	Sc 45
Unsubstituted HAp by precipitation	707795	401240	103797	-
5% ScHAp by precipitation	589319	315216	105800	1992.9
Unsubstituted HAp by hydrolysis	769928	423970	78396	-
5% ScHAp by hydrolysis	652509	366970	63700	357.7

The starting (calculated) and actual (measured) degree of chemical composition of the prepared powders in terms of wt.% of Sc^{3+}ions, the calcium/phosphorus (Ca/P) molar ratios as well as (Ca+Na+Sc)/P molar ratio were determined by ICP-MS and presented in **Table 6-26.**

Table 6-26: The chemical analysis data of sintered 5% ScHAp (5 wt.% Sc^{3+}) materials by ICP-MS measurements after sintering at 900 ˚C.

Sample	Ca/P Theoretical	Ca/P Measured	(Ca+Na+Sc)/P	Wt.% Sc^{3+} ions theoretical	Wt.% Sc^{3+} ions measured	Wt.% Na^{+} ions measured
Unsubstituted HAp by precipitation	1.67	1.36	1.71	-	-	5.2%
5% ScHAp by precipitation	1.47	1.45	1.90	5%	0.10%	5.3%
Unsubstituted HAp by hydrolysis	1.67	1.40	1.65	-	-	3.9%
5%ScHAp by hydrolysis	1.47	1.35	1.61	5%	0.02%	3.2%

As shown in **Table 6-26** the doped concentration of Sc^{3+} ions (0.1 and 0.02% by the precipitation and the novel hydrolysis methods) in the prepared samples were very low compared to the expected one (5.00%) this can be attributed to the low concentration of Sc_2O_3 material that was used as a source of scandium ions (0.2 g of Sc_2O_3 were dissolved in 30 ml of 6M HCl). The Ca:P mole ratio of the prepared 5%ScHAp samples was also found to be lower than the expected value of stochiometric HAp (1.67 due to the presence of sodium ions in the samples which are substituting into the calcium ion sites in the HAp lattice as discussed previously (see Chapter four for details), whereas the measured **(**Ca+Na+Sc)/P mole ratios of the prepared 5%ScHAp samples by precipitation method were found to be higher than the stochiometric value of HAp (1.67). This observation can be ascribed to the formation of carbonated HAp as confirmed by FTIR spectra.

6.4.3.3 FTIR of 5% ScHAp (5 wt.% Sc^{3+}) materials prepared by precipitation and hydrolysis methods.

FTIR of non-sintered of 5% ScHAp (5 wt.% Sc^{3+}) materials prepared by hydrolysis and precipitation methods.

The FTIR spectra of non-sintered 5% ScHAp powders prepared by precipitation and hydrolysis methods are shown in **Fig. 6-25.**

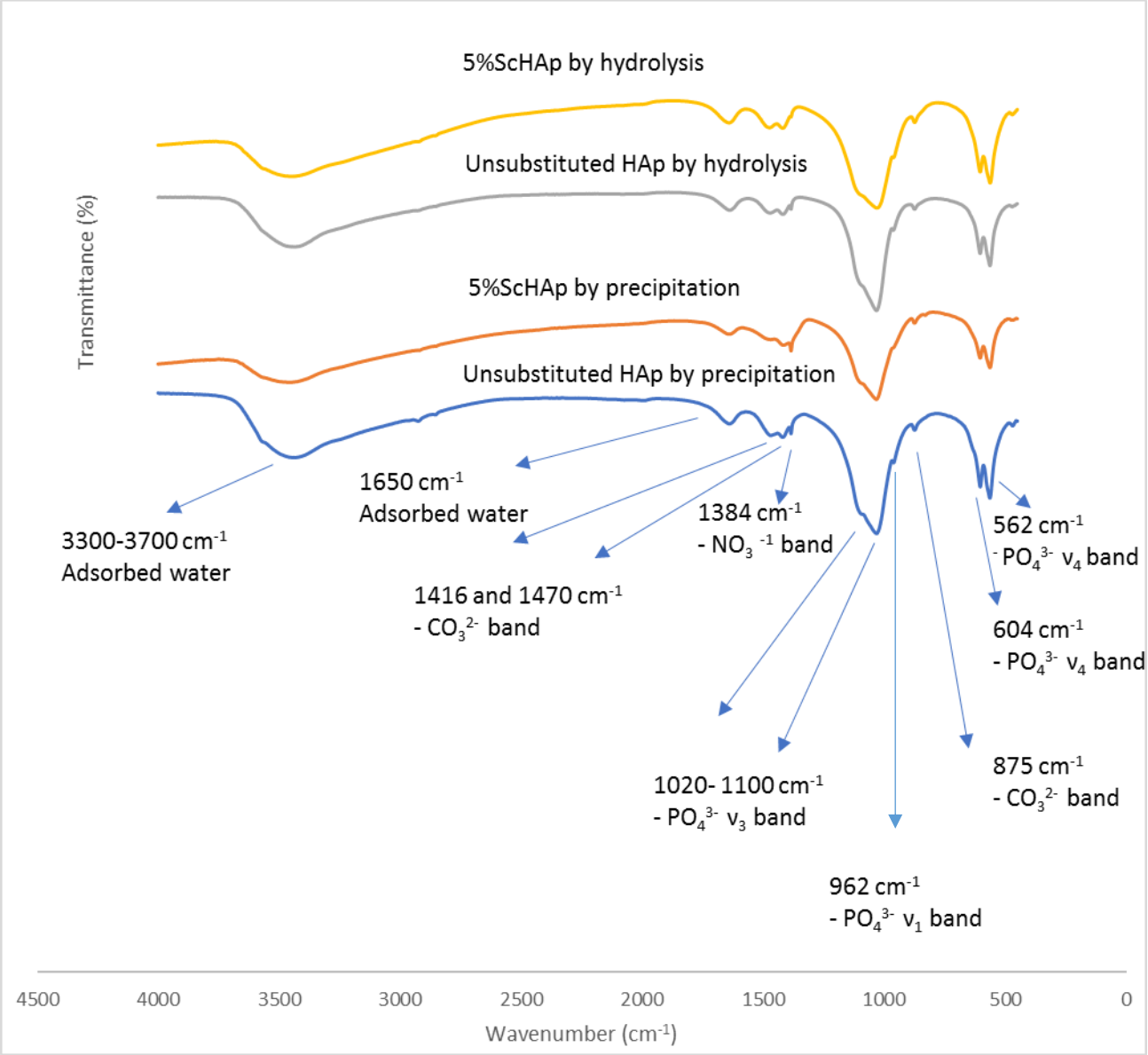

Figure 6-25: FTIR spectra of sintered 5% ScHAp (5 wt.% Sc^{3+}) materials prepared by precipitation and hydrolysis methods.

The FTIR spectra of 5%ScHAp powders at room temperature are shown in **Fig. 6-25**. The characteristic peaks of phosphate group were displayed at (562, 603, 962, 1028 and 1093 cm^{-1}). The absence of the stretching and librational modes of hydroxyl groups at (630 and 3572 cm^{-1}) as evidence of nanocrystalline materials had been confirmed by the FTIR spectra. The presence of adsorbed water was recorded by detecting the characteristic peaks of water at (1630 and 3000-3700 cm^{-1}). The characteristic bands of carbonate were also detected at 875, 1415 and

1465 cm^{-1} as evidence of substitution of phosphate group by carbonate and confirming the presence of the B-type of carbonated HAp.

FTIR of 5% ScHAp (5 wt.% Sc^{3+}) materials prepared by hydrolysis and precipitation methods after sintering at 900 ˚C:

Fig. 6-26 shows the FTIR spectra of sintered 5%ScHAp materials prepared by precipitation and hydrolysis methods.

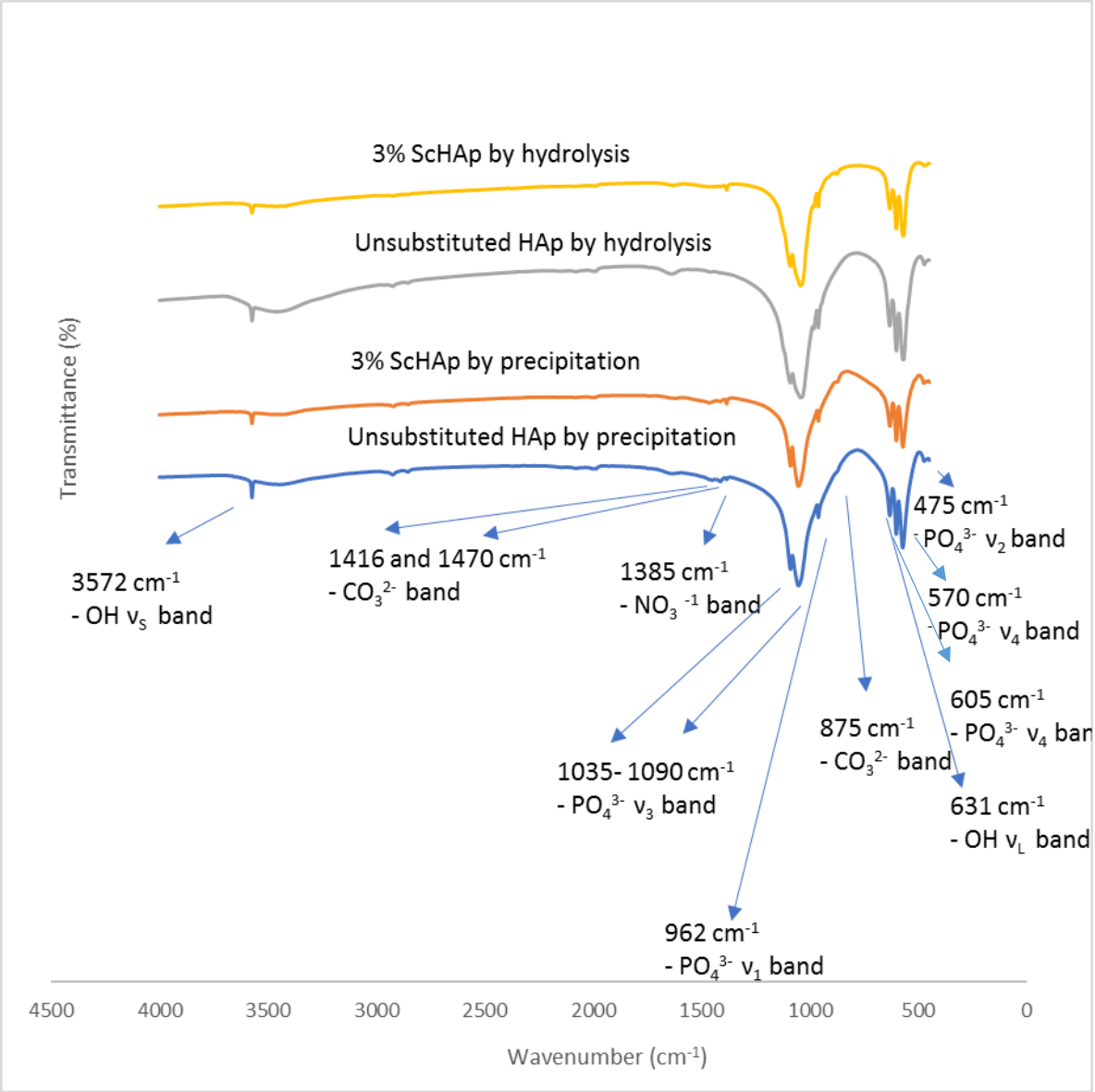

Figure 6-26: FTIR of 5% ScHAp (5 wt.% Sc^{3+}) materials prepared by precipitation and hydrolysis methods after sintering at 900 ˚C.

The presence of the apatitic phase was confirmed by FTIR through detecting the fundamental modes of phosphate bands at (562, 603, 962, 1035 and 1095 cm^{-1}) as well as the typical modes of hydroxyl groups at (631 and 3572 cm^{-1}).

Also, **Fig. 6-26** revealed an obvious reduction in the intensity of the stretching mode of OH- group at 3572 cm^{-1} due to substitution process by precipitation and hydrolysis routes. This observation as discussed previously, resulted from:

1- The partial substitution of hydroxyl group by chloride ions as a result of using $ScCl_3$ as a precursor to substitute Sc^{3+} ions into HAp crystals.
2- The presence of sodium ions as confirmed by ICP-MS analysis coupled with formation CO_3HAp powders as detected by FTIR spectra in the whole prepared 5% ScHAp powders. As a result, the OH^- ion content was derived by the requirement to keep charge balance and to restore the neutrality of HAp crystals (see FTIR of RbHAp for details).
3- Although, the results of ICP-MS analysis showed that the measured wt.% of Sc^{3+} ions that associated with the HAp was very low by both routes (the precipitation and the novel hydrolysis). The reduction in the intensity of the stretching mode of OH^- group at 3572 cm^{-1} that was obtained by both preparation methods, was thought to be due to the substitution process of a trivalent cation into HAp samples as explained by Serret et al. [232] (see the FTIR of EuHAp materials)

6.4.3.4 XRD diffraction patterns of 5% ScHAp (5 wt.% Sc^{3+}) materials prepared by hydrolysis and precipitation methods:

Phase Identification of 5% ScHAp (5% wt. $Sc3^{+}$) materials:

The XRD patterns of non-sintered and sintered 5% ScHAp (5 wt.% Sc^{3+}) materials prepared by precipitation and hydrolysis routes are displayed in **Fig.6-27 and Fig.6-28**, respectively.

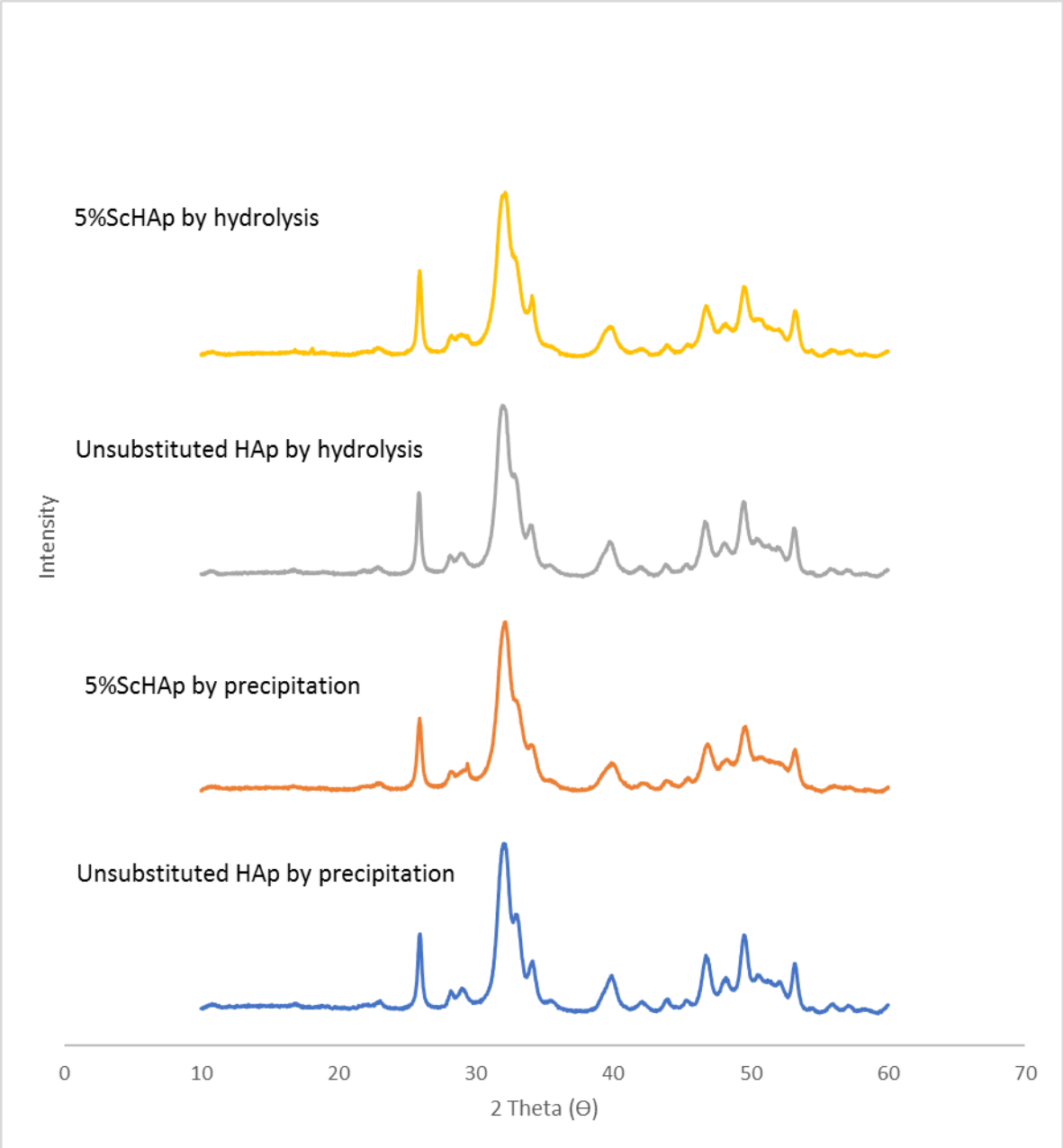

Figure 6-27: The XRD diffraction patterns of non-sintered 5% ScHAp (5 wt.% Sc^{3+}) materials as prepared by the conventional precipitation and novel hydrolysis methods.

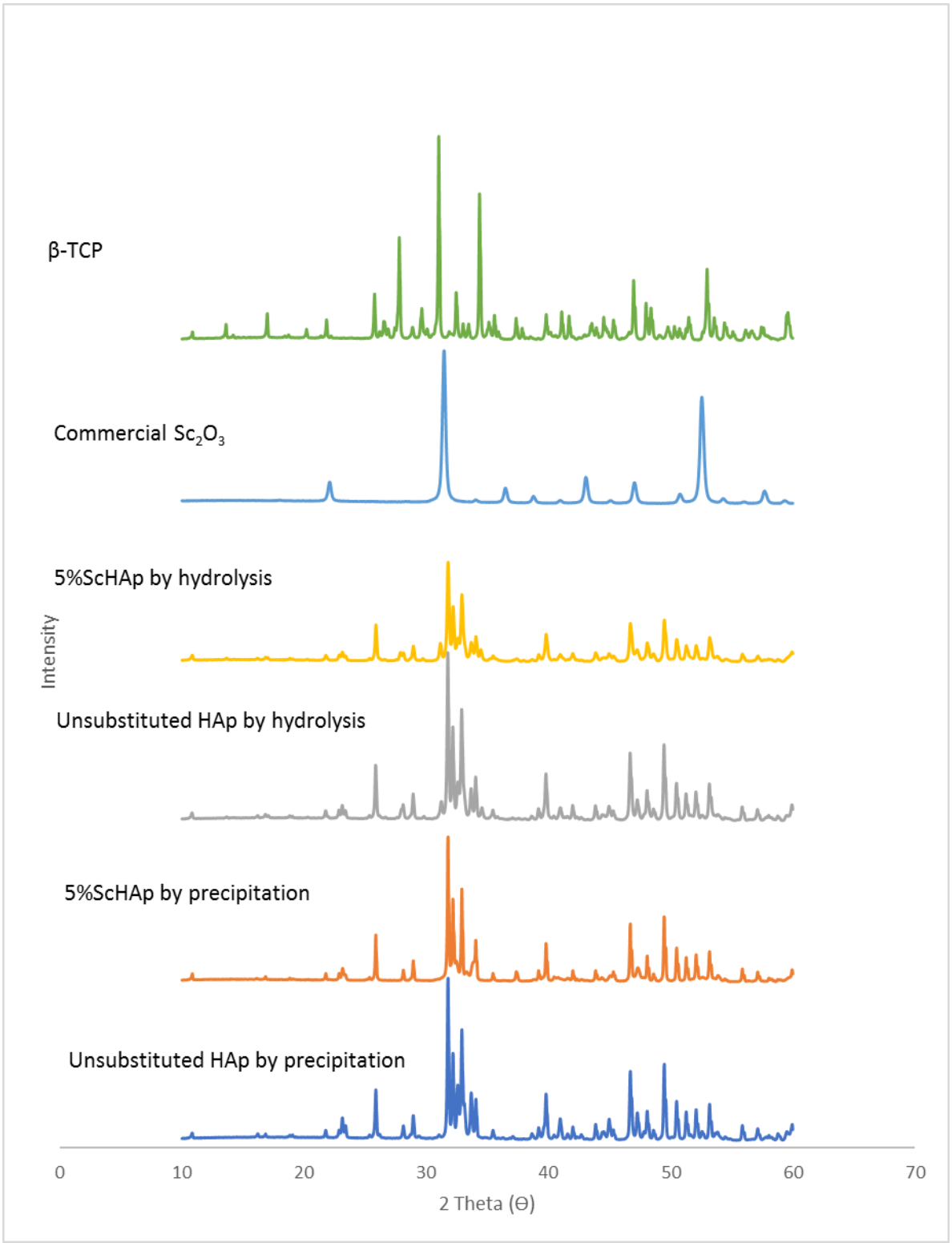

Figure 6-28: The XRD diffraction patterns of 5% ScHAp (5 wt.% Sc^{3+}) materials prepared by precipitation and hydrolysis methods after sintering at 900 ˚C.

Fig. 6-28, showed that the XRD diffraction patterns of the prepared 5% ScHAp powders by both methods were very similar to that of 3%ScHAp materials, but an enhancement in the intensities of the typical peaks that were related to HAp powders were detected by XRD analysis especially in the case of hydrolysis method.

Crystallinity and crystallite size of sintered 5% ScHAp (5 wt.% Sc^{3+}) materials:

Table 6-27 shows the degree of crystallinity and the crystallite size of sintered 5% ScHAp (5 wt.% Sc^{3+}) materials prepared by the conventional precipitation and novel hydrolysis methods.

Table 6-27: The degree of crystallinity and the crystallite size of 5% ScHAp (5 wt.% Sc^{3+}) materials prepared by precipitation and hydrolysis methods after sintering at 900 ˚C.

Sample	D_{002} (Å)	Crystallinity %
Unsubstituted HAp by precipitation	618.3±3.2	84.15±2.4
5% ScHAp by precipitation	711.0±6.6	79.43±4.6
Unsubstituted HAp by hydrolysis	549.8±3.6	82.57±2.1
5% ScHAp by hydrolysis	444.4±3.2	73.83±3.8

As shown in **Table 6-27**, a clear reduction in the degree of crystallinity of the 5% ScHAp powders was achieved due to the substitution process of scandium ions by both routes.

The results of crystallite size of the prepared 5%ScHAp samples displayed an increase by precipitation route, while a reduction was detected in samples prepared using the novel hydrolysis method. The variation in the values of crystallinity and crystallite size of the prepared 5% ScHAp samples, which were prepared by the conventional and the novel hydrolysis methods can be attributed to the effect of the preparation method and the chemical composition.

Lattice parameter and volume of unit cell of sintered 5% ScHAp (5 wt.% Sc^{3+}) materials:

Table 6-28 shows the lattice parameters and the volume of hexagonal unit cell of 5% ScHAp (5 wt. % Sc^{3+}) materials prepared by the precipitation and hydrolysis methods after sintering at 900 ˚C

Table 6-28: The lattice parameters and the volume of hexagonal unit cell of 5% ScHAp (5 wt.% Sc^{3+}) materials prepared by precipitation and hydrolysis methods after sintering at 900 ˚C.

Sample	a [Å]	c [Å]	V[Å³]
Unsubstituted HAp by precipitation	9.416±0.004	6.879±0.003	1579±0.004
5% ScHAp by precipitation	9.420±0.003	6.883±0.002	1581±0.003
Unsubstituted HAp by hydrolysis	9.421±0.003	6.882±0.005	1581±0.004
5% ScHAp by hydrolysis	9.421±0.002	6.882±0.002	1581±0.002

Table 6-28, showed the unit cell parameters and volume of unit cell of the calcined 5% ScHAp materials prepared by precipitation and hydrolysis methods at 900 ˚C.

An increase in the both lattice parameters (a and c) were recorded by the precipitation method, and this may be ascribed to the replacement process of chloride ions with bigger ionic radius (1.81 Å) compared to hydroxyl group (1.68 Å). On the other hand, no clear effect on the lattice parameters were produced by hydrolysis method.

6.4.3.5 SEM of 5% ScHAp (5 wt.% Sc^{3+}) materials prepared by hydrolysis and precipitation methods.

SEM of non-sintered 5% ScHAp (5 wt.% $Sc3^{+}$) materials prepared by hydrolysis and precipitation methods.

Fig. 6-29 shows the SEM images of the non-sintered 5%ScHAp powders prepared by hydrolysis and precipitation methods.

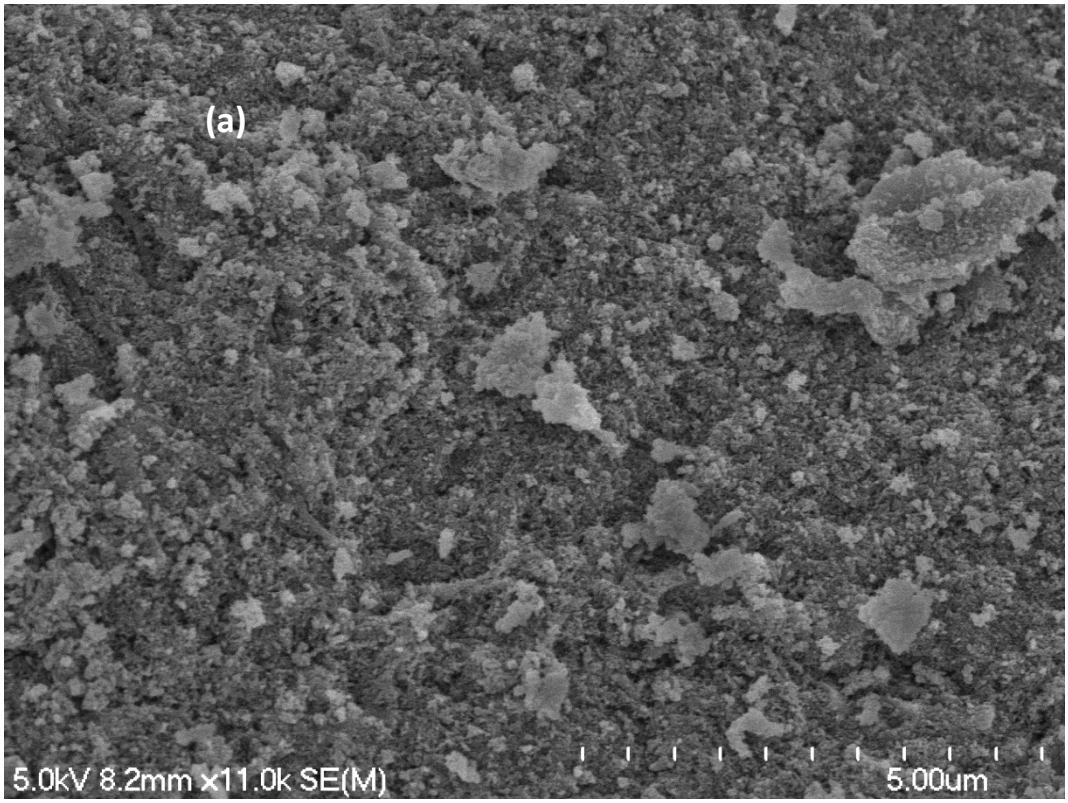
(a)
5.0kV 8.2mm x11.0k SE(M)
5.00um

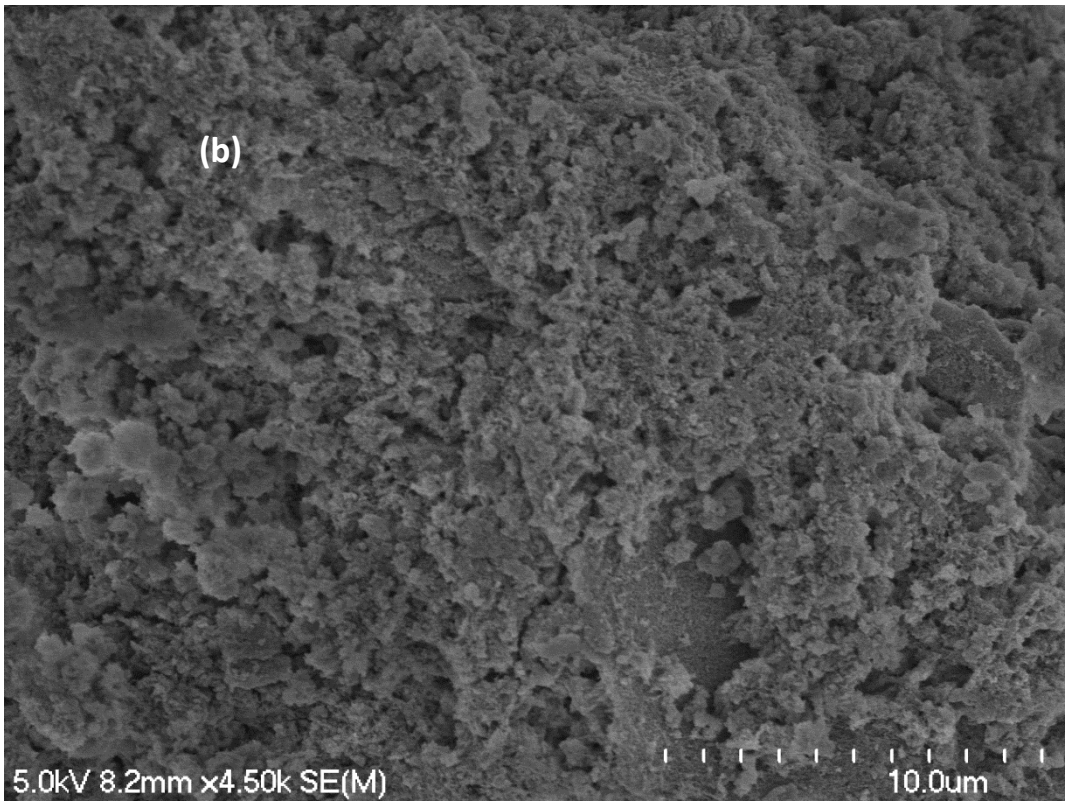
(b)
5.0kV 8.2mm x4.50k SE(M)
10.0um

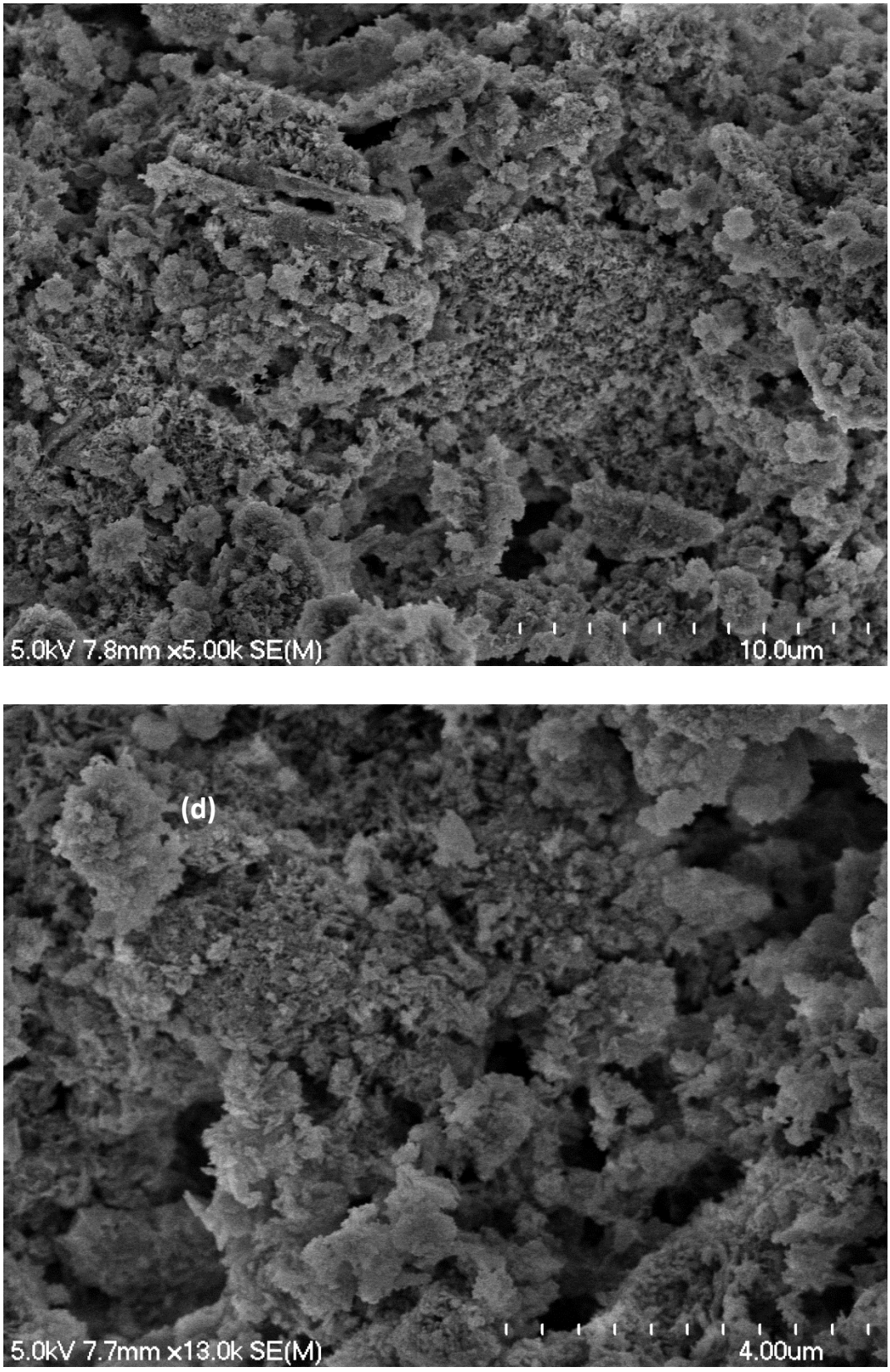

Figure 6-29: SEM images of non-sintered (a) unsubstituted HAp by precipitation (b) unsubstituted HAp by hydrolysis (c) 5% ScHAp by precipitation (d) 5% ScHAp by hydrolysis.

Fig. 6-29, showed the effect of the increasing level of Sc^3 addition on the morphology, in that porous material with anirregular structure associated with ability to agglomerate were recorded by both methods.

SEM of 5% ScHAp (5 wt.% Sc^{3+}) materials prepared by hydrolysis and precipitation methods after sintering at 900 ˚C:

Fig.6-30 displays SEM images of the sintered 5% ScHAp powders prepared by hydrolysis and precipitation methods.

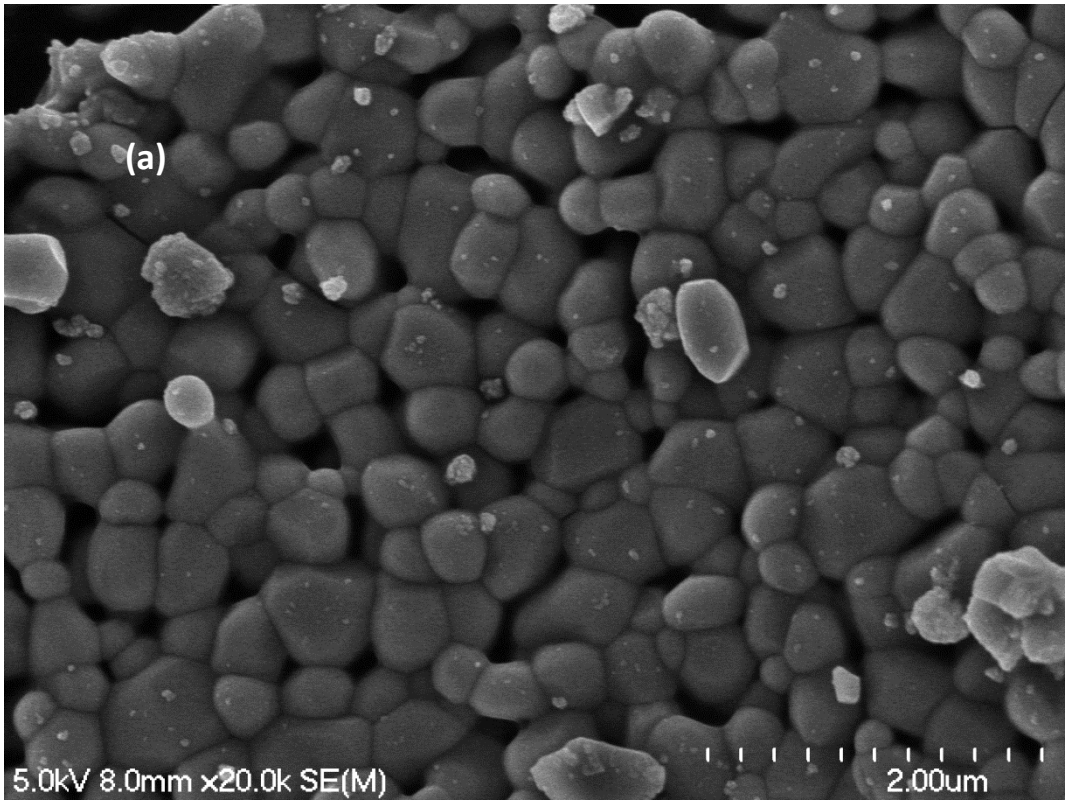

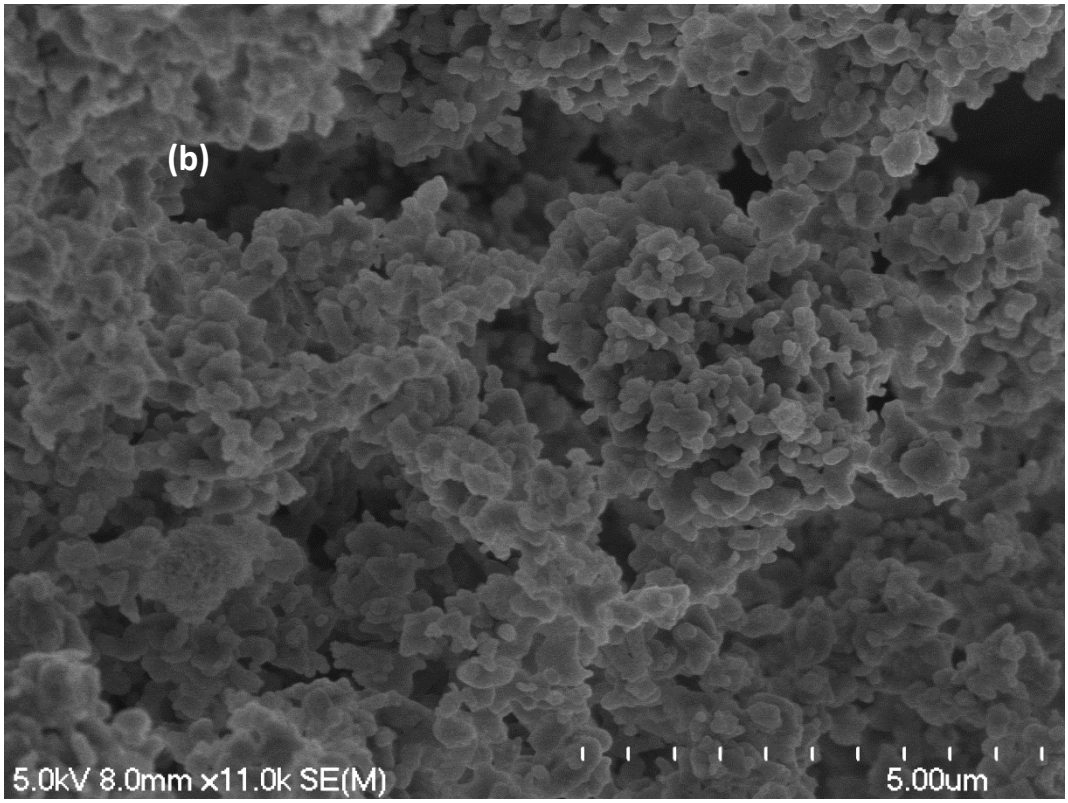
(b)
5.0kV 8.0mm x11.0k SE(M)
5.00um

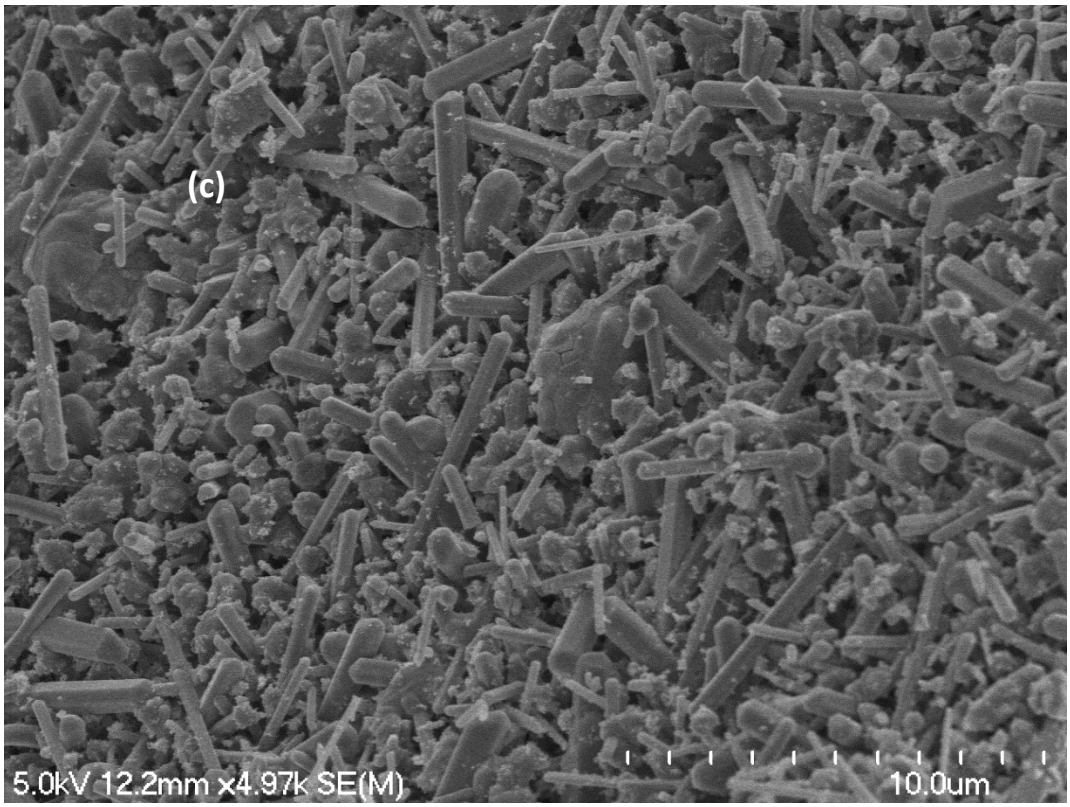
(c)
5.0kV 12.2mm x4.97k SE(M)
10.0um

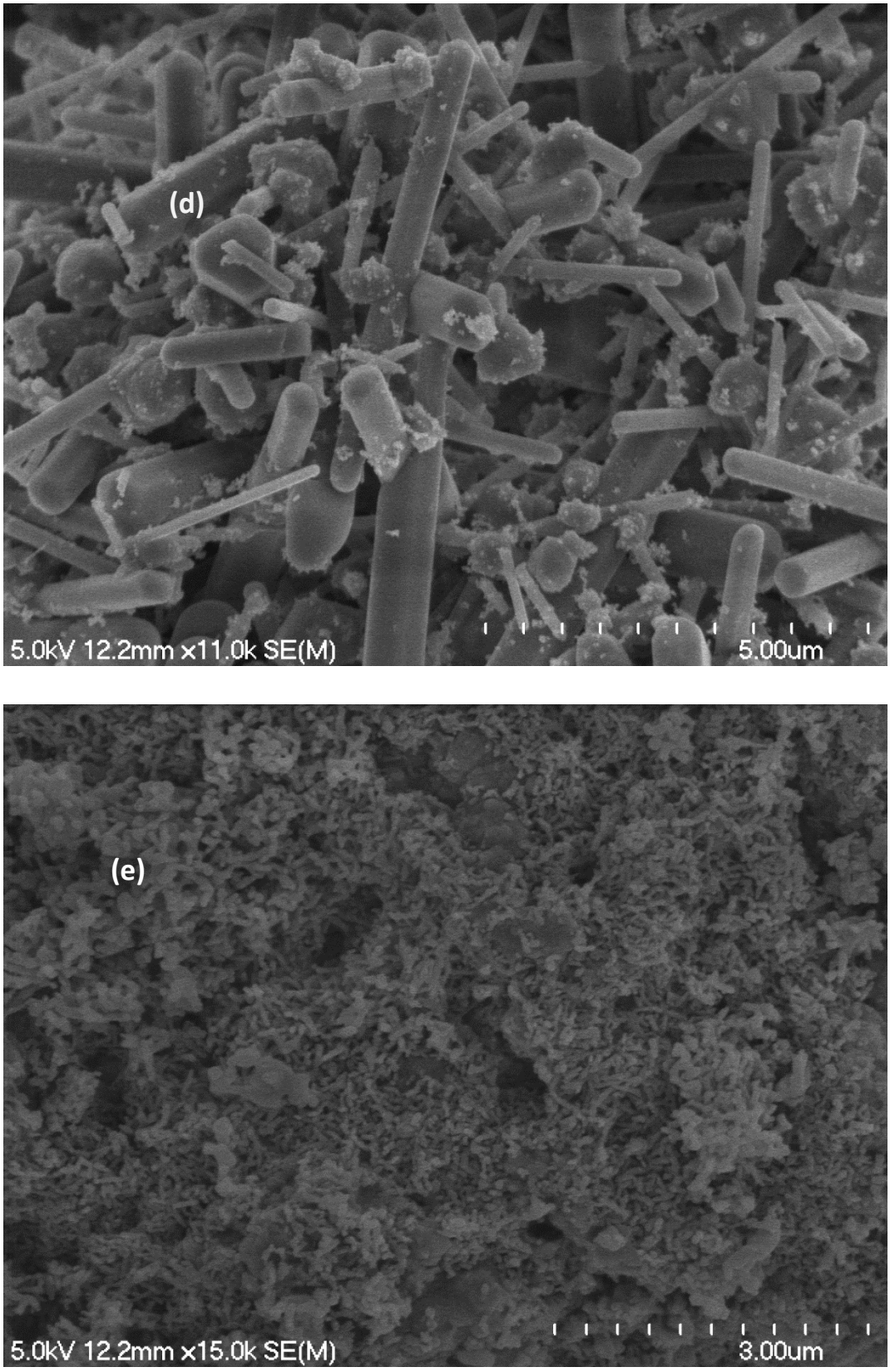

Figure 6-30: SEM of (a) unsubstituted HAp by precipitation (b) unsubstituted HAp by hydrolysis (c+d) 5 % ScHAp by precipitation (e) 5% ScHAp by hydrolysis, after sintering at 900 ˚C.

The SEM images showed the sintered 5%ScHAp powders prepared by the precipitation method consist of particles with a rod like shape, indicating the effect of the preparation method, the chemical composition as well as phase purity on the morphology. On the other hand, the preparation of 5% ScHAp by the hydrolysis method produced spherical like shapes with an irregular distribution. Also, the ability to agglomerate and to form porous material was confirmed by the SEM images.

6.5 Summary:

1- Different systems of cationic substituted HAp, namely 1% RbHAp (1 wt.% Rb^{+}), 1%EuHAp (1 wt.% Eu^{3+}) and 1,3 and 5% ScHAp(1, 3 and 5 wt.% Sc^{3+}), were prepared by using two different methods (precipitation and hydrolysis).

2- Different techniques were used to characterize the samples such as SEM, FTIR, XRD and ICP-MS.

The result of using these techniques showed:

- The presence of Rb^{+}, Eu^{3+} and Sc^{3+} ions into HAp samples were detected by using ICP-MS analysis. This technique could not prove substitution of the aforementioned ions but if they were present as substituted ions, the level of substitution was either very low or non existent. The following Table (**Table 6-29**) summaries the measured wt.% of doped ions (Rb^{+}, Eu^{3+} and Sc^{3+}) into HAp samples:

Table 6-29: The measured wt.% of doped ions (Rb^{+}, Eu^{3+}, Sc^{3+} and Na^{+}) into HAp structure as confirmed by ICP-MS analysis.

Sample	Wt.% Rb^{+} ions measured	Wt.% Eu^{3+} ions measured	Wt.% Sc^{3+} ions measured
1%RbHAp by precipitation	0.05%	-	-
1%RbHAp by hydrolysis	0.01%	-	-
1%EuHAp by precipitation	-	0.74%	-
1%EuHAp by hydrolysis	-	0.25%	-
1%ScHAp by precipitation	-	-	0.01
1%ScHAp by hydrolysis	-	-	0.01
3%ScHAp by precipitation	-	-	0.03
3%ScHAp by hydrolysis	-	-	0.01
5%ScHAp by precipitation	-	-	0.10
5%ScHAp by hydrolysis	-	-	0.02

- The effect of preparation method on the morphology were confirmed by SEM images. While all samples that prepared by the novel hydrolysis method (1%RbHAp, 1%EuHAp as well as 1, 3, and 5% ScHAp) resulted in spherical particles. the precipitation method led to the formation of different morphologies. As an example: 1% RbHAp powders consist of spherical particles with fine grain, but the prepared 1%EuHAp materials consisted of particles with spherical shape and small quantity of whiskers. The SEM images showed that the morphology of ScHAp materials prepared by the precipitation route depend on the levels of Sc salts introduced at point of preparation. As an example: 1% ScHAp materials were found to contain particles with spherical shape and small quantity of whiskers, but 3% and 5% ScHAp samples consist of particle with rod like shape. (These results were detected by using the SEM technique). The variation in the morphology of 1,3 and 5% ScHAp samples that were prepared by

precipitation route can be ascribed to the chemical composition, since the presence of other ions such as Na^{+}, CO_3^{2-} and Cl^{-} were detected by FTIR and ICP-MS analysis.

- The presence of the apatite phase in the whole prepared powders was confirmed through detecting the fundamental vibrational modes of PO_4^{3-} group at 562, 602, 962 and 1032-1095 cm^{-1}, as well as by recording the typical bands of the OH^{-} group at 3572 and 631 cm^{-1}. On the other hand a reduction of the intensities of stretching and librational modes of the OH^{-} group at (3572 and 630 cm^{-1}) due putatively to the replacement process of calcium site by trivalent cation (Eu^{3+}) and monovalent cation (Rb^{+}) had been produced in order to keep charge balance. (These results were detected by using FTIR analysis).
- The effect of the replacement process of calcium site by the following cation (Rb^{+}, Eu^{3+} and Sc^{3+}) on the crystallinity, crystallite size and lattice parameters were varied and the details of these values were discussed in the Chapter (these results were confirmed by using XRD technique).

Chapter Seven

Specific systems of anionic substituted HAp powders.

7.1 Introduction:

As discussed in the current literature [132], stoichiometric HAp is not regarded as suitable as a bone graft material because HAp does not dissolve over time and remodel in vivo but instead remains as a permanent fixture means it can be susceptible to failure in the long-term due to displacement or non union with other bone. Natural bone differs from stoichiometric HAp in that natural bone contains other ions substituted into the HAp lattice, such as carbonate, silicate, magnesium, etc. Therefore, the addition process of ions such as CO_3^{2-}, F^-, SiO_4^{4-} and other anions (which are present in native hard tissue) into the HAp crystal lattice enhances biomaterial properties, such as solubility and dissolution rate [132]. In terms of anionic substitution, which is the subject of this chapter, the way this occurs can be divided into three categories [29]:

1- Type A substitution : in this kind of replacement process a hydroxyl group would be replaced by other anions such as a larger halide ion (Cl^-) [29].
2- Type B substitution : this type of substitution occurs when the phosphate group is replaced by another group, such as a silicate group for instance [29].
3- Type AB substitution : occurs when hydroxyl and phosphate groups are replaced by other anions such as the carbonate ion [10].

This Chapter serves to outline the preparation method of new systems of anionic substituted hydroxyapatite materials. Specific systems of novel anionic substituted HAp materials were prepared using three synthetic approaches, namely the novel hydrolysis approach, as well as the more conventional precipitation and ion exchange methods. No studies to the author's knowledge on the synthesis of NbHAp, B_4O_7HAp, Br_2Ap, SAp and NaCl co substituted HAp (synthesized by the hydrolysis method using MCP/$Ca(OH)_2$ as a starting materials) have been published before in the chemical literature. While, limited attempts have been carried out to prepare NbHAp powders as discussed in the literature [32,240], one work was reported to prepare NaClHAp co substituted HAp materials in the chemical literature by using the precipitation method [28]. No previous works to the author's knowledge have been reported

for the preparation of B_4O_7HAp by the precipitation route. Also, no previous works to the author's knowledge was reported on synthesising Br_2Ap and SAp by using the precipitation method, however, calcium-bromapatite (Br_2Ap) and calcium- sulfoapatite (SAp) materials were prepared by using other methods [23,25]. The details of possible benefits of studying the substitution processes of these ions into the HAp crystal lattice were discussed elsewhere (see Chapter 1).

This chapter outlines the detailed results for:

1- The preparation process of specific systems of anionic and co substituted HAp, namely:
   - 1, 3 and 5% NbHAp.
   - 1% B_4O_7HAP.
   - Calcium-bromapatite ($Ca_{10}(PO_4)_6Br_2$).
   - Calcium- sulfoapatite ($Ca_{10}(PO_4)_6S$).
   - NaClHAp ($Ca_9Na(PO_4)_6(OH)Cl$). Different preparation methods were employed for that purpose such as precipitation, hydrolysis and ion exchange routes. The procedures of the preparation methods were described elsewhere (see Chapter 3 for details).
2- The evaluation of the effect of the synthesis route on some properties of HAp materials such as the morphology, chemical composition, substitution levels, crystallinity, crystallite size, lattice parameters and phase purity.

The following techniques were used to characterize the above substituted HAp powders and the results were discussed extensively.

1- Scanning electron microscope materials.
2- FTIR spectroscopy.
3- Powder X-ray diffraction (XRD).
4- Inductively coupled plasma mass spectrometry (ICP-MS) analysis.

7.2 1%, 3% and 5% NbHAp (1%, 3% and 5 wt.% niobate ions) powders prepared by precipitation and hydrolysis methods.

Three different series of NbHAp material (known as 1, 3 and 5% wt Nb) were prepared by using two different synthesis routes (i.e. the conventional precipitation and novel hydrolysis methods) as used in other studies reported by this thesis.

The structure of "Nb ions" in aqueous media is not fully understood at present [32]. Jehng et al. [241]reported the niobium ions in solutions do not exist as Nb^{5+} but as a hexaniobate ionic species [$H_xNb_6O_{19}^{(8-x)-}$, x=0-3] at pH>7. The hexaniobate ionic species starts to degrade into another ionic species such as the monomeric species with the following chemical formula : $NbO_2(OH)_4^{3-}$[$H_4NbO_6^{3-}$][241], and therefore this monomeric species [$H_4NbO_6^{3-}$] can exist only in very basic and dilute Nb solutions (< 0.08 M)[32].

Sommers [242] reported that the dissolution of $NbCl_5$ in (12 N HCl) is an endothermic process, resulting in a clear yellow solution, so in order to convert Nb_2O_5 to $NbCl_5$, 0.2 g of Nb_2O_5 was dissolved in 30 mL HCl (12 M) for that purpose. Afterwards the solution was heated at 200 ˚C with reflux for 10 hours, and the obtained yellow $NbCl_5$ solution (as shown below in **Fig. 7-1**) was used as a precursor to generate niobate ions.

NbHAp powders were prepared based on the following:

1- Niobium precursors (e.g., $NbCl_5$) undergo hydrolysis in alkaline aqueous solutions leading to the formation of oxyanions (generic formula $Nb_xO_y^{z-}$) instead of (Nb^{5+}) [31], and this report was also extensively discussed in the literature [32,241]
2- The density of $NbCl_5$ is 2.75 g/cm^3 and molecular weight= 270.2 g/mol.

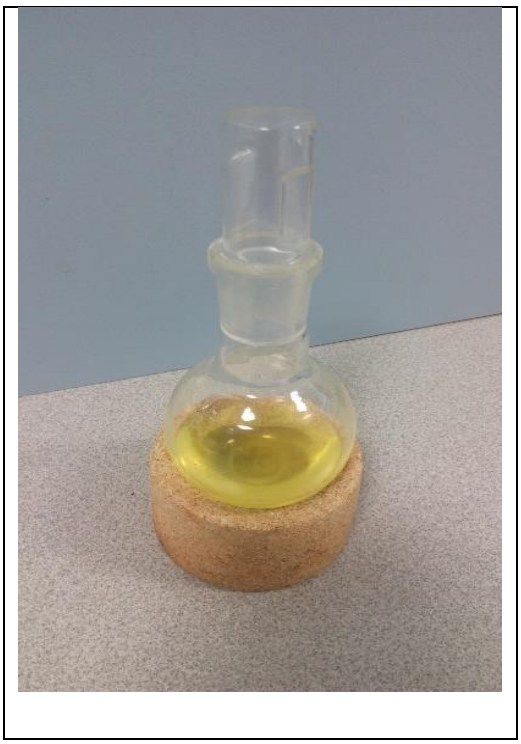

Figure 7-1: $NbCl_5$ solution that resulted from dissolving Nb_2O_5 in 12 M HCl and heated at 200 ˚C with reflux for 10 hours.

The detailed amounts of the reagents that used to prepare 1%, 3% and 5% NbHAp powders are listed in the **Tables 7-1, 7-2 and 7-3.**

Table 7-1: Synthesis details of 1% NbHAp powders by precipitation and hydrolysis methods.

Sample	MCPM (g)	$Ca(OH)_2$ (g)	$Ca(NO_3)_2$ (g)	Na_2HPO_4 (g)	$NbCl_5$ (g)	MCPM $Ca(H_2PO_4)_2.H_2O$ (mol)	$Ca(OH)_2$ (mol)	$Ca(NO_3)_2$ (mol)	Na_2HPO_4 (mol)	$NbCl_5$ (mol)
1% NbHAp by precipitation	-	-	8.1156	4.1722	0.0825	-	-	0.0495	0.0294	0.0003
1% NbHAp by hydrolysis	12.4552	3.6616	-	-	0.0825	0.0494	0.0494	-	-	0.0003

Table 7-2: Synthesis details of 3% NbHAp powders by precipitation and hydrolysis methods.

Sample	MCPM (g)	$Ca(OH)_2$ (g)	$Ca(NO_3)_2$ (g)	Na_2HPO_4 (g)	$NbCl_5$ (g)	MCPM $Ca(H_2PO_4)_2.H_2O$ (mol)	$Ca(OH)_2$ (mol)	$Ca(NO_3)_2$ (mol)	Na_2HPO (mol)	$NbCl_5$ (mol)
3% NbHAp by precipitation	-	-	8.0348	4.0545	0.2200	-	-	0.0490	0.0286	0.0008
3% NbHAp by hydrolysis	12..3496	3.6259	-	-	0.2200	0.0490	0.0489	-	-	0.0008

Table 7-3: Synthesis details of 5% NbHAp powders by precipitation and hydrolysis methods.

Sample	MCPM (g)	$Ca(OH)_2$ (g)	$Ca(NO_3)_2$ (g)	Na_2HPO_4 (g)	$NbCl_5$ (g)	MCPM $Ca(H_2PO_4)_2.H_2O$ (mol)	$Ca(OH)_2$ (mol)	$Ca(NO_3)_2$ (mol)	Na_2HPO_4 (mol)	$NbCl_5$ (mol)
5%NbHAp by precipitation	-	-	7.9325	3.9326	0.3300	-	-	0.0483	0.0277	0.0012
55NbHAp by hydrolysis	12.1785	3.5818	-	-	0.3300	0.0483	0.0483	-	-	0.0012

7.2.1 1% NbHAp (1 wt.% niobate ions) powders prepared by precipitation and hydrolysis methods:

One series of 1% NbHAp materials (1 wt.% niobate ions) was prepared by using two different synthesis routes (i.e. the precipitation and hydrolysis methods), and the detailed amounts of the reagents were listed in the **Table 7-1** (see page 5 for details)

7.2.1.1 Characterization techniques of prepared 1% NbHAp (1 wt.% niobate ions) materials by the precipitation and hydrolysis methods:

ICP-MS of 1%NbHAp (1 wt.% niobate ions) materials prepared by precipitation and hydrolysis methods after sintering at 900 ˚C:

The results of the elemental analyses of 1% NbHAp samples that were prepared by the precipitation and hydrolysis routes are displayed in **Table 7-4.**

Table 7-4: ICP-MS results of 1% NbHAp samples prepared by the precipitation and hydrolysis methods after sintering at 900 ˚C. The concentration was in ppb (ug/L):

Sample	Ca 44	P 31	Na 23	Nb 93
Unsubstituted HAp by precipitation	707795	401240	103797	-
1%NbHAp by precipitation	735373	369440	115490	N/D
Unsubstituted HAp by hydrolysis	769928	423970	78396	-
1%NbHAp by hydrolysis	704990	392719	81562	N/D

The starting (calculated) and actual (measured) degree of chemical composition of the prepared powders in terms of wt% of niobate ions, the calcium/phosphorus (Ca/P) molar ratios as well as (Ca+Na)/P molar ratio were determined by ICP-MS and presented in **Table 7-5.**

Table 7-5: The chemical analysis data of 1% NbHAp materials by ICP-MS measurements after sintering at 900 ˚C.

Sample	Ca/P Theoretical	Ca/P Measured	(Ca+Na+Nb)/P	Wt.% niobate ions theoretical	Wt.% niobate ions measured
Unsubstituted HAp by precipitation	1.67	1.36	1.71	-	-
1% NbHAp by precipitation	1.68	1.54	1.96	1.00%	0.00%
Unsubstituted HAp by hydrolysis	1.67	1.40	1.65	-	-
1% NbHAp by hydrolysis	1.68	1.39	1.67	1.00%	0.00%

As shown in **Table 7-5**, niobate ions were not detected (**N/D**) by ICP-MS analysis, suggesting the substitution of niobate ion (had it occurred if Nb were present or associated with the HAp sample) had not occurred. These results may be attributed to the lower concentration of $NbCl_5$ that was used as a source of niobate ions (0.2 g of Nb_2O_5 were dissolved in 30 mL of 12 M HCl to obtain $NbCl_5$ solution). Therefore, increasing the amount of Nb introduced to the preparation at time of synthesis was performed (as shown later) to see whether a higher level of substitution could be achieved in the samples. The reduction in the measured value of Ca:P mole ratios for the whole prepared 1%NbHAp powders can be ascribed to the presence of Na^+ ions, whereas the (Ca+Na)/ P in solids prepared by the precipitation method were recorded to be higher than the expected value of stoichiometric HAp (1.67), due to the formation process of B-type of CO_3HAp powders as confirmed by the FTIR spectra (see later), but the (Ca+Na)/ P by hydrolysis method were found to be the same as the theoretical value of stoichiometric HAp (1.67).

FTIR of 1%NbHAp (1 wt.% niobate ions) materials prepared by precipitation and hydrolysis methods:

FTIR of non-sintered 1% NbHAp (1 wt.% niobate ions) materials prepared by precipitation and hydrolysis methods:

FTIR spectra of the non-sintered 1% NbHAp powders prepared by precipitation and hydrolysis methods are shown in **Fig.7-2.**

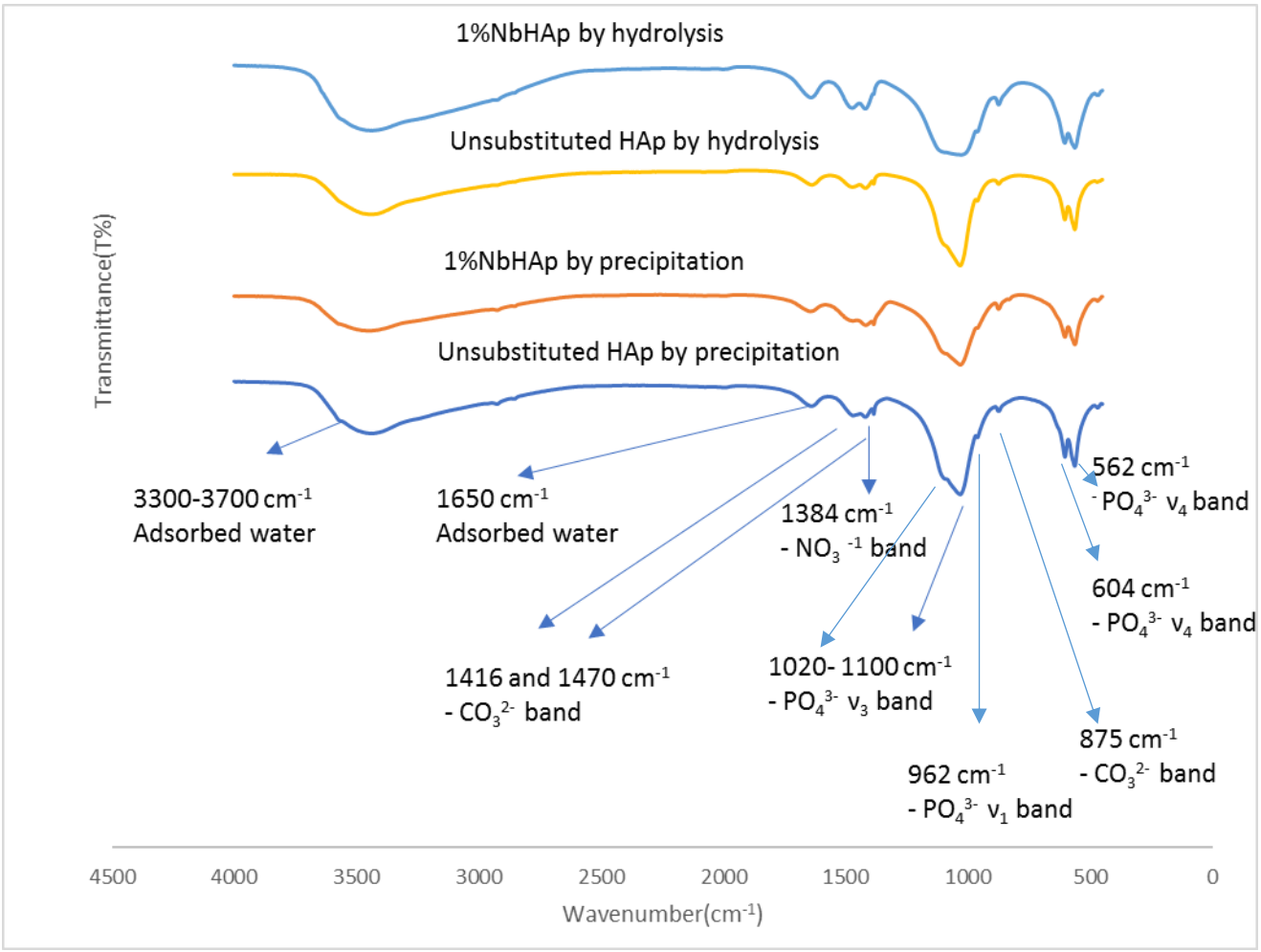

Figure 7-2: FTIR spectra of non-sintered 1% NbHAp (1 wt.% niobate ions) materials prepared by precipitation and hydrolysis methods.

The spectra consist of the typical bands ascribed to HAp material. PO_4^{3-} bands were detected at 562, 603, 963, and 1030–1098 cm^{-1}. The absence of fundamental bands of the OH^- group at 630 and 3570 cm^{-1} were confirmed by FTIR analysis due to the presence of adsorbed water, whereas the typical modes of adsorbed water appeared clearly at 1640 and 3000–3700 cm^{-1}. The characteristic bands of carbonate were also detected at 875, 1415 and 1465 cm^{-1} as evidence of

the substitution of the phosphate group by carbonate and confirming the presence of B-type carbonated HAp.

FTIR spectra of 1%NbHAp(1 wt.% niobate ions) materials prepared by precipitation and hydrolysis methods after sintering at 900 ˚C:

Fig.7-3 shows the FTIR spectra of the sintered NbHAp powders prepared by precipitation and hydrolysis methods.

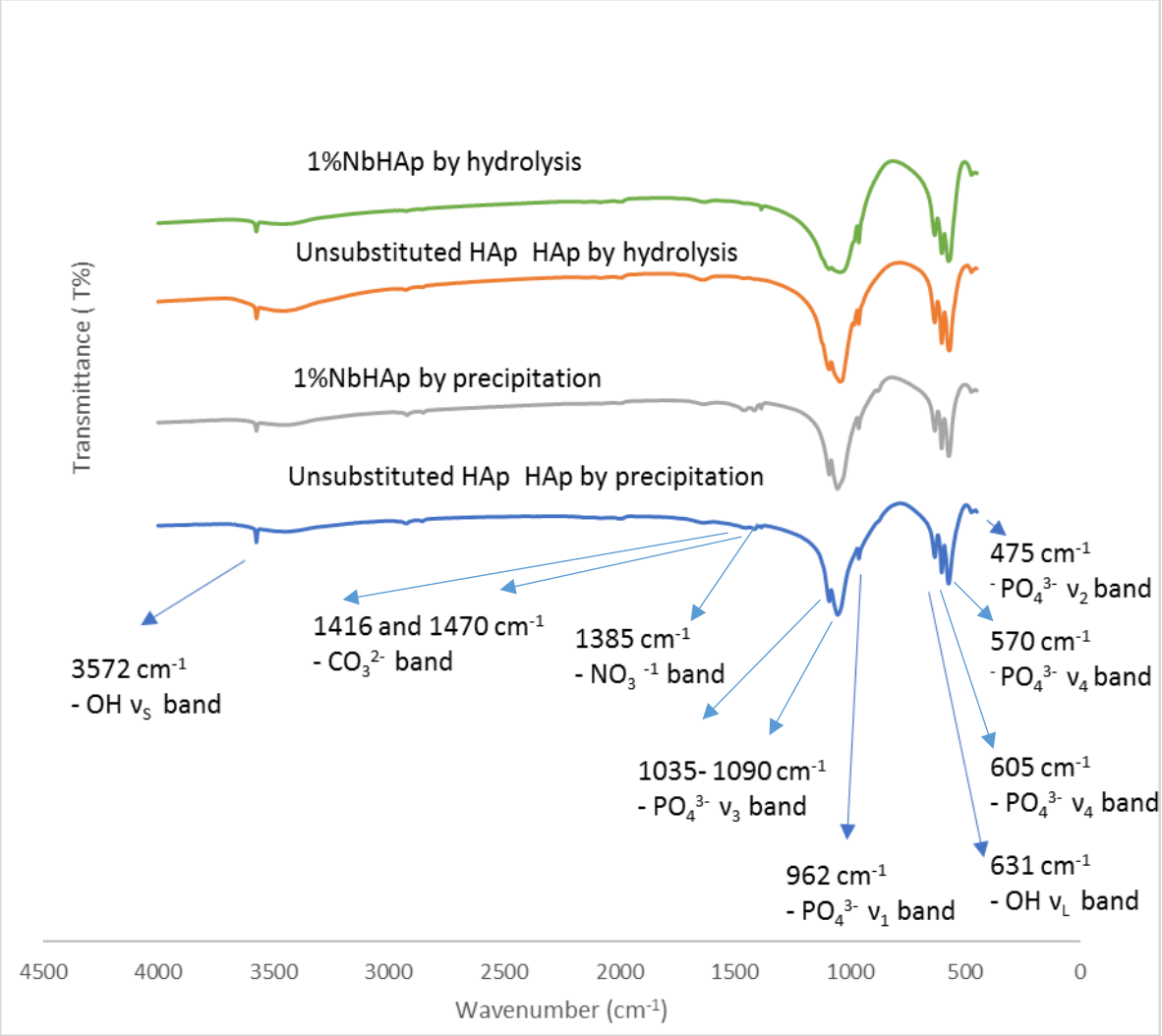

Figure 7-3: FTIR spectra of 1%NbHAp (1 wt.% niobate ions) materials prepared by precipitation hydrolysis methods after sintering at 900 ˚C.

The characteristic bands of HAp are exhibited in all prepared materials. The vibrational and stretching modes of hydroxyl group appeared at 632 and 3571 cm^{-1}, indicating highly crystalline

powders. The typical bands of the phosphate group were recorded at 570, 603, 963, 1028-1070 cm^{-1}, whereas the fundamental peaks of the carbonate group appeared in the prepared NbHAp powders, which were prepared by the precipitation method at 875, 1411 and 1452 cm^{-1}. These results suggest the carbonate uptake has occurred from the reaction solutions. The bands that appeared at 1384 cm^{-1} by hydrolysis method is believed to be due to the N-O stretching vibration of the nitrate group.

A further remarkable observation had also been recorded by FTIR spectra, that a clear reduction in the intensity of stretching modes of OH^- group at 3572 cm^{-1} was obtained in the whole prepared 1%NbHAp powders, especially in those prepared by the precipitation method, while the librational band of OH^- at 632 cm^{-1} did not display any significant difference. This reduction in the intensity of stretching mode was also associated with the appearance of a well- defined peak which corresponded to the carbonate group at 875 cm^{-1}. This reduction can be ascribed to:

1- The partial substitution of hydroxyl group (OH^-) by chloride ions (Cl^-). The substitution of Cl^- ions occurred as a result of using $NbCl_5$ as a starting material to insert niobate ions into HAp crystal. So, Cl may have substituted instead of niobate ions. Therefore, reduction in the stretching mode of lattice OH at (3752 cm^{-1}) was observed.

2- The presence of sodium ions, coupled with the formation of CO_3HAp powders in the whole 1%NbHAp powders which were prepared by the precipitation method. Therefore, the OH^- ion content was derived by the requirement to keep charge balance and to restore the neutrality of HAp crystals as discussed earlier in Chapter 6 (see FTIR of 1%RbHAp samples for details).

XRD diffraction analysis of 1%NbHAp (1 wt.% niobate ions) materials prepared by precipitation and hydrolysis methods:

Phase Identification of 1% NbHAp materials:

Figures 7-4 and 7-5 show that the XRD diffraction patterns of the non-sintered and sintered 1% NbHAp (1 wt.% niobate ions) materials prepared by two different methods (precipitation and hydrolysis routes).

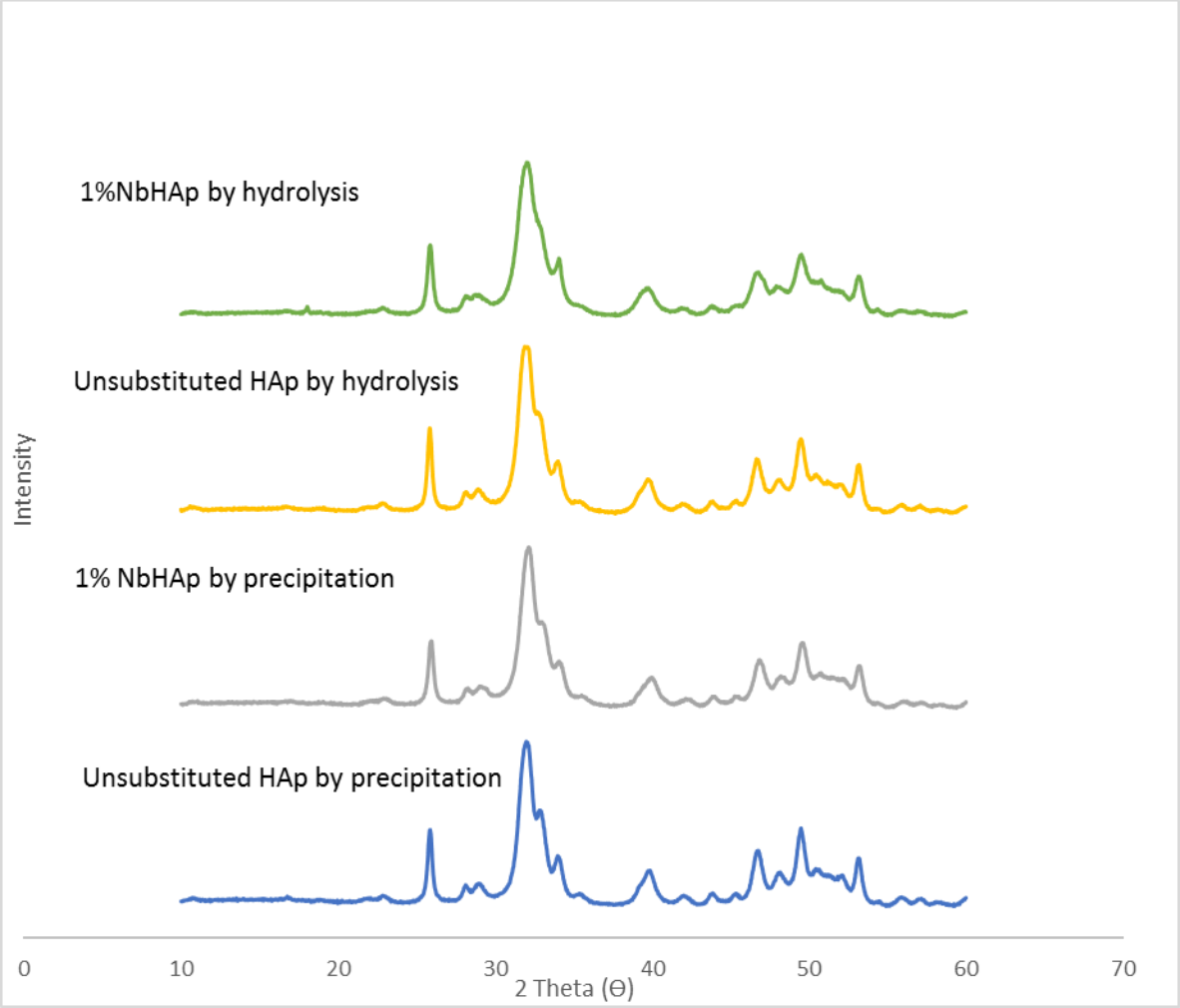

Figure 7-4: The XRD diffraction patterns of non-sintered 1% NbHAp (1 wt.% niobate ions) materials prepared by precipitation and hydrolysis methods.

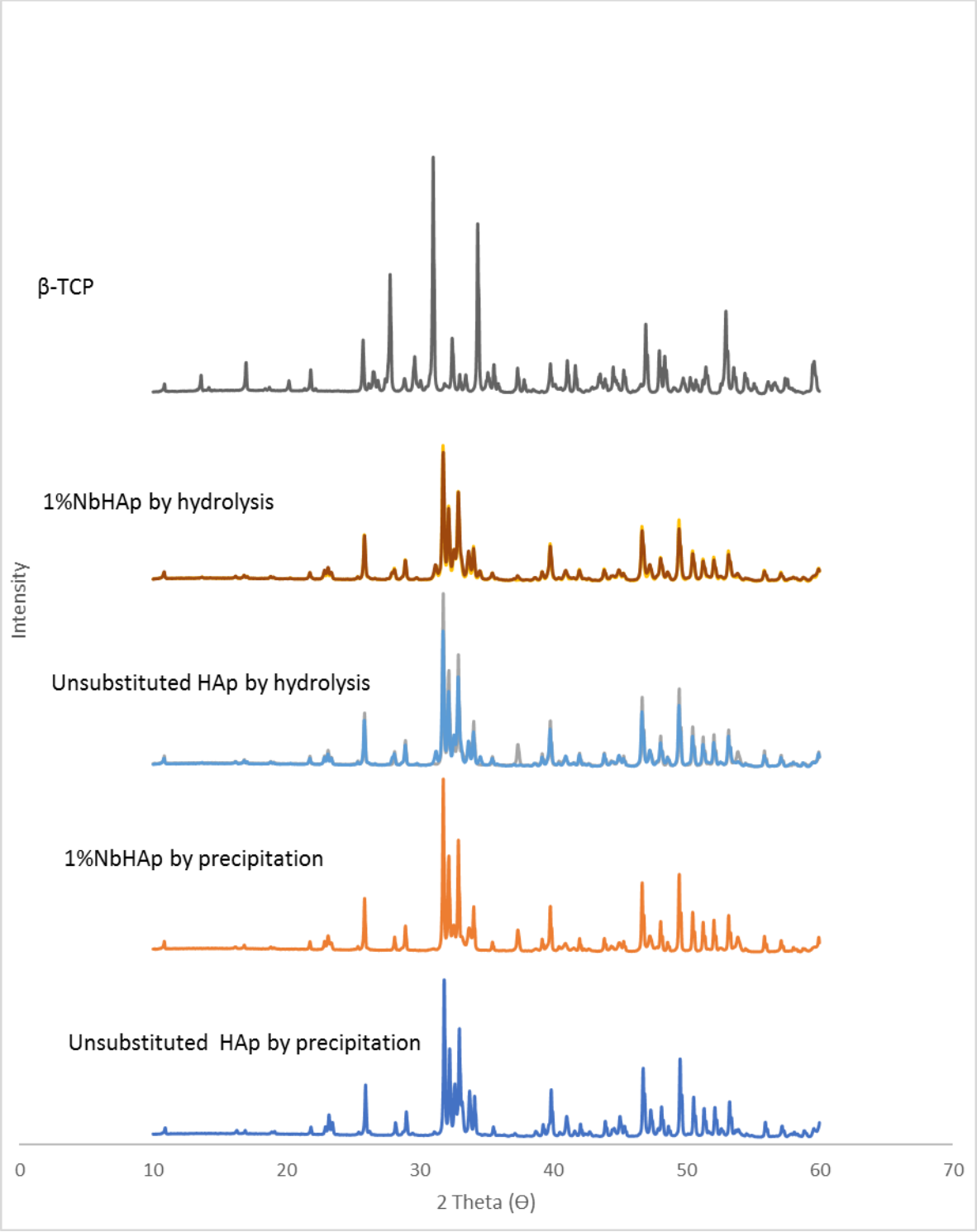

Figure 7-5: The XRD diffraction patterns of 1%NbHAp (1 wt.% niobate ions) materials prepared by precipitation and hydrolysis methods after sintering at 900 ˚C.

Although most of the XRD patterns showed the mean peaks of hydroxyapatite, we can see in the case of the precipitation route that a reduction in the intensity of some peaks, that were related

to a β-TCP at 2 Theta = 33.60˚ and 47.36˚, was observed. Also, an increase in the intensity of one peak that belongs to HAp at 2 Theta =34.10˚ was associated with the appearance of new peak at 2Theta= 37.40˚. This peak that appeared at 37.40 ˚ peak can be attributed to CaO (reference card number 04-017-9575). In the case of the hydrolysis method, the XRD analysis had not shown any detectable difference in the phase purity, since the only recorded variation between the prepared powders was a very slight increase in the intensity of one typical peak due to a β-TCP impurity phase at 2 Theta = 33.6˚.

Crystallinity and crystallite size of sintered 1% NbHAp materials:

Table 7-6 shows the degree of crystallinity and the crystallite size of sintered 1% NbHAp (1 wt.% niobate ions) materials prepared by precipitation and hydrolysis methods.

Table 7-6: The degree of crystallinity and the crystallite size of 1% NbHAp (1 wt.% niobate ions) materials by precipitation and hydrolysis methods after sintering at 900 ˚C.

Sample	D_{002} (Å)	Crystallinity %
Unsubstituted HAp by precipitation	618.3±3.2	84.15±2.4
1%NbHAp by precipitation	751.7±2.4	80.49±4.1
Unsubstituted HAp by hydrolysis	549.8±3.6	82.57±2.1
1%NbHAp by hydrolysis	473.6±3.2	76.09±3.4

The numerical value of the crystallinity of the 1%NbHAp powders which was prepared by different methods, displayed a clear reduction as confirmed in **Table 7-6,** suggesting that it is difficult to substitute one ion, such as niobate, because of the larger ionic radius of that monomer

($H_4NbO_6^{3-}$) compared to PO_4^{3-} ions (0.30 nm and 0.23 nm [32], respectively).

Also, **Table 7-6** shows the crystallite size of 1%NbHAp powders that were prepared by precipitation route was significantly increased. The hydrolysis method had a completely different effect on the crystallite size in that there was a decrease in size, indicating the effect of the synthesis route on the numerical value of crystallite size.

Lattice parameters and volume of unit cell of 1%NbHAp materials:

Table 7-7 displays the lattice parameters and the volume of hexagonal unit cell of the sintered 1% NbHAp (1 wt.% niobate ions) materials prepared by precipitation and hydrolysis methods.

Table 7-7: The lattice parameters and the volume of hexagonal unit cell of 1% NbHAp (1 wt.% niobate ions) prepared by precipitation and hydrolysis methods, after sintering at 900 ˚C.

Sample	a [Å]	c [Å]	V[Å^3]
Unsubstituted HAp by precipitation	9.416±0.004	6.879±0.003	1579±0.004
1%NbHAp by precipitation	9.422±0.003	6.884±0.003	1582±0.003
Unsubstituted HAp by hydrolysis	9.421±0.003	6.882±0.005	1581±0.004
1%NbHAp by hydrolysis	9.422±0.001	6.883±0.003	1581±0.002

Table 7-7 shows a clear increase in both values of lattice constants (a and c), especially with the precipitation method. This expansion obtained by both methods can be ascribed to the substitution of chloride ions which have larger ionic radius (1.81 Å) [123] compared to hydroxyl group(1.68 Å). The presence of Cl^- ions into HAp crystal can be determined through using other techniques such as XRD analysis and FTIR spectra (see latter, NaClHAp materials).

SEM of prepared 1%NbHAp(1 wt.% niobate ions) materials prepared by precipitation and hydrolysis methods:

The SEM was used to analyze the surface morphology of the substituted HAp compounds to check whether they were of porous or crystalline character, see below:

SEM of non-sintered 1% NbHAp (1 wt.% niobate ions) materials prepared by precipitation and hydrolysis methods:

Figure 6-7 shows the morphology of the non-sintered 1% NbHAp powders prepared by precipitation and hydrolysis methods.

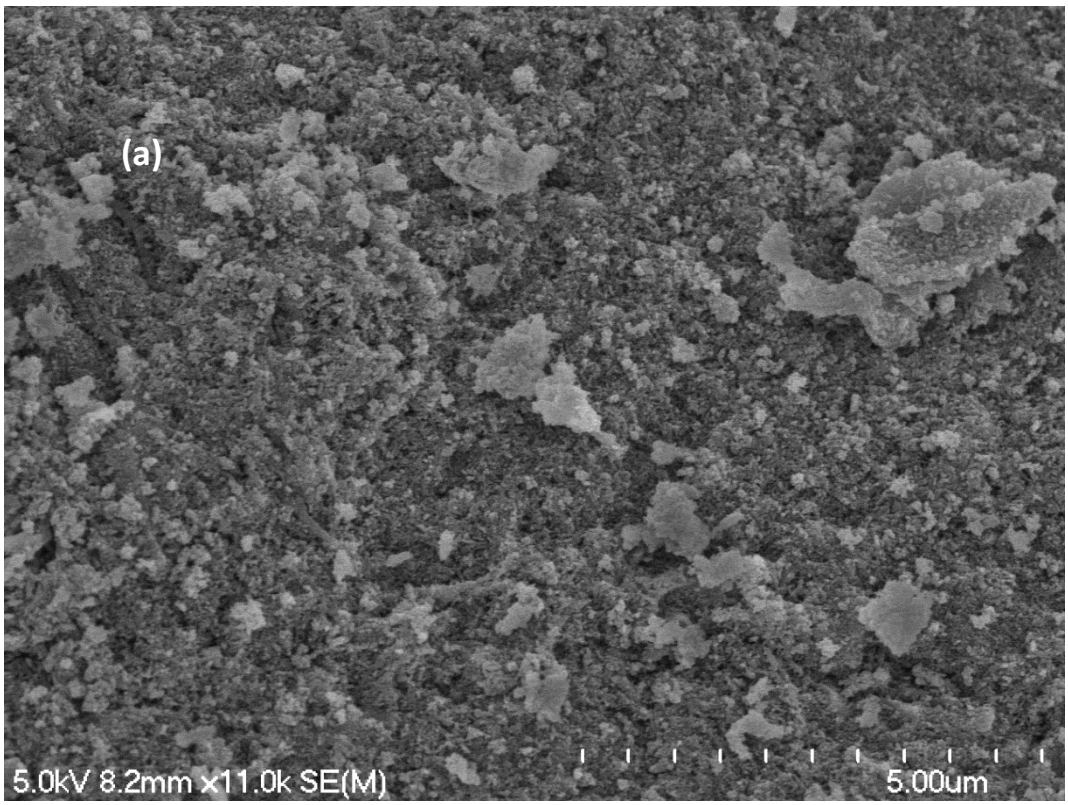
(a)
5.0kV 8.2mm x11.0k SE(M)
5.00um

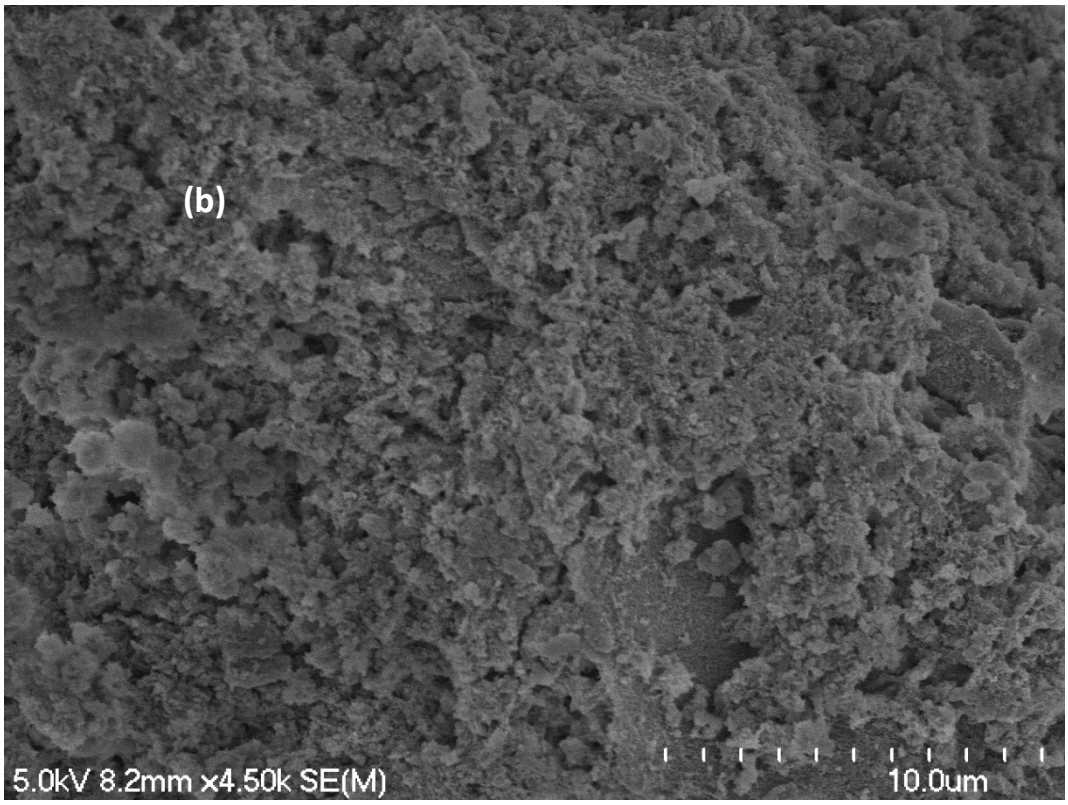
(b)
5.0kV 8.2mm x4.50k SE(M)
10.0um

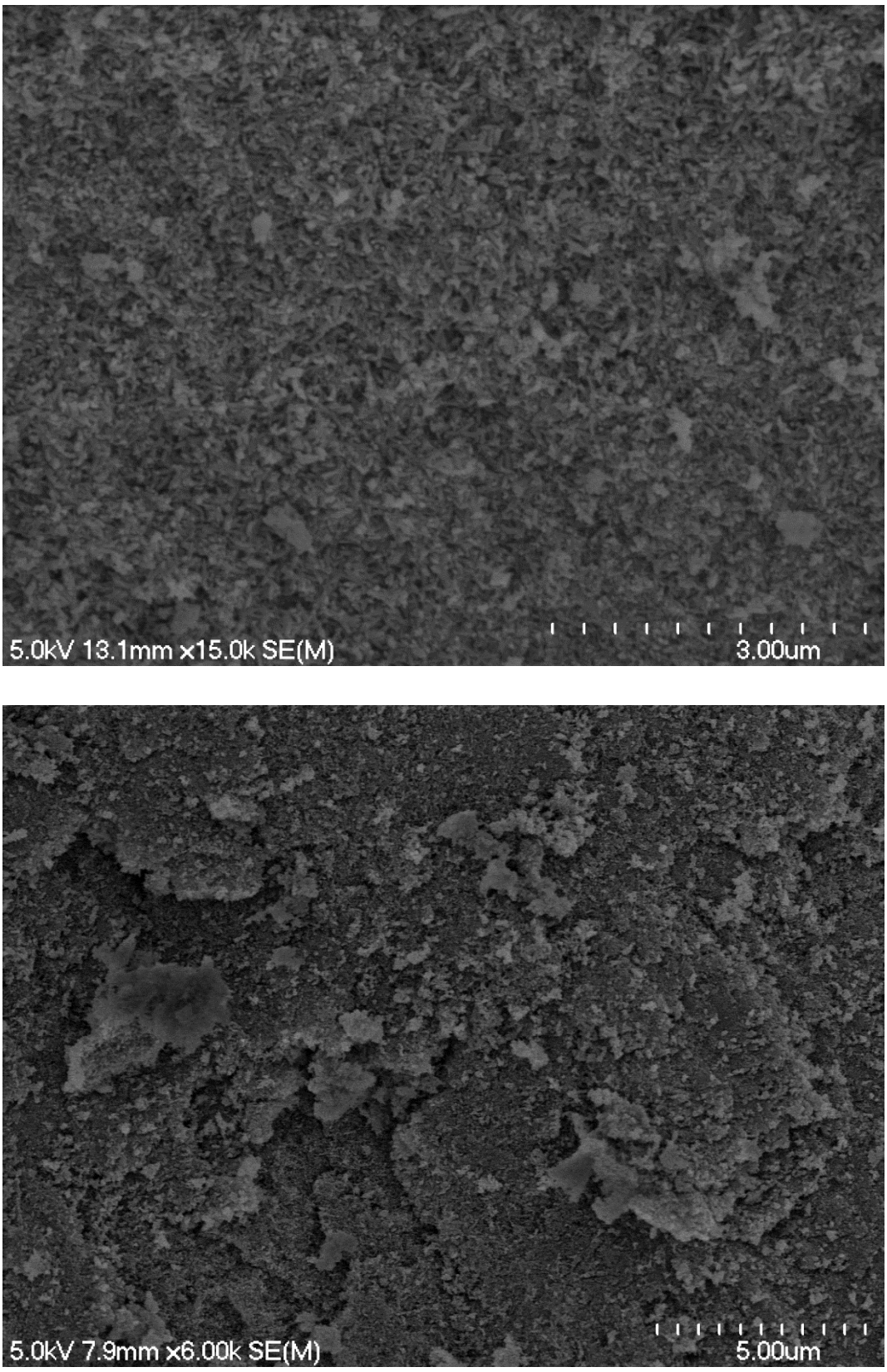

Figure 7-6: SEM images of non-sintered (a)unsubstituted HAp by precipitation (b) unsubstituted HAp by hydrolysis (c) 1%NbHAp by precipitation (d) 1%NbHAp by hydrolysis.

As recorded by SEM images, the morphology of the prepared materials had not varied by the synthesis methods due to the attempted substitution of niobate ions into HAp samples. Irregular distribution, porous materials and a trend to agglomerate were recorded for these samples by both methods as shown in **Fig 7-**6 but this would have occurred due to other reasons.

SEM of 1% NbHAp (1 wt.% niobate ions) materials prepared by precipitation and hydrolysis methods after sintering at 900 ˚C:

Figure 7-7 shows the morphology of the sintered NbHAp materials as prepared by precipitation and hydrolysis methods.

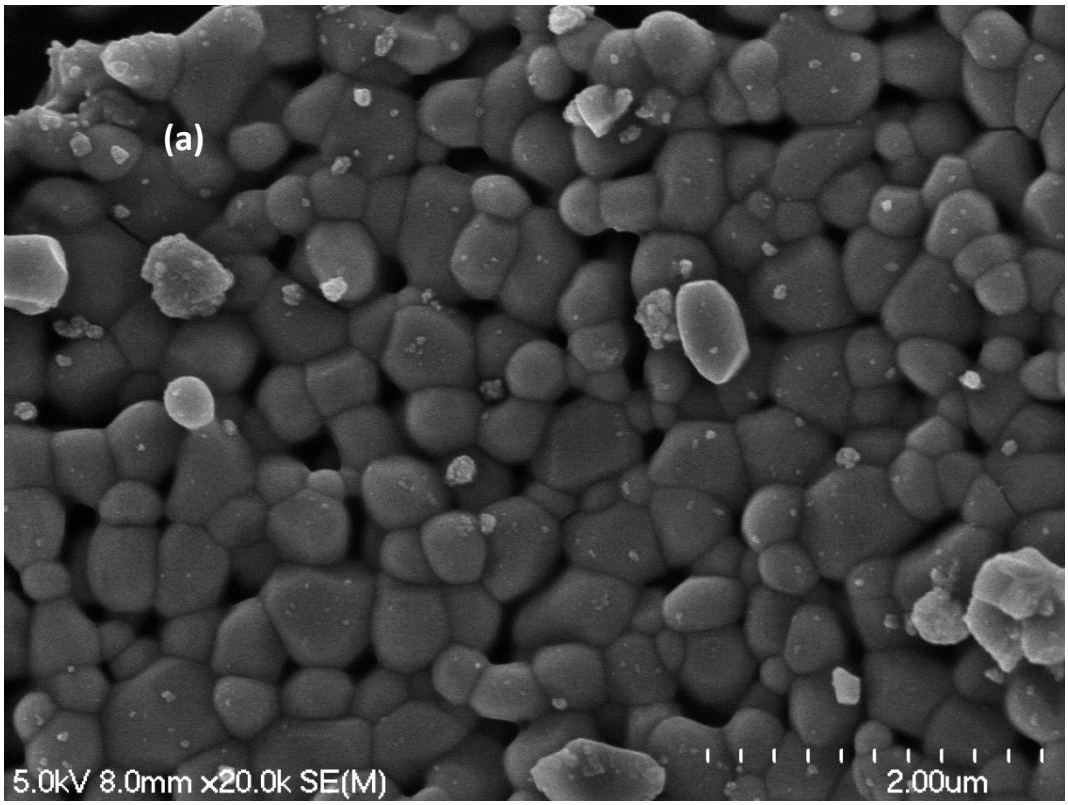

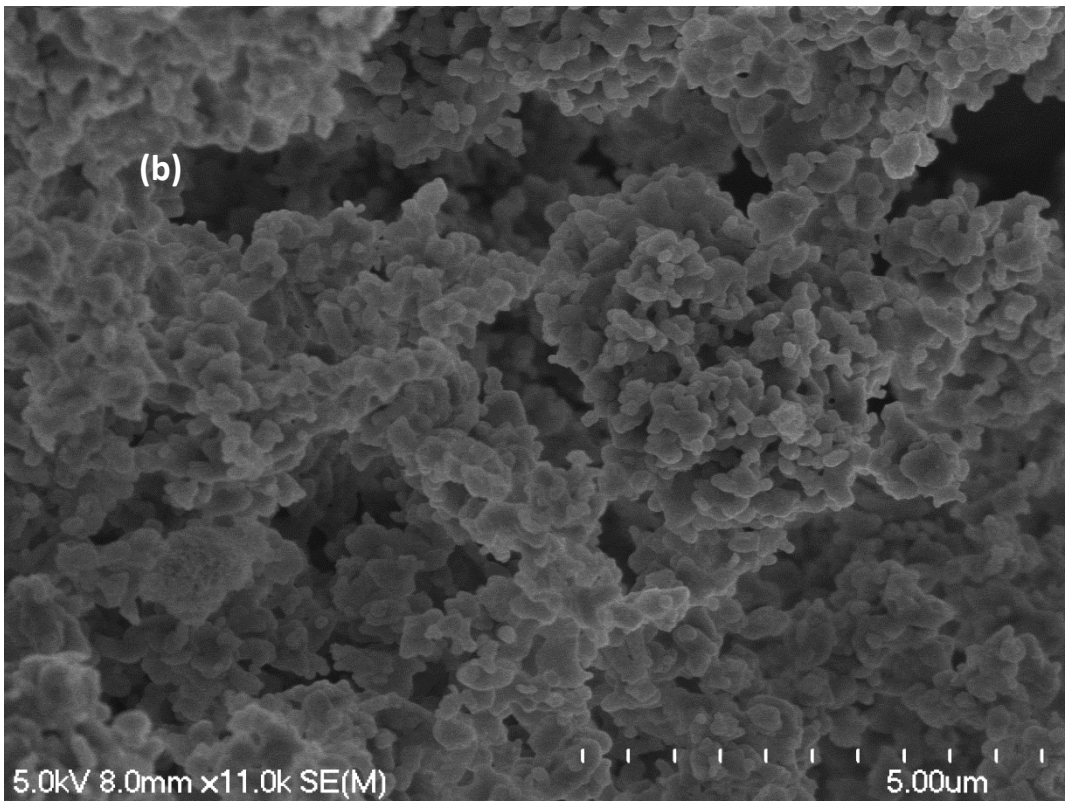
(b)
5.0kV 8.0mm x11.0k SE(M)
5.00um

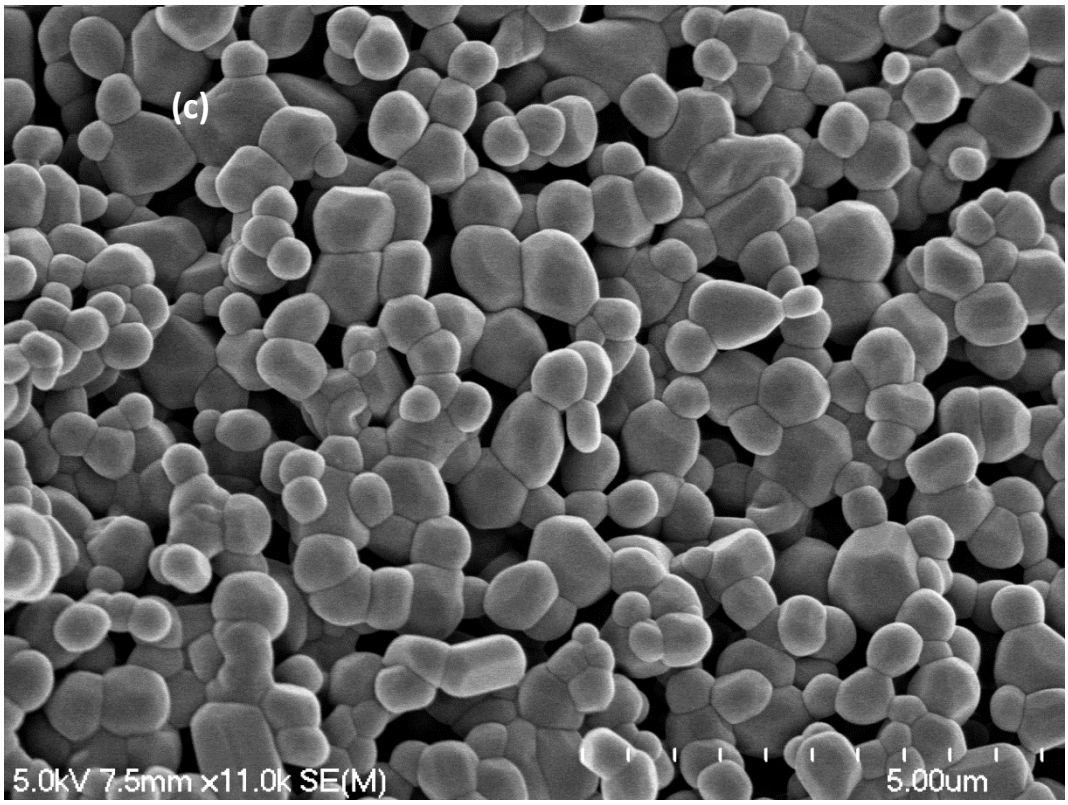
(c)
5.0kV 7.5mm x11.0k SE(M)
5.00um

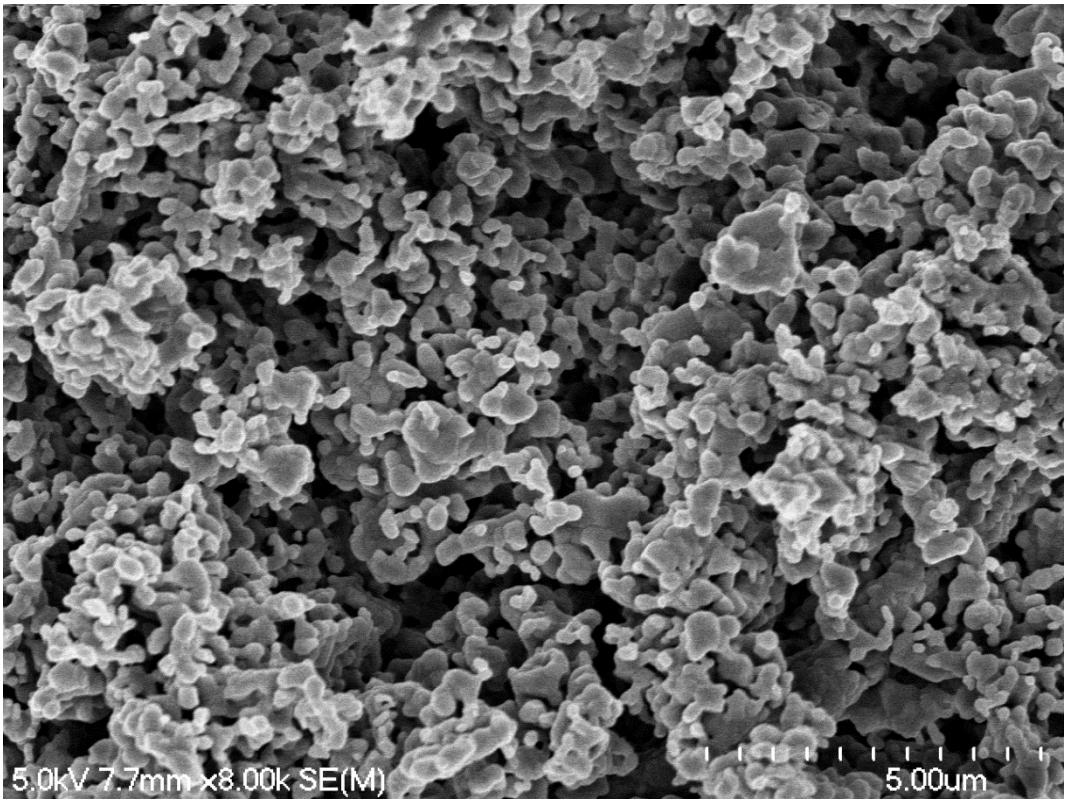

Figure 7-7: SEM images of (a) unsubstituted HAp by precipitation (b)unsubstituted HAp by hydrolysis (c) 1% NbHAp by precipitation (d) 1% NbHAp by hydrolysis after sintering at 900 ˚C.

Fig.7-7 shows that the 1% NbHAp materials which were prepared by the precipitation method have a much more uniform structure with a lesser tendency to agglomerate compared to the hydrolysis method. The hydrolysis process as recorded by SEM images showed irregular structure, a high level of porosity and a high capacity to agglomerate.

7.2.2 3% NbHAp (3 wt.% niobate ions) powders prepared by the precipitation and hydrolysis methods:

One series of 3%NbHAp materials (3 wt.% niobate ions) was prepared by using two different synthesis routes (precipitation and hydrolysis), and the detailed amounts of the reagents were listed in the **table 7-2.**

7.2.2.1 Characterization techniques of 3% NbHAp (3 wt.% niobate ions) materials prepared by precipitation and hydrolysis methods.

ICP-MS of 3% NbHAp *(3 wt.% niobate ions) materials prepared by precipitation and hydrolysis methods after sintering at 900 ˚C*.

The results of the elemental analyses of sintered 3%NbHAp samples prepared by precipitation and hydrolysis routes are displayed in **Table 7-8 .**

Table 7-8: ICP-MS results of 3%NbHAp (3 wt.% niobate ions) materials prepared by precipitation and hydrolysis methods after sintering at 900 ˚C. The concentration was in ppb unit (ug/L):

Sample	Ca 44	P 31	Na 23	Nb 93
Unsubstituted HAp by precipitation	707795	401240	103797	-
3%NbHAp by precipitation	622596	335522	125100	-
Unsubstituted HAp by hydrolysis	769928	423970	78396	-
3%NbHAp by hydrolysis	634459	387761	116100	-

The starting (calculated) and actual (measured) degree of chemical composition of the prepared powders in terms of wt.% of niobate ions, the calcium/phosphorus (Ca/P) molar ratios as well as (Ca+Na)/P molar ratio were determined by ICP-MS and presented in **Table 7-9.**

Table 7-9: The chemical analysis data of 3%NbHAp (3 wt.% niobate ions) materials by ICP-MS measurements after sintering at 900 ˚C.

Sample	Ca/P Theoretical	Ca/P Measured	(Ca+Na+Nb)/P Mole ratio	Wt.% niobate ions theoretical	Wt.% niobate ions measured
Unsubstituted HAp by precipitation	1.67	1.36	1.71	-	-
5% NbHAp by precipitation	1.71	1.54	1.94	5%	-
Unsubstituted HAp by hydrolysis	1.67	1.40	1.65	-	-
5% NbHAp by hydrolysis	1.71	1.39	1.67	5%	-

As discussed previously, the niobate ions were not detected in the prepared 1%NbHAp materials through using ICP-MS techniques. Such an observation was attributed to the lower concentration

of niobium ions used in the syntheses, therefore increasing the amount of niobate ions in the synthesis was done in order to evaluate such results and to determine whether any Nb substitution had occurred in the HAp samples. However, **Tables 7-8** and **7-9** show clearly that there was still no evidence from ICP-MS that Nb was even associated with the HAp samples indicating that the substitution process was not achieved at this level of Nb addition either. A reduction in the measured value of Ca:P mole ratios for the whole prepared 3% NbHAp powders were confirmed due to the presence of Na^+ ions, whereas the (Ca+Na)/ P by precipitation method were measured to be higher than the expected value (1.67), due to the presence of carbonate in the prepared materials as confirmed by the FTIR spectra, but the (Ca+Na)/ P mole ratio by hydrolysis method were found to be at the same level as would be seen in stoichiometric HAp (1.67).

FTIR of prepared 3% NbHAp (3 wt.% niobate ions) materials prepared by precipitation and hydrolysis methods:

FTIR of non-sintered 3%NbHAp (3 wt.% niobate ions) materials prepared by precipitation and hydrolysis methods:

Figure 7-8 displays the FTIR spectra of the non-sintered 3%NbHAp powders prepared by precipitation and hydrolysis methods.

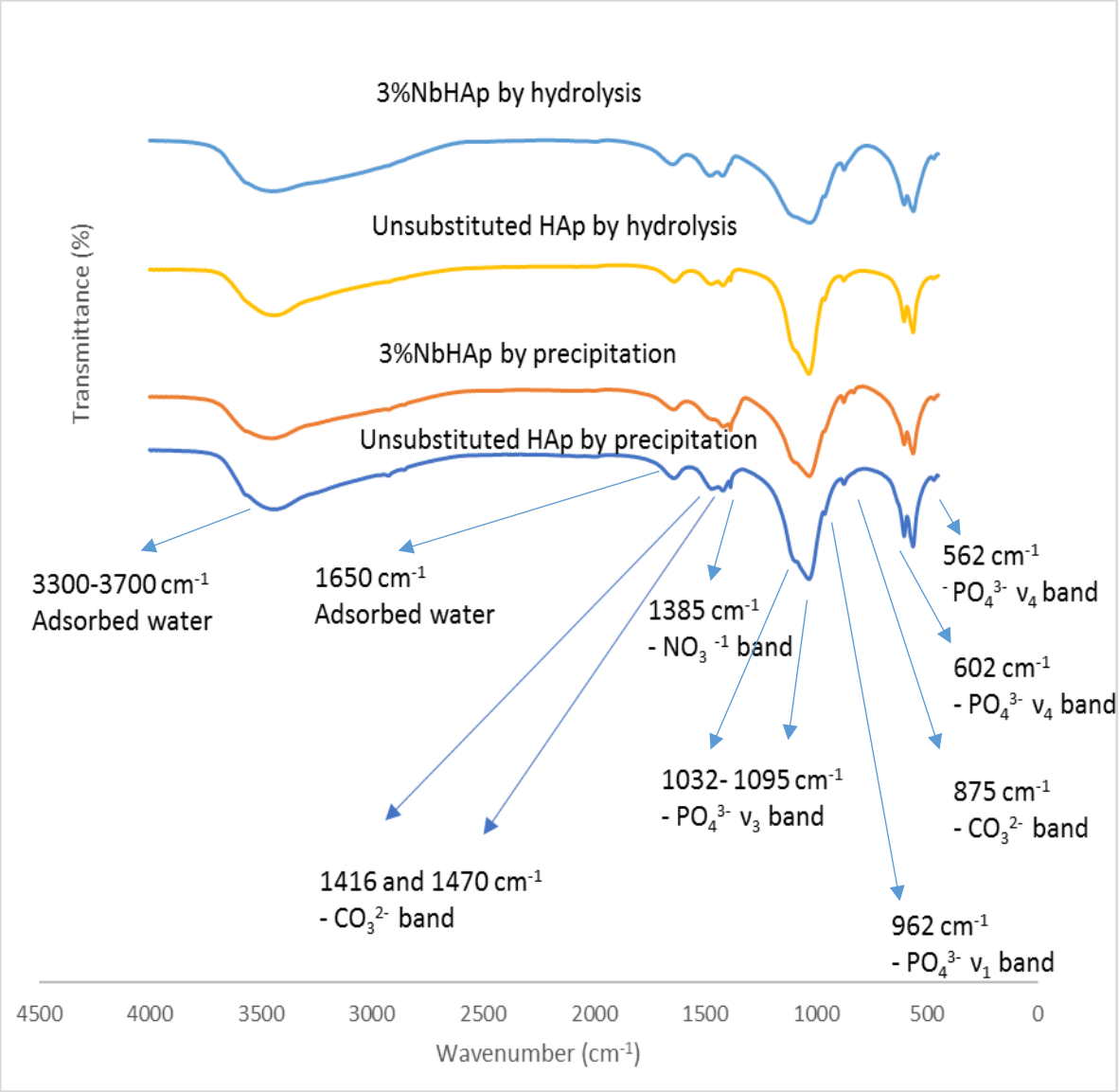

Figure 7-8: FTIR of non-sintered 3%NbHAp (3 wt.% niobate ions) materials prepared by precipitation and hydrolysis methods.

While the characteristic bands of the phosphate group stood out at (562, 603, 962, 1032 and 1092 cm^{-1}), the carbonate substitution was detected at (875, 1415 and 1452 cm^{-1}) as and showed that B-type substituted CO_3HAp had occurred. Also, in all phases prepared by the precipitation method, the typical band of nitrate group which came from the starting material (calcium nitrate) appeared clearly at 1385 cm^{-1}, however, in the case of phases prepared by the hydrolysis route (nitrate free preparations), it is likely to have come about from contamination of the KBr powder used to prepare the KBr disks for IR analysis.

FTIR of 3% NbHAp (3%wt. Nb^{5+}) materials prepared by precipitation and hydrolysis methods after sintering at 900 ˚C:

Fig.7-9 shows the FTIR spectra of the sintered 3% NbHAp powders prepared by different methods (precipitation and hydrolysis).

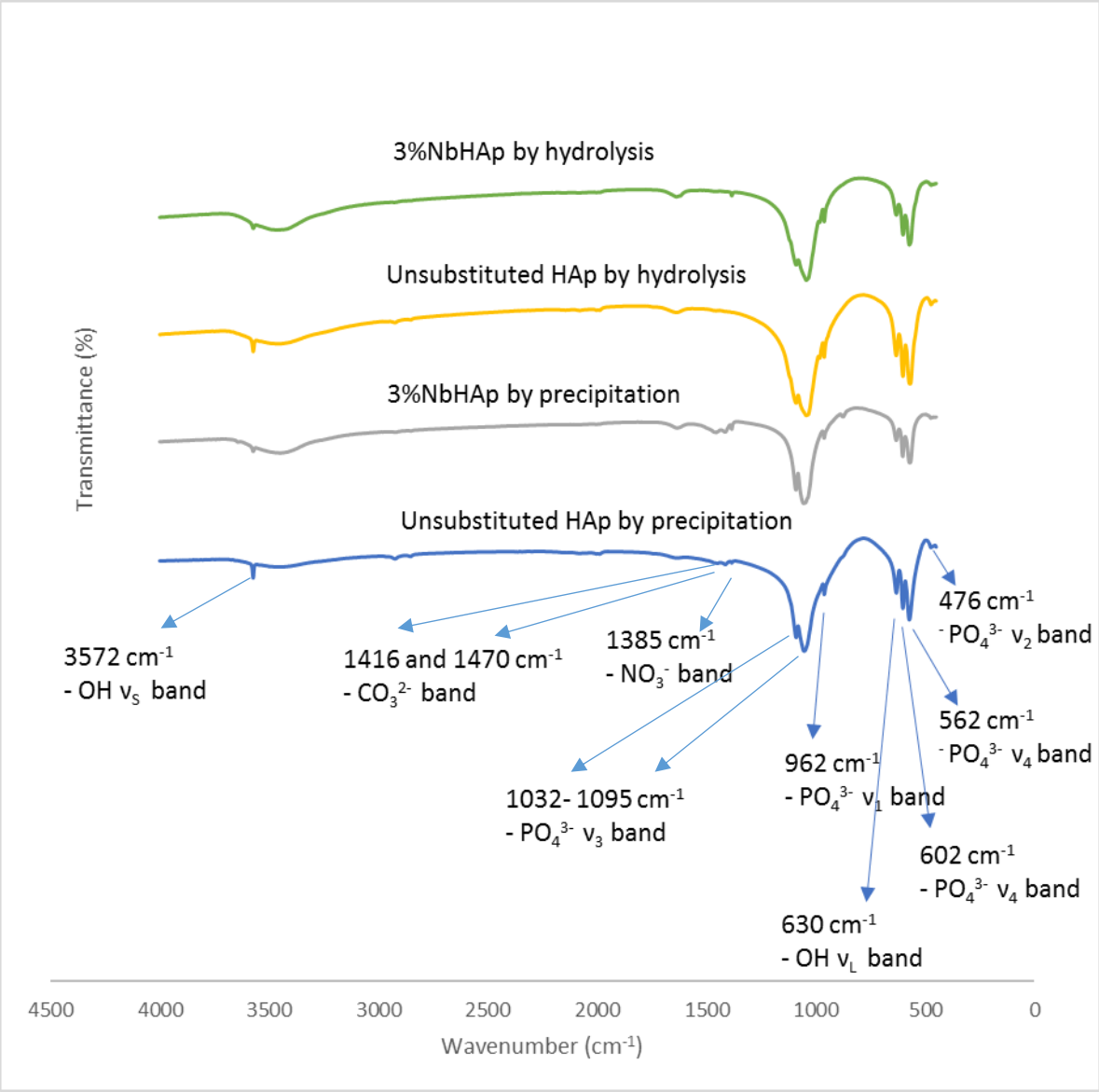

Figure 7-9: FTIR spectra of 3%NbHAp (3 wt.% niobate ions) materials prepared by precipitation and hydrolysis methods after sintering at 900 ˚C.

The characteristic IR bands of HAp were confirmed in the whole prepared materials. The vibrational and stretching modes of the hydroxyl group appeared at 632 and 3571 cm^{-1} confirmed

that the powders were of high crystallinity, and the typical bands of the phosphate group were recorded at 570, 603, 963, 1028-1070 cm^{-1}. Also, the fundamental peaks of the carbonate group appeared in the whole prepared 3% NbHAp powders that were synthesized by the precipitation method at 875, 1411 and 1452 cm^{-1} as an indication of the formation of carbonated HAp.,

Also, **Fig. 7-9** shows that a clear reduction in the intensity of stretching modes of OH^- group at 3572 cm^{-1} in the whole prepared 3% NbHAp samples that were synthesized by precipitation and hydrolysis methods. However, the intensity of the librational mode of OH^- at 632 cm^{-1} displayed a slight reduction, and this reduction in the intensity of the stretching and librational modes is associated with the appearance of a well-defined peak corresponding to carbonate group at 875 cm^{-1}. This reduction can be ascribed to:

1- The partial substitution of hydroxyl group by chloride ions. The substitution of Cl^- ions occurred as a result of using $NbCl_5$ in the synthesis. Though Nb species had not substituted it is possible that Cl substitution had occurred instead. Therefore, reduction in the stretching mode of lattice OH at (3752 cm^{-1}) was observed.
2- The presence of sodium ions, coupled with the formation of CO_3HAp powders in the whole 3%NbHAp materials which were prepared by the precipitation method. Therefore, the OH^- ion content was derived by the requirement to keep charge balance and to restore the neutrality of HAp crystals as discussed earlier in chapter 6 (see FTIR of sintered RbHAp samples for details).

XRD diffraction patterns of 3%NbHAp (3 wt.% niobate ions) materials prepared by precipitation and hydrolysis methods:

Phase Identification of 3% NbHAp materials:

The XRD patterns of the non-sintered and sintered 3%NbHAp powders prepared by different methods (precipitation and hydrolysis) are shown in **Fig.7-10 and Fig.7-11,** respectively.

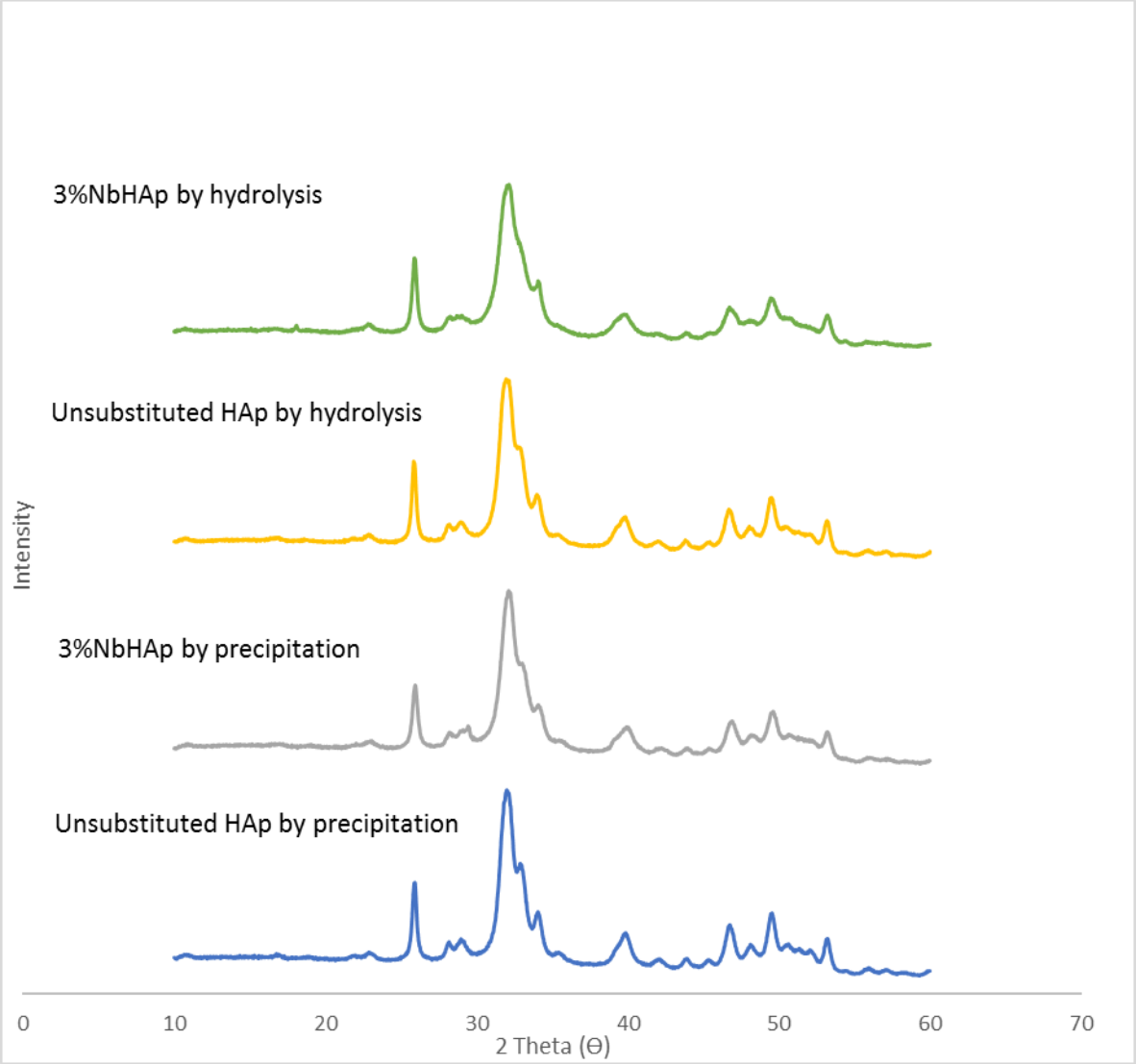

Figure 7-10: The XRD diffraction patterns of the non-sintered 3%NbHAp (3 wt.% niobate ions) materials prepared by precipitation and hydrolysis methods.

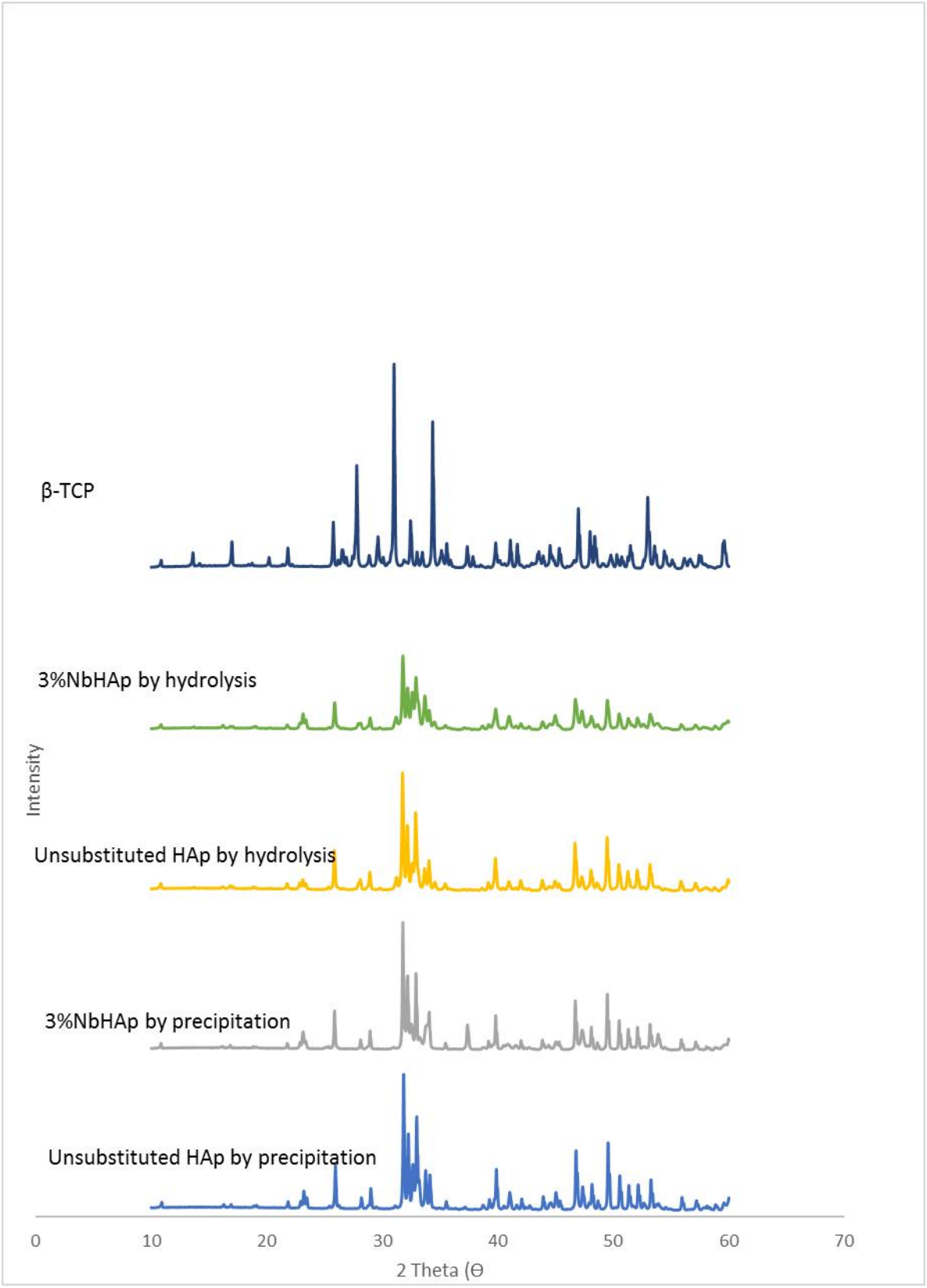

Figure 7-11: The XRD diffraction patterns of 3%NbHAp (3 wt.% niobate ions) materials prepared by precipitation and hydrolysis methods after sintering at 900˚C.

Fig. 7-11, displays the impact of substituting increasing levels of niobate ions from 1%NbHAp to 3%NbHAp, which caused:

1- A new peaks to appear when using the precipitation method at 2Θ = 37.40˚, coupled with a decreased intensity of two typical peaks that is related to an impurity phase β-TCP) at 2 Θ= 32.80˚ and 33.60˚. The new peak that appeared at 2 Θ = 37.40 ˚ can be ascribed to the CaO phase (reference card number 04-017-9575).

2- Also, an increase in the intensity of one typical peak that was ascribed to HAp phase at 2 Θ = 34.1˚ had been detected by the precipitation method.

On the other hand, the hydrolysis methods had not displayed an obvious difference that can be ascribed to an increase in the concentration of niobate ions which is supported by ICP-MS which showed there was no Nb associated with the HAp samples The only observation that was detected was an increase in the intensity of one peak related to the impurity phase at 2 Θ= 33.60˚, associated with a reduction in the intensity of one peak that can be attributed to HAp samples at 2 Θ = 34.10˚.

Crystallinity and crystallite size of 3% materials:

Table 7-10 displays the degree of crystallinity and the crystallite size of sintered 3% NbHAp (3 wt.% niobate ions) materials prepared by precipitation and hydrolysis methods.

Table 7-10: The degree of crystallinity and the crystallite size of 3% NbHAp (3 wt.% niobate ions) materials prepared by precipitation and hydrolysis methods after sintering at 900 ˚C.

Sample	D_{002} (Å)	Crystallinity %
Unsubstituted HAp by precipitation	618.3±3.2	84.15±2.4
3%NbHAp by precipitation	711.0±6.2	75.03±5.2
Unsubstituted HAp by hydrolysis	549.8±3.6	82.57±2.1
3%NbHAp by hydrolysis	418.3±4.4	72.97±3.8

Table 7-10 shows that the numerical values of the crystallinity have been reduced, this can be ascribed to the presence of Na^+ and CO_3^{2-} ions as confirmed by ICP-MS and FTIR analysis. In addition to the partial substitution of hydroxyl group by chloride ions as a result of using $NbCl_5$ in the synthesis. On the other hand, the value of crystallite size of the prepared 3%NbHAp samples

by precipitation method was enlarged due to the (Cl) substitution process, whereas a reduction in the value of crystallite size was produced by hydrolysis method.

Lattice parameters and volume of unit cell of prepared 3% NbHAp materials:

Table 7-11 shows the lattice parameters and the volume of hexagonal unit cell of the sintered 3% NbHAp (3 wt.% niobate ions) materials prepared by the precipitation and hydrolysis methods.

Table 7-11: The lattice parameters and the volume of hexagonal unit cell of 3% NbHAp (3 wt.% niobate ions) prepared by precipitation and hydrolysis methods after sintering at 900 ˚C.

Sample	a [Å]	c [Å]	V[Å^3]
Unsubstituted HAp by precipitation	9.416±0.004	6.879±0.003	1579±0.004
3% NbHAp by precipitation	9.419±0.005	6.885±0.003	1581±0.004
Unsubstituted HAp by hydrolysis	9.421±0.003	6.882±0.005	1581±0.004
3% NbHAp by hydrolysis	9.422±0.002	6.883±0.004	1582±0.003

An increase in both lattice parameters (a and c) were recorded by both methods, which caused an expansion in the volume of unit cell of the whole prepared materials, especially when the precipitation method was used. As discussed previously, this result could not be ascribed to the replacement of phosphate by niobate ions, since niobate ions were not detected by ICP-MS analysis. This expansion obtained by both methods can be ascribed to the substitution of chloride ions which have larger ionic radius (1.81 Å) [123] compared to hydroxyl group(1.68 Å).

SEM of 3% NbHAp (3 wt.% niobate ions) materials prepared by precipitation and hydrolysis methods:

SEM of non-sintered 3% NbHAp (3 wt.% niobate ions) materials prepared by precipitation and hydrolysis methods:

Fig.7-12. displays the SEM images of non-sintered 3% NbHAp powders prepared by hydrolysis and precipitation methods.

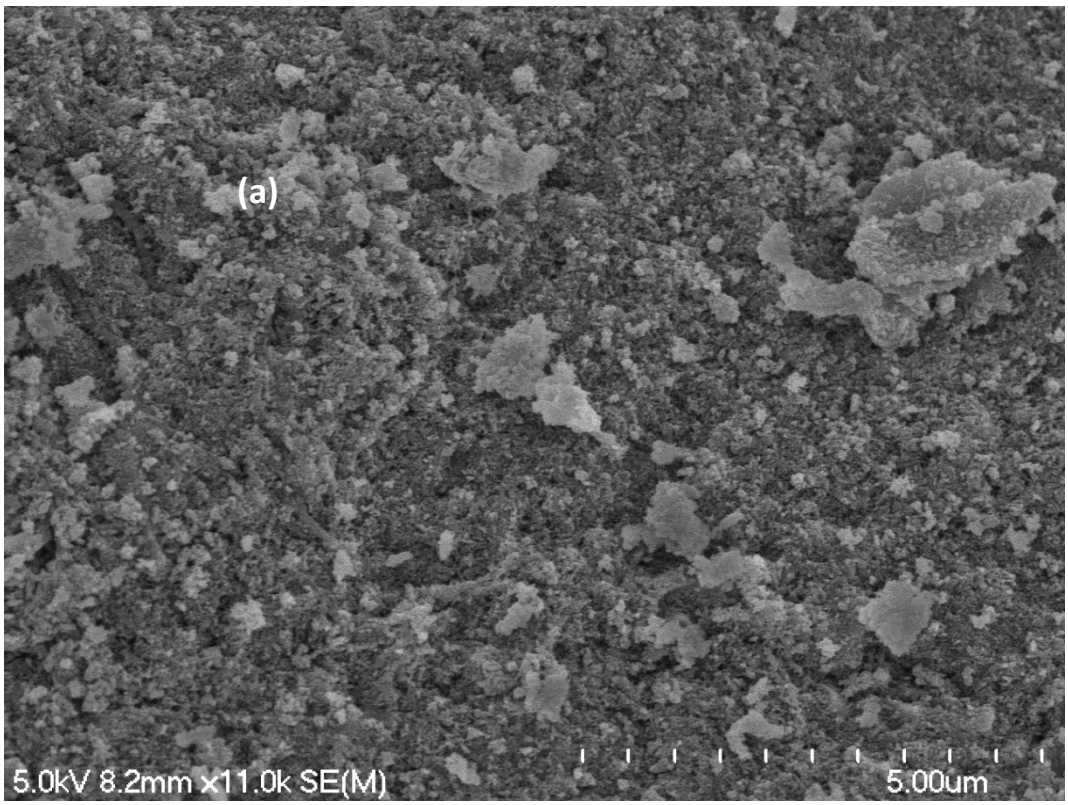
(a)
5.0kV 8.2mm x11.0k SE(M)
5.00um

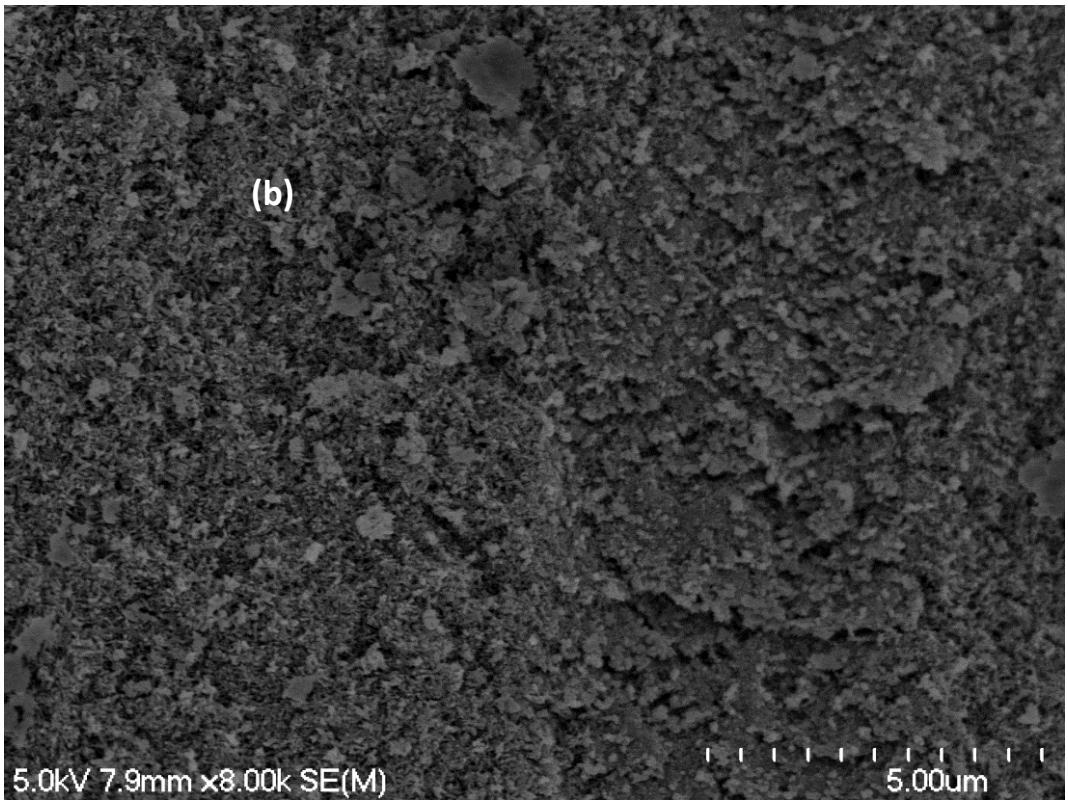
(b)
5.0kV 7.9mm x8.00k SE(M)
5.00um

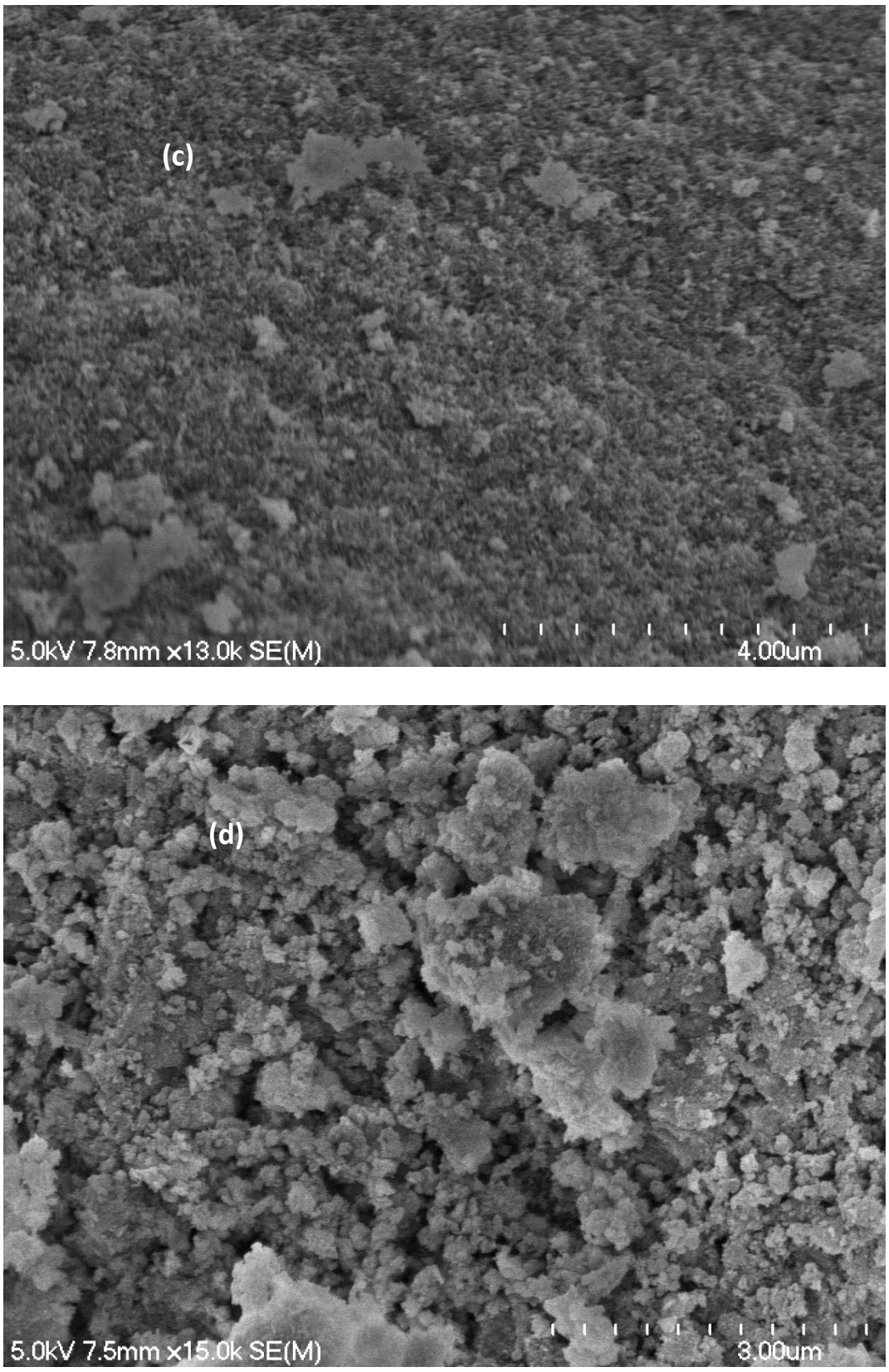

Figure 7-12: SEM images of non-sintered (a) Unsubstituted HAp by precipitation (b)Unsubstituted HAp by hydrolysis (c) 3%NbHAp by precipitation (d)3%NbHAp by hydrolysis.

As detected by SEM images, the observed morphology of the samples which were prepared by both methods were not different from each other. The spheroidal-like shape associated with a trend to agglomerate were produced by both routes (precipitation and hydrolysis methods).

SEM of 3% NbHAp (1 wt.% niobate ions) materials prepared by precipitation and hydrolysis methods after sintering at 900 ˚C:

Figure 7-13 shows the morphology of the sintered 3%NbHAp materials prepared by using different synthesis routes (the conventional precipitation and novel hydrolysis methods).

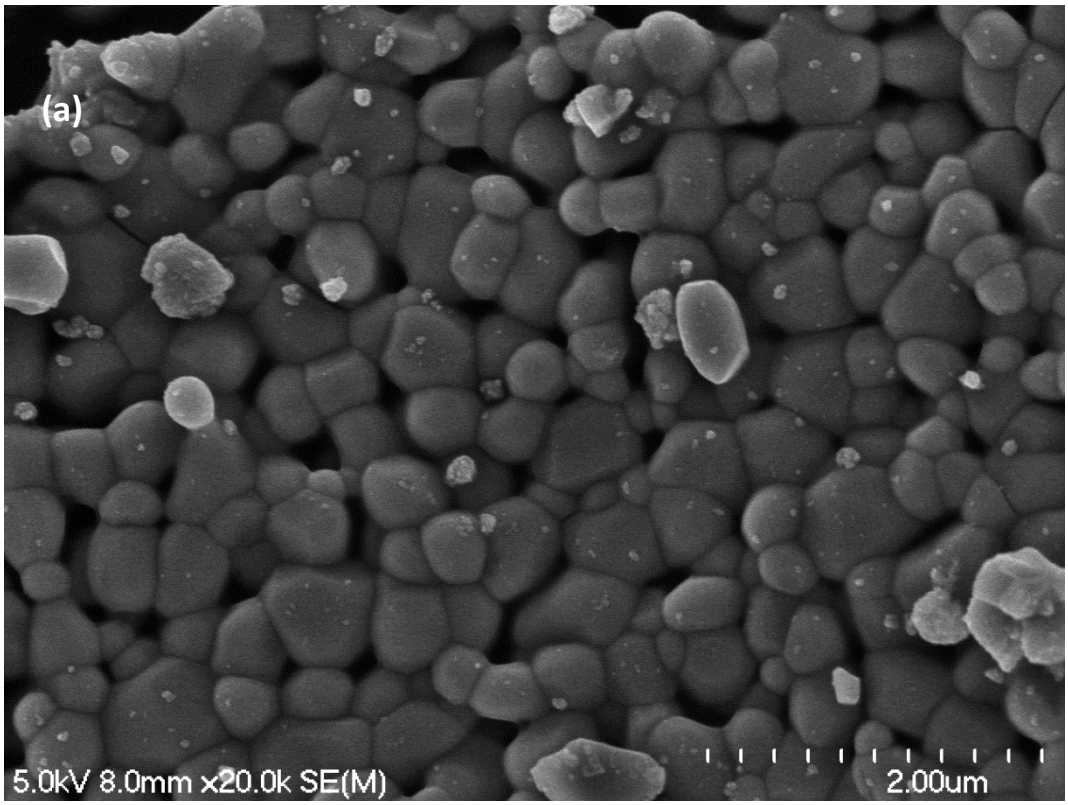

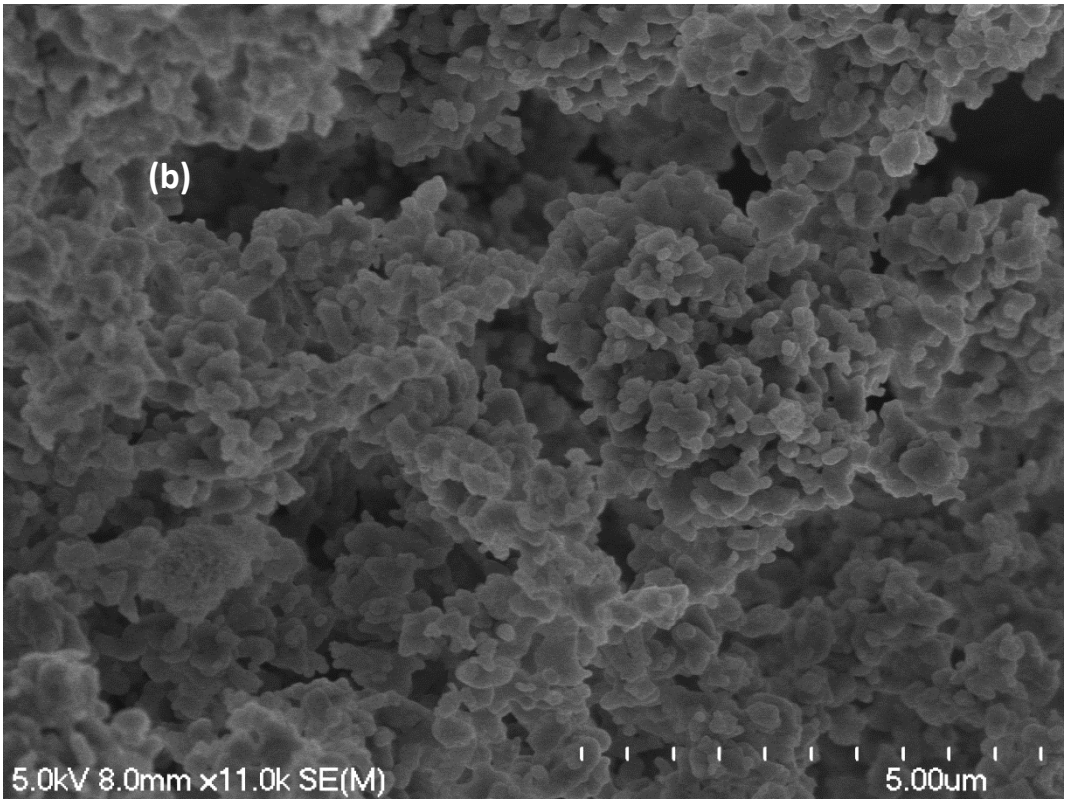
(b)
5.0kV 8.0mm x11.0k SE(M)
5.00um

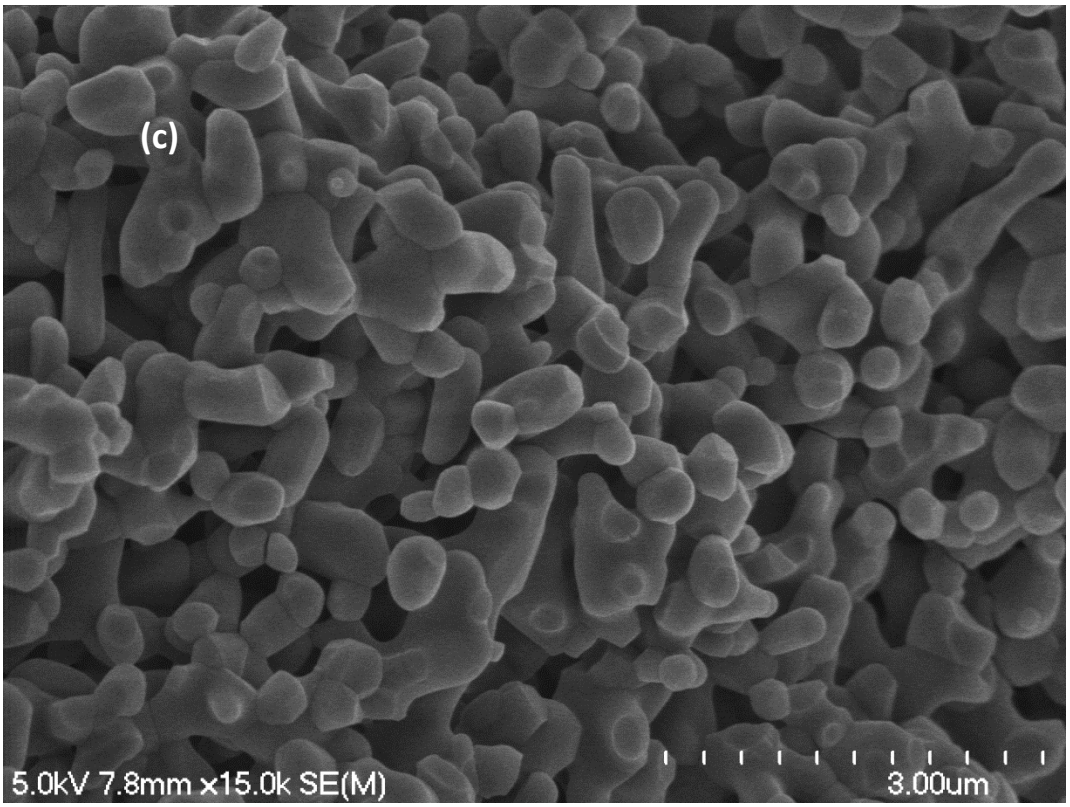
(c)
5.0kV 7.8mm x15.0k SE(M)
3.00um

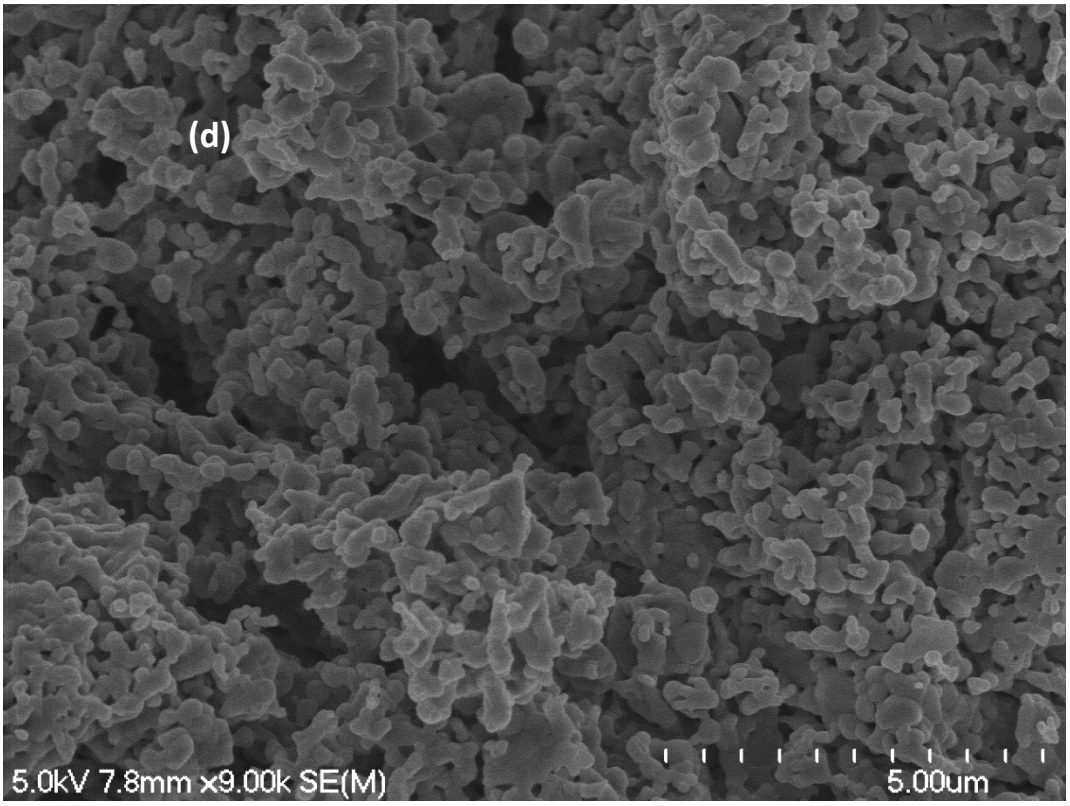

Figure 7-13: SEM of (a) Unsubstituted HAp by precipitation (b)Unsubstituted HAp by hydrolysis (c) 3%NbHAp by precipitation (d) 3%NbHAp by hydrolysis, after sintering at 900 ˚C.

The spheroidal shape with small quantity of rod-like shapes resulted from the precipitation method. On the other hand, the SEM images showed that the hydrolysis method produced spherical shaped particles coupled with an irregular distribution, a high level of porosity coupled with a high ability to agglomerate.

7.2.3 5% NbHAp (5 wt.% niobate ions) powders prepared by precipitation and hydrolysis methods:

One series of 5% NbHAp material (5 wt.% niobate ions) was prepared by using two different synthesis routes (precipitation and hydrolysis), and the detailed amounts of the reagents were listed in the **table 7-3**.

7.2.3.1 Characterization techniques of 5% NbHAp (*5* wt.% niobate ions) materials prepared by precipitation and hydrolysis methods.

ICP-MS of* 5% NbHAp *(5 wt.% niobate ions) materials prepared by precipitation and hydrolysis methods, after sintering 900 ˚C.

The results of the elemental analyses of 5% NbHAp samples that were prepared by precipitation and hydrolysis routes are displayed in **Table 7-12 .**

Table 7-12: ICP-MS results of *5*% NbHAp (5 wt.% niobate ions) materials prepared by precipitation and hydrolysis methods after sintering at 900 C˚. The concentration was in ppb (ug/L):

Sample	Ca 44	P 31	Na 23	Nb 93
Unsubstituted HAp by precipitation	707795	401240	103797	-
5% NbHAp by precipitation	678563	359133	114200	-
Unsubstituted HAp by hydrolysis	769928	423970	78396	-
5% NbHAp by hydrolysis	673498	399577	97200	-

The starting (calculated) and actual (measured) degree of chemical composition of the prepared powders in terms of wt.% of niobate ions, the calcium/phosphorus (Ca/P) molar ratios as well as (Ca+Na)/P molar ratio were determined by ICP-MS and presented in **Table 7-13.**

Table 7-13: The chemical analysis data of 5%NbHAp (5 wt.% niobate ions) materials by ICP-MS measurements after sintering at 900 ˚C.

Sample	Ca/P Theoretical	Ca/P Measured	(Ca+Na+Nb)/P	Wt.% niobate ions theoretical	Wt.% niobate ions Measured
Unsubstituted HAp by precipitation	1.67	1.36	1.71	-	-
5% NbHAp by precipitation	1.74	1.46	1.89	5%	-
Unsubstituted HAp by hydrolysis	1.67	1.40	1.65	-	-
5% NbHAp by hydrolysis	1.74	1.30	1.63	5%	-

Once again, the increase in substitution levels of niobium ions has not made any difference , since **Tables 7-12** and **7-13** show clearly that Nb was not detected in the prepared samples. The Ca: P mole ratios were lower than expected due to the existence of sodium ions. The (Ca+Na)/ P by precipitation were found to be higher than supposed value (1.67) due to the replacement process of carbonate group, but that value achieved by hydrolysis method was found to be close to the expected value.

FTIR of 5% NbHAp (5 wt.% niobate ions) materials prepared by precipitation and hydrolysis methods:

*FTIR of non-sintered 5%NbHAp (**5** wt.% niobate ions) materials prepared by precipitation and hydrolysis:*

The FTIR spectra of the non-sintered 5%NbHAp samples prepared by precipitation and hydrolysis methods are shown in **Fig. 7-14**

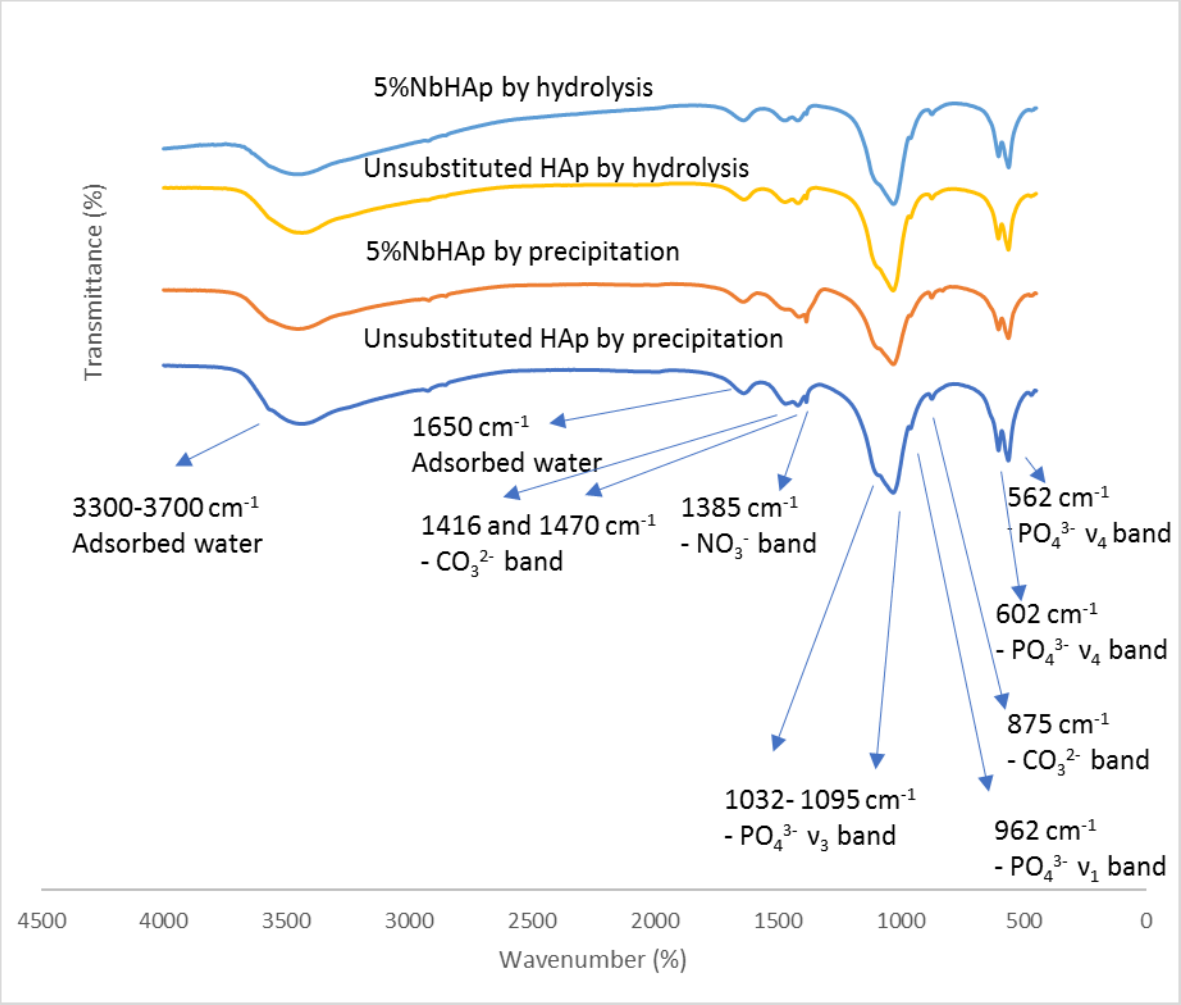

Figure 7-14: FTIR of non-sintered 5% NbHAp (5 wt.% niobate ions) materials prepared by precipitation and hydrolysis methods.

The broad band at 3300 - 3700 cm^{-1} and the peak at 1635 cm^{-1} in the whole prepared powders can be attributed to the absorbed water. The doublet band at 1028–1090 cm^{-1} was assigned to the P–O stretching vibration of the phosphate groups (PO_4^{3-}), while the band at 568–605 cm^{-1} which appears as a doublet was also ascribed to the PO_4^{3-} bending mode. The small bands at about 1416 and 1465 cm^{-1} are related to CO_3^{2-} group indicating the formation of CO_3HAp (B-type). In the case of the precipitation method, the visible band recorded at 1385 cm^{-1} refers to the nitrate group (NO_3^-), that may be present as a result of either the starting materials or contamination in the KBr used to make the pellets.

*FTIR of 5% NbHAp (**5** wt.% niobate ions) materials prepared by precipitation and hydrolysis methods after sintering at 900 ˚C:*

The FTIR spectra of the sintered 5%NbHAp powders prepared by different methods (the precipitation and hydrolysis) are shown in **Fig.7-15**.

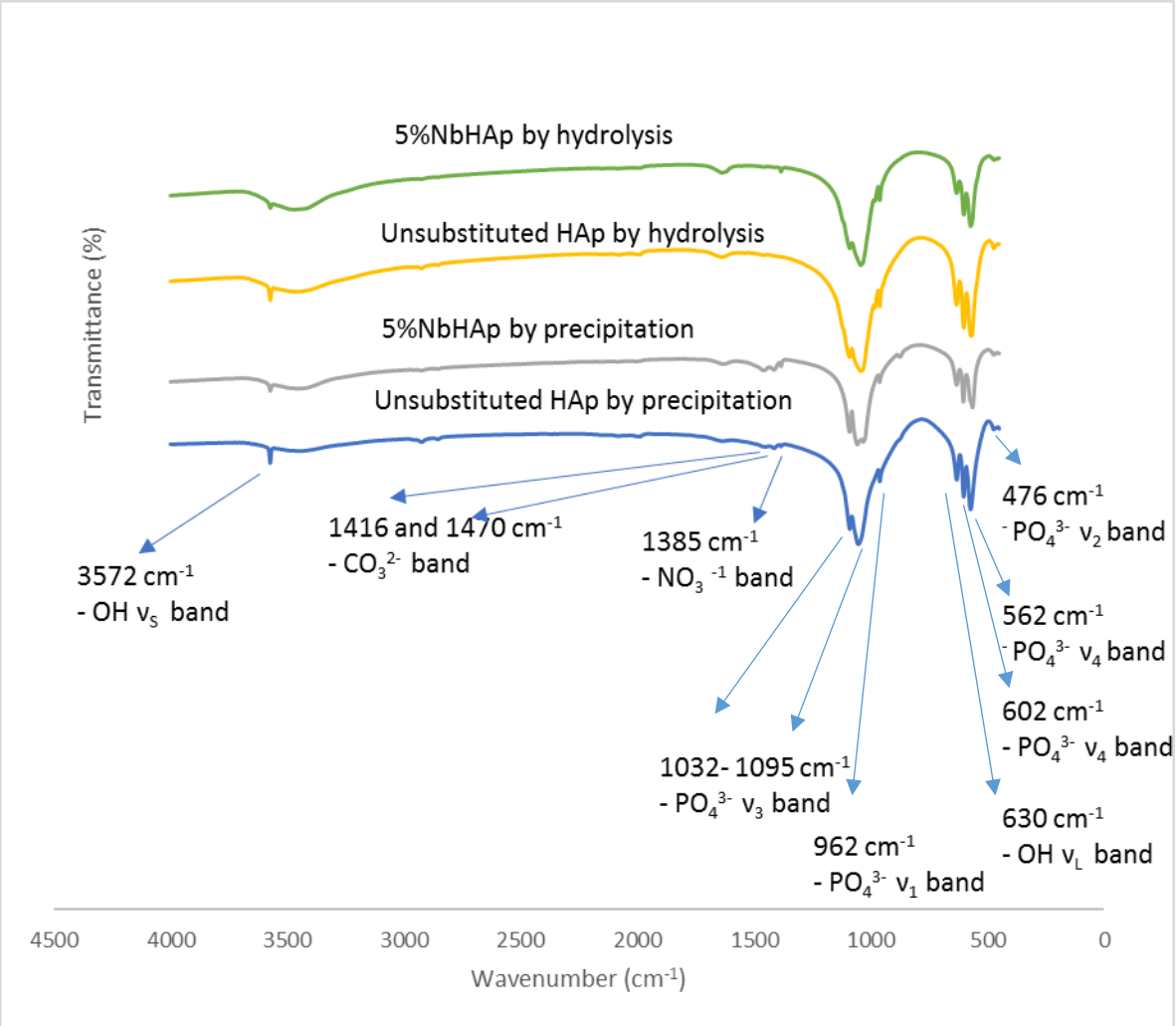

Figure 7-15: FTIR of 5% NbHAp (5 wt.% niobate ions) materials prepared by precipitation and hydrolysis methods after sintering at 900 ˚C.

The characteristic bands of HAp were confirmed in the whole prepared materials. The vibrational and stretching modes of hydroxyl group appeared at 632 and 3571 cm^{-1}, while the characteristic bands of phosphate group were recorded at 570, 603, 963, 1028-1070 cm^{-1}. In contrast, the fundamental peaks of the carbonate group appeared in the whole prepared 5% NbHAp powders that were synthesized by the precipitation method at 875, 1411 and 1452 cm^{-1} so indicating the

formation of carbonated HAp, but in the case of hydrolysis method the carbonate bands disappeared due to the heating process. Also, **Fig. 7-15** showed that a clear reduction in the intensity of the stretching modes of the OH^- group at 3572 cm^{-1} in the whole prepared 5%NbHAp samples. This reduction in the intensity of stretching mode are associated with the appearance of a well-defined peak, which corresponded to carbonate group at 875 cm^{-1}. The reduction in intensity can be ascribed to:

1- The partial substitution of hydroxyl group by chloride ions. The substitution of Cl^- ions occurred as a result of using $NbCl_5$ in the synthesis of HAp. Therefore, reduction in the stretching mode of lattice OH at (3752 cm^{-1}) was observed.
2- The presence of sodium ions, coupled with the formation of CO_3HAp materials in the whole 5% NbHAp samples which were prepared by the precipitation method. Therefore, the OH^- ion content was derived by the requirement to keep charge balance and to restore the neutrality of HAp crystals as discussed earlier in Chapter 6 (see FTIR of sintered RbHAp samples for details).

XRD diffraction patterns of 5% NbHAp (5 wt.% niobate ions) materials prepared by precipitation and hydrolysis methods:

Phase Identification of 5% NbHAp materials:

The XRD patterns of the non-sintered and sintered 5% NbHAp samples prepared by different methods (precipitation and hydrolysis) are shown in **Fig.7-16 and Fig.7-17,** respectively.

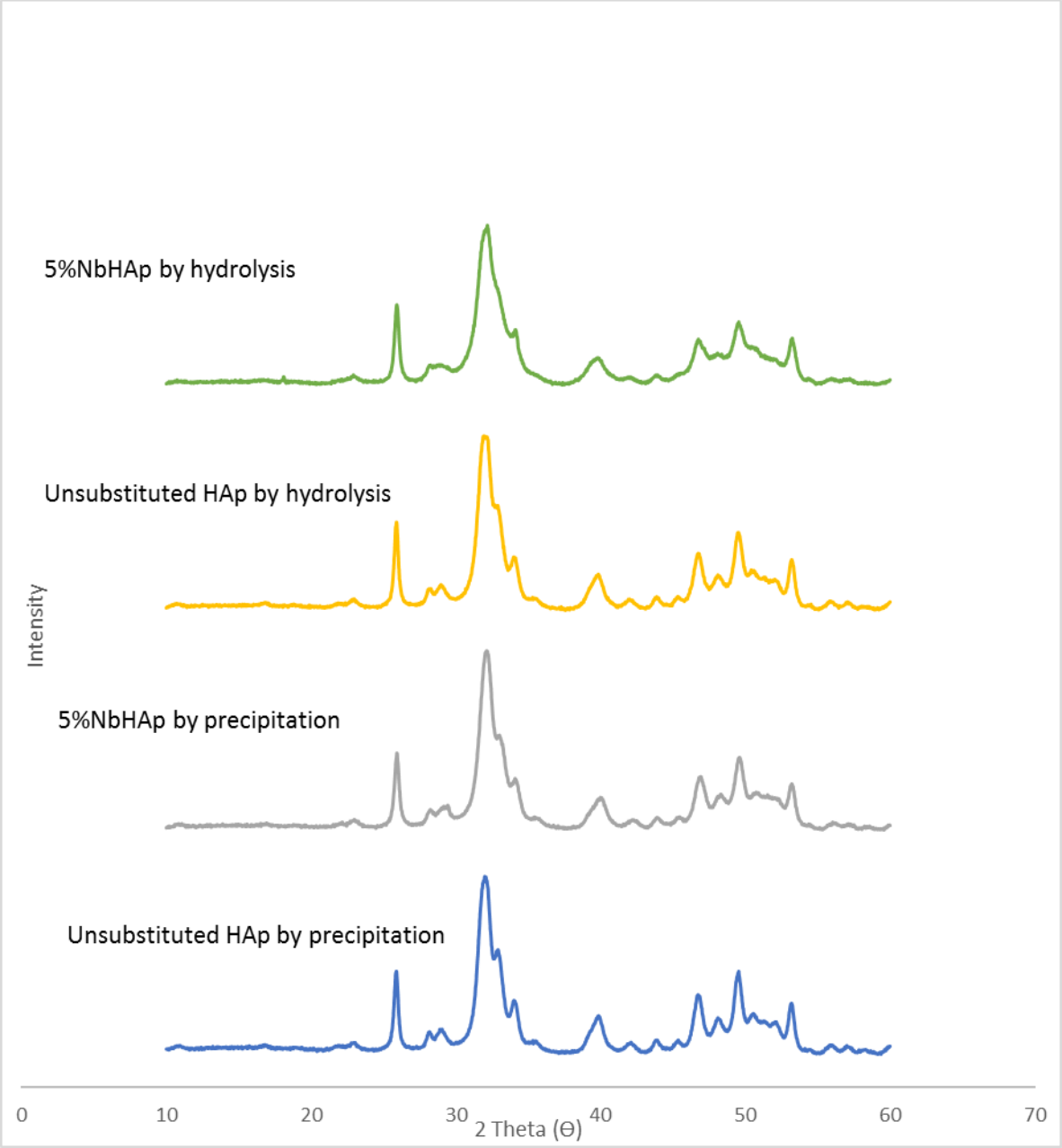

Figure 7-16: The XRD diffraction patterns of the non-sintered 5%NbHAp (5 wt.% niobate ions) materials prepared by precipitation and hydrolysis methods.

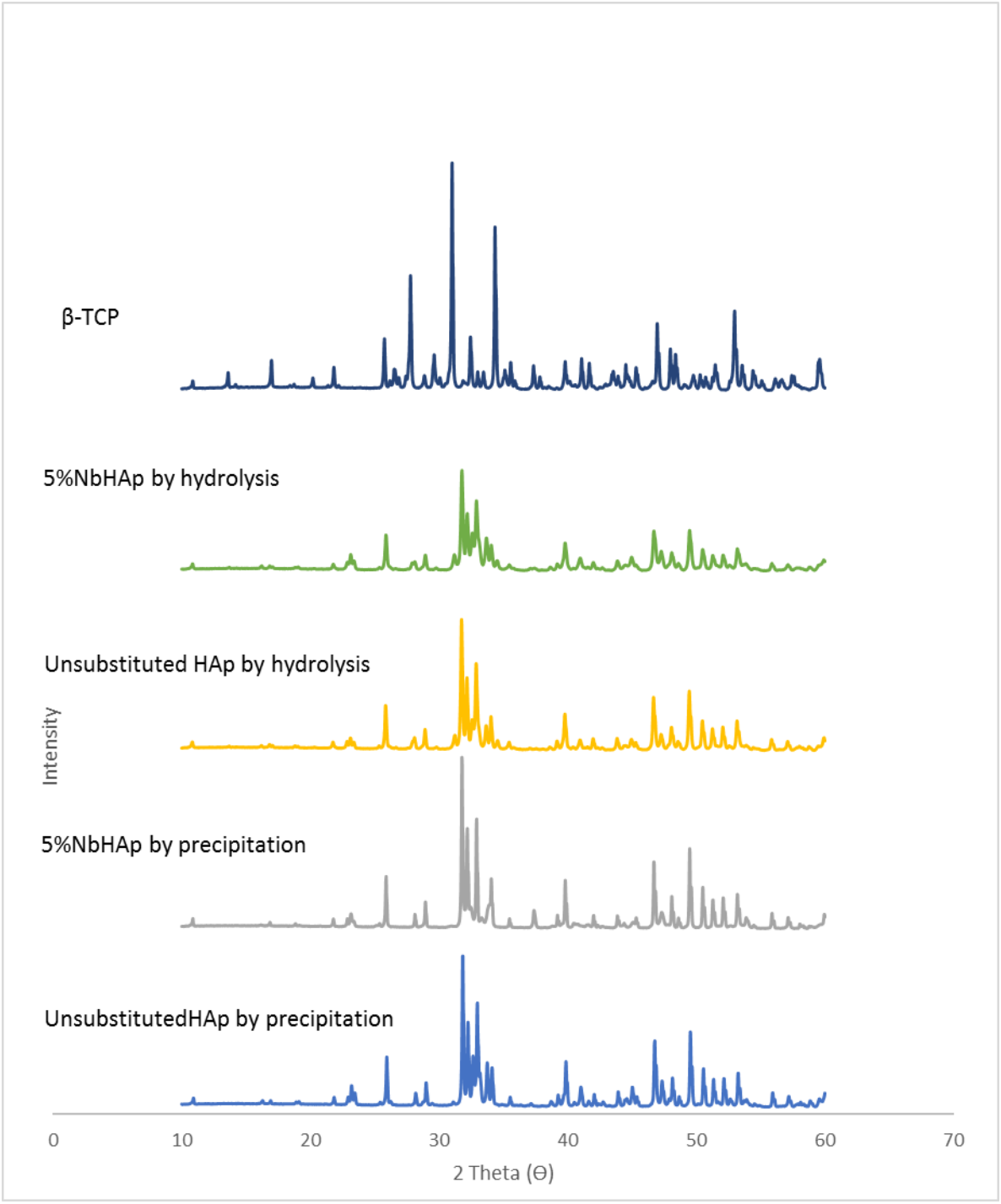

Figure 7-17: The XRD diffraction patterns of 5% NbHAp (5 wt.% niobate ions) materials prepared by precipitation and hydrolysis methods after sintering at 900 ˚C.

Fig. 7-17, which displays the increased level of substitution from 1%NbHAp to 5%NbHAp in the HAp samples by the precipitation method caused the following:

1- A new peak to appear by precipitation method at 2Θ = 37.40°. This peak that appeared at 37.40˚ is attributable to CaO (reference card number 04-017-9575).
2- The disappearance of two typical peaks that are related to impurity phase (β-TCP) at 2 Θ= 32.80˚ and 33.60˚, and also an increase in the intensity of one typical peaks of HAp phase at 2Θ= 34.10˚.

On the other hand, the substitution process by hydrolysis methods showed an increase in the intensity of one peak that was related to an impurity phase at 33.6˚, coupled with a reduction in the intensity of one peak that can be attributed to HAp samples at 2Θ = 34.1˚.

Crystallinity and crystallite size of prepared 5%NbHAp materials:

Table 7-14 shows the degree of crystallinity and crystallite size of the sintered 5% NbHAp (5 wt.% niobate ions) materials prepared by precipitation and hydrolysis methods.

Table 7-14: The degree of crystallinity and crystallite size of 5%NbHAp (5 wt.% niobate ions) materials prepared by precipitation and hydrolysis methods after sintering at 900 ˚C.

Sample	D_{002} (Å)	Crystallinity %
Unsubstituted HAp by precipitation	618.3±3.2	84.15±2.4
5% NbHAp by precipitation	836.5±6.6	78.83±6.2
Unsubstituted HAp by hydrolysis	549.8±3.6	82.57±2.1
5% NbHAp by hydrolysis	418.3±4.6	68.80±4.2

The numerical values of crystallinity of the whole prepared samples were varied due to an increase in the substitution level, as shown in (**Table 7-14**). A clear reduction in the value of crystallinity by hydrolysis route had been achieved, whereas a slight reduction was recorded by precipitation route. The calculated value of the crystallite size of the prepared 5%NbHAp samples by using the precipitation route showed an increase. On the other hand, the hydrolysis route led to a clear reduction in the value of crystallite size, which reflects the effect of synthesis route on the crystallinity as well as crystallite size. In the present study, the effect of substitution process on the numerical values of crystallinity and crystallite size can be ascribed to:

1- The presence of Na^+ and CO_3^{2-} ions into HAp samples as confirmed by ICP-MS analysis and FTIR spectra. 2- The partial substitution of hydroxyl group by chloride ions as a result of using $NbCl_5$ as a starting material.

Lattice parameters and volume of unit cell of prepared 5%NbHAp materials:

Table 7-15 displays the lattice parameters and the volume of hexagonal unit cell of the sintered 5% NbHAp (5 wt.% niobate ions) prepared by precipitation and hydrolysis methods.

Table 7-15: The lattice parameters and the volume of hexagonal unit cell of 5% NbHAp (5 wt.% niobate ions) prepared by precipitation and hydrolysis methods after sintering at 900 ˚C.

Sample	a [Å]	c [Å]	V[Å^3]
Unsubstituted HAp by precipitation	9.416±0.004	6.879±0.003	1579±0.004
5%NbHAp by precipitation	9.422±0.005	6.884±0.005	1582±0.005
Unsubstituted HAp by hydrolysis	9.421±0.003	6.882±0.005	1581±0.004
5%NbHAp by hydrolysis	9.423±0.003	6.882±0.004	1582±0.004

An increase in both lattice parameters (a and c) and in the volume of unit cell were recorded by the both routes, This result can be attributed to replacement process of chloride ions with bigger ionic radius (1.81 Å) compared to hydroxyl group(1.68 Å) [123].

SEM of 5%NbHAp (5 wt.% niobate ions) materials prepared by precipitation and hydrolysis methods:

SEM of the non-sintered 5% NbHAp (5 wt.% niobate ions) materials prepared by precipitation and hydrolysis methods powders:

Fig.7-18. displays the SEM images of the non-sintered 5% NbHAp powders prepared by hydrolysis and precipitation methods.

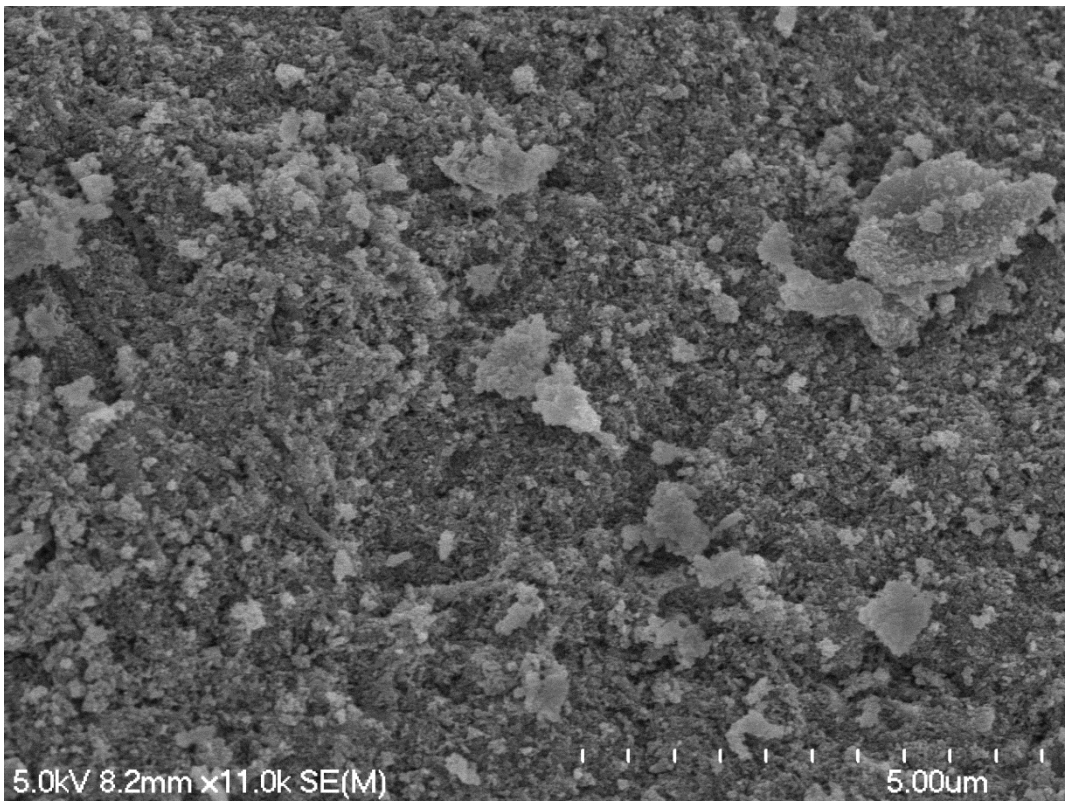
5.0kV 8.2mm x11.0k SE(M)
5.00um

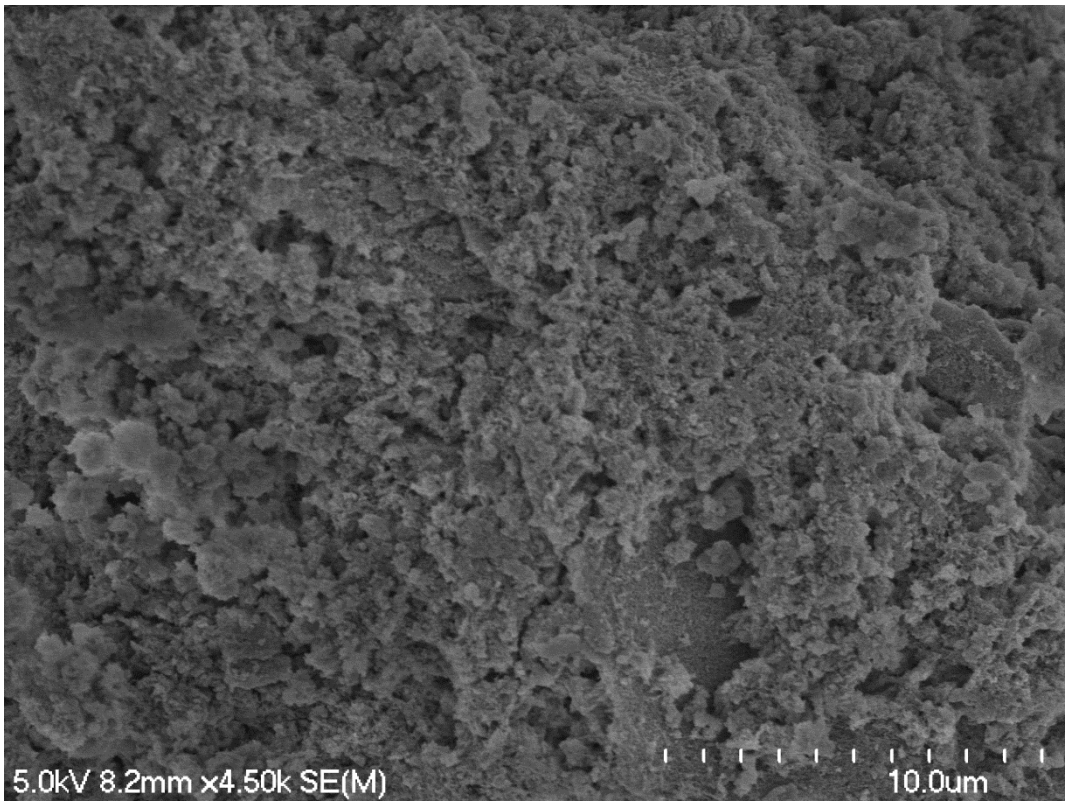
5.0kV 8.2mm x4.50k SE(M)
10.0um

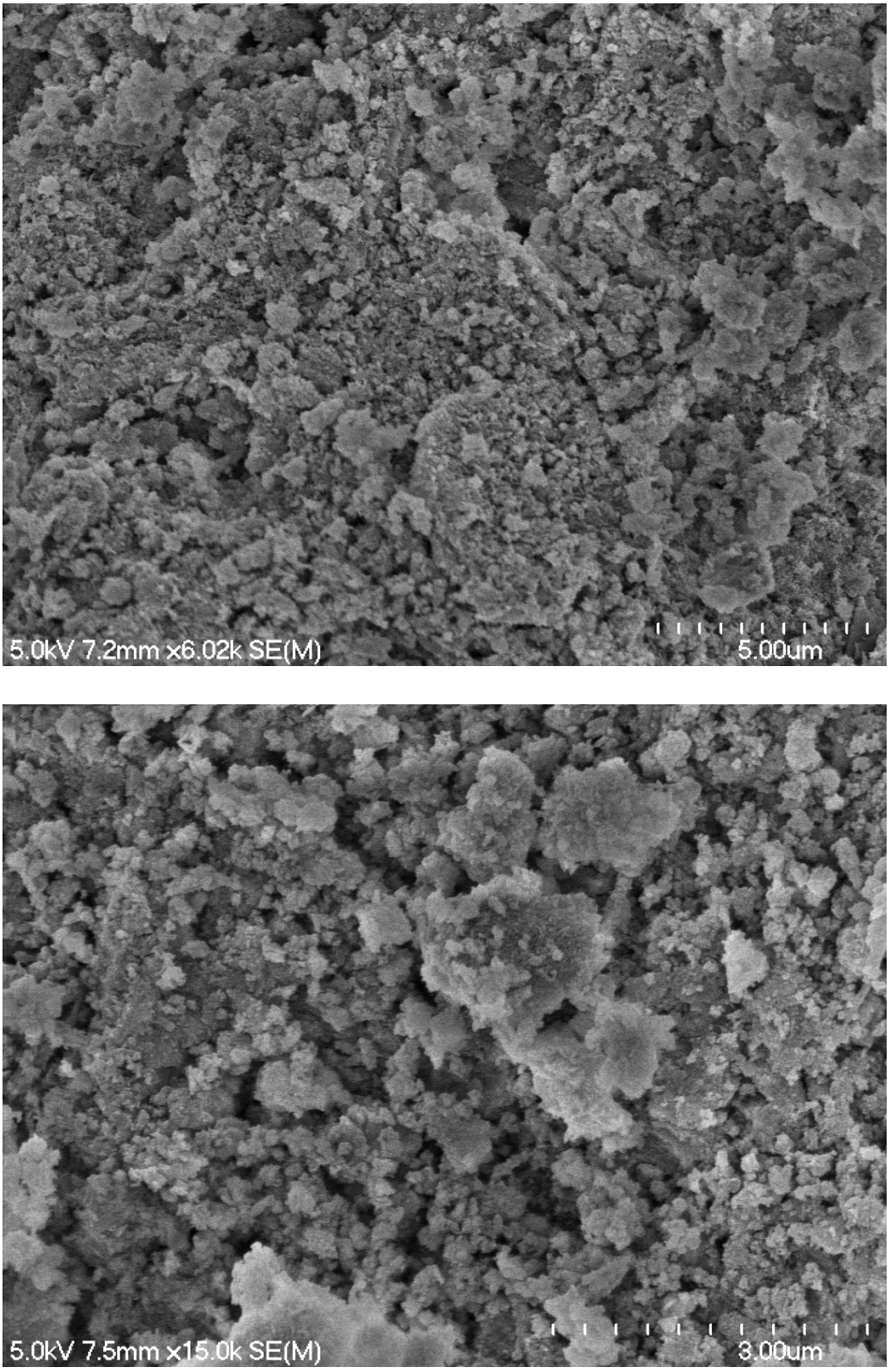

Figure 7-18: SEM images of (a)Unsubstituted HAp by precipitation (b)Unsubstituted HAp by hydrolysis (c) 5%NbHAp by precipitation (d)5%NbHAp by hydrolysis.

SEM images showed the observed morphology of the prepared samples by both routes had not varied due to substitution process of niobate ions into HAp samples. A spheroidal-- like shape associated with a trend to agglomerate was recorded.

SEM of 5%NbHAp (5 wt.% niobate ions) materials prepared by precipitation and hydrolysis methods after sintering at 900 ˚C:

Fig.7-19 shows the SEM images of the sintered 5% NbHAp powders as prepared by the novel hydrolysis and precipitation methods.

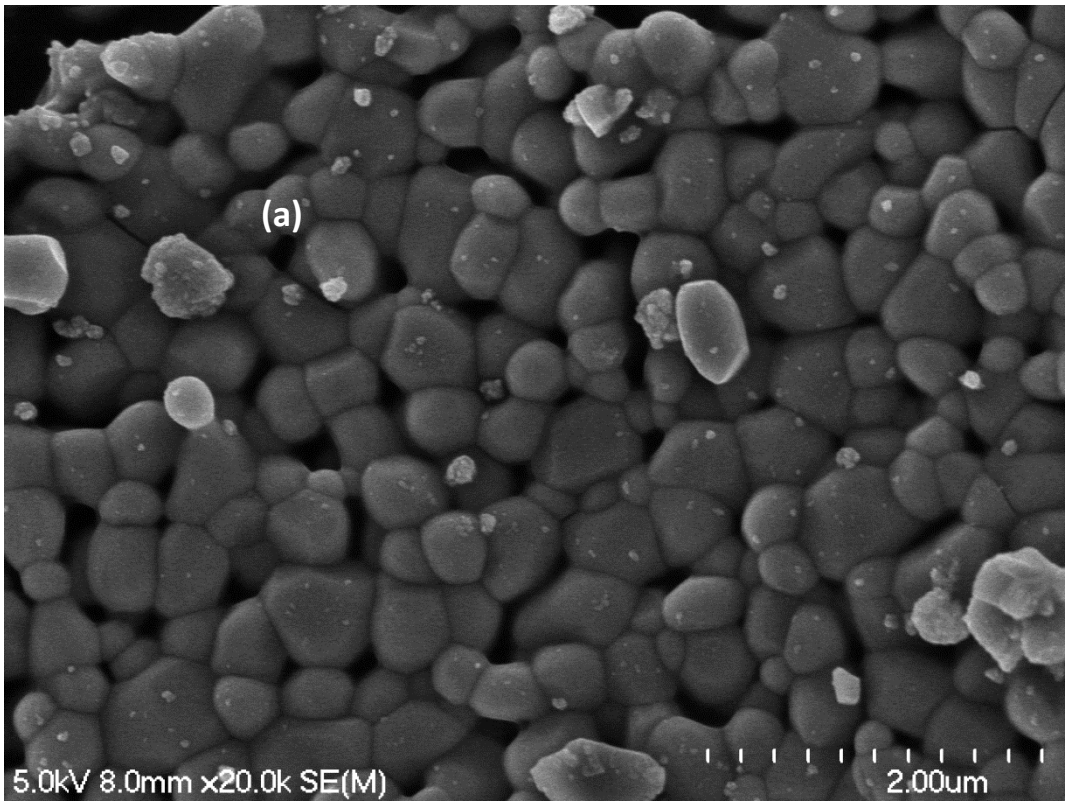

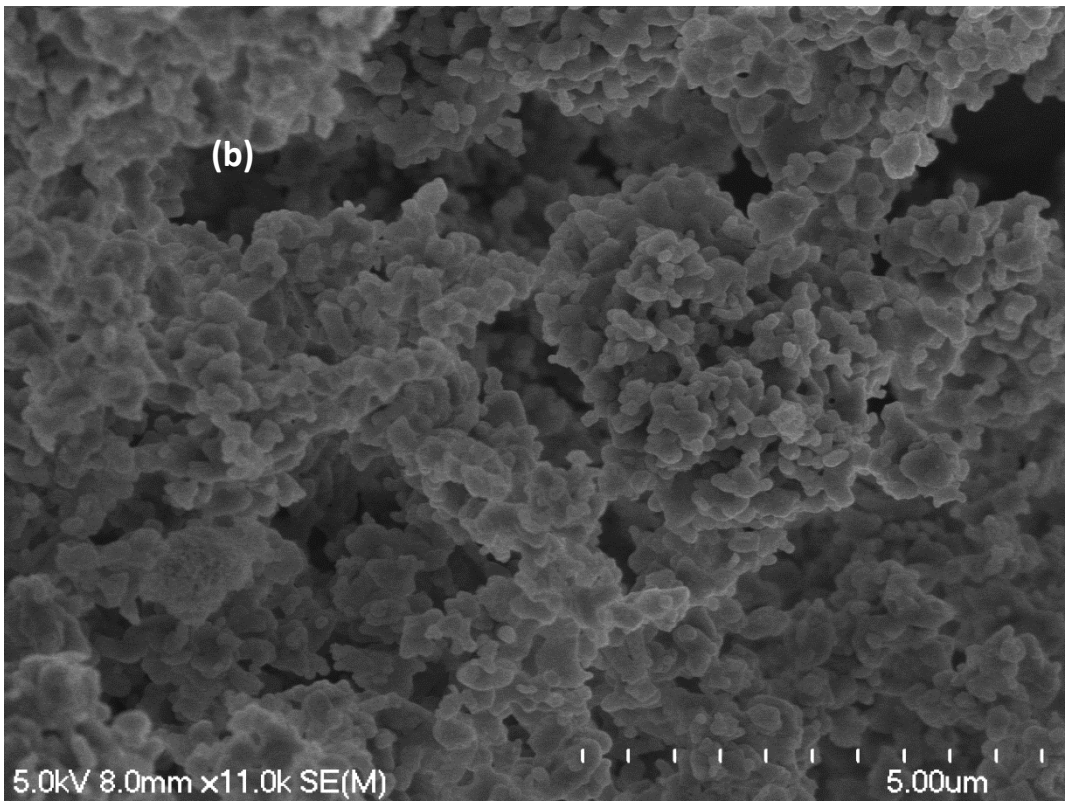
(b)
5.0kV 8.0mm x11.0k SE(M)
5.00um

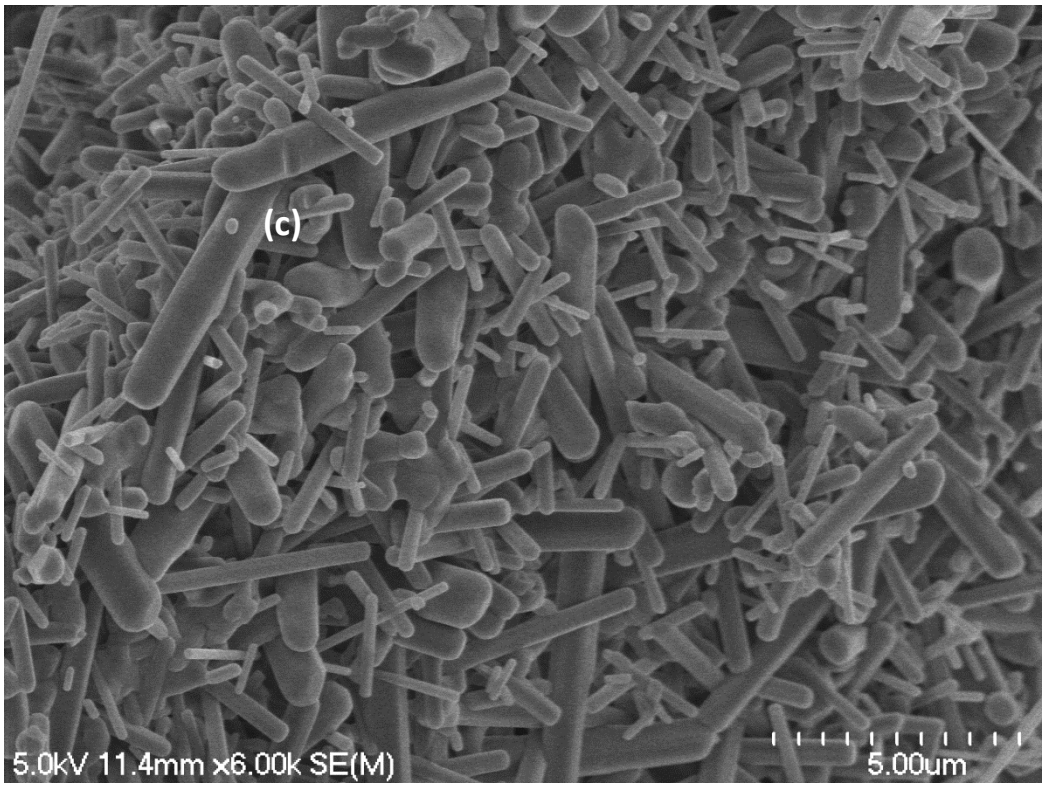
(c)
5.0kV 11.4mm x6.00k SE(M)
5.00um

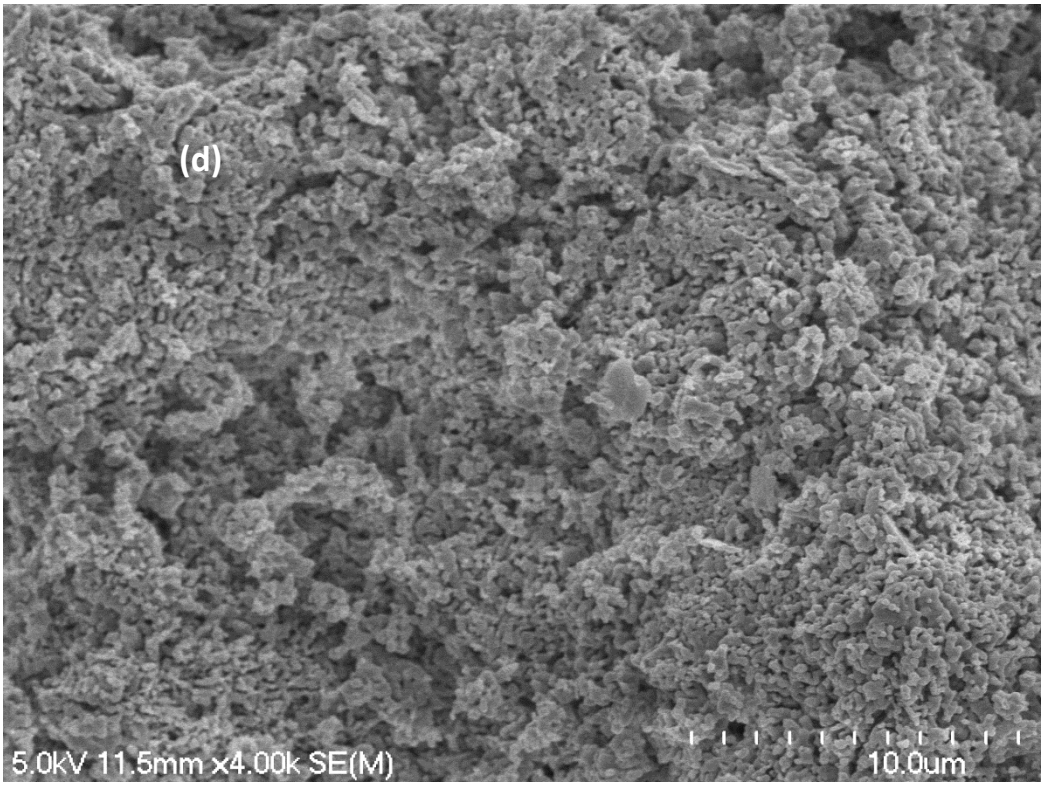

Figure 7-19: SEM images of (a) Unsubstituted HAp by precipitation (b) Unsubstituted HAp by hydrolysis (c) 5%NbHAp by precipitation (d) 5%NbHAp by hydrolysis, after sintering at 900 ˚C.

While the rod-like shape was produced by precipitation method, the hydrolysis method led to the production of an irregular structure with a high tendency to agglomerate, and an enhancement in the level of porosity was recorded by SEM images. Such a result confirmed the effect of the preparation method on the morphology.

7.3 1% B_4O_7HAp (1 wt.% $B_4O_7^{2-}$) powders prepared by precipitation and hydrolysis methods:

In this project, one series of 1% B_4O_7HAp (1 wt.% $B_4O_7^{2-}$) materials were prepared by using precipitation and hydrolysis methods. The detailed amounts of the reagents that used to prepare 1% B_4O_7HAp powders are listed in the **Table 7-16.**

Table 7-16: Synthesis details of 1% B_4O_7HAp (1 wt.% $B_4O_7^{2-}$) materials prepatred by precipitation and hydrolysis methods.

Sample name	MCPM (g)	$Ca(OH)_2$ (g)	$Ca(NO_3)_2$ (g)	Na_2HPO_4 (g)	$Na_2B_4O_7.10H_2O$ (g)	MCPM ($Ca(H_2PO_4)_2.H_2O$) (mol)	$Ca(OH)_2$ (mol)	$Ca(NO_3)_2$ (mol)	Na_2HPO_4 (mol)	$Na_2B_4O_7.10H_2O$ (mol)
B_4O_7HAp by hydrolysis	12.5013	3.6697	-	-	0.1230	0.0496	0.0495	-	-	0.0003
B_4O_7HAp by precipitation	-	-	8.1365	4.1784	0.1239	-	-	0.0496	0.0294	0.0003

7.3.1 Characterization techniques of prepared 1% B_4O_7HAp (1 wt.% B_4O_7) materials prepared by precipitation and hydrolysis methods:

7.3.1.1 ICP-MS of 1% B_4O_7HAp (1 wt.% $B_4O_7^{2-}$) materials prepared by precipitation and hydrolysis methods, after sintering at 900 ˚C:

The results of the elemental analyses of 1%B_4O_7HAp samples that were prepared by precipitation and hydrolysis routes are displayed in **Table 7-17 .**

Table 7-17: ICP-MS results of 1%B_4O_7HAp (1 wt.% $B_4O_7^{2-}$) materials prepared by precipitation and hydrolysis methods after sintering at 900 ˚C. The concentration is reported in ppb (ug/L):

Sample	Ca 44	P 31	Na 23	B 11
Unsubstituted HAp by precipitation	707795	401240	103797	-
1% B_4O_7HAp by precipitation	768865	362636	88590	5890.2
Unsubstituted HAp by hydrolysis	759928	423970	78396	-
1% B_4O_7HAp by hydrolysis	676696	391910	127512	901.5

The starting (calculated) and actual (measured) degree of chemical composition of the prepared powders in terms of wt.% of $B_4O_7^{2-}$ ions, the calcium/phosphorus (Ca/P) molar ratios as well as (Ca+Na)/P molar ratio were determined by ICP-MS and presented in **Table 7-18.**

Table 7-18: The chemical analysis data of 1% B_4O_7HAp (1 wt.% $B_4O_7^{2-}$) materials by ICP-MS measurements after sintering at 900 ˚C.

Sample	Ca/P Theoretical	Ca/P Measured	(Ca+Na)/(P+B)	Wt. % $B_4O_7^{2-}$ ions theoretical	Wt. % $B_4O_7^{2-}$ ions measured
Unsubstituted HAp by precipitation	1.67	1.36	1.71	-	-
1% B_4O_7HAp by precipitation	1.69	1.64	1.88	1%	0.30%
Unsubstituted HAp by hydrolysis	1.67	1.40	1.65	-	-
1% B_4O_7HAp by hydrolysis	1.69	1.33	1.76	1%	0.05%

Tables 7-17 and 7-18, show the presence of borate and Na^+ ions in the HAp samples, whereas the experimental values of (Ca+Na)/(P+B) mole ratios for the prepared borate substituted hydroxyapatite powders by precipitation and hydrolysis methods were (1.88 and 1.76), respectively. However, these values were higher than the expected values of stoichiometric HAp, indicating the substitution of phosphate site by carbonate group (as detected by FTIR spectra), as well (possibly) as by the borate group.

7.3.1.2 FTIR of 1% B_4O_7HAp (1 wt.% B_4O_7) materials prepared by precipitation and hydrolysis methods.

FTIR of the non-sintered 1% B_4O_7HAp (1 wt.% B_4O_7) materials prepared by precipitation and hydrolysis methods at room temperature.

Fig.7-20 shows the FTIR spectra of the non-sintered 1%B_4O_7HAp material prepared by different synthesis routes.

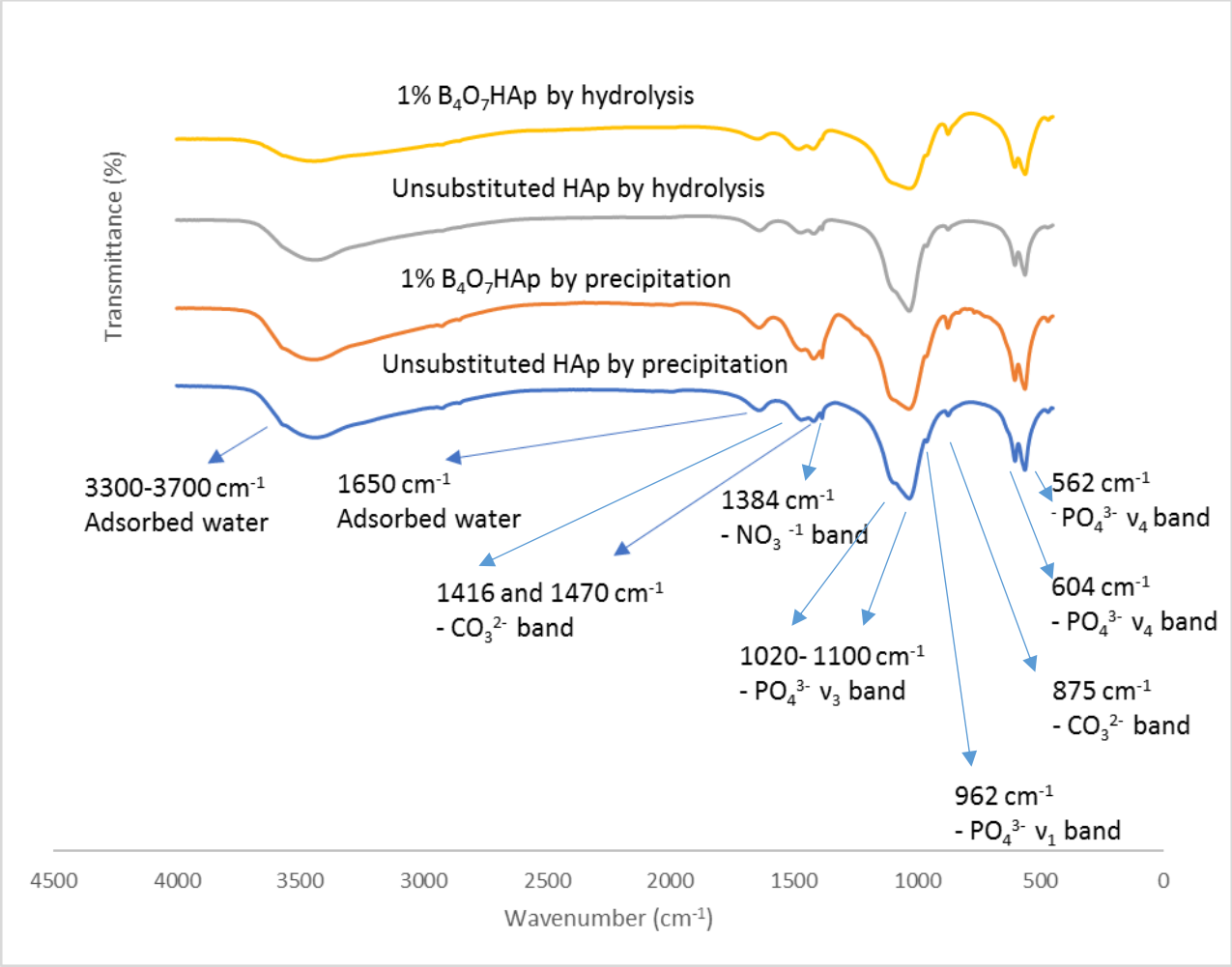

Figure 7-20: FTIR spectra of the non-sintered 1%B_4O_7HAp (1 wt.% B_4O_7) materials prepared by precipitation and hydrolysis methods.

An amorphous/poorly crystalline material was produced, which was confirmed by FTIR through the absence of fundamental peaks of hydroxyl group at 630 and 3572 cm^{-1} and broadening of the observed peaks. The characteristic peaks that are related to PO_4^{3-} group appeared at 1098 and 1029cm^{-1} (v_3), 605 and 564 cm^{-1} (v_4). The adsorbed H_2O appeared at 1650 cm^{-1}, whereas the broad bands at 3300-3700 cm^{-1} were also assigned to the adsorbed water. However, the presence of typical peaks of carbonate groups at 875, 1416 and 1474 cm^{-1} can be considered as evidence of replacement of the PO_4^{3-}group by carbonate and formation of B-type carbonated HAp.

FTIR of 1% B_4O_7HAp (1 wt.% $B_4O_7^{2-}$) materials prepared by precipitation and hydrolysis methods after sintering at 900 ˚C.

Fig.7-21 displays the FTIR spectra of the sintered 1%B_4O_7HAp material as prepared by different synthesis routes (the precipitation and hydrolysis).

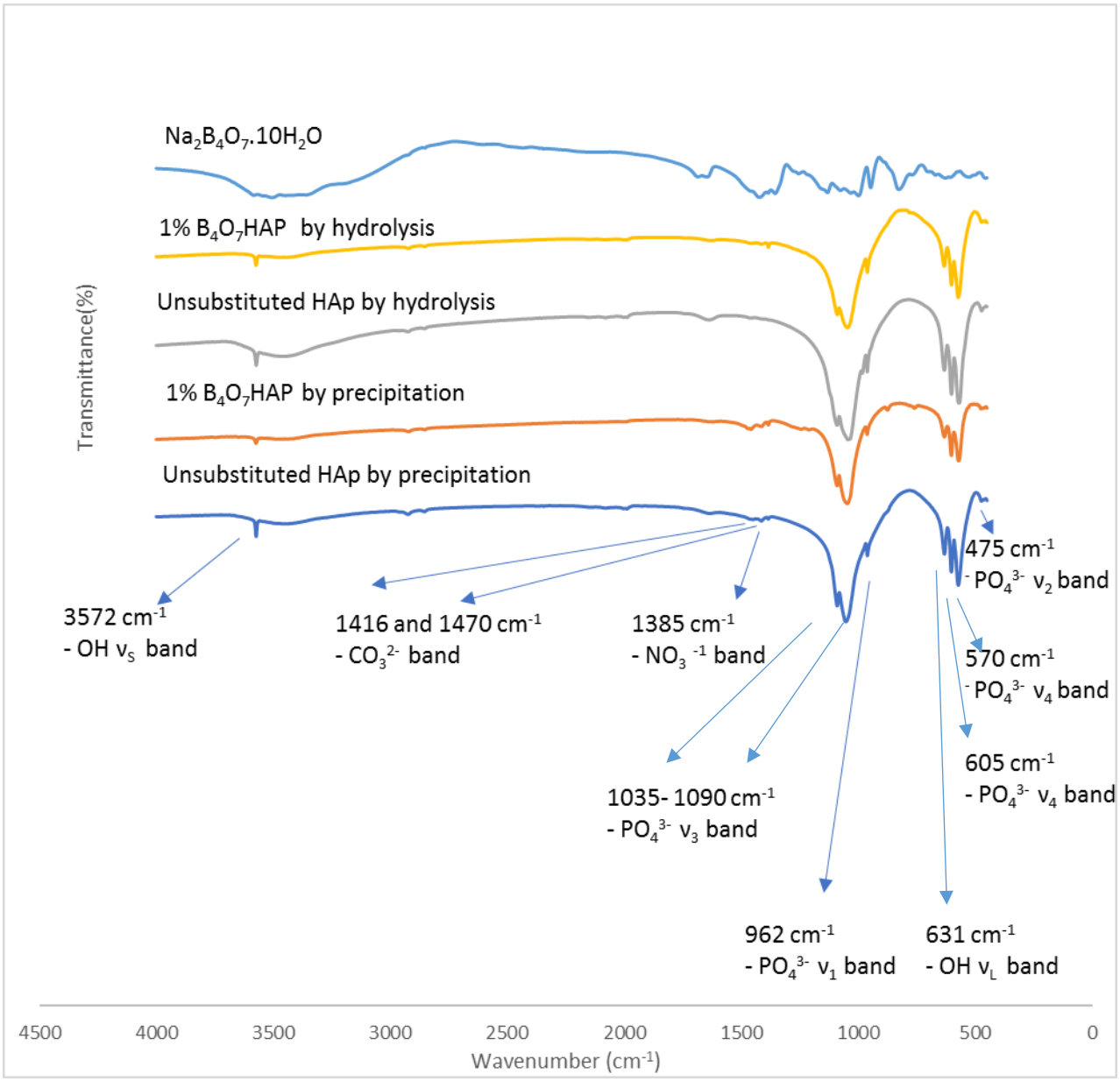

Figure 7-21: FTIR spectra of 1% B_4O_7HAp (1 wt.% B_4O_7) materials prepared by precipitation and hydrolysis methods after sintering at 900 ˚C.

Ternane et al. [243] introduced boron into the HAp structure by a solid state method using $CaCO_3$, $(NH_4)_2HPO_4$ and H_3BO_3 as starting materials with the following proposed nominal stoichiometry : Ca_{10} [$(PO_4)_{6-x}$ $(BO_3)_x][(BO_3)_y(BO_2)_z(OH)_{2-3y-z}$. They suggested that phosphate and OH groups would be partially substituted by borate groups. The IR spectra of BHAp (where X=0.5) compared to free boron hydroxyapatite revealed clear bands that can be assigned to borate group vibrations. The results showed several bands attributed to antisymmetric stretching v_3 of BO_3^{3-} group at 1304, 1253, 1208 cm^{-1}, whereas the peaks at 784, 771 and 755 cm^{-1} were assigned to the symmetric bending v_2 mode of the BO_3^{3-} group.

In the present study, the FTIR spectrum of the prepared 1% B_4O_7HAp materials as shown in **Fig. 7-21** displayed the characteristic absorption bands of HAp materials. The vibrational modes of thePO_4^{3-} ions appeared at 572, 604 cm^{-1} (υ_4); 963 cm^{-1} (υ_1); 1045 cm^{-1} (υ_3), while the fundamental OH^- peaks at 630 and 3572 cm^{-1} are clearly visible in the whole samples indicating highly crystalline materials. However, FTIR spectra of prepared HAp and 1% B_4O_7HAp by using precipitation route confirmed the substitution of CO_3^{2-} groups in B-site through observing the carbonate bands at 874, 1416 and 1470 cm^{-1}. The band at 1384 cm^{-1} can be assigned to the nitrate group (NO_3^-) due to the starting materials using metal nitrate salts.

A clear reduction in the intensity of stretching and librational modes of the lattice OH^- group at 3572 and 630 cm^{-1} by both methods were also observed. This reduction in the intensities of stretching and librational modes is associated with the appearance of a well-defined peak and corresponded to the carbonate group at 875 cm^{-1} by using the precipitation route. This reduction of intensities can be ascribed to the presence of sodium ions as confirmed by ICP-MS analysis, coupled with formation of CO_3HAp powders as detected by FTIR spectra in the case of precipitation route. Therefore, the OH- ion content was derived by the requirement to keep the charge balance and to restore the neutrality of HAp crystals (see Chapter 6 for details)[-].

In the present study, the FTIR spectra showed another important observation was that a new peak with very slight intensity appeared at 757 cm^{-1} by using precipitation route, while no evidence of that peak was seen by hydrolysis method. This peak may be attributed to the $B_4O_7^{2-}$ group.

7.3.1.3 XRD diffraction patterns of 1% B_4O_7HAp (1 wt.% $B_4O_7^{2-}$) materials prepared by precipitation and hydrolysis methods:

Phase Identification of 1% B_4O_7HAp materials:

The X-ray diffraction patterns of the non-sintered and sintered 1% B_4O_7HAp materials prepared by precipitation and hydrolysis are given in **Figures 7-22 and 7-23**, respectively**.**

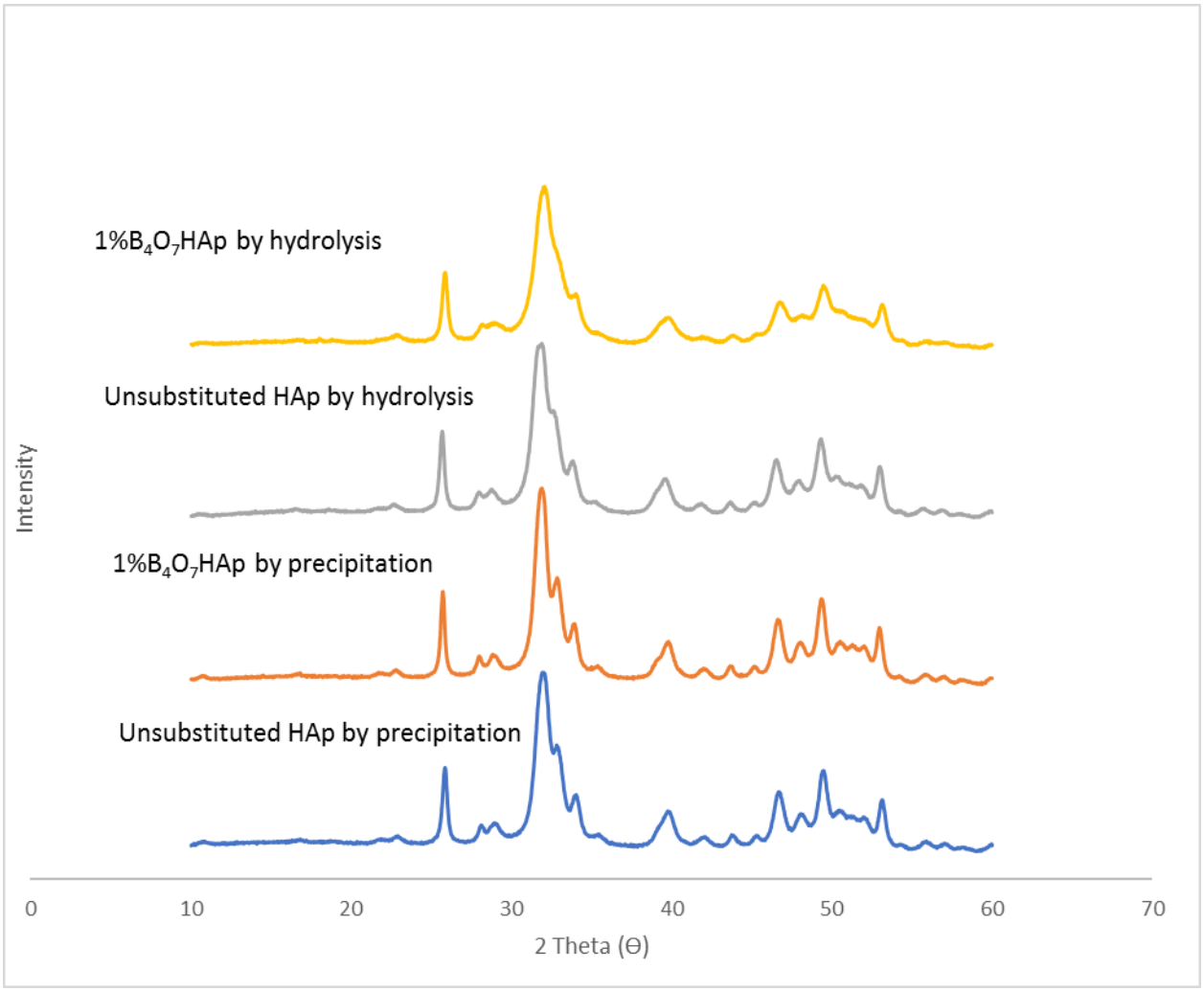

Figure 7-22: **XRD diffraction patterns of the non-sintered of 1% B_4O_7HAp (1 wt.% $B_4O_7^{2-}$) materials prepared by precipitation and hydrolysis methods.**

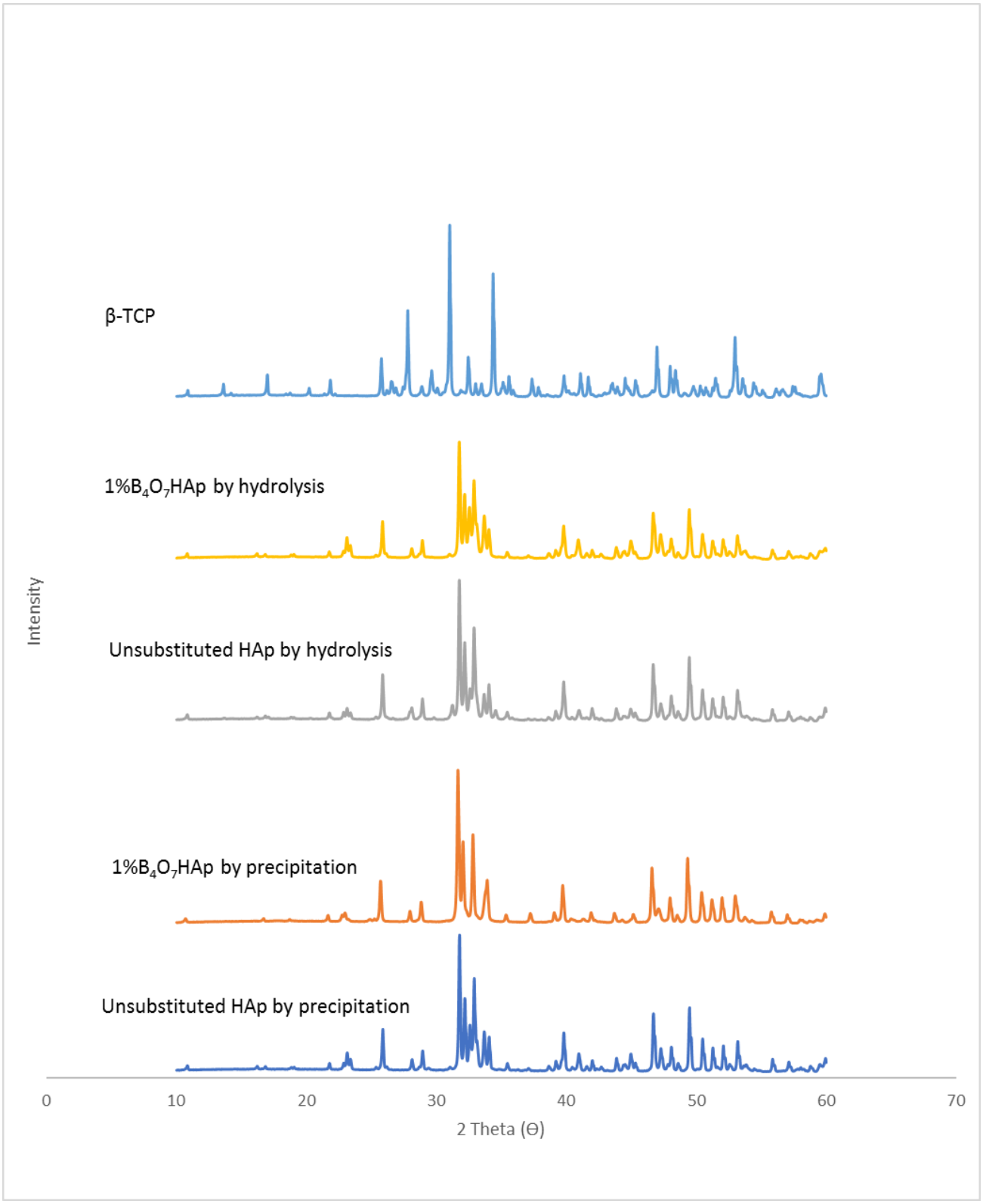

Figure 7-23: **XRD diffraction patterns of 1% B_4O_7HAp (1 wt.% $B_4O_7^{2-}$) materials prepared by precipitation and hydrolysis methods after sintering at 900 ˚C.**

Fig.7-23. showed the disappearance of the major peaks that were related to impurity phase (β-TCP), except two typical peaks of β-TCP with very slight intensity appeared at 2 Theta = 41.14˚ and 47.36. This observation was associated with the appearance of a new peak at 2 Theta = 37.40˚. This peak appearing at 37.40˚ can be attributed to a CaO phase (reference card number 04-017-9575). In the case of the hydrolysis method, **Fig.7-25** displayed some peaks that are related to the impurity phase (β-TCP) at 2 Theta = 31.20˚ and the peak at 34.57˚ disappeared, while at the same time there was an increase in the other intensities of the impurity peaks (β-TCP), especially those at 2 Theta = 32.80˚ and 33.60˚.

Crystallinity and crystallite size of 1% B_4O_7HAp materials:

Table 7-19 displays the degree of crystallinity and crystallite size of the sintered 1% B_4O_7HAp materials prepared by precipitation and hydrolysis methods.

Table 7-19: The degree of crystallinity and crystallite size of 1% B_4O_7HAp (1 wt.% $B_4O_7^{2-}$) materials prepared by precipitation and hydrolysis methods after sintering at 900 ˚C.

Sample	D_{002} (Å)	Crystallinity %
Unsubstituted HAp by precipitation	618.3±3.2	84.15±4.2
1%B_4O_7HAp by precipitation	568.4±4.4	85.62±5.2
Unsubstituted HAp by hydrolysis	549.8±3.6	82.57±2.1
1%B_4O_7HAp by hydrolysis	507.9±7.4	72.78±5.2

Also, **Table 7-19** shows a slight increase in the numerical value of crystallinity obtained due to prepared 1% B_4O_7HAp powders by precipitation route, whereas a significant reduction in the calculated value of crystallinity was recorded in the case of hydrolysis method. This observation was also confirmed by XRD diffraction patterns (**Fig.7-25)**, which shows a decrease in the intensities of the major peaks of HAp materials combined with peak broadening achieved through preparing 1% B_4O_7HAp samples by the hydrolysis method. The values of the crystallite size displayed a reduction by both routes.

Lattice Parameters and volume of unit cell of 1% B_4O_7HAp materials:

Table 7-20 displays the lattice parameters and the volume of hexagonal unit cell of the sintered 1% B_4O_7HAp prepared by precipitation and hydrolysis methods.

Table 7-20: The lattice parameters and the volume of hexagonal unit cell of 1% B_4O_7HAp (1 wt.% $B_4O_7^{2-}$) materials prepared by precipitation and hydrolysis methods after sintering at 900 ˚C.

Sample	a [Å]	c [Å]	V[Å^3]
Unsubstituted HAp by precipitation	9.416±0.004	6.879±0.003	1579±0.004
1%B_4O_7HAp by precipitation	9.428±0.005	6.911±0.005	1590±0.005
Unsubstituted HAp by hydrolysis	9.421±0.003	6.882±0.005	1581±0.004
1%B_4O_7HAp by hydrolysis	9.434±0.002	6.896±0.004	1588±0.003

The refined crystal lattice constants (a and c) of the prepared materials using various synthesis routes are listed in **Table 7-20.** We can notice the substitution of $B_4O_7^{2-}$ ions into HAp samples was characterized by an expansion in the both lattice constants (a and c). This observation can be attributed to the general fact that $B_4O_7^{2-}$ ions have bigger ionic radius (3.507 Å) [244] compared to phosphate (2.3 Å) [32] and hydroxyl group (1.68 Å)[123], which lead to an increase the unit cell in both directions. The presence of other ions such as Na^+ and CO_3^{2-} group in the HAp samplewas confirmed by using ICP-MS and the FTIR analysis. But the expansion in the lattice parameters could not be ascribed to these ions (Na^+ and CO_3^{2-} group). Because the ionic radius of Na^+ ions (0.99 Å) and Ca^{2+} (1.00 Å) are very close [136], also the substitution of phosphate anion by CO_3^{2-} will not cause an increase in the lattice constants. The replacement of PO_4^{3-} group by CO_3^{2-} will cause a reduction in the lattice constants, simply because the phosphate site is characterized by a larger ionic radius (0.23 nm) compared to the smaller ionic radius carbonate group (0.189 nm) [216].

7.3.1.4 SEM of 1% B_40_7HAp (1 wt.% B_4O_7) materials prepared by precipitation and hydrolysis methods.

SEM of the non-sintered 1% B4O7HAp (1 wt.% B_4O_7) materials prepared by precipitation and hydrolysis methods.

Fig.7-24. displays the SEM images of the non-sintered 1% B_4O_7HAp powders prepared by hydrolysis and precipitation methods.

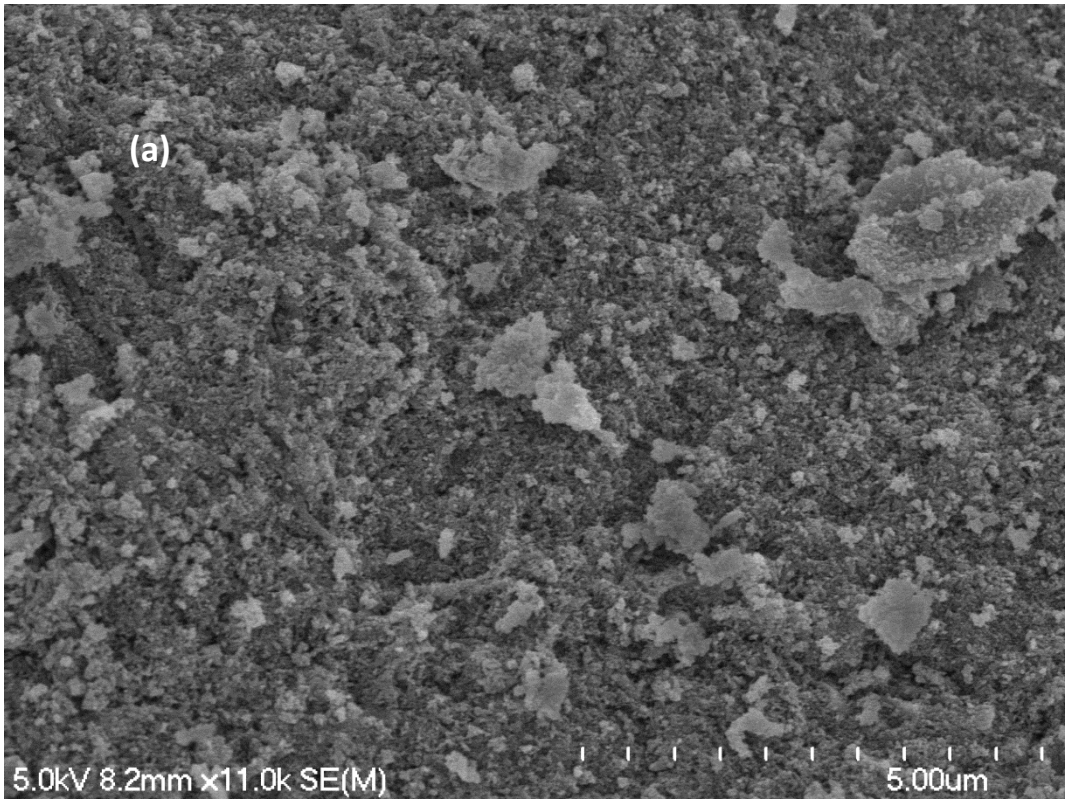
(a)
5.0kV 8.2mm x11.0k SE(M)
5.00um

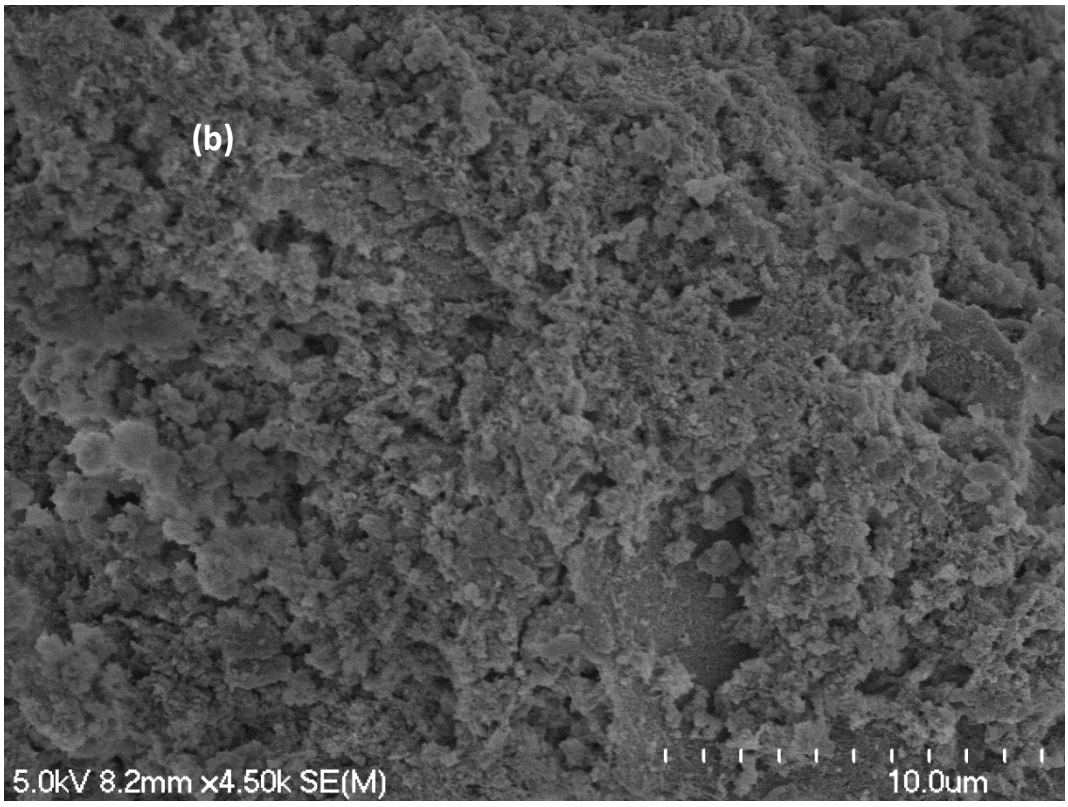
(b)
5.0kV 8.2mm x4.50k SE(M)
10.0um

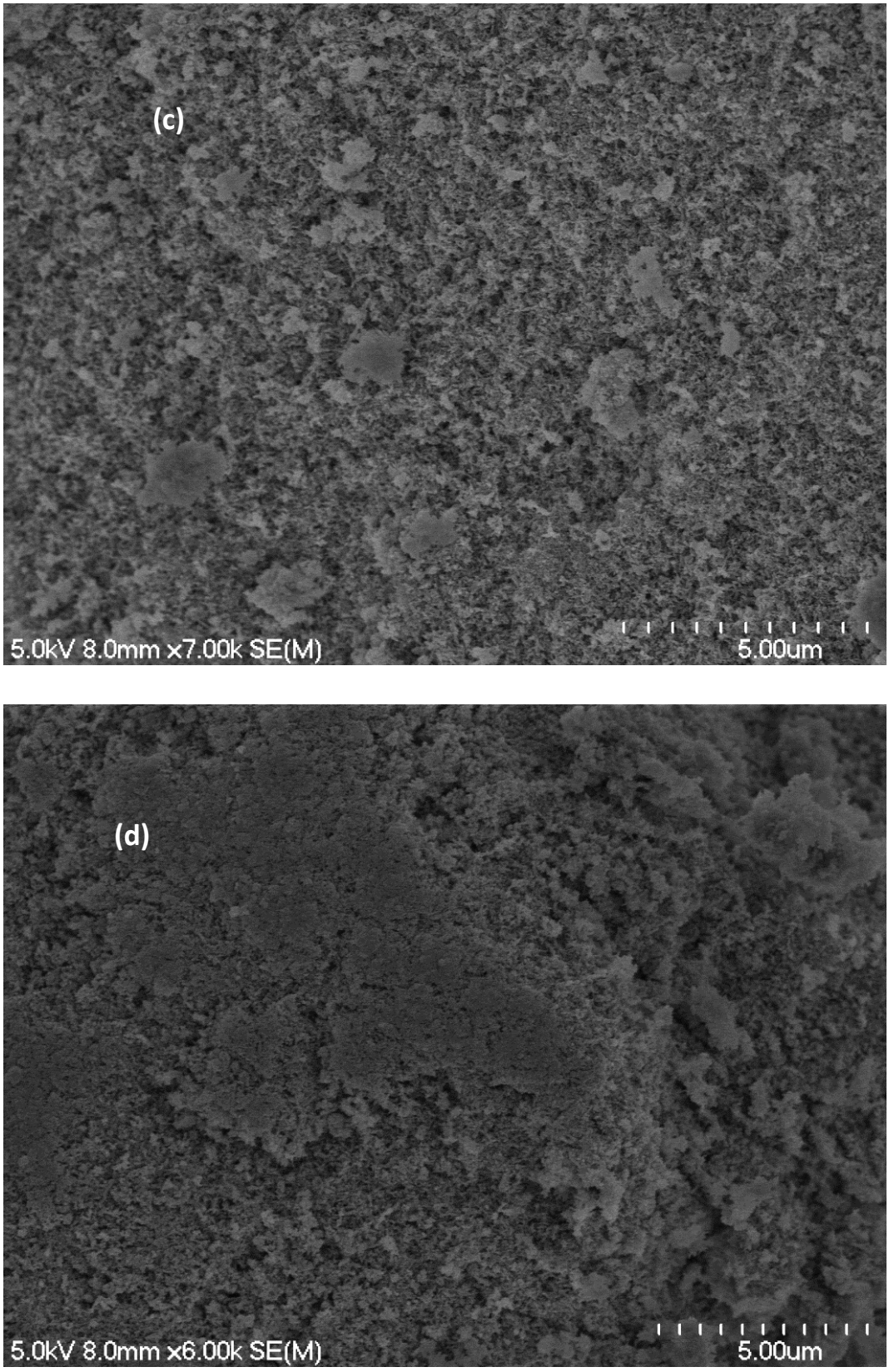

Figure 7-24: SEM images of non-sintered (a) Unsubstituted HAp by precipitation (b) Unsubstituted HAp by hydrolysis (c) 1%B_4O_7HAp by precipitation (e) 1%B_4O_7HAp by hydrolysis.

The surface morphology of the prepared 1% B_4O_7HAp materials at room temperature was observed by using SEM technique. The SEM images displayed the morphology of HAp materials which had not been affected by substitution process, and the B_4O_7HAp materials prepared by both methods were recorded to be generally spherical-like shape coupled with a trend to agglomerate.

SEM of 1% B_4O_7HAp (1 wt.% B_4O_7) materials prepared by precipitation and hydrolysis methods after sintering at 900 ˚C.

Fig.7-25 displays the SEM images of the sintered 1% B_4O_7HAp powders as prepared by the hydrolysis and precipitation methods.

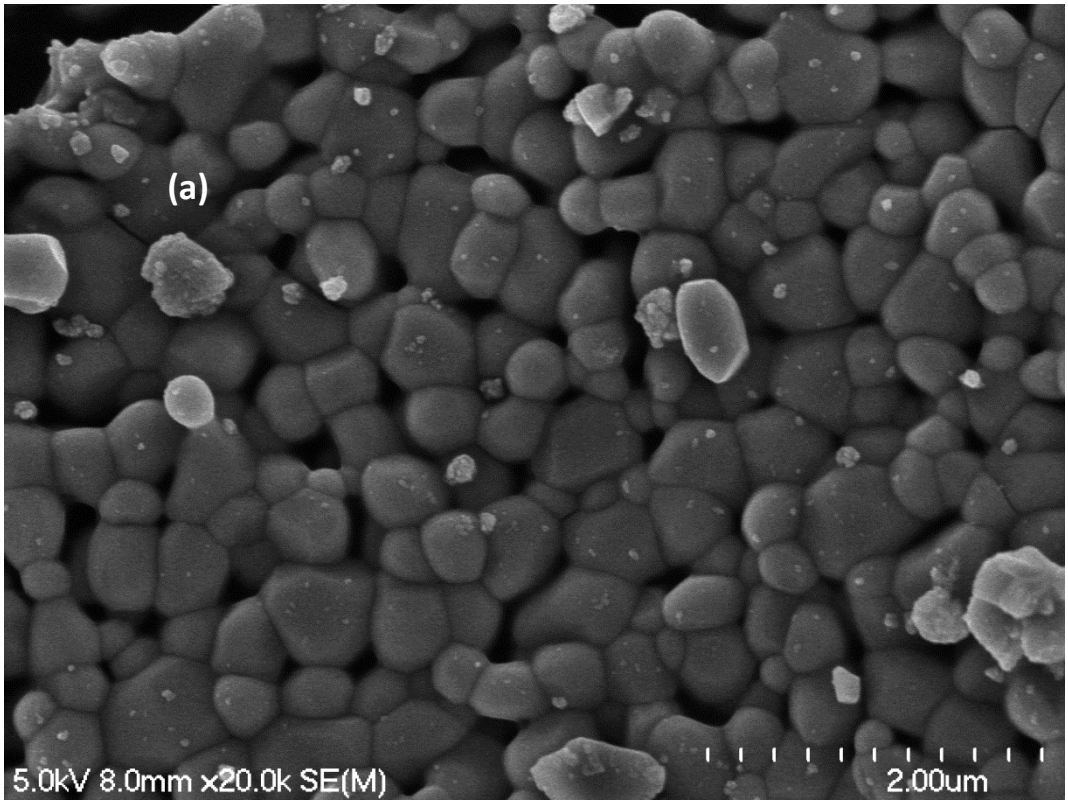

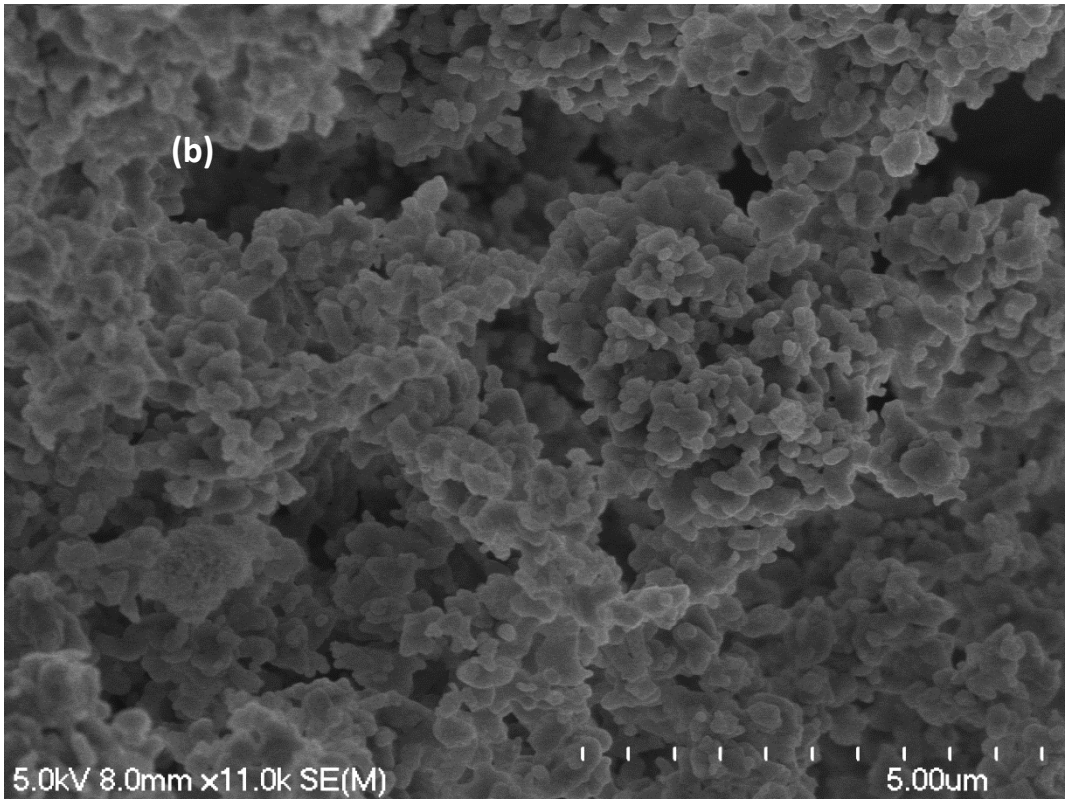
(b)
5.0kV 8.0mm x11.0k SE(M)
5.00um

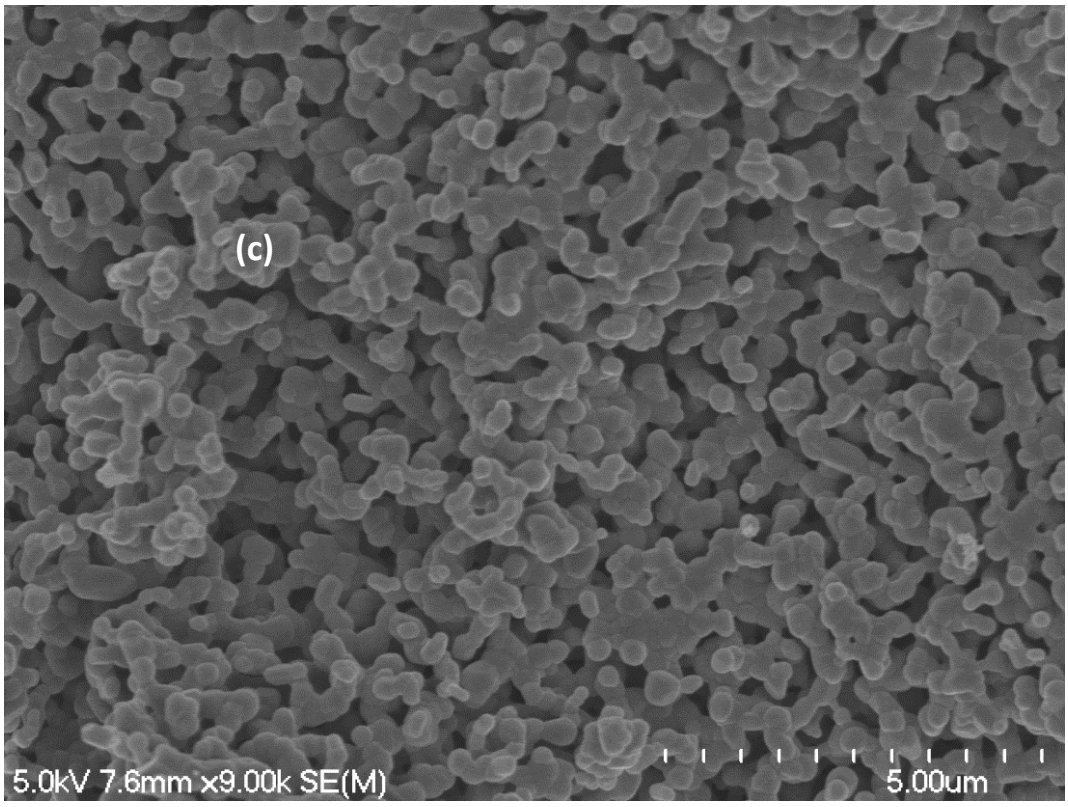
(c)
5.0kV 7.6mm x9.00k SE(M)
5.00um

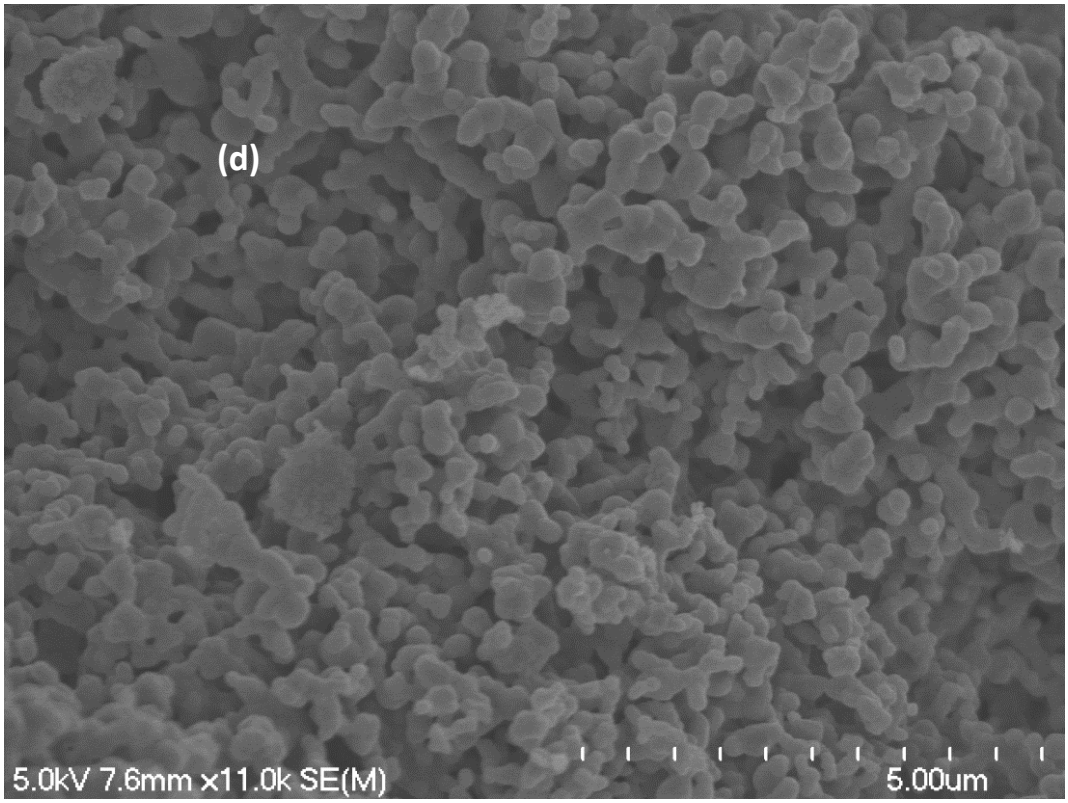

Figure 7-25: SEM imaged of (a) Unsubstituted HAp by precipitation (b) Unsubstituted HAp by hydrolysis (c) 1% B_4O_7HAp by precipitation (d) 1%B_4O_7HAp by hydrolysis, after sintering at 900 ˚C.

The SEM images of the sintered materials by different synthesis methods at 900 ˚C are shown in **Fig. 7-25.** These had spheroid-like shapes with a clear ability to agglomerate which were obtained by using the precipitation method.

The hydrolysis method was also characterized by particles which formed spheroid like shape materials, and a visible trend to agglomerate, but the effect of the replacement process by using hydrolysis method was obviously recorded, indicating that a visible enhancement in the level of porosity was obtained.

7.4 Br_2Ap powders prepared by precipitation and hydrolysis:

E. Dykes prepared bromapatite [23] with the following chemical formula: $Ca_{10}(PO_4)_6Br_2$ through two stages. The first stage was the preparation of HAp by refluxing H_3PO_4 and calcium carbonate for one week, after which the precipitate was filtered and dried at 900 ˚C for one hour. The second step can be summarized in heating the HAp powders at 900 ˚C in a flow of hydrogen bromide for 10 hours. As a result, bromoapatite powders were obtained with the following chemical formula: $Ca_{10}(PO_4)_6Br_2$. In

this project, BrHAp and Br_2Ap materials were prepared by using three different preparation methods, namely precipitation, hydrolysis and ion exchange methods. The detailed amounts of the reagents are listed in the **Table 7-21**, see below for details:

Table 7-21: Synthesis details of BrHAp and Br_2Ap materials prepared by precipitation, hydrolysis and ion exchange methods

Sample	MCP $Ca(H_2PO_4)_2$ (g)	$Ca(OH)_2$ (g)	$Ca(NO_3)_2$ (g)	Na_2HPO_4 (g)	NaBr (g)	MCP($Ca(H_2PO_4)$ (mol)	Ca(OH)2 (mol)	$Ca(NO_3)_2$ (mol)	Na_2HPO_4 (mol)	NaBr (mol)
$Ca_{10}(PO_4)_6Br_2$ by soaking	-	-	-	-	102.89	-	-	-	-	1.0000
$Ca_{10}(PO_4)_6Br_2$ by hydrolysis	10.345	3.2615	-	-	0.9172	0.0442	0.0440	-	-	0.0089
$Ca_{10}(PO_4)_6Br_2$ by precipitation	-	-	7.2610	3.7658	0.9096	-	-	0.0443	0.0265	0.0088
$Ca_{10}(PO_4)_6Br(OH)$ By precipitation	-	-	7.6855	3.9855	0.4911	-	-	0.0468	0.0281	0.0048

7.4.1 Characterization methods of prepared Br_2Ap materials prepared by precipitation, hydrolysis and ion exchange methods.

7.4.1.1 ICP/MS of Br_2Ap materials prepared by precipitation, hydrolysis and ion exchange methods:

The results of the elemental analyses of Br_2Ap and BrHAp samples that were prepared by precipitation, hydrolysis and ion exchange routes are displayed in **Table 7-22 .**

Table 7-22: ICP-MS results of Br_2Ap and BrHAp materials prepared by precipitation, hydrolysis and ion exchange methods after sintering at 900 ˚C. The concentration is in ppb (ug/L):

Sample	Ca 44	P 31	Na 23
Unsubstituted HAp by precipitation	707795	401240	103797
BrHAp by precipitation	827512	419428	86237
Br_2Ap by precipitation	696613	374532	94984
Unsubstituted HAp by hydrolysis	769928	423970	78396
Br_2Ap by hydrolysis	737458	386470	64942
Br_2Ap by ion exchange	753172	384554	3230
Commercial HAp (Fluka)	557227	262446	298

The calcium/phosphorus (Ca/P) molar ratios as well as (Ca+Na)/P molar ratio were determined by ICP-MS and presented in **Tables 7-23.**

Table 7-23: The chemical analysis data of Br_2Ap materials by ICP-MS measurements after sintering at 900 ˚C.

Sample	Ca/P Theoretical	Ca/P Measured	(Ca+Na)/ P
Unsubstituted HAp by precipitation	1.67	1.36	1.71
BrHAp by precipitation	1.67	1.52	1.80
Br_2Ap by precipitation	1.67	1.44	1.77
Unsubstituted HAp by hydrolysis	1.67	1.40	1.65
Br_2Ap by hydrolysis	1.67	1.47	1.70
Br_2Ap by ion exchange	1.67	1.51	1.52
Commercial HAp (Fluka)	1.67	1.64	1.64

Tables 7-22 and 7-23, show the presence of sodium ions in the whole prepared materials. The calculated values of (Ca+Na)/ P, for the whole prepared materials by precipitation and hydrolysis methods, were found to be higher than the stoichiometric HAp. Such results can be ascribed to the formation of carbonated HAp with B-type as confirmed by FTIR spectra in the case of precipitation method. The higher value in the case of hydrolysis method may be attributed to the phase purity, but in the case of the soaking method the calculated value of (Ca+Na)/ P was found to be lower (1.52) than the expected value (1.67) of the stoichiometric HAp. Such results merit further investigation.

Tables 7-22 and **7-23** showed that Br^- ions were not detected by using the ICP-MS analysis. The presence of Br^- ions into HAp lattice were confirmed by using other techniques such as XRD and FTIR spectra (see later). Several researchers confirmed the presence of Br^- ions into HAp structure by using various techniques rather than the ICP-MS analysis. As an example, E. Dykes prepared bromapatite [23] with the following chemical formula: $Ca_{10}(PO_4)_6Br_2$ as mentioned previously. The FTIR spectra showed that no evidence of any remaining OH^- ions in the bromapatite spectra because the stretching and the librational modes at 630 and 3572 cm^{-1} had disappeared. The result of FTIR spectra suggested the replacement of OH^- group by the Br^- ions. Also, the XRD analysis showed that the lattice constants a and c were increased due to the substitution of Br^- ions into HAp lattice. The lattice constants of hydroxyapatite were (9.428 and 6.881 Å) compared to (9.7614 and 6.7386 Å) for bromapatite. The expansion of lattice constants

can be ascribed to the replacement process of Br^- ions with larger ionic radius of Br^- ions (0.190 nm) [216] compared to OH^- group (0.152 nm). Therefore, the XRD and FTIR spectra confirmed the replacement of hydroxyl group (OH^-) by Br^- ions.

7.4.1.2 FTIR of Br_2Ap materials prepared by precipitation, hydrolysis, and ion exchange methods:

FTIR of the non-sintered Br_2Ap and BrHAp materials prepared by precipitation, hydrolysis, and ion exchange methods.

Fig.7-26 displays the FTIR spectra of the non-sintered Br_2Ap and BrHAp material prepared by different synthesis routes.

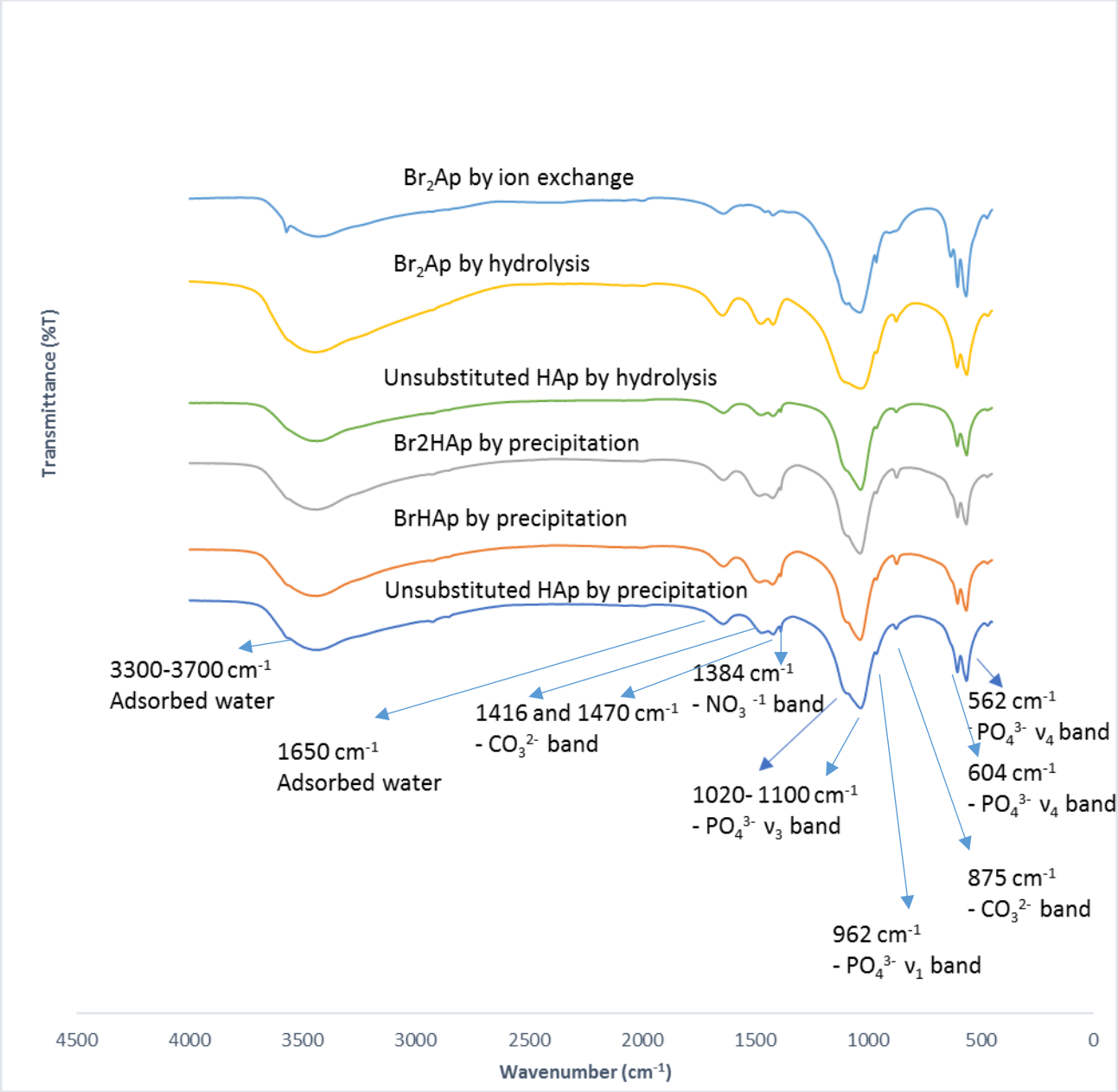

Figure 7-26: FTIR spectra of the non-sintered Br_2Ap and BrHAp materials prepared by precipitation, hydrolysis and ion exchange methods.

The characteristic peaks that are related to PO_4^{3-} group appeared in the whole prepared powders at 1098 and 1029cm^{-1} (v_3), 605 and 564 cm^{-1} (v_4). The adsorbed H_2O appeared at 1650 cm^{-1}, whereas the broad bands at 3300-3700 cm^{-1} were also assigned to the adsorbed water. The presence of typical peaks of carbonate groups at 875, 1416 and 1474 cm^{-1} confirmed the formation of B type carbonated HAp.

FTIR of Br_2Ap and BrHAp materials prepared by hydrolysis, precipitation, and ion exchange methods after sintering at 900 ˚C:

Fig.7-27 displays the FTIR spectra of the sintered Br_2Ap and BrHAp material prepared by different synthesis routes.

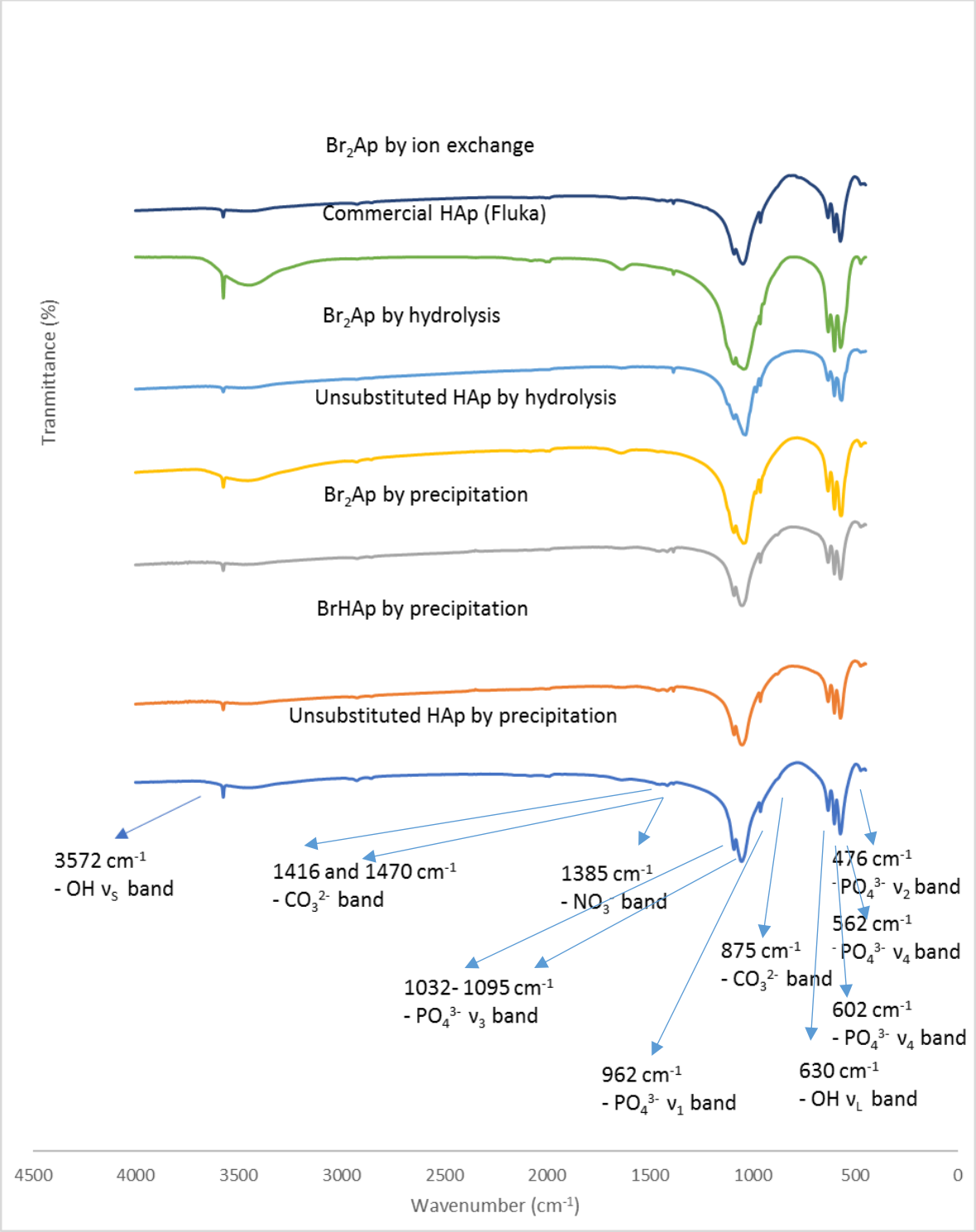

Figure 7-27: FTIR spectra of Br_2Ap and BrHAp materials prepared by precipitation, hydrolysis and ion exchange methods after sintering at 900 ˚C.

The functional groups of the prepared HAp, BrHAp and Br_2Ap powders that were produced as a result of different synthesis routes and calcination process at 900 ˚C were displayed in **Fig.7-27.** The bands at 3572 and 632 were attributed to the stretching and vibrational modes of the hydroxyl group. The bands at 1025- 1090 and 961cm^{-1} were related to the stretching vibration modes of phosphate group, whereas the doublet at 572 and 602 cm^{-1} corresponds to the PO_4^{3-} bending modes. Another important observation was recorded by FTIR analysis, which was that the intensity of the librational mode of OH^- group at 630 cm^{-1} was not affected by substitution of bromide ions, whereas an obvious decrease in the intensity of stretching mode of OH^- group at 3752cm^{-1} was shown. This observation can be attributed to the partial substitution of Br^- by OH^- in hydroxyapatite crystal, whereas the Br_2Ap crystal as confirmed by FTIR analysis had not been reached as proposed by our theoretical calculation, due to the appearance of typical peaks of OH^- group at 630 and 3572 cm^{-1}. E. Dykes [23] prepared bromapatite as mentioned previously, and the result of this investigation showed that the stretching and vibrational bands of hydroxyl group were not observed by the FTIR analysis, confirming preparation of single crystal of Br_2Ap material.

Also, we can see the bands that were related to carbonate group at 875, 1416 and 1474 cm^{-1} were detected in the Br_2Ap and Br_2HAp powders prepared by precipitation route, but the absence of these peaks were confirmed by using hydrolysis and ion exchange routes due to the heat treatment. Also, the bands that appeared at 1385 cm^{-1} in the case of the precipitation route can be attributed to nitrate group due to the starting materials using metal (nitrate) salts.

7.4.1.3 XRD diffraction analysis of Br_2Ap and BrHAp materials prepared by precipitation, hydrolysis and ion exchange methods.

Phase Identification of BrHAp and Br_2Ap materials prepared by precipitation, hydrolysis as well as ion exchange methods.

The XRD patterns of the non-sintered and sintered Br_2Ap and BrHAp materials prepared by using different synthesis routes are shown in **Figures 7-28**, **7-29 and 7-30.**

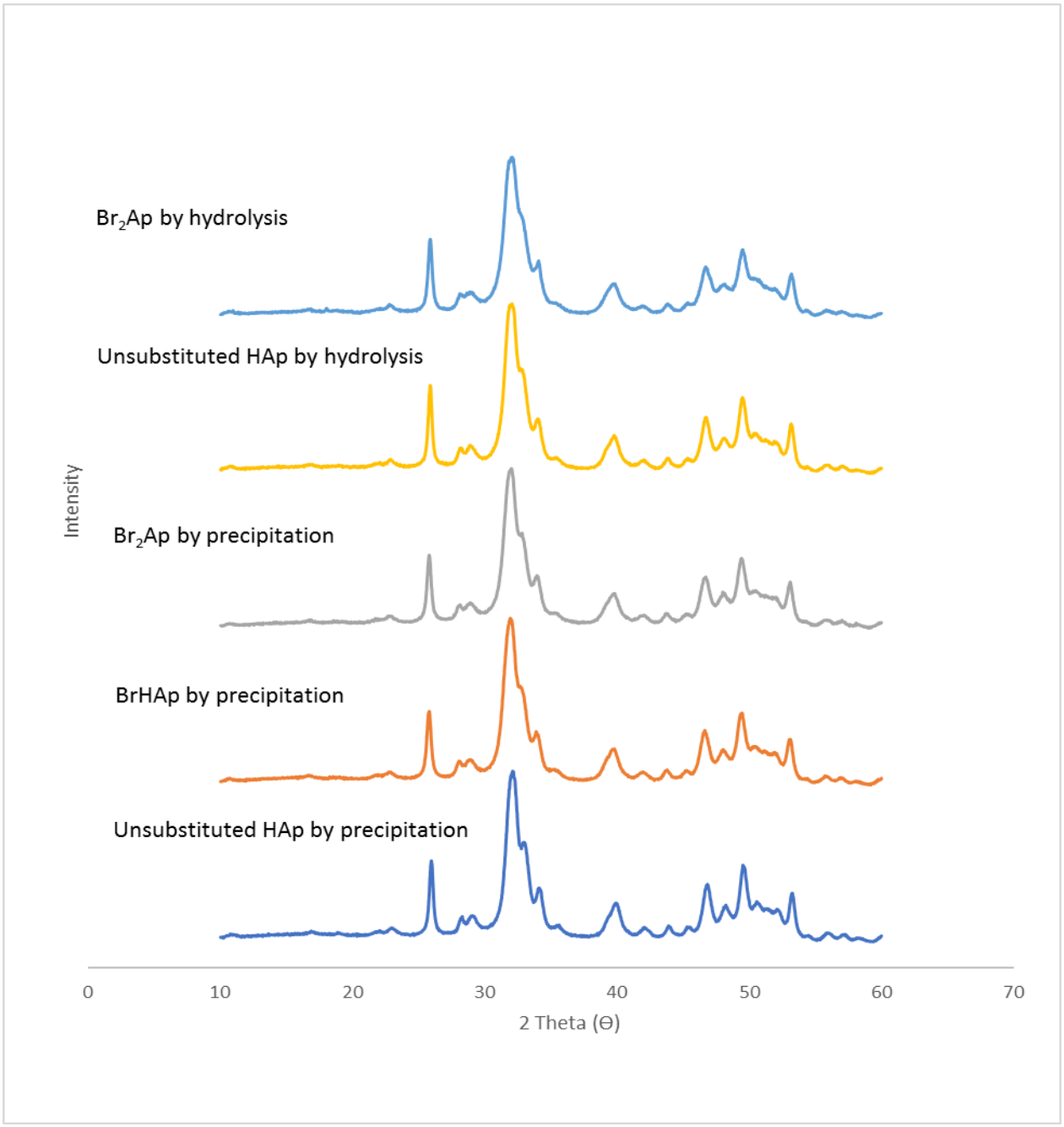

Figure 7-28: The XRD diffraction patterns of the non-sintered Br_2Ap and BrHAp materials prepared by precipitation and hydrolysis methods.

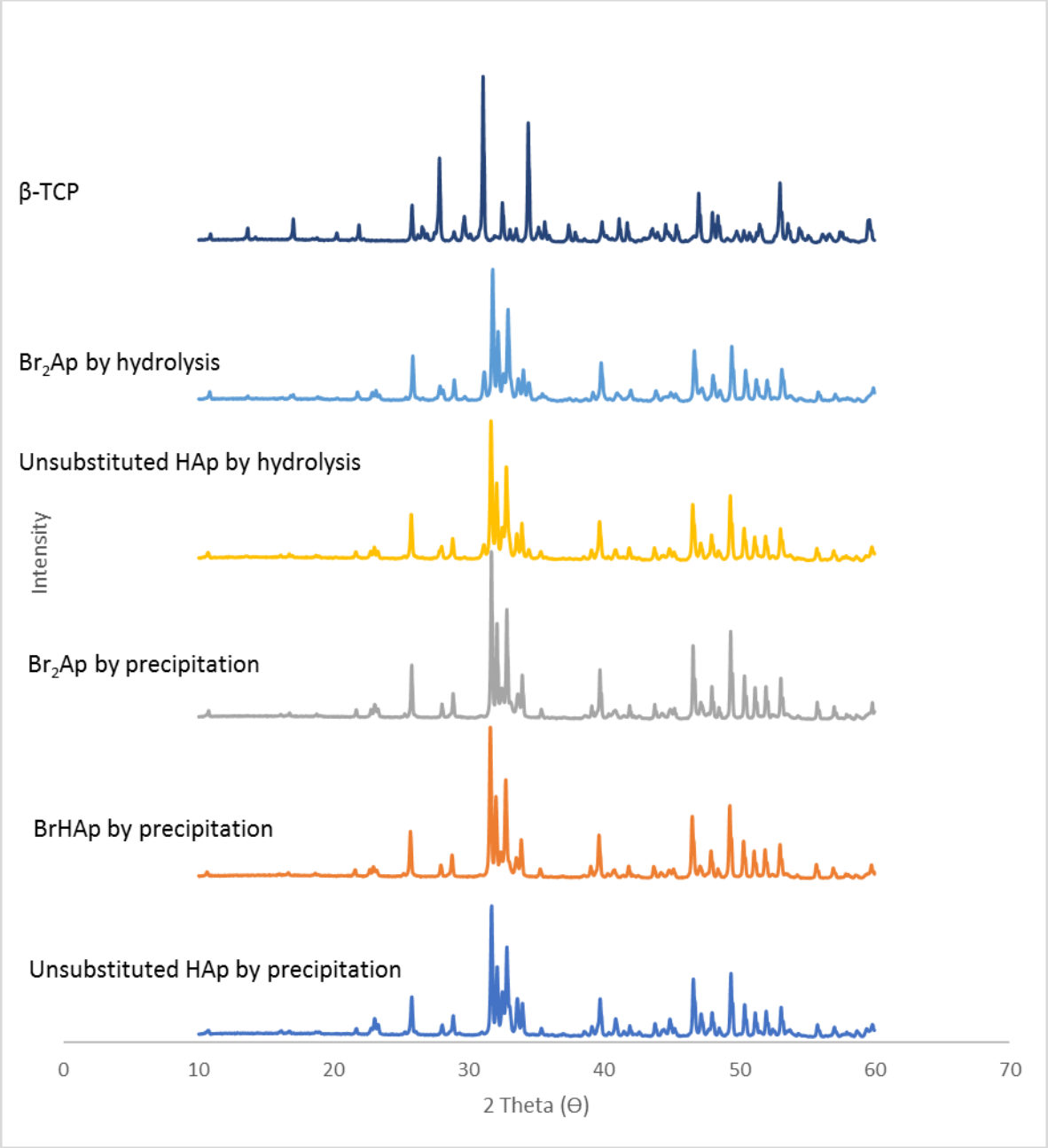

Figure 7-29: The XRD diffraction patterns Br_2Ap and BrHAp materials prepared by precipitation and hydrolysis methods after sintering at 900 ˚C.

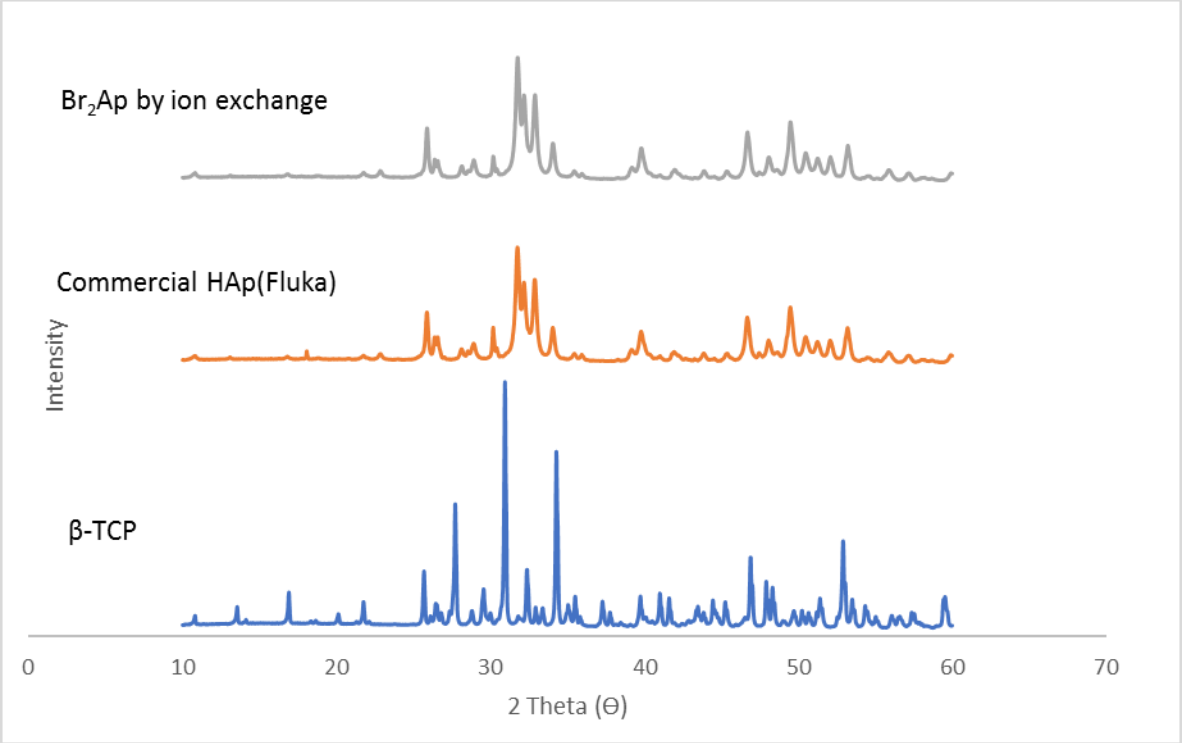

Figure 7-30: The XRD diffraction patterns of commercial HAp (fluka) and Br_2Ap materials prepared by ion exchange method.

Fig.7-29 displays the effect of synthesis route on the phase purity. The substitution process of Br^- ions by precipitation route led to a decrease in the intensity of the major peaks that corresponded to impurity phase such as those at 2 Theta = 31.2˚, 32.8˚, 33.6, 38.8˚, 41.14˚ and 47.36˚, indicating a greater degree phase purity of the HAP was obtained by using the precipitation method.

The replacement process of Br^- ions in HAp through using the ion exchange process showed a reduction in the intensity of one typical peak of β-TCP at 2 Theta = 31.2˚. On the other hand, preparation of Br_2Ap materials by the hydrolysis method displayed an increase in the intensities of some typical peaks that are related to β-TCP at 2 Theta = 31.2˚ and 34.57˚, indicating the effect of the preparation method as well as the chemical composition on the phase purity of the prepared samples.

Crystallinity and crystallite size of prepared Br_2Ap and BrHAp materials:

Table 7-24 displays the degree of crystallinity and crystallite size of Br_2Ap and BrHAp materials prepared by precipitation, hydrolysis and ion exchange methods after sintering at 900 ˚C.

Table 7-24: The degree of crystallinity and crystallite size of Br_2Ap and BrHAp materials prepared by precipitation, hydrolysis and ion exchange methods after sintering at 900 ˚C.

Sample	D_{002} (Å)	Crystallinity %
Unsubstituted HAp by precipitation	618.3±3.2	84.15±2.4
BrHAp by precipitation	592.5±6.2	81.53±4.8
Br_2Ap by precipitation	807.1±4.4	81.10±5.2
Unsubstituted HAp by hydrolysis	549.8±3.6	82.57±2.1
Br_2Ap by hydrolysis	547.7±3.6	83.03±3.2
Commercial HAp (Fluka)	395.0±2.8	77.31±4.2
Br_2Ap by ion exchange	263.3±4.6	79.90±4.4

While the crystallization process as presented in **Table 7-24** displayed a reduction in the values of crystallinity of Br_2Ap and BrHAp powders prepared by the precipitation method, an increase in the numerical values of crystallinity was recorded due to the substitution process of bromide ions into the HAp crystal by hydrolysis and ion exchange methods. Also, as confirmed by the Debye Scherrer formula, an increase in the numerical value of crystallite size was produced by precipitation, whereas a very slight reduction resulted from the hydrolysis and ion exchange methods.

Lattice parameters and volume of unit cell of prepared Br_2Ap and BrHAp materials:

Table 7-25 displays the lattice parameters and the volume of hexagonal unit cell of the sintered Br_2Ap and Br_2HAp prepared by precipitation and hydrolysis methods.

Table 7-25: The lattice parameters and the volume of hexagonal unit cell of Br_2Ap and BrHAp materials prepared by precipitation, hydrolysis and ion exchange methods after sintering at 900 ˚C.

Sample	a [Å]	c [Å]	V[Å^3]
Unsubstituted HAp by precipitation	9.416±0.004	6.879±0.003	1579±0.004
BrHAp by precipitation	9.417±0.003	6.879±0.002	1579±0.003
Br_2Ap by precipitation	9.422±0.002	6.884±0.004	1582±0.003
Unsubstituted HAp by hydrolysis	9.421±0.003	6.882±0.005	1581±0.004
Br_2Ap by hydrolysis	9.422±0.003	6.885±0.003	1582±0.003
Commercial HAp (Fluka)	9.391±0.005	6.861±0.005	1566±0.005
Br_2Ap by ion exchange	9.393±0.002	6.863±0.004	1568±0.003

Table 7.25 shows both lattice constants (a and c) of Br_2Ap materials increased as a result of substitution of bromide ions by precipitation, hydrolysis and ion exchange methods. This expansion in the values of lattice constants by using the precipitation, hydrolysis and ion exchange methods can be ascribed to the replacement process of Br^- ions with larger ionic radius of Br^- ions (0.190 nm) [216] compared to OH^- group (0.152 nm).

7.4.1.4 SEM of Br_2Ap and BrHAp materials prepared by precipitation, hydrolysis and ion exchange methods.

SEM of the non- sintered Br_2Ap and BrHAp materials prepared by precipitation, hydrolysis and ion exchange methods.

Fig.7-31. displays the SEM images of the non-sintered Br_2Ap and BrHAp powders prepared by hydrolysis, precipitation and ion exchange methods.

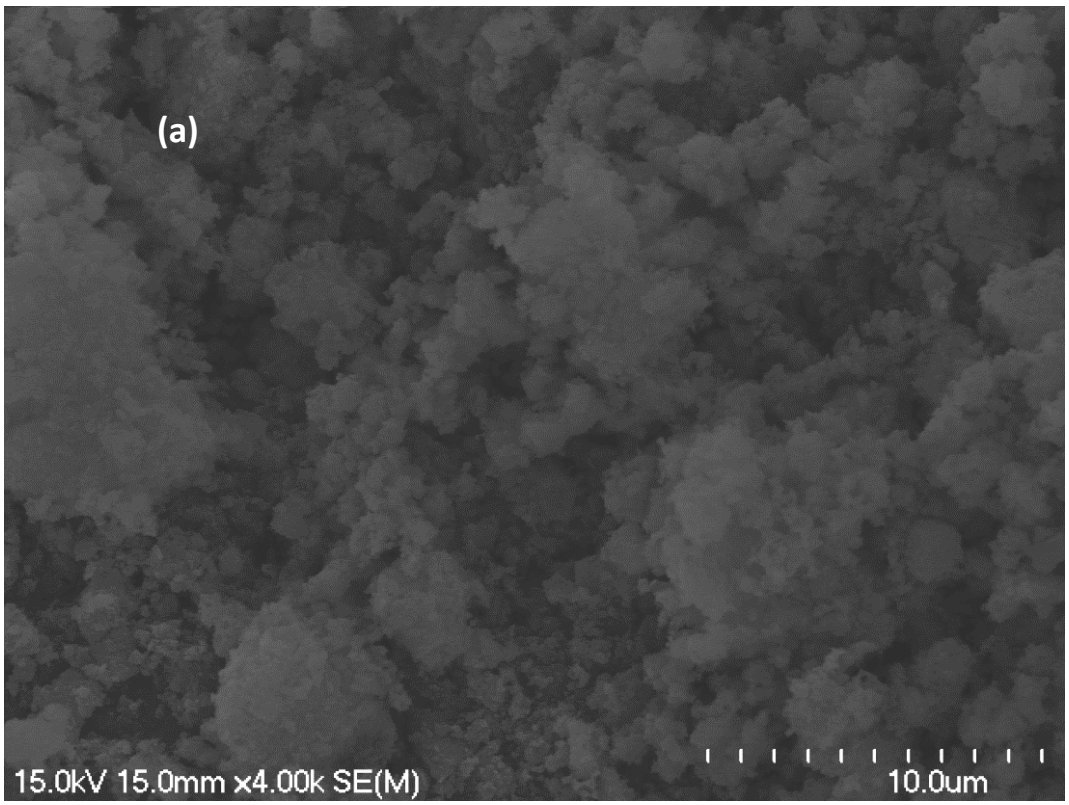
(a)
15.0kV 15.0mm x4.00k SE(M)
10.0um

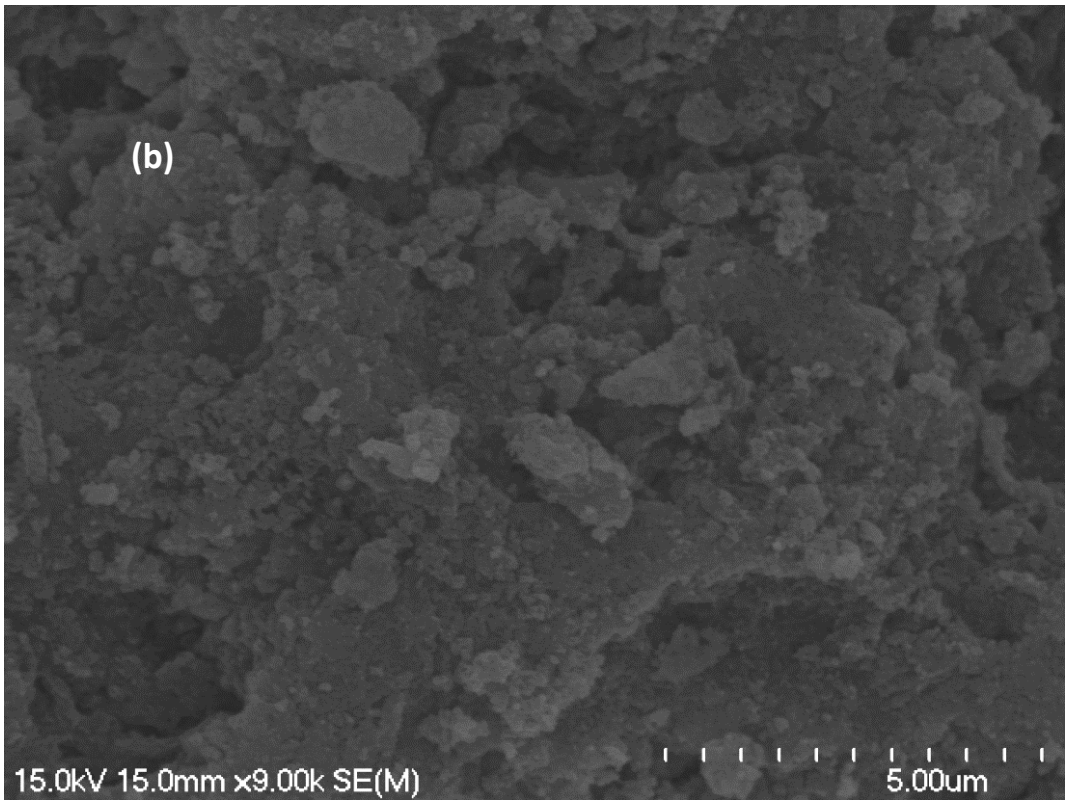
(b)
15.0kV 15.0mm x9.00k SE(M)
5.00um

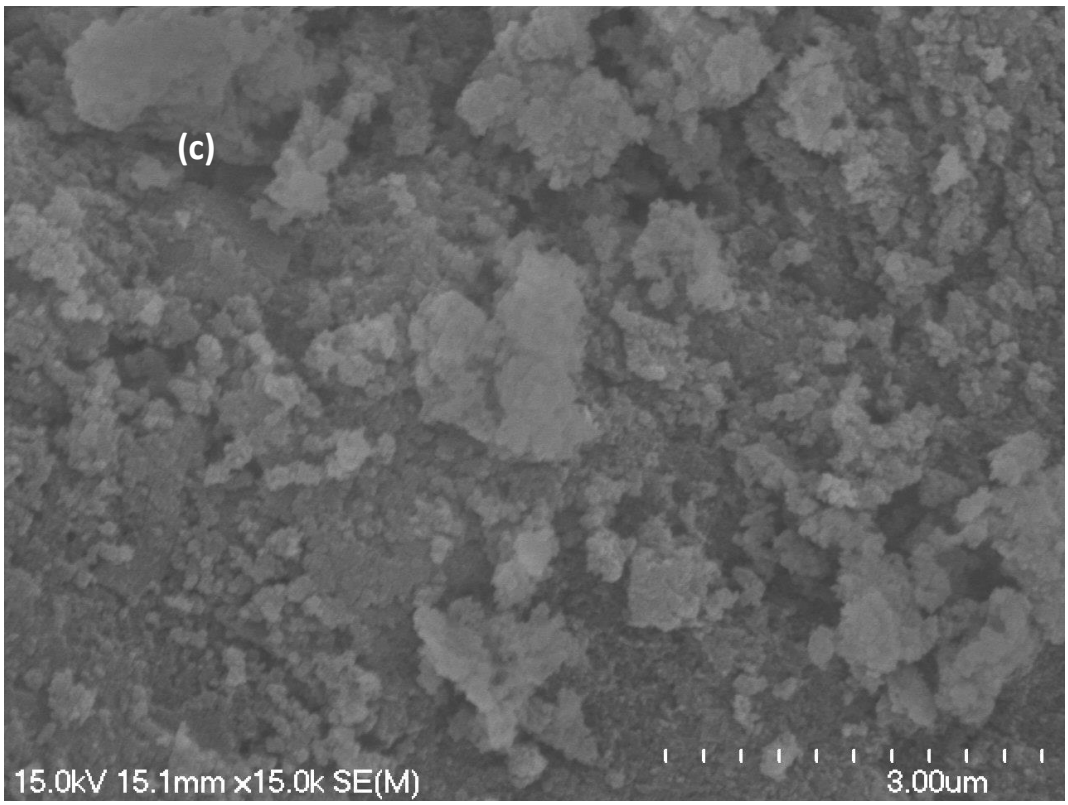
(c)
15.0kV 15.1mm x15.0k SE(M)
3.00um

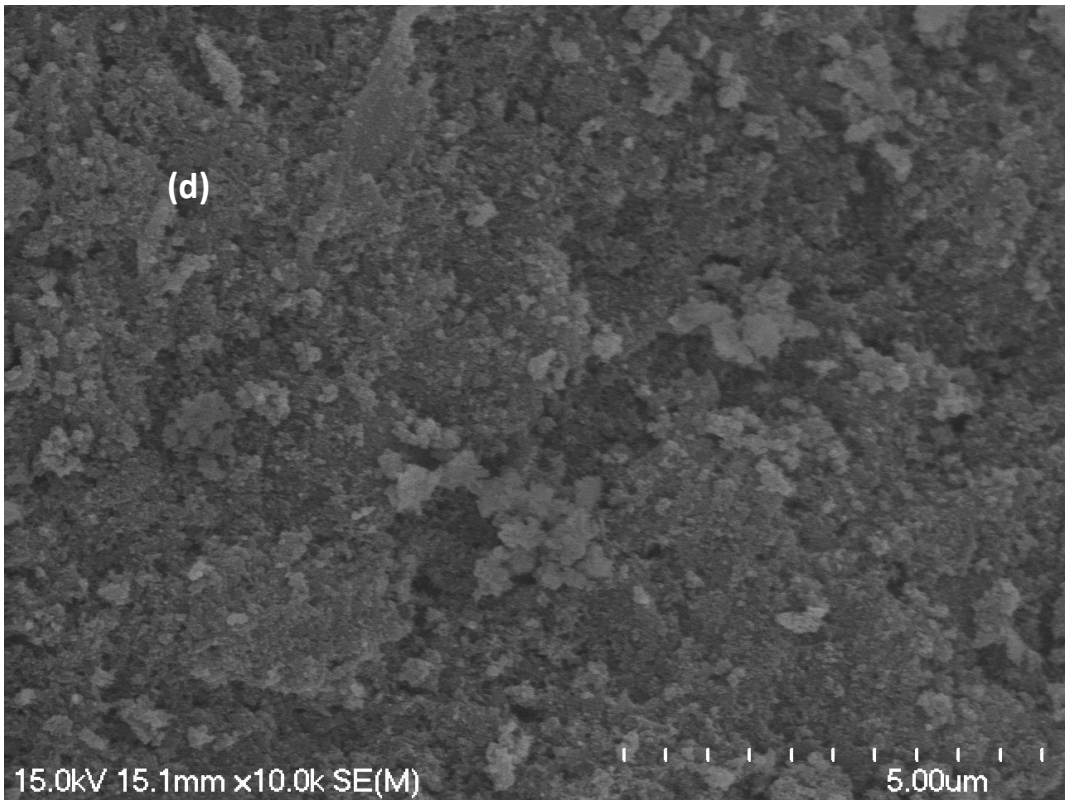
(d)
15.0kV 15.1mm x10.0k SE(M)
5.00um

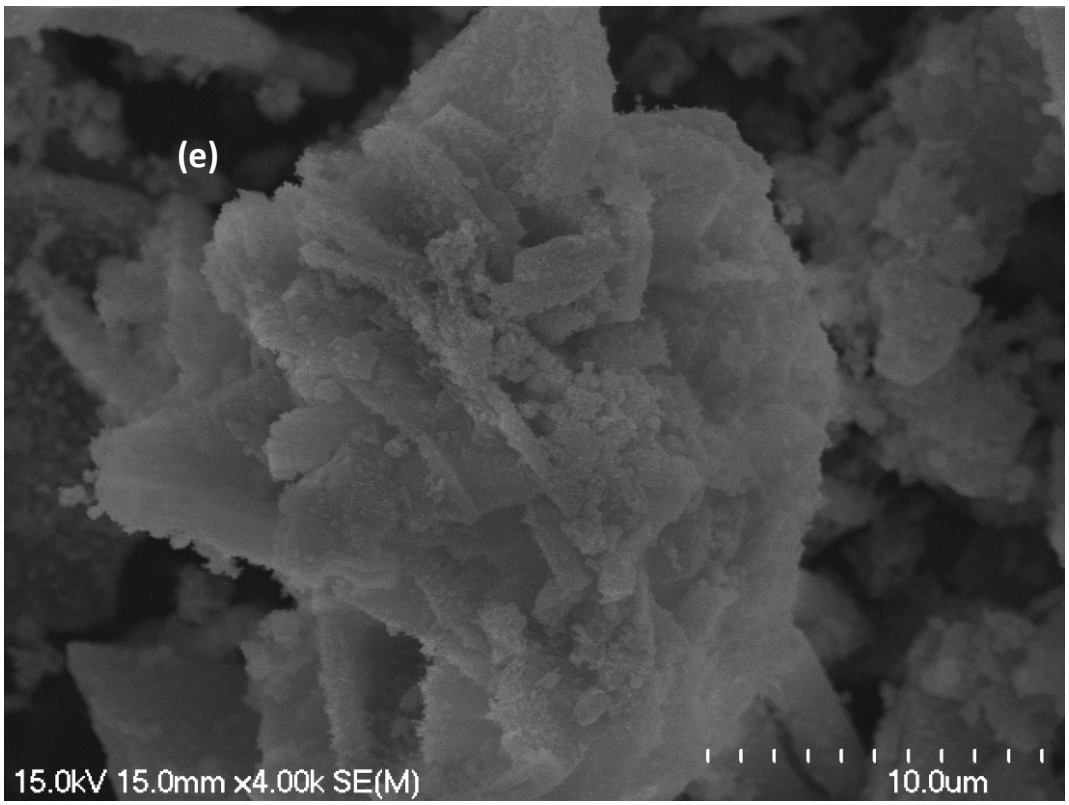
(e)
15.0kV 15.0mm x4.00k SE(M)
10.0um

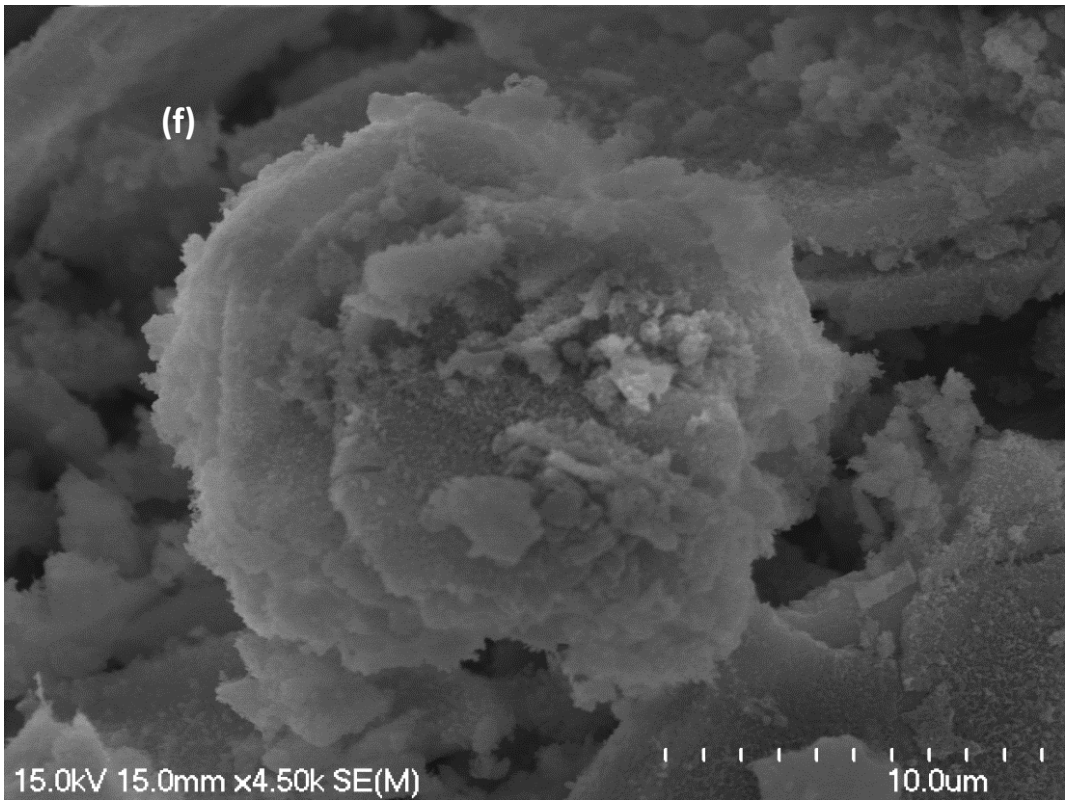
(f)
15.0kV 15.0mm x4.50k SE(M)
10.0um

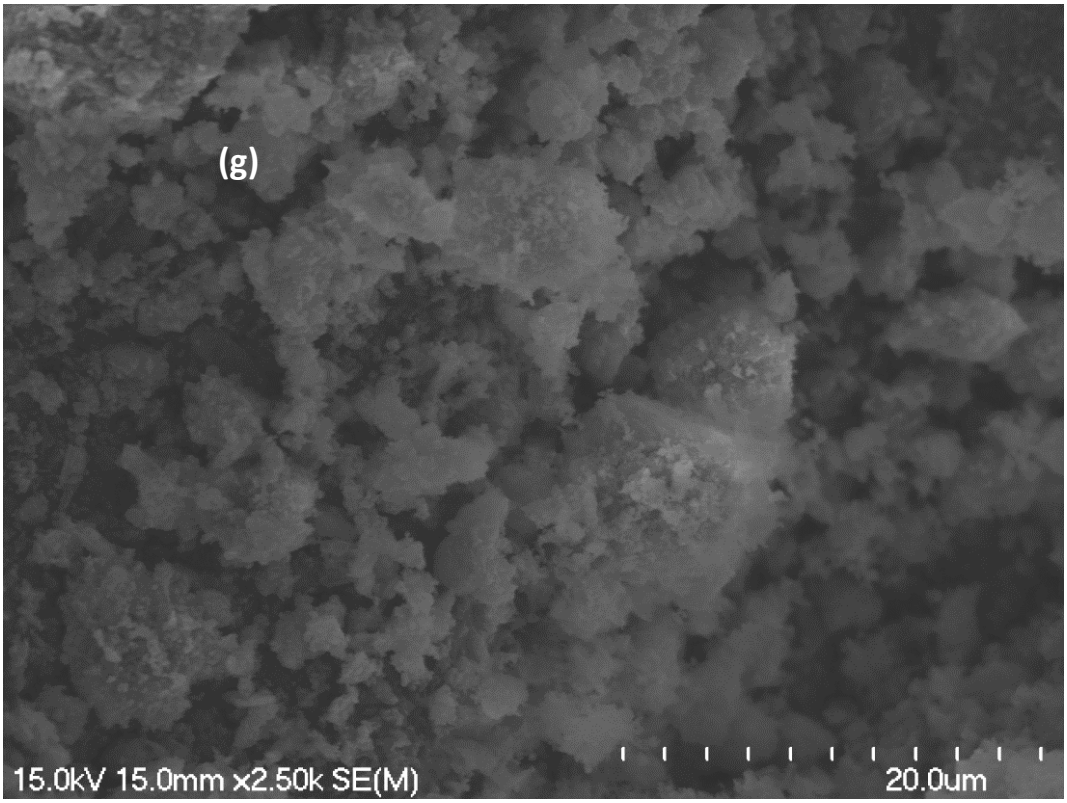

Figure 7-31: SEM images of the non-sintered (a) Unsubstituted HAp by hydrolysis (b) Unsubstituted HAp by precipitation (c) BrHAp by precipitation (d) Br_2Ap by precipitation (e,f) Br_2Ap by hydrolysis (g) Br_2Ap by ion exchange.

As recorded by SEM images, the morphology had not varied due to substitution of bromide ions by the precipitation route, irregular distribution of particles, and as well, the spheroidal shape can be considered as a major characteristic of precipitation route. On the other hand, **a** flower-like morphology was obtained by the hydrolysis method but in the case of the ion exchange preparation method, particles possessed a spherical like shape and were porous with irregular structure.

SEM of Br_2Ap and BrHAp materials prepared by precipitation, hydrolysis and ion exchange methods after sintering at 900 ˚C:

Fig.7-32 displays the SEM images of the sintered Br_2Ap and BrHAp powders as prepared by the hydrolysis, precipitation and ion exchange methods.

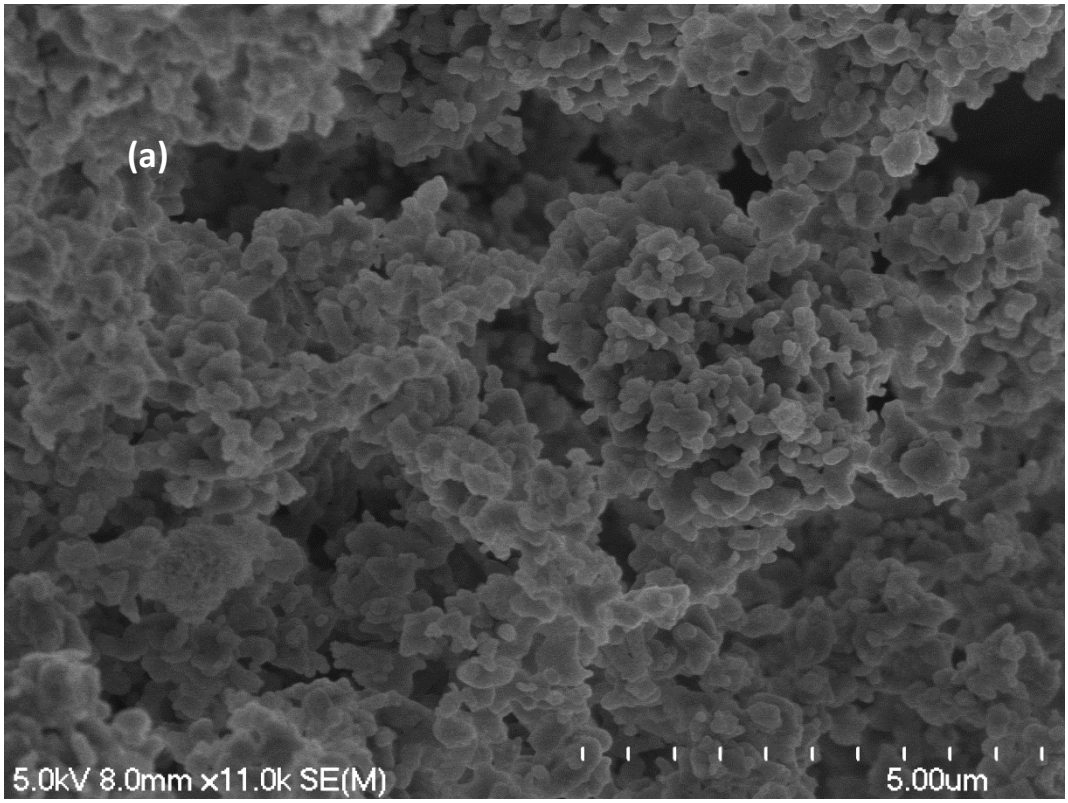
(a)
5.0kV 8.0mm x11.0k SE(M)
5.00um

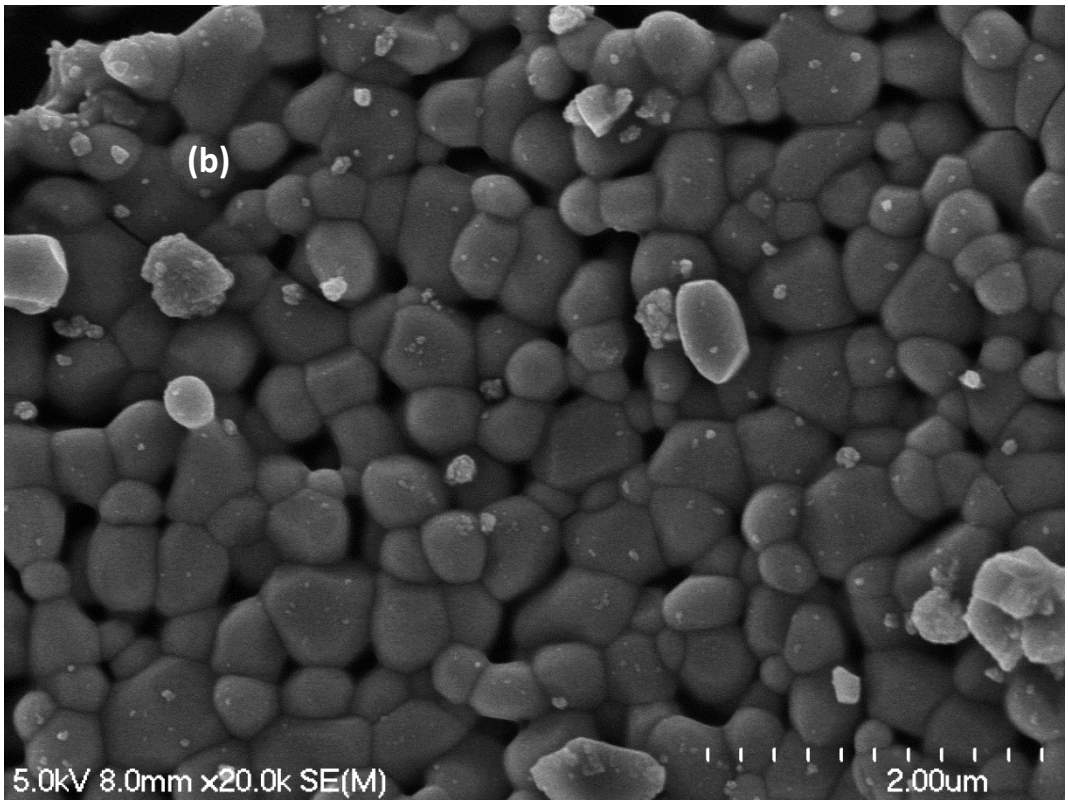
(b)
5.0kV 8.0mm x20.0k SE(M)
2.00um

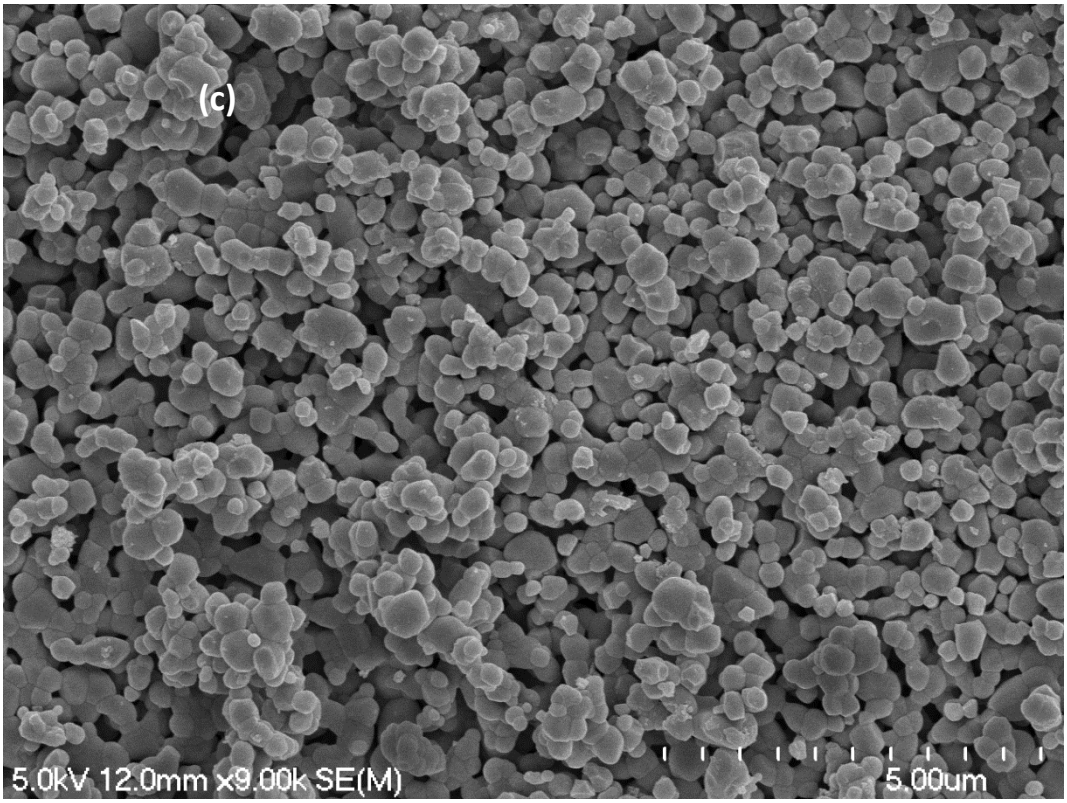
(c)
5.0kV 12.0mm x9.00k SE(M)
5.00um

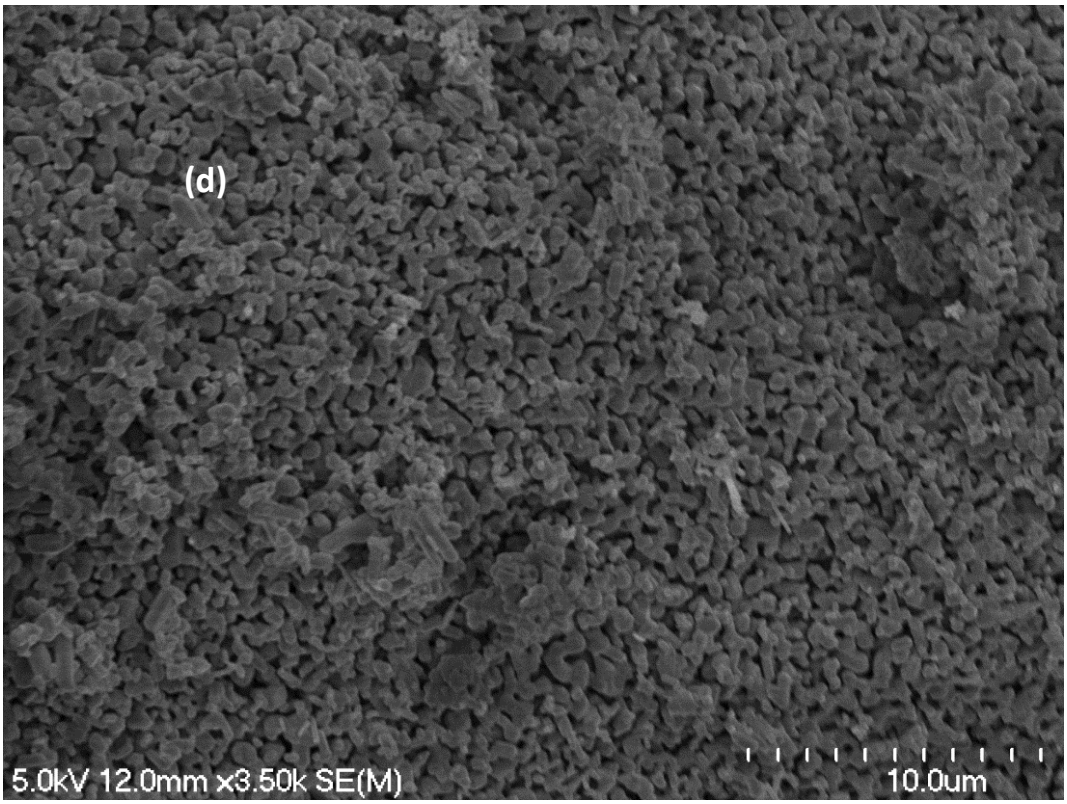
(d)
5.0kV 12.0mm x3.50k SE(M)
10.0um

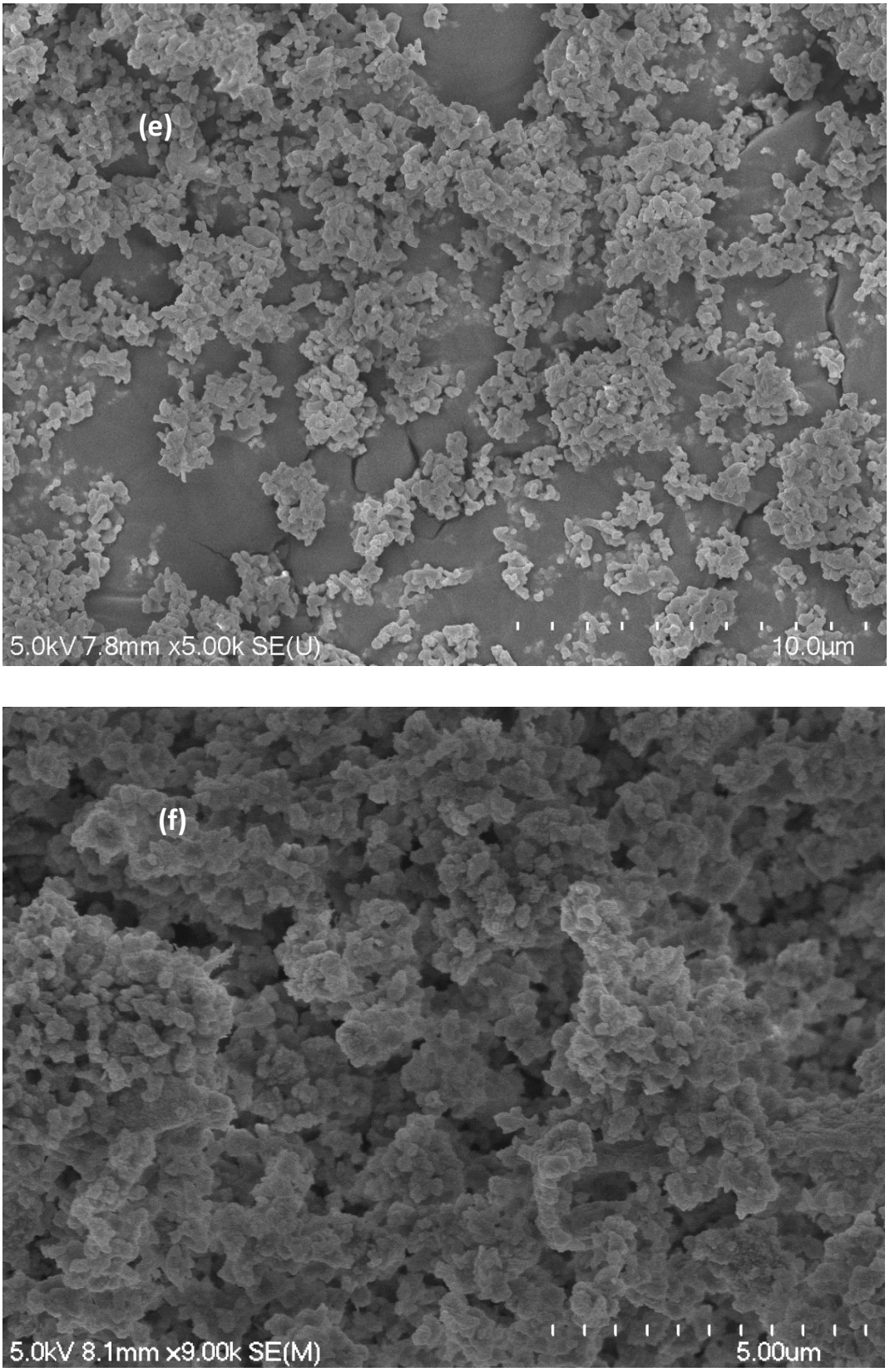

Figure 7-32: SEM images of (a) Unsubstituted HAp by hydrolysis (b) Unsubstituted HAp by precipitation (c) Br_2Ap by precipitation (d) Br_2Ap by hydrolysis (e) Commercial HAp (Fluka) (f) Br_2Ap by ion exchange, after sintering at 900 ˚C.

The morphology of the prepared powders was not affected by substitution of Br^- ions through different synthesis routes, since spheroidal like shapes with irregular distributed particles were detected by SEM images, coupled with an enhancement in the level of porosity especially in the cases of precipitation and hydrolysis methods. On the other hand, **Fig. 7-32** displays that the ion exchange method produced porous materials with a visible tendency to agglomerate. The same result was observed by other researchers. As an example Cho et al. [245] prepared chloride-substituted hydroxyapatites with the following formula $Ca_{10}(PO_4)_6(OH)_{2-x}(Cl)_x$, (x = 0.0, 0.5 and 1.0) by precipitation method. The SEM images showed that the morphology of the prepared materials had not varied due to substitution of Cl^- ions into HAp structure and remained similar to each other.

7.5 SHAp powders prepared by precipitation, hydrolysis and ion exchange methods:

In this project calcium sulfoapatite powders with the following chemical formula: $Ca_{10}(PO_4)_6S$ were prepared by three different synthesis routes (precipitation, hydrolysis and ion exchange), 5 g of each sample was prepared as mentioned previously (see Chapter three for details). The detailed amounts of the reagents are listed in **Table 7-26.**

Table 7-26: Synthesis details of SAp materials prepared by precipitation, hydrolysis and ion exchange methods.

Sample name	MCP $Ca(H_2PO_4)_2$ (g)	$Ca(OH)_2$ (g)	$Ca(NO_3)_2$ (g)	Na_2HPO_4 (g)	NaSH (g)	MCP (mol)	$Ca(OH)_2$ (mol)	$Ca(NO_3)_2$ (mol)	Na_2HPO_4 (mol)	NaSH (mol)
SAp by ion exchange $Ca_{10}(PO_4)_6S$	-	-	-	-	56.060	-	-	-	-	1.0000
SAp by hydrolysis $Ca_{10}(PO_4)_6S$	11.6721	3.7173	-	-	0.2863	0.0499	0.0502	-	-	0.0051
SAp by precipitation $Ca_{10}(PO_4)_6S$	-	-	8.1958	4.2513	0.2749	-	-	0.0499	0.0299	0.0049

7.5.1 Characterization techniques of prepared SAp materials by precipitation, hydrolysis and ion exchange methods.

7.5.1.1 ICP/MS of SAp materials prepared by precipitation, hydrolysis and ion exchange methods after sintering at 900 ˚C.

The results of the elemental analyses of SAp samples that were prepared by precipitation, hydrolysis and ion exchange routes are displayed in **Table 7-27**.

Table 7-27: ICP-MS results of SAp materials prepared by precipitation, hydrolysis and ion exchange methods after sintering at 900 ˚C. The concentration was in ppb unit (ug/L):

Sample	Ca 44	P 31	Na 23	S 34
Unsubstituted HAp by precipitation	707795	401240	103797	-
SAp by precipitation	711449	383124	79368	31843.1
Unsubstituted HAp by hydrolysis	769928	423970	78396	-
SAp by hydrolysis	728367	413363	157026	50605
SAp by ion exchange	750507	371647	11202	11587.7
Commrcial HAp (Fluka)	557227	262446	298	-

The calcium/phosphorus (Ca/P) molar ratios as well as (Ca+Na)/P molar ratio for whole prepared SHAp samples were determined by ICP-MS and presented in **Table 7-28.**

Table 7-28: The chemical analysis data of SAp materials by ICP-MS measurements after sintering at 900 ˚C.

Sample	Ca/P Theoretical	Ca/P Measured	(Ca+Na)/ P Measured	Wt.% of S^{2-} ions theoretical	Wt.% of S^{2-} ions measured
Unsubstituted HAp by precipitation	1.67	1.36	1.71	-	-
SAp by precipitation	1.67	1.43	1.59	3.2%	1.6%
Unsubstituted HAp by hydrolysis	1.67	1.40	1.65	-	-
SAp by hydrolysis	1.67	1.36	1.67	3.2%	2.5%
Commercial HAp (Fluka)	1.67	1.64	1.64	-	-
SAp by ion exchange	1.67	1.56	1.55	3.2%	0.6%

Table 7-28 displays the measured values of Ca/P and (Ca+Na)/ P mole ratios for the whole prepared SAp materials. The presence of S^{2-} ions into HAp samples was confirmed by ICP-MS analysis though this did not necessarily prove that S was substituted in the lattice. The results as shown in **Table 7-28** displayed that Ca/P mole ratios for the prepared powders by precipitation and hydrolysis were lower than the expected value of stoichiometric HAp due to presence of sodium ions, but the (Ca+Na)/ P for the prepared powders by hydrolysis method was found to be identical with the stoichiometric HAp. In the case of precipitation and ion exchange routes, the experimental results showed that the measured values were (1.59 and 1.55) respectively, which are lower than the expected value of stoichiometric HAp (1.67).

7.5.1.2 FTIR of SAp materials prepared by precipitation, hydrolysis and ion exchange methods.

FTIR of the non-sintered SAp materials prepared by precipitation, hydrolysis and ion exchange methods.

Fig.7-33 displays the FTIR spectra of the non-sintered SAp material prepared by different synthesis routes.

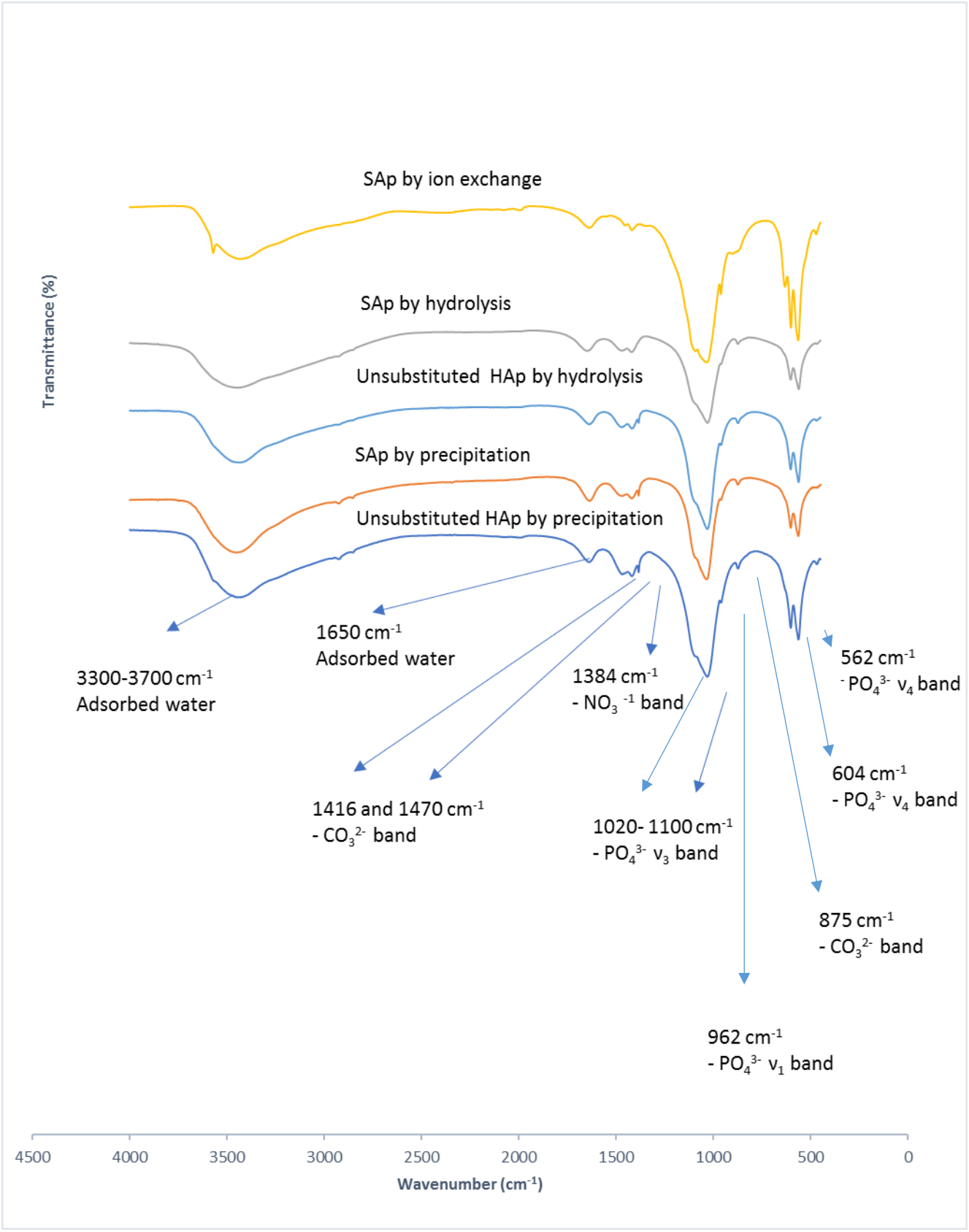

Figure 7-33: FTIR spectra of the non-sintered SAp materials prepared by precipitation, hydrolysis and ion exchange methods.

The recorded peaks at 562 and 604 cm^{-1} referred to the bending vibrational mode in PO_4^{3-}. The stretching modes of PO_4^{3} bonds were observed at 963 and 1035-1075 cm^{-1}. The characteristic bands at 875, 1470 and 1415 cm^{-1} that appeared in the case of precipitation and hydrolysis methods were attributed to a/the carbonate group. A typical peak of nitrate at 1384 cm^{-1} was obtained as a result of using calcium nitrate as a starting material in the case of precipitation route. The fundamental band of the hydroxyl group at 630 cm^{-1} in the prepared SAp powders by soaking method were confirmed by FTIR, while a stretching band was obscured by the presence of a broad peak of H_2O at 3000-3700 cm^{-1}. Also, the absence of hydroxyl bands at 630 and 3572cm^{-1} in the SAp materials by other synthesis routes were recorded and can be considered as evidence of obtaining amorphous samples by precipitation and hydrolysis methods.

FTIR of SHAp materials prepared by precipitation, hydrolysis and ion exchange, after sintering at 900 ˚C:

Fig.7-34 displays the FTIR spectra of the sintered SAp material prepared by different synthesis routes.

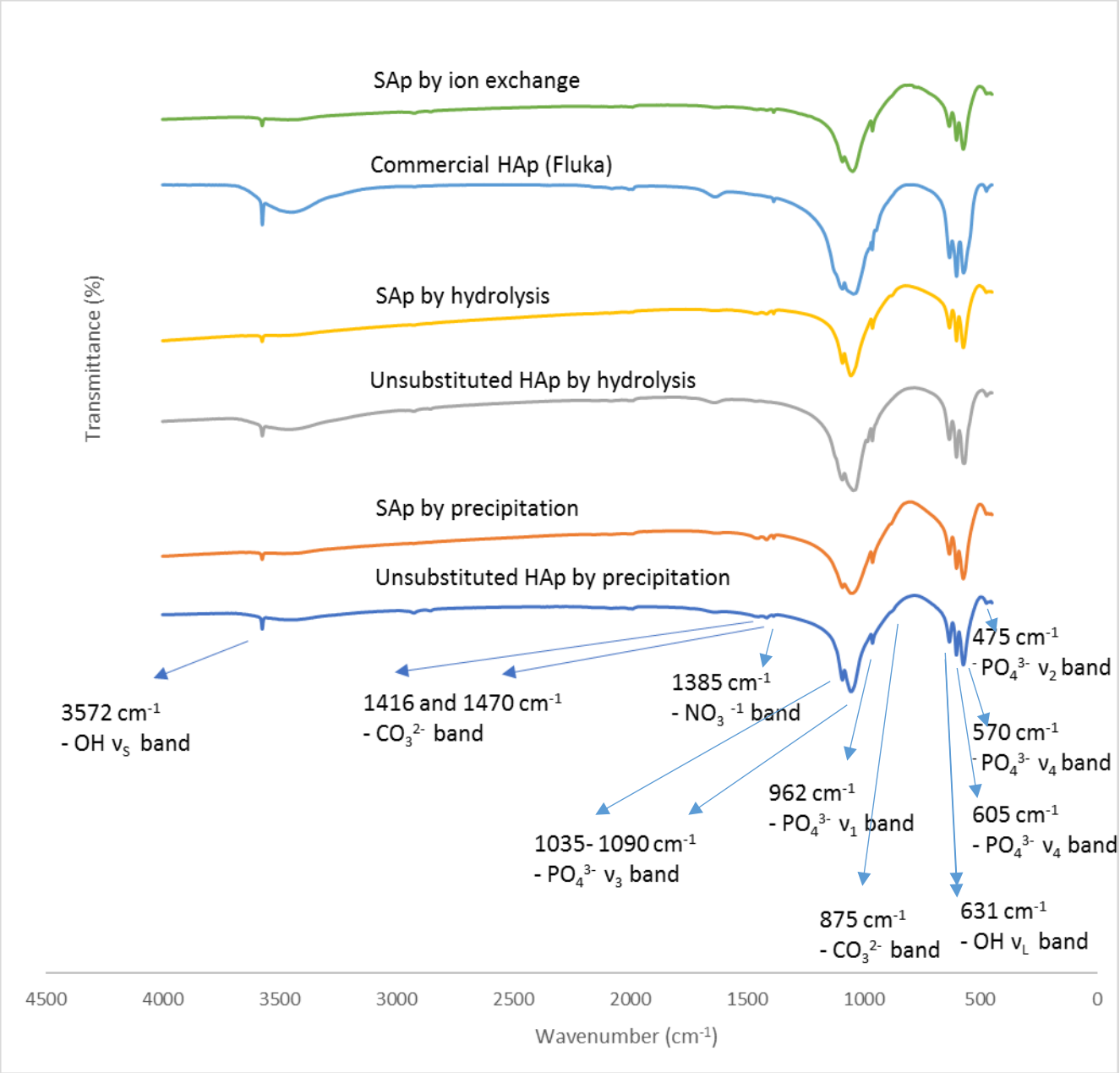

Figure 7-34: ***FTIR spectra SAp materials prepared by precipitation, hydrolysis and ion exchange methods after sintering at 900 ˚C.***

The peaks corresponding to the bending and stretching bands of PO_4^{3-} group at (574 and 604 cm^{-1}, 962, 1035-1090 cm^{-1}) and to the hydroxyl group at 630 and 3572 cm^{-1} were observed in all samples. The substitution of CO_3^{2-} group in prepared SAp powders by using three different preparation methods was confirmed by FTIR through the existence of the characteristic bands of carbonate at 1416 and 1450 $cm^{-1,}$ suggesting that some CO_2 gas in the

atmosphere had been introduced through the preparation process. While the intensity of the librational mode of OH^- group at 630 cm^{-1} has not shown any significant difference, **Fig 7-34** revealed an obvious decrease in the intensity of the stretching mode of the OH^- group at 3752 cm^{-1} in samples of HAp prepared by the hydrolysis, precipitation and ion exchange methods had taken place. This observation can be attributed to the partial substitution of S^{2-} by OH^- in hydroxyapatite crystal.

Also, the reduction in the intensity of the stretching mode of the OH^- group at 3752cm^{-1} can be ascribed to the presence of sodium ions as confirmed by ICP-MS analysis (see Chapter four), coupled with the formation of CO_3HAp powders as detected by FTIR spectra in the cases of precipitation and hydrolysis methods. Therefore, the OH^- ion content was determined by the requirement to keep charge balance and to restore the neutrality of HAp crystals.

7.5.1.3 XRD diffraction patterns of SAp materials prepared by precipitation, hydrolysis and ion exchange methods.

Phase Identification of the non-sintered and sintered SAp materials prepared by precipitation, hydrolysis and ion exchange methods.

Figures 7-35 and 7-36 show the typical XRD patterns of the non-sintered and sintered SAp powders prepared by precipitation, hydrolysis and ion exchange methods.

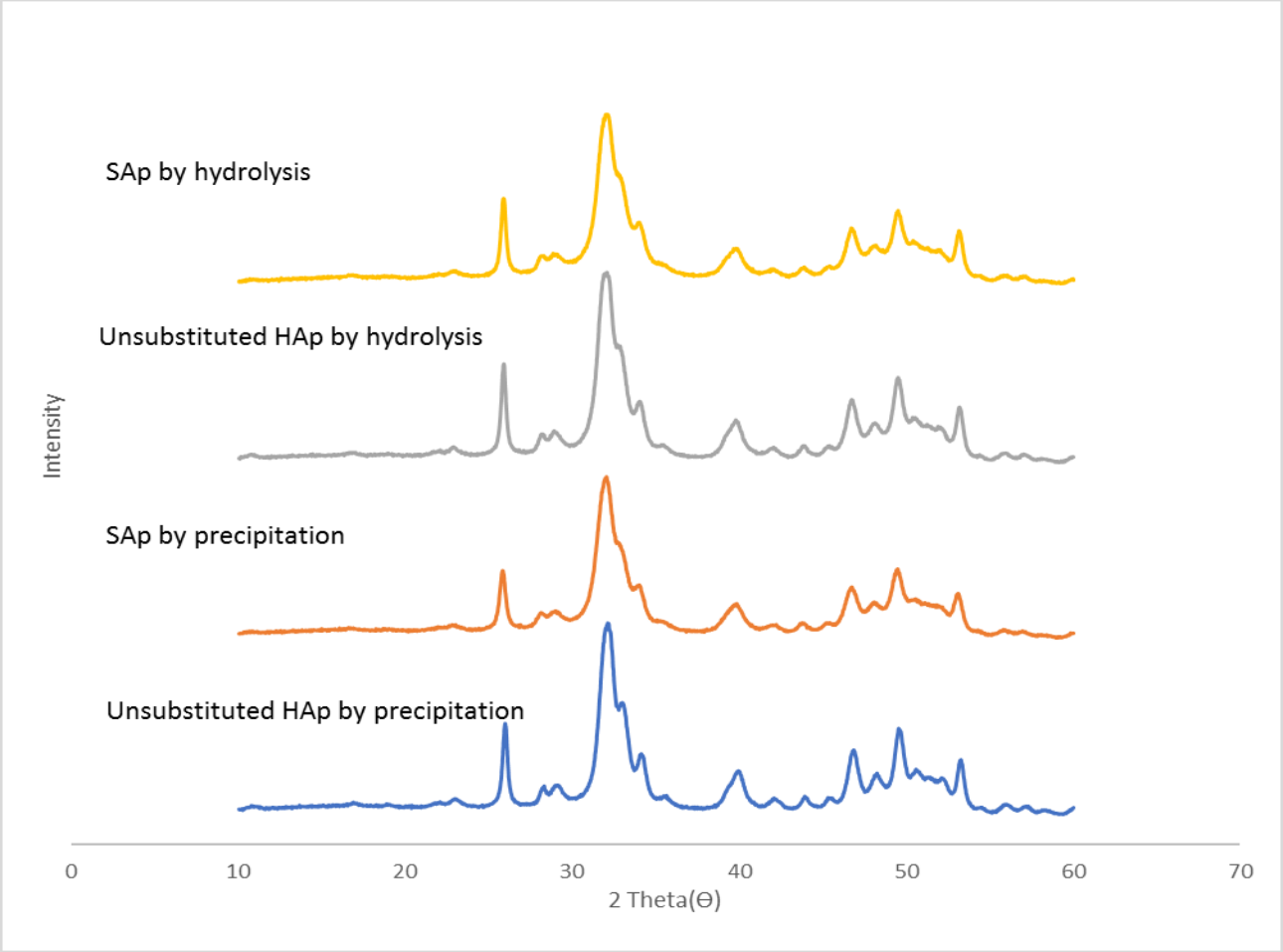

Figure 7-35: The XRD diffraction patterns of non-sintered SAp materials by precipitation and hydrolysis methods.

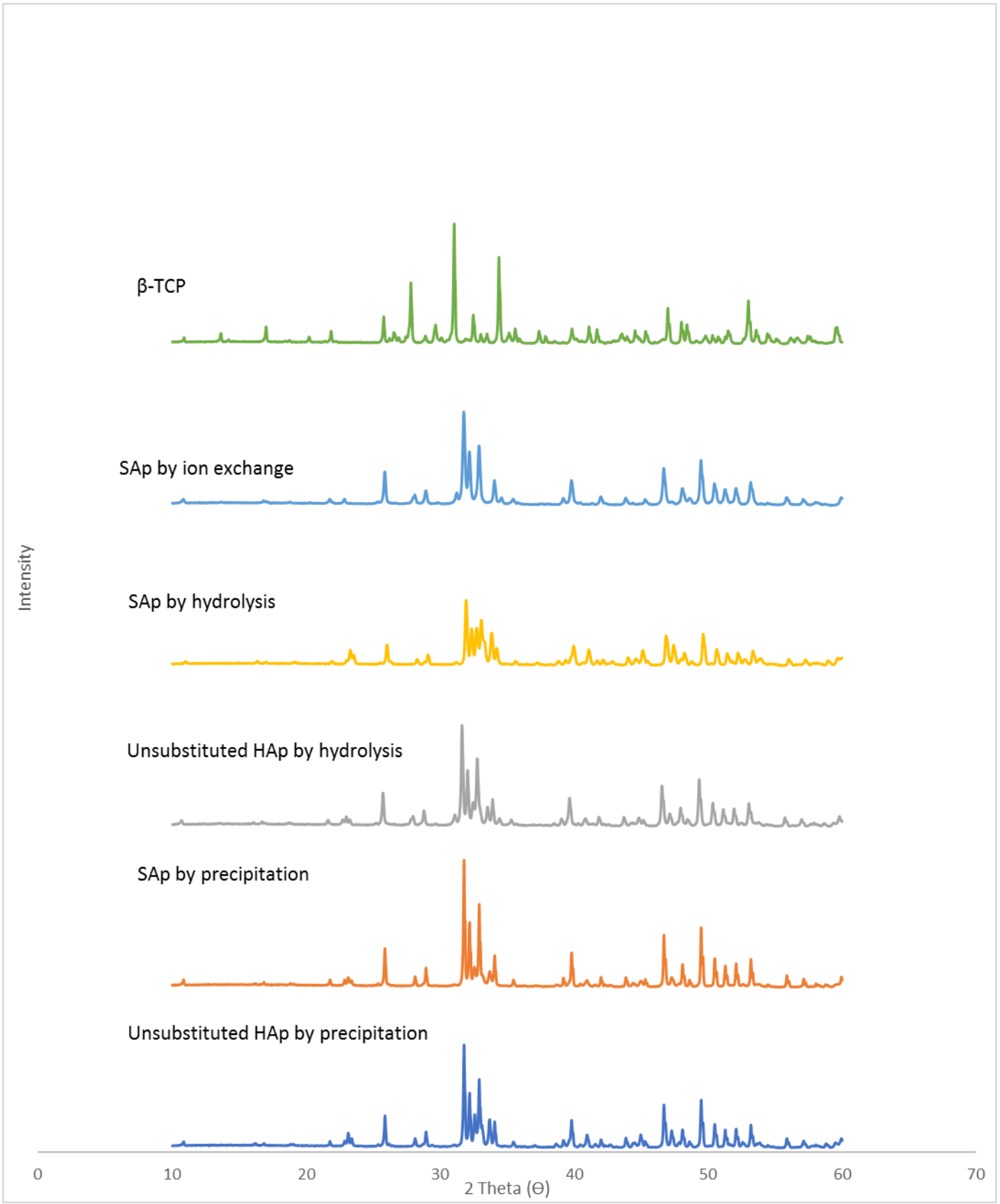

Figure 7-36: The XRD diffraction patterns of SAp materials prepared by precipitation, hydrolysis and ion exchange methods after sintering at 900 ˚C.

A significant variation in the XRD patterns of the prepared samples by using different synthesis approaches was detected, which reflects the effect of synthesis route on the phase purity. While the majority of the diffraction patterns of the produced SAp powders by various preparation methods indicate a mostly HAp phase, we can see some peaks corresponding to a β-TCP phase impurity, indicating the formation of biphasic material, especially in the case of SAp samples, which was prepared by the novel hydrolysis method that were characterized by a clear reduction in the intensities of some peaks at 2 Theta = 21.7˚, 32.3˚, 33.1˚ and 34.3˚ and that are attributed to the HAp phase, combined with an increase in the intensities of other peaks that correspond to impurity phase (β-TCP) at 2 Theta = 32.8˚, 33.6˚, 41.14˚ and 47.36˚. In the case of the precipitation method, a decrease in the intensities of major peaks of β-TCP, coupled with disappearance of some peaks that are attributed to impurity phase at 2 Theta = 31.2˚ and 38.8˚, were recorded, suggesting a much purer phase of SHAp materials, and indicating that the substitution of S^{2-} ions had enhanced thermal stability of hydroxyapatite. On the other hand, the only effect that was detected through using the ion exchange route was the reduction in the intensity of one of the typical peaks of β-TCP at 2 Theta =31.2˚.

Crystallinity and crystallite size of prepared SAp materials by precipitation, hydrolysis and ion exchange methods:

Table 7-29 displays the degree of crystallinity and crystallite size of sintered SAp materials prepared by precipitation, hydrolysis and ion exchange methods.

Table 7-29: The degree of crystallinity and crystallite size of SAp materials prepared by precipitation, hydrolysis and ion exchange methods, after sintering at 900 ˚C.

Sample	D_{002} (Å)	Crystallinity %
Unsubstituted HAp by precipitation	618.3±3.2	84.15±2.4
SAp by precipitation	791.1±6.4	85.56±2.2
Unsubstituted HAp by hydrolysis	549.8±3.6	82.57±2.1
SAp by hydrolysis	507.9±4.4	70.44±4.1
Commercial HAp (Fluka)	395.0±2.8	77.31±4.2
SAp by soaking	268.6±3.2	83.91±3.1

The substitution process of S^{2-} ions into HAp samples by the precipitation and ion exchange methods enhances the numerical values of crystallinity, as confirmed by (**Table 7-29**). On the other hand, **Fig.7-36** shows that the peaks of SAp powders became much broader, and as well there was a reduction in their intensities which occurred as a result of using the hydrolysis method indicating a decrease in the crystallinity. The calculated value of crystallinity of SHAp materials, which were prepared by the novel hydrolysis method hydrolysis was decreased (70.43) due to the replacement process of S^{2-} ions into HAp structure.

Also, **Table 7-29** shows the effect of synthesis route on the value of the crystallite size, where an increase was recorded following precipitation method. In contrast, a reduction was achieved by hydrolysis and ion exchange methods, indicating the effect of the preparation method and the chemical composition on the numerical value of the crystallite

Lattice parameters and volume of unit cell of the sintered SAp materials prepared by precipitation, hydrolysis and ion exchange methods:

Table 7-30 displays the lattice parameters and the volume of hexagonal unit cell of sintered SHAp materials prepared by the precipitation, hydrolysis and ion exchange methods.

Table 7-30: The lattice parameters and the volume of hexagonal unit cell of SHAp materials prepared by precipitation, hydrolysis and ion exchange methods, after sintering at 900 ˚C.

Sample	a [Å]	c [Å]	V[Å^3]
Unsubstituted HAp by precipitation	9.416±0.004	6.879±0.003	1579±0.004
SAp by precipitation	9.420±0.006	6.882±0.004	1580±0.005
Unsubstituted HAp by hydrolysis	9.421±0.003	6.882±0.005	1581±0.004
SAp by hydrolysis	9.422±0.004	6.883±0.002	1582±0.003
Commercial HAp (Fluka)	9.391±0.005	6.861±0.005	1566±0.005
SAp by ion exchange	9.392±0.002	6.864±0.002	1568±0.002

Table 7-30 displays an increase in the both values of lattice parameters (a and c) due to substituting S^{2-} ions by the whole preparation methods. These results are related to the ionic radius of S^{2-} (0.189 nm) [216]compared to OH^- (0.152 nm). Also, Henning et al. [25] prepared sulfoapatite by solid state reactions of CaS and $Ca_3(PO_4)_2$ at 1373 K in an evacuated quartz tube

for 24 hours. The XRD results showed the value of lattice constants (a) and (c) were found to be 9.4619(6) Å and 6.8342(8) Å, respectively.

7.5.1.4 SEM of SAp materials prepared by precipitation, hydrolysis and ion exchange methods.

SEM of the non-sintered SAp materials prepared by precipitation, hydrolysis and ion exchange methods.

Fig.7-37. displays the SEM images of the non-sintered SAp powders prepared by hydrolysis, precipitation, and ion exchange methods.

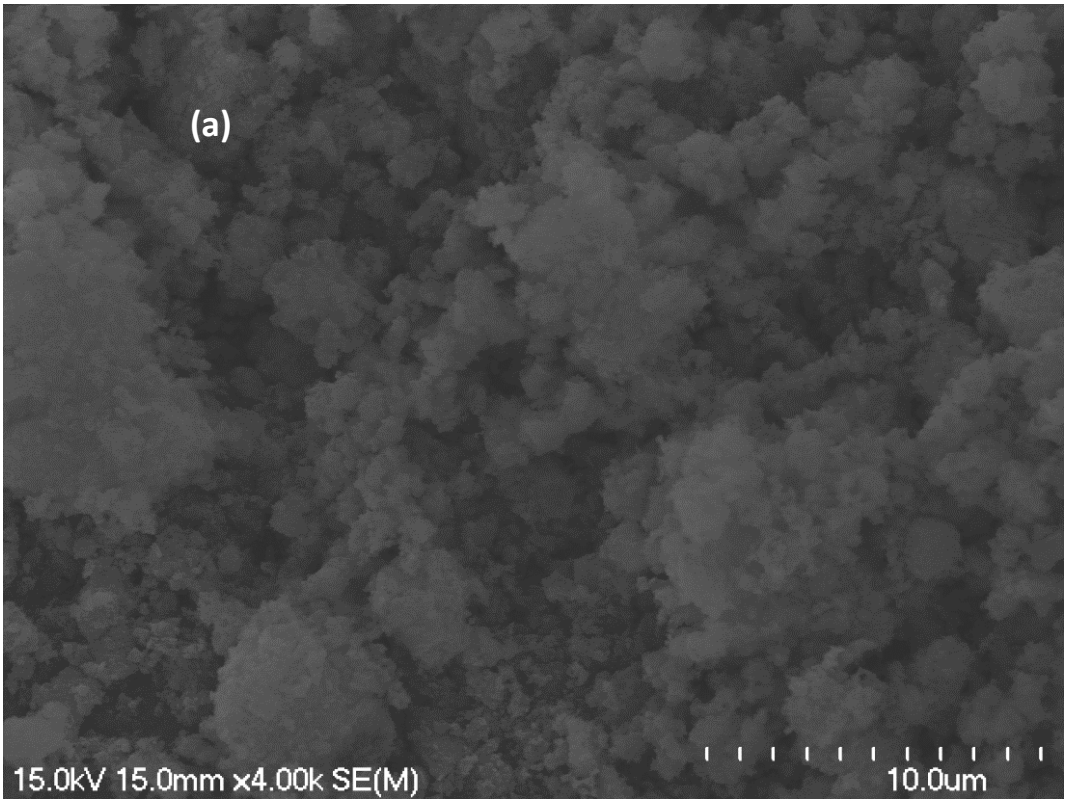

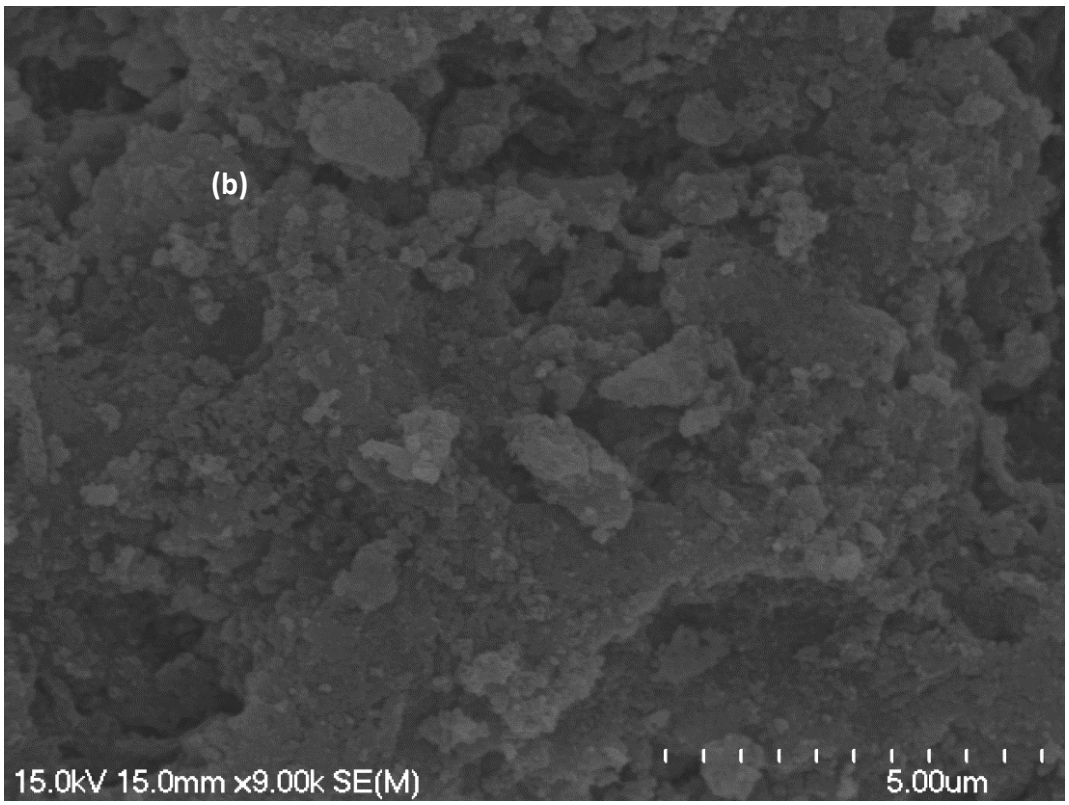
(b)
15.0kV 15.0mm x9.00k SE(M)
5.00um

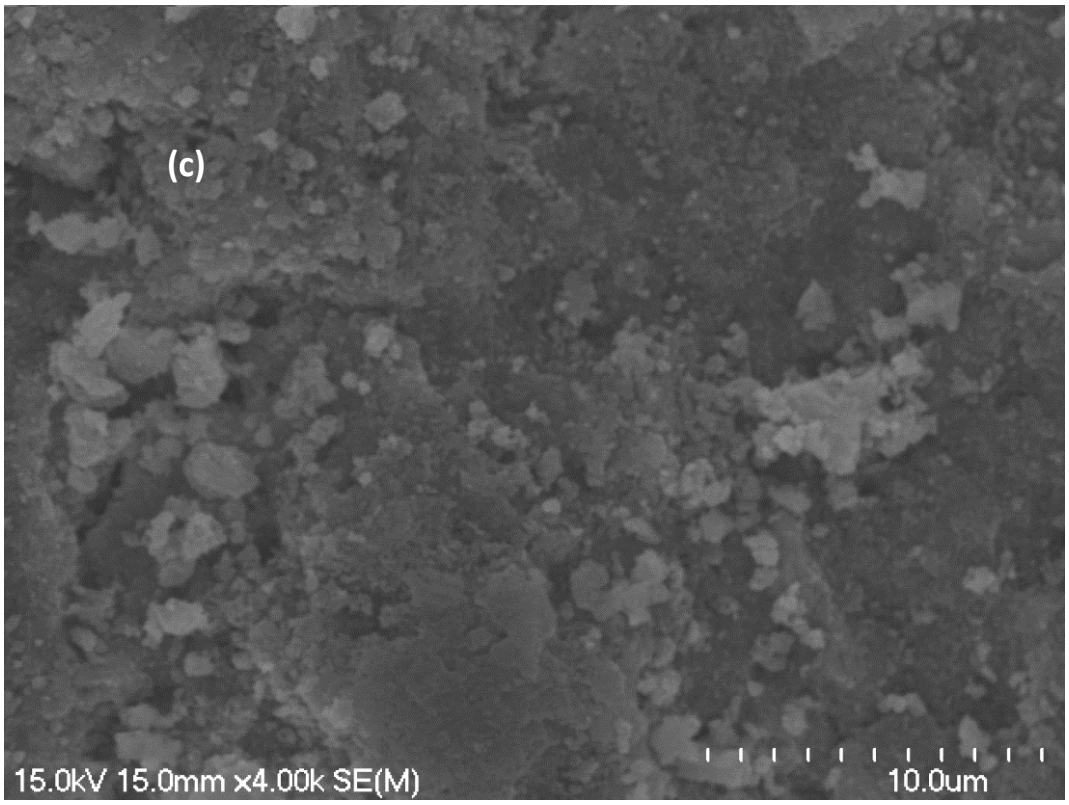
(c)
15.0kV 15.0mm x4.00k SE(M)
10.0um

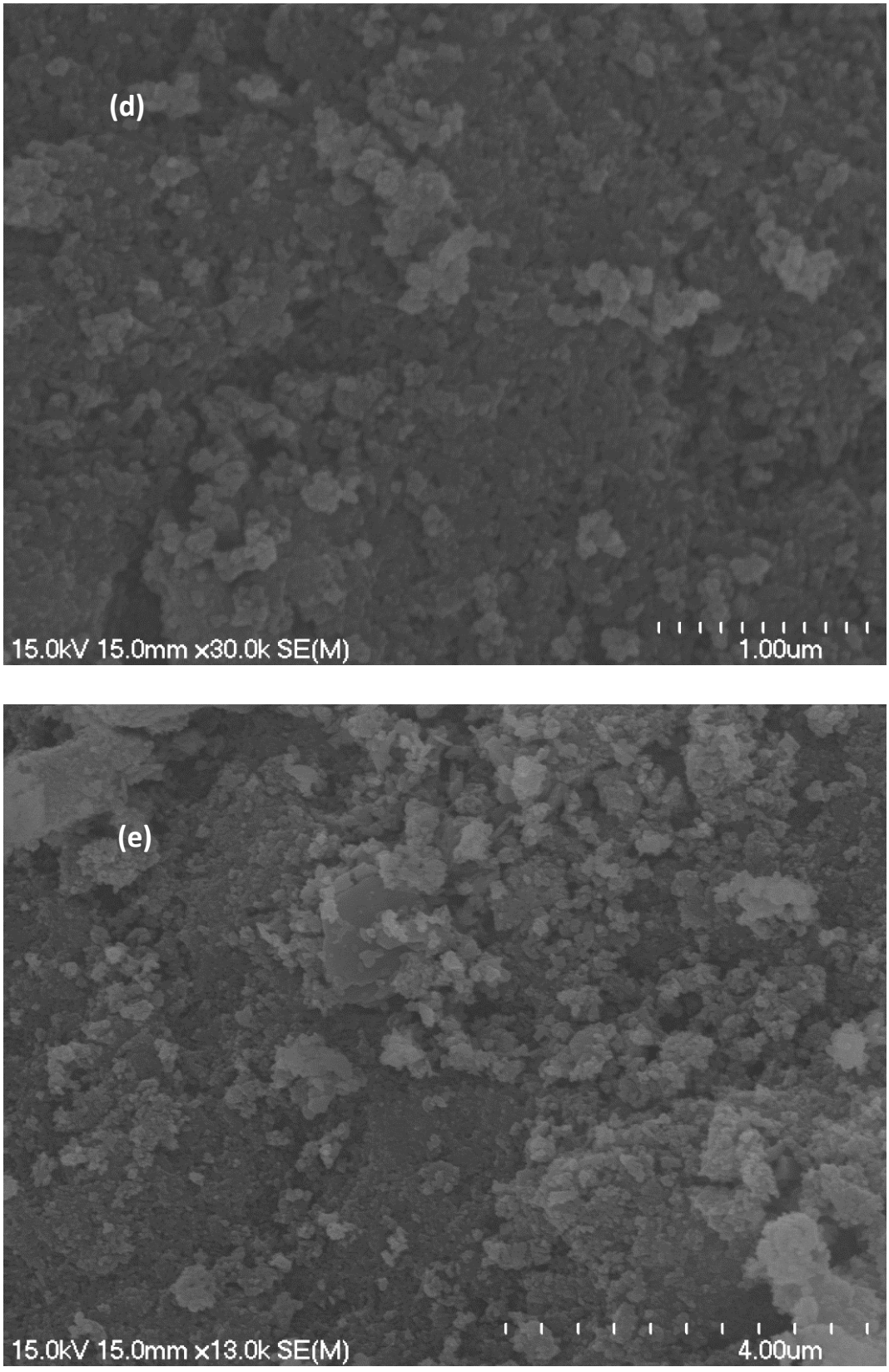

Figure 7-37: SEM mages of the non-sintered (a) Unsubstituted HAp by hydrolysis (b) Unsubstituted HAp by precipitation (c)SAp by hydrolysis (d) SAp by precipitation (e) SAp by ion exchange.

Fig. 7-37 shows the morphology of SAp powders, which were prepared by several synthesis methods. SEM images revealed that the morphology of the prepared materials by different methods did not change due to the substitution process, and in addition spheroid shapes were produced. Irregular distribution, and a clear ability to agglomerate and to form a porous powders were recorded for the whole prepared SAp samples.

SEM of SAp materials prepared by precipitation, hydrolysis and ion exchange methods after sintering at 900 ˚C:

Fig.7-38 displays the SEM images of the sintered S_2Ap powders as prepared by the hydrolysis, precipitation and ion exchange methods.

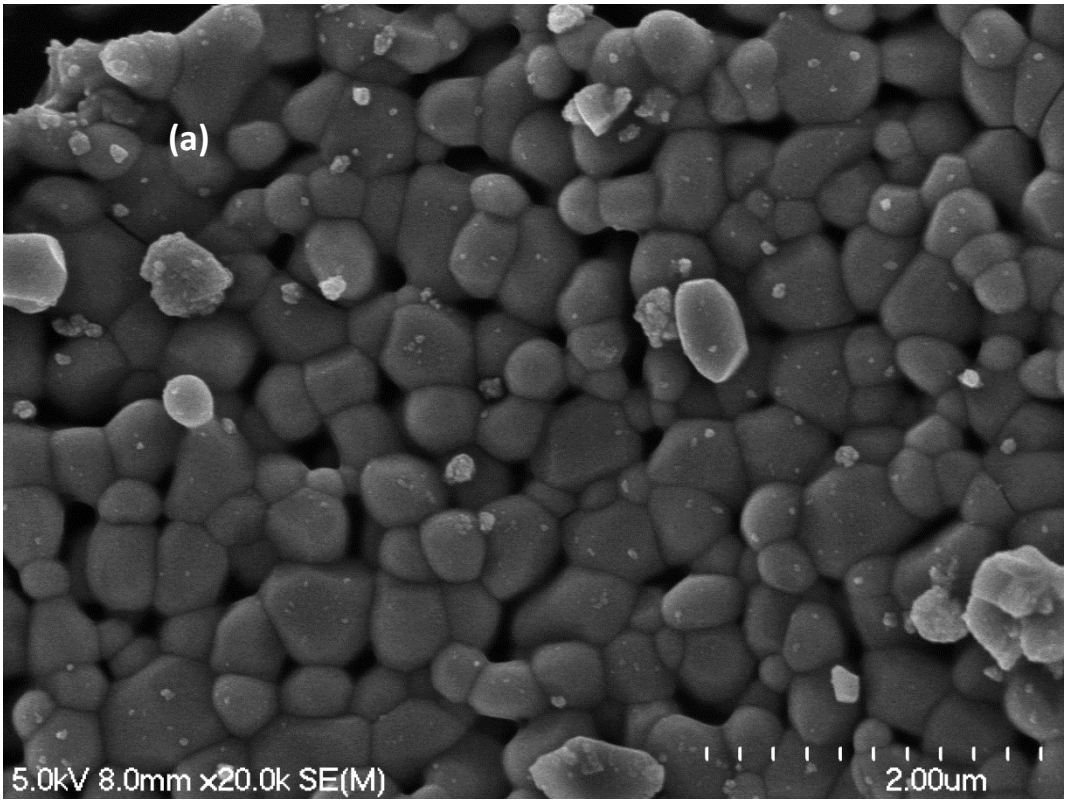

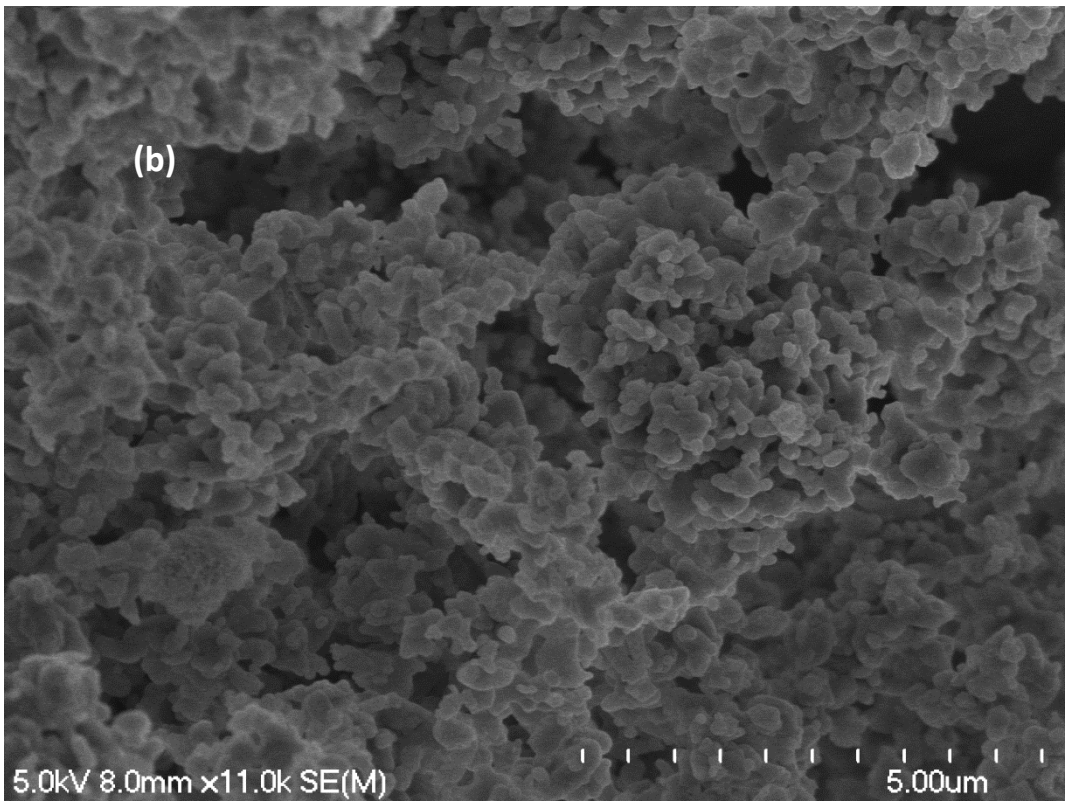
(b)
5.0kV 8.0mm x11.0k SE(M)
5.00um

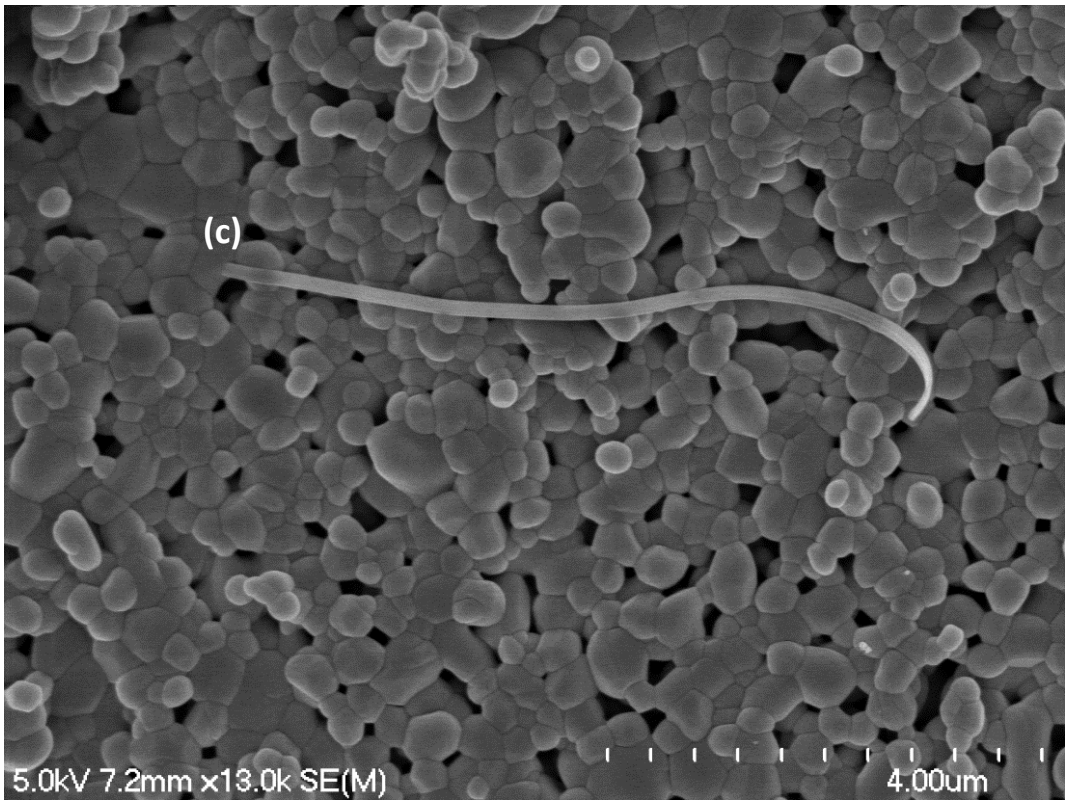
(c)
5.0kV 7.2mm x13.0k SE(M)
4.00um

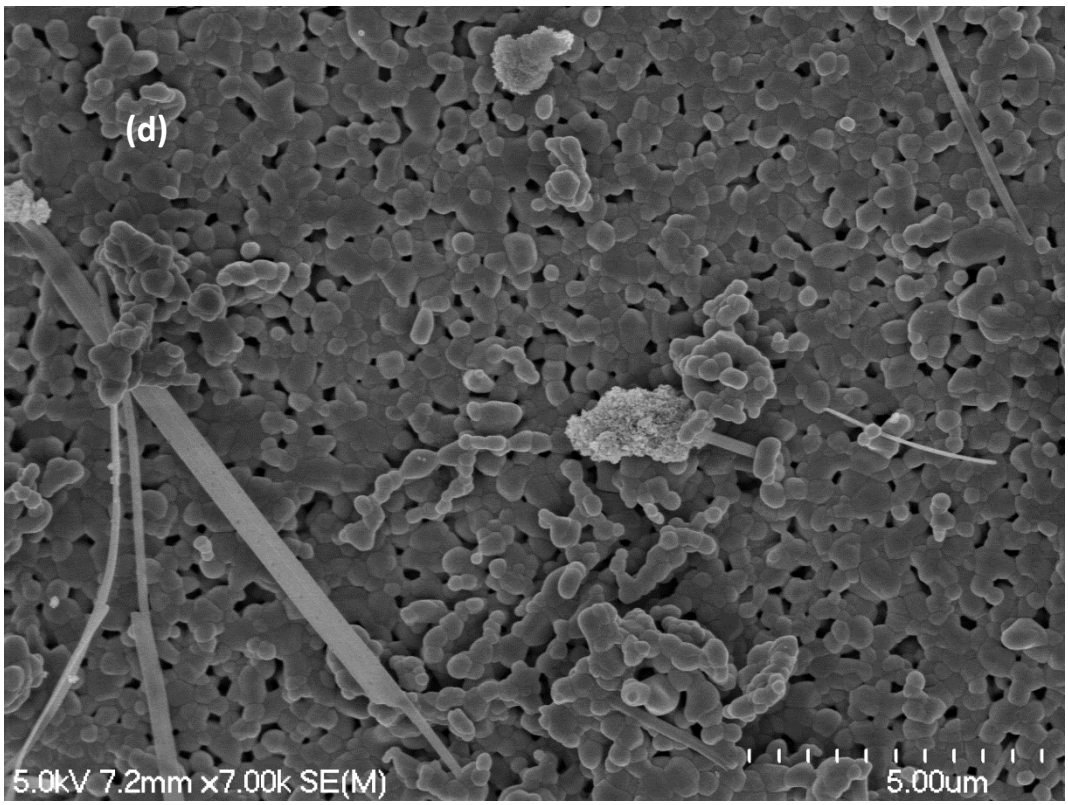
(d)
5.0kV 7.2mm x7.00k SE(M)
5.00um

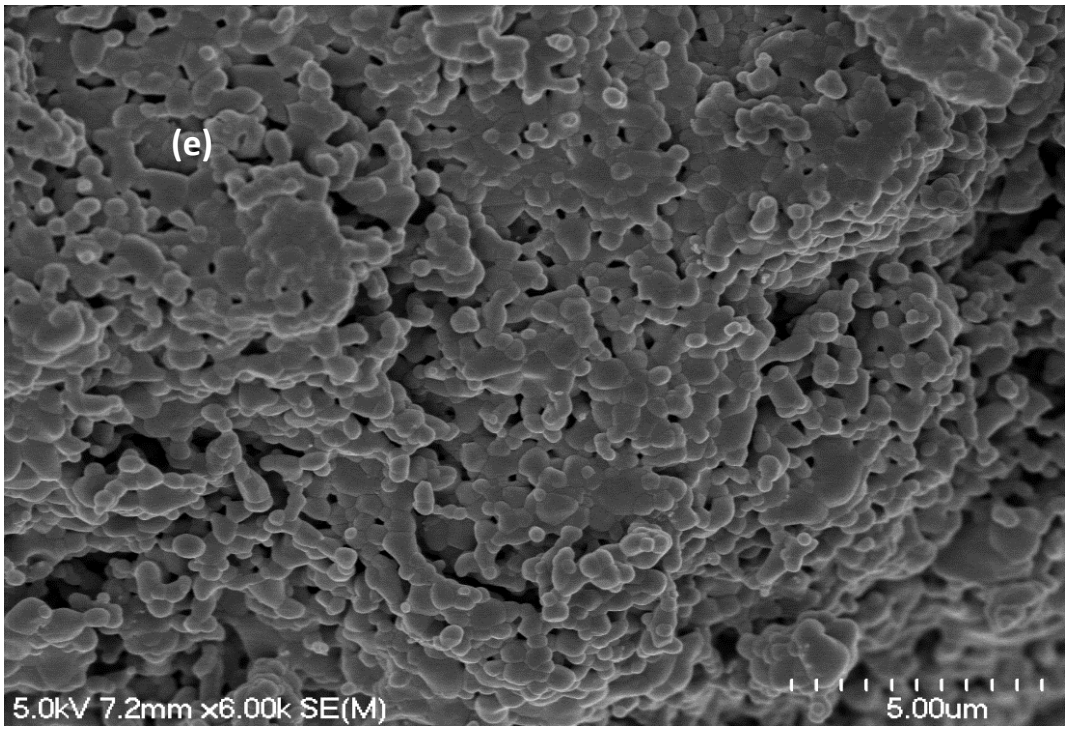
(e)
5.0kV 7.2mm x6.00k SE(M)
5.00um

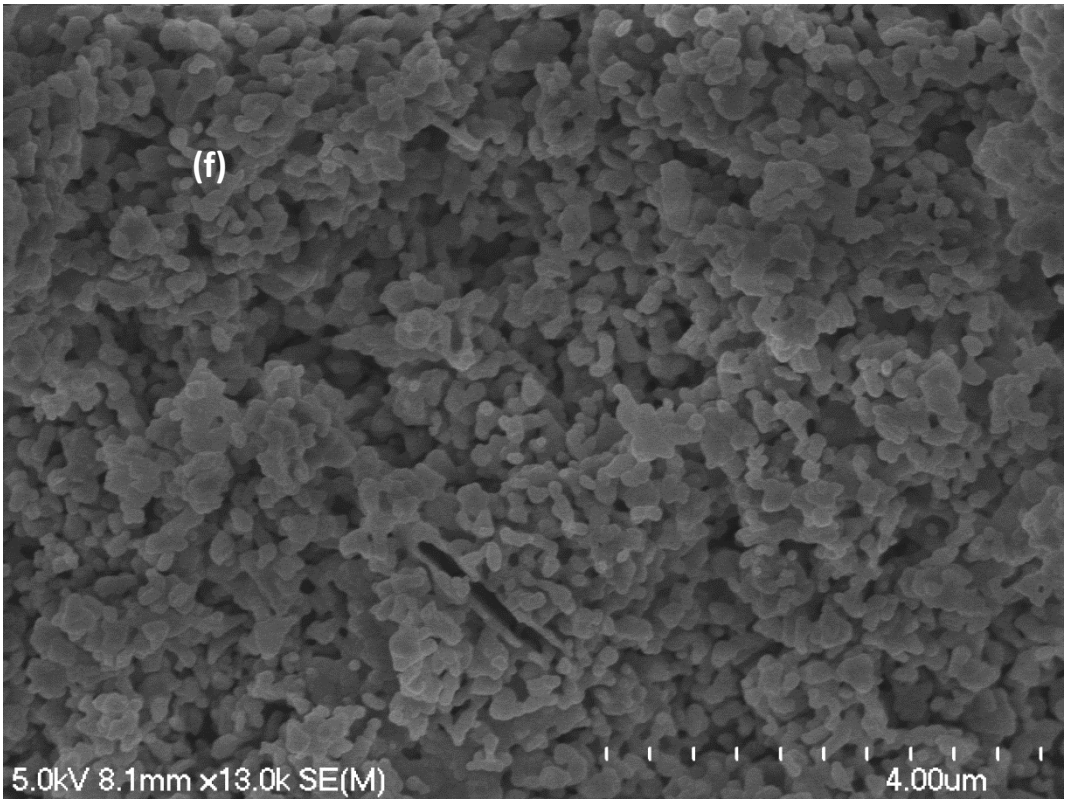

Figure 7-38: SEM images of: (a) Unsubstituted HAp by precipitation (b) Unsubstituted HAp by hydrolysis (c and d) SAp by precipitation (e) SAp by hydrolysis (f) SAp by ion exchange, after sintering at 900 ˚C.

Fig.7-38 shows the SEM images of the prepared SAp materials by three different synthesis routes, namely precipitation, hydrolysis as well as ion exchange methods**.** We can see that the particles of SAp by precipitation have spheroid like shape with a small quantity of whiskers, which reflect the ability of sulfide ions to form whiskers. The SEM/EDX techniques was also used to get a better idea about the elemental composition of the SAp samples that was prepared by the conventional precipitation method. The results of SEM/EDX analysis for the above-mentioned system can be found in the Appendix (see appendix A). The SEM/EDX results showed that:

1- The whiskers consist of Ca^{2+}, PO_4^{3-}, OH^-, CO_3^{2-} and Na^+ ions.

2- Also, the weight percent of Na^+ ions (4.44 and 3.86%) in the whiskers were found to be higher than the spherical particles (1.39%).

3- The Ca/P mole ratio of the whiskers are (1.78 and 1.62) compared to (1.64) of the spherical particles.

On the other hand, a spheroid shape, and an ability to agglomerate with porous powders was confirmed for SAp materials by soaking, while the irregular structure coupled with porous material was recorded in in the case of hydrolysis method.

7.6 Co-substitution of NaClHAp ($Ca_9Na(PO_4)_6(OH)Cl$) powders prepared by precipitation and hydrolysis methods:

There is a limited number of studies that describe the co-substitution process of sodium and chloride ions into HAp structure [28] but it appears no reports referring to co-substitution of these ions into HAp has been published or taken place by using a hydrolysis method for generating HAp. Hence 5g of co-substituted NaClHAp with the following chemical formula: $Ca_9Na(PO_4)_6(OH)Cl$ was prepared by precipitation and hydrolysis routes using the mentioned procedures in Chapter 3. The detailed amounts of the reagents are listed in **Table 7-31**

Table 7-31: Synthesis details of prepared NaClHAp materials by precipitation and hyfdrolysis methods.

Sample	$Ca(NO_3)_2$ (g)	$Ca(OH)_2$ (g)	MCPM (g)	Na_2HPO_4 (g)	NaCl (g)	$Ca(NO_3)_2$ (mol)	$Ca(OH)_2$ (mol)	MCPM (mol)	Na_2HPO_4 (mol)	NaCl (mol)	NaCL (mol)
NaClHAp by precipitation	7.3348	-	-	4.2350	0.2903	0.0447	-	-	0.0298	.0.0050	0.0036
NaClHAp by hydrolysis	-	3.3054	11.203	-	0.2902		0.0446	0.0446		0.0050	0.0036

7.6.1 Characterization techniques of prepared NaClHAp ($Ca_9Na(PO_4)_6(OH)Cl$) materials prepared by precipitation and hydrolysis methods.

7.6.1.1 ICP/MS of NaClHAp materials prepared by precipitation and hydrolysis methods after sintering at 900 ˚C:

The results of the elemental analyses of NaCl co substituted HAp samples that were prepared by ppt and hydrolysis routes are displayed in **Table 7-32 .**

Table 7-32: ICP-MS results of NaCl co substituted HAp materials prepared by precipitation and hydrolysis methods after sintering at 900 ˚C. The concentration was in ppb unit(ug/l):

Sample	Ca 44	P 31	Na 23
Unsubstituted HAp by precipitation	707795	401240	103797
NaClHAp by precipitation	748191	370392	55852
Unsubstituted HAp by hydrolysis	769928	423970	78396
NaClHAp by hydrolysis	728324	382589	111829

The starting (calculated) and actual (measured) degree of chemical composition of the prepared powders in terms of wt.% of Na^+ ions, the calcium/phosphorus (Ca/P) molar ratios as well as (Ca+Na)/P molar ratio were determined by ICP-MS and presented in **Table 7-33**

Table 7-33: The chemical analysis data of prepared NaClHAp materials by precipitation and hydrolysis methods by ICP-MS measurements

Sample	Ca/P Theoretical	Ca/P Measured	(Ca+Na)/ P	Wt.% of Na^+ ions theoretical	Wt.% of Na^+ ions measured
Unsubstituted HAp by precipitation	1.67	1.36	1.71	-	5.2%
NaClHAp by precipitation	1.50	1.56	1.76	2.3%	2.8%
Unsubstituted HAp by hydrolysis	1.67	1.40	1.65	-	3.9%
NaCl co-substituted HAp by hydrolysis	1.50	1.47	1.86	2.3%	5.6%

Tables 7-32 and 7-33 show clearly that presence of sodium ions into HAp structure, whereas the Ca:P mole ratios for the prepared samples were lower than (1.67). However, the measured values of (Ca+Na)/ P for the whole powders were higher than stoichiometric values, evidence of the replacement process of phosphate site by CO_3^{2-} group as shown by FTIR spectra.

As shown **i**n **Tables 7-32** and **7-33** Cl^- ions were not detected by ICP-MS analysis. The presence of Cl^- ions into HAp lattice were confirmed by using other techniques such as XRD and FTIR spectra (see later). Some elements like Cl and Br could not be detected by ICP-MS analysis. Therefore, the presence of these ions(Cl^- and Br^-) into HAp crystal can be determined through using other techniques such as XRD analysis. As an example:

Cho et al. [245] prepared chloride-substituted hydroxyapatites with the following formula $Ca_{10}(PO_4)_6(OH)_{2-x}(Cl)_x$, (x = 0.0, 0.5 and 1.0) by precipitation method through using calcium hydroxide , phosphoric acid and ammonium chloride as starting materials. The presence of Cl^- ions into hydroxyapatite crystal was confirmed by using XRD. The lattice parameters (a and c) of Cl substituted HAp samples were varied due to the substitution process. The Rietveld results showed that the lattice constants a and c of hydroxyapatite were (9.421 and 6.881 Å) compared to (9.457 and 6.870 Å) for 0.5 ClHAp and (9.541 and 6.843 Å) for 1.0 ClHAp.

7.6.1.2 FTIR of NaClHAp ($Ca_9Na(PO_4)_6(OH)Cl$) materials prepared by precipitation and hydrolysis methods.

FTIR of the non-sintered NaClHAp ($Ca_9Na(PO_4)_6(OH)Cl$) materials prepared by precipitation and hydrolysis methods.

Fig.7-39 displays the FTIR spectra of the non-sintered NaClHAp material prepared by different synthesis routes.

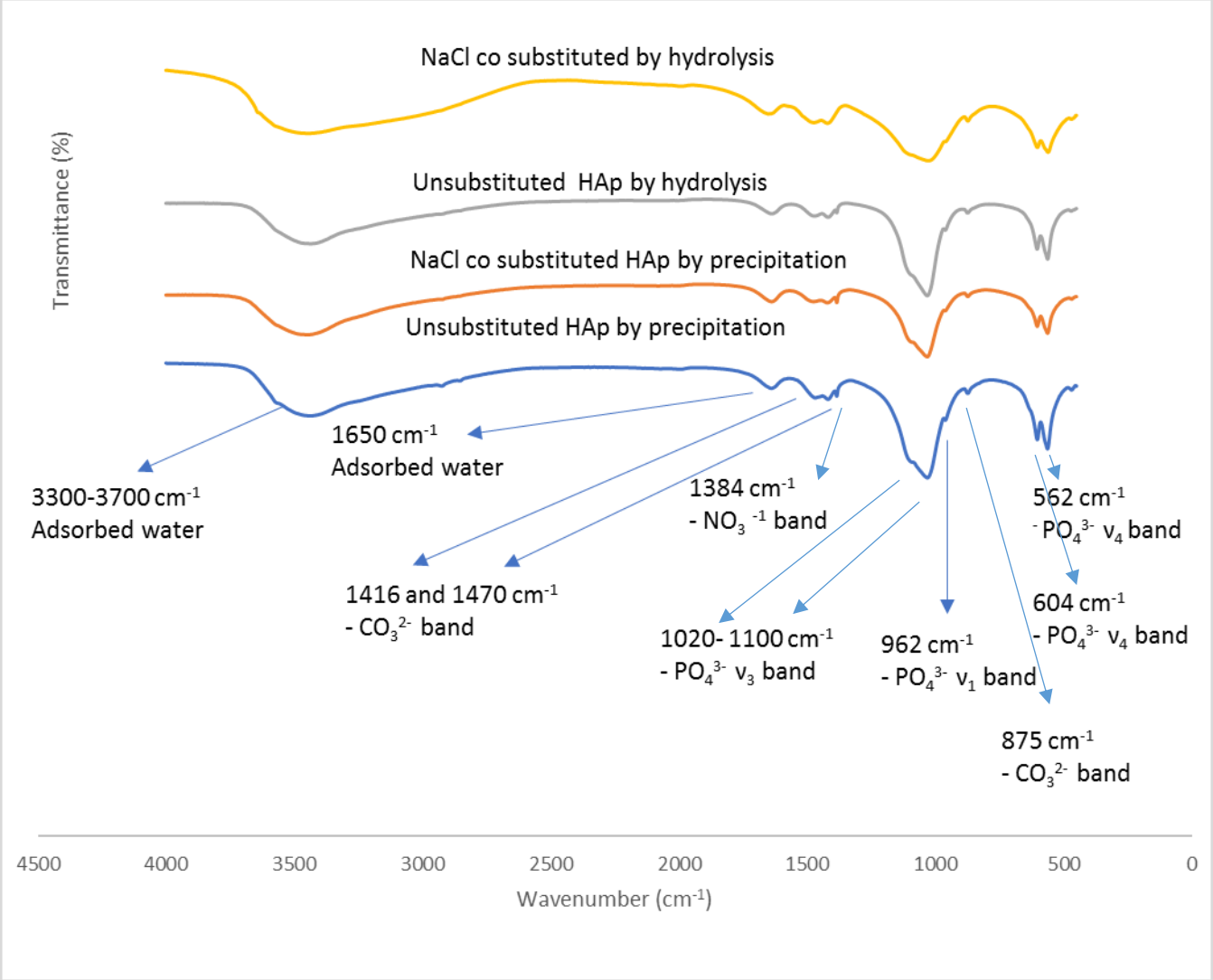

Figure 7-39: FTIR spectra of non-sintered NaClHAp materials prepared by precipitation and hydrolysis methods.

Fig.7-39 displayed that the recorded peaks at 562, 602, 962, 1028 and 1090 cm^{-1} can be attributed to phosphate groups. The carbonate bands appeared at 872,1416 and 1470 cm^{-1}, where the

characteristic peaks of hydroxyl group at 630 and 3572 cm^{-1} completely disappeared. In addition, the peak at 1630 cm^{-1} can be ascribed to adsorbed water as an indication of amorphous materials.

FTIR spectra of NaClHAp materials prepared by precipitation and hydrolysis methods after sintering at 900 ˚C.

Fig.7-40 displays the FTIR spectra of the sintered NaClHAp_material prepared by different synthesis routes.

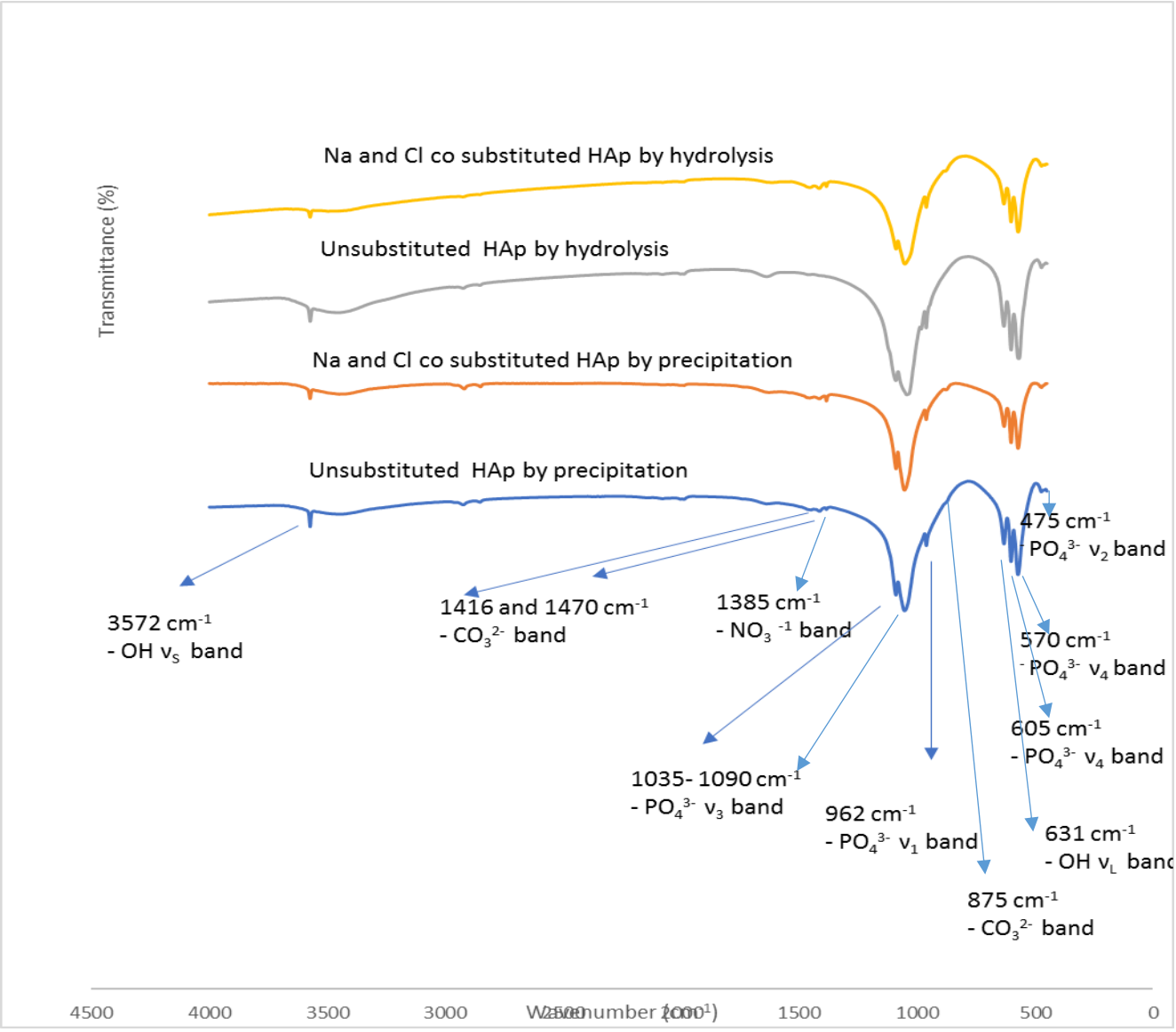

Figure 7-40: FTIR of NaClHAp materials prepared by precipitation and hydrolysis methods after sintering at 900 ˚C.

All prepared samples displayed the characteristic bands of hydroxyapatite. The bands at 3572 and 633 cm^{-1} correspond to the stretching and vibrational modes of the hydroxyl group. While the intensity of the librational mode of OH^- group at 630 cm^{-1} has not shown any significant difference compared to unsubstituted HAp powders that were prepared by two preparation methods (precipitation and hydrolysis), a clear reduction in the intensity of the stretching modes of OH^- group at 3752 cm^{-1} was observed for co substituted HAp powders (NaCl HAp) that prepared by precipitation and hydrolysis methods. This reduction in the intensity can be assigned to the partial substitution of Cl^- by OH^- in HAp crystal. The typical bands at 1090, 1050, and 962 cm^{-1} correspond to P –O stretching vibration modes, whereas the doublet at 603 – 572 cm^{-1} corresponds to the O-P-O bending mode. Carbonate peaks were recorded by FTIR spectra in both methods at 875, 1411 and 1453 $cm^{-1,}$ evidence of obtaining CO_3HAp samples, and keeping the charge balance that resulted due to the substitution process of monovalent cation. The peak that was detected by FTIR at 1384 cm^{-1} by precipitation can be attributed to the nitrate from either starting materials or trace nitrate impurities in the KBr powder.

7.6.1.3 XRD diffraction analysis of sodium chloride co- substituted hydroxyapatite (NaClHAp) prepared by precipitation and hydrolysis methods:

<u>Phase Identification of sintered NaClHAp materials prepared by precipitation and hydrolysis methods.</u>

The XRD pattern of the non-sintered and sintered NaCl co substituted HAp materials prepared by different synthesis routes are shown in **Fig.7-41 and 7-42.**

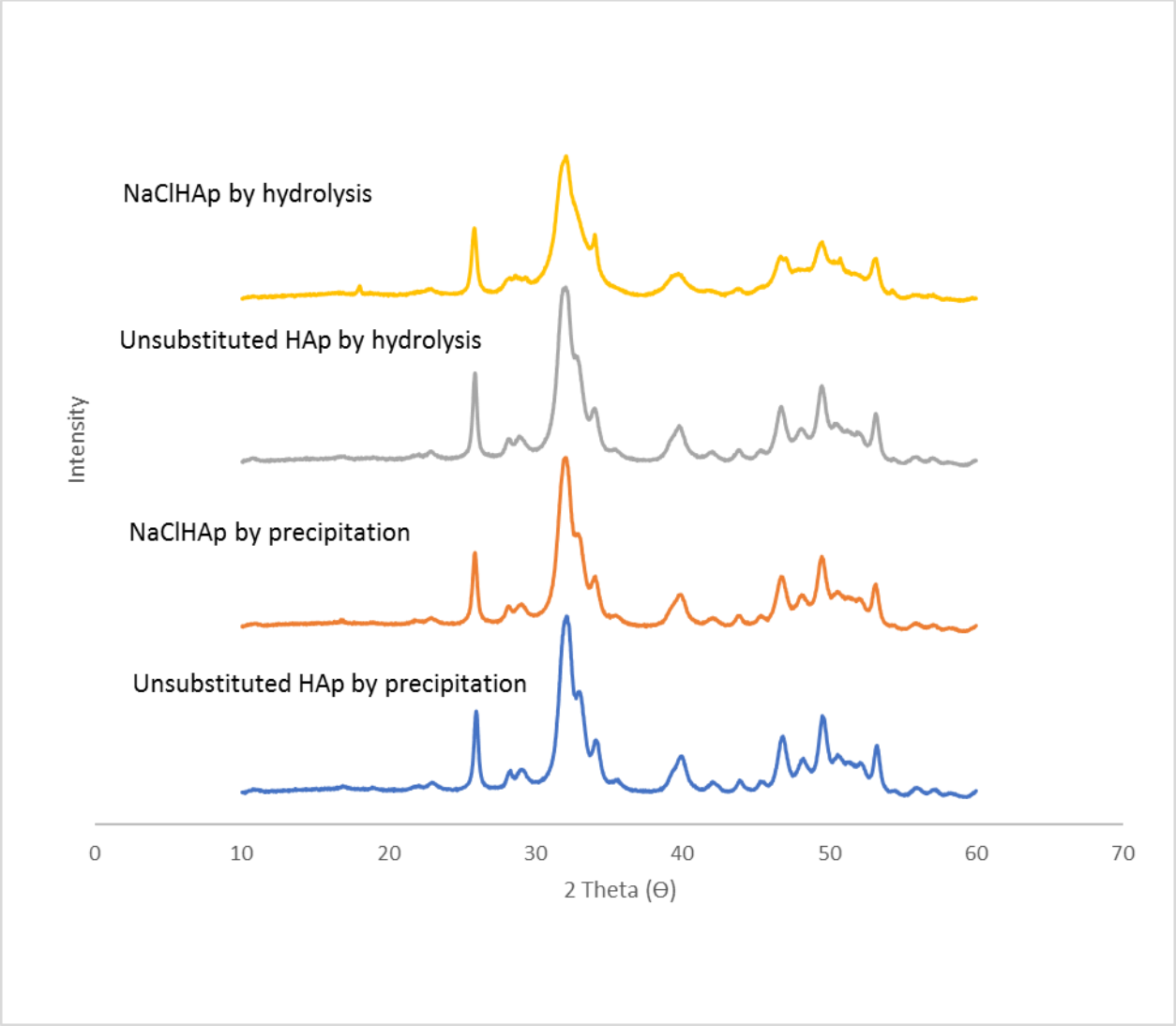

Figure 7-41: XRD diffraction patterns of the sintered NaClHAp materials prepared by precipitation and hydrolysis methods.

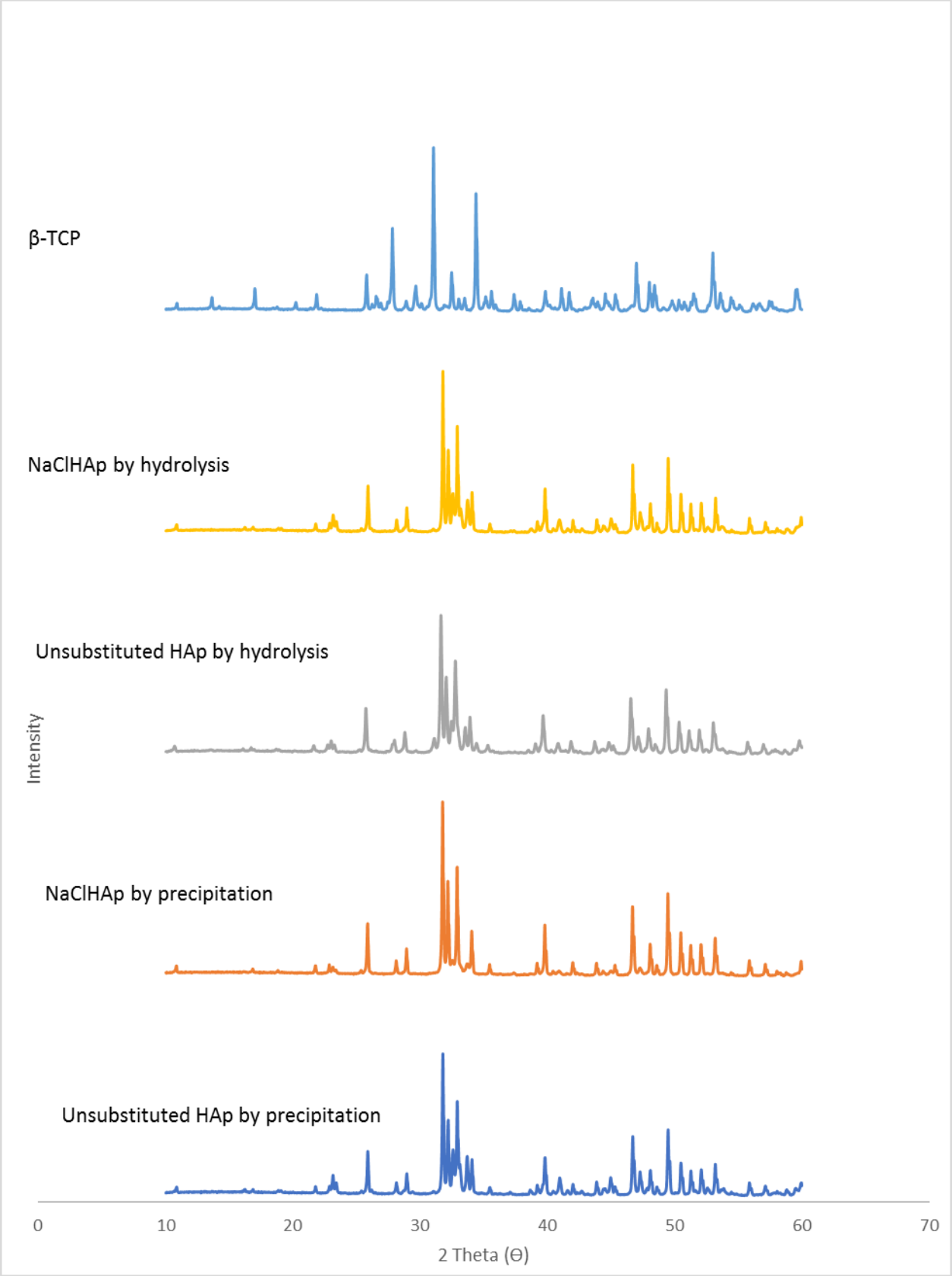

Figure 7-42: XRD diffraction patterns of NaClHAp materials prepared by precipitation and hydrolysis methods after sintering at 900 ˚C.

A highly pure phase was produced due to the substitution of Na^+ and Cl^- ions into HAp by precipitation route, as confirmed by XRD patterns,. This was due to the absence of some peaks that were related to an impurity phase (β-TCP) at 2 Theta = 31.20˚, 38.60˚, 41.14˚, and 45.20˚ coupled with a clear decrease in the whole other peaks that are attributed to β- tricalcium phosphate. On the other hand, use of the hydrolysis method caused the disappearance of two characteristic peaks of β-TCP at 2 Theta = 31.20˚ and 34.57˚. But, an increase in the intensity of another peak that can be assigned to β-TCP at 2 Theta = 33.60˚ was observed.

Crystallinity and crystallite size of NaClHAp materials prepared by precipitation and hydrolysis methods:

Table 7-34 displays the degree of crystallinity and crystallite size of the sintered NaClHAp materials prepared by precipitation and hydrolysis methods.

Table 7-34: The degree of crystallinity and crystallite size of NaClHAp materials prepared by precipitation and hydrolysis methods after sintering at 900 ˚C.

Sample	D_{002} (Å)	Crystallinity %
Unsubstituted HAp by precipitation	618.3±±3.2	84.15±2.4
NaClHAp by precipitation	748.6±2.8	85.31±2.6
Unsubstituted HAp by hydrolysis	549.8±3.6	82.57±2.1
NaClHAp by hydrolysis	790.0±4.4	85.65±5.2

An improvement in the numerical value of crystallinity as shown in (**Table 7-34**) was recorded for all NaClHAp samples, due to the co-substitution process of Na^+ and Cl^- ions.

On the other hand, the crystallite size was increased as a result of co-substitution process of Na^+ and Cl^- ions by both methods, namely precipitation and hydrolysis.

Lattice parameters and volume of unit cell of NaClHAp materials prepared by precipitation and hydrolysis methods:

Table 7-35 displays the lattice parameters and the volume of hexagonal unit cell of the sintered NaClHAp materials prepared by precipitation and hydrolysis methods.

Table 7-35: The lattice parameters and the volume of hexagonal unit cell of NaClHAp materials prepared by precipitation and hydrolysis methods after sintering at 900 ˚C.

Sample	a [Å]	c [Å]	V[Å^3]
Unsubstituted HAp by precipitation	9.416±0.004	6.879±0.003	1579±0.004
NaClHAp by precipitation	9.420±0.002	6.882±0.001	1581±0.002
Unsubstituted HAp by hydrolysis	9.421±0.003	6.882±0.005	1581±0.004
NaClHAp by hydrolysis	9.425±0.001	6.881±0.001	1582±0.001

The lattice parameters (a and b) of the prepared samples by the hydrolysis and the precipitation methods exhibited an increase in their values. Such an expansion in the lattice parameters could not be attributed to the Na^+ ions, since as discussed previously Na^+ ions and Ca^{2+} have approximately the same ionic radius (0.99 Å for Na^+ compared to 1.00 Å for Ca^{2+}) [136]. Also, the substitution of phosphate site by CO_3^{2-} will not cause an increase in the lattice parameters. The replacement of PO_4^{3-} group by CO_3^{2-} will cause a reduction in the lattice constants, simply because the phosphate site is characterized by a larger ionic radius (0.23 nm) compared to the smaller ionic radius carbonate group (0.189 nm) [216]. This expansion in the volume of unit cell of NaCl co substituted HAp in the present study can be ascribed to the larger ionic radius of Cl^- (0.168 nm) [216] compared to the OH^- group (0.153 nm).

7.6.1.4 SEM of NaClHAp materials prepared by precipitation and hydrolysis methods.

SEM of the non-sintered NaClHAp materials prepared by precipitation and hydrolysis methods.

Fig.7-43. displays the SEM images of the non-sintered NaClHAp powders prepared by hydrolysis and precipitation methods.

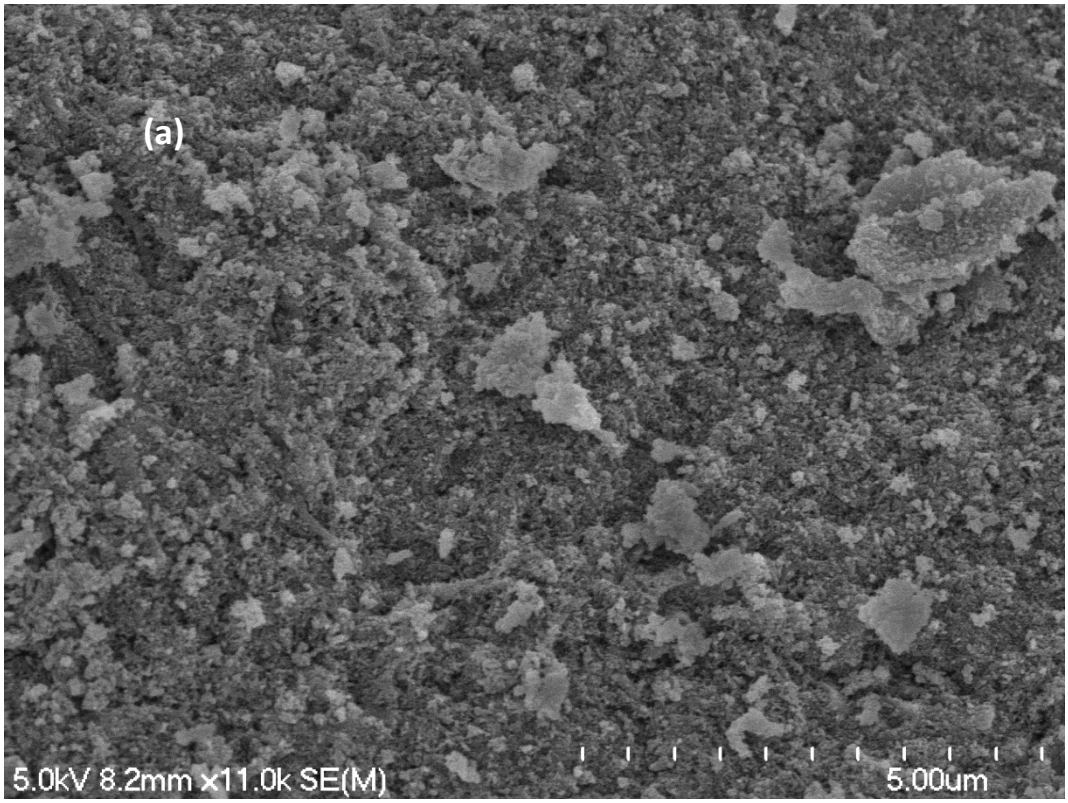
(a)
5.0kV 8.2mm x11.0k SE(M)
5.00um

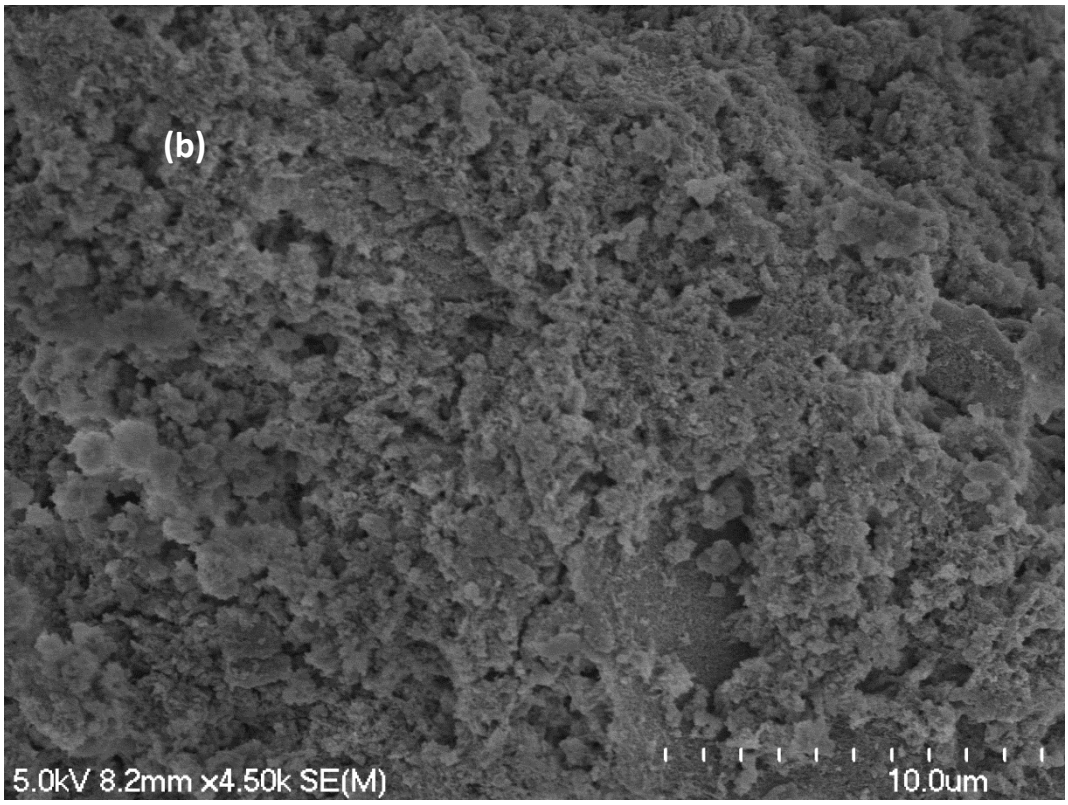
(b)
5.0kV 8.2mm x4.50k SE(M)
10.0um

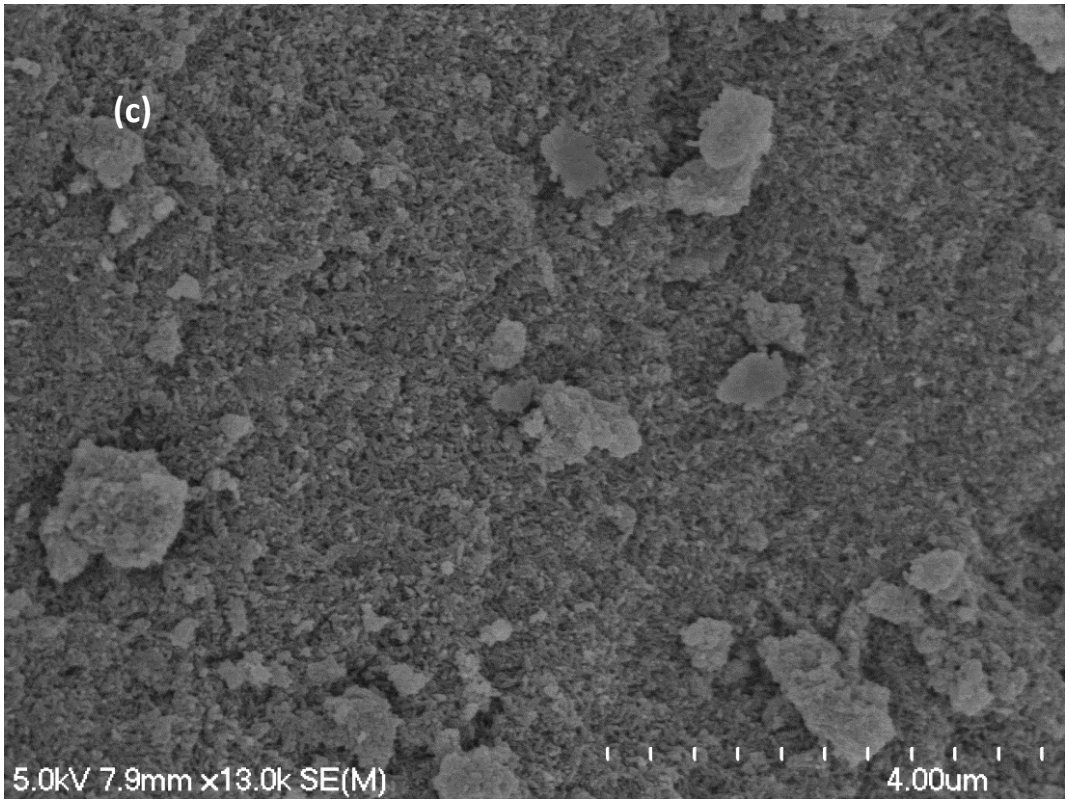
(c)
5.0kV 7.9mm x13.0k SE(M)
4.00um

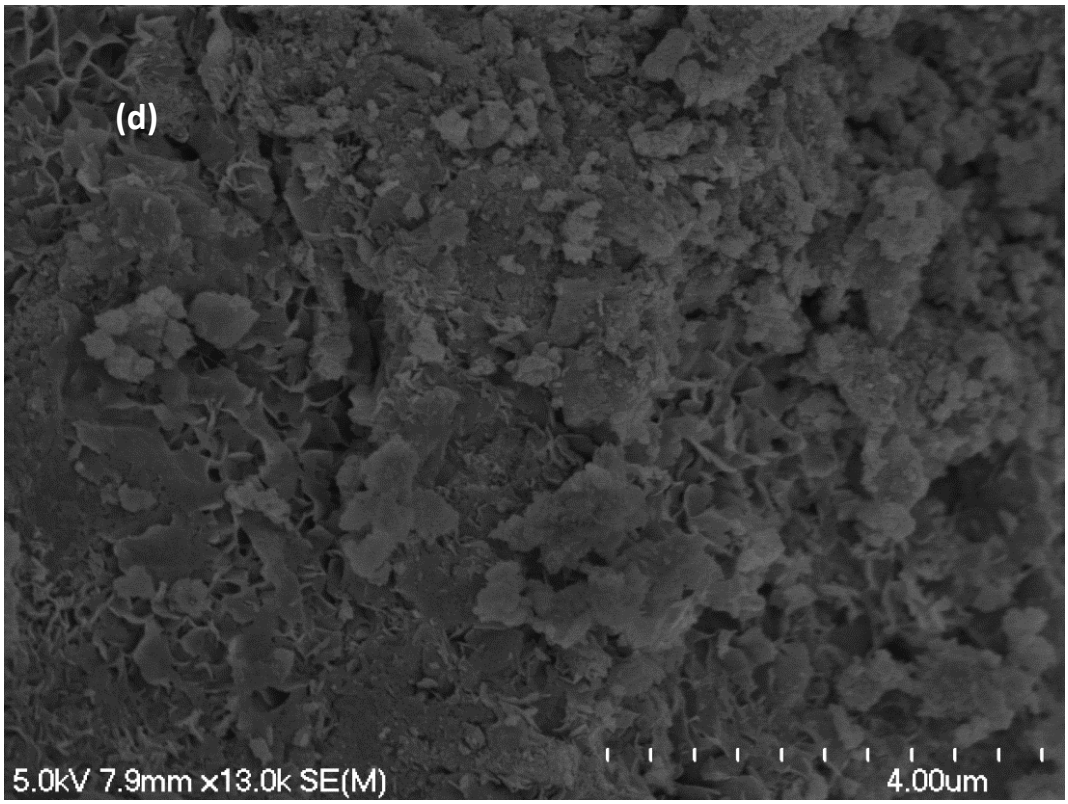
(d)
5.0kV 7.9mm x13.0k SE(M)
4.00um

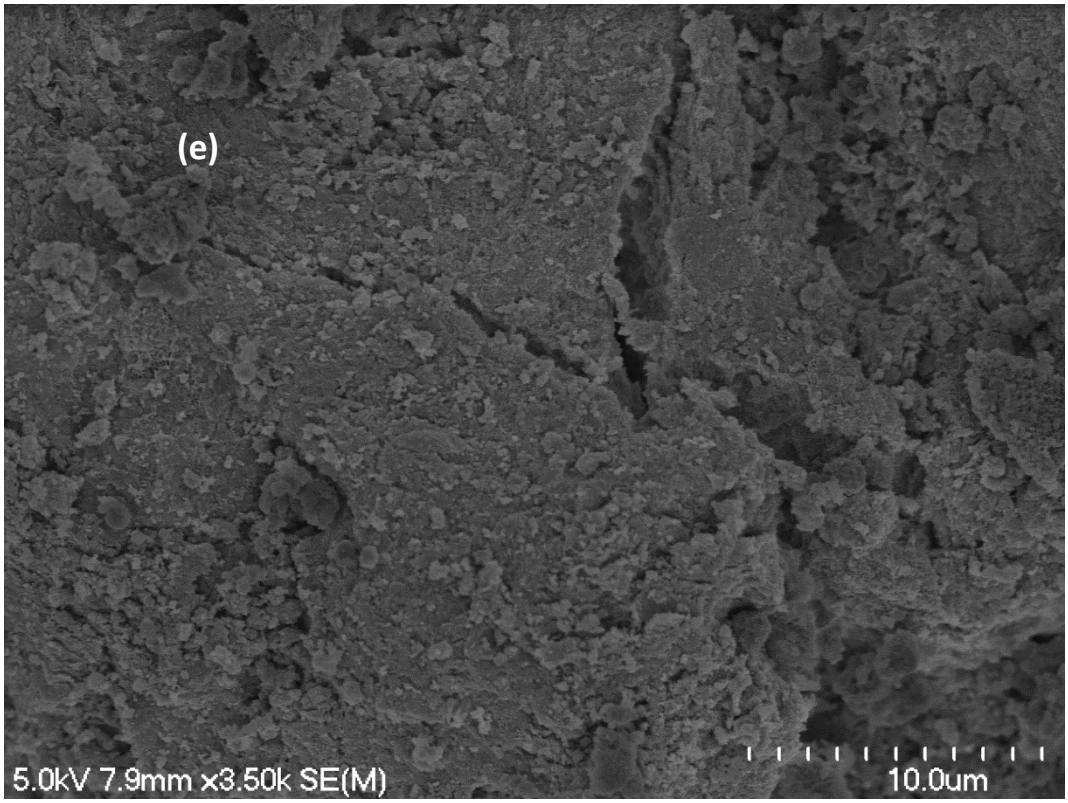

Figure 7-43: SEM images of the non-sintered (a) Unsubstituted HAp by precipitation (b) Unsubstituted HAp by hydrolysis (c)NaClHAp by precipitation (d and e) NaClHAp by hydrolysis.

While a clear tendency to agglomerate with porous and irregular structure was proven by SEM images for hydrolysis method, we can see the co-substitution of Na^+ and Cl^- ions by precipitation produced spheroid like shape with a trend to agglomerate, but in the case of hydrolysis route different morphologies were produced, namely flake-like flowers and spheroid like shapes, which reflected the effect of the synthesis method on the morphology.

SEM of NaClHAp materials prepared by precipitation and hydrolysis methods after sintering at 900 ˚C.

Fig.7-44 displays the SEM images of the sintered NaClHAp powders as prepared by the novel hydrolysis and conventional precipitation methods.

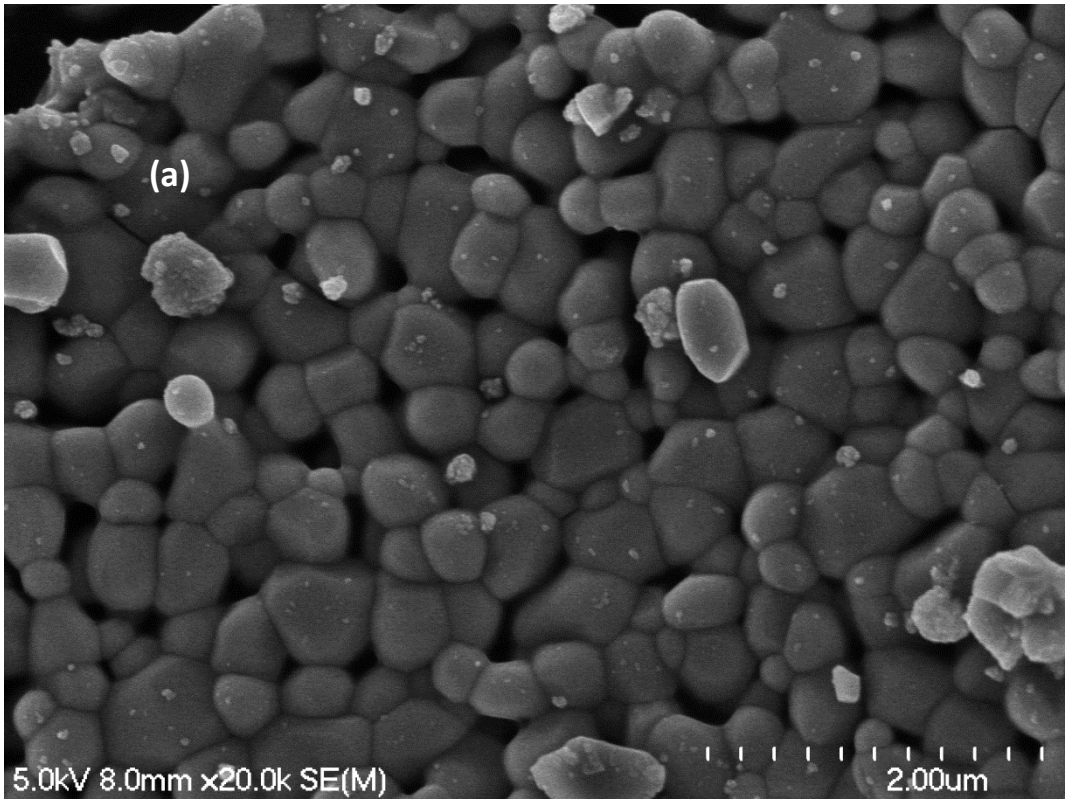
(a)
5.0kV 8.0mm x20.0k SE(M)
2.00um

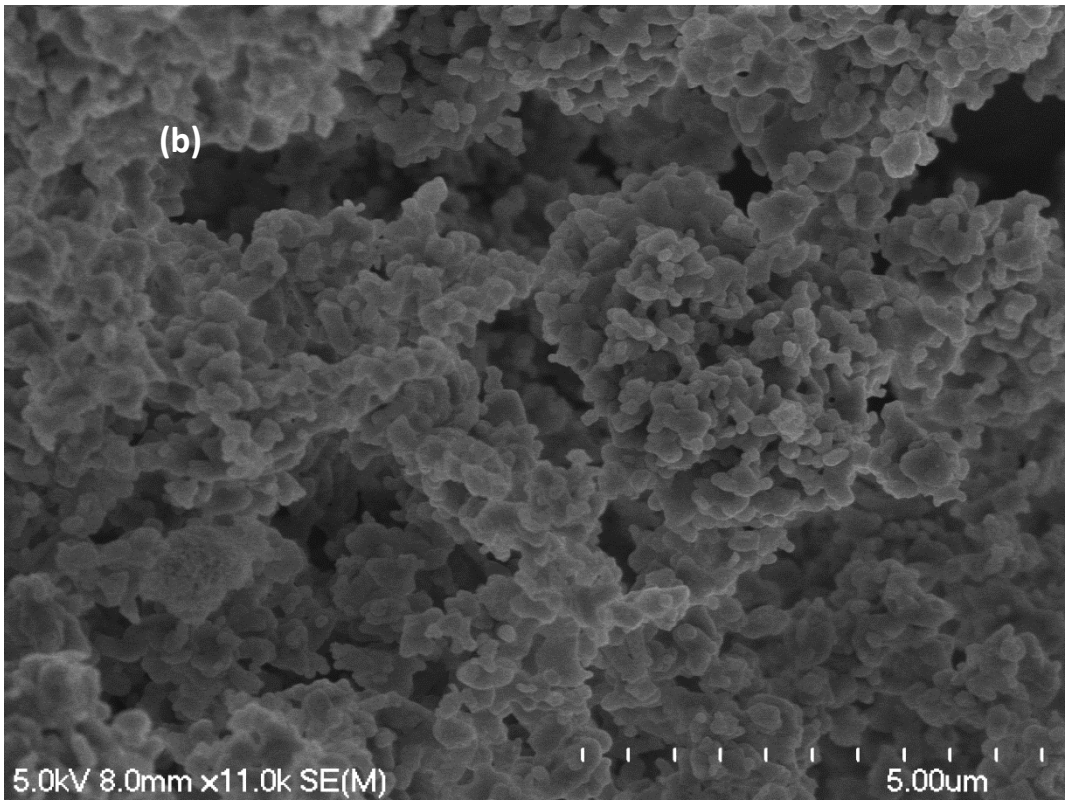
(b)
5.0kV 8.0mm x11.0k SE(M)
5.00um

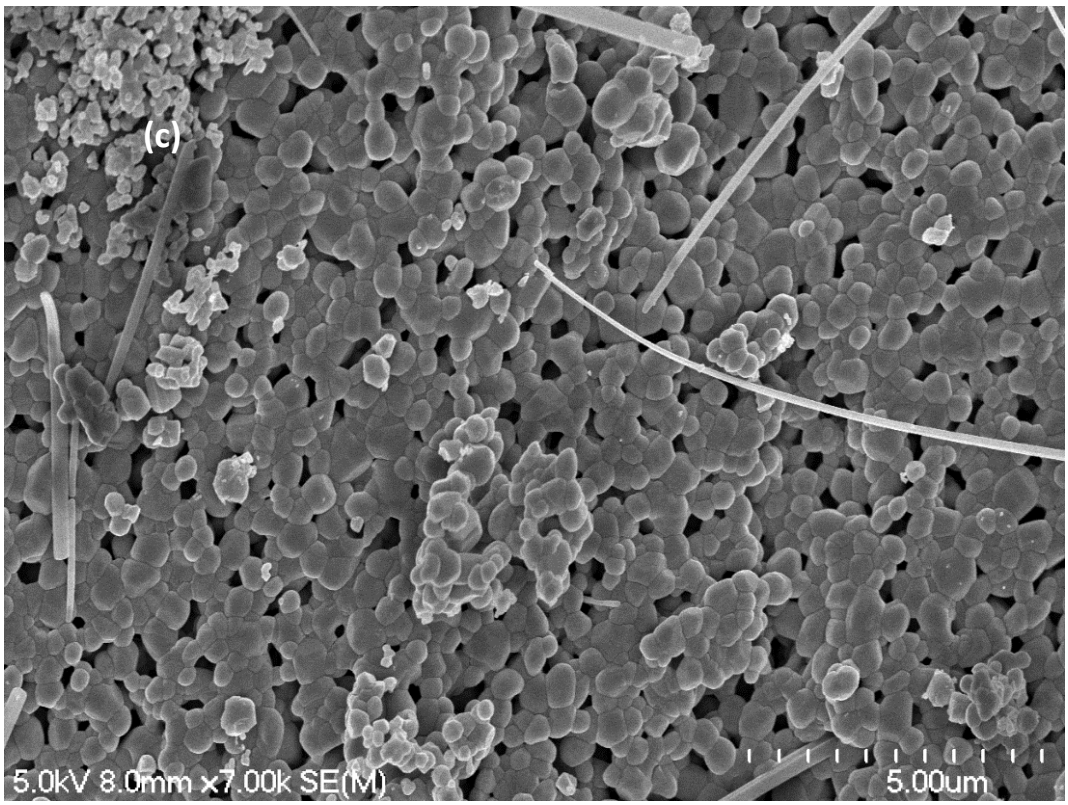
(c)
5.0kV 8.0mm x7.00k SE(M)
5.00um

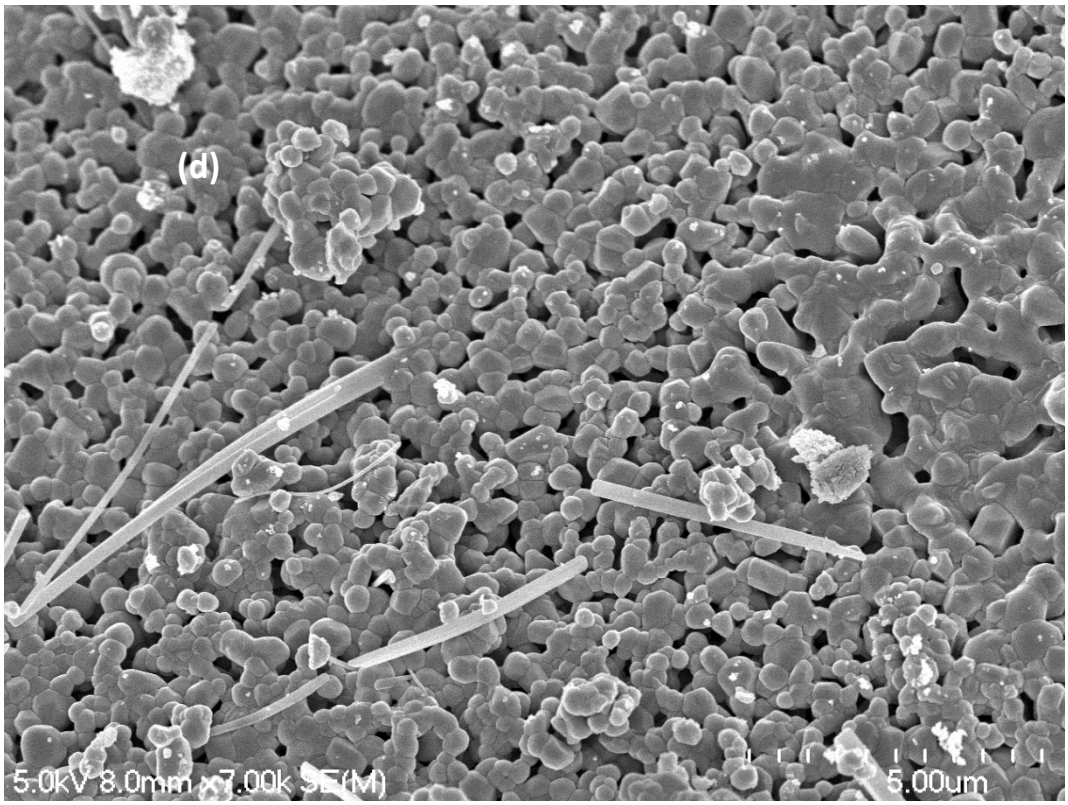
(d)
5.0kV 8.0mm x7.00k SE(M)
5.00um

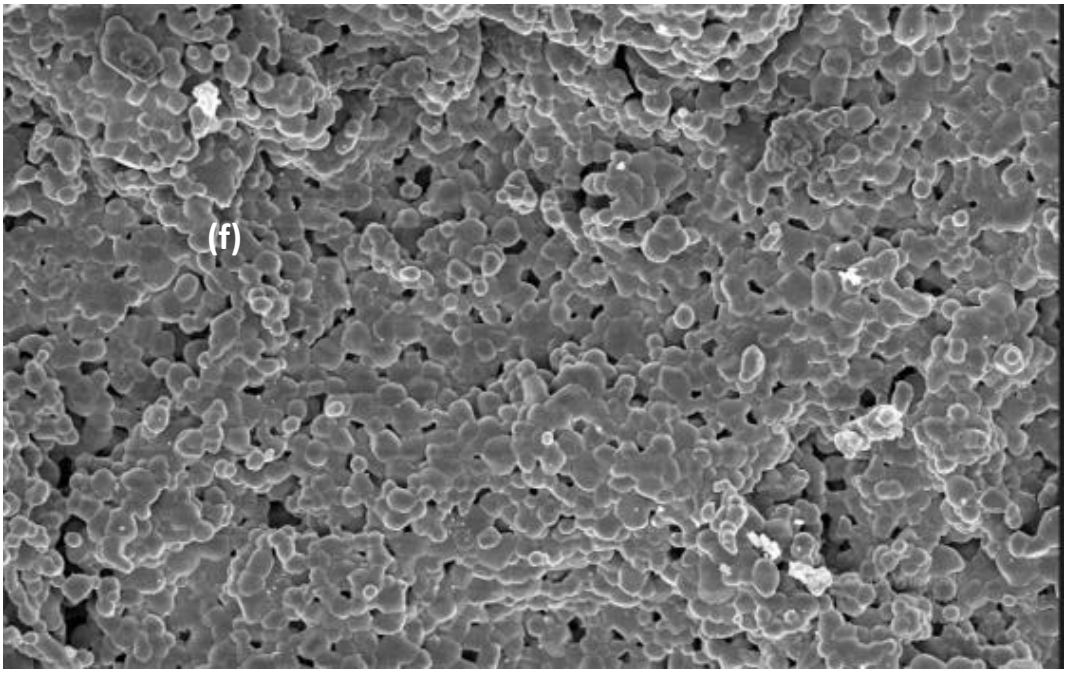

Figure 7-44: SEM images of (a) Unsubstituted HAp by precipitation (b) Unsubstituted HAp by hydrolysis (c + d) NaClHAp by precipitation (f) NaClHAp by hydrolysis, after sintering at 900 ˚C.

The effect of synthesis method on the morphology of NaClHAp powders were confirmed by SEM images. We can see that, as a result of heat treatment, the obtained NaClHAp powders by precipitation have a well-defined morphology such that the prepared materials consist of a spherical shape and a small quantity of whiskers with the ability to agglomerate, while spherical shaped particles with an irregular distribution were recorded in samples prepared by the hydrolysis method, but enhancement in the level of porosity was also seen as a result of co substitution NaCl by hydrolysis.

The SEM/EDX techniques was also used to get a better idea about the elemental composition of the 1%NaClHAp that was prepared by the conventional precipitation method. The results of SEM/EDX analysis for the above-mentioned system can be found in the Appendix (see appendix A). The SEM/EDX results showed that:

1- The whiskers consist of Ca^{2+}, PO_4^{3-}, OH^-, CO_3^{2-} and Na^+ ions.

2- Also, the weight percent of Na^+ ions (1.69%) in the whiskers were found to be higher than the spherical particles (1.38%).

3- The Ca/P mole ratio of the whiskers is (1.47) compared to (1.37) of the spherical particles.

7.7 Summary:

1- Different systems of anionic and co substituted HAp, namely 1, 3 and 5% NbHAp, 1% B_4O_7HAp, bromapatite, sulfoapatite and NaClHAp were prepared by using different preparation methods (precipitation, hydrolysis and ion exchange routes).
2- Different techniques were used to characterize the prepared samples such as SEM, FTIR, XRD and ICP-MS.

The result of using these techniques showed:

- The effect of preparation method on the morphology:
  In particular, the hydrolysis method of all prepared materials produced spherical shaped particles which had a tendency to agglomerate, but the precipitation method, in contrast, formed several kinds of morphologies. For example: 1, 3 and 5% NbHAp, 1%B_4O_7HAp and bromapatite powders produced spheroidal like shape particles, whereas sulfoapatite and NaClHAp formed spherical shape with small quantity of whiskers. These results were obtained through SEM investigations.
- The presence of apatite phase in the whole prepared powders had been confirmed through detecting the fundamental vibrational modes of PO_4^{3-} group at 562, 602, 962 and 1032-1095 cm^{-1}, as well as by recording the typical bands of OH^- group at 3572 and 631 cm^{-1}. On the other hand, a reduction of the intensities of the stretching and librational modes of the lattice OH^- group at (3572 and 630 cm^{-1}) due to the replacement process of the monovalent and bivalent ions (Br^-, S^{2-} and $B_4O_7^{2})^-$ was observed in order to keep charge balance. These results were detected by using FTIR analysis.
- The effect of the replacement process of phosphate and/or hydroxyl groups by the ions that were used to substitute HAp structure on the crystallinity, crystallite size and lattice parameters were varied, and the details of these values were discussed in the chapter (these results were confirmed by using XRD).
- The presence of some of these such as $B_4O_7^{2-}$, Na^+, S^{2-} ions into HAp samples was confirmed by using ICP-MS analysis, whereas the theoretical and experimental values

of Ca/P mole ratios as well as the wt.% percent of substitution were discussed. ICP-MS does not offer conclusive proof of substitution, however. The presence of other ions such as Cl^- and Br^- were not detected by ICP-MS analysis. Therefore, the substitution of these ions (Cl^- and Br^-) into HAp structure were confirmed by XRD and FTIR spectra, the details about the results of these tests (XRD and FTIR) were discussed.

Chapter Eight

Mechanical properties of unsubstituted, substituted and co substituted HAp powders prepared by the Hydrolysis of monocalcium phosphate (MCP)/$Ca(OH)_2$.

8.1 Mechanical Properties:

The mechanical properties of materials are properties such as strength, used to describe how well a material withstands applied forces [50]. As a common mineral component of human bones, hydroxyapatite $Ca_{10}(PO_4)_6(OH)_2$ has been widely used in various biomedical fields such as bone repair and orthopedic prosthesis, due to its biocompatibility and bioactivity characteristics [246]. However, the poor mechanical performance of hydroxyapatite materials limits their application in load-bearing situations [6]. Therefore, several works have been carried out as discussed in the literature to improve the mechanical strength of HAp materials through incorporation of various ions, even functional groups into the HAp crystal [247-249].

It was reported the value of mechanical properties of synthetic HAp materials depend on several factors such as crystallinity, agglomeration, chemical composition, substitution process, substitution levels, porosity and grain size [35,153]. Therefore, in the context of the present study, the mechanical properties of the following systems had been studied. These systems have been described previously in earlier chapters (see chapters 4, 5, 6 and 7 for details).

1- Unsubstituted HAp samples prepared by the novel hydrolysis method involving MCP/$Ca(OH)_2$.
2- MHAp samples with the following chemical formula: $Ca_{10-x}M_xHAp$ (where M=Zn, Sr and Cu, X=0.5, 1.0 and 1.5) prepared by the hydrolysis of monocalcium phosphate (MCP) and calcium hydroxide.
3- 1%EuHAp (1 wt.% Eu^{3+}) and 1%ScHAp(1 wt% Sc^{3+}) samples prepared by the hydrolysis of MCP/$Ca(OH)_2$.

4- 1% B_4O_7HAp (1 wt.% $B_4O_7^{2-}$) and NaClHAp($Ca_9Na(PO_4)_6ClOH$) samples prepared by the hydrolysis of MCP/$Ca(OH)_2$.
5- SAp samples prepared by the novel hydrolysis method.

This chapter aimed to:

1. To investigate the mechanical properties of specific systems of substituted and co substituted materials prepared by using the hydrolysis method through performing the compression test. The Laser Diffraction Particle Size Analyzer was also employed to measure the particle size of these systems in order to investigate the effect of particle size on the mechanical strength.
2. To study the effect of substitution levels for specific systems of substituted HAp (MHAp) with the following chemical formula $Ca_{10-x}M_x(PO_4)_6(OH)_2$, where M= Zn, Sr and Cu, X=0.5, 1.0 and 1.5) on the value of mechanical properties.
3. To study the effect of particle size on the value of mechanical strength.

8.1.1 Mechanical properties of sintered unsubstituted HAp powders at 900 ˚C prepared by the novel hydrolysis method using MCP and $Ca(OH)_2$ as starting materials:

Table 8-1 shows the mechanical results of unsubstituted HAp material prepared by the hydrolysis of MCP/$Ca(OH)_2$.

Table 8-1: Mechanical results of unsubstituted HAp powders prepared by the hydrolysis of MCP/$Ca(OH)_2$.

Sample	Maximum load (N)	Maximum load (N)	Maximum load (N)	Average of maximum load (N)	Particle size (um)	Compression strength (MPa)
Unsubstituted HAp by hydrolysis	2129	2145	2245	2137	26.1	22.38

As well known, the CaPs ceramics provide limited mechanical support simply because they have little tensile strength and are brittle in nature due to their high strength ionic bonds[250]. The mechanical properties of CaPs powders were found to be affected by several parameters such as crystallinity, grain size, grain boundaries, porosity as well as substitution process [35,153]. As an example when the microstructure contains small grains, the number of grain boundaries will be decreased significantly, suggesting an enhancement in the mechanical strength[251]. Le Huec et al. [252] studied the influence of porosity on the mechanical strength of calcium phosphate ceramics. They tested 150 cylindrical hydroxyapatite samples. The total porous volume of the ceramics was varied from 20% to 60%. The result of that investigation showed that the compressive strength decreases as porosity increases. Dean-Mo Liu [253] investigated the effect of porosity and pore size on the compressive strength of hydroxyapatite ceramic. The result of that investigation showed clearly the compressive strength behaves linearly with macropore size, that a smaller macropore corresponds to a higher compressive strength. Another factor that causes an obvious effect on the mechanical strength is the packing density. Spath et al. [254] investigated the relationship between the mechanical strength of 3D printed ceramic scaffolds and the following parameters: the particle size and the packing density. Hydroxyapatite granule blend with a wide particle size distribution was used for that goal. Different fractions of hydroxyapatite granule blends were used (<32 μm, 32–45 μm, 45–63 μm, 63–80 μm, 80–100 μm, 100–125 μm and >125 μm). The result of that investigation showed that an optimized arrangement of fractions with large and small particles can provide 3D printed specimens with good mechanical strength due to a higher packing density.

In the present investigation, the effect of the following parameters: the porosity, the pore size and the packing density on the mechanical strength had not been investigated. The only parameter that was studied during this project is the relationship between the particle size and the compressive strength. The details of the compression strength calculations and the particle size measurement report can be found in Appendix A (see appendix A) through one computed example involving 1%B_4O_7HAp samples (1 wt.% B_4O_7) prepared by the novel hydrolysis method using (hydrolysed) MCP/$Ca(OH)_2$ as starting materials.

8.1.2 Mechanical properties of ZnHAp powders at 900 ˚C ($Ca_{10-x}Zn_x(PO_4)_6(OH)_2$, where x= 0.5, 1.0 and 1.5) prepared by the novel hydrolysis of MCP/Ca(OH)2.:

Table 8-2 displays the mechanical results of ZnHAp powders prepared by the hydrolysis method with different substitution levels.

Table 8-2: Mechanical results of ZnHAp powders prepared by hydrolysis method with different substitution levels.

Sample	Trial one Maximum load (N)	Trial Two Maximum load (N)	Trial Three Maximum load (N)	Average of maximum load (N)	Particle size (um)	Compression strength (MPa)
Unsubstituted HAp by hydrolysis	2129	2145	2245	2137	26.1	22.38
0.5ZnHAp	2099	2148	2150	2132	29.0	21.96
1.0ZnHAp	3139	3145	3125	3136	17.0	32.31
1.5ZnHAp	3120	3125	3128	3124	16.9	32.19

Fig.8-1 displays the effect of the particle size of ZnHAp powders on the value of the compression test.

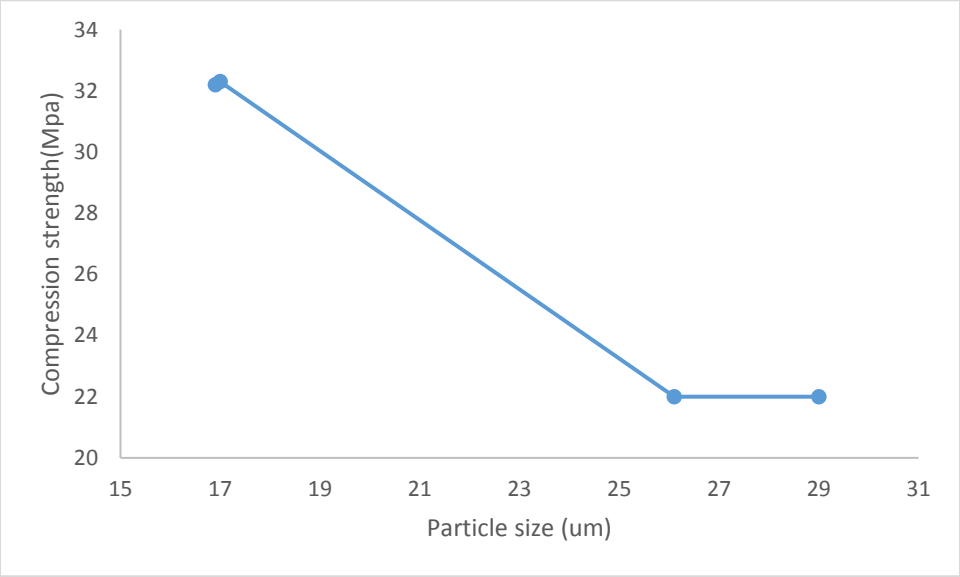

Figure 8-1: Compression strength against particle size of ZnHAp powders prepared by hydrolysis method with different substitution levels.

The result of mechanical tests showed a visible increase in the compression strength values with increasing the level of Zn^{2+} contents, coupled with a reduction in the measured values of particle size. It was reported the replacement process of Zn^{2+} ions with smaller ionic radius (0.074 nm) compared to Ca^{2+} (0.099 nm) into HAp structure, will enhance the mechanical properties [255], due to the difference in ionic radius between Zn^{2+} and Ca^{2+} ions . The improvement in the measured values of the mechanical strength in this study can be ascribed to the smaller ionic radius of Zn^{2+} compared to Ca^{2+} ions, which caused a decrease in the grain size. As a result, a reduction in the particle size would be recorded suggesting an increase in the strength values.

8.1.3 Mechanical properties of sintered SrHAp powders ($Ca_{10-x}Sr_x(PO_4)_6(OH)_2$ at 900 ˚C, where x= 0.5, 1.0 and 1.5) prepared by the novel hydrolysis of MCP/$Ca(OH)_2$:

Table 8-3 displays the mechanical results of SrHAp powders prepared by hydrolysis method with different substitution levels.

Table 8-3: Mechanical results of SrHAp powders prepared by hydrolysis method with different substitution levels.

Sample	Trial one Maximum load (N)	Trial Two Maximum load (N)	Trial Three Maximum load (N)	Average of maximum load (N)	Particle size (um)	Compression strength (MPa)
Unsubstituted HAp by hydrolysis	2129	2145	2245	2137	26.1	22.38±1.7
0.5 SrHAp	1697	1684	1696	1692	33.8	17.43±1.3
1.0 SrHAp	2146	2111	2095	2117	28.0	21.81±2.8
1.5 SrHAp	1725	1748	1735	1736	32.6	17.88±3.1

Fig.8-2 displays the effect of the particle size of SrHAp powders prepared by the hydrolysis method on the value of the compression test.

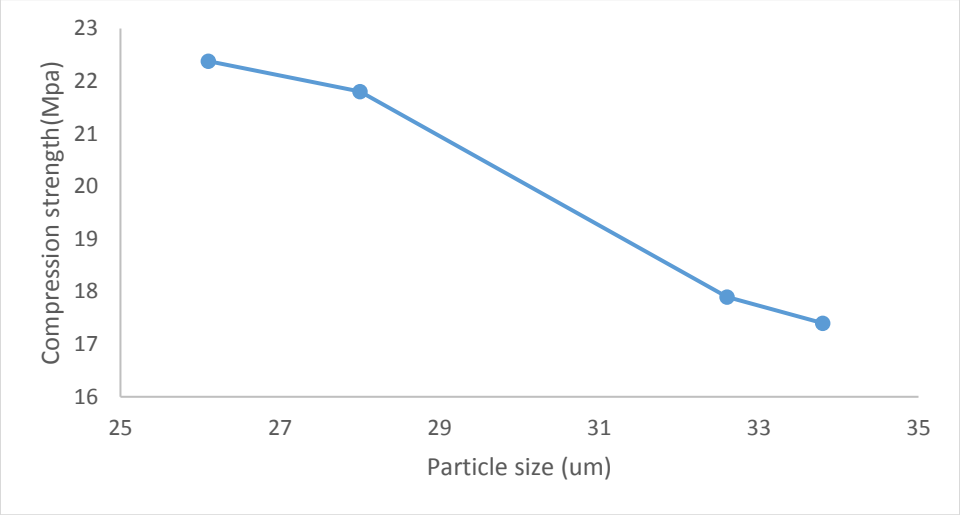

Figure 8-2: Compression strength against particle size for SrHAp powders prepared by the hydrolysis method at different substitution levels.

Table 8-3 shows a small decrease in the values of compression strength due to the substitution of Sr^{2+} ions and a slight increase in the value of the particle size of the prepared SrHAp samples. This result can be explained in terms of the larger ionic radius of Sr^{2+}(0.118 nm) compared to Ca^{2+} (0.100 nm) [131](see chapter 5 for details) which caused an increase in the grain size. As a result, an increase in the particle size would be recorded suggesting a reduction in the strength values. In the case of 1.0 SrHAp materials, the results showed a slight reduction in the value of particle size causing an enhancement in the mechanical strength. This result can be ascribed to the effect of phase purity and chemical composition on the value of mechanical strength. It has been reported that the mechanical properties of biphasic calcium phosphate (BCP) can be modified by parameters like the ratio of HAp/β-TCP [256]. So, it seems that the HAp/β-TCP ratio in the BCP can be adjusted to control mechanical characteristics. Increasing the substitution level of Sr^{2+} ions as in the case of 1.5 SrHAp materials, resulted in a slight increase in the particle size. This result can be explained in terms of larger ionic radius of Sr^{2+} ions $^{+}$(0.118 nm) compared to Ca^{2+} (0.100 nm) [131], which caused an increase in the grain size. As a result, an increase in the particle size would be recorded suggesting a reduction in the strength values.

Aoki et al. [257] prepared SrHAp powders with different Sr/Ca molar ratio (0.0006 and 0.006) and studied the effect of substitution process on mechanical properties. They reported that the

mechanical properties of sintered SrHAp powders slightly decreased as the level of Sr^{2+} ions increased in the HAp, and this agrees with the result obtained through the present investigation.

8.1.4 Mechanical properties of sintered CuHAp powders at 900 ˚C ($Ca_{10-x}Cu_x(PO_4)_6(OH)_2$, where x= 0.5, 1.0 and 1.5) prepared by the novel hydrolysis of MCP/$Ca(OH)_2$:

Table 8-4 displays the mechanical results of CuHAp powders prepared by hydrolysis method with different substitution levels.

Table 8-4: Mechanical results of CuHAp powders prepared by hydrolysis method with different substitution levels.

Sample	Trial one Maximum load (N)	Trial Two Maximum load (N)	Trial Three Maximum load (N)	Average of maximum load (N)	Particle size (um	Compression strength (MPa)
Unsubstituted HAp by hydrolysis	2129	2145	2245	2137	26.1	22.38
0.5CuHAp	2752	2820	2765	2229	22.9	28.62
1.0CuHAp	3096	3110	3128	3111	17.3	32.05
1.5CuHAp	2197	2156	2160	2171	29.8	22.37

Fig.8-3 displays the effect of the particle size of CuHAp powders prepared by hydrolysis method on the value of compression test.

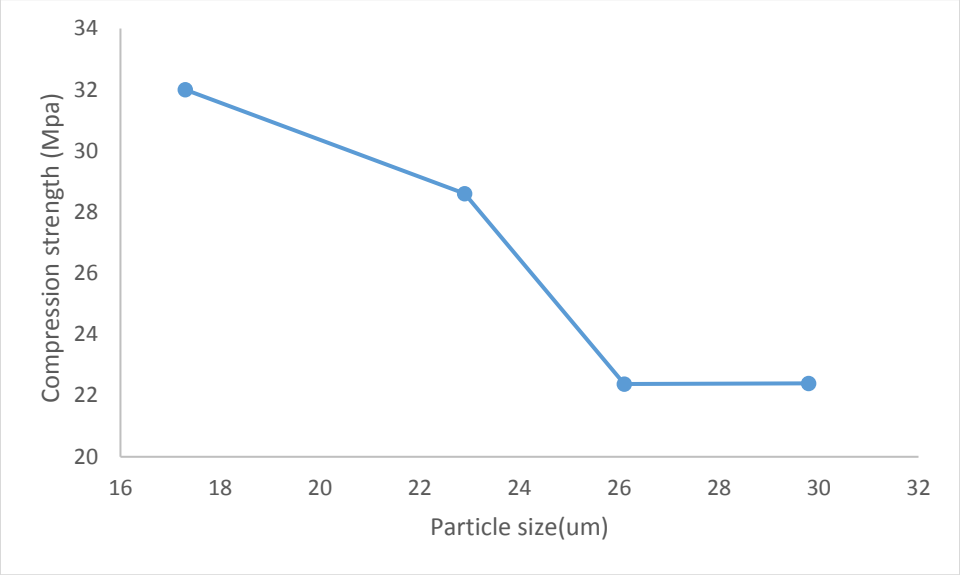

Figure 8-3: Compression strength against particle size of CuHAp powders prepared by hydrolysis method with different substitution levels.

The result of present investigation shows increasing the level of substitution of copper ions into HAp crystal caused an improvement in the value of the mechanical strength of CuHAp powders. These results can be attributed to the substitution process of the calcium ionin the lattice by Cu^{2+} ions. The smaller ionic radius of Cu^{2+} ions (73 pm) compared to Ca^{2+} ions (100 pm), would reduce the grain and particle sizes of CuHAp powders, and thus increase their strength.

In the case of the 1.5 CuHAp powder a clear decrease in the mechanical strength was recorded. This result may be attributed to the phase purity. As confirmed by the XRD analysis, the presence of biphasic material had been observed, and the percent of β-TCP was raised increasing the amount of substitution levels of Cu^{2+} ions into HAp crystal (see chapter 5 for details). Therefore, the value of strength may be affected, depending on the composition range of HAp and β-TCP in the prepared powders. It has been reported that the mechanical properties of biphasic calcium phosphate (BCP) can be modified by parameters like the ratio of HAp/β-TCP [256]. So, it seems that the HAp/β-TCP ratio in the BCP can be adjusted to control mechanical characteristics, since that ratio was also used to determine its reactivity [258] as stated in the literature.

8.1.5 Mechanical properties of sintered 1%EuHAp (1 wt.% Eu^{3+}) and 1% ScHAp(1 wt.% Sc^{3+}) powders at 900 ˚C prepared by the novel hydrolysis of MCP/$Ca(OH)_2$:

Table 8-5 displayed the mechanical results of 1%EuHAp and 1%ScHAp powders prepared by the hydrolysis method.

Table 8-5: Mechanical results of 1%EuHAp (1% wt. Eu^{3+}) and 1% ScHAp(1% wt. Sc^{3+}) powders prepared by hydrolysis method.

Sample	Trial one Maximum load (N)	Trial Two Maximum load (N)	Trial Three Maximum load (N)	Average of maximum load (N)	Particle size (um)	Compression strength (MPa)
Unsubstituted HAp by hydrolysis	2129	2145	2245	2137	26.1	22.38
1%EuHAp by hydrolysis	2577	2547	2630	2585	23.3	26.63
1%ScHAp by hydrolysis	2696	2750	2724	2723	21.2	28.06

Fig. 8-4 displays the effect of the particle size of 1%EuHAp (1 wt.% Eu^{3+}) and 1% ScHAp(1 wt.% Sc^{3+}) powders prepared by hydrolysis method on the value of compression test.

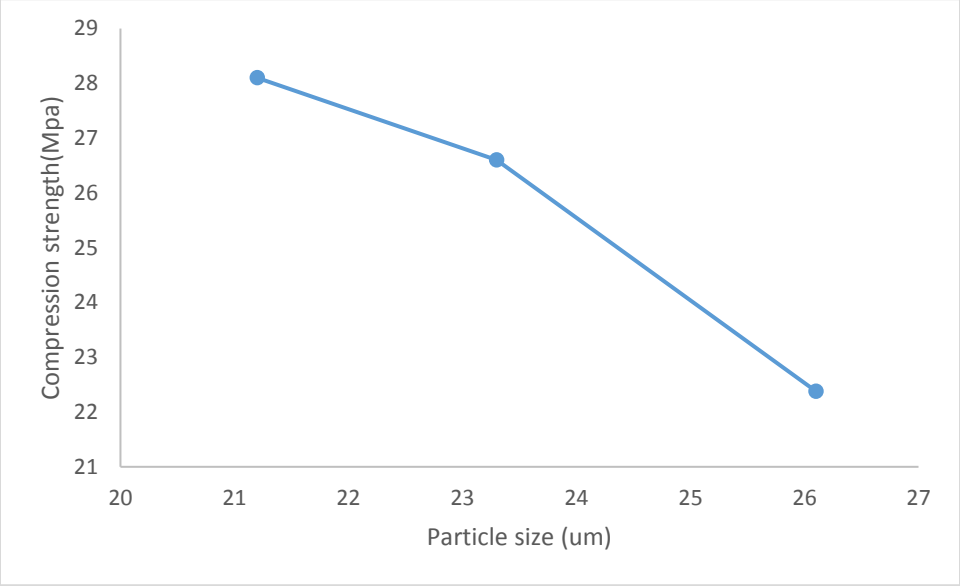

Figure 8-4: Compression strength against particle size of of 1%EuHAp (1% wt. Eu^{3+}) and 1% ScHAp(1% wt. Sc^{3+}) powders prepared by hydrolysis method.

In the case of 1%ScHAp powders, we can see the replacement process caused a small improvement in strength value. This result can be attributed to the smaller particle size. The reduction in the particle size could not be attributed to the substitution of Sc^{3+} ions into HAp crystal, since the substitution level was very low as confirmed by ICP-MS analysis (0.01 wt.% Sc^{3+} ions). But the reduction in the value of particle size can be ascribed to the presence of CO_3^{2-} (as confirmed by FTIR spectra, see chapter 6 for details). The replacement process of phosphate site with larger ionic radius (0.23 nm) compared to carbonate group (0.189 nm) [216], caused a reduction in the value of particle size. As a result, an enhancement in the mechanical strength was recorded.

The 1%EuHAp powders also, showed slightly higher value of strength compared to unsubstituted HAp samples. This result, can be ascribed to the smaller particle size and a decrease in the level of porosity as confirmed by SEM images due to the substitution process of europium ions (Eu^{3+}) into HAp crystal (see chapter 6 for details) It was reported that the mechanical strength of hydroxyapatite materials are affected by the porosity [251]. For example, the strength of HAp bodies decreases gradually as porosity increases [251]. Therefore, the slight increase in the mechanical strength of 1%EuHAp samples was the result of a reduction in the level of porosity.

8.1.6 Mechanical properties of sintered 1% B_4O_7HAp (1 wt.% $B_4O_7^{2-}$) and NaClHAp ($Ca_9Na(PO_4)_6ClOH$)powders at 900 ˚C prepared by the novel hydrolysis of MCP/$Ca(OH)_2$:

Table 8-6 displays the mechanical results of 1% B_4O_7HAp (1 wt.% $B_4O_7^{2-}$) and NaClHAp ($Ca_9Na(PO_4)_6ClOH$)powders prepared by the hydrolysis method.

Table 8-6: Mechanical results of 1% B_4O_7HAp (1 wt.% $B_4O_7^{2-}$) and NaClHAp ($Ca_9Na(PO_4)_6ClOH$) powders prepared by hydrolysis method.

Sample	Trial one Maximum load (N)	Trial Two Maximum load (N)	Trial Three Maximum load (N)	Average of maximum load (N)	Particle size (um)	Compression strength (MPa)
Unsubstituted HAp by hydrolysis	2129	2145	2245	2137	26.1	22.38
B_4O_7HAp by hydrolysis	3220	3135	3250	3202	13.9	32.98
NaClHAp by hydrolysis	1039	1021	1035	1032	54.4	10.62

Fig. 8-5 displays the effect of the particle size of 1% B_4O_7HAp (1 wt.% $B_4O_7^{2-}$) and NaClHAp ($Ca_9Na(PO_4)_6ClOH$) powders prepared by the hydrolysis method on the value of the compression test.

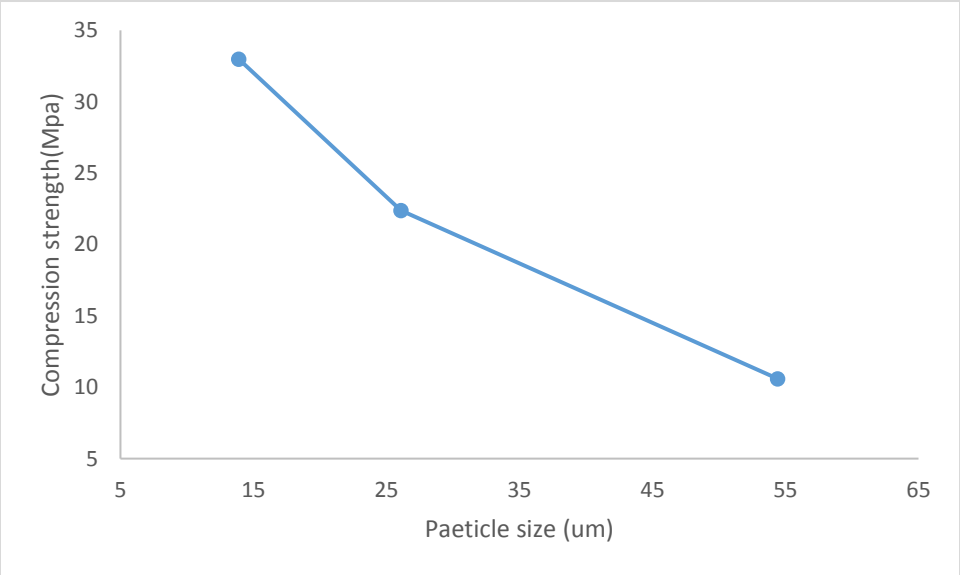

Figure 8-5: Compression strength against particle size of 1% B_4O_7HAp (1 wt.% $B_4O_7^{2-}$) and NaClHAp ($Ca_9Na(PO_4)_6ClOH$) powders prepared by hydrolysis method..

In the case of NaClHAp samples with the following chemical formula : $Ca_9Na_1(PO_4)_6(OH)Cl$, a clear reduction in the value of strength was produced as a result of substitution of both ions, namely Na^+ and Cl^- ions The reduction in the mechanical strength can be ascribed to the enhancement in the value of the particle size. The increase in the measured value of particle size could not be attributed to the substitution of calcium site by Na^+ ion (as confirmed by ICP-MS analysis, see

chapter 7 for details), because the ionic radius of both ions are so close to each other, it is [0.99 Å] for Na^+ compared to Ca^{2+} (1.00 Å) [259]. But the obvious increase in the value of particle size of NaClHAp materials can be ascribed to the substitution of Cl^- ions with larger ionic radius (0.168 nm) compared to the OH^- group (0.153 nm) [216]. The substitution of hydroxyl group by Cl^- ions was not proven by the ICP-MS analysis, but confirmed through using other kinds of analysis tests such as FTIR and XRD techniques (see chapter 7 for details).

On the other hand, the substitution process of $B_4O_7^{2-}$ ions caused an obvious enhancement in the mechanical properties. The enhancement in the mechanical strength of 1% B_4O_7HAp can be attributed to the obvious decrease in the value of particle size. The reduction in the particle size was resulted from the substitution process of phosphate site with larger ionic radius (0.23 nm) compared to carbonate group (0.189 nm) [216] (see chapter 7 for details). As a result, an increase in the measured value of the mechanical strength was achieved.

8.1.7 Mechanical properties of sintered SAp powders at 900 ˚C prepared by the novel hydrolysis of MCP/$Ca(OH)_2$:

Table 8-7 displays the mechanical results of SAp powders prepared by the novel hydrolysis method.

Table 8-7: Mechanical results of SAp powders prepared by the novel hydrolysis methods.

Sample	Trial one Maximum load (N)	Trial Two Maximum load (N)	Trial Three Maximum load (N)	Average of maximum load (N)	Particle size (um)	Compression strength (MPa)
Unsubstituted HAp by hydrolysis	2129	2145	2245	2137	26.1	22.38
SAp by hydrolysis	1427	1470	1458	1452	47.5	14.96

Fig. 8-6 displays the effect of the particle size of SAp powders prepared by hydrolysis method on the value of compression test.

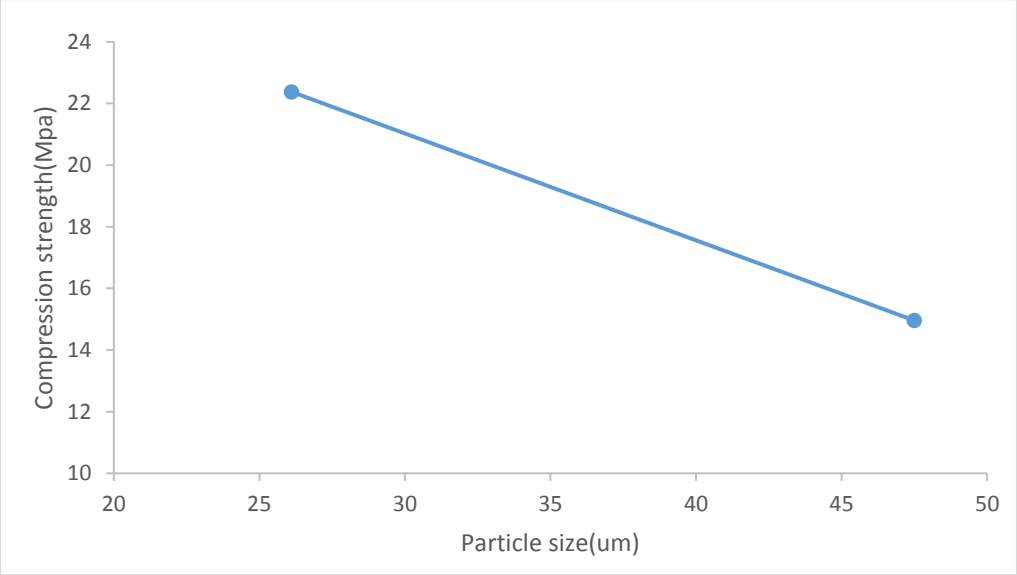

Figure 8-6: Compression strength against particle size of SAp powders prepared by hydrolysis methods

During this project, the required samples of SAp powders that were prepared by the ion exchange method were excluded from our consideration for mechanical testing , because the sintering process caused an obvious mass decrease and sample shrinkage. A similar observation was made by Dorozhkin et al. [156]. The authors prepared cylindrical samples of dense HAp in order to analyse them mechanically. They attributed that result to the sintering process of HAp cylinders, since it always leads to mass decreasing and sample shrinkage because of several factors such as evaporation of water as well as burning out of other volatile compounds such as binder[156].

In the present study, the results of substitution S^{2-} ions into HAp crystal showed a clear reduction in the compression values. This reduction can be explained in terms of the following:

1- The bigger particle size that resulted from the replacement process of S^{2-} ions with larger ionic radius (0.189 nm) into HAp structure compared to OH^{-} ions (0.152 nm).
2- The phase purity. As discussed earlier, the mechanical properties of biphasic calcium phosphate (BCP) ceramics can be modified by parameters like the ratio of HAp/β-TCP [256].

8.2 Summary:

Based on the outcome of the mechanical results of this project, it is clear that several factors can affect the mechanical strength of the prepared substituted and co substituted HAp samples other than the substitution levels. Because the results displayed a clear difference in the calculated values of compression strength. The results of the tests for mechanical properties in this project showed that particle size plays a fundamental role in the value of mechanical strength, since an enhancement in strength was recorded with a reduction in particle size.

Chapter Nine

Conclusions and Future work

9.1 Conclusion of this work:

The conclusions resulting from this research are summarized into sections as follows:

9.1.1 The development of a novel method to prepare (unsubstituted) HAp by hydrolysis of monocalcium phosphate (MCP) using calcium hydroxide (Chapter 4):

The main finding at this stage can be summarized as the following:1- The novel hydrolysis method using monocalcium phosphate and calcium hydroxide as precursors displayed clearly that it can be considered as an effective approach to prepare unsubstituted HAp powders.

2- The presence of an apatitic phase was confirmed by FTIR spectra.

3- The XRD diffraction patterns of sintered, unsubstituted HAp powders were in good agreement with the current literature ([8], [80], [190]), the standard HAp (reference card number 01-074-9780) as well as commercial HAp (Fluka) and showed the characteristic peaks of the HAp phase. A slight decomposition of the HAp to the β-TCP phase was observed due to the sintering process at 900 ˚C.

4- SEM images show that the sintered samples of unsubstituted HAp powders consist of particles with fine grains which are spheroidal in shape and associated with an irregular distribution of components.

5- The ICP-MS measurements revealed that the Ca/P mole ratio of unsubstituted HAp samples was 1.40, which is lower than the theoretical value of stochiometric HAp, but the value of (Ca+Na)/P was found to be 1.65 which is very close to the stoichiometric HAp.

9.1.2 Preparation of MHAp powders with the chemical formula: $Ca_{10-x}M_xHAp$ (where M=Zn, Sr and Cu, X=0.5, 1.0 and 1.5) by the novel hydrolysis method(Chapter 5):

The main findings in this chapter (Chapter five) can be summarized as follows:

1- The novel hydrolysis method using monocalcium phosphate and calcium hydroxide as starting materials was proven to be an effective route for preparing substituted HAp powders.
2- FTIR displayed i- the presence of apatite phase. ii- a clear relation between the amount of M ions, and the intensities of OH^- vibration modes at 3572 cm^{-1} (stretching) and 630 cm^{-1}. iii- an obvious shift of phosphate bands at 572 and 604 cm^{-1} to a lower wave number due to substitution of Sr^{2+} ions. This shift increases as the amount of Sr ions increases.
3- The phase purity, crystallinity, crystallite size and lattice parameters of the prepared MHAp materials varied with increasing substitution levels.
4- SEM images showed that ZnHAp and CuHAp substituted materials consist of agglomerated crystals which are spheroidal in shape. Spheroidal particles were seen in 0.5 SrHAp and 1.0 SrHAp samples, but a combination of spheroidal and rod like particles was recorded in the case of the 1.5 SrHAp materials.
5- The results of ICP-MS measurements displayed the presence of Zn^{2+}, Sr^{2+} and Cu^{2+} ions into HAp samples but was not necessarily indicative of substitution.

9.1.3 Cationic substituted HAp powders:

The main findings at this Chapter (Chapter six) can be summarized as the following:

1- The presence of Rb^+, Eu^{3+} and Sc^{3+} ions in HAp samples was detected by using ICP-MS analysis with low wt.%. Although the technique cannot prove substitution of these ions, it appears that if there is substitution occurring, it would be at low level.
2- FTIR analysis displayed i- the presence of the apatite phase in the prepared powders ii- a reduction of the intensities of the stretching and librational modes of the OH^- group at (3572 and 630 cm^{-1}) due to the replacement process of calcium site by trivalent cation (Eu^{3+}) and monovalent cation (Rb^+).
3- The effects of the replacement process of calcium site by the cation (Rb^+, Eu^{3+} and Sc^{3+}) on the crystallinity crystallite size and lattice parameters were varied.
4- The effects of preparation method used on the morphology were confirmed by SEM images.

9.1.4 Anionic substituted HAp and co-substituted HAp powders:

The main findings of Chapter 7 were as follows:

1- FTIR spectra showed i- the presence of the apatite phase in the prepared powders ii- a reduction of the intensities of the stretching and librational modes of OH- group at 3572 and 630 cm^{-1} due to the replacement process of monovalent and bivalent ions(Br^-, S^{2-} and $B_4O_7^{2})^-$.
2- The effect of the replacement process of phosphate and/or hydroxyl groups by the ions used to substitute HAp structure on the crystallinity, crystallite size and lattice parameters were varied, and the details of these values were discussed in Chapter 7
3- SEM images displayed the effect of preparation method on the morphology.

9.1.5 Mechanical properties:

The mechanical strength and the particle size of unsubstituted HAp, substituted and co substituted HAp powders prepared by the hydrolysis process of MCP and $Ca(OH)_2$ were studied**.** The results of the mechanical properties in the present investigation showed clearly that particle size plays a fundamental rule in the value of mechanical strength, since an enhancement in the mechanical strength was recorded because of the reduction in particle size that occurred in some preparations.

9.2 Further work:

Three main areas to focus on in future work in order to reach the maximum benefits of these biomaterials in biomedical areas are:

1- The thermal stability: many variables were found to play a fundamental role in the thermal stability of the prepared substituted HAp powders such as the substitution of calcium ion by other cations, replacement of phosphate and hydroxyl groups by other anions, the preparation method, the substitution level and the chemical composition. Therefore, the effect of these parameters should be further investigated in order to produce substituted HAp materials with high thermal stability properties. High thermal stability of substituted HAp is an essential requirement in the biological

environment, since decomposition of HAp into other phases such as β-TCP will cause an undesirable fast dissolution rate in vivo [260].

2- The biological tests: these kinds of tests must be done if the main goal of the produced materials was application as biomedical materials, because cytotoxic effects can easily occur at any level of substitution [261]. As an example, Copper is an essential micronutrient in living organisms since it is involved in metabolic processes. Hence copper substituted HAps could be of some use as an antibacterial against E. coli for CuHAp (3.3 wt. % Cu) has been revealed from several studies. But, 1 at.% doped CuHAp has been found to be cytotoxicfor human foetal osteoblasts (hFOB1.19 cell line)as reported in the literature [221] .

3- The mechanical properties: more work is still needed to well understand the effect of substitution levels on the mechanical strength. Several factors should be eliminated such as the particle size and the cooling rate, because these parameters can also affect the mechanical properties.

References

[1] Malysheva, A. Y.; Beletskii, B. I.; Vlasova, E. B. Structure and Properties of Composite Materials for Medical Application. *Glass and Ceramics* **2001**, *58*, 66-69.

[2] Gallo, R. Synthesis and characterization of substituted apatites for biomedical applicationsThesis, Universitas Studii Patavini, 2011.

[3] Williams, D. F.; European Society for, B.; Consensus Conference of the European Society for, B. *Definitions in biomaterials : proceedings of a Consensus Conference of the European Society for Biomaterials, Chester, England, March 3-5, 1986*; Elsevier, 1987.

[4] Vallet-Regi, M. *Bio-Ceramics with Clinical Applications*; John Wiley & Sons, Incorporated: New York, UNITED KINGDOM, 2014.

[5] Šupová, M. Substituted hydroxyapatites for biomedical applications: A review. *Ceramics International* **2015**, *41*, 9203-9231.

[6] Ratnayake, J.; Mucalo, M.; Dias, G. Substituted hydroxyapatites for bone regeneration:A review of current trends. *Journal of Biomedical Materials Research Part B Applied Biomaterials* **2016**, *105*.

[7] Stanić, V.; Janaćković, D.; Dimitrijević, S.; Tanasković, S. B.; Mitrić, M.; Pavlović, M. S.; Krstić, A.; Jovanović, D.; Raičević, S. Synthesis of antimicrobial monophase silver-doped hydroxyapatite nanopowders for bone tissue engineering. *Applied Surface Science* **2011**, *257*, 4510-4518.

[8] Stanić, V.; Dimitrijević, S.; Antić-Stanković, J.; Mitrić, M.; Jokić, B.; Plećaš, I. B.; Raičević, S. Synthesis, characterization and antimicrobial activity of copper and zinc-doped hydroxyapatite nanopowders. *Applied Surface Science* **2010**, *256*, 6083-6089.

[9] Tampieri, A.; D'Alessandro, T.; Sandri, M.; Sprio, S.; Landi, E.; Bertinetti, L.; Panseri, S.; Pepponi, G.; Goettlicher, J.; Bañobre-López, M.; Rivas, J. Intrinsic magnetism and hyperthermia in bioactive Fe-doped hydroxyapatite. *Acta Biomaterialia* **2012**, *8*, 843-851.

[10] Germaini, M.-M.; Detsch, R.; Grünewald, A.; Magnaudeix, A.; Lallou, F.; Boccaccini, A.; Champion, E. Osteoblast and osteoclast responses to A/B type carbonate-substituted hydroxyapatite ceramics for bone regeneration. *Biomedical materials (Bristol, England)* **2017**, *12*.

[11] Bianco, A.; Cacciotti, I.; Lombardi, M.; Montanaro, L. Si-substituted hydroxyapatite nanopowders: Synthesis, thermal stability and sinterability. *Materials Research Bulletin* **2009**, *44*, 345-354.

[12] Jiménez-Flores, Y.; Suárez-Quezada, M.; Rojas-Trigos, J.; Lartundo-Rojas, L.; Suárez, V.; Mantilla, A. Characterization of Tb-doped hydroxyapatite for biomedical applications: optical properties and energy band gap determination. *Journal of Materials Science* **2017**, *52*, 9990-10000.

[13] Mucalo, M.; Bandyopadhyay, A. *Hydroxyapatite (HAp) for biomedical applications*; Amsterdam, Netherlands : Woodhead Publishing, 2015.

[14] Bhattacharjee, B.; Mishra, V.; Rai, S.; Parkash, O.; Kumar, D. Study of Morphological Behavior of Hydroxyapatite, EDTA Hydroxyapatite and Metal Doped EDTA Hydroxyapatite Synthesized by Chemical Co-Precipitation Method via Hydrothermal Route. *Key Engineering Materials* **2016**, *720*, 210-214.

[15] Zorenko, Y.; Gorbenko, V.; Zorenko, T.; Voznyak, T.; Voloshynovskii, A.; Vistovskiy, V.; Paprocki, K.; Mosińska, L.; Bilski, P.; Twardak, A.; Fedorov, A.; Nikl, M.; Mares, J. A.

Luminescent and scintillation properties of Sc3+and La3+doped Y2SiO5 powders and single crystalline films. *Journal of Luminescence* **2016**, *179*, 445-450.
[16] Tite, T.; Popa, A.-C.; Balescu, L.; Bogdan, I.; Pasuk, I.; Ferreira, J.; Stan, G. Cationic Substitutions in Hydroxyapatite: Current Status of the Derived Biofunctional Effects and Their In Vitro Interrogation Methods. *Materials (Basel)* **2018**, *11*, 2081.
[17] Liu, Y.; Tan, Y.; Wu, J. Rubidium doped nano-hydroxyapatite with cytocompatibility and antibacterial. *Journal of Asian Ceramic Societies* **2021**, *9*, 323-333.
[18] Han, Y.; Wang, X.; Dai, H.; Li, S. Synthesis and luminescence of Eu3+ doped hydroxyapatite nanocrystallines: Effects of calcinations and Eu3+ content. *Journal of Luminescence* **2013**, *135*, 281-287.
[19] Xuan, T.-C.; Trung, N. N.; Pham, V.-H. Comparative characterization of microstructure and luminescence of europium doped hydroxyapatite nanoparticles via coprecipitation and hydrothermal method. *Optik* **2015**, *126*, 5019-5021.
[20] Ciobanu, C. S.; Iconaru, S. L.; Massuyeau, F.; Constantin, L. V.; Costescu, A.; Predoi, D. Synthesis, Structure, and Luminescent Properties of Europium-Doped Hydroxyapatite Nanocrystalline Powders. *Journal of Nanomaterials* **2012**, *2012*, 942801.
[21] Kataoka, T.; Shiba, K.; Tagaya, M. Preparation of europium(III)-doped hydroxyapatite nanocrystals in the presence of cationic surfactant. *Colloid and Interface Science Communications* **2016**, *13*, 1-5.
[22] Wiglusz, R. J.; Bednarkiewicz, A.; Lukowiak, A.; Strek, W. Synthesis and Optical Properties of Eu3+ Ion Doped Nanocrystalline Hydroxyapatites. *Spectroscopy Letters* **2010**, *43*, 333-342.
[23] Dykes, E. Preparation and characterisation of calcium bromapatite. *Materials Research Bulletin* **1974**, *9*, 1227-1236.
[24] Green, J. Phosphorus-bromine flame retardant synergy in engineering thermoplastics. In *Industrial Chemistry Library*; J.-R. Desmurs; B. Gérard and M. J. Goldstein, Eds.; Elsevier, 1995; pp 341-354.
[25] Henning, P.; Adolfsson, E.; Grins, J. The chalcogenide phosphate apatites Ca10(PO4)6S, Sr10(PO4)6S, Ba10(PO4)6S and Ca10(PO4)6Se. *Zeitschrift fur Kristallographie* **2000**, *215*, 226.
[26] Olofsson, K. Thiol-Ene CHemistry and Dopa-Functional Materials towards Biomedical Applications. Doctoral thesis, comprehensive summary Thesis, KTH Royal Institute of Technology, Stockholm, 2016.
[27] Alshemary, A. Z.; Goh, Y.-F.; Akram, M.; Razali, I. R.; Abdul Kadir, M. R.; Hussain, R. Microwave assisted synthesis of nano sized sulphate doped hydroxyapatite. *Materials Research Bulletin* **2013**, *48*, 2106-2110.
[28] Yoo, D. S.; Cho, J. S.; Chung, Y.-C.; Rhee, S.-H. Defect structures of sodium and chloride co-substituted hydroxyapatite and its osseointegration capacity. *Journal of Materials Science* **2021**, *56*, 5493-5508.
[29] Ratnayake, J. T. B.; Mucalo, M.; Dias, G. J. Substituted hydroxyapatites for bone regeneration: A review of current trends. *J Biomed Mater Res B Appl Biomater* **2017**, *105*, 1285-1299.
[30] Yılmaz, B.; Evis, Z. Boron-substituted bioceramics: A review. **2016**.
[31] Capanema, N.; Mansur, A.; Carvalho, S.; Silva, A.; Ciminelli, V.; Mansur, H. Niobium-Doped Hydroxyapatite Bioceramics: Synthesis, Characterization and In Vitro Cytocompatibility. *Materials* **2015**, *8*, 4191-4209.

[32] Tamai, M.; Isama, K.; Nakaoka, R.; Tsuchiya, T. Synthesis of a novel b-tricalcium phosphate/hydroxyapatite biphasic calcium phosphate containing niobium ions and evaluation of its osteogenic properties. *Journal of Artificial Organs* **2007**, *10*, 22-28.
[33] Weinmann, M.; Schnitter, C.; Stenzel, M.; Markhoff, J.; Schulze, C.; Bader, R. Development of bio-compatible refractory Ti/Nb(/Ta) alloys for application in patient-specific orthopaedic implants. *International Journal of Refractory Metals and Hard Materials* **2018**, *75*.
[34] Dorozhkin, S. V. Calcium Orthophosphates in Nature, Biology and Medicine. *Materials* **2009**, *2*, 399-498.
[35] Shi, D. *Introduction to Biomaterials*; Tsinghua University Press: Singapore, UNITED STATES, 2006.
[36] Suchanek, W.; Yoshimura, M. Processing and Properties of HAp Based Biomaterials for Use as Hard Tissue Replacement Implants. *Journal of Materials Research* **1998**, *13*, 94-117.
[37] Mucalo, M. *BOOK: Hydroxyapatite (HAp) for Biomedical Applications*, 2015.
[38] Heimann, R. B.; Lehmann, H. *Bioceramic Coatings for Medical Implants: Trends and Techniques*, 2015; 1-467.
[39] Niimi, M.; Masuda, T.; Kaihatsu, K.; Kato, N.; Nakamura, S.; Nakaya, T.; Arai, F. Virus purification and enrichment by hydroxyapatite chromatography on a chip. *Sensors and Actuators B: Chemical* **2014**, *201*, 185-190.
[40] Cakmak, I. Plant nutrition research: Priorities to meet human needs for food in sustainable ways. *Plant and Soil* **2002**, *247*, 3-24.
[41] Liu, R.; Lal, R. Synthetic apatite nanoparticles as a phosphorus fertilizer for soybean (Glycine max). *Sci Rep* **2014**, *4*, 5686-5686.
[42] Safatian, F.; Doago, Z.; Torabbeigi, M.; Rahmani Shams, H.; Ahadi, N. Lead ion removal from water by hydroxyapatite nanostructures synthesized from egg sells with microwave irradiation. *Applied Water Science* **2019**, *9*, 108.
[43] Jiménez-Flores, Y.; Suárez-Quezada, M.; Rojas-Trigos, J. B.; Lartundo-Rojas, L.; Suárez, V.; Mantilla, A. Characterization of Tb-doped hydroxyapatite for biomedical applications: optical properties and energy band gap determination. *Journal of Materials Science* **2017**, *52*, 9990-10000.
[44] Domínguez, M. I.; Romero-Sarria, F.; Centeno, M. A.; Odriozola, J. A. Gold/hydroxyapatite catalysts: Synthesis, characterization and catalytic activity to CO oxidation. *Applied Catalysis B: Environmental* **2009**, *87*, 245-251.
[45] Dong, Q. X.; Chen, Q.; Yang, W.; Zheng, Y. L.; Liu, X.; Li, Y. L.; Yang, M.-B. Thermal properties and flame retardancy of polycarbonate/hydroxyapatite nanocomposite. *Journal of Applied Polymer Science* **2008**, *109*, 659-663.
[46] Plūduma, L. HYDROXYL ION QUANTIFICATION IN HYDROXYAPATITE AND THE EFFECT ON THE BIOLOGICAL RESPONSEThesis, RIGA TECHNICAL UNIVERSITY, 2017.
[47] Eliaz, N.; Metoki-Shlubsky, N. *Calcium Phosphate Bioceramics: A Review of Their History, Structure, Properties, Coating Technologies and Biomedical Applications*, 2017.
[48] Mucalo, M. R. *Hydroxyapatite (HPA) for Biomedical Applications*; Elsevier Science & Technology: Cambridge, UNITED KINGDOM, 2015.
[49] Ma, G.; Liu, X. Hydroxyapatite: Hexagonal or Monoclinic? *Crystal Growth & Design - CRYST GROWTH DES* **2009**, *9*.

[50] Askeland, D. R. *The science and engineering of materials*; 5th ed.. ed.; Thomson Learning: Toronto : London, 2006.
[51] Elliott, J. C. *Structure and chemistry of the apatites and other calcium orthophosphates*; Elsevier: Amsterdam [The Netherlands] : New York, 1994.
[52] Oshida, Y. *Hydroxyapatite : synthesis and applications*; Biomaterials engineering collection; Momentum Press: New York, [New York] (222 East 46th Street, New York, NY 10017), 2015.
[53] Sadat-Shojai, M.; Khorasani, M.-T.; Dinpanah-Khoshdargi, E.; Jamshidi, A. Synthesis methods for nanosized hydroxyapatite with diverse structures. *Acta Biomaterialia* **2013**, *9*, 7591-7621.
[54] Cox, S. Synthesis methods of hydroxyapatite. **2014**.
[55] Nayak, A. Hydroxyapatite synthesis methodologies: An overview. *International Journal of ChemTech Research* **2010**, *2*, 903-907.
[56] Dou, L.; Zhang, Y.; Sun, H. *Advances in Synthesis and Functional Modification of Nanohydroxyapatite*, 2018; 1-7.
[57] Gomes, D.; Santos, A.; Neves, G.; Menezes, R. A brief review on hydroxyapatite production and use in biomedicine. *Cerâmica* **2019**, *65*, 282-302.
[58] Gopi, D.; Kavitha, L.; Rajeswari, D. Synthesis of Pure and Substituted Hydroxyapatite Nanoparticles by Cost Effective Facile Methods. In *Handbook of Nanoparticles*; M. Aliofkhazraei, Ed.; Springer International Publishing: Cham, 2016; pp 167-190.
[59] Anitha, P.; , H. M. P. Comprehensive Review of Preparation Methodologies of Nano Hydroxyapatite. *J. Environ. Nanotechnol* **2014**, *3*, 101-121.
[60] Basu, S.; Basu, B. Doped biphasic calcium phosphate: synthesis and structure. *Journal of Asian Ceramic Societies* **2019**, *7*, 265-283.
[61] Mutis, R. *Nanoparticles of hydroxyapatite: preparation, characterization and cellular approach - An Overview*, 2013.
[62] Beganskienė, A.; Dudko, O.; Sirutkaitis, R.; Giraitis, R. Water based sol-gel synthesis of hydroxyapatite. *Mater Sci* **2003**, *9*.
[63] Daculsi, G.; Bouler, J. M.; LeGeros, R. Z. Adaptive Crystal Formation in Normal and Pathological Calcifications in Synthetic Calcium Phosphate and Related Biomaterials. In *International Review of Cytology*; K. W. Jeon, Ed.; Academic Press, 1997; pp 129-191.
[64] Tõnsuaadu, K.; Gross, K. A.; Plūduma, L.; Veiderma, M. A review on the thermal stability of calcium apatites. *Journal of Thermal Analysis and Calorimetry* **2012**, *110*, 647-659.
[65] Gibson, I. R.; Best, S. M.; Bonfield, W. Chemical characterization of silicon-substituted hydroxyapatite. *Journal of Biomedical Materials Research* **1999**, *44*, 422-428.
[66] Bigi, A.; Cojazzi, G.; Panzavolta, S.; Ripamonti, A.; Roveri, N.; Romanello, M.; Noris Suarez, K.; Moro, L. Chemical and structural characterization of the mineral phase from cortical and trabecular bone. *Journal of Inorganic Biochemistry* **1997**, *68*, 45-51.
[67] Racquel, Z.-L. Effect of Carbonate on the Lattice Parameters of Apatite. *Nature* **1965**, *206*, 403.
[68] Maeyer, E.; Verbeeck, R.; Naessens, D. Stoichiometry of Na+- and CO2- 3-Containing Apatites Obtained by Hydrolysis of Monetite. *Inorganic Chemistry - INORG CHEM* **1993**, *32*.
[69] Carlisle, E. M. Silicon: A possible factor in bone calcification. *Science* **1970**, *167*, 279-280.
[70] Schwarz, K.; Milne, D. B. Growth-promoting Effects of Silicon in Rats. *Nature* **1972**, *239*, 333-334.

[71] Nakata, K.; Kubo, T.; Numako, C.; Onoki, T.; Nakahira, A. Synthesis and Characterization of Silicon-Doped Hydroxyapatite. *Materials Transactions* **2009**, *50*, 1046-1049.
[72] Ewald, A.; Hösel, D.; Patel, S.; Grover, L. M.; Barralet, J. E.; Gbureck, U. Silver-doped calcium phosphate cements with antimicrobial activity. *Acta Biomaterialia* **2011**, *7*, 4064-4070.
[73] Bouts, B. A. Argyria. *New England Journal of Medicine* **1999**, *340*, 1554-1554.
[74] Bir, F.; Khireddine, H.; Touati, A.; Sidane, D.; Yala, S.; Oudadesse, H. Electrochemical depositions of fluorohydroxyapatite doped by Cu2+, Zn2+, Ag+ on stainless steel substrates. *Applied Surface Science* **2012**, *258*, 7021-7030.
[75] Iqbal, N.; Abdul Kadir, M. R.; Nik Malek, N. A. N.; Humaimi Mahmood, N.; Raman Murali, M.; Kamarul, T. Rapid microwave assisted synthesis and characterization of nanosized silver-doped hydroxyapatite with antibacterial properties. *Materials Letters* **2012**, *89*, 118-122.
[76] Yamada, Y.; Ito, A.; Kojima, H.; Sakane, M.; Miyakawa, S.; Uemura, T.; LeGeros, R. Inhibitory effect of Zn 2+ in zinc-containing ??-tricalcium phosphate on resorbing activity of mature osteoclasts. *Journal of biomedical materials research. Part A* **2008**, *84*, 344-352.
[77] Chen, X.; Tang, Q.-L.; Zhu, Y.-J.; Zhu, C.-L.; Feng, X.-P. Synthesis and antibacterial property of zinc loaded hydroxyapatite nanorods. *Materials Letters* **2012**, *89*, 233-235.
[78] Jallot, E.; Nedelec, J.-M.; Grimault-Jacquin, A. S.; Chassot, E.; Grandjean-Laquerriere, A.; Laquerriere, P.; Laurent-Maquin, D. STEM and EDXS characterisation of physic chemical reactions at the periphery of sol-gel derived Zn substituted hydroxyapatites during interactions with biological fluids. *Colloids and surfaces. B, Biointerfaces* **2005**, *42*, 205-210.
[79] Li, Y.; Widodo, J.; Lim, S.; Ooi, C. P. Synthesis and cytocompatibility of manganese (II) and iron (III) substituted hydroxyapatite nanoparticles. *Journal of Materials Science* **2012**, *47*, 754-763.
[80] Kramer, E.; Zilm, M. A Comparative Study of the Sintering Behavior of Pure and Iron-Substituted Hydroxyapatite. *Bioceramics Development and Applications* **2013**, *3*.
[81] Trinkunaite-Felsen, J.; Prichodko, A.; Semasko, M.; Skaudzius, R.; Beganskienė, A.; Kareiva, A. Synthesis and characterization of iron-doped/substituted calcium hydroxyapatite from seashells Macoma balthica (L.). *Advanced Powder Technology* **2015**, *26*.
[82] Kramer, E.; Itzkowitz, E.; Wei, M. Synthesis and characterization of cobalt-substituted hydroxyapatite powders. *Ceramics International* **2014**, *40*, 13471-13480.
[83] Ignjatovic, N.; Ajdukovic, Z.; Rajkovic, J.; Najman, S.; Mihailovic, D.; Uskokovic, D. Enhanced Osteogenesis of Nanosized Cobalt-substituted Hydroxyapatite. *Journal of Bionic Engineering* **2015**, *12*, 604-612.
[84] S, S.; R, A.; R, P.; Rani, M. Structural, Optical and Antimicrobial Activity of Cu Doped HAp: Synthesized by Solgel Method for Biomedical Applications. *Research & Reviews: Journal of Material Sciences* **2017**, *05*.
[85] Li, J.; Li, Y. B.; Zuo, Y.; Lu, G. Y.; Yang, W. H.; Mo, L. R. Preparation and antibacterial properties valuation of copper-substituted nano-hydroxyapatite. *Gongneng Cailiao/Journal of Functional Materials* **2006**, *37*, 635-638.
[86] Li, Y.; Ho, J.; Ooi, C. P. Antibacterial efficacy and cytotoxicity studies of copper (II) and titanium (IV) substituted hydroxyapatite nanoparticles. *Materials Science and Engineering: C* **2010**, *30*, 1137-1144.

[87] Sopyan, I.; Pusparini, E.; Ramesh, S.; Tan, C. Y.; Ching, Y. C.; Wong, Y. H.; Abidin, N. I. Z.; Chandran, H.; Ramesh, S.; Bang, L. T. Influence of sodium on the properties of sol-gel derived hydroxyapatite powder and porous scaffolds. *Ceramics International* **2017**, *43*, 12263-12269.

[88] Cho, J.; Um, S.-H.; Yoo, D.; Chung, Y.-C.; Chung, S.; Lee, J.-C.; Rhee, S.-H. Enhanced osteoconductivity of sodium-substituted hydroxyapatite by system instability. *Journal of biomedical materials research. Part B, Applied biomaterials* **2014**, *102*.

[89] Oshida, Y. *Hydroxyapatite : Synthesis and Applications*; New York: Momentum Press: New York, 2014.

[90] Li, C.; Paris, O.; Siegel, S.; Roschger, P.; Paschalis, L.; Klaushofer, K.; Fratzl, P. Strontium Is Incorporated Into Mineral Crystals Only in Newly Formed Bone During Strontium Ranelate Treatment. *Journal of bone and mineral research : the official journal of the American Society for Bone and Mineral Research* **2009**, *25*, 968-975.

[91] Landi, E.; Tampieri, A.; Celotti, G.; Sprio, S.; Sandri, M.; Logroscino, G. Sr-substituted hydroxyapatites for osteoporotic bone replacement. *Acta Biomaterialia* **2007**, *3*, 961-969.

[92] Xue, W.; Moore, J.; Hosick, H.; Bose, S.; Bandyopadhyay, A.; Lu, W.; Cheung, K.; Luk, K. Osteoprecursor Cell Response to Strontium-Containing Hydroxyapatite Ceramics. *Journal of biomedical materials research. Part A* **2006**, *79*, 804-814.

[93] Cox, S. C.; Jamshidi, P.; Grover, L. M.; Mallick, K. K. Preparation and characterisation of nanophase Sr, Mg, and Zn substituted hydroxyapatite by aqueous precipitation. *Materials Science and Engineering: C* **2014**, *35*, 106-114.

[94] Liangzhi, G.; Zhang, W.; Shen, Y. Magnesium substituted hydroxyapatite whiskers: synthesis, characterization and bioactivity evaluation. *RSC Adv.* **2016**, *6*.

[95] Andrés, N.; D'Elía, N.; Ruso, J.; Campelo, A.; Massheimer, V.; Messina, P. Manipulation of Mg2+-Ca2+ Switch on the Development of Bone Mimetic Hydroxyapatite. *ACS Applied Materials & Interfaces* **2017**, *9*.

[96] Ren, F.; Leng, Y.; Xin, R.; Ge, X. Synthesis, characterization and ab initio simulation of magnesium-substituted hydroxyapatite. *Acta biomaterialia* **2010**, *6*, 2787-2796.

[97] Mehrjoo, M.; Javadpour, J.; Shokrgozar, M.; Farokhi, M.; Javadian, S.; Bonakdar, S. Effect of magnesium substitution on structural and biological properties of synthetic hydroxyapatite powder. *Materials Express* **2015**, *5*.

[98] Sopyan, I.; Nawawi, N.; Shah, Q.; Singh, R.; Y, T.; Abd Shukor, M. Sintering and Properties of Dense Manganese-Doped Calcium Phosphate Bioceramics Prepared Using Sol-Gel Derived Nanopowders. *Materials and Manufacturing Processes* **2011**, *26*, 908-914.

[99] Zilm, M.; Thomson, S.; Wei, M. A Comparative Study of the Sintering Behavior of Pure and Manganese-Substituted Hydroxyapatite. *Materials* **2015**, *8*, 6419-6436.

[100] Chen, F.; Huang, P.; Zhu, Y.-J.; Wu, J.; Zhang, C.-L.; Cui, D.-X. The photoluminescence, drug delivery and imaging properties of multifunctional Eu3+/Gd3+ dual-doped hydroxyapatite nanorods. *Biomaterials* **2011**, *32*, 9031-9039.

[101] Guo, D. G.; Wang, A. H.; Han, Y.; Xu, K.-W. Characterization, physicochemical properties and biocompatibility of La-incorporated apatites. *Acta biomaterialia* **2009**, *5*, 3512-3523.

[102] Li, Y.; Ooi, C.; Ning, C.; Khor, K. Synthesis and Characterization of Neodymium(III) and Gadolinium(III)-Substituted Hydroxyapatite as Biomaterials. *International Journal of Applied Ceramic Technology* **2008**, *6*, 501-512.

[103] Ergun, C. Effect of Ti ion substitution on the structure of hydroxylapatite. *Journal of the European Ceramic Society* **2008**, *28*, 2137-2149.

[104] Marshall, B. J. The use of bismuth in gastroenterology. The ACG Committee on FDA-Related Matters. American College of Gastroenterology. *American Journal of Gastroenterology* **1991**, *86*, 16-25.
[105] Stoltenberg, M.; Juhl, S.; Danscher, G. Bismuth ions are metabolized into autometallographic traceable bismuth-sulphur quantum dots. *European journal of histochemistry : EJH* **2007**, *51*, 53-57.
[106] Ciobanu, G.; Bargan, A. M.; Luca, C. New Bismuth-Substituted Hydroxyapatite Nanoparticles for Bone Tissue Engineering. *JOM* **2015**, *67*, 2534-2542.
[107] Kikuchi, M.; Yamazaki, A.; Akao, M.; Aoki, H. Cytotoxicity of synthetic barium hydroxyapatite. *Bio-Medical Materials and Engineering* **1996**, *6*, 405-413.
[108] Zhu, Q.-X.; Li, Y.-M.; Han, D. Co-substitution of carbonate and fluoride in hydroxyapatite: Effect on substitution type and content. *Frontiers of Materials Science* **2015**, *9*, 192-198.
[109] CASS, R. M.; CROFT, J. D., JR.; PERKINS, P.; NYE, W.; WATERHOUSE, C.; TERRY, R. New Bone Formation in Osteoporosis Following Treatment With Sodium Fluoride. *Archives of Internal Medicine* **1966**, *118*, 111-116.
[110] Gross, K. A.; Rodríguez-Lorenzo, L. M. Sintered hydroxyfluorapatites. Part II: Mechanical properties of solid solutions determined by microindentation. *Biomaterials* **2004**, *25*, 1385-1394.
[111] Chander, S.; Fuerstenau, D. W. An XPS study of the flouride uptake by hydroxyapatite. *Colloids and Surfaces* **1985**, *13*, 137-144.
[112] Tredwin, C. J.; Georgiou, G.; Kim, H.-W.; Knowles, J. C. Hydroxyapatite, fluor-hydroxyapatite and fluorapatite produced via the sol–gel method: Bonding to titanium and scanning electron microscopy. *Dental Materials* **2013**, *29*, 521-529.
[113] Ohno, M.; Kimoto, K.; Toyoda, T.; Kawata, K.; Arakawa, H. Fluoride-Treated Bio-Resorbable Synthetic Hydroxyapatite Promotes Proliferation and Differentiation of Human Osteoblastic MG-63 Cells. *The Journal of oral implantology* **2011**, *39*.
[114] Kim, H.-W.; Li, L.; Koh, Y.-H.; Knowles, J.; Kim, H. J. *Sol–Gel Preparation and Properties of Fluoride-Substituted Hydroxyapatite Powders*, 2004; 1939-1944.
[115] Monmaturapoj, N.; Luang, K. Nano-size Hydroxyapatite Powders Preparation by Wet-Chemical Precipitation Route. *Journal of Metals, Materials and Minerals* **2008**, *18*.
[116] Cho, J.; Yoo, D.; Chung, Y.-C.; Rhee, S.-H. Enhanced bioactivity and osteoconductivity of hydroxyapatite through chloride substitution. *Journal of biomedical materials research. Part A* **2014**, *102*.
[117] Geng, Z.; Wang, R.; Li, Z.; Cui, Z.; Zhu, S.; Liang, Y.; Liu, Y.; Huijing, B.; Li, X.; Huo, Q.; Liu, Z.; Yang, X. Synthesis, characterization and biological evaluation of strontium/magnesium-co-substituted hydroxyapatite. *Journal of biomaterials applications* **2016**, *31*.
[118] Kulanthaivel, S.; Mishra, U.; Agarwal, T.; Giri, S.; Pal, K.; Pramanik, K.; Banerjee, I. Improving the osteogenic and angiogenic properties of synthetic hydroxyapatite by dual doping of bivalent cobalt and magnesium ion. *Ceramics International* **2015**, *41*.
[119] Lowry, N.; Han, Y.; Meenan, B. J.; Boyd, A. R. Strontium and zinc co-substituted nanophase hydroxyapatite. *Ceramics International* **2017**, *43*, 12070-12078.
[120] Gopi, D.; Ramya, S.; Rajeswari, D.; Karthikeyan, P.; Kavitha, L. Strontium, cerium co-substituted hydroxyapatite nanoparticles: Synthesis, characterization, antibacterial activity towards prokaryotic strains and in vitro studies. *Colloids and Surfaces A: Physicochemical and Engineering Aspects* **2014**, *451*, 172-180.

[121] Huang, Y.; Hao, M.; Nian, X.; Qiao, H.; Zhang, X.; Zhang, X.; Song, G.; Guo, J.; Pang, X.; Zhang, H. Strontium and copper co-substituted hydroxyapatite-based coatings with improved antibacterial activity and cytocompatibility fabricated by electrodeposition. *Ceramics International* **2016**, *42*.
[122] Tamm, T.; Peld, M. Computational study of cation substitutions in apatites. *Journal of Solid State Chemistry* **2006**, *179*, 1581-1587.
[123] Kannan, S.; Rebelo, A.; Ferreira, J. M. F. Novel synthesis and structural characterization of fluorine and chlorine co-substituted hydroxyapatites. *Journal of Inorganic Biochemistry* **2006**, *100*, 1692-1697.
[124] Ibrahim, D.; Mostafa, A.; Korowash, S. Chemical characterization of some substituted hydroxyapatites. *Chemistry Central journal* **2011**, *5*, 74.
[125] Landi, E.; Uggeri, J.; Sprio, S.; Tampieri, A.; Guizzardi, S. Human osteoblast behavior on as-synthesized SiO(4) and B-CO(3) co-substituted apatite. *Journal of biomedical materials research. Part A* **2010**, *94*, 59-70.
[126] Okada, M.; Matsumoto, T. Synthesis and modification of apatite nanoparticles for use in dental and medical applications. *Japanese Dental Science Review* **2015**, *51*, 85-95.
[127] Anitha, P.; Pandya, H. Comprehensive Review of Preparation Methodologies of Nano Hydroxyapatite. Presented at.
[128] Dou, L.; Zhang, Y.; Sun, H. Advances in Synthesis and Functional Modification of Nanohydroxyapatite. *Journal of Nanomaterials* **2018**, *2018*, 3106214.
[129] Evis, Z.; Yilmaz, B.; Usta, M.; Levent Aktug, S. X-ray investigation of sintered cadmium doped hydroxyapatites. *Ceramics International* **2013**, *39*, 2359-2363.
[130] Gibson, I. R.; Best, S. M.; Bonfield, W. Chemical characterization of silicon-substituted hydroxyapatite. *Journal of Biomedical Materials Research* **1999**, *44*, 422-428.
[131] Bigi, A.; Boanini, E.; Capuccini, C.; Gazzano, M. Strontium-substituted hydroxyapatite nanocrystals. *Inorganica Chimica Acta* **2007**, *360*, 1009-1016.
[132] Bang, L. T.; Ramesh, S.; Purbolaksono, J.; Ching, Y. C.; Long, B. D.; Chandran, H.; Ramesh, S.; Othman, R. Effects of silicate and carbonate substitution on the properties of hydroxyapatite prepared by aqueous co-precipitation method. *Materials & Design* **2015**, *87*, 788-796.
[133] Bianco, A.; Cacciotti, I.; Lombardi, M.; Montanaro, L.; Bemporad, E.; Sebastiani, M. F-substituted hydroxyapatite nanopowders: Thermal stability, sintering behaviour and mechanical properties. *Ceramics International* **2010**, *36*, 313-322.
[134] Kramer, E. R.; Morey, A. M.; Staruch, M.; Suib, S. L.; Jain, M.; Budnick, J. I.; Wei, M. Synthesis and characterization of iron-substituted hydroxyapatite via a simple ion-exchange procedure. *Journal of Materials Science* **2013**, *48*, 665-673.
[135] Zilm, M. E.; Chen, L.; Sharma, V.; McDannald, A.; Jain, M.; Ramprasad, R.; Wei, M. Hydroxyapatite substituted by transition metals: experiment and theory. *Physical chemistry chemical physics : PCCP* **2016**, *18*, 16457-16465.
[136] Zyman, Z.; Tkachenko, M. Sodium-carbonate co-substituted hydroxyapatite ceramics. *Processing and Application of Ceramics* **2013**, *7*, 153-157.
[137] Sinitsyna, O.; Veresov, A. G.; Kovaleva, E.; Kolen'ko, Y. V.; I. Putlyaev, V.; Tretyakov, Y. *Synthesis of hydroxyapatite by hydrolysis of α-Ca3(PO4)2*, 2005; 79-86.
[138] Bandhyopadhya, A.; Bose, S. *Characterization of biomaterials*; Amsterdam : Elsevier: Amsterdam, 2013.

[139] Synthesis, Processing, and Characterization of Ceramic Nanobiomaterials for Biomedical Applications. CRC Press, 2011; pp 67-108.
[140] Mackintosh, L. J. Characterisation and applications of marine derived calcium phosphates and carbonatesThesis, University of Waikato, Hamilton, New Zealand, 2018.
[141] Mitić, Ž.; Stolić, A.; Stojanović, S.; Najman, S.; Ignjatović, N.; Nikolić, G.; Trajanović, M. Instrumental methods and techniques for structural and physicochemical characterization of biomaterials and bone tissue: A review. *Materials Science and Engineering: C* **2017**, *79*, 930-949.
[142] Yoshida, Y.; Van Meerbeek, B.; Nakayama, Y.; Yoshioka, M.; Snauwaert, J.; Abe, Y.; Lambrechts, P.; Vanherle, G.; Okazaki, M. Adhesion to and Decalcification of Hydroxyapatite by Carboxylic Acids. *Journal of dental research* **2001**, *80*, 1565-1569.
[143] El Hadad, A. A.; Peón, E.; García-Galván, F. R.; Barranco, V.; Parra, J.; Jiménez-Morales, A.; Galván, J. C. Biocompatibility and Corrosion Protection Behaviour of Hydroxyapatite Sol-Gel-Derived Coatings on Ti6Al4V Alloy. *Materials (Basel, Switzerland)* **2017**, *10*, 94.
[144] Fifield, F. W. *Principles and practice of analytical chemistry*; Blackwell Science, 2000.
[145] Cullity, B. D. *Elements of X-ray diffraction*; Scholar's Choice, 2015.
[146] Kaygili, O.; Dorozhkin, S. V.; Keser, S. Synthesis and characterization of Ce-substituted hydroxyapatite by sol–gel method. *Materials Science and Engineering: C* **2014**, *42*, 78-82.
[147] Webster, T. J.; Massa-Schlueter, E. A.; Smith, J. L.; Slamovich, E. B. Osteoblast response to hydroxyapatite doped with divalent and trivalent cations. *Biomaterials* **2004**, *25*, 2111-2121.
[148] Vamvakeros, A. Operando chemical tomography of packed bed and membrane reactors for methane processingThesis, 2017.
[149] White, M. A. High Pressure SynchrotronY XRD, NFS, and NRIXS Studies OF FeSb2Thesis, University of Nevada, Las Vegas, 2016.
[150] Bandyopadhyay, A.; Bose, S. *Characterization of Biomaterials*; Elsevier: San Diego, UNITED STATES, 2013.
[151] Baradaran, S. Mechanical and Biological Evaluations of Hydroxyapatite Composite for Orthopedic ApplicationsThesis, University of Malaya, Kula Lumpur, 2015.
[152] Zyman, Z.; Tkachenko, M.; Epple, M.; Polyakov, M.; Naboka, M. Magnesium-substituted hydroxyapatite ceramics. *Materialwissenschaft und Werkstofftechnik* **2006**, *37*, 474-477.
[153] Song, J.; Liu, Y.; Zhang, Y.; Jiao, L. Mechanical properties of hydroxyapatite ceramics sintered from powders with different morphologies. *Materials Science and Engineering: A* **2011**, *528*, 5421-5427.
[154] Hernandez, E.; Robles-Vazquez, O.; Orozco, I.; Sánchez-Díaz, J. An Overview of Mechanical Tests for Polymeric Biomaterial Scaffolds Used in Tissue Engineering. *Journal of Research Updates in Polymer Science* **2015**, *4*, 168-178.
[155] Canillas, M.; Pena, P.; de Aza, A. H.; Rodríguez, M. A. Calcium phosphates for biomedical applications. *Boletín de la Sociedad Española de Cerámica y Vidrio* **2017**, *56*, 91-112.
[156] Dorozhkin, S.; Gunduz, O.; Oktar, F. Variations in the Compression Strength of Cylindrical Samples Made of Dense Hydroxyapatite. *Key Engineering Materials* **2008**, *361 - 363*, 103-106.
[157] Singer, J. K.; Anderson, J. B.; Ledbetter, M. T.; McCave, I. N.; Jones, K. P. N.; Wright, R. An assessment of analytical techniques for the size analysis of fine-grained sediments. *Journal of sedimentary petrology* **1988**, *58*, 534-543.

[158] Huseynova, S. K. Determination of particle size distributions of industrial side streams by using laser diffraction and sieving methods. Presented at.
[159] Merck. anhydrous mono calcium phosphate. https://www.sigmaaldrich.com/NZ/en/search/anhydrous-mono-calcium-phosphate?focus=products&page=1&perpage=30&sort=relevance&term=anhydrous%20mono%20calcium%20phosphate&type=product (accessed 31 July 2022)
[160] Merck. Calcium phosphate monobasic monohydrate. https://www.sigmaaldrich.com/NZ/en/search/10031-30-8?focus=products&page=1&perpage=30&sort=relevance&term=10031-30-8&type=cas_number (accessed 31 July 2022)
[161] Merck. β-tri-Calcium phosphate. https://www.sigmaaldrich.com/NZ/en/product/sigald/49963 (accessed 31 July 2022)
[162] Merck. Alpha-Tricalcium phosphate. https://www.sigmaaldrich.com/NZ/en/product/aldrich/918601 (accessed 31 July 2022)
[163] Made-in-China. Monocalcium phosphate. https://www.made-in-china.com/price/monocalcium-phosphate-price.html (accessed 20 August 2022)
[164] Made-in-China. Tricalcium phosphate. https://www.made-in-china.com/productdirectory.do?word=b-TCP&file=&searchType=0&subaction=hunt&style=b&mode=and&code=0&comProvince=nolimit&order=0& (accessed 20 August 2022 2022)
[165] Ernani, P. R.; Barber, S. A. Comparison of P- availability from monocalcium and diammonium phosphates using a mechanistic nutrient uptake model. *Fertilizer research* **1990**, *22*, 15-20.
[166] Vetter, J. L. LEAVENING AGENTS. In *Encyclopedia of Food Sciences and Nutrition (Second Edition)*; B. Caballero, Ed.; Academic Press: Oxford, 2003; pp 3485-3490.
[167] Sobczak-Kupiec, A.; Malina, D.; Kijkowska, R.; Wzorek, Z. *Comparative study of hydroxyapatite prepared by the authors with selected commercially available ceramics*, 2012.
[168] Xidaki, D.; Agrafioti, P.; Diomatari, D.; Kaminari, A.; Tsalavoutas-Psarras, E.; Alexiou, P.; Psycharis, V.; Tsilibary, E.; Silvestros, S.; Sagnou, M. Synthesis of Hydroxyapatite, β-Tricalcium Phosphate and Biphasic Calcium Phosphate Particles to Act as Local Delivery Carriers of Curcumin: Loading, Release and In Vitro Studies. *Materials* **2018**, *11*, 595.
[169] Koutsopoulos, S. Synthesis and characterization of hydroxyapatite crystals: A review study on the analytical methods. *Journal of Biomedical Materials Research* **2002** *62*, 600--612.
[170] Freund, F.; Knobel, R. M. Distribution of fluorine in hydroxyapatite studied by infrared spectroscopy. *Journal of the Chemical Society, Dalton Transactions* **1977**, 1136-1140.
[171] Ren, F.; Ding, Y.; Leng, Y. Infrared spectroscopic characterization of carbonated apatite: A combined experimental and computational study. *Journal of biomedical materials research. Part A* **2014**, *102*, 496-505.
[172] Gadaleta, S. J.; Mendelsohn, R.; Paschalis, E. L.; Camacho, N. P.; Betts, F.; Boskey, A. L. Fourier Transform Infrared Spectroscopy of Synthetic and Biological Apatites. In *Mineral Scale Formation and Inhibition*; Z. Amjad, Ed.; Springer US: Boston, MA, 1995; pp 283-294.
[173] Fowler, B. O. Infrared studies of apatites. I. Vibrational assignments for calcium, strontium, and barium hydroxyapatites utilizing isotopic substitution. *Inorganic Chemistry* **1974**, *13*, 194-207.

[174] Arends, J.; Christoffersen, J.; Christoffersen, M. R.; Eckert, H.; Fowler, B. O.; Heughebaert, J. C.; Nancollas, G. H.; Yesinowski, J. P.; Zawacki, S. J. A calcium hydroxyapatite precipitated from an aqueous solution: An international multimethod analysis. *Journal of Crystal Growth* **1987**, *84*, 515-532.

[175] Laird, D. F.; Mucalo, M.; Dias, G. *Reinforced sintered cancellous bovine bone as a potential bone implant material*, 2007.

[176] Mavropoulos, E.; Rossi, A. M.; da Rocha, N. C. C.; Soares, G. A.; Moreira, J. C.; Moure, G. T. Dissolution of calcium-deficient hydroxyapatite synthesized at different conditions. *Materials Characterization* **2003**, *50*, 203-207.

[177] LeGeros, R. Z.; Lin, S.; Rohanizadeh, R.; Mijares, D.; LeGeros, J. P. Biphasic calcium phosphate bioceramics: preparation, properties and applications. *Journal of Materials Science: Materials in Medicine* **2003**, *14*, 201-209.

[178] Othmani, M.; Bachoua, H.; Ghandour, Y.; Aissa, A.; Debbabi, M. Synthesis, characterization and catalytic properties of copper-substituted hydroxyapatite nanocrystals. *Materials Research Bulletin* **2018**, *97*, 560-566.

[179] Louyeh, M. A. Silver, Magnesium and Zinc Substituted Hydroxyapatite for Orthopaedic Applications. PhD Thesis, University of Birmingham Birmingham, U.K., 2016.

[180] Stojanovic, Z.; Veselinovi, L.; Markovic, S.; Ignjatovic, N.; Uskokovi, D. Hydrothermal Synthesis of Nanosized Pure and Cobalt-Exchanged Hydroxyapatite. *Materials and Manufacturing Processes* **2009**, *24*, 1096–1103.

[181] Mostafa, N. Y. Characterization, thermal stability and sintering of hydroxyapatite powders prepared by different routes. *Materials Chemistry and Physics* **2005**, *94*, 333-341.

[182] Tang, X. L.; Xiao, X. F.; Liu, R. F. Structural characterization of silicon-substituted hydroxyapatite synthesized by a hydrothermal method. *Materials Letters* **2005**, *59*, 3841-3846.

[183] Balamurugan, A.; Rebelo, A. H. S.; Lemos, A. F.; Rocha, J. H. G.; Ventura, J. M. G.; Ferreira, J. M. F. Suitability evaluation of sol–gel derived Si-substituted hydroxyapatite for dental and maxillofacial applications through in vitro osteoblasts response. *Dental Materials* **2008**, *24*, 1374-1380.

[184] Adzila, S.; Sopyan, I.; Singh, R.; Pusparini, E.; Abd Shukor, M. *Mechanochemical synthesis of sodium doped hydroxyapatite powder*, 2013; 739-743.

[185] Tian, T.; Jiang, D.; Zhang, J.; Lin, Q. Synthesis of Si-substituted hydroxyapatite by a wet mechanochemical method. *Materials Science and Engineering: C* **2008**, *28*, 57-63.

[186] Martínez-Castañon, G.-A.; Loyola-Rodriguez, J.; Zavala-Alonso, V.; Hernandez, S.; Nino, N.; Ortega-Zarzosa, G.; Ruiz, F. Preparation and characterization of nanostructured powders of hydroxyapatite. *Superficies y vacío* **2012**, *25*, 101-105.

[187] Graham, S.; Brown, P. W. Reactions of octacalcium phosphate to form hydroxyapatite. *Journal of Crystal Growth* **1996**, *165*, 106-115.

[188] Fulmer, M. T.; Brown, P. W. Hydrolysis of dicalcium phosphate dihydrate to hydroxyapatite. *Journal of materials science. Materials in medicine* **1998**, *9*, 197-202.

[189] Monma, H.; Kamiya, T. Preparation of hydroxyapatite by the hydrolysis of brushite. *Journal of Materials Science* **1987**, *22*, 4247-4250.

[190] Li, Y.; Ooi, C.; Philip Hong Ning, C.; Khor, K. Synthesis and Characterization of Neodymium(III) and Gadolinium(III)-Substituted Hydroxyapatite as Biomaterials. *International Journal of Applied Ceramic Technology* **2008**, *6*, 501-512.

[191] Miyaji, F.; Kono, Y.; Suyama, Y. Formation and structure of zinc-substituted calcium hydroxyapatite. *Materials Research Bulletin* **2005**, *40*, 209-220.
[192] Frasnelli, M.; Cristofaro, F.; Sglavo, V. M.; Dirè, S.; Callone, E.; Ceccato, R.; Bruni, G.; Cornaglia, A. I.; Visai, L. Synthesis and characterization of strontium-substituted hydroxyapatite nanoparticles for bone regeneration. *Materials Science and Engineering: C* **2017**, *71*, 653-662.
[193] Nikitina, Y. O.; Petrakova, N. V.; Ashmarin, A. A.; Titov, D. D.; Shevtsov, S. V.; Penkina, T. N.; Kuvshinova, E. A.; Barinov, S. M.; Komlev, V. S.; Sergeeva, N. S. Preparation and Properties of Copper-Substituted Hydroxyapatite Powders and Ceramics. *Inorganic Materials* **2019**, *55*, 1061-1067.
[194] Thian, E.; Konishi, T.; Kawanobe, Y.; Lim, P. N.; Choong, C.; Ho, B.; Aizawa, M. Zinc-substituted hydroxyapatite: A biomaterial with enhanced bioactivity and antibacterial properties. *Journal of materials science. Materials in medicine* **2012**, *24*.
[195] Ofudje, E. A.; Adeogun, A. I.; Idowu, M. A.; Kareem, S. O. Synthesis and characterization of Zn-Doped hydroxyapatite: scaffold application, antibacterial and bioactivity studies. *Heliyon* **2019**, *5*, e01716.
[196] Imrie, F.; Ms Skakle, J. *Preparation of Copper-Doped Hydroxyapatite with Varying x in the Composition Ca10(PO4)6CuxOyHz*, 2013.
[197] Barinov, S. M.; Rau, J. V.; Cesaro, S. N.; Ďurišin, J.; Fadeeva, I. V.; Ferro, D.; Medvecky, L.; Trionfetti, G. Carbonate release from carbonated hydroxyapatite in the wide temperature rage. *Journal of Materials Science: Materials in Medicine* **2006**, *17*, 597-604.
[198] Bulina, N. V.; Chaikina, M. V.; Prosanov, I. Y. Mechanochemical Synthesis of Sr-Substituted Hydroxyapatite. *Inorganic Materials* **2018**, *54*, 820-825.
[199] Suchita Kohli, U. B. a. S. K. Influence of Zinc Substitution on Physicochemical and In-vitro Behaviour of Nanodimensional Hydroxyapatite. *Asian Journal of Engineering and Applied Technology* **2014**, *3*, 63-67.
[200] C. Paikaew, P. L., W. Kaewwiset and K. Naemchanthara Temperature effect on Zinc Substituted Hydroxyapatite Investigated by XRD, FTIR and FESEM Technique. *Siam Physics Congress 2016 proceedings* **2016**, 41-45.
[201] Nuamsrinuan, N.; Naemchanthara, P.; Limsuwan, P.; Naemchanthara, K. Influence of Zinc Substitution on Hydroxyapatite Structure Prepared by Chemical Precipitation Method. *Applied Mechanics and Materials* **2018**, *879*, 3-7.
[202] Ren, F.; Xin, R.; Ge, X.; Leng, Y. Characterization and Structural Analysis of Zinc-Substituted Hydroxyapatites. *Acta biomaterialia* **2009**, *5*, 3141-3149.
[203] Predoi, D.; Iconaru, S. L.; Deniaud, A.; Chevallet, M.; Michaud-Soret, I.; Buton, N.; Prodan, A. M. Textural, Structural and Biological Evaluation of Hydroxyapatite Doped with Zinc at Low Concentrations. *Materials (Basel, Switzerland)* **2017**, *10*, 229.
[204] Peñaflor Galindo, T. G.; Kataoka, T.; Tagaya, M. Morphosynthesis of Zn-Substituted Stoichiometric and Carbonate Hydroxyapatite Nanoparticles and Their Cytotoxicity in Fibroblasts. *Journal of Nanomaterials* **2015**, *2015*, 376045.
[205] LeGeros, R. Z.; Bonel, G.; Legros, R. Types of "H2O" in human enamel and in precipitated apatites. *Calcified Tissue Research* **1978**, *26*, 111-118.
[206] Predoi, D.; Iconaru, S. L.; Deniaud, A.; Chevallet, M.; Michaud-Soret, I.; Buton, N.; Prodan, A. *Textural, Structural and Biological Evaluation of Hydroxyapatite Doped with Zinc at Low Concentrations*, 2017; 229.

[207] Li, M. O.; Xiao, X.; Liu, R.; Chen, C.; Huang, L. Structural characterization of zinc-substituted hydroxyapatite prepared by hydrothermal method. *Journal of Materials Science: Materials in Medicine* **2008**, *19*, 797-803.
[208] Predoi, D.; Iconaru, S. L.; Deniaud, A.; Chevallet, M.; Michaud-Soret, I.; Buton, N.; Prodan, A. Textural, Structural and Biological Evaluation of Hydroxyapatite Doped with Zinc at Low Concentrations. *Materials* **2017**, *10*, 229.
[209] Zhang, W.; Shen, Y.; Pan, H.; Lin, K.; Liu, X.; Darvell, B. W.; Lu, W. W.; Chang, J.; Deng, L.; Wang, D.; Huang, W. Effects of strontium in modified biomaterials. *Acta Biomaterialia* **2011**, *7*, 800-808.
[210] Guo, D.; Hao, Y.; Li, H.; Fang, C.; Sun, L.; Zhu, H.; Wang, J.; Huang, X.; Ni, P.; Xu, K.-W. Influences of Sr dose on the crystal structure parameters and Sr distributions of Sr-incorporated hydroxyapatite. *Journal of biomedical materials research. Part B, Applied biomaterials* **2013**, *101*.
[211] Tavares, D. d. S.; Resende, C. X.; Quitan, M. P.; Castro, L. d. O.; Granjeiro, J. M.; Soares, G. d. A. Incorporation of strontium up to 5 Mol. (%) to hydroxyapatite did not affect its cytocompatibility. *Materials Research* **2011**, *14*, 456-460.
[212] Geng, Z.; Li, Z. Y.; Cui, Z. D.; Zhu, S.; Liang, Y.; Lu, W.; Yang, X. J. Synthesis, characterization and formation mechanism of magnesium- and strontium-substituted hydroxyapatite. *J. Mater. Chem. B* **2015**, *3*.
[213] O'Donnell, M. D.; Fredholm, Y.; de Rouffignac, A.; Hill, R. G. Structural analysis of a series of strontium-substituted apatites. *Acta Biomaterialia* **2008**, *4*, 1455-1464.
[214] Xu, Y.; An, L.; Chen, L.; Xu, H.; Zeng, D.; Wang, G. Controlled hydrothermal synthesis of strontium-substituted hydroxyapatite nanorods and their application as a drug carrier for proteins. *Advanced Powder Technology* **2018**, *29*, 1042-1048.
[215] Raul, P.; Senapati, S.; Sahoo, A.; Umlong, I.; Devi, R.; Thakur, A. J.; Veer, V. CuO Nanorods: A potential and Efficient Adsorbent in Water Purification. *RSC Adv.* **2014**, *4*.
[216] Haynes, W. M. *CRC Handbook of Chemistry and Physics, 95th Edition*; CRC Press LLC: Oakville, UNITED KINGDOM, 2014.
[217] Kazin, P.; Karpov, A.; Jansen, M.; Nuss, J.; Tretyakov, Y. Crystal Structure and Properties of Strontium Phosphate Apatite with Oxocuprate Ions in Hexagonal Channels. *Zeitschrift für anorganische und allgemeine Chemie* **2003**, *629*, 344-352.
[218] Pujari, M.; Patel, P. N. Strontium-copper-calcium hydroxyapatite solid solutions: Preparation, infrared, and lattice constant measurements. *Journal of Solid State Chemistry* **1989**, *83*, 100-104.
[219] Bhattacharjee, A.; Fang, Y.; Hooper, T. J. N.; Kelly, N. L.; Gupta, D.; Balani, K.; Manna, I.; Baikie, T.; Bishop, P. T.; White, T. J.; Hanna, J. V. Crystal Chemistry and Antibacterial Properties of Cupriferous Hydroxyapatite. *Materials* **2019**, *12*, 1814.
[220] Kolmas, J.; Velard, F.; Jaguszewska, A.; Lemaire, F.; Kerdjoudj, H.; Gangloff, S. C.; Kaflak, A. Substitution of strontium and boron into hydroxyapatite crystals: Effect on physicochemical properties and biocompatibility with human Wharton-Jelly stem cells. *Materials Science and Engineering: C* **2017**, *79*, 638-646.
[221] Tite, T.; Popa, A.-C.; Balescu, L. M.; Bogdan, I. M.; Pasuk, I.; Ferreira, J. M. F.; Stan, G. E. Cationic Substitutions in Hydroxyapatite: Current Status of the Derived Biofunctional Effects and Their In Vitro Interrogation Methods. *Materials (Basel, Switzerland)* **2018**, *11*, 2081.

[222] Sun, Y.; Yang, H.; Tao, D. Microemulsion process synthesis of lanthanide-doped hydroxyapatite nanoparticles under hydrothermal treatment. *Ceramics International* **2011**, *37*, 2917-2920.
[223] Carmen, C.; Iconaru, S. L.; Massuyeau, F.; Constantin, L.; Costescu, A.; Predoi, D. Synthesis, Structure, and Luminescent Properties of Europium-Doped Hydroxyapatite Nanocrystalline Powders. *Journal of Nanomaterials* **2012**.
[224] Liu, Y.; Tan, Y.; Wu, J. Rubidium doped nano-hydroxyapatite with cytocompatibility and antibacterial. *Journal of Asian Ceramic Societies* **2020**, *9*, 1-11.
[225] Rothenberger, A. Advanced Structural Inorganic Chemistry. By Wai-Kee Li, Gong-Du Zhou and Thomas C. W. Mak. *Angewandte Chemie International Edition* **2008**, *47*, 8343-8343.
[226] Santos, E.; Santos, I.; Noel, L.; Resende, C.; Soares, G. Crystallographic Aspects Regarding the Insertion of Ag+Ions into a Hydroxyapatite Structure. *Materials Research* **2015**, *18*, 881-890.
[227] Yao, F.; LeGeros, J. P.; LeGeros, R. Z. Simultaneous incorporation of carbonate and fluoride in synthetic apatites: Effect on crystallographic and physico-chemical properties. *Acta Biomaterialia* **2009**, *5*, 2169-2177.
[228] Wilson, R. M.; Elliott, J. C.; Dowker, S. E. P.; Smith, R. I. Rietveld structure refinement of precipitated carbonate apatite using neutron diffraction data. *Biomaterials* **2004**, *25*, 2205-2213.
[229] Goldberg, M. A.; Protsenko, P. V.; Smirnov, V. V.; Antonova, O. S.; Smirnov, S. V.; Konovalov, A. A.; Vorckachev, K. G.; Kudryavtsev, E. A.; Barinov, S. M.; Komlev, V. S. The enhancement of hydroxyapatite thermal stability by Al doping. *Journal of Materials Research and Technology* **2020**, *9*, 76-88.
[230] Qiao, W.; Liu, Q.; Li, Z.; Zhang, H.; Chen, Z. Changes in physicochemical and biological properties of porcine bone derived hydroxyapatite induced by the incorporation of fluoride. *Science and Technology of Advanced Materials* **2017**, *18*, 110-121.
[231] Gibson, I.; Bonfield, W. Novel Synthesis and Characterization of an AB-Type Carbonate-Substituted Hydroxyapatite. *Journal of biomedical materials research* **2002**, *59*, 697-708.
[232] Serret, A.; Cabañas, M. V.; Vallet-Regí, M. Stabilization of Calcium Oxyapatites with Lanthanum(III)-Created Anionic Vacancies. *Chemistry of Materials* **2000**, *12*, 3836-3841.
[233] Lin, C.-Y.; Yang, S.-H.; Lin, J.-L.; Yang, C.-F. *Effects of the Concentration of Eu3+ Ions and Synthesizing Temperature on the Luminescence Properties of Sr2−xEuxZnMoO6 Phosphors*, 2016; 30.
[234] Carmen, C.; Iconaru, S. L.; Massuyeau, F.; Violeta Constantin, L.; Costescu, A.; Predoi, D. *Synthesis, Structure, and Luminescent Properties of Europium-Doped Hydroxyapatite Nanocrystalline Powders*, 2012.
[235] Complexes of Bulky β-Diketiminate Ligands. In *Inorganic Syntheses*, 2010; pp 1-55.
[236] Wang, P.; Li, C.; Gong, H.; Jiang, X.; Wang, H.; Li, K. Effects of synthesis conditions on the morphology of hydroxyapatite nanoparticles produced by wet chemical process. *Powder Technology* **2010**, *203*, 315-321.
[237] Rodriguez Lugo, V.; Karthik, T. V. K.; Mendoza-Anaya, D.; Rubio-Rosas, E.; Cerón, L.; Reyes-Valderrama, M.; Salinas, E. Wet chemical synthesis of nanocrystalline hydroxyapatite flakes: Effect of pH and sintering temperature on structural and morphological properties. *Royal Society Open Science* **2018**, *5*, 180962.

[238] Rohani, S.; Al-Qasas, N. Synthesis of Pure Hydroxyapatite and the Effect of Synthesis Conditions on its Yield, Crystallinity, Morphology and Mean Particle Size. *Separation Science and Technology - SEPAR SCI TECHNOL* **2005**, *40*, 3187-3224.
[239] Joseph Nathanael, A.; Mangalaraj, D.; Hong, S. I.; Masuda, Y.; Rhee, Y. H.; Kim, H. W. Influence of fluorine substitution on the morphology and structure of hydroxyapatite nanocrystals prepared by hydrothermal method. *Materials Chemistry and Physics* **2013**, *137*, 967-976.
[240] Capanema, N. S. V.; Mansur, A. A. P.; Carvalho, S. M.; Silva, A. R. P.; Ciminelli, V. S.; Mansur, H. S. Niobium-Doped Hydroxyapatite Bioceramics: Synthesis, Characterization and In Vitro Cytocompatibility. *Materials (Basel, Switzerland)* **2015**, *8*, 4191-4209.
[241] Jehng, J.-M.; Wachs, I. E. Niobium oxide solution chemistry. *Journal of Raman Spectroscopy* **1991**, *22*, 83-89.
[242] Sommers, J. A. *Hydrolysis of niobium pentachloride solutions*; The Metallurgical Society Inc: United States, 1992.
[243] Ternane, R.; Cohen-Adad, M. T.; Panczer, G.; Goutaudier, C.; Kbir-Ariguib, N.; Trabelsi-Ayedi, M.; Florian, P.; Massiot, D. Introduction of boron in hydroxyapatite: synthesis and structural characterization. *Journal of Alloys and Compounds* **2002**, *333*, 62-71.
[244] Ayata, S. Estimation of limiting equivalent conductivity and ionic radius of tetraborate anion from conductivity measurements of concentrated tetraborate solutions. *Chemical Engineering Communications - CHEM ENG COMMUN* **2007**, *194*, 893-900.
[245] Cho, J. S.; Yoo, D. S.; Chung, Y.-C.; Rhee, S.-H. Enhanced bioactivity and osteoconductivity of hydroxyapatite through chloride substitution. *Journal of biomedical materials research. Part A* **2014**, *102*, 455-469.
[246] Elrayah, A.; Weng, J.; Suliman, E. *Effect-of-Copper-Ions-Doped-Hydroxyapatite-3D-Fiber-Scaffold*, 2019.
[247] Teraoka, K.; Ito, A.; Maekawa, K.; Onuma, K.; et al. Mechanical properties of hydroxyapatite and OH-carbonated hydroxyapatite single crystals. *Journal of Dental Research* **1998**, *77*, 1560-1568.
[248] Curran, D. J.; Fleming, T. J.; Towler, M. R.; Hampshire, S. Mechanical parameters of strontium doped hydroxyapatite sintered using microwave and conventional methods. *Journal of the Mechanical Behavior of Biomedical Materials* **2011**, *4*, 2063-2073.
[249] Bang, L. T.; Long, B. D.; Othman, R. Carbonate Hydroxyapatite and Silicon-Substituted Carbonate Hydroxyapatite: Synthesis, Mechanical Properties, and Solubility Evaluations. *The Scientific World Journal* **2014**, *2014*, 969876.
[250] Hannink, G.; Arts, J. Bioresorbability: Porosity and mechanical strength of bone substitutes: What is optimal for bone regeneration? *Injury* **2011**, *42 Suppl 2*, S22-25.
[251] Prakasam, M.; Locs, J.; Salma-Ancane, K.; Loca, D.; Largeteau, A.; Berzina-Cimdina, L. Fabrication, Properties and Applications of Dense Hydroxyapatite: A Review. *J Funct Biomater* **2015**, *6*, 1099-1140.
[252] Le Huec, J. C.; Schaeverbeke, T.; Clement, D.; Faber, J.; Le Rebeller, A. Influence of porosity on the mechanical resistance of hydroxyapatite ceramics under compressive stress. *Biomaterials* **1995**, *16*, 113-118.
[253] Liu, D.-M. Influence of porosity and pore size on the compressive strength of porous hydroxyapatite ceramic. *Ceramics International* **1997**, *23*, 135-139.
[254] Spath, S.; Drescher, P.; Seitz, H. Impact of Particle Size of Ceramic Granule Blends on Mechanical Strength and Porosity of 3D Printed Scaffolds. *Materials* **2015**, *8*, 4720-4732.

[255] Saxena, V.; Hasan, A.; Pandey, L. Effect of Zn/ZnO integration with hydroxyapatite: a review. *Materials Technology* **2017**.
[256] Pecqueux, F.; Tancret, F.; Payraudeau, N.; Bouler, J. M. Influence of microporosity and macroporosity on the mechanical properties of biphasic calcium phosphate bioceramics: Modelling and experiment. *Journal of the European Ceramic Society* **2010**, *30*, 819-829.
[257] Aoki, H.; Okayama, S.; Akao, M. Effect of Strontium Content on the Mechanical Properties of Bone and Sintered Hydroxyapatite. In *Bioceramics*; W. Bonfield; G. W. Hastings and K. E. Tanner, Eds.; Butterworth-Heinemann, 1991; pp 87-90.
[258] Narayan, R.; Colombo, P.; Salem, J.; Singh, D. *Advances in Bioceramics and Porous Ceramics II : A collection of papers presented at the 33rd International Conference on Advanced Ceramics and Composites, January 18-23, 2009, Daytona Beach, Florida*; John Wiley & Sons, Incorporated: Hoboken, UNITED STATES, 2009.
[259] Zyman, Z.; Tkachenko, M. *Sodium-carbonate co-substituted hydroxyapatite ceramics*, 2013; 153-157.
[260] Chen, Y.; Miao, X. Thermal and chemical stability of fluorohydroxyapatite ceramics with different fluorine contents. *Biomaterials* **2005**, *26*, 1205-1210.
[261] Teddy, T.; Popa, A.-C.; Trinca, L.; Bogdan, I.; Pasuk, I.; Ferreira, J.; Stan, G. Cationic Substitutions in Hydroxyapatite: Current Status of the Derived Biofunctional Effects and Their In Vitro Interrogation Methods. *Materials* **2018**, *11*, 2081.

Appendix A

Theoretical chemical calculations of unsubstituted HAp and 1% EuHAp samples:

Below are some examples of calculations that were performed to calculate the theoretical weights of the reactants that were used to synthesize unsubstituted HAp and 1%substituted EuHAp samples by the precipitation route:

1- Unsubstituted HAp materials: The following chemical equation, represents the reaction involved in the formation of unsubstituted HAp through using precipitation route:
$10\ Ca(NO_3)_2 + 6\ Na_2HPO_4 + 8\ NaOH \rightarrow Ca_{10}(PO_4)_6(OH)_2 + 20\ NaNO_3 + 6\ H_2O$.

5 g of unsubstituted HAp was prepared.

We used calcium nitrate $Ca(NO_3)_2$ as a source of Ca^{2+} ions (molecular weight = 164.09 g/mol) and disodium phosphate Na_2HPO_4 as a source of phosphate ions (molecular weight = 141.96 g/mol). The molecular weight of HAp is 1004.64g/mol.

The balanced equation was used to calculate the theoretical amounts of reactants, as the following:

5 g HAp X 1 mol HAp / 1004.64 g HAp X 10 mol $Ca(NO_3)_2$ / 1 mol HAp = 0.0498 mol $Ca(NO_3)_2$

0.0498 mol $Ca(NO_3)_2$ X 164.09 = 8.1666 g $Ca(NO_3)_2$.

0.0498 mol $Ca(NO_3)_2$ X 6 mol Na_2HPO_4 / 10 mol $Ca(NO_3)_2$ X 141.96 (molecular weight of Na_2HPO_4) = 4.2418 g Na_2HPO_4.

2- Unsubstituted HAp materials: The following chemical equation, represents the reaction involved in the formation of unsubstituted HAp through using the novel hydrolysis of MCP/$Ca(OH)_2$.

10 MCP → $Ca_{10}(PO_4)_6(OH)_2$.

5 g of unsubstituted HAp was prepared by the novel hydrolysis:

In the present study, calcium hydroxide ($Ca(OH)_2$) was used with monocalcium phosphate ($Ca(H_2PO_4)_2$) to supplement the calcium level in any resultant HAp products (and hence avoid the production of calcium deficient HAp).

The molecular weight of MCP and $Ca(OH)_2$ are 234.05 and 74.093 g/mol, respectively. The molecular weight of HAp is 1004.64g/mol.

5 g HAp X 1 mol HAp / 1004.64 g HAp X 10 mol MCP / 1 mol HAp = 0.0498 mol MCP.

0.0498 mol MCP X 234.05 g/mol = 11.655 g MCP.

0.0498 mol $Ca(OH)_2$X 74.093 g/mol =3.6898 g $Ca(OH)_2$.

3- Substituted HAp materials: The reaction of the formation of 1% EuHAp can be expressed as the following:

(10-x) Ca^{2+} + x Eu^{3+} + 6 PO_4^{3-} + 2 OH^- → $Ca_{9.93}$ $Eu_{0.07}$ $(PO_4)_6$ $(OH)_2$, where x = 0.07.

5 g of 1% EuHAp (1 wt.% Eu^{3+}) was prepared.

Calcium nitrate $Ca(NO_3)_2$ was used as a source of Ca^{2+} ions (molecular weight = 164.09 g/mol), disodium phosphate Na_2HPO_4 as a source of phosphate ions (molecular weight = 141.96 g/mol) and Europium (III) nitrate pentahydrate $Eu(NO_3)_3.5H_2O$ (molecular weight = 428.06 g/mol).

The molecular weight of 0.07 EuHAp is 1012.45 g/mol

The balanced equation was used to calculate the theoretical amounts of reactants, as the following:

5 g HAp X 1 mol EuHAp / 1012.45 g HAp X 9.93 mol $Ca(NO_3)_2$ / 1 mol EuHAp = 0.0490 mol $Ca(NO_3)_2$.

0.0490 mol $Ca(NO_3)_2$ X 164.09 = 8.0467 g $Ca(NO_3)_2$.

0.0490 mol $Ca(NO_3)_2$ X 6 mol Na_2HPO_4 / 9.93 mol $Ca(NO_3)_2$ X 141.96 (molecular weight of Na_2HPO_4) = 4.2030 g Na_2HPO_4.

0.0490 mol $Ca(NO_3)_2$ X 0.07 mol $Eu(NO_3)_3.5H_2O$ / 9.93 mol $Ca(NO_3)_2$ X 428.06 (molecular weight of $Eu(NO_3)_3.5H_2O$) = 0.1479 g $Eu(NO_3)_3.5H_2O$.

%Eu = (0.07X151.96) / 1012.45 X100% = 1%.

4- Substituted HAp materials: The reaction of the formation of 0.5 ZnHAp can be expressed as the following:
$(10-x)\ Ca^{2+} + x\ Zn^{2+} + 6\ PO_4^{3-} + 2\ OH^- \rightarrow Ca_{9.5}\ Zn_{0.5}\ (PO_4)_6\ (OH)_2$, where x = 0.5.

5 g of 0.5 ZnHAp (molecular weight = 1017.29 g/mol) was prepared by the novel hydrolysis method using MCP (molecular weight = 234.05 g/mol), $Ca(OH)_2$ (molecular weight = 74.093 g/mol) and $Zn(NO_3)_2.6H_2O$ (molecular weight = 297.48 g/mol).

The balanced equation was used to calculate the theoretical amounts of reactants, as the following:

5 g 0.5 ZnHAp X 1 mol of 0.5 ZnHAp / 1017.29 g 0.5 ZnHAp X 9.5 mol MCP / 1 mol 0.5 ZnHAp = 0.0467 mol MCP.

0.0467 mol MCP X 234.05 g/mol = 10.9301 g MCP.

0.0467 mol $Ca(OH)_2$X 74.093 g/mol =3.4601 g $Ca(OH)_2$.

0.0467 mol MCP X 0.5 $Zn(NO_3)_2.6H_2O$/9.5 MCP X 297.48 g/mol = 0.7312.

ICP-MS calculations of unsubstituted HAp samples:

Below are given some examples that were performed to calculate the measured Ca/P and (Ca+Na)/P mole ratios of the sintered unsubstituted HAp powders prepared by hydrolysis method:

The following result was detected by ICP-MS analysis of sintered unsubstituted HAp materials at 900 ˚C by hydrolysis method. The concentration was in ppb (ug/L):

Sample	Ca 44	P 31	Na 23
Unsubstituted HAp by hydrolysis	769928	423970	78396

the chemical analysis data of commercial HAp (Fluka) and sintered unsubstituted HAp materials prepared by precipitation and hydrolysis methods at 900 ˚C by ICP-MS measurements.

Sample	Ca/P Theoretical	Ca/P Measured	(Ca+Na)/ P Mole ratio
Unsubstituted HAp by hydrolysis	1.67	1.40	1.65

The weight of calcium in 1 L= (769928ug/L)X(1g/1000,000ug)X1L= 0.769928 g.

The number of moles of calcium =(0.769928 g)X(mole/ 40.078 g)= 0.0192 mole Ca.

The weight of phosphorus in I L= (423970 ug/L) X(1g/1000,000ug)X1L = 0.423970 g.

The number of moles of phosphorus = (0.423970 g)X (mole/ 30.974 g) = 0.0137 mole P.

The weight of sodium in 1 L = (78396 ug/L) X(1g/1000,000ug)X1L = 0.078396 g.

The number of moles of sodium = (0.078396 g)X (mole/ 22.99 g) =0.0034 mole Na.

Ca/P =(0.0192 mole Ca / 0.0137 mole P)= 1.40.

(Ca+Na)/P= (0.0192 mole Ca + 0.0034 mole Na)/ 0.0137 mole P= 1.65.

ICP-MS calculations of 0.5ZnHAp samples:

Below are given some examples that were performed to calculate the measured Ca/P and (Ca+Na+Zn)/P mole ratios of the sintered 0.5 ZnHAp samples, as well as the measured wt.% of Zn^{2+} that had been substituted into HAp crystal.

ICP-MS results of O.5 ZnHAp materials from the present study which were at 900 ˚C as prepared by the hydrolysis reaction. Concentrations are quoted in ppb (ug/L):

Sample	**Ca 44**	**P 31**	**Na 23**	**Zn 66**
0.5 ZnHAp by hydrolysis	697527	380678	112772	30472.3

The chemical analysis data of prepared sintered 0.5ZnHAp materials by ICP-MS measurements

Sample	**Ca/P Expected**	**Ca/P Measured**	**(Ca+Na+Zn)/ P Measured**	**Wt.% of Zn^{2+} ions Theoretical**	**Wt.% of Zn^{2+} ions Measured**
0.5 ZnHAp by hydrolysis	**1.58**	**1.42**	**1.85**	**3.2%**	**1.5%**

The weight of calcium in 1 L= (697527ug/L)X(1g/1000,000ug)X1L= 0. 697527 g.

The number of moles of calcium =(0.697527 g)X(mole/ 40.078 g)= 0.0174 mole Ca.

The weight of phosphorus in I L= (380678 ug/L) X(1g/1000,000ug)X1L = 0.380678 g.

The number of moles of phosphorus = (0.380678 g)X (mole/ 30.974 g) = 0.0123 mole P.

The weight of sodium in 1 L = (112772 ug/L) X(1g/1000,000ug)X1L = 0.112772 g.

The number of moles of sodium = (0.112772 g)X (mole/ 22.99 g) =0.0049 mole Na.

The weight of zinc in 1 L= (30472.3ug/L)X(1g/1000,000ug)X1L= 0. 0304723 g.

The number of moles of zinc =(0304723g)X(mole/ 65.38 g)= 0.00047 mole Zn.

Ca/P =(0.0174 mole Ca / 0.0123 mole P)= 1.42.

(Ca+Na+Zn)/P= (0.0174 mole Ca + 0.0049 mole Na+ 0.00047)/ 0.0123 mole P= 1.85.

In order to do perform the ICP-MS measurements, 0.1 g of 0.5 ZnHAp was dissolved in 50 mL. Therefore, the concentration of 0.5 ZnHAp = 0.1/0.05= 2 g/L.

The measured concentration of 0.5 ZnHAp by using ICP-MS = 0. 0304723 g/L.

The measured wt.% of Zn^{2+} ions = (0. 0304723/2)*100%= 1.5%

The result of SEM/EDX analysis of the 1%EuHAp samples:

Below are given some example that were performed to calculate the measured Ca/P mole ratio of the sintered 1% EuHAp powders at 900 ˚C as prepared by the precipitation method:

The following result was detected by SEM/EDX analysis of sintered 1% EuHAp materials at 900 ˚C by the precipitation method.

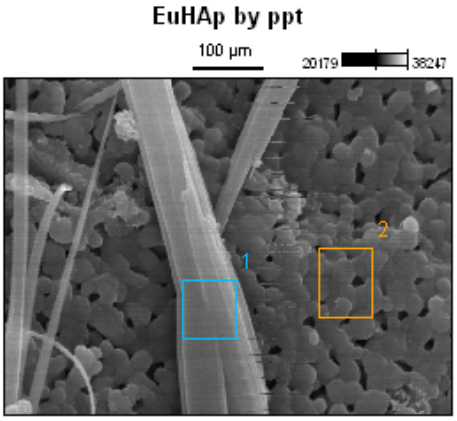

Image Name: EuHAp by ppt

Accelerating Voltage: 15.0 kV

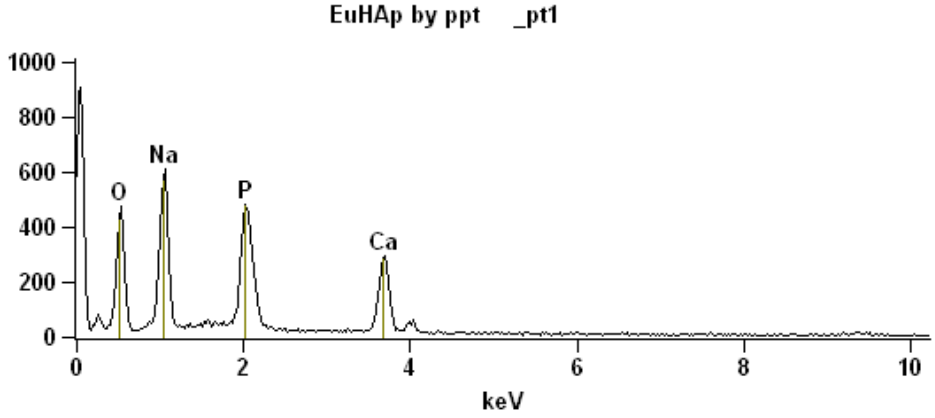

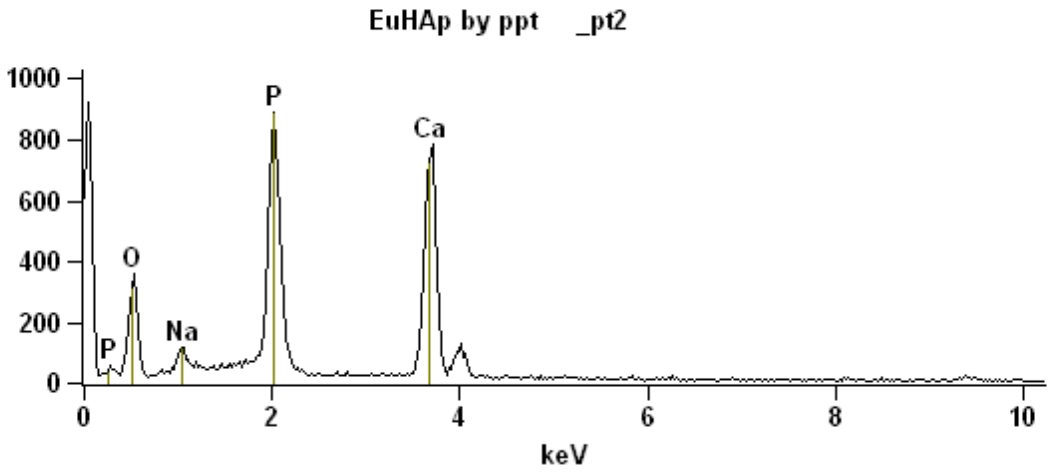

Weight %

	O-K	Na-K	P-K	Ca-K
EuHAp by ppt _pt1	32.76	23.74	19.86	23.64
EuHAp by ppt _pt2	25.25	2.22	25.75	46.79

Weight % Error (+/- 1 Sigma)

	O-K	Na-K	P-K	Ca-K
EuHAp by ppt _pt1	+/-0.61	+/-0.41	+/-0.46	+/-0.68
EuHAp by ppt _pt2	+/-0.58	+/-0.21	+/-0.41	+/-0.76

Atom %

	O-K	Na-K	P-K	Ca-K
EuHAp by ppt _pt1	47.49	23.95	14.87	13.68
EuHAp by ppt _pt2	42.97	2.62	22.63	31.78

Atom % Error (+/- 1 Sigma)

	O-K	*Na-K*	*P-K*	*Ca-K*
EuHAp by ppt _pt1	+/-0.88	+/-0.42	+/-0.35	+/-0.40
EuHAp by ppt _pt2	+/-0.98	+/-0.25	+/-0.36	+/-0.52

The chemical analysis data of sintered EuHAp samples that contain the whiskers (labelled as EuHAp by ppt_pt1) and the spherical particles (labelled as EuHAp by ppt_pt2) at 900 ˚C by SEM/EDX technique.

Sample	**Ca/P**
	Measured
Whiskers	0.91
Spherical particle	1.40

The number of moles of calcium in the whiskers = 23.64/ 40.078 = 0.58598 mole.

The number of moles of phosphorus in the whiskers = 19.86/ 30.97 = 0.6413 mole.

Ca/P mole ratio in the whiskers = 0.58598/0.6413= 0.91.

The number of moles of calcium in the spherical particles = 46.79/ 40.078 = 1.1675 mole.

The number of moles of phosphorus in the spherical particles = 25.75/ 30.97 = 0.8314 mole.

Ca/P mole ratio in the spherical particles = 1.1675 /0.8314 = 1.40.

The result of SEM/EDX analysis of 1%ScHAp samples:

The following result was detected by SEM/EDX analysis of sintered 1% ScHAp materials at 900 ˚C by the precipitation method.

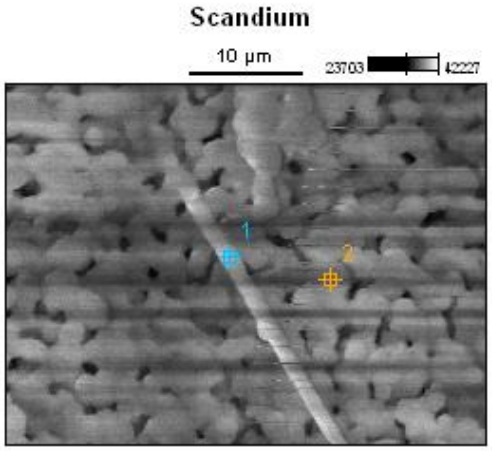

Image Name: Scandium

Accelerating Voltage: 20.0 kV

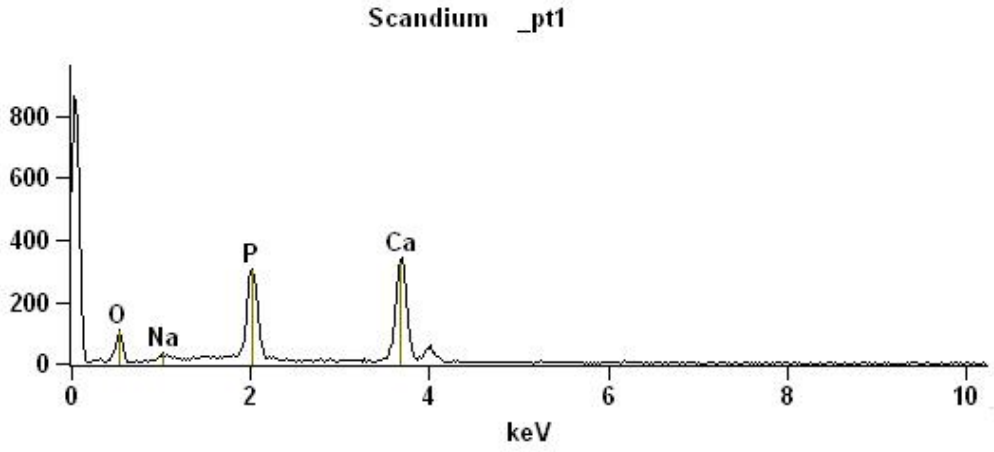

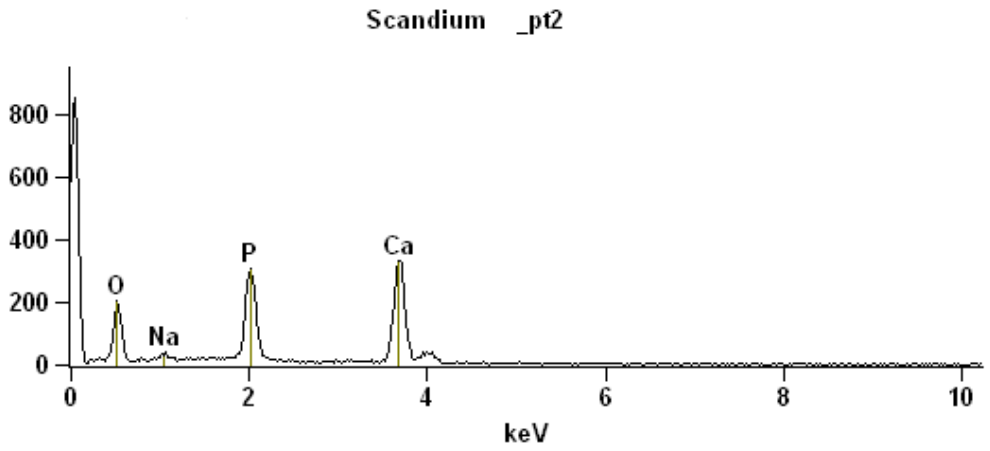

Weight %

	O-K	Na-K	P-K	Ca-K
Scandium_pt1	29.37	2.17	23.56	44.91
Scandium_pt2	42.75	1.59	18.95	36.71

Weight % Error (+/- 1 Sigma)

	O-K	Na-K	P-K	Ca-K
Scandium(2)_pt1	+/-1.20	+/-0.36	+/-0.58	+/-1.05
Scandium(2)_pt2	+/-1.18	+/-0.19	+/-0.47	+/-0.84

Atom %

	O-K	Na-K	P-K	Ca-K
Scandium_pt1	48.17	2.47	19.96	29.40
Scandium_pt2	62.60	1.62	14.33	21.46

Atom % Error (+/- 1 Sigma)

	O-K	Na-K	P-K	Ca-K
Scandium_pt1	+/-1.97	+/-0.41	+/-0.49	+/-0.69
Scandium_pt2	+/-1.73	+/-0.20	+/-0.35	+/-0.49

The result of SEM/EDX analysis of SAp samples:

The following result was detected by SEM/EDX analysis of sintered SAp materials at 900 ˚C by the precipitation method.

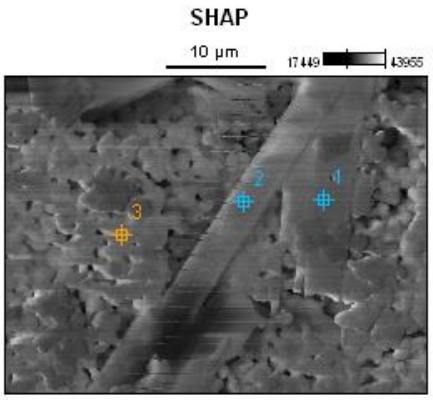

Image Name: SHAP

Accelerating Voltage: 20.0 kV

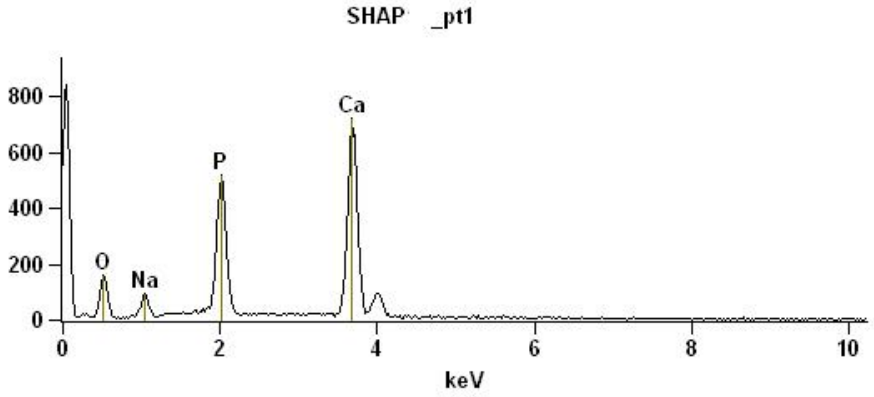

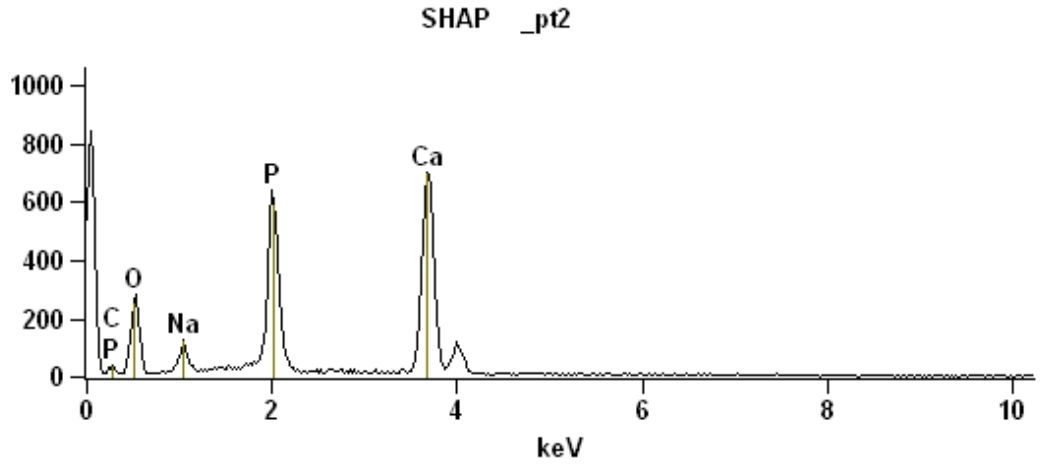
SHAP _pt2
1000
800
600
400
200
0
C
O
P
Na
P
Ca
0
2
4
6
8
10
keV

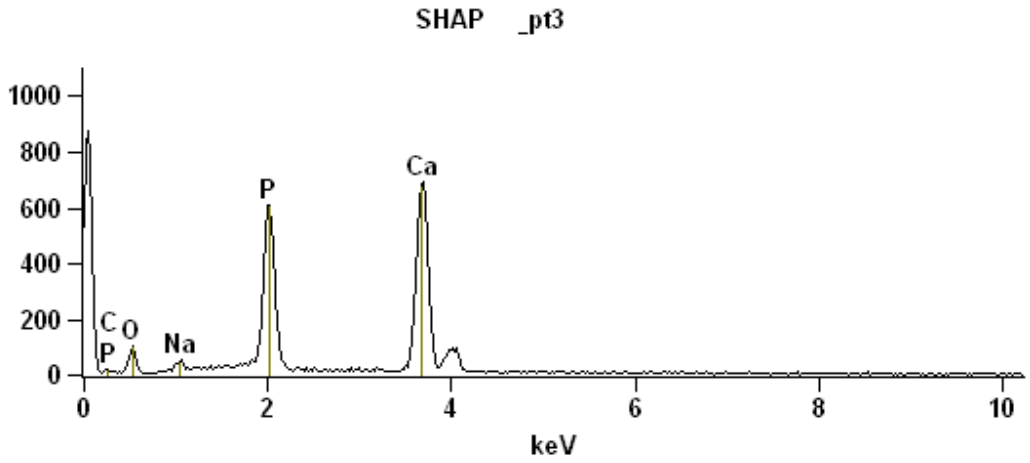
SHAP _pt3
1000
800
600
400
200
0
C
P
O
Na
P
Ca
0
2
4
6
8
10
keV

Weight %

	C-K	O-K	Na-K	P-K	Ca-K
SHAP_pt1		27.91	4.44	20.44	47.21
SHAP_pt2	4.87	34.29	3.86	18.39	38.59
SHAP_pt3	3.38	17.44	1.93	24.71	52.55

Weight % Error (+/- 1 Sigma)

	C-K	O-K	Na-K	P-K	Ca-K
SHAP_pt1		+/-0.82	+/-0.24	+/-0.38	+/-0.76
SHAP_pt2	+/-0.63	+/-0.81	+/-0.23	+/-0.33	+/-0.61
SHAP_pt3	+/-0.44	+/-0.78	+/-0.23	+/-0.43	+/-0.82

Atom %

	C-K	O-K	Na-K	P-K	Ca-K
SHAP_pt1		46.21	5.11	17.48	31.20
SHAP_pt2	9.49	50.15	3.93	13.89	22.53
SHAP_pt3	7.89	30.59	2.35	22.38	36.79

Atom % Error (+/- 1 Sigma)

	C-K	O-K	Na-K	P-K	Ca-K
SHAP_pt1		+/-1.36	+/-0.28	+/-0.33	+/-0.50
SHAP_pt2	+/-1.23	+/-1.18	+/-0.23	+/-0.25	+/-0.36
SHAP_pt3	+/-1.03	+/-1.37	+/-0.28	+/-0.39	+/-0.58

The result of SEM/EDX analysis of NaClHAp samples:

The following result was detected by SEM/EDX analysis of the sintered NaClHAp materials at 900 ˚C which was originally prepared by the precipitation method.

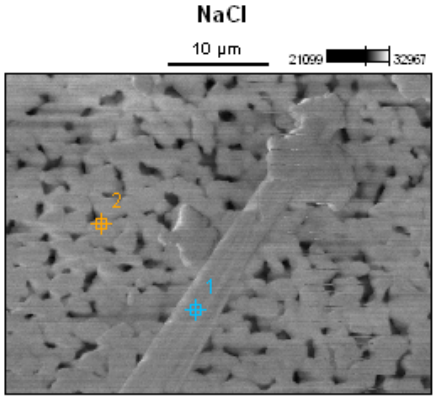

Image Name: NaCl

Accelerating Voltage: 20.0 kV

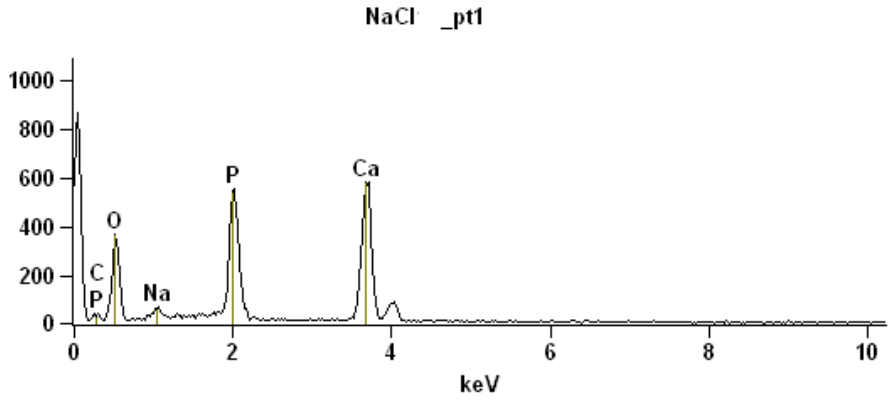

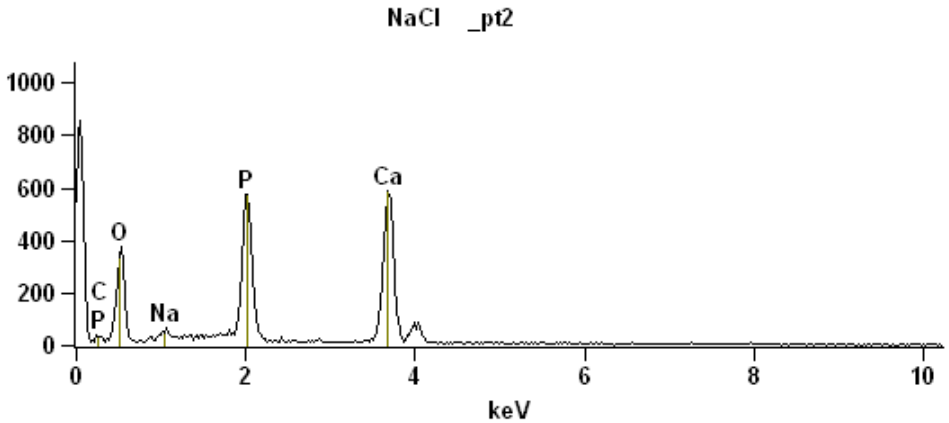

Weight %

	C-K	O-K	Na-K	P-K	Ca-K
NaCl_pt1	2.63	42.44	1.69	18.37	34.88
NaCl_pt2	4.52	42.98	1.38	18.43	32.69

Weight % Error (+/- 1 Sigma)

	C-K	O-K	Na-K	P-K	Ca-K
NaCl_pt1	+/-0.46	+/-0.86	+/-0.14	+/-0.34	+/-0.60
NaCl_pt2	+/-0.74	+/-0.89	+/-0.23	+/-0.33	+/-0.59

Atom %

	C-K	O-K	Na-K	P-K	Ca-K
NaCl_pt1	4.96	60.17	1.66	13.45	19.75
NaCl_pt2	8.30	59.25	1.32	13.13	17.99

Atom % Error (+/- 1 Sigma)

	C-K	O-K	Na-K	P-K	Ca-K
NaCl_pt1	+/-0.86	+/-1.22	+/-0.14	+/-0.25	+/-0.34
NaCl_pt2	+/-1.35	+/-1.23	+/-0.22	+/-0.24	+/-0.33

The calculations of the compression strength:

Below is given one example that were performed to calculate the compressive strength of the sintered cylindrical specimen of B_4O_7HAp powders, which was prepared by the hydrolysis method:

The **load versus extension** graph of B_4O_7HAp as recorded by the Instron mechanical tester is presented below:

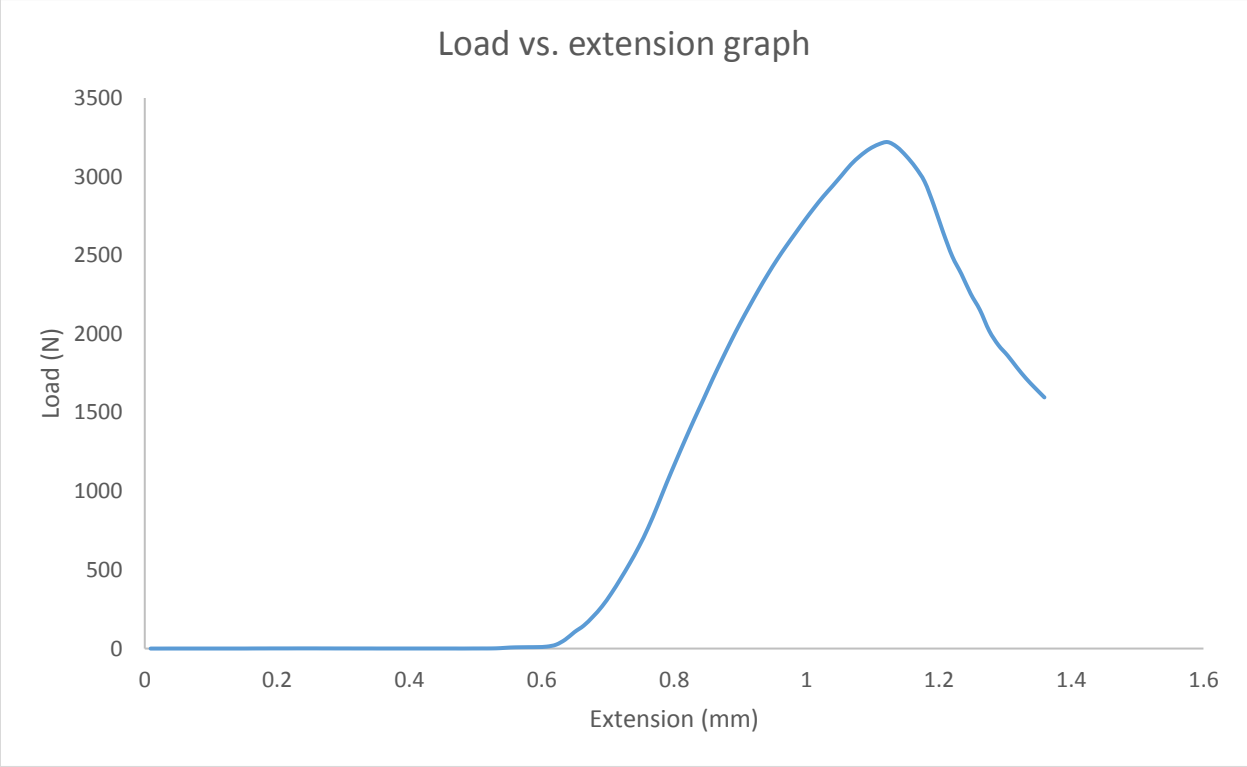

The maximum Load (N) as shown by the graph is 3220 N.

The diameter of the cylindrical specimen of B_4O_7HAp powders is 11.12 mm. Therefore, the radius is 11.12/2 = 5.56 mm.
The cross sectional area of the cylindrical specimen of B_4O_7HAp powders = πr^2, where π =3.14 and r (radius) = 5.56 mm. Therefore, the area = $3.14(5.56)^2$ = 97.0687 mm^2.

Compressive strength = F/A, where F is a failure load (in Newtons, N), and A is the sample cross-sectional area (mm^2). Therefore, Compressive strength = 3220 N / 97.0687 mm^2 = 33.17 MPa.

Analysis - Under

Measurement Details	
Sample Name	BHAp
SOP File Name	Hydroxyapatite.SOP.msop
Lab Number	
Operator Name	instrument

Measurement Details	
Analysis Date Time	28/02/2020 10:15:12 AM
Measurement Date Time	28/02/2020 10:15:12 AM
Result Source	Measurement

Analysis	
Particle Name	Calcium Apatite (Hydroxyapatite)
Particle Refractive Index	1.640
Particle Absorption Index	0.010
Dispersant Name	Water
Dispersant Refractive Index	1.330
Scattering Model	Mie
Analysis Model	General Purpose
Weighted Residual	0.49 %
Laser Obscuration	7.92 %

Result	
Concentration	0.0060 %
Span	5.321
Uniformity	1.973
Specific Surface Area	473.8 m^2/kg
D [3,2]	6.33 µm
D [4,3]	35.3 µm
Dv (10)	2.63 µm
Dv (50)	14.7 µm
Dv (90)	80.6 µm

Frequency (compatible)

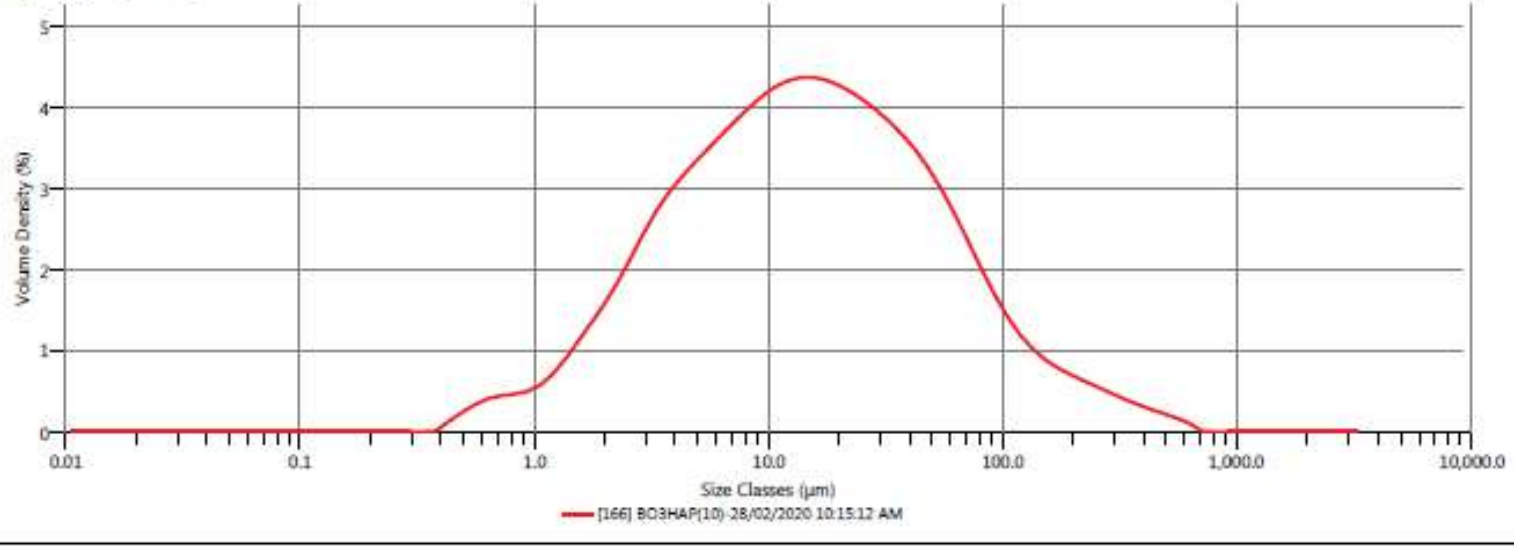

Result

Size (µm)	% Volume Under	Size (µm)	% Volume Under	Size (µm)	% Volume Under	Size (µm)	% Volume Under	Size (µm)	% Volume Under	Size (µm)	% Volume Under	Size (µm)	% Volume Under	Size (µm)	% Volume Under
0.0100	0.00	0.0597	0.00	0.357	0.00	2.13	7.30	12.7	45.98	76.0	88.22	454	99.57	2710	100.00
0.0114	0.00	0.0679	0.00	0.405	0.00	2.42	8.84	14.5	49.61	86.4	90.91	516	99.76	3080	100.00
0.0129	0.00	0.0771	0.00	0.460	0.11	2.75	10.62	16.4	53.27	98.1	92.33	586	99.90	3500	100.00
0.0147	0.00	0.0876	0.00	0.523	0.31	3.12	12.66	18.7	56.89	111	93.52	666	100.00		
0.0167	0.00	0.0995	0.00	0.594	0.59	3.55	14.96	21.2	60.47	127	94.51	756	100.00		
0.0189	0.00	0.113	0.00	0.675	0.93	4.03	17.43	24.1	63.97	144	95.36	859	100.00		
0.0215	0.00	0.128	0.00	0.767	1.31	4.58	20.07	27.4	67.38	163	96.09	976	100.00		
0.0244	0.00	0.146	0.00	0.872	1.69	5.21	22.85	31.1	70.69	186	96.74	1110	100.00		
0.0278	0.00	0.166	0.00	0.991	2.11	5.92	25.77	35.3	73.88	211	97.33	1260	100.00		
0.0315	0.00	0.188	0.00	1.13	2.58	6.72	28.83	40.1	76.93	240	97.85	1430	100.00		
0.0358	0.00	0.214	0.00	1.28	3.17	7.64	32.03	45.6	79.83	272	98.31	1630	100.00		
0.0407	0.00	0.243	0.00	1.45	3.92	8.68	35.35	51.8	82.54	310	98.71	1850	100.00		
0.0463	0.00	0.276	0.00	1.65	4.86	9.86	38.80	58.9	85.02	352	99.05	2100	100.00		
0.0526	0.00	0.314	0.00	1.88	5.98	11.2	42.34	66.9	87.26	400	99.33	2390	100.00		

Analysis - Under

Measurement Details	
Sample Name	BHAp
SOP File Name	Hydroxyapatite.SOP.msop
Lab Number	
Operator Name	instrument

Measurement Details	
Analysis Date Time	28/02/2020 10:15:44 AM
Measurement Date Time	28/02/2020 10:15:44 AM
Result Source	Measurement

Analysis	
Particle Name	Calcium Apatite (Hydroxyapatite)
Particle Refractive Index	1.640
Particle Absorption Index	0.010
Dispersant Name	Water
Dispersant Refractive Index	1.330
Scattering Model	Mie
Analysis Model	General Purpose
Weighted Residual	0.54 %
Laser Obscuration	7.99 %

Result	
Concentration	0.0059 %
Span	4.850
Uniformity	1.840
Specific Surface Area	486.2 m^2/kg
D [3,2]	6.17 µm
D [4,3]	31.5 µm
Dv (10)	2.61 µm
Dv (50)	13.8 µm
Dv (90)	69.4 µm

Frequency (compatible)

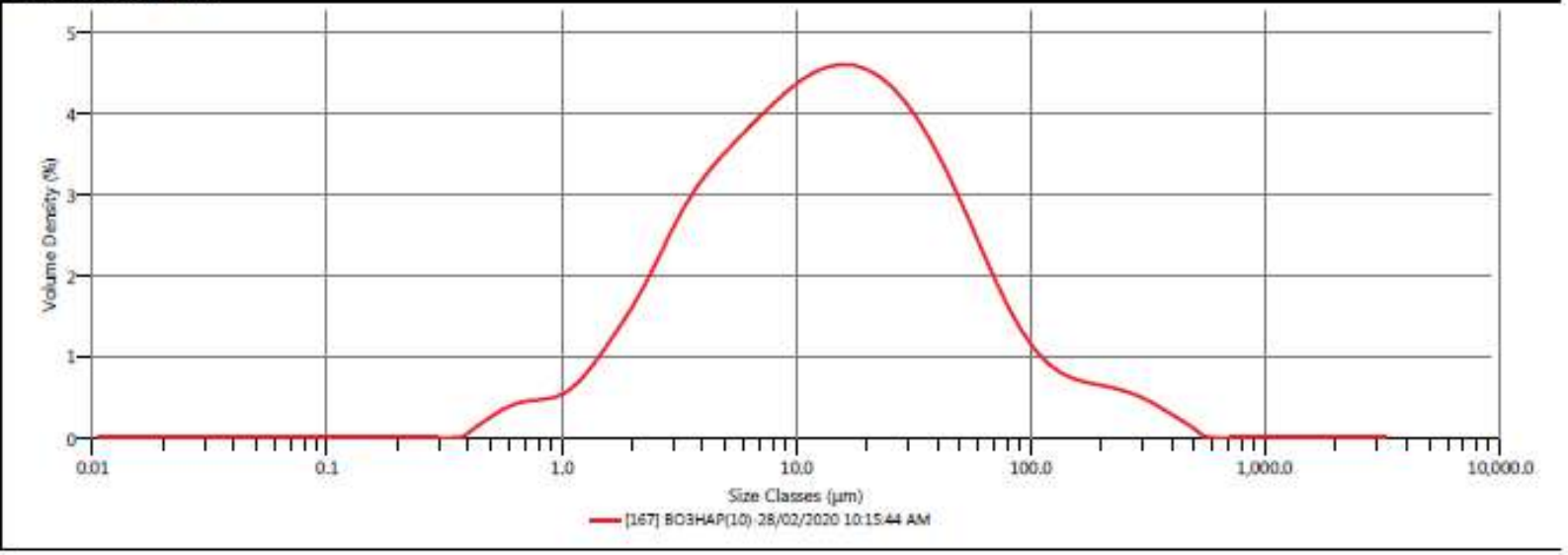

Result

Size (µm)	% Volume Under	Size (µm)	% Volume Under	Size (µm)	% Volume Under	Size (µm)	% Volume Under	Size (µm)	% Volume Under	Size (µm)	% Volume Under	Size (µm)	% Volume Under	Size (µm)	% Volume Under
0.0100	0.00	0.0597	0.00	0.357	0.00	2.13	7.36	12.7	47.63	76.0	91.14	454	99.88	2710	100.00
0.0114	0.00	0.0679	0.00	0.405	0.00	2.42	8.94	14.5	51.45	86.4	92.47	516	100.00	3080	100.00
0.0129	0.00	0.0771	0.00	0.460	0.11	2.75	10.78	16.4	55.30	98.1	93.56	588	100.00	3500	100.00
0.0147	0.00	0.0876	0.00	0.523	0.32	3.12	12.90	18.7	59.14	111	94.46	668	100.00		
0.0167	0.00	0.0995	0.00	0.594	0.61	3.55	15.28	21.2	62.95	127	95.22	756	100.00		
0.0189	0.00	0.113	0.00	0.675	0.96	4.03	17.87	24.1	66.67	144	95.89	859	100.00		
0.0215	0.00	0.128	0.00	0.767	1.34	4.58	20.64	27.4	70.29	163	96.49	976	100.00		
0.0244	0.00	0.146	0.00	0.872	1.74	5.21	23.55	31.1	73.76	186	97.06	1110	100.00		
0.0278	0.00	0.166	0.00	0.991	2.15	5.92	26.61	35.3	77.04	211	97.60	1260	100.00		
0.0315	0.00	0.188	0.00	1.13	2.62	6.72	29.81	40.1	80.09	240	98.12	1430	100.00		
0.0358	0.00	0.214	0.00	1.28	3.20	7.64	33.14	45.6	82.89	272	98.60	1630	100.00		
0.0407	0.00	0.243	0.00	1.45	3.95	8.68	36.60	51.8	85.41	310	99.03	1850	100.00		
0.0463	0.00	0.276	0.00	1.65	4.89	9.86	40.18	58.9	87.61	352	99.39	2100	100.00		
0.0526	0.00	0.314	0.00	1.88	6.02	11.2	43.87	66.9	89.54	400	99.68	2390	100.00		

Analysis - Under

Measurement Details	
Sample Name	BHAp
SOP File Name	Hydroxyapatite.SOP.msop
Lab Number	
Operator Name	instrument

Measurement Details	
Analysis Date Time	28/02/2020 10:16:17 AM
Measurement Date Time	28/02/2020 10:16:17 AM
Result Source	Measurement

Analysis	
Particle Name	Calcium Apatite (Hydroxyapatite)
Particle Refractive Index	1.640
Particle Absorption Index	0.010
Dispersant Name	Water
Dispersant Refractive Index	1.330
Scattering Model	Mie
Analysis Model	General Purpose
Weighted Residual	0.51 %
Laser Obscuration	8.03 %

Result	
Concentration	0.0059 %
Span	4.590
Uniformity	1.764
Specific Surface Area	492.3 m^2/kg
D [3,2]	6.09 µm
D [4,3]	29.3 µm
Dv (10)	2.60 µm
Dv (50)	13.2 µm
Dv (90)	63.3 µm

Frequency (compatible)

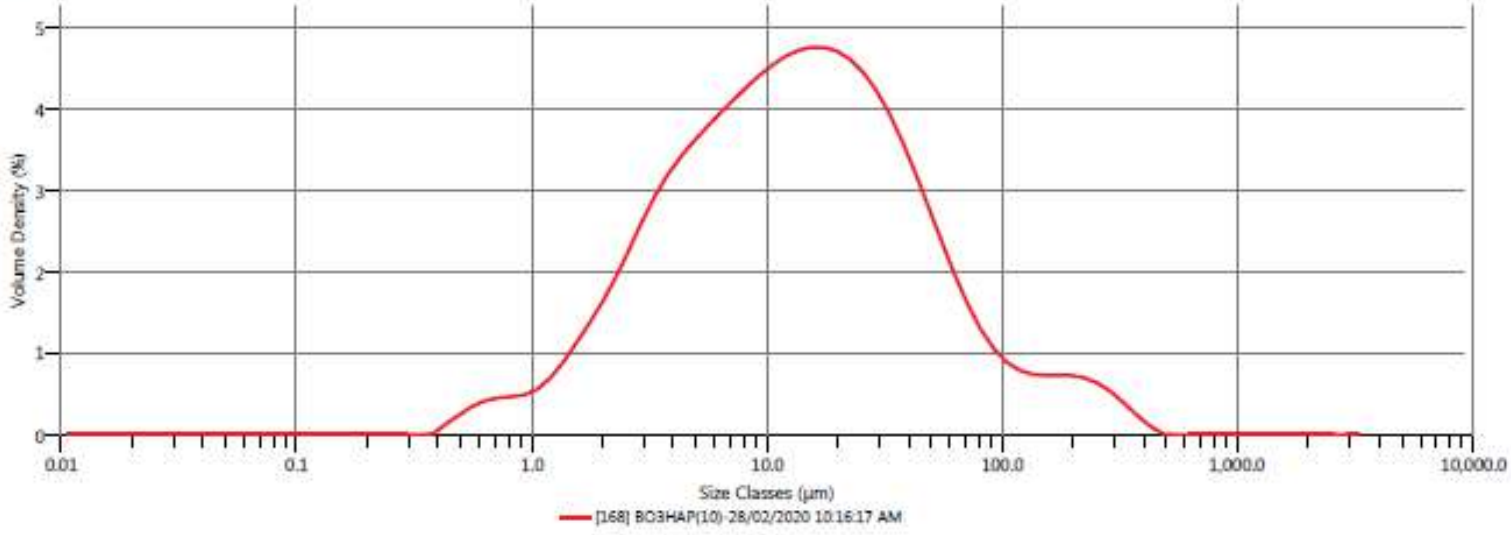

Result

Size (µm)	% Volume Under	Size (µm)	% Volume Under	Size (µm)	% Volume Under	Size (µm)	% Volume Under	Size (µm)	% Volume Under	Size (µm)	% Volume Under	Size (µm)	% Volume Under	Size (µm)	% Volume Under
0.0100	0.00	0.0597	0.00	0.257	0.00	2.13	7.35	12.7	48.79	76.0	92.04	454	100.00	2710	100.00
0.0114	0.00	0.0679	0.00	0.405	0.00	2.42	8.95	14.5	52.73	86.4	93.12	516	100.00	3080	100.00
0.0129	0.00	0.0771	0.00	0.460	0.11	2.75	10.84	16.4	56.71	98.1	93.99	586	100.00	3500	100.00
0.0147	0.00	0.0876	0.00	0.523	0.31	3.12	13.01	18.7	60.69	111	94.74	666	100.00		
0.0167	0.00	0.0995	0.00	0.594	0.60	3.55	15.46	21.2	64.63	127	95.39	756	100.00		
0.0189	0.00	0.113	0.00	0.675	0.96	4.03	18.13	24.1	68.48	144	96.01	859	100.00		
0.0215	0.00	0.128	0.00	0.767	1.34	4.58	20.98	27.4	72.21	163	96.61	976	100.00		
0.0244	0.00	0.146	0.00	0.872	1.72	5.21	23.99	31.1	75.74	186	97.22	1110	100.00		
0.0278	0.00	0.166	0.00	0.991	2.13	5.92	27.15	35.3	79.04	211	97.83	1260	100.00		
0.0315	0.00	0.188	0.00	1.13	2.59	6.72	30.44	40.1	82.05	240	98.42	1430	100.00		
0.0358	0.00	0.214	0.00	1.28	3.17	7.64	33.87	45.6	84.74	272	98.95	1630	100.00		
0.0407	0.00	0.243	0.00	1.45	3.91	8.68	37.43	51.8	87.08	310	99.39	1850	100.00		
0.0463	0.00	0.276	0.00	1.65	4.85	9.86	41.12	58.9	89.06	352	99.72	2100	100.00		
0.0526	0.00	0.314	0.00	1.88	5.99	11.2	44.91	66.9	90.70	400	99.91	2390	100.00		

Analysis - Under

Measurement Details	
Sample Name	Average of 'B HAP
SOP File Name	Hydroxyapatite.SOP.msop
Lab Number	
Operator Name	instrument

Measurement Details	
Analysis Date Time	28/02/2020 10:15:12 AM
Measurement Date Time	28/02/2020 10:15:12 AM
Result Source	Averaged

Analysis	
Particle Name	Calcium Apatite (Hydroxyapatite)
Particle Refractive Index	1.640
Particle Absorption Index	0.010
Dispersant Name	Water
Dispersant Refractive Index	1.330
Scattering Model	Mie
Analysis Model	General Purpose
Weighted Residual	0.51 %
Laser Obscuration	7.98 %

Result	
Concentration	0.0059 %
Span	4.964
Uniformity	1.867
Specific Surface Area	484.1 m^2/kg
D [3,2]	6.20 µm
D [4,3]	32.0 µm
Dv (10)	2.61 µm
Dv (50)	13.9 µm
Dv (90)	71.4 µm

Frequency (compatible)

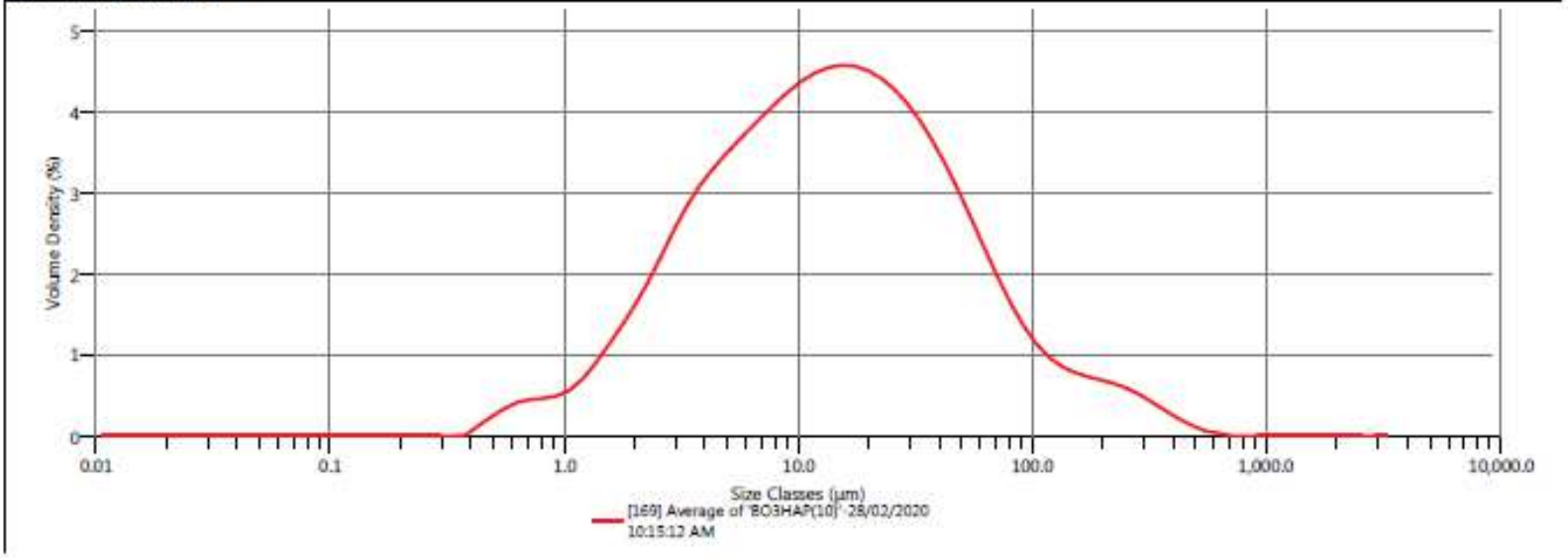

Result

Size (µm)	% Volume Under	Size (µm)	% Volume Under	Size (µm)	% Volume Under	Size (µm)	% Volume Under	Size (µm)	% Volume Under	Size (µm)	% Volume Under	Size (µm)	% Volume Under	Size (µm)	% Volume Under
0.0100	0.00	0.0597	0.00	0.357	0.00	2.13	7.34	12.7	47.46	76.0	90.80	454	99.81	2710	100.00
0.0114	0.00	0.0679	0.00	0.405	0.00	2.42	8.91	14.5	51.27	86.4	92.16	516	99.92	3080	100.00
0.0129	0.00	0.0771	0.00	0.460	0.11	2.75	10.75	16.4	55.09	98.1	93.29	586	99.97	3500	100.00
0.0147	0.00	0.0876	0.00	0.523	0.31	3.12	12.86	18.7	58.91	111	94.24	666	100.00		
0.0167	0.00	0.0995	0.00	0.594	0.60	3.55	15.23	21.2	62.68	127	95.04	756	100.00		
0.0189	0.00	0.113	0.00	0.675	0.95	4.03	17.81	24.1	66.38	144	95.75	859	100.00		
0.0215	0.00	0.128	0.00	0.767	1.33	4.58	20.56	27.4	69.98	163	96.40	976	100.00		
0.0244	0.00	0.146	0.00	0.872	1.72	5.21	23.47	31.1	73.40	186	97.01	1110	100.00		
0.0278	0.00	0.166	0.00	0.991	2.13	5.92	26.51	35.3	76.65	211	97.59	1260	100.00		
0.0315	0.00	0.188	0.00	1.13	2.60	6.72	29.69	40.1	79.69	240	98.13	1430	100.00		
0.0358	0.00	0.214	0.00	1.28	3.18	7.64	33.01	45.6	82.49	272	98.62	1630	100.00		
0.0407	0.00	0.243	0.00	1.45	3.93	8.68	36.46	51.8	85.01	310	99.04	1850	100.00		
0.0463	0.00	0.276	0.00	1.65	4.88	9.86	40.03	58.9	87.24	352	99.39	2100	100.00		
0.0526	0.00	0.314	0.00	1.88	6.00	11.2	43.71	66.9	89.17	400	99.64	2390	100.00		